DOE Grant No: DE-FE-0026041

Office of Fossil Energy

Assessment of CO_2 Storage Resources in Depleted Oil and Gas Fields in the Ship Shoal Area, Gulf of Mexico

Final Report

DOE-GMT-0026041-F

Dr. Michael S. Bruno (PI)
GeoMechanics Technologies
103 E. Lemon Ave.,
Monrovia, CA 91016
Phone: 626 305-8460
Fax: 626 305-8462

March 14, 2018

DUNS Number: 848908356

Project Period: September 15, 2015 to March 14, 2018

Submitted by Jean Young, Project Manager

jtyoung@geomechanicstech.com

Disclaimer:

This report was prepared as an account of work sponsored by an agency of the United States Government. Neither the United States Government nor any agency thereof, nor any of their employees, makes any warranty, express or implied, or assumes any legal liability or responsibility for the accuracy, completeness, or usefulness of any information, apparatus, product, or process disclosed, or represents that its use would not infringe privately owned rights. Reference herein to any specific commercial product, process, or service by trade name, trademark, manufacturer, or otherwise does not necessary constitute or imply its endorsement, recommendation, or favoring by the United States Government or any agency thereof. The views and opinions of authors expressed herein does not necessarily state or reflect those of the United States Government or any agency thereof.

1 Abstract

GeoMechanics Technologies has completed a detailed characterization study of the northern Ship Shoal area, offshore Gulf of Mexico for large scale CO_2 sequestration. This effort included: a detailed review and interpretation of publicly available geologic data to identify targets and seals; development of an integrated 3D geologic, geomechanics and fluid flow models for the Ship Shoal Block 84 and 107 fields area; simulation of long-term injectivity, fluid flow migration, storage permanence, and induced fault reactivation; risk assessment for CO_2 injection, analysis of existing hydrocarbon infrastructure for CO_2 transport, and an estimation of potential CO_2 storage volume. Our analysis indicates that:

- The fluid flow simulation results for Block 107 and Block 84 show a very low risk of CO_2 leakage and a good containment of the injected CO_2 for 30 million metric tons within the 60 years of injection and observation simulated. Most of the cases show that the CO_2 injected will be contained in either the Pliocene or the Miocene Formation.
- The geomechanical model results indicate low to no risks for fault slips or fault reactivation after 30 years of CO_2 injection and migration with relatively small induced stresses and displacements.
- 12 well bores and 76 well bores for Ship Shoal Block 84 and 107 respectively were reviewed for their cement history. Most wells have good integrity. Some wells with no top plug, incomplete cement or Plug and Abandonment information are given yellow cautionary indicators. These cautionary wells may provide leakage paths of CO_2 through the well bores to the USDWs.
- Using our Quantitative Risk & Decision Analysis Tool (QRDAT) for caprock integrity evaluation, we compared Ship Shoal's risk to that of In Salah, Sleipner, Kevin Dome, Loudon, Illinois Industrial CCS and Wilmington Graben. We found the risk at the Ship Shoal Blocks 84 and 107 fields is similar to the known CO_2 active sequestration sites, but lower than the Wilmington Graben turbidities offshore California studied site.
- GeoMechanics Technologies has documented the top 25 CO_2 emission sources within the close proximity of the Ship Shoal Block 84 and 107 fields. All the offshore and onshore pipelines have been digitized and can be viewed in an interactive website (http://www.geomechanicstech.com/shipshoal.html). There are abandoned, idled and retired onshore and offshore pipelines. However, there is no standard specification for maximum pipeline pressures needed for CO_2 transport; thus it will be the responsibility of the pipeline operator to correctly determine, maintain and operate within the limits of the pipelines. There are a few transit corridors extending from onshore Louisiana to offshore trunk-lines. The cost for constructing a pipeline has increased about 46% from 2015 to an average cost of $5,064,046 per mile in 2016.
- The NETL CO_2 storage resource mass estimation underestimate the storage potential but the resource calculation using the sand volume obtained through geologic modeling overestimate the capacity as the model accounts for all sand within the formation and not just interconnected sand.

Table of Contents

List of Figures

List of Tables

List of Appendices

2 Introduction

The Gulf of Mexico is one of the most important regions in the United States for energy resources and infrastructure. Gulf of Mexico federal offshore oil and gas production accounts for 17% of total U.S. crude oil production and 5% of total U.S. gas production (EIA Gulf of Mexico Fact Sheet). Over 45% of total U.S. petroleum refining capacity is located along the Gulf coast, as well as 51% of total U.S. natural gas processing plant capacity. This region presents an excellent combination of high need and significant opportunity for large scale geologic storage of CO_2.

The Ship Shoal Area is located about 20 miles offshore Louisiana within the Gulf Coast federal waters. Miocene and Pliocene sediments in the Ship Shoal Area are proven to provide excellent and secure traps for oil and gas. The Ship Shoal Area contains a large number of depleted oil and gas fields either currently abandoned, or planned for abandonment by 2025, which may provide very significant potential CO_2 storage capacity.

Through DOE Grant No: DE-FE-0026041, GeoMechanics Technologies are conducting a comprehensive research project to better characterize the Neogene sediments in the Ship Shoal Area for high volume CO_2 storage. Figure 1 shows our study area. Two fields – Ship Shoal Block 107 and Ship Shoal Block 84 fields were studied. The research program included well data review and analysis, the preparation of two high resolution 3D geologic models and integrated geomechanics and fluid flow models, and an analysis of the existing offshore infrastructure of oil and gas for CO_2 transportation. The results of the modeling efforts from the 2 fields will provide refined storage capacity estimation for the Ship Shoal Area. The research efforts funded by this DOE grant included the following:

- Completed a detailed review and interpretation of publicly available geologic data to identify targets and seals;
- Provided an estimation of storage volume for each oil/gas field within northern Ship Shoal area using the NETL approved calculation;
- Developed a geologic model of the northern Ship Shoal Area (producing Pliocene and Miocene structure maps) including a detailed lithologic model of the Ship Shoal Blocks 84 and 107 fields;
- Developed an integrated 3D fluid-flow and geomechanics model of the Ship Shoal Blocks 84 and 107 fields to simulate long-term injectivity, migration, storage permanence, and induced fault reactivation;
- Completed a risk assessment to evaluate the potential of leakage during CO_2 injection;
- Analyzed existing infrastructure of oil and gas for CO_2 transport.

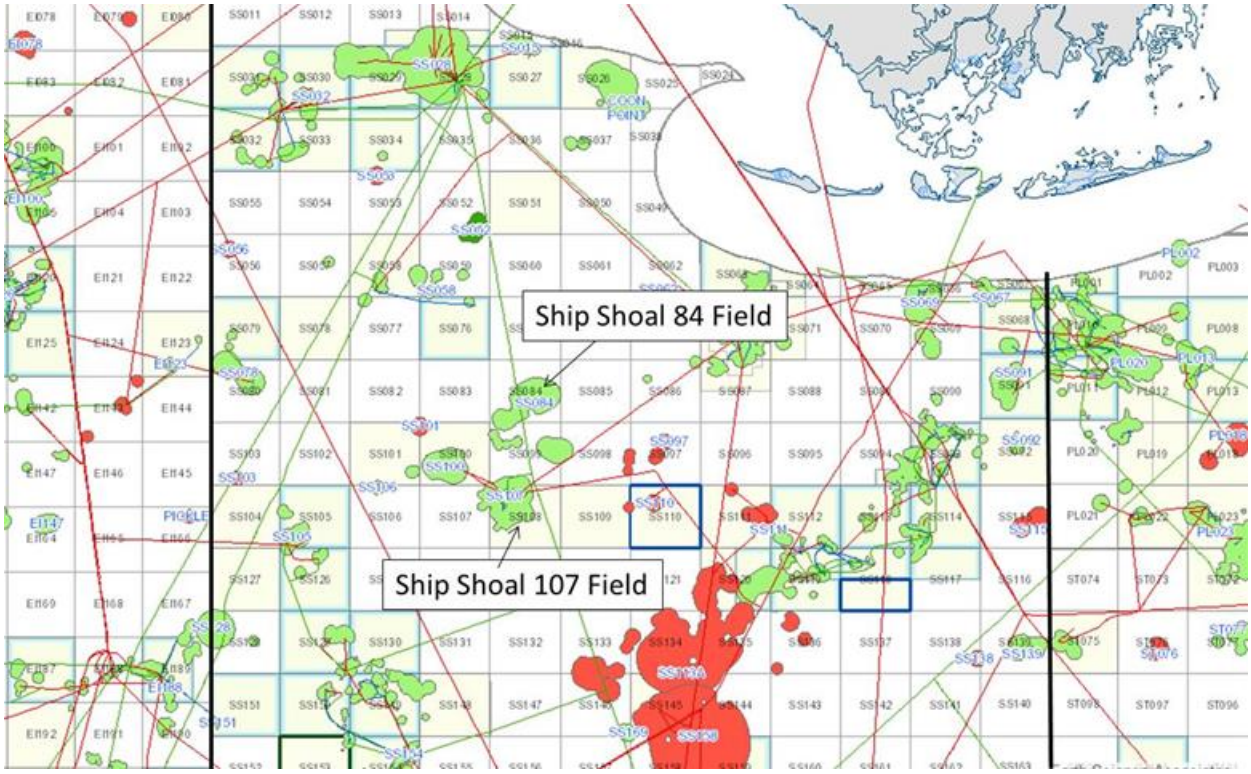

Figure 1: Ship Shoal Block 84 Field and Block 107 Field

Modified from GOMSmart.com

3 Well data review and formation evaluation

GeoMechanics Technologies have review all publically available pertinent literature and have collected all available well data in the public domain, including those reside with the Bureau of Ocean Energy Management (BOEM), for the Ship Shoal Block 84 and Block 107 evaluation. We also purchased Ship Shoal well data and maps from two commercial databases -- GOMSMART, and I.H.S. Global, online data portals for well data in the offshore Gulf of Mexico. The geologic characterization effort included assembly and analysis of log data from over a hundred wells, mapping several key geologic horizons at each well location. Lithology versus depth was also identified for each well.

3.1 Well Logs Review

We have reviewed and correlated 12 well logs within the Ship Shoal Block 84 field and 76 well logs within the Block 107 field plus major outlier wells for key horizon markers and lithology. These logs were obtained through subscription in IHS and GOMsmart database. The gamma ray, spontaneous potential, resistivity and porosity curves were examined. These logs were correlated, and lithologies from over a hundred wells were assessed. The data were input into the Rockwork 16 Geologic Software. Lithologies at 10 ft increments separated into sand, silt and shale were interpreted to create a detailed geologic model.

3.2 Stratigraphic Horizon Analysis

The key horizons from log picks were compared to the commercial paleo database and maps. All discrepancies were reviewed and resolved. All stratigraphic data were input into the geologic software for development of the Ship Shoal geologic model. Five key stratigraphic horizons (Top Pliocene, Textularia X, Top Miocene, Bigenerina A and Cristellaria K) were created. The general stratigraphy and chronologic age for the different horizons are shown in Figure 2. For detailed interpretation please see Stratigraphy (Miocene to Holocene).

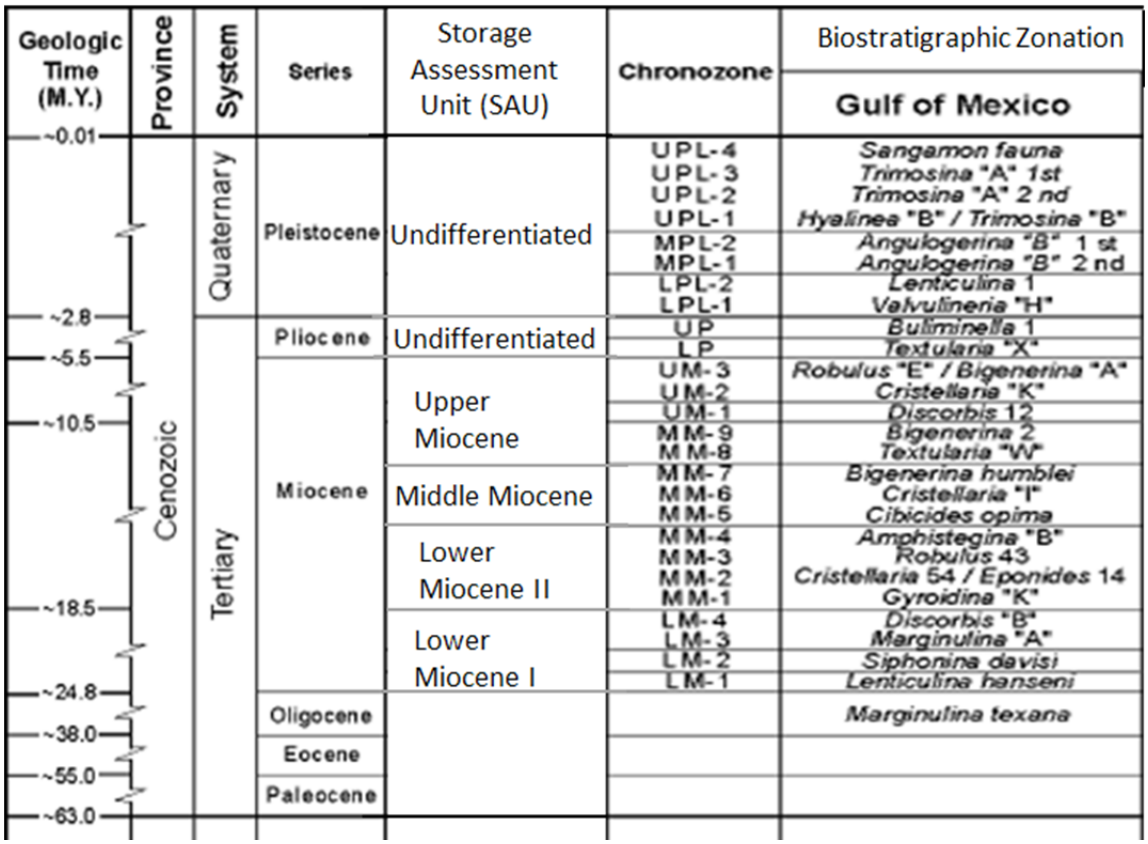

Figure 2: Biostratigraphic zonation and corresponding Storage Assessment Unit for Cenozoic in the Gulf of Mexico

Modified from MMS, 1999

3.3 Porosity and Permeability Data

The porosities and permeabilities for all 48 fields within the northern Ship Shoal area have been assessed. The Ship Shoal Reservoir porosity values range from 14 to 37 percent with the average reservoir porosity at about 27 percent (BOEM, 2014). The permeability ranges from 3 mD to maximum 2,105 mD, with the average permeability of all the reservoirs within the Ship Shoal area at about 280 mD (BOEM, 2014). Graphical representations of the porosities and permeabilities for all 48 fields are shown in Table 1 and Table 2. Red symbols are porosity and permeability values for the Ship Shoal Block 107 field, while green symbols are for the Ship Shoal Block 84 field.

Table 1: Porosity versus Depth for northern Ship Shoal

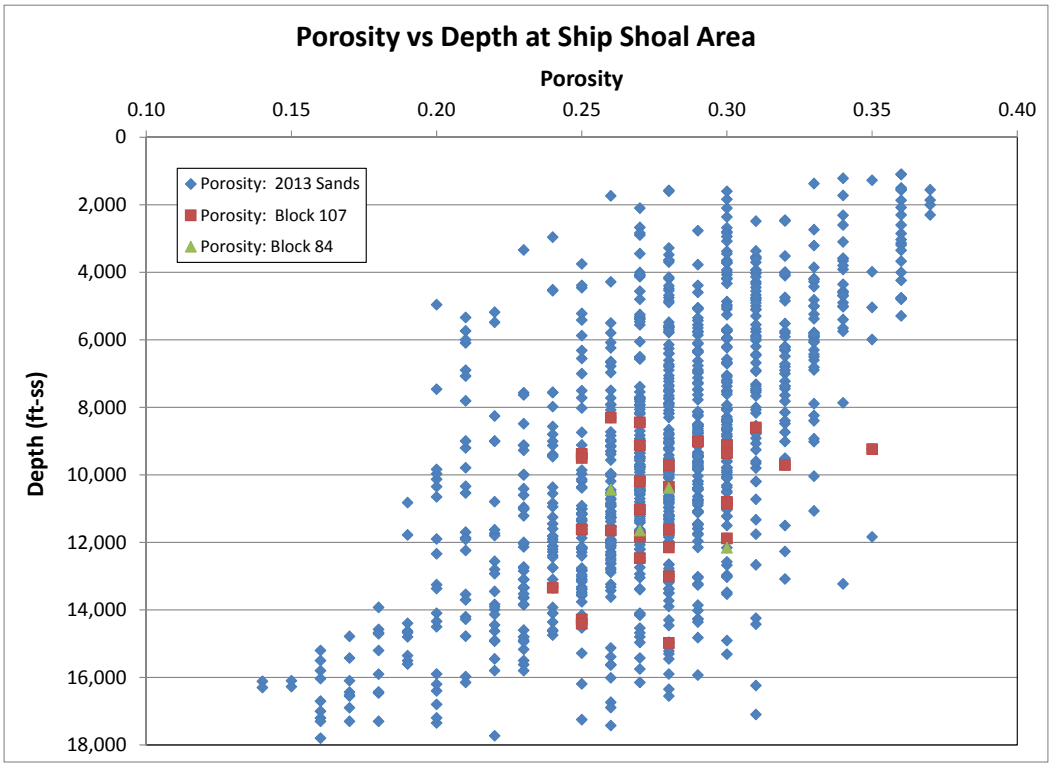

BOEM, 2014

Table 2: Permeability versus Depth for northern Ship Shoal

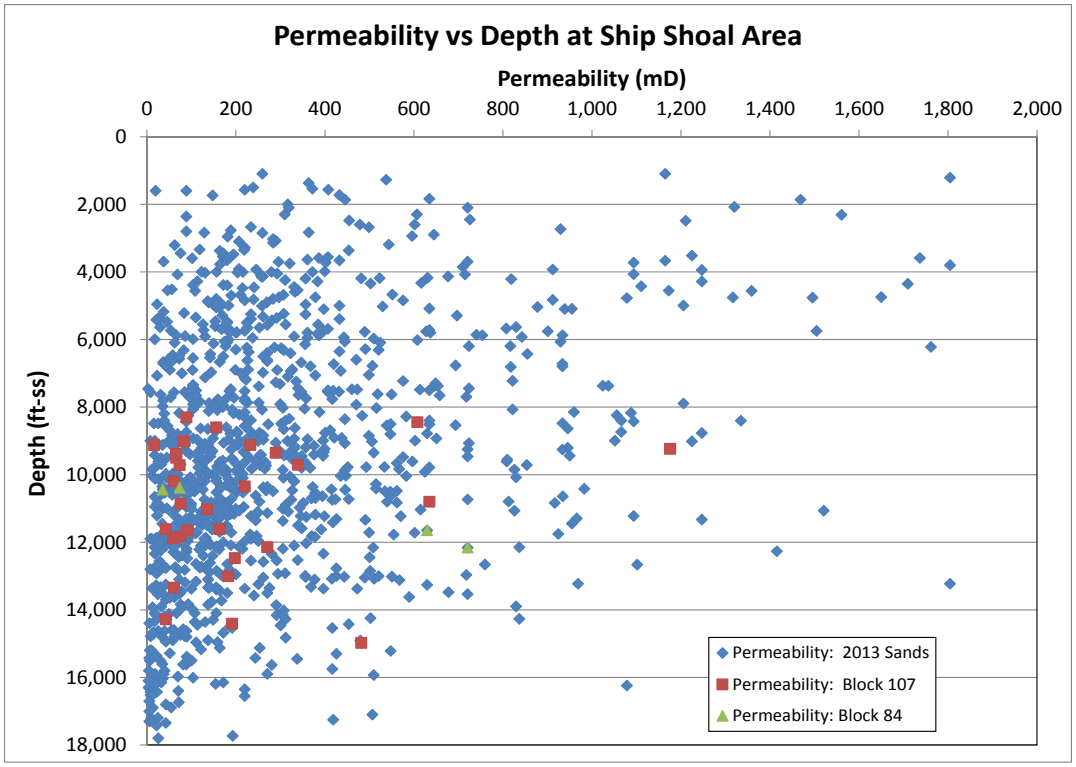

BOEM, 2014

3.3.1 Ship Shoal Block 107 Field

For the Ship Shoal Block 107 field, the porosity ranges from 24 to 36 percent with average at about 28 percent. Permeability ranges from 17 mD to 1,176 mD, with the average reservoir permeability listed as 213 mD (BOEM, 2014). These numbers compare very well with Russel's (1973) average porosity and permeability of 25% and over 100 mD respectively.

Next we analyzed the average porosity and permeability data of each sand reservoir according to their respective formations. Table 3 shows the porosity and permeability of interest to this study (BOEM, 2014). These data will be used to represent the flow properties of sand per formation in Task 4. There is no data for silt and shale provided from BOEM for this field.

Table 3: Average porosity and permeability for sand in different formations for the Ship Shoal Block 107 Field

Formation	Av. Porosity (%)	Average Permeability (mD)
Top Pliocene	29	261.9
Top Tex X	29	261.9
Top Miocene	28	108.8
Top Big A	27	228.2

BOEM (2014)

No core data is available for the wells inside the Ship Shoal Block 107 field; however, we found some core data from wells (Murphy 101-G-9612 #2 and Exxon 123-G-5546 #1 wells) in nearby fields. To obtain average porosity and permeability data for silt and shale per formation in Block 107, we used an empirical correlation based on the Kozeny-Carman (Carman, 1997 & Taylor, 1948) equation. The best fitting equation for each lithology was then used to calculate average permeability from average estimated porosity.

Core data and estimated permeability for Murphy 101-G-9612 #2 and Exxon 123-G-5546 #1 wells, respectively, are show in Table 4 and Table 5. The following permeability and porosity correlation for silt and shale was used for the estimation:

Shale/Silt permeability P (mD)= 700*Φ^3/ (1- Φ)^2;

where Φ is the porosity

As can be seen from Figure 3, the comparison between the measured permeability and the estimated permeability are very close, suggesting that the correlation equation is reasonable.

Table 4: Core measurement data and estimated permeability comparison for Exxon 123-G-5546 #1 well

Depth (ft)	Core porosity (%)	Lithology	Core permeability (MD)	Estimated Permeability for silt and shale (MD)
9320	24	Silt	77	16.8
11856	19.7	Silt	3.4	8.3
12105	21.9	Silt	17	12.1
12543	17.7	Silt	2.1	5.7
12729	30.8	Silt	21	42.7
12940	22.6	Shale	3.3	13.5
13177	16.1	Shale	0.1	4.2
13343	23.5	Silt	4.4	15.5
13346	19.7	Silt	1.8	8.3
13380	20.3	Silt	2.5	9.2
13825	23.2	Silt	8.7	14.8
13962	19.9	Silt	1.9	8.6
13962	19.9	Silt	1.9	8.6

Table 5: Core measurement data and estimated permeability comparison for Murphy 101-G-9612-#2 well

Depth (ft)	Core porosity (%)	Lithology	Core permeability (MD)	Estimated Permeability for shale and silt (MD)
11716	15.7	Shale	2.4	3.8
11720	18.5	Shale	6.9	6.7
11721	16.3	Shale	3.8	4.3
11723	18.1	Shale	7	6.2
11732	23.3	Shale	25	15.1
11733	20.1	Shale	9.5	8.9
11828	19.7	Silt	9.1	8.3
11831	23	Silt	18	14.4
11832	17.6	Silt	5.4	5.6
11836	17.2	Silt	6.4	5.2
11838	16.6	Silt	4.4	4.6
11843	15.6	Silt	3.2	3.7
11844	21.7	Silt	15	11.7
11847	16.2	Silt	4.1	4.2
11850	17.2	Silt	6.7	5.2
11853	20	Silt	9	8.8
11856	15.5	Silt	2.4	3.7
11879	20	Silt	21	8.8
11880	22.3	Silt	26	12.9
11881	17	Silt	6.6	5.0
11885	17.7	Silt	7.2	5.7
11886	22.8	Silt	24	13.9
11887	18.8	Silt	5.7	7.1
11890	20.1	Silt	12	8.9
11897	19.4	Silt	8.8	7.9
11898	18.4	Silt	7.1	6.5
11899	20	Silt	9.6	8.8
11902	21.2	Silt	4	10.7
11905	20.8	Silt	3.2	10.0
11914	23.9	Silt	9.1	16.5
11924	22.3	Silt	7.1	12.9

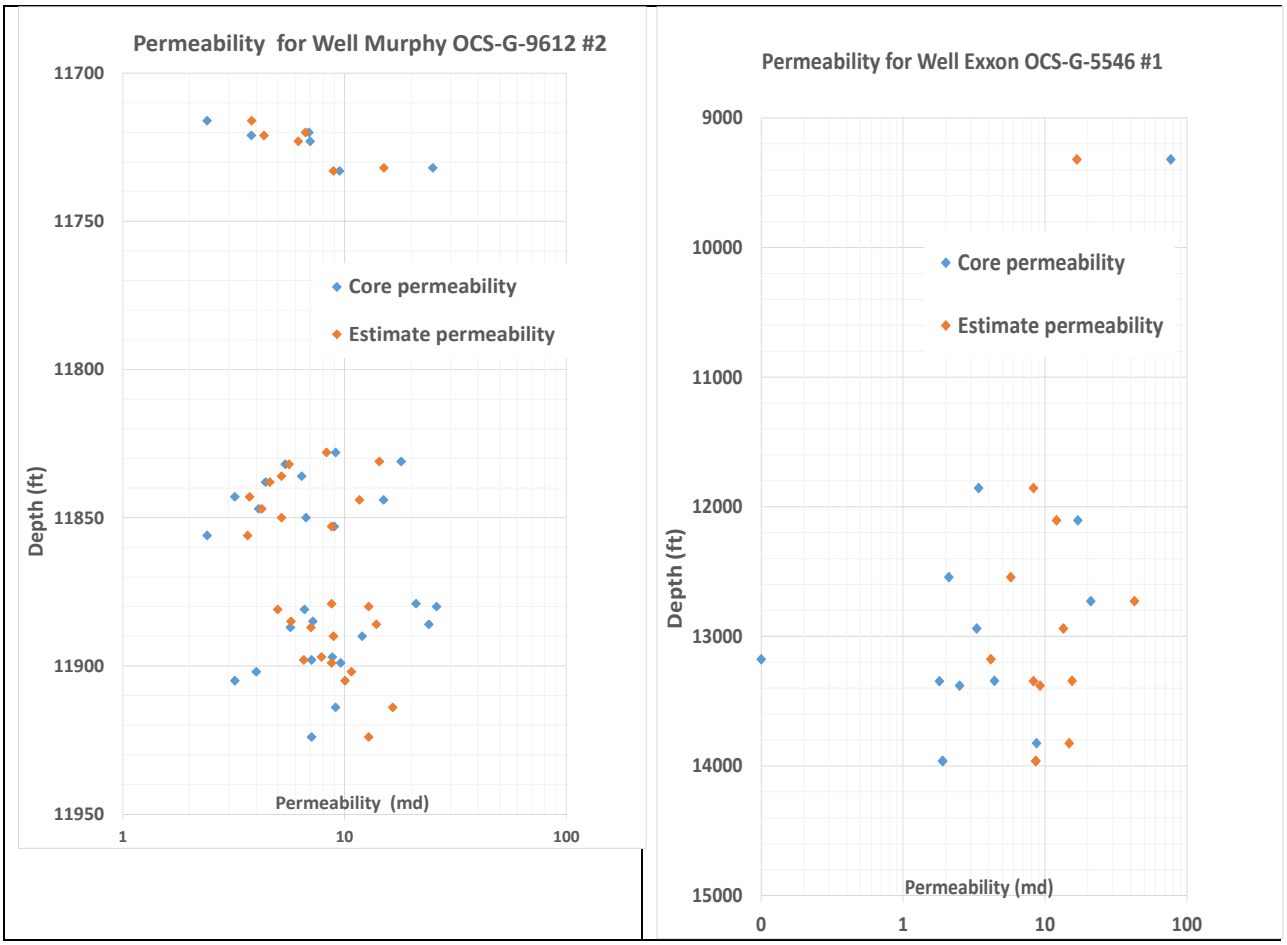

Figure 3: Correlation of measured and estimated permeability for Murphy 101-G-9612#2 (left) and Exxon 123-5546#1 (right) wells

The above correlation was applied to wells with porosity log data within the Block 107 field to obtain the permeability for silt and shale. Only two wells have porosity log data; Stone 99-1ST1 well and Stone 99-A1. The estimated permeability for each well is shown in Figure 4 and Figure 5. The average porosity and permeability for silt and shale for each formation from each well is then calculated based on its respective lithology. Table 6 and Table 7 show the average porosity and permeability in each formation for Stone 99-1ST1 and Stone 99-A1 wells, respectively. The final porosity and permeability for silt and shale per formation were then assigned from the average value obtained from these two wells.

The final result of porosity and permeability for sand, silt, and shale for each formation are summarized in Table 8

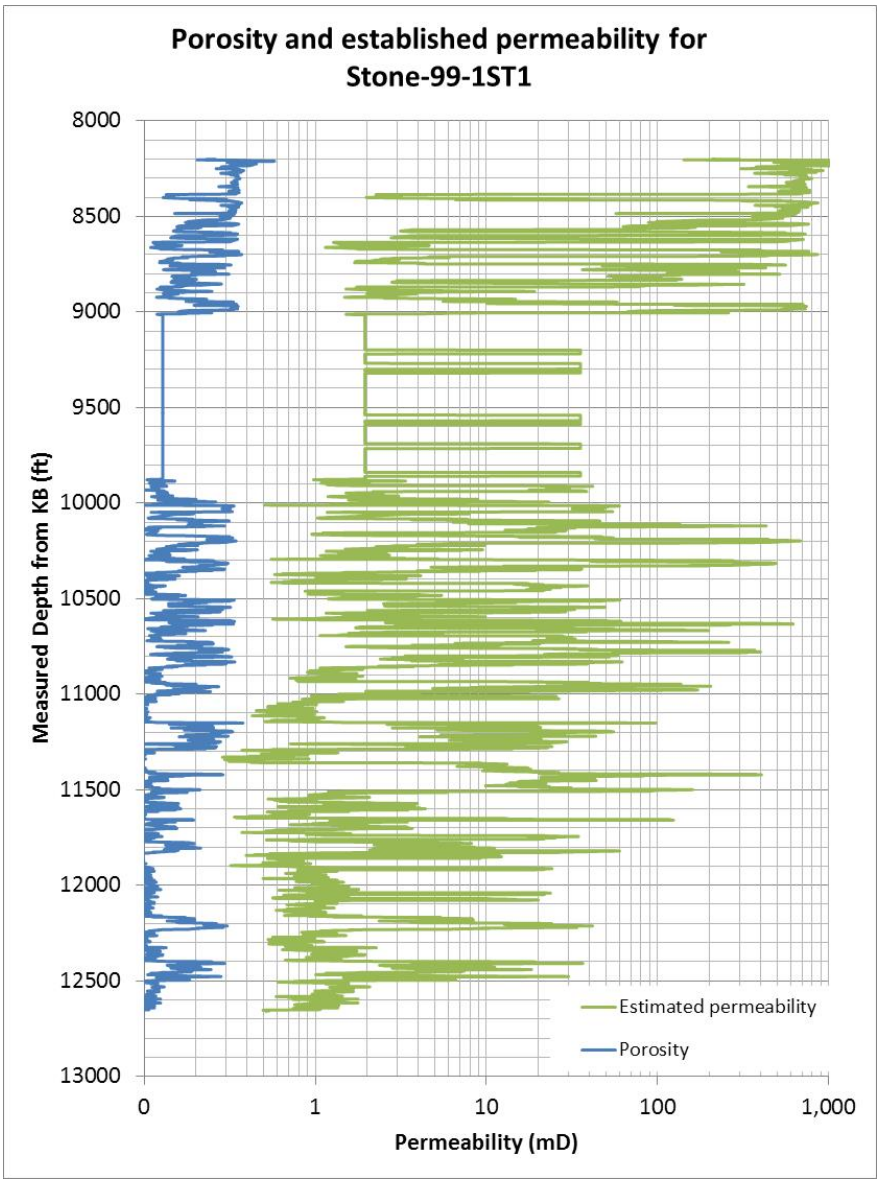

Figure 4: Estimated permeability for Well Stone 99-1ST1

Table 6: Average porosity and estimated permeability for silt and shale per formation from Stone-99-1ST1

	Silt		Shale	
Formation	Av porosity	Av permeability	Av porosity	Av permeability
	(%)	(md)	(%)	(md)
Top Pliocene	0.14	4.5	0.15	7.1
Tex X	0.14	4.5	0.15	7.1
Top Miocene	0.10	1.2	0.11	1.4
Big A	0.11	1.2	0.13	3.3

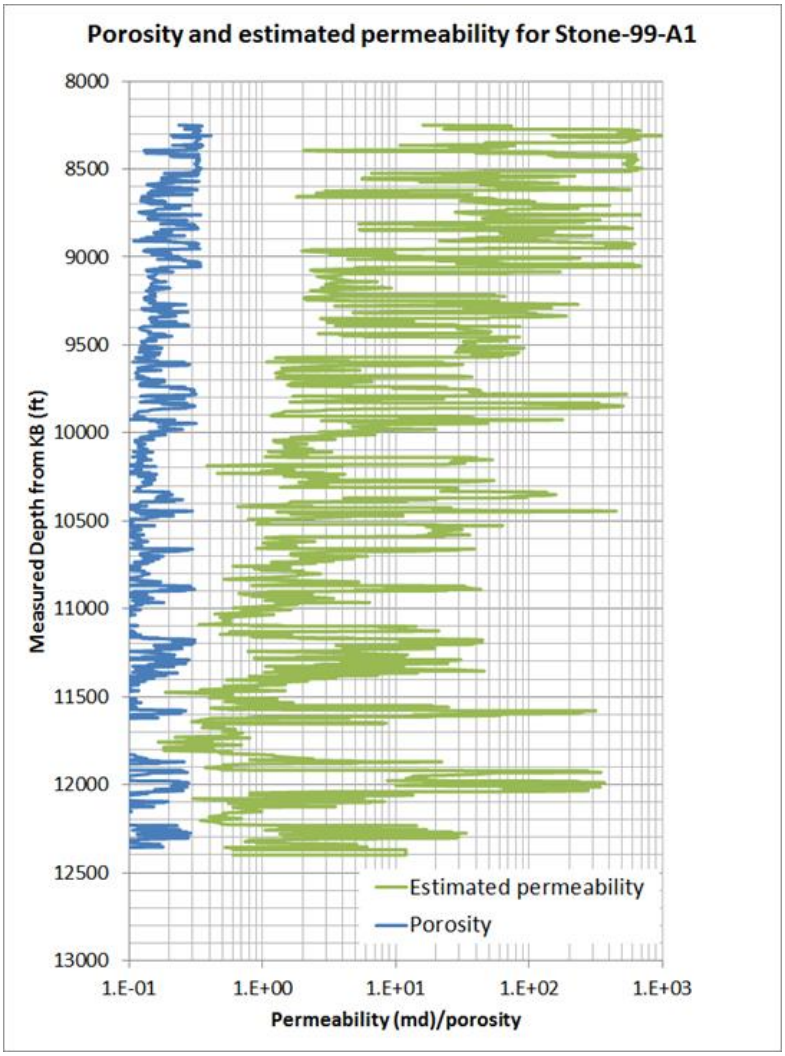

Figure 5: Estimated permeability for Well Stone 99-A1

Table 7: Average porosity and estimated permeability for silt and shale per formation from Stone 99-A1

	Silt		Shale	
Formation	Av. porosity	Av. permeability (md)	Av. porosity	Av. permeability (md)
Top Pliocene	0.31	49.0	0.26	30
Tex X	0.15	6.2	0.16	6.7
Big A	0.11	1.2	0.12	4

Table 8: Final estimated Porosity and Permeability for Ship Shoal Block 107 Field per lithology type

	Sand		Silt		Shale	
Formation	Av. porosity	Av. permeability (md)	Av. porosity	Av. permeability (md)	Av. porosity	Av. permeability (md)
Top Pliocene	0.29	261.9	0.23	26.8	0.21	18.6
Top Tex X	0.29	261.9	0.15	5.4	0.16	6.9
Top Miocene	0.28	108.8	0.10	1.2	0.11	1.4
Top Big A	0.27	228.2	0.11	1.2	0.13	3.7

3.3.2 Ship Shoal Block 84 Field

The depleted Ship Shoal Block 84 field produced only in the Miocene. The average porosity and permeability for Block 84 field ranges from 27% and 55 mD for the Big A horizon, to 29% and 676 mD for the Cristellaria K horizon respectively (BOEM, 2014). The core data from Chevron 85-1 (Taylor 85-1) a nearby well, recorded maximum 32% porosity and 1500 mD permeability from sidewall cores obtained below 10,000 ft. Table 9 summarizes the porosity and permeability for the Pliocene and Miocene cores. We look at the described lithology and compared that to the gamma ray log response for each individual depth. Some very fine grained shaly sand cores have been reclassified as silt. No shale core had been recovered.

Table 9: Porosity and Permeability from Chevron (Taylor) 85-1 sidewall cores

	Pliocene			**Miocene**	
Type	porosity (%)	permeability (mD)		porosity (%)/AV	permeability (mD)/AV
Sand	29	105		20 - 31/27	3 - 1500/425
Silt	22 - 23	7 - 9		19 - 32/24	4 - 500/57

AV = average

To obtain average porosity and permeability data for shale per formation for Block 84, we again used the Kozeny-Carman (Carman, 1997 & Taylor, 1948) equation. The best fitting equation for shale was then used to calculate average permeability from average estimated porosity.

Shale/Silt permeability P= 700*Φ^3/ (1- Φ)^2;

where Φ is the porosity

The density porosity and the neutron porosity from the same well (Chevron 85-1) were compared to the core porosity. We find the average of the density and neutron porosity better match the core data (Figure 6). Table 10 and the graphic presentation shown in Figure 7 are the comparison between the core permeability and estimated permeability using the same Kozeny-Carmen equation on core data. As can be seen, the estimated permeability has a reasonably good match to the core permeability.

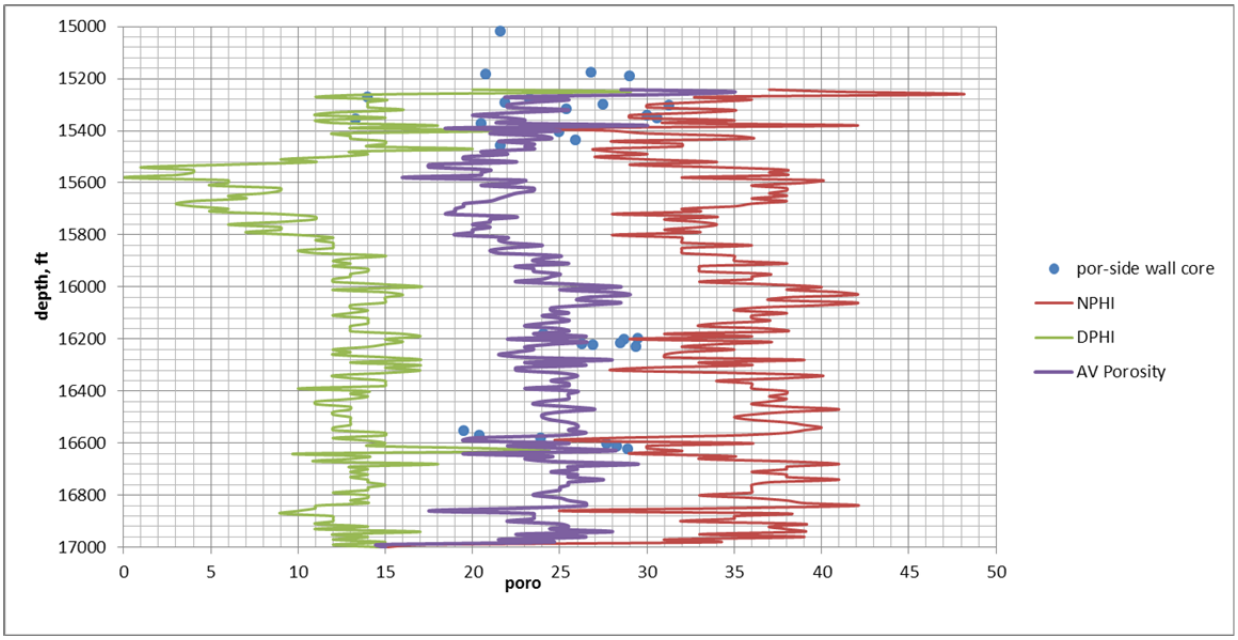

Figure 6: Comparison between NPHI, DPHI, Average porosity and Core porosity for Chevron (Taylor) 85-1 well

Table 10: Core measurement data and estimated permeability comparison for silt in Chevron (Taylor) 85-1 well

Depth (ft)	core Permeability (MD)	core Porosity (%)	permeability estimated
8524	8.9	23.3	15.1
9716	6.9	21.9	12.1
12192	41	25.4	20.6
12198	125	30	38.6
13051	5	20.5	9.5
13515	3.8	24.1	17.0
15074	500	32.2	50.8
15190	100	29.4	35.7
15350	8.1	19.5	8.0
15356	9.2	20.4	9.4
15372	25	23.9	16.5
16237	70	28.5	31.7
16253	7.6	19.9	8.6
16270	49	24.1	17.0
16275	7.5	21.7	11.7
16280	7.9	19.9	8.6
16286	5.5	20.6	9.7
16305	3.6	18.5	6.7
16570	6.9	21	10.4

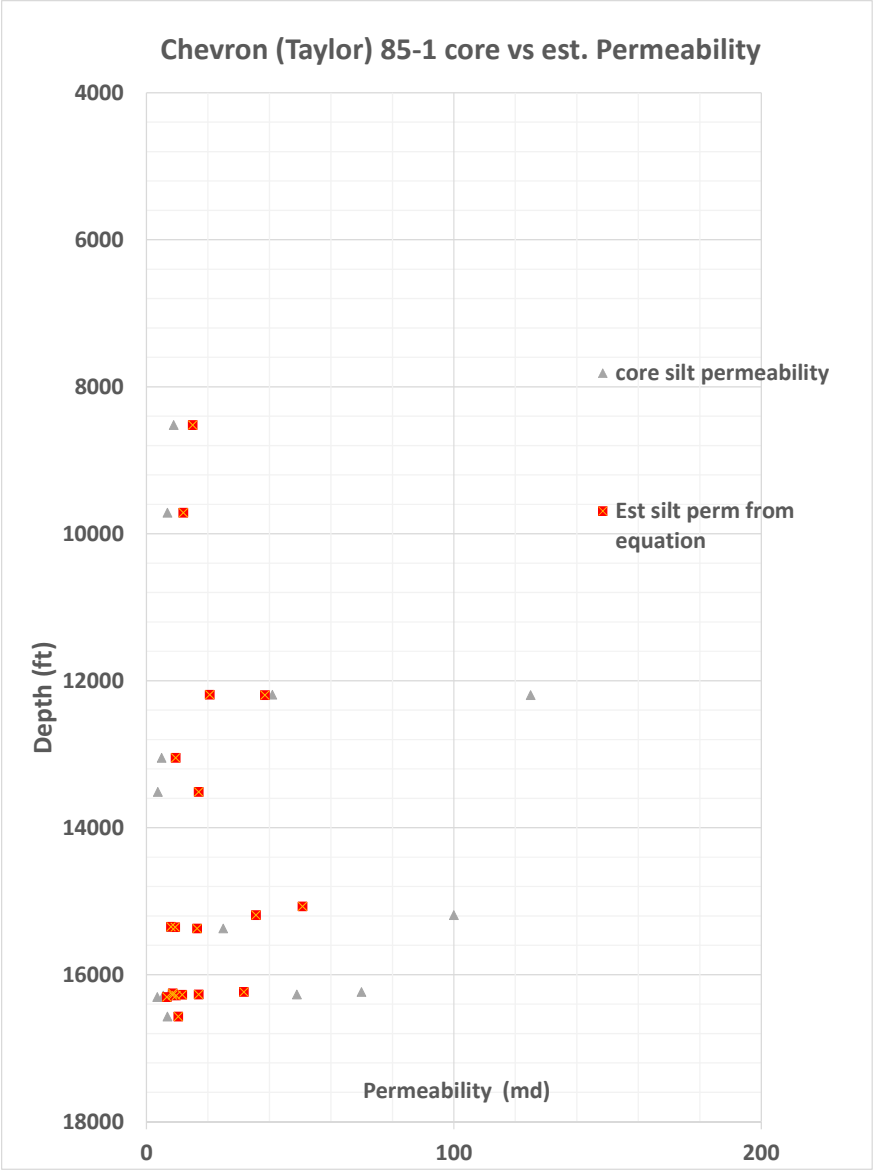

Figure 7: Correlation of measured and estimated permeability for silt cores for Chevron (Taylor) 85-1 well

The Chevron (Taylor) 85-1 well porosity log was digitized and the estimated permeability calculated. Figure 8 shows the estimated permeability calculated using the Kozeny-Carmen equation. The porosity log started from 15,261 ft only which is in the "Discorbis 12" horizon (below the base of our model), in the lower section of the upper Miocene; thus, no log porosity is available for the Pliocene or top Miocene section.

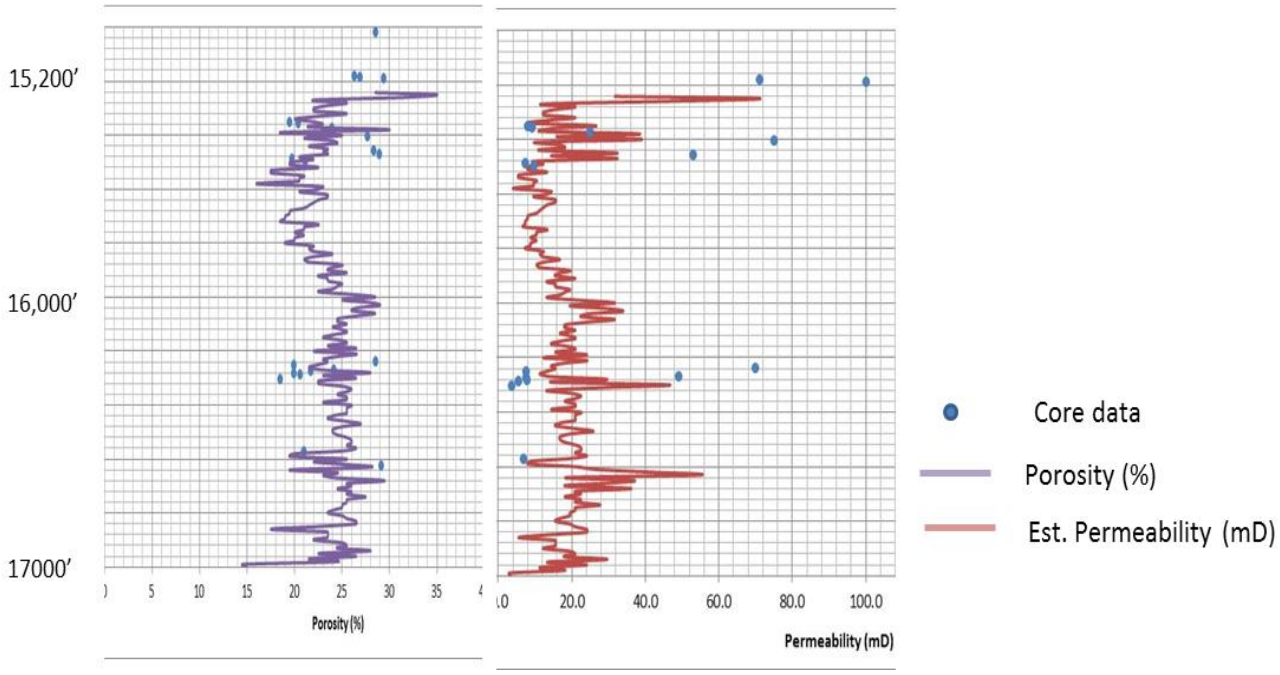

Figure 8: Estimated permeability using Kozeny-Carman equation from Chevron (Taylor) 85-1 well porosity log

We then digitized the porosity logs for BP 84-A1 and 84-A-3 wells. The same constant derived from matching the Kozeny Carmen equation to the cores from Chevron 85-1 well was used to calculate the permeability for the 2 wells. Figure 9 and Figure 10 are the graphic representations of the relative permeability calculated and the density porosity curve used for BP 84-A1 and 84-A3 wells. Note the permeability corresponded well with the sand lenses. The porosity and permeability for each stratigraphic horizon and lithologic type are broken down as shown in Table 11, and will be used in Task 5, CO_2 injection modeling.

Table 11: Final estimated Porosity and Permeability for Ship Shoal Block 84 Field per lithology type

	Sand		Silt		Shale	
Formation	Av Por (%)	Av Perm (mD)	Av Por (%)	Av Perm (mD)	Av Por (%)	Av Perm (mD)
Top Pliocene	32.34	88.9	27.44	31.52	28.74	38.36
Tex X	28.17	61.08	23.32	16.78	23.66	16.78
Top Miocene	26.57	50.39	21.78	12.76	22.61	14.84
Big A	24.94/27	42.13/55	18.86	13.37	22.21	15.8
Cris K to base of model	27.32/29	59.03/663.5	17.37	6.06	17.54	7.2

Data from BP 84-A1 porosity (DPHI) log and permeability using Kozeny Carmen equation

Red is from BOEM (2014) sand data

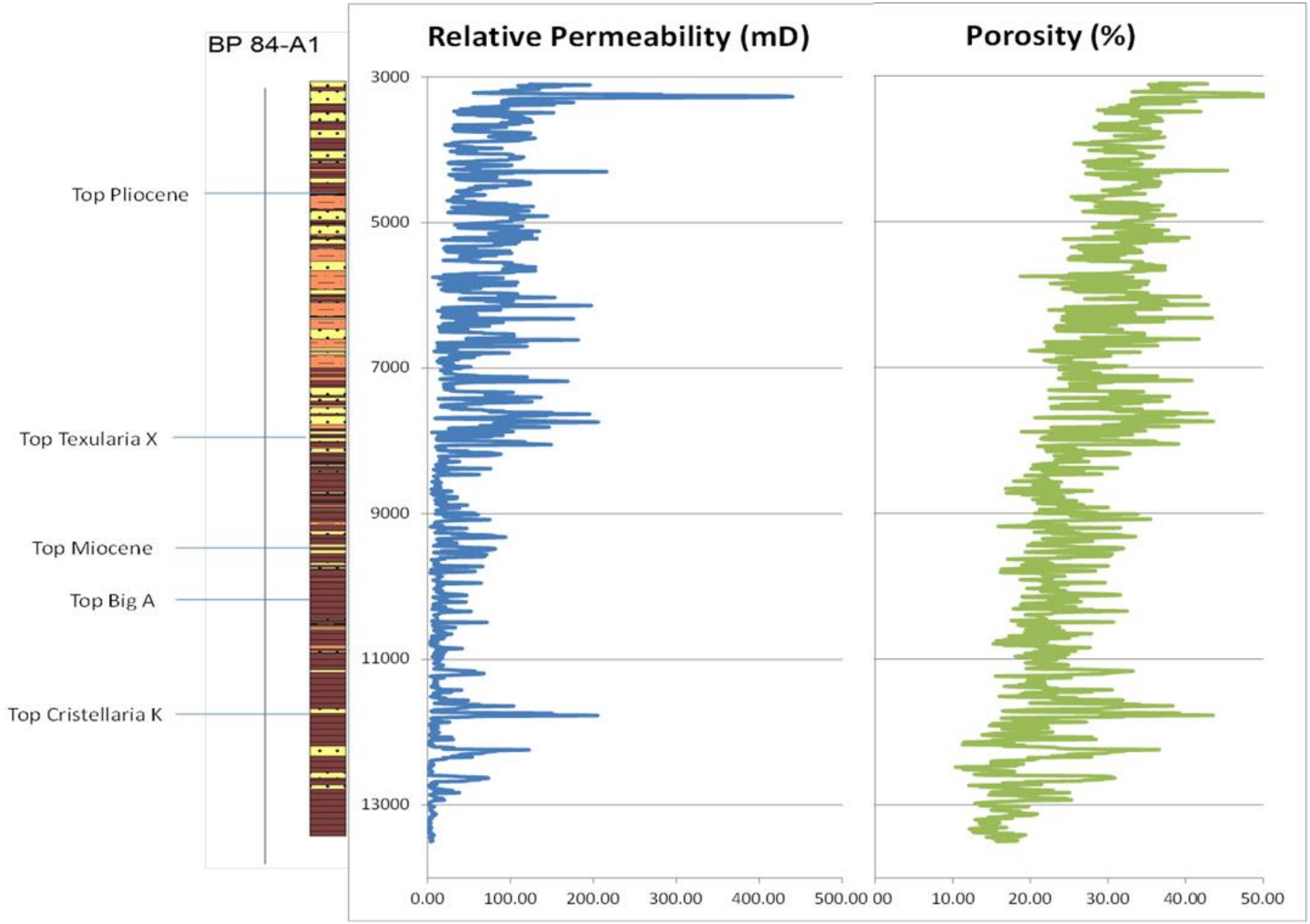

Figure 9: Relative permeability calculated using DPHI for BP 84-A1 well

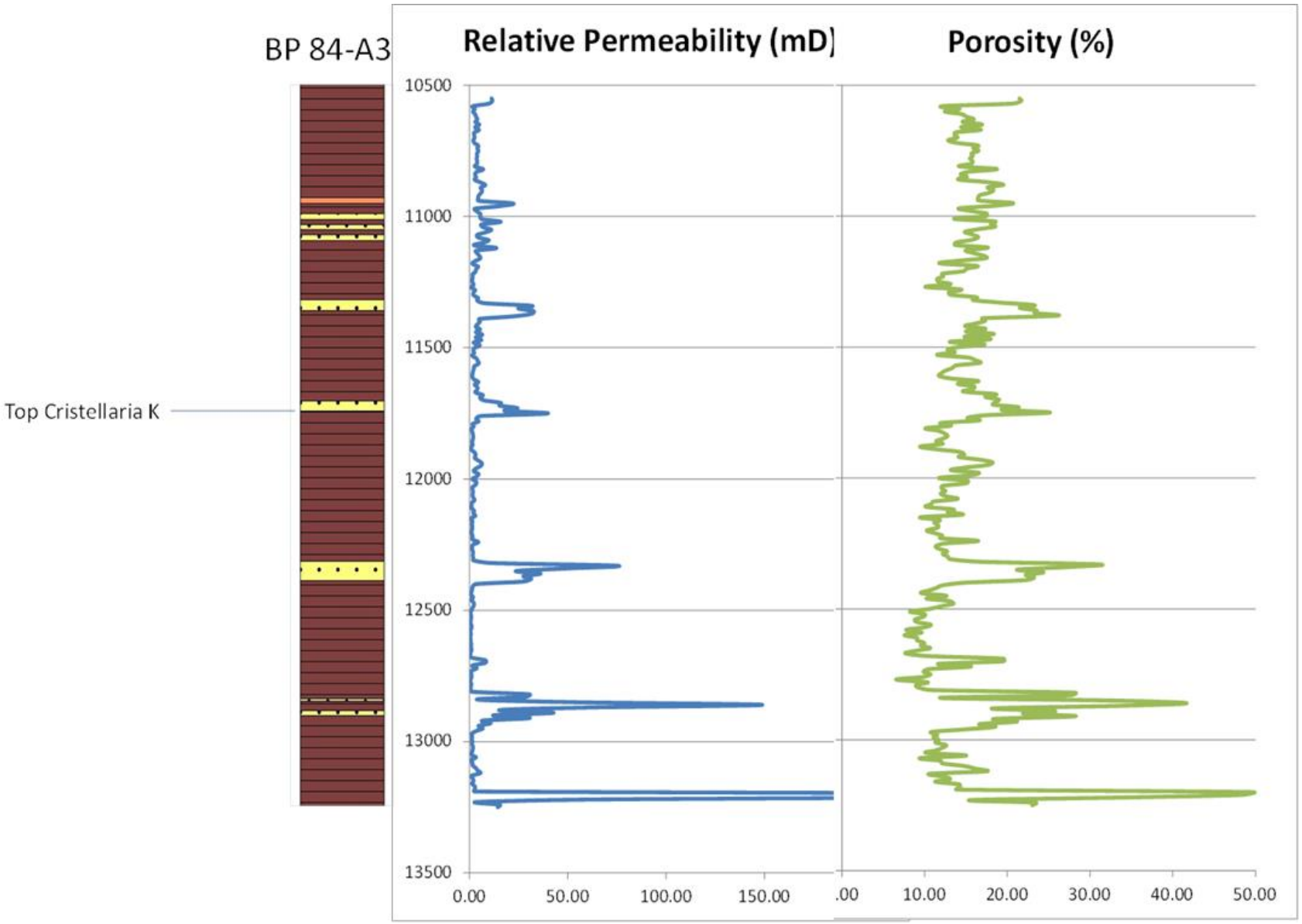

Figure 10: Relative permeability calculated using DPHI for BP 84-A3 well

3.4 Conclusions

The data generated from literature and well log review, and formation evaluation were input into Rockwork 16 geologic software to create a detailed geologic model for the Ship Shoal studied area. The geologic grids were then fed into TOUGH2, the gas migration model software and FLAC 3D, the geomechanical model software.

We analyzed the average porosity and permeability data for each lithology (sand, silt and shale) according to their respective stratigraphy. The core porosity was analyzed and compared to the log porosity. The core permeability was analyzed and compared to the permeability curve generated by using an empirical correlation based on the Kozeny-Carman equation (Carman, 1997 & Taylor, 1948). The best fitting equation for sand, silt and shale was then used to calculate the average permeability for the different lithologies for each horizon if there are no available data.

4 Geologic model development

4.1 Geology

The Gulf of Mexico (GOM) evolved in Late Triassic to Middle Jurassic time when the North American plate separated from the South American plate, and rifting spread southward along the Atlantic spreading ridge (Edring, C.H., 2008, Galloway, W.E., 2008, Salvador, A., 1991). Late Jurassic was continuation of the sea floor spreading and the development of the passive margin. The marine incursion in the later part of the Middle Jurassic is the precursor for the accumulation of the thick salt deposits into the subsiding rift basin. During Cretaceous, the GOM passive margin evolved into a carbonate shelf and platform environment, linking GOM to the Western Interior Seaway. By the beginning of Cenozoic time, siliciclastic sediment dominates from the progradation of the passive continental margin (Edring, C. H., 2008, Galloway, W.E., 2008, Salvador, A., 1999).

During Paleogene, the depocenters were located in East Texas and South Texas and progradation was concentrated on the western and northwestern shelf margins. By Miocene, the fluvial sediment input shifted eastwards to the present day Mississippi embayment (Galloway, W.E., 2008, and 2009). During Pliocene time, there was rejuvenation of the Rockies, and the glaciation in Pleistocene which resulted in the renewal of the sediment sources and development of the present day Mississippi drainage system (Edring, C.H., 2008).

The thick Tertiary sedimentation contains multiple episodes of sand reservoirs and regional seals building gulf-ward. These episodes are related to the multiple transgression and regression of the depositional cycles (Wallace, K. J. et al., 2013, Galloway, W.E., et al, 1991). Boundaries are generally transitional and subjective, making correlation difficult. Stratigraphic classification relies heavily on biostratigraphic zonation using benthic and planktonic foraminifera, and supplemented by nannoplankton and palynomorphs. Figure 11 shows the stratigratigraphic zonation and the corresponding CO_2 Storage Assessment Unit (USGS, 2012).

The northern GOM shelf is well known for high pressure zone (geopressured zone) occurring at about 2700 m (8858 ft) to 5500 m (18,044 ft) in Louisiana. Temperature gradient increased from 1.0 – 1.5 °F /100 ft to 1.8 – 3.5 °F/100 ft in the geopressured zone. Temperature at the top of geopressured zone ranges from 200 – 250 °F (Galloway, W.E. et al, 1991, MMS, 1999). Salinity however decreases from 100,000 – 250,000 ppm in the hydro-pressured zone to 50,000 - 150,000 ppm in the geopressured zone (Galloway, W.E., et al, 1991).

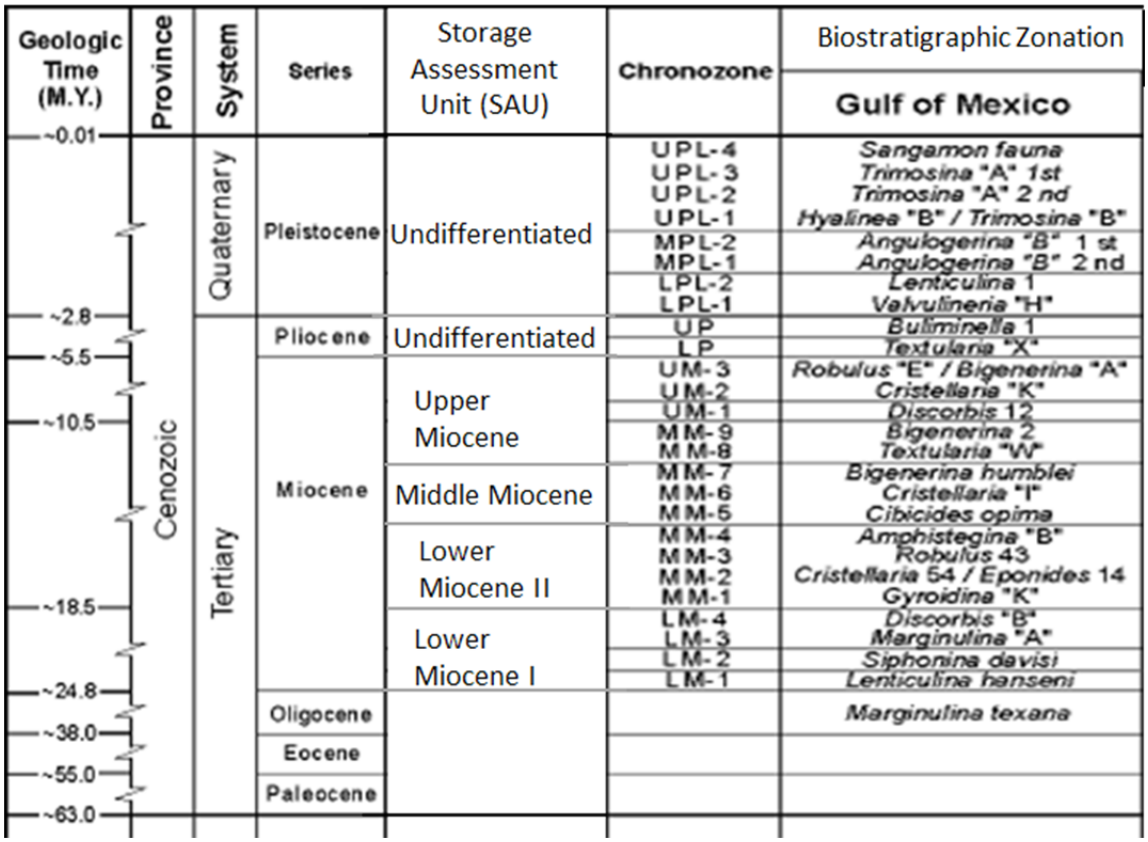

Figure 11: Biostratigraphic zonation and corresponding Storage Assessment Unit for Cenozoic in the Gulf of Mexico

Modified from MMS, 1999

4.2 Stratigraphy (Miocene to Holocene)

We are primarily interested in the Miocene and Pliocene sections for CO_2 sequestration. Our stratigraphy will begin from the Miocene.

Miocene sediment in the offshore Louisiana is dominated by deltaic and shallow marine deposition. It is mainly composed of sand, silt, shale/clay with localized carbonates. Average thickness about 2400 m (7873 ft) is reported. In offshore Louisiana, a maximum thickness of 7600 m (24,924 ft) has been recorded (Edring, C.H., 2008, Galloway, W.E. et al, 1991). In Miocene, the continental shelf prograded about 200 km (124 miles) onto the continental shelf margin (Galloway, W.E., 2000). The depocenter was located in the southwestern Louisiana during the early Miocene time, and shifted to the east by the Late Miocene time (Edring, C.H., 2008).

Numerous transgressive - regressive cycles occurred within the Miocene leaving major regional shale horizons during the transgressive phase. Each cycle grades from a fluvial to deltaic to marine depositional environment (Wallace, K.J., et al, 2013). For example, the Anahuac shale formation was deposited during a transgressive eustatic sea level rise (Haq, et al,

1987) and this event correlates to the beginning of the Miocene epoch. Four other prominent transgressive shale tongues in the Miocene are:

- Lower Miocene I -- Marginulina A (correlates to the top of Lower Miocene I),
- Lower Miocene II -- Amphestigina B (correlates to the top of Lower Miocene II),
- Middle Miocene -- Textularia W (marks the beginning of the Middle Miocene), and
- Upper Miocene -- Robulus E (marks the end of the Miocene epoch)

As shown in Figure 12. Each cycle was related to a transgressive shale layer. Using the biostratigraphic zonation, the Miocene section is divided into the Lower Miocene I Storage Assessment Unit (SAU); Lower Miocene II SAU; Middle Miocene SAU and Upper Miocene SAU section (USGS, 2014). Each of the SAU is marked by the extinction of the specific paleo marker (IHS database, MMS, 1999).

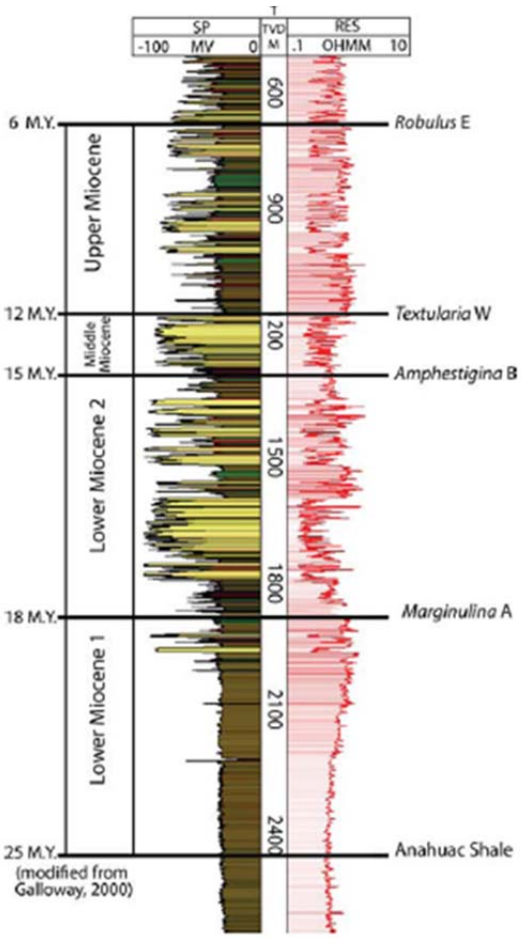

Figure 12: Type log for Miocene interval showing Storage Assessment Units and corresponding paleo markers

Wallace, K.J. et al, 2013

The **Pliocene** was marked by progradation of the shelf margin by an additional 80 km or 50 miles (Edring, C.H., 2008). The depocenter was located in the east – central offshore Louisiana. A total thickness of 3600 m (11,810 ft) was measured. The Pliocene – Pleistocene boundary is not firmly established (Galloway, W.E. et al, 1991), and is positioned at the extinction of Bullminella 1 biostratigraphic marker (I.H.S. database, MMS, June 1999). Rare Bullminella 1 bio-markers are found mainly in the southern portion of our study area, and not found at all in Block 107 field. We can consistently pick the Valvulineria H marker in the electronic logs and this log pick is supported by I.H.S. paleo data. We decided to map the Valvulineria H marker as the top of our Pliocene. Valvulineria H marker is found on average 1500 ft above the Bullminella 1 marker in the southern portion of the studied area, below 1370 m (4500 ft) depth, which is below the supercritical phase for CO_2, thus still a viable target for CO_2 sequestration.

The **Quaternary** was dominated by continental glaciation and associated eustatic sea level changes. The formation of ice volume to the north and significantly lowering of the sea level provide major sediment source into the GOM (Galloway, W.E., et al., 1991).

4.2.1 Ship Shoal Block 107 Field

Ship Shoal Block 107 Field is a large salt associated structure related to an east-west trending, down to the south growth fault. The regional fault and structure grew throughout the late Miocene through Pliocene time, with a major growth occurring in the late Pliocene (Russell, E.L., 1973). The generalized stratigraphic column with type log from Block 107 field is shown in Figure 13.

Miocene

The Energy XXI #43 well, which is the deepest well drilled in the studied only reached into the upper Miocene section at 5029 m (16,500 ft) depth (IHS database). Upper Miocene clastics were deposited in the outer neritic environment. The top of Miocene is marked by the extinction of Robulus E which coincides with the deposition of the transgressive shale. Productive sands are very fine grained, with porosities ranging between 17 – 30%, and permeabilities up to 1800 mD. Average porosity and permeability is measured at 25% and between 50-250 mD respectively (Russell, E.L., 1973). Please also see 3.3.1 Ship Shoal Block 107 Field above. Maximum oil column is 30 m (100 ft) thick and reservoir pressures up to 12,800 psi were recorded (Russell, E.L., 1973). The top of Miocene in the studied area is found below 3260 m (10,700 ft).

Pliocene

Lower Pliocene sediments were deposited in a middle neritic environment. The sands are very fined grained, with some shaling out locally. Porosities range from 25 to 30%, while permeabilities range from 0 – 2700 mD, commonly is between 250 – 500 mD. Oil columns can range up to 22 m (75 ft) thick producing at normal hydrostatic reservoir pressure. In the study area, top Pliocene is found below 1462 m (4700 ft). At the boundary between Pliocene and Miocene is the onset of the geopressured zone.

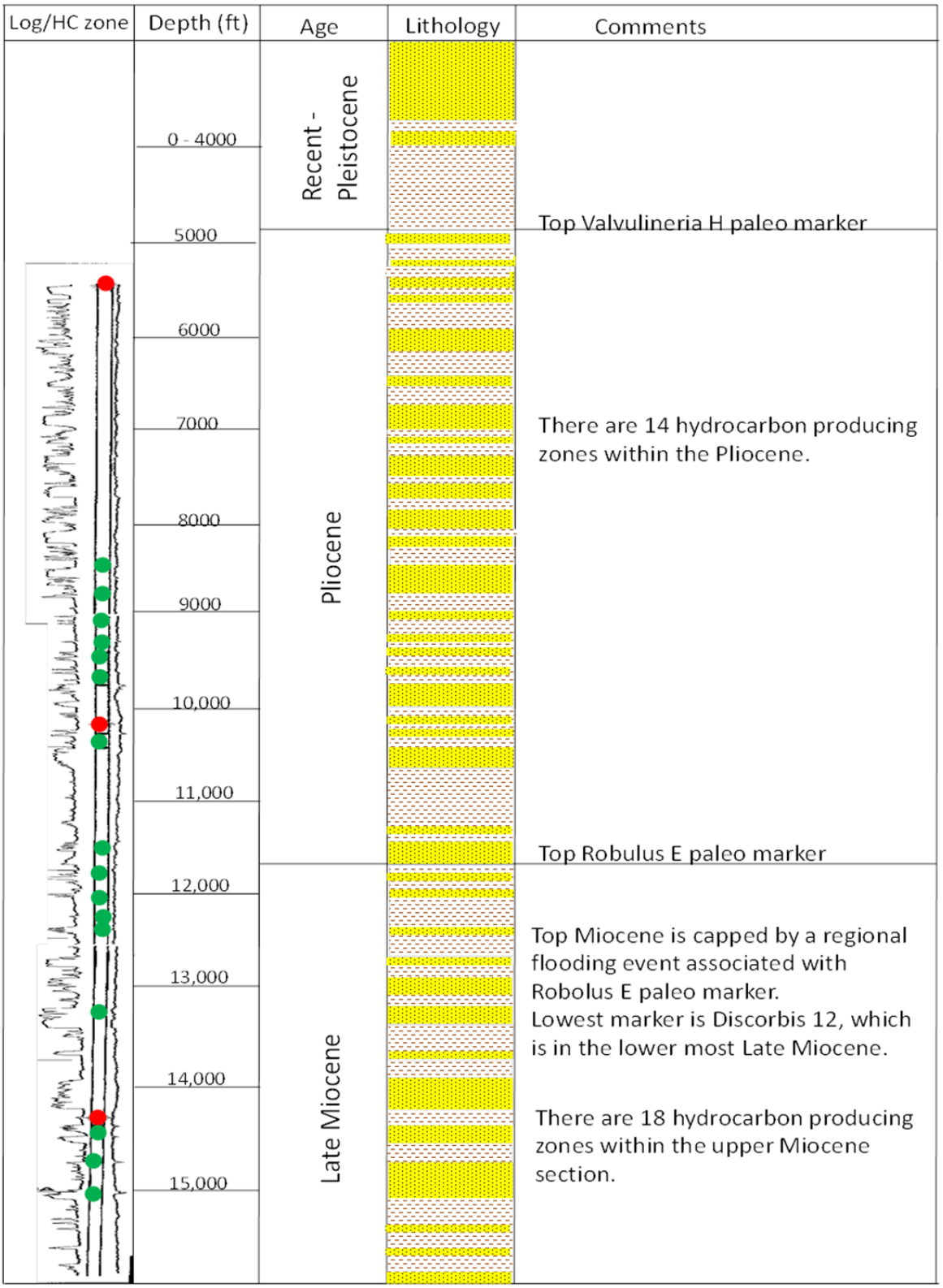

Figure 13: Generalized stratigraphic column and type log for Block 107 field

Modified from Russell, E.L., 1973; green dot – oil producing zone, red dot – gas producing zone

4.2.2 Ship Shoal Block 84 Field

Ship Shoal Block 84 Field is a small depleted oil field on the up-thrown side of the east-west trending major fault. Only six hydrocarbon producing wells are recorded in IHS database. Similar to the Block 107 Field, this ridge-like structure is associated with the growth of the nearby salt dome. The generalized stratigraphic column with type log for Block 84 field is shown in Figure 14.

Miocene

We only have deviation surveys for the BP 84-A5 and Prime 84-A7 wells within this field. The BP 84-A1 well is a straight hole and presumed to be the deepest well drilled. This well was drilled to 4226 m (13,866 ft) and reached the top Miocene at approximately 2895 m (9500 ft) subsea. This well was drilled below the base for our model, which we defined as the economic basement for CO_2 injection and storage. Three producing zones were reported by BOEM (2014); all producing zones were found within the Big A and Cris K stratigraphic layers.

The porosity and permeability for the Miocene producing zone average 27% and 55 mD respectively for the Big A horizon; and 29% and 663 mD for the Cris K horizon. Please also see 3.3.2 Ship Shoal Block 84 Field section above.

Pliocene

Pliocene is dry, and consists of shales at the base and increasingly sandy towards the top of the section. Cores from a nearby dry Chevron 85-1 well show the sand to be very fine grained and containing shale.

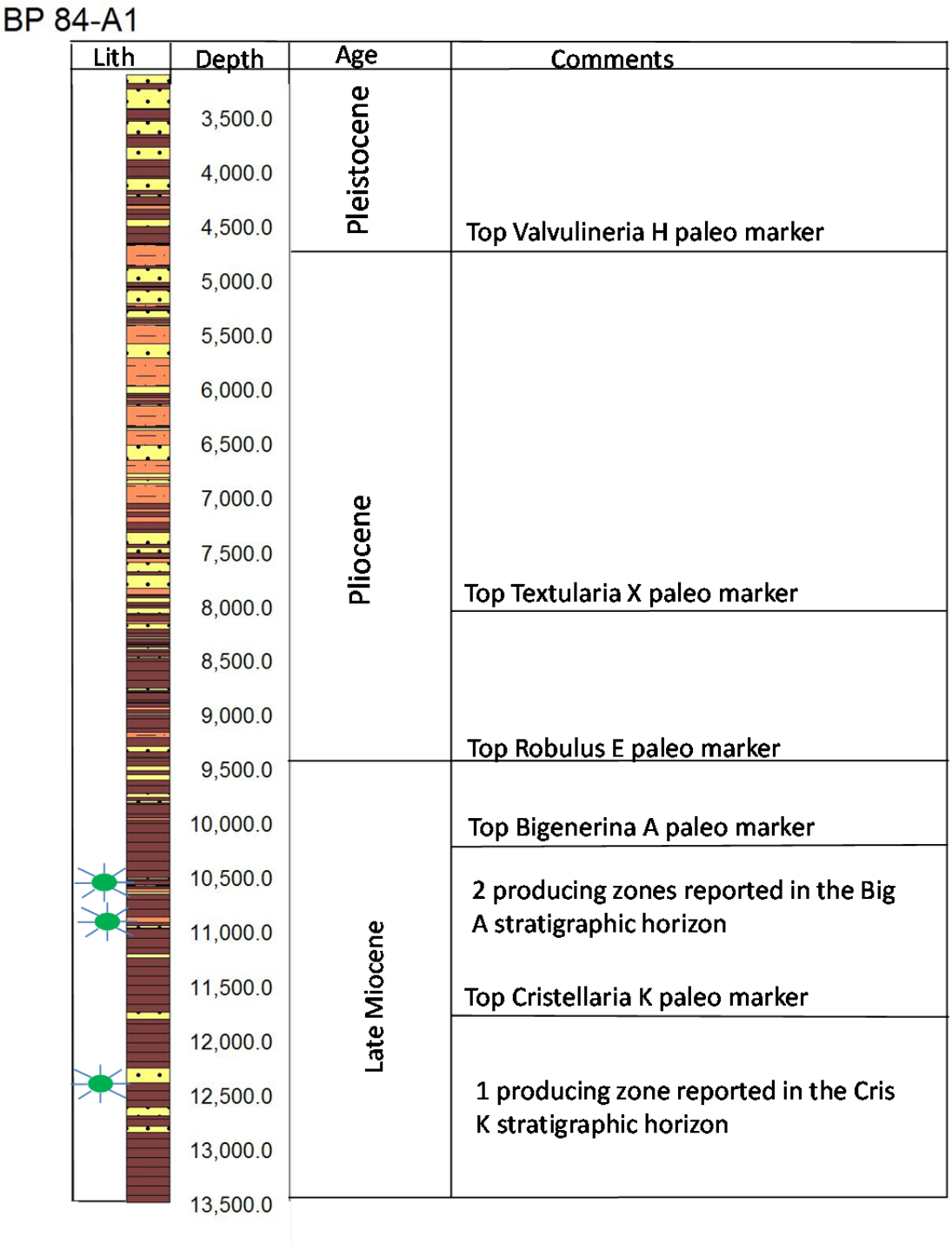

Figure 14: Generalized stratigraphic column for Block 84 field

BP 84-A1 well shown as type log; green dot – oil and gas producing zone

4.3 Geologic Model

The geological model spans about 24,688 m (82,000 ft) in the x-direction, 21,336 m (70,000 ft) in the y-direction, and 4,267 m (14,000 ft) in the z-direction. We have input all 121 vertical wellbore locations and wellbore with deviation surveys within and surrounding the Ship Shoal Block 84 and 107 fields into the Rockwork 16 geologic modeling software program. The structure maps for the top of the Pliocene (Figure 15) and top of the Miocene (Figure 16) formations were digitized and input into the geological modeling program. These two structure maps were modified using I.H.S. Tex X and Big A paleo datum. Using these two primary horizons, we developed the structure maps for the Pliocene Tex-X, and the Miocene Big-A and Cris-K formations. Tex X on average is 1066 m (3500 ft) below the top of Pliocene; while Big A and Top Cris K are on average 243 m (800 ft) and 670 m (2200 ft) below top of Miocene respectively. These structures are used for lithology model development, to constrain and warp the lithology according to the geologic structures of the area.

The 5 stratigraphic grids -- Top Pliocene, Textularia X, Top Miocene, Bigenerina A and Cristellaria K were stitched together to form a comprehensive stratigraphic model for the area. We also created a 3D lithologic model for the Ship Shoal study area. Lithologies obtained from well logs were used to create the lithologic model. This model is geologically sound and consistent with our interpretation and the regional geology within the Gulf of Mexico.

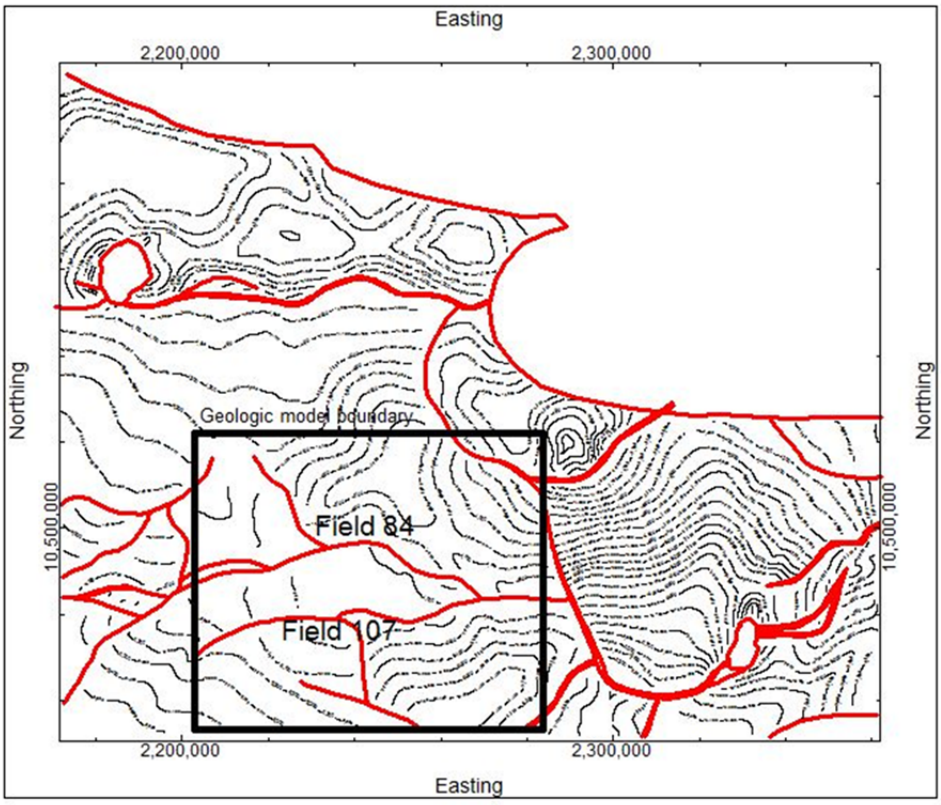

Figure 15: Structure map for the top of Pliocene formation

Fault in red

Modified from I.H.S. Textularia X structure map

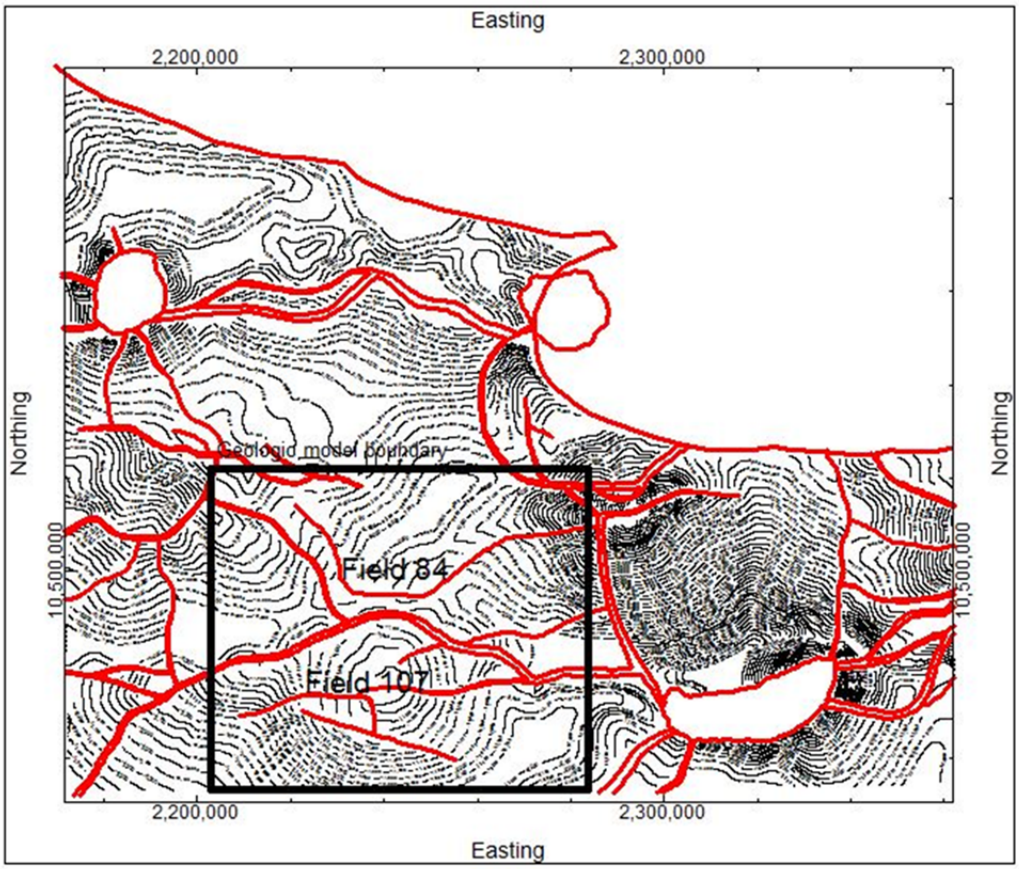

Figure 16: Structure map for the top of the Miocene formation

Fault in red

Modified from I.H.S. Bigenerina A structure map

4.3.1 Ship Shoal Block 107 Field

Figure 17 shows the 3D stratigraphic model and Figure 18 shows the lithology model of Block 107. Figure 20 and Figure 21 are the north-south and east-west cross sections through the proposed injection site in Block 107. Location for the two cross sections is shown in Figure 19.

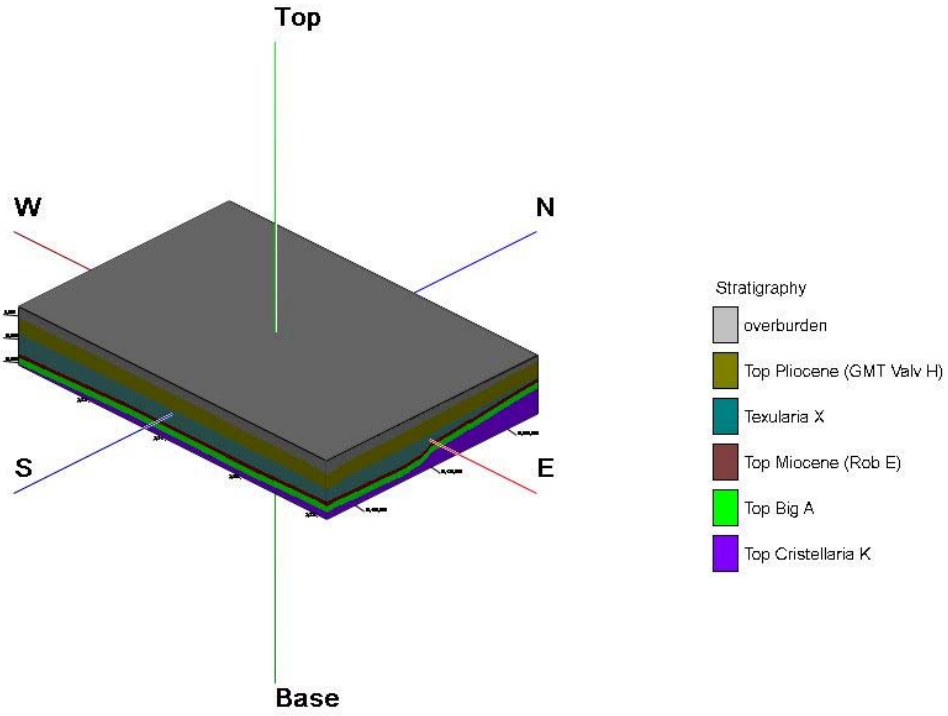

Figure 17: 3D stratigraphy model for Ship Shoal Block 107 field

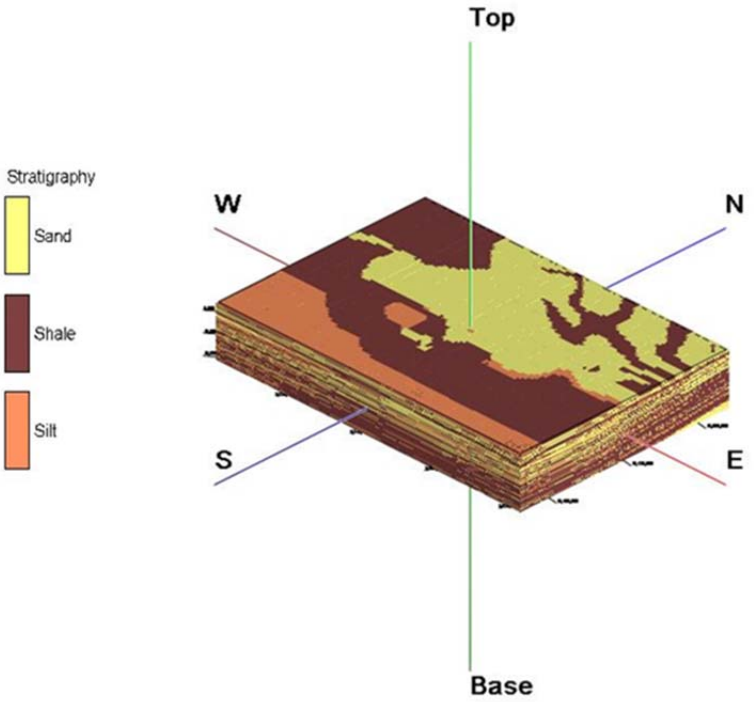

Figure 18: 3D lithology model for Ship Shoal Block 107 field

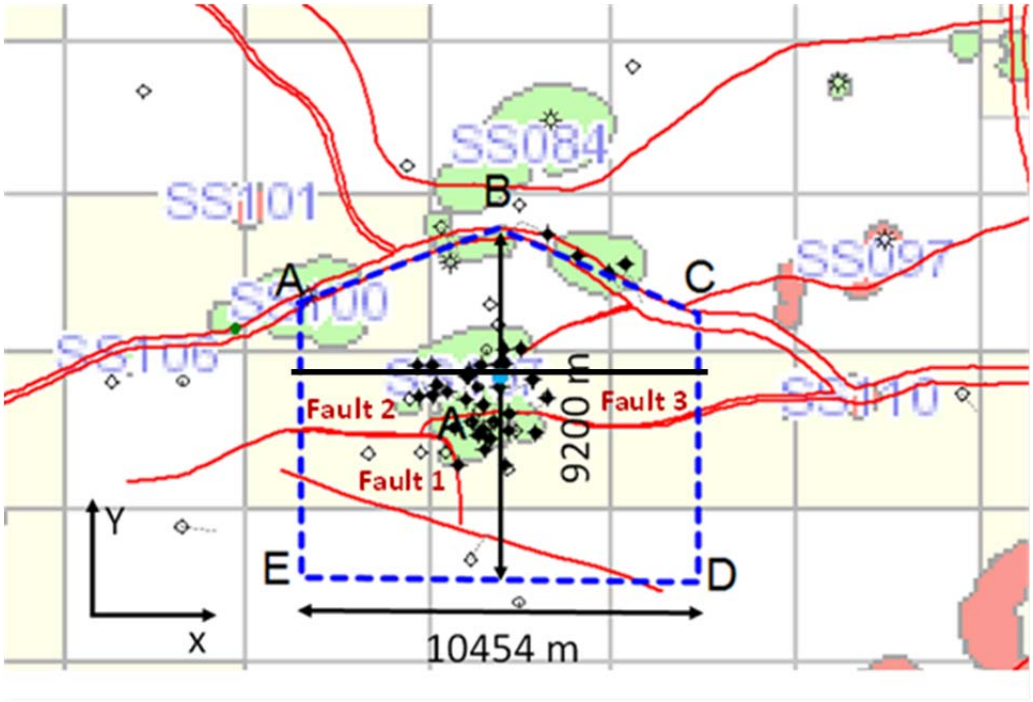

Figure 19: Location map showing N-S and W-E cross section lines through SS Block 107 field

Injection well – blue dot

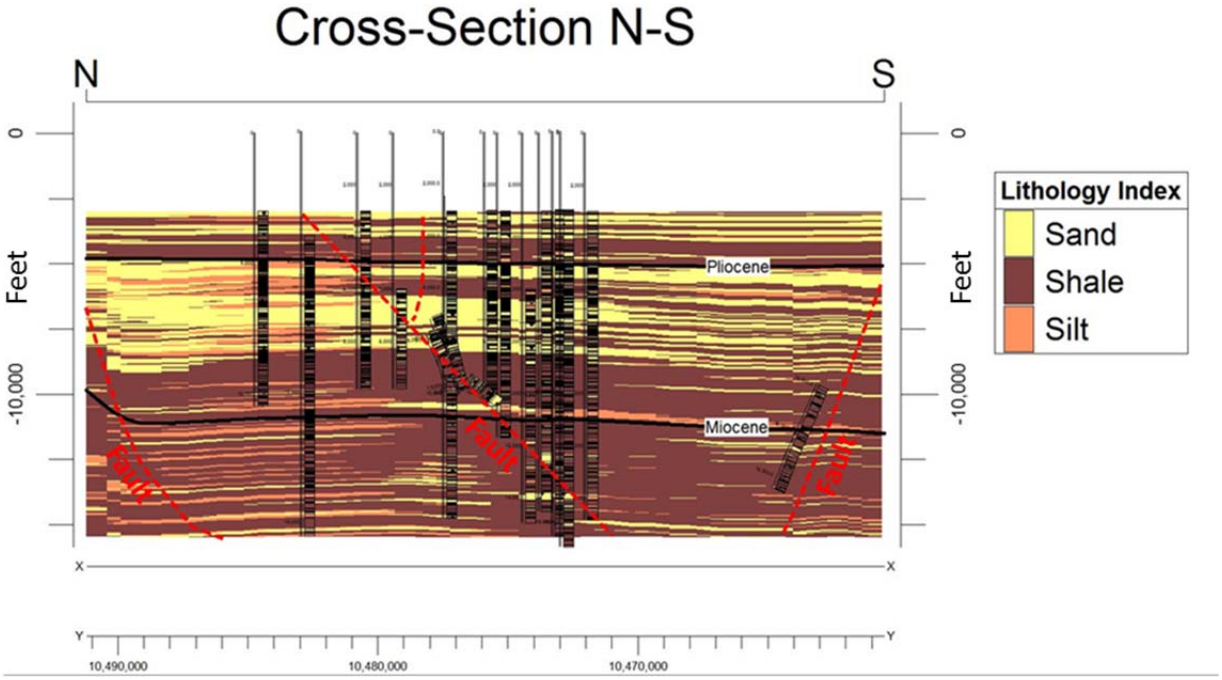

Figure 20: North - South cross section across Ship Shoal Block 107 field

Fault – red dash line

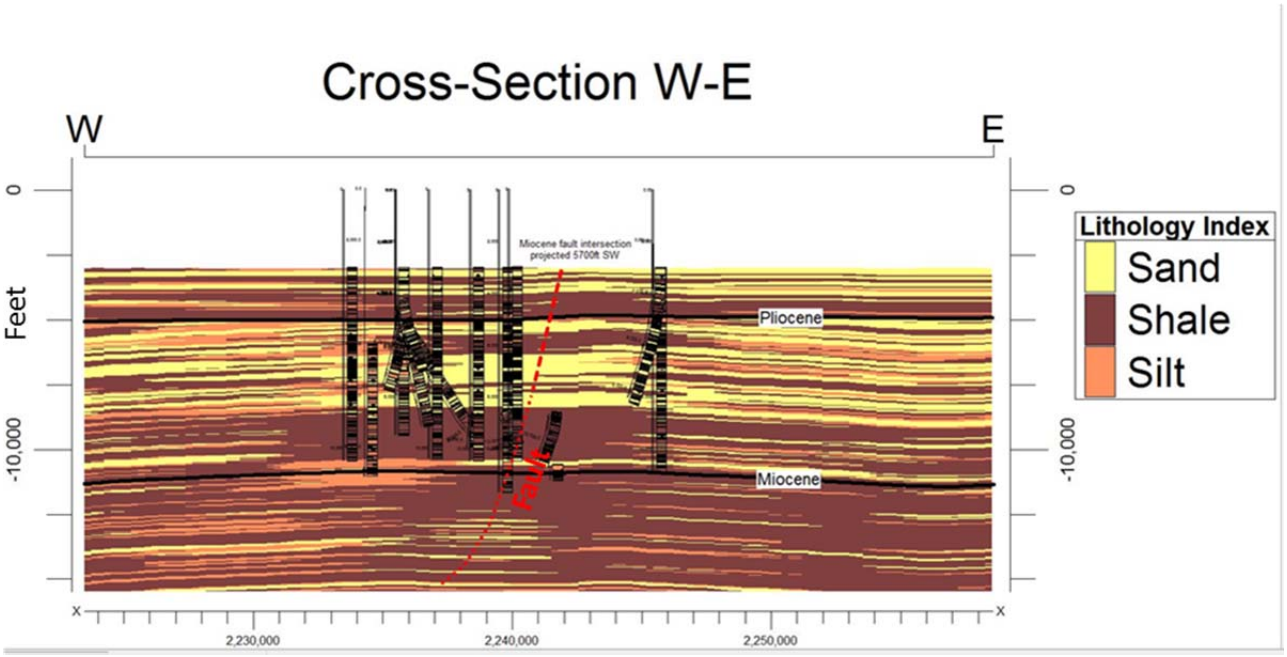

Figure 21: East – West cross section across Ship Shoal Block 107 field

Fault – red dash line

4.3.2 Ship Shoal Block 84 Field

We identified and recorded the lithology for sixteen wells throughout the Ship Shoal Block 84 Field area. This data was used to generate the lithology model. Figure 22 is the stratigraphic model for Ship Shoal Block 84 Field and Figure 23 shows a 3D view of the lithology model developed for the field and its surrounding area. Two cross sections were developed that run North-South and West-East that helped with fluid flow and geomechanical model developments. The cross section location map is shown in Figure 24. The north-south and west-east cross sections are shown in Figure 25 and Figure 26, respectively.

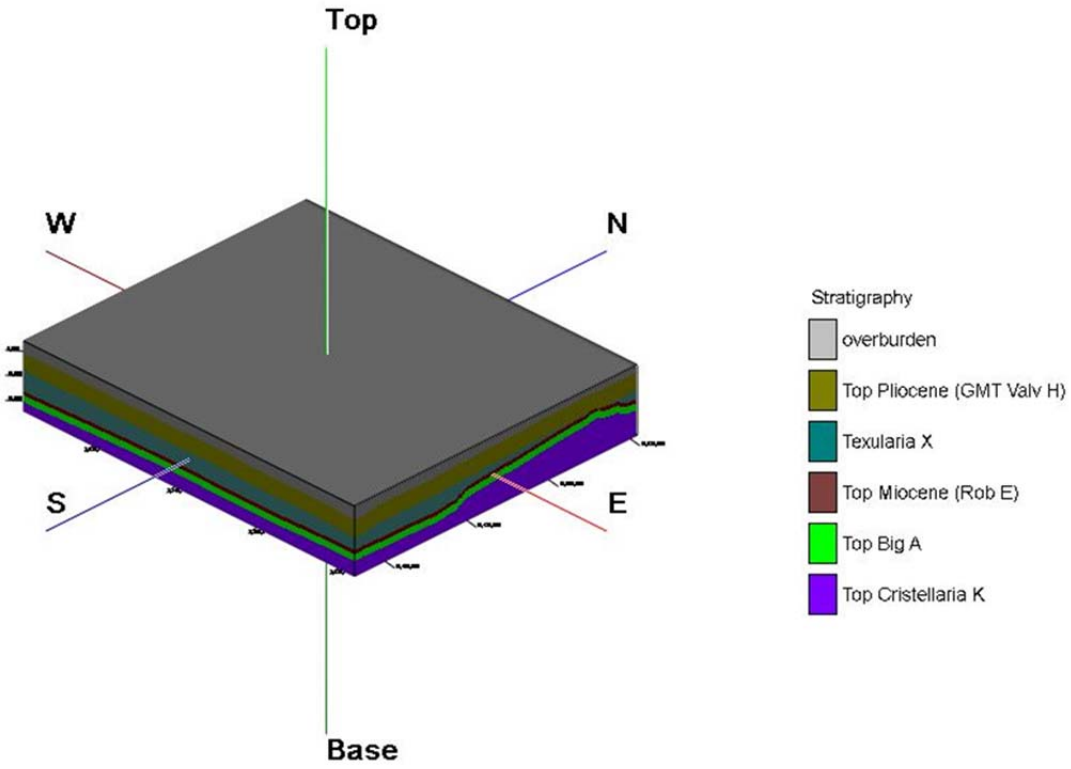

Figure 22: Stratigraphic model for the Ship Shoal Block 84 field

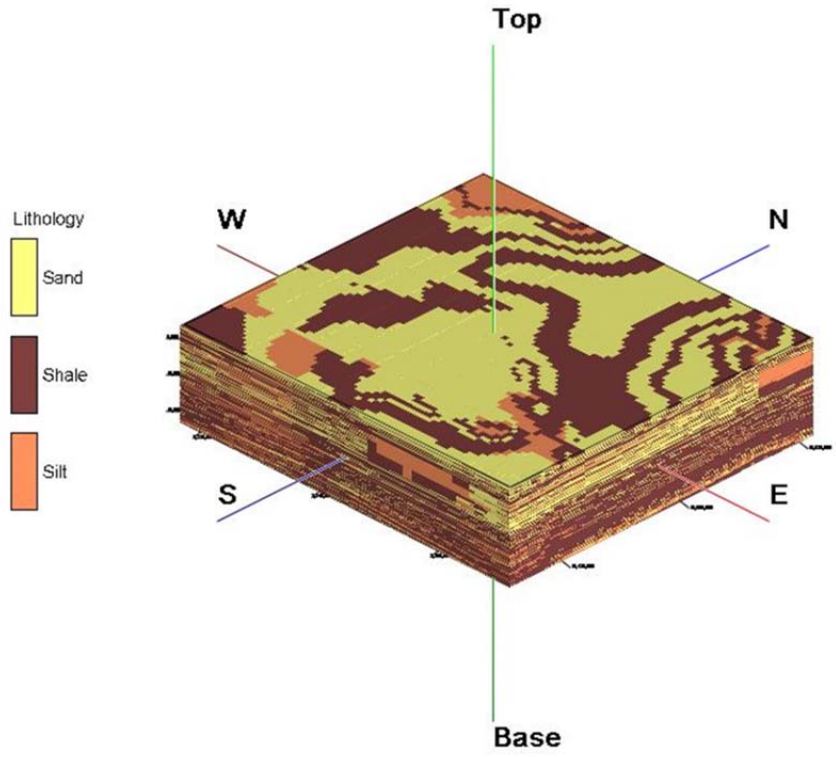

Figure 23: Lithology model for SS Block 84 field

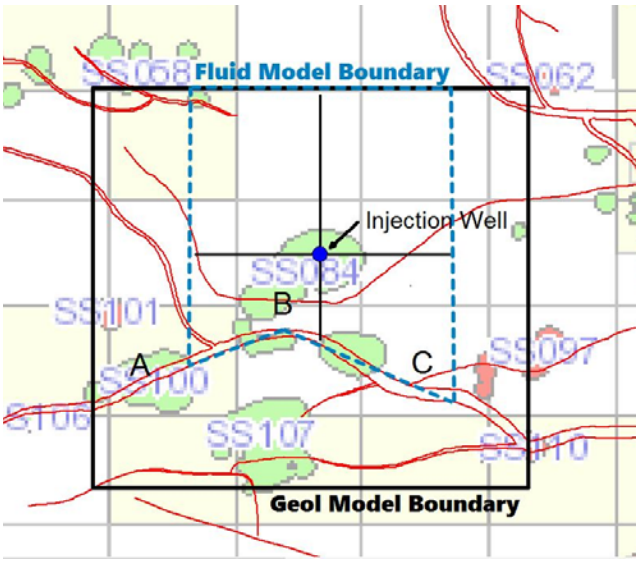

Figure 24: Location map showing N-S and W-E cross section lines through SS Block 84 field

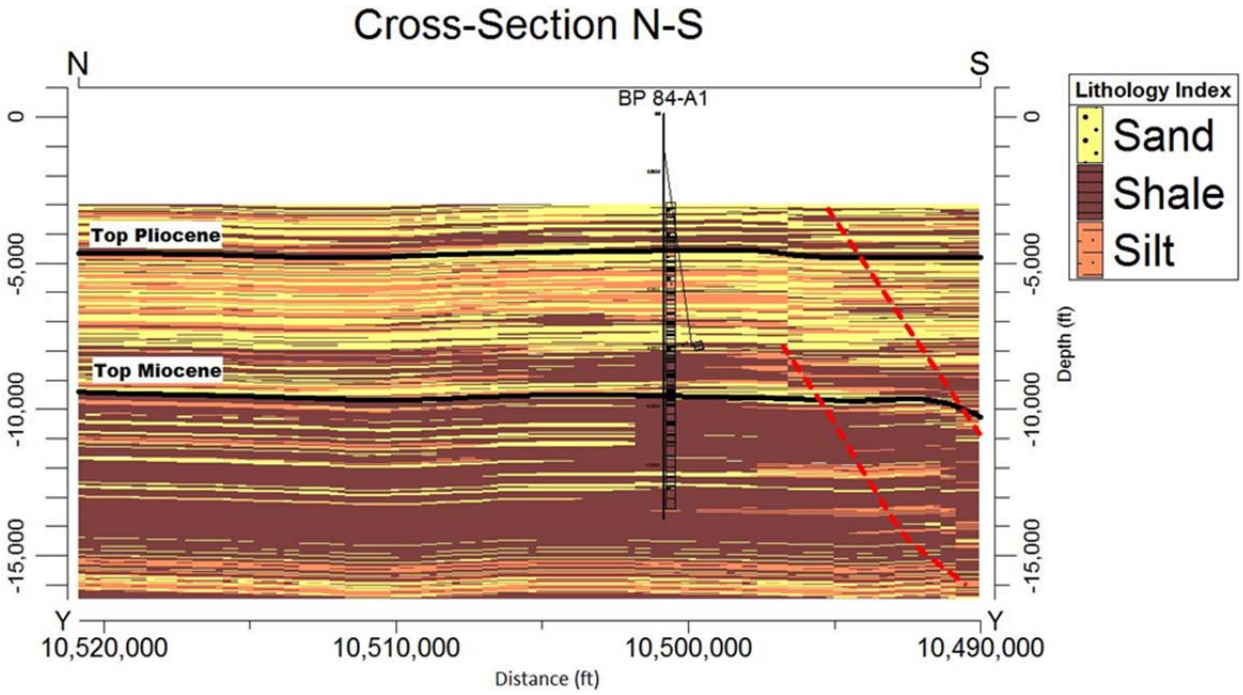

Figure 25: Cross section north-south through SS Block 84 field

Faults – red dash line

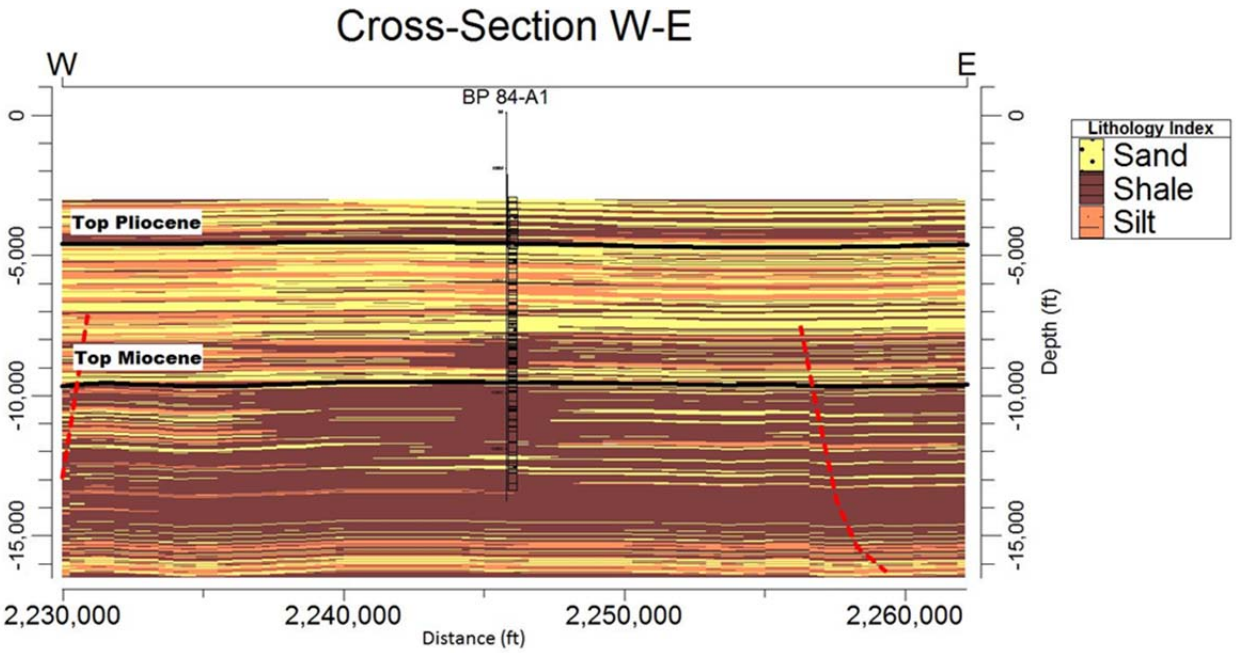

Figure 26**: Cross section west-east through SS Block 84 field**

Faults – red dash line

4.4 Conclusions

A detailed geological model spanning about 24,688 m (81,000 ft) in the x-direction, 21,336 m (70,000) ft in the y-direction, and 4267 m (14,000 ft) in the z-direction was created. A total of 121 wells were input into a database using Rockwork 16 geologic software program. We have input all vertical wellbore locations and wellbore with deviation surveys within and surrounding the Ship Shoal Block 84 and 107 fields. The structure maps for the top of the Pliocene and top of the Miocene were created by modifying I.H.S. Tex X and Big A paleo datum. Using these two primary horizons, we developed the structure maps for the Pliocene Tex-X, and the Miocene Big-A and Cris-K formations. These structures are used for lithology model development, to constrain and warp the lithology according to the geologic structures of the area. Five stratigraphic grids -- Top Pliocene, Textularia X, Top Miocene, Bigenerina A and Cristellaria K were stitched together to form a comprehensive stratigraphic model for the area.

We also created a 3D lithologic model for the Ship Shoal study area. Lithologies obtained from well logs were used to create the lithologic model. This model is geologically sound and consistent with our interpretation and the regional geology within the Gulf of Mexico.

5 CO_2 injection and migration modeling

TOUGH2 (Pruess et al., 1999) modeling software was used to simulate CO_2 migration and fluid flow during and after CO_2 injection. Both Modulus ECO_2N and EOS7C were used in the simulations. ECO_2N equations of state can model the three component system of water, CO_2, salt in liquid, gaseous, or solid states. For the Pliocene Model, ECO_2N Modulus was used. For the Miocene Model, since the injection depth is deep and the temperature already exceeds the limit of Modulus ECO2N of TOUGH2 (2.0 version), Modulus EOS7C TOUGH2 (2.0 version) was used instead. EOS7C is a fluid-property module for the TOUGH2 simulator (Version 2.0) that was developed for applications involving geologic storage of CO_2 in formations containing water and methane. It includes a comprehensive description of the thermodynamics and thermophysical properties of H_2O-CO_2-CH_4 mixtures that reproduces fluid properties largely within experimental error for the temperature and pressure conditions of interest. In particular, CO_2 and CH_4 can exist in a gas-like phase (CO_2 is actually supercritical if pressure and temperature are above the critical point (72 bars or 1044 psi, 31°C) or dissolved in the aqueous phase, and water can evaporate into the gas-like phase. Ship Shoal field is a depleted oil reservoir, thus it is applicable to use Modulus EOS7C. Experiments have been performed by LBNL (Lawrence Berkeley National Lab) showing that simulation results of EOS7C and ECO2N for the same condition are almost identical.

Figure 27 shows a map with the outline of the two blocks modeled. Each block is described in a separate section.

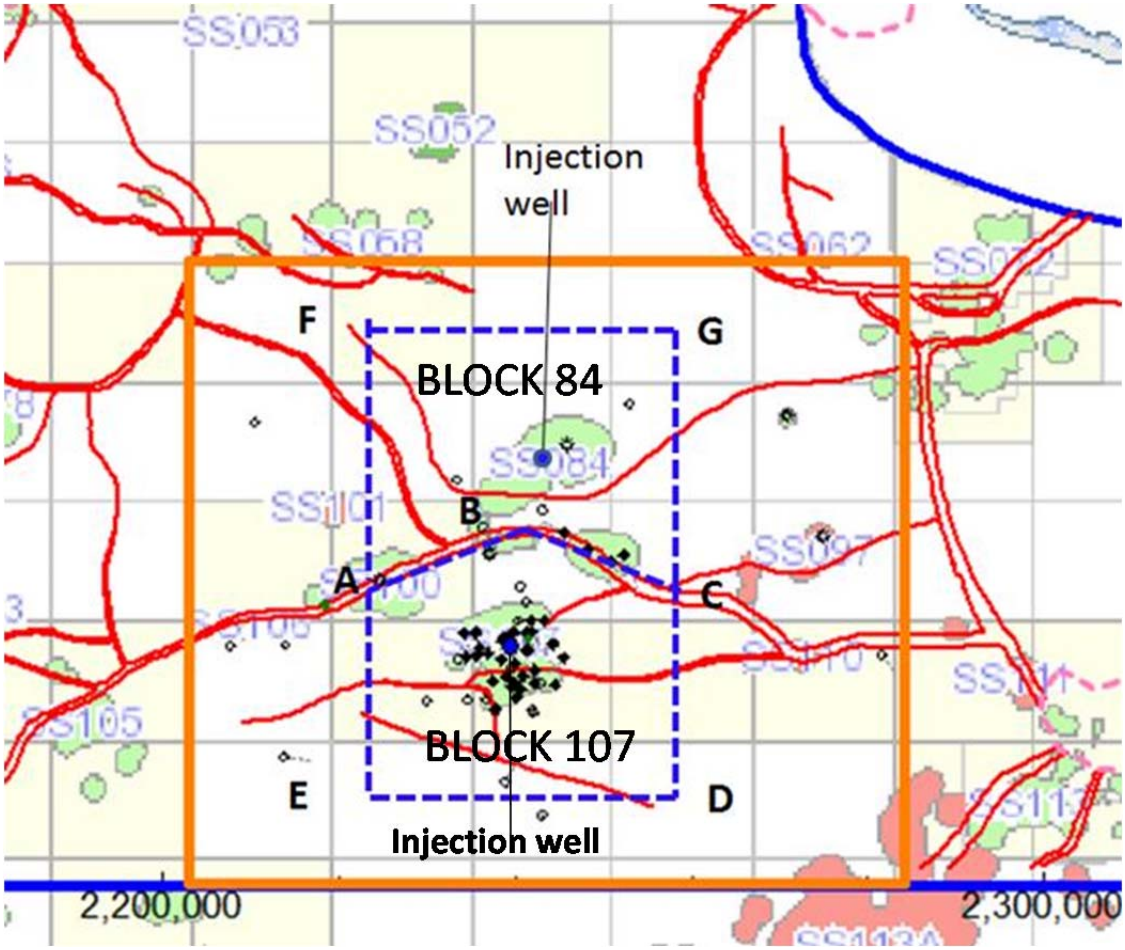

Figure 27: Outline (blue dashed) of Ship Shoal Block 84 (North of major fault 'A-B-C') and Block 107 (South of major fault) fluid flow models

Geologic model boundary: Orange boundary

5.1 Ship Shoal Block 107 Field

As stated in the proposal, two target injection zones, one within the base of the Pliocene and another within the upper Miocene formation have been selected for fluid flow simulation for evaluating the capacity potential for the CO_2 injection.

Figure 28 shows the fluid flow model boundary top view in Block 107. The reservoir model covers a lateral area of approximately 4.8 km or 3 miles in radius. The big fault (AB and BC in Figure 28) is used as the model boundary. Figure 29 presents the two target zone injection intervals in the fluid flow simulation. The sand at the bottom of the Pliocene target zone seems to have better lateral continuity than the upper Miocene Formation target zone.

GeoMechanics Technologies developed the fluid flow model for the bottom of Pliocene Formation. The results are summarized below.

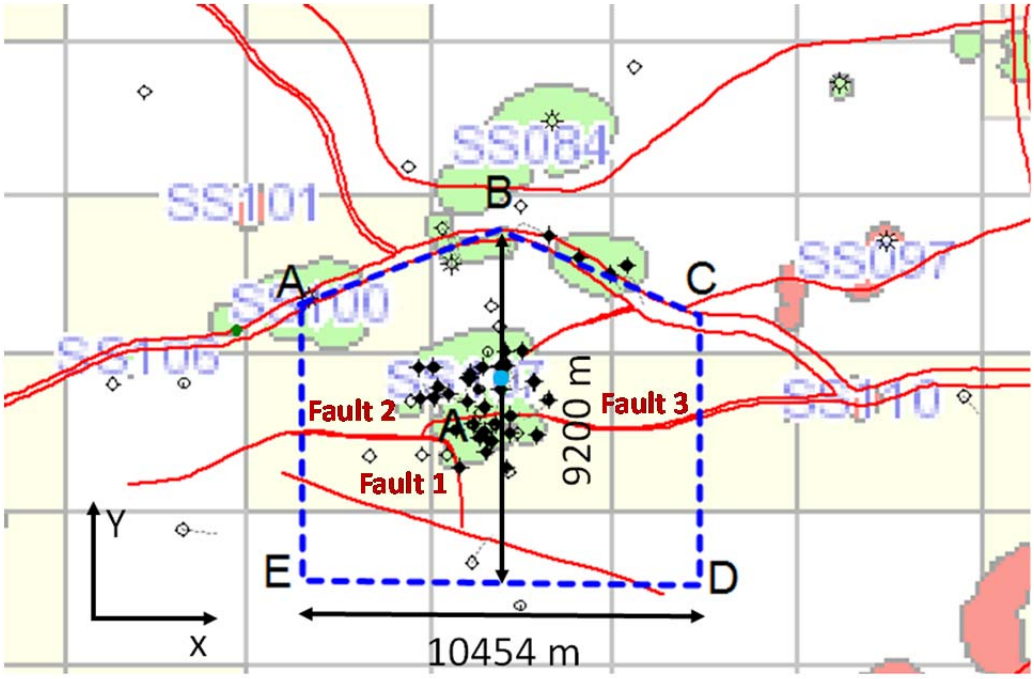

Figure 28: Fluid flow and geomechanical models boundary shown in blue dash lines. Injection well (blue) is assumed to be in the center of the model – SS Block 107 field.

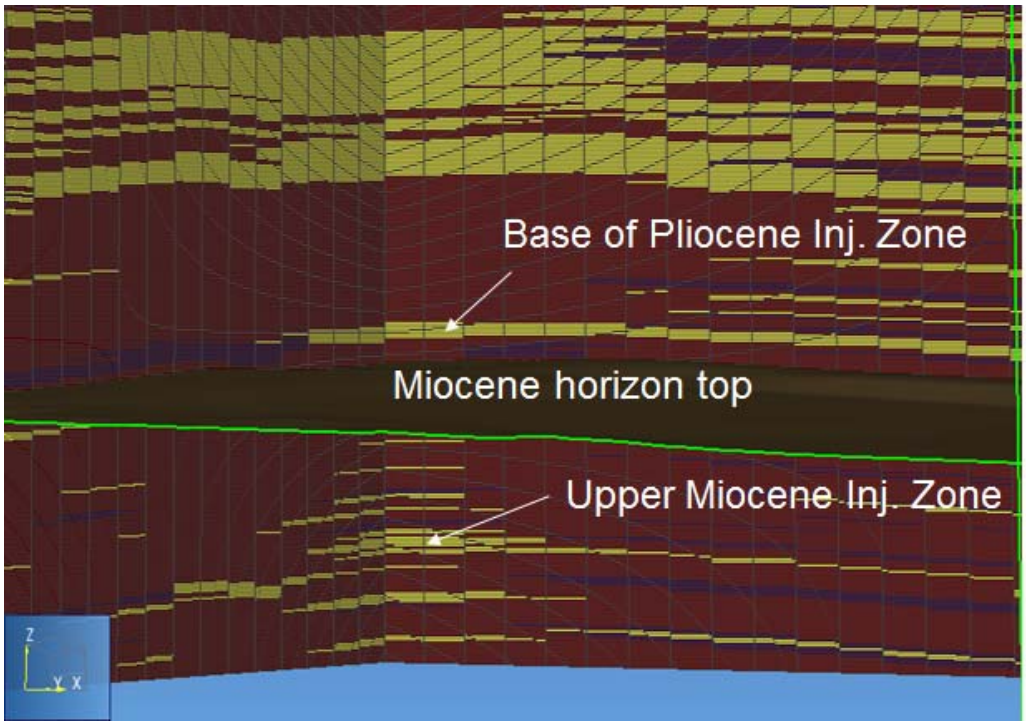

Figure 29: Target injection zones of Ship Shoal Block 107 field

5.1.1 Design and Assemble CO_2 injection model

5.1.1.1 Material Properties

Porosity and permeability for each formation used in the baseline simulations have been documented and presented in Table 8. All the detailed fluid flow properties used in the baseline simulation is listed in Table 12.

Table 12: Baseline fluid flow properties for various formations

Formation	Top Plioce			TexX			Top Miocene			BigA		
Material name	Sand	Shale	Silt	Sand	Shale	Silt	Sand	Shale	Silt	Sand	Shale	Silt
Density [kg/m³]	2650	2500	2400	2650	2500	2400	2650	2500	2400	2650	2500	2400
Wet heat conductivity [W/mC]	2.51	2.51	2.51	2.51	2.51	2.51	2.51	2.51	2.51	2.51	2.51	2.51
Specific heat [J/kg-C]	920	920	920	920	920	920	920	920	920	920	920	920
Total porosity [-]	0.28	0.2	0.22	0.28	0.16	0.15	0.28	0.1	0.1	0.27	0.12	0.11
Effective porosity (-)	0.28	0.1	0.11	0.28	0.08	0.075	0.28	0.05	0.05	0.27	0.06	0.055
x permeability [mD]	261.0	18	26.7	261	7	5.4	108	1.4	1.2	228	3.6	1.2
y permeability [mD]	261.0	18	26.7	261	7	5.4	108	1.4	1.2	228	3.6	1.2
z permeability [mD]	130.5	9	13.4	131	3.5	2.7	54	0.7	0.6	114	1.8	0.6

The relative permeability curve for CO_2 in the Ship Shoal area was not found in the literature review; however, we were able to find some relative permeability curves for CO_2 in other areas, including different kinds of rock formations. Due to the lack of detailed information regarding relative permeability and capillary pressure curves for different material types, we distinguish mainly sand and shale characteristics. We applied sand characteristics to all sand and silt material types, and shale characteristics to the shale material types used.

As found from the paper review (Doughty, 2010; Bennion and Bachu, 2007, Krevor et al., 2012 and Nathan David Moodie, undated), the different relative permeability curves and capillary pressure curves were shown in Figure 30 and Figure 31, respectively. There are several permeability curves found for different sand formations, however, only one permeability curve was found for a shale formation. In this study, based on the comparatively similar porosity and permeability properties, we use the relative permeability curve and capillary pressure curve from Berea rock for the sand and silt. For shale formation, the Kimberlina shale relative permeability curve and capillary pressure curve were used. The detailed parameters for each curve used in TOUGH2 simulation input is listed in Table 13.

Table 13: Baseline relative permeability and capillary pressure curve for various formations

Formation		Top Plioce			TexX			Top Miocene			BigA		
Material name		Sand	Shale	Silt	Sand	Shale	Silt	Sand	Shale	Silt	Sand	Shale	Silt
Rel. perm. /van Genuchten	λ		0.9170			0.9170			0.9170			0.9170	
	S_{lr}		0.30			0.30			0.30			0.30	
	S_{ls}		1.00			1.00			1.00			1.00	
	S_{gr}		0.29			0.29			0.29			0.29	
Rel. perm. /Corey	S_{lr}	0.20		0.20	0.20		0.20	0.20		0.20	0.20		0.20
	S_{gr}	0.00		0.00	0.00		0.00	0.00		0.00	0.00		0.00
Cap pressure /van Genuchten	λ	0.6700	0.4120	0.6700	0.6700	0.4120	0.6700	0.67	0.4120	0.6700	0.67		0.6700
	S_{lr}	0.11	0.3	0.11	0.11	0.3	0.11	0.11	0.3	0.11	0.11		0.11
	$1/P_0$ (1/Pa)	4.0E-04	1.2E-06	4.0E-04	4.0E-04	1.2E-06	4.0E-04	4.0E-04	1.2E-06	4.0E-04	4.0E-04		4.0E-04
	P_{max}(Pa)	1.0E+07	1.0E+09	1.0E+07	1.0E+07	1.0E+09	1.0E+07	1.0E+07	1.0E+09	1.0E+07	1.0E+07		1.0E+07
	S_{ls}	1.00	1.00	1.00	1.00	1.00	1.00	1.00	1.00	1.00	1.00		1.00

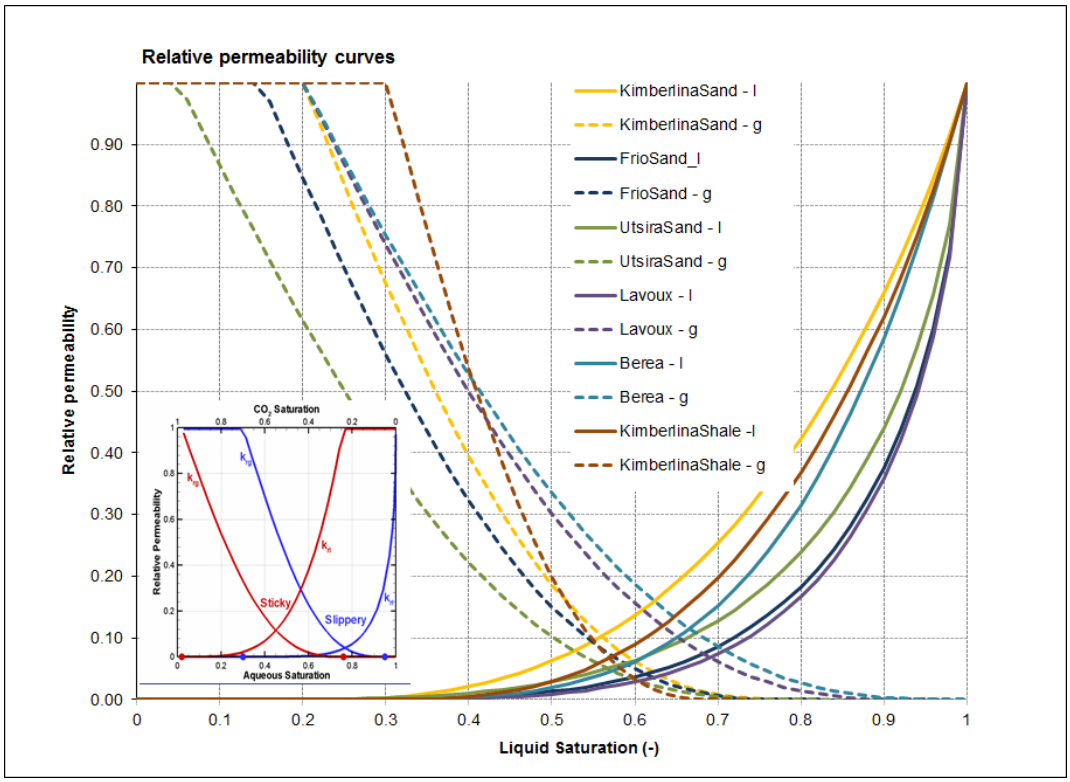

Figure 30: Relative permeability curves from literature review for CO2

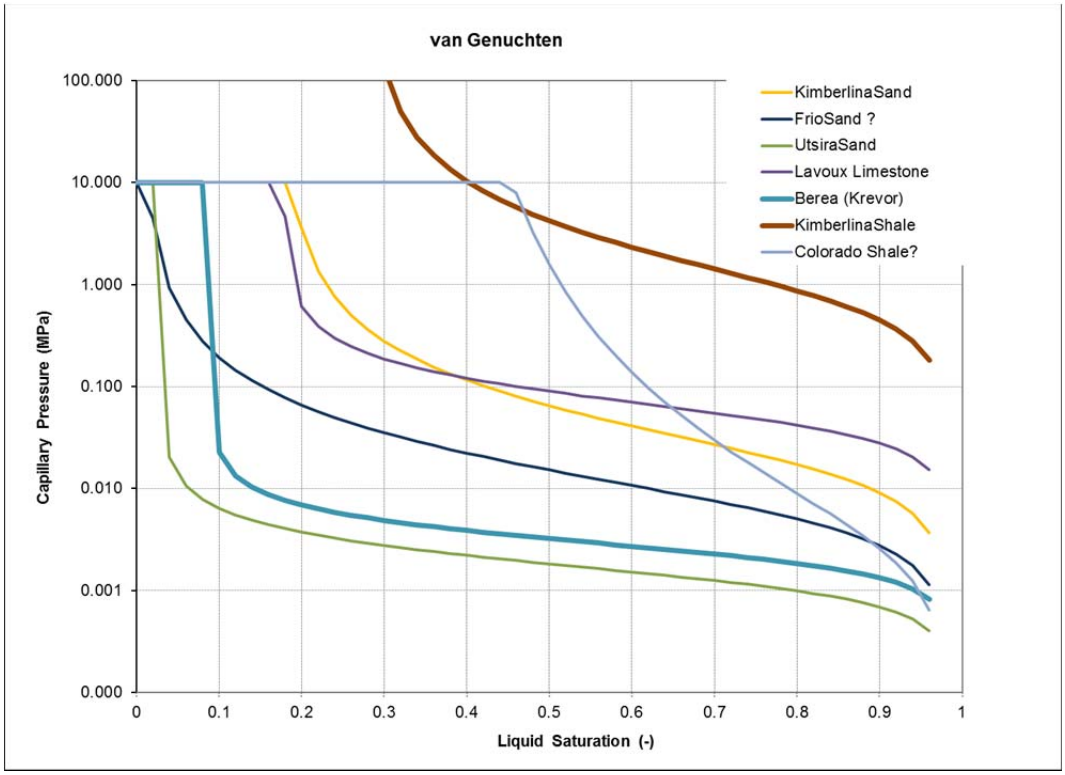

Figure 31: Capillary pressure curves evaluated from literature

5.1.1.2 Base of Pliocene Model Assembly

The base of Pliocene fluid flow model covers approximately 10,400 m (34,120 ft) in the x direction, 9,200 m (30,183 ft) in the y direction, and 3,000 m (9,842 ft) in the z direction (-1524 m to -4572 m or -5000 ft to 15,000 ft SSL.).The detailed dimensions and boundary conditions of the model can be found in Figure 32. A no-flow boundary condition has been applied to the two sides of the fault, and the top and bottom of the model; while constant-pressure has been applied to the other 3 sides.

Figure 33 shows the injection location and perforation interval for this simulation. Close to the injection well, the mesh is more refined, while the mesh coarsens away from the injection well. Around the injection well area, the cell dimensions in the x and y direction are 50 m, while the cell dimensions in the x and y direction outside of the injection area is 200 m. The z spacing in the injection zone is 10 m, and it gradually increases towards the top and bottom of the model.

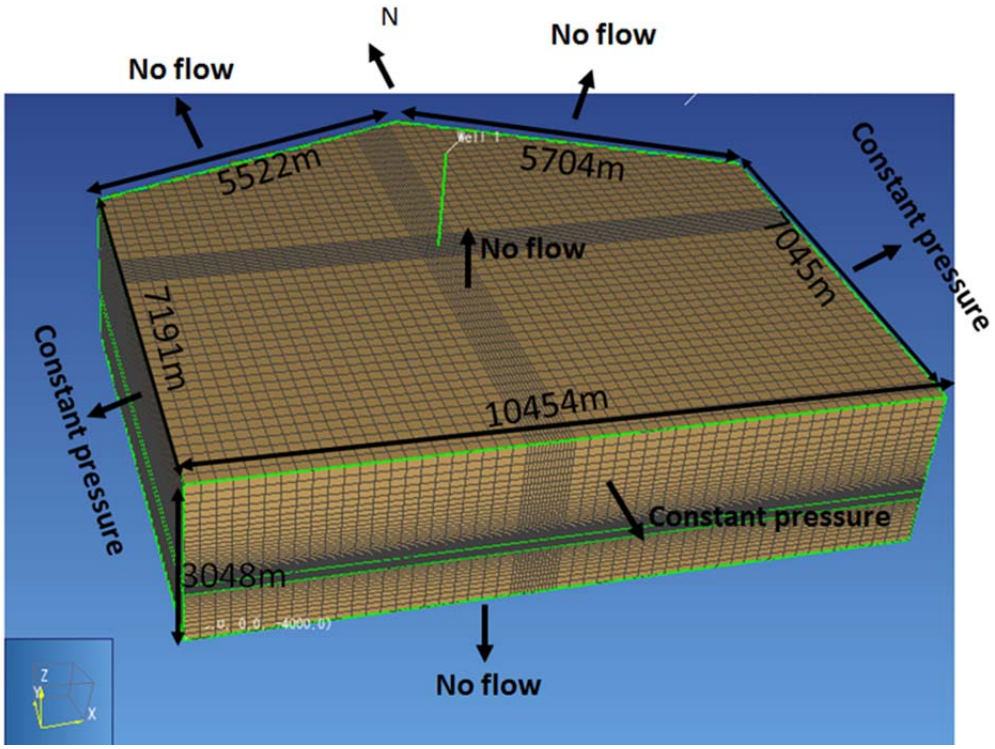

Figure 32: Base Pliocene fluid flow model boundary size and boundary conditions – SS Block 107 field

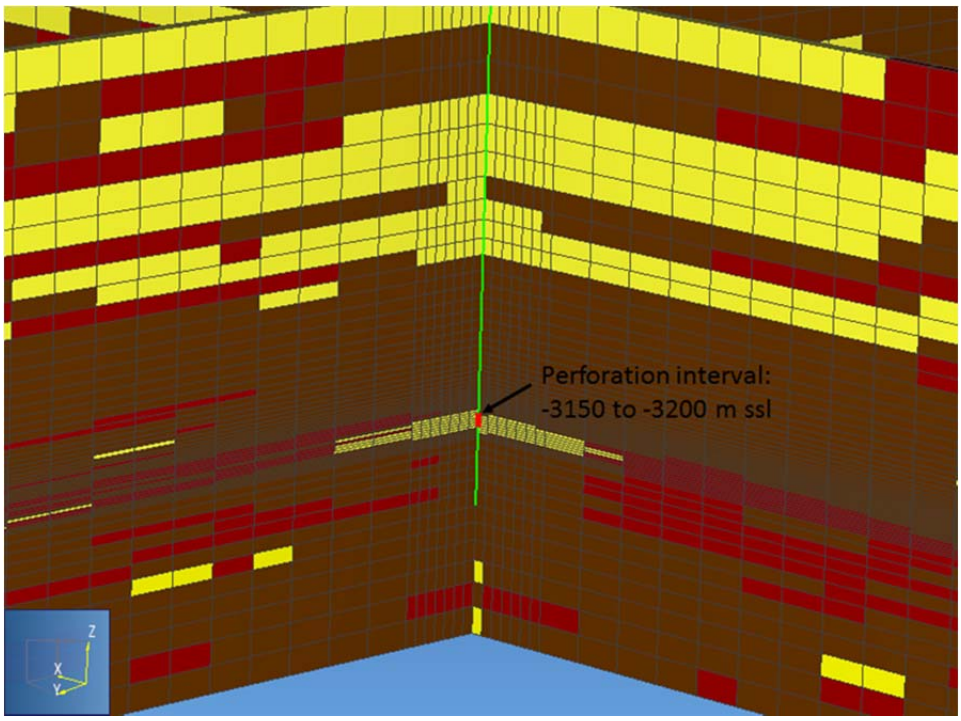

Figure 33: Injection location and perforation interval for Bottom of Pliocene fluid flow model 3D cut out view looking from S-- SS Block 107 field

5.1.1.3 Upper Miocene Model Assembly

The Upper Miocene fluid flow model covers approximately 10,400 m (34,120 ft) in the x direction, 9,200 m (30,183 ft) in the y direction, and 1,800 m (5905 ft) in the z direction (-2700 m to -4500 m or -8858 ft to -14,763 ft SSL.). The detailed dimensions and boundary conditions of the model can be found in Figure 32. A no-flow boundary condition has been applied to the two sides of the fault, and to the top and bottom of the model; while constant-pressure has been applied to the other 3 sides.

Figure 35 shows the injection location and perforation interval for this simulation. The perforation interval for this well is -4070 to -4080 m or -13,353 to -13,386 ft SSL. Close to the injection well, the mesh is more refined, while the mesh coarsens away from the injection well. Around the injection well area, the cell dimensions in the x and y direction are about 30 m. The z spacing in the injection zone is 10 meters, and it gradually increases towards the top and bottom of the model.

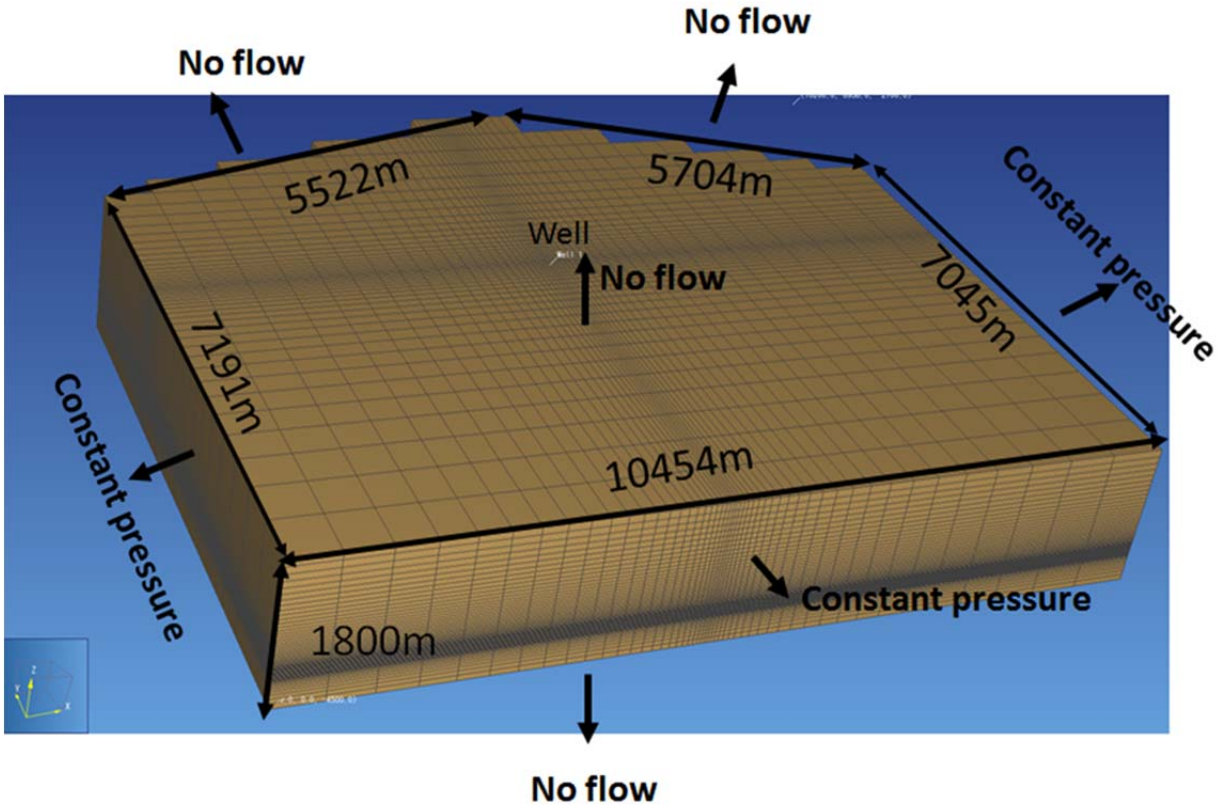

Figure 34: Upper Miocene fluid flow model boundary size and boundary conditions -- SS Block 107 field

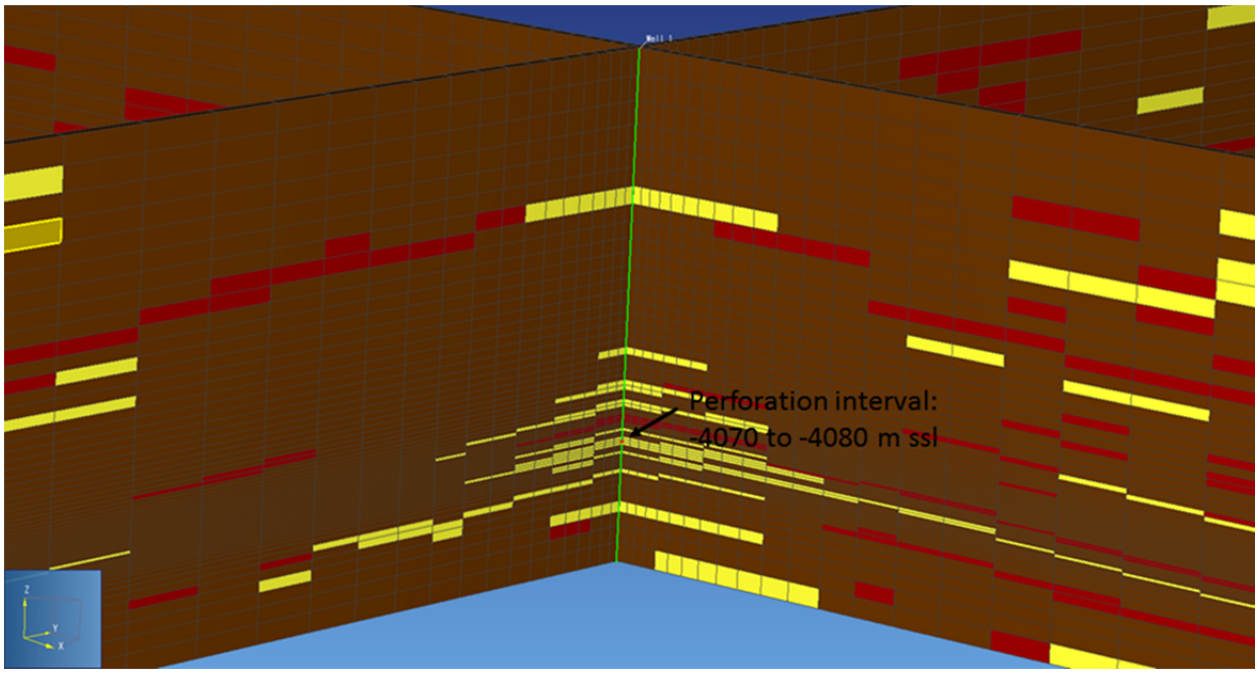

Figure 35: Injection location and perforation interval for Upper Miocene fluid flow model -- SS Block 107 field

5.1.2 Simulate varying injection scenarios

5.1.2.1 Pliocene Model Simulation

5.1.2.1.1 Simulation matrix

Six (6) scenarios have been simulated for the Pliocene fluid flow model. The following conditions were used for the baseline case:

- Assume an initial reservoir pore pressure gradient of 0.435 psi/ft and initial reservoir temperature gradient of 24 degree/km with surface temperature of 25 degree C.
- Assume the salt mass fraction of 0.02148 for the reservoir fluid.
- Assume no initial mass fraction of CO_2 in the reservoir
- Simulation is run in isothermal mode
- Relative permeability for sand is based on the Berea Sandstone lab data.
- An injection rate of 1 million metric tons of CO_2 per year is applied for 30 years
- Additional 30 years of plume migration are modeled after injection ceased
- Capillary pressure was included

Besides the baseline case (sim01), different sensitivity scenarios including different relative permeability for sand (sim02), different pore pressure gradient (sim03), no salt (sim04), non-isothermal (sim05), and no capillary pressure (sim06) effects were also included. The simulation matrix is listed in Table 14 in detail.

Table 14: Simulation Matrix for Pliocene Model - SS Block 107 field

Model	Scenarios	Relative Permeability for Sand	Capillary Pressure	Injection Rate (million ton/y)	Isothermal?	Salt?	PP Gradient (psi/ft)
Pliocene	107_P_Sim01 (Baseline)	Based on Berea Sandstone	Yes	1	Yes	Yes	0.435
	107_P_Sim02 (Different Relative Permeability for Sand)	Based on Utsira Sandstone	Yes	1	Yes	Yes	0.435
	107_P_Sim03 (Different PP Gradient)	Based on Berea Sandstone	Yes	1	Yes	Yes	0.3
	107_P_Sim04 (No Salt)	Based on Berea Sandstone	Yes	1	Yes	No	0.435
	107_P_Sim05 (Non-isothermal)	Based on Berea Sandstone	Yes	1	No	Yes	0.435
	107_P_Sim06 (No capillary pressure)	Based on Berea Sandstone	No	1	Yes	Yes	0.435

5.1.2.1.2 Baseline case (107_P_sim01) result

Figure 36 and Figure 37 show the gas saturation distribution results for the baseline case simulation after 30 years injection and after another 30 years observation, respectively. Simulation results show that the injected CO_2 migrates about 2414 m or 1.5 mile radius in lateral direction over 30 years injection. The injected CO_2 is contained in the bottom of Pliocene Formation within a 100 meters (328 ft) interval. Figure 38 shows the CO_2 plume lateral migration from top view after 30 years of injection and another 30 years of observation.

Figure 39 shows the pressure change in the model after 30 years injection. A maximum pressure change of about 90 psi is observed in the injection interval. Simulation results suggest that the 30 Million tons of CO_2 injected is contained within the Pliocene Formation.

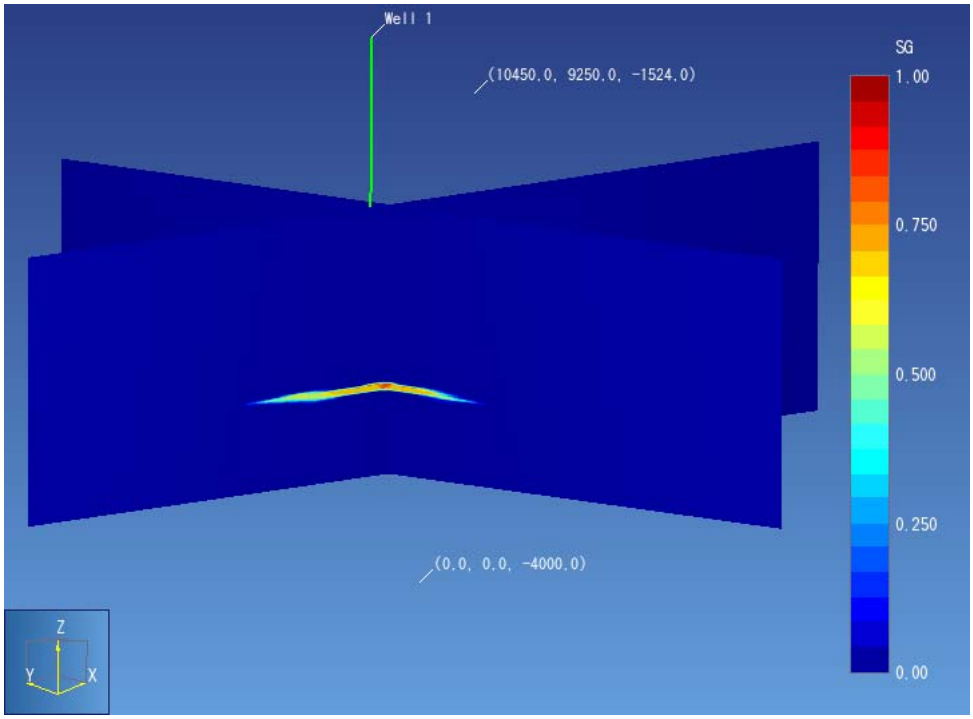

Figure 36: Gas saturation distribution after 30 year injection for baseline case (107_P_sim01)-Pliocene Model in SS Block 107 field

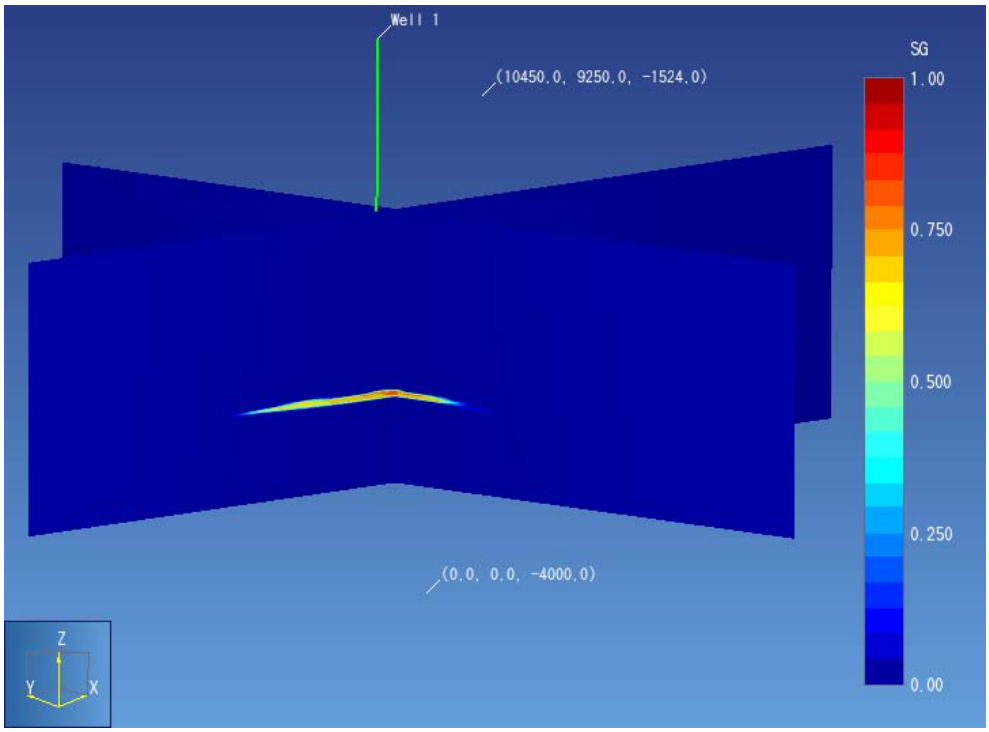

Figure 37: Gas saturation distribution after 30 year of observation for baseline case (107_P_sim01)-Pliocene Model in SS Block 107 field

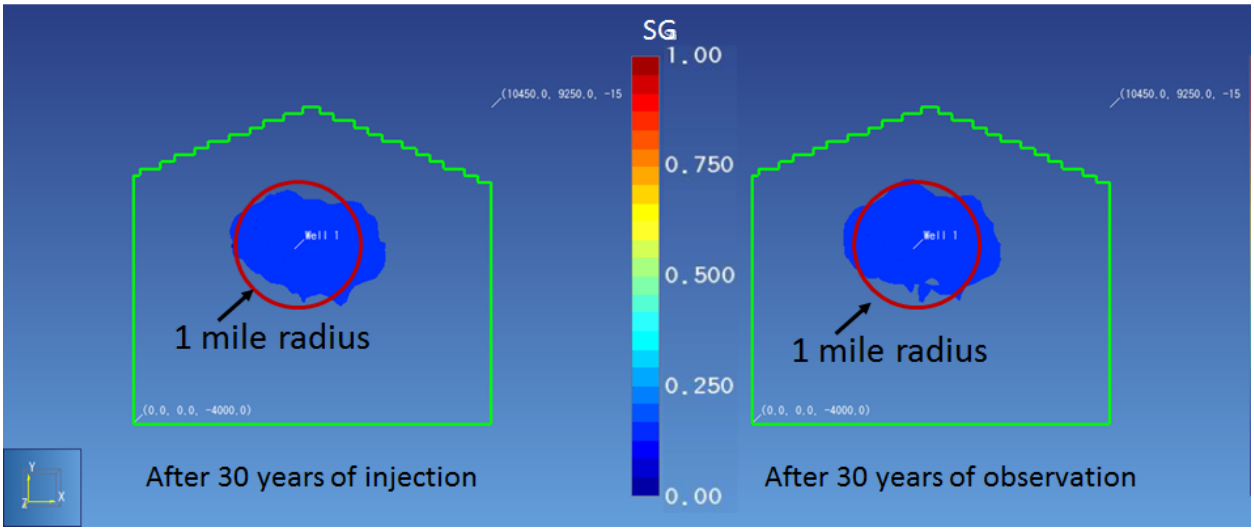

Figure 38: CO2 plume migration front from top view for baseline case after 30 years injection (left) and after 30 years observation (right) for Pliocene Model (107_P_sim01)– SS Block 107 field

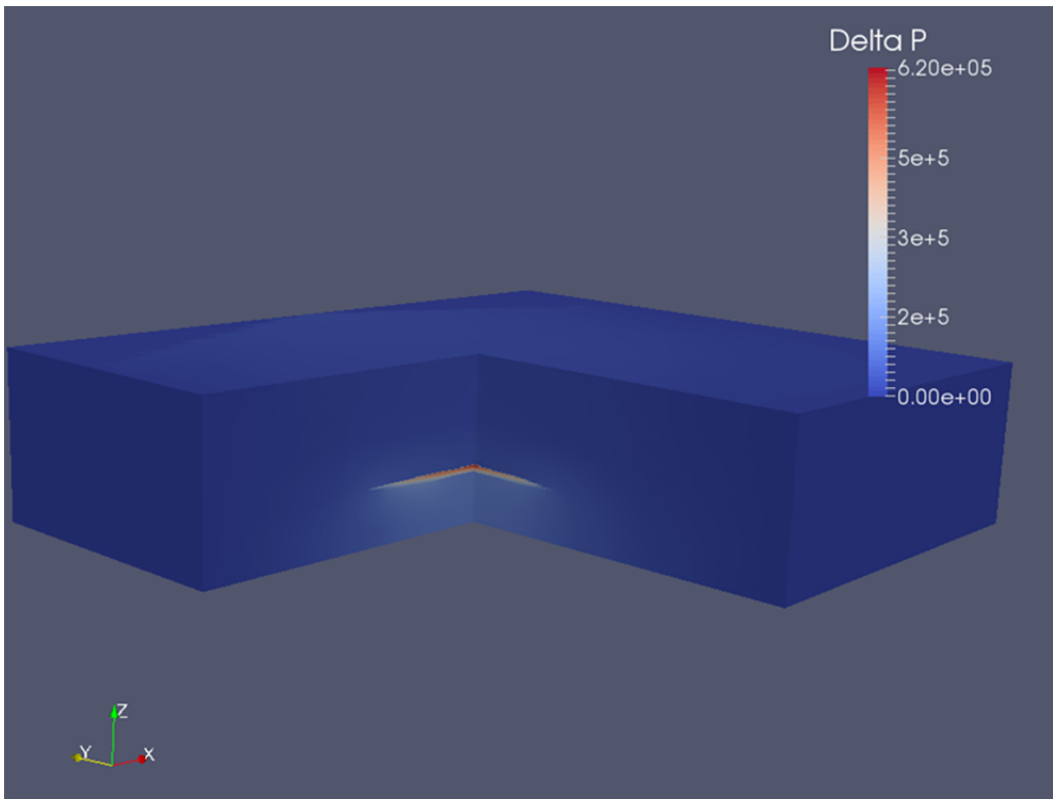

Figure 39: Pore pressure distribution (pascal) after 30 year injection for baseline case (107_P_sim01)-Pliocene Model in SS Block 107 field

5.1.2.1.3 Different relative permeability for sand and silt case (107_P_sim02) result

In the baseline simulation, we use the relative permeability curve from Berea sandstone for all the sand and silt formations in the model. To investigate how relative permeability curve affects the result, we use a different relative permeability curve from Utsira sandstone as shown in Figure 30 for all sand and silt formation. Since there is only one relative permeability curve for the shale formation, we use the same Kimberlina shale curve for all shale formations in the model.

The model set up and injection parameters are the same as the baseline case except the relative permeability curve for silt and sand formations. Figure 40 shows the CO_2 distribution and migration front from top view after 30 years of observation. Simulation results show that the injected CO_2 migrates about 2,253 m or 1.4 mile radius in lateral direction after 30 years of injection and another 30 years of observation. The injected CO_2 is contained in the bottom of Pliocene Formation within a 100 meters interval.

The pressure change comparison between the baseline cases at the end of the 30 year injection is shown in Figure 41. The simulation results show that the maximum pressure change for both cases are very similar with a 600,000 pascal (87psi) increase for the different relative permeability case (sim02)and 620,000 pascal (90psi) increase for the baseline case (sim01). The gas saturation for the sim02 case show a higher concentration around the injection area since the residual water saturation is lower than the baseline case. However, the gas saturation distribution area is very similar for both cases. The simulation result also suggests that the injected CO_2 is

contained in the injection zone in the bottom of Pliocene Formation within a 100 meters (328 ft) interval.

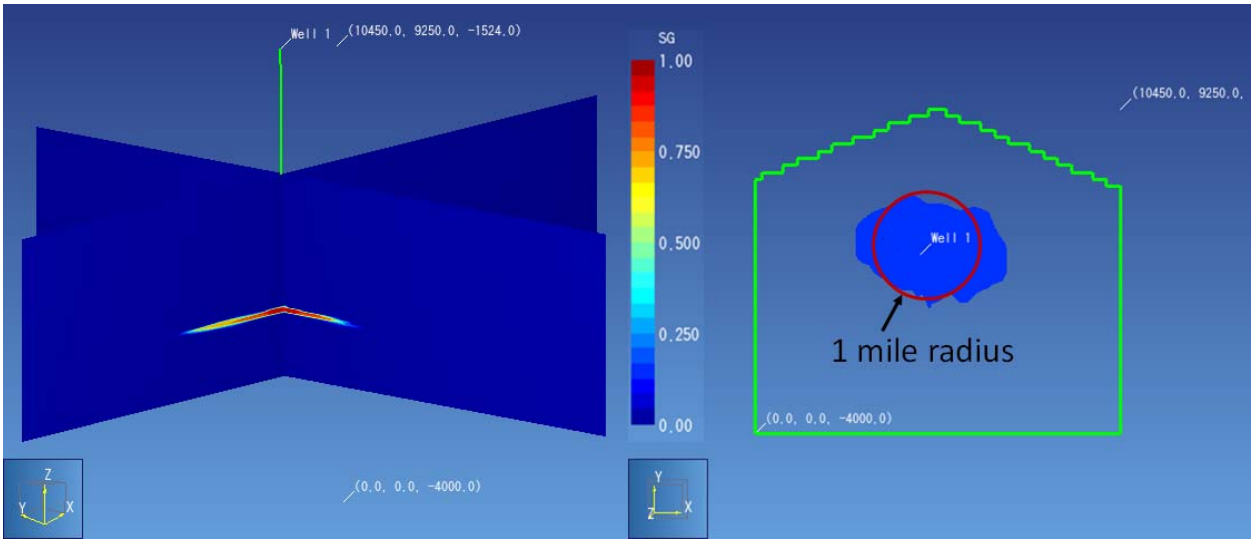

Figure 40: CO2 distribution (left) and migration front from top view (right) after 30 years of observation -- SS Block 107 field

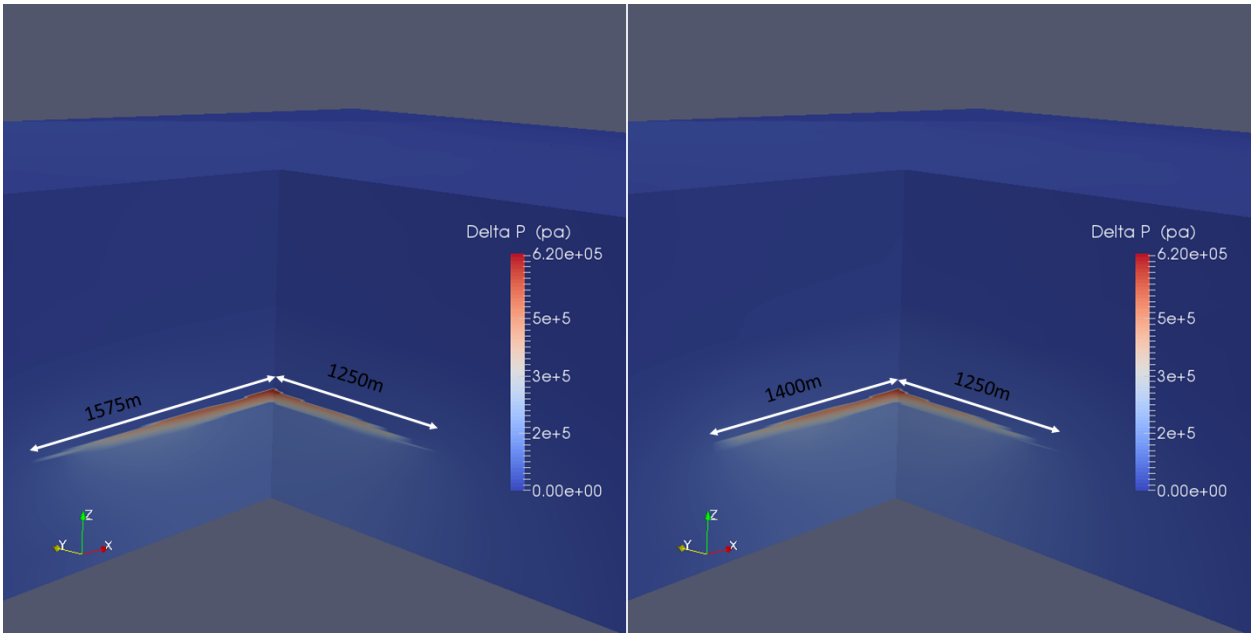

Figure 41: Pressure change comparison between Pliocene model baseline case (left) and different relative permeability case (right) after 30 years of injection -- SS Block 107 field

5.1.2.1.4 Different reservoir pore pressure (107_P_sim03) result

In the baseline case, a normal reservoir pore pressure gradient of 0.435 psi/ft at the initial condition is used in the model. Since this is a depleted oil reservoir, we want to investigate how different initial reservoir pore pressures affect the capability of CO_2 injection and sequestration. For this sensitivity analysis, a smaller pressure gradient in the reservoir section is assumed to be 0.3 psi/ft. The caprock and underburden formation pressure gradient is the same as the baseline case at 0.435 psi/ft.

The model set up and injection parameters are the same as the baseline case except reservoir pore pressure gradient. Figure 44 shows the CO_2 distribution and migration front from top view after 30 years of observation. Simulation results show that the injected CO_2 migrates about 2,253 m or 1.4 mile radius in lateral direction after 30 years of observation. The injected CO_2 is also contained in the bottom of Pliocene Formation within a 100 m (328 ft) interval.

The simulation results show that the maximum pressure change over the 30 years of injection for this case is 608,600 pascal (88.6 psi), which is very similar to baseline case of 90 psi. The simulation results show that the gas saturation distribution for this case is also very similar to the baseline case. The simulation result also suggests that the injected CO_2 is contained in the injection zone in the bottom of Pliocene Formation within a 100 m (328 ft) interval.

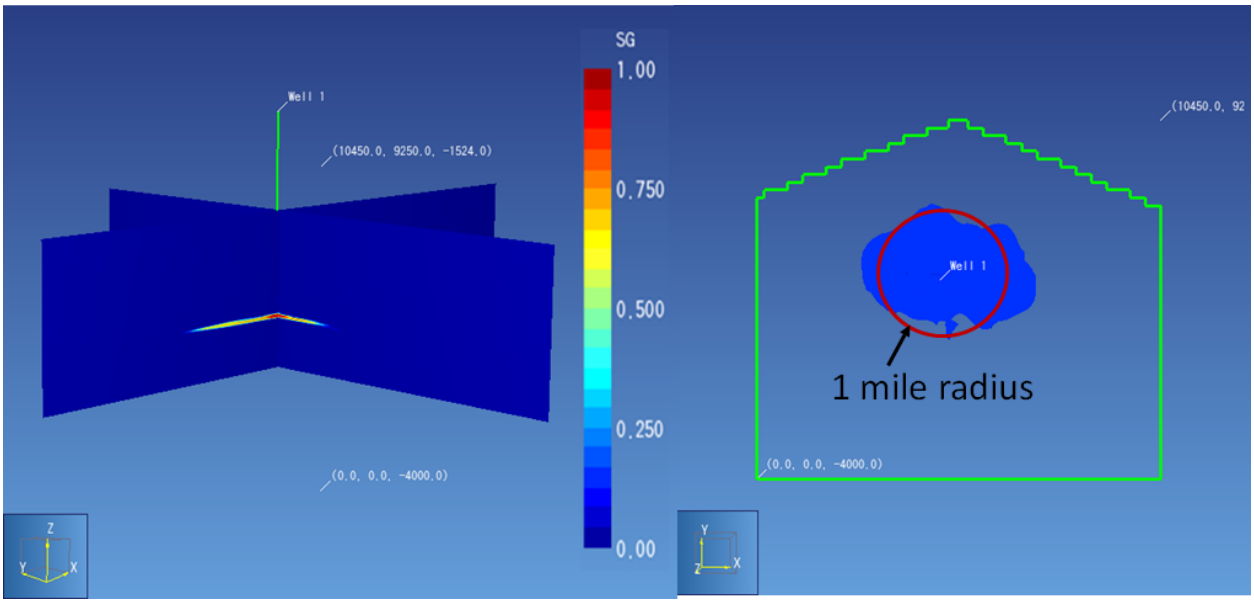

Figure 42: CO2 distribution (left) and migration front from top view (right) after 30 years of observation for 107_P_sim03 -- SS Block 107 field

5.1.2.1.5 No salt mass fraction (107_P_sim04) result

The baseline case assumes a salt mass fraction of 0.02148 for the reservoir fluid. To evaluate the effect of salt on CO_2 sequestration, another sensitivity of no salt in the fluid (sim04) was run in this study.

Figure 43 presents the comparison result of gas saturation after 30 years of injection between baseline case (sim01) and the no salt case (sim04). Figure 42 shows the comparison result of CO_2 migration front from top view after 30 years of observation between baseline case (sim01) and no salt case (sim04). The results indicate that the gas saturation from both cases is almost identical. The pressure distribution is also very similar with a maximum pressure difference of less than 2 psi over the 30 year injection period. This suggests that the salt mass fraction has very little impact in CO_2 sequestration.

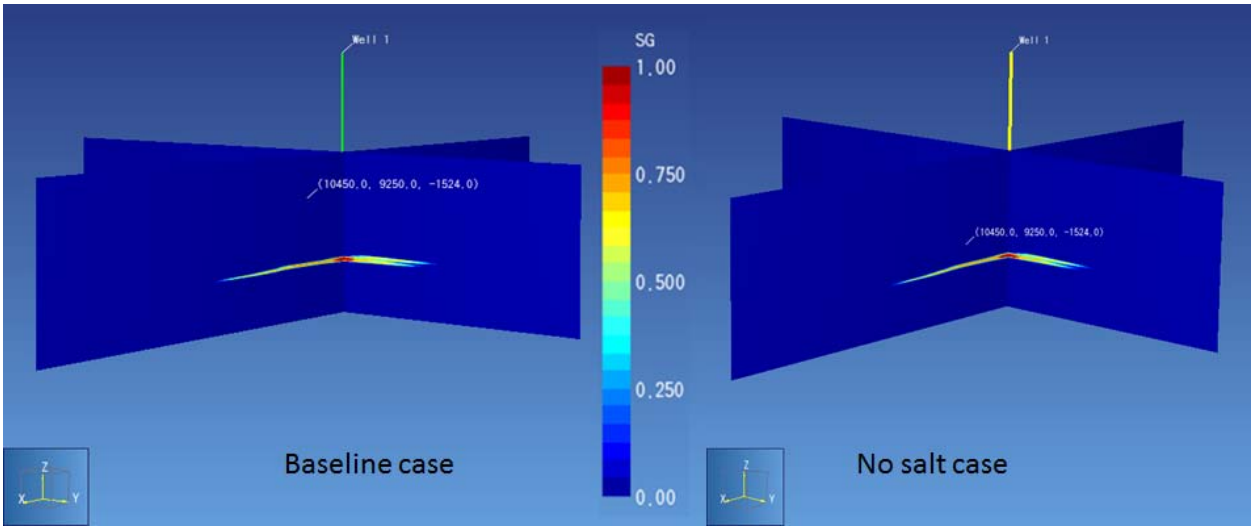

Figure 43: Comparison of gas saturation distribution at year 30 of injection for baseline case (left) and no salt case (right) -- SS Block 107 field

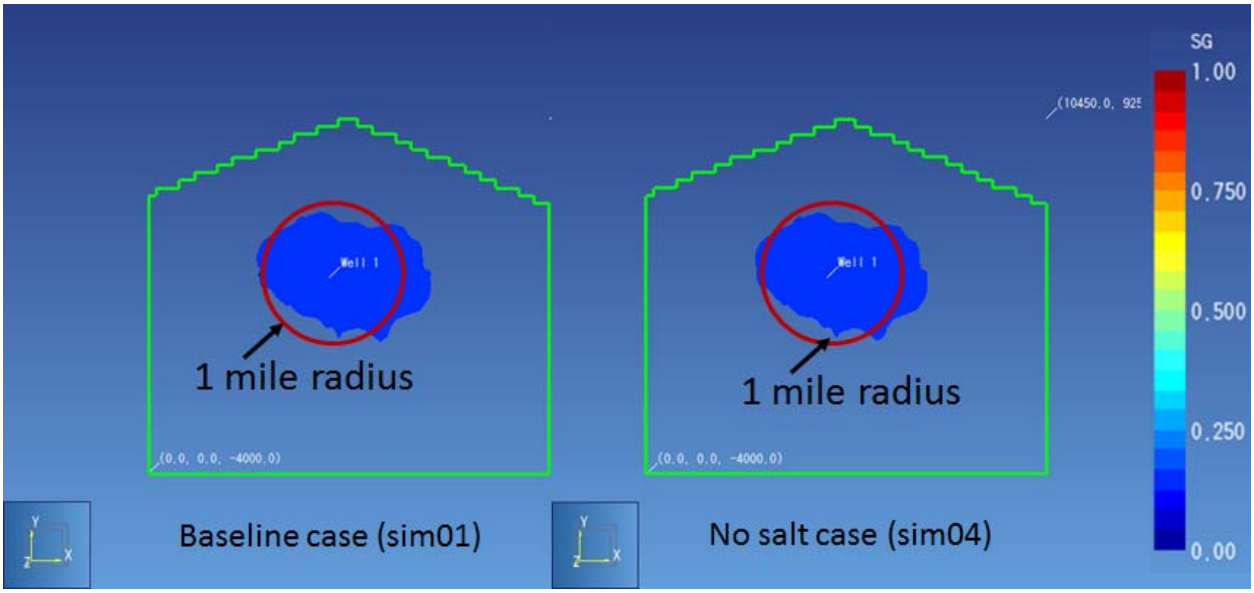

Figure 44: CO2 plume migration front from top view for no salt case (sim04) after 30 years injection (left) and after 30 years observation (right) for Pliocene Model – SS Block 107 field

5.1.2.1.6 Non-isothermal effect case (107_P_sim05) result

In the baseline case, isothermal conditions were used in the simulation. To investigate thermal effects on CO_2 injection capacity, the sensitivity of a non-isothermal case was simulated assuming the injected CO_2 temperature is 60 °C at the injection point in the reservoir. A cooling effect to the reservoir formation with original 103°C temperature was simulated. A simulation time of 10 years were performed for both cases.

Figure 45 shows the comparison result of the baseline (sim01) and the non-isothermal case (sim05) for gas saturation distribution after injection of 10 years. The temperature at the end of 10 years of injection is presented in Figure 46. As can be seen from the temperature plot, the temperature is affected in the area within a radius of approximately 350 m (1148 ft). Pressure and gas saturation along y direction at the mid perforation depth of -3175m (-10,416 ft) at the end of 10 years is presented in Figure 47 and Figure 48, respectively. The simulation results show that the gas saturation close to the injection cell is slightly lower for the non-isothermal case (sim05) than that in the baseline case (sim01), however, the gas saturation distribution area for both cases are almost identical. The pressure changes over the 10 year injection period for both cases are also very similar. Thus we conclude that the thermal effect is not significant for CO_2 injection.

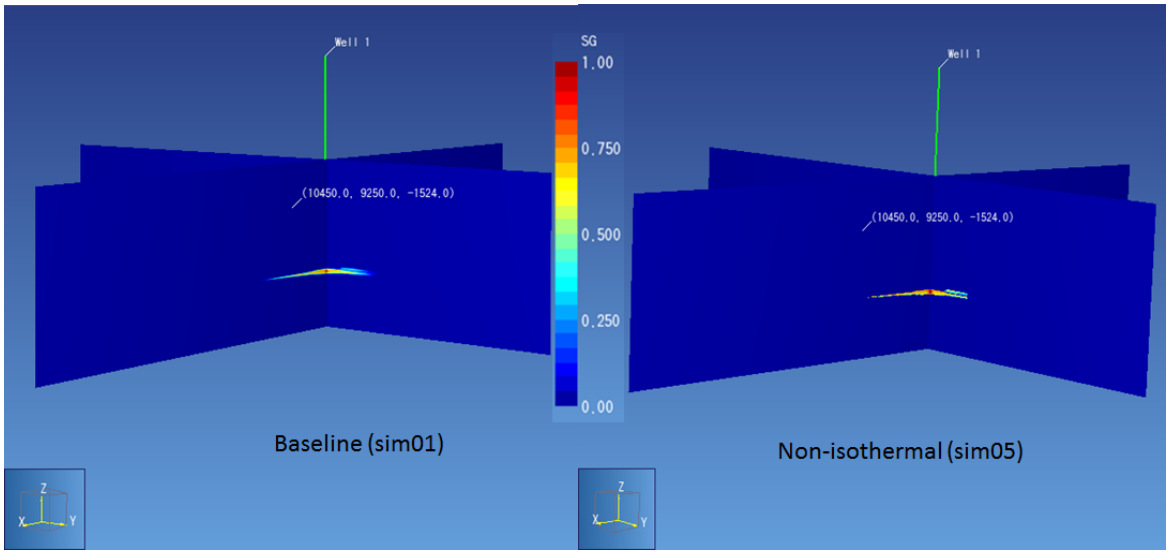

Figure 45: Comparison of gas saturation distribution after 10 years of injection for baseline case (sim01) (left) and non-isothermal case (sim05) (right) -- SS Block 107 field

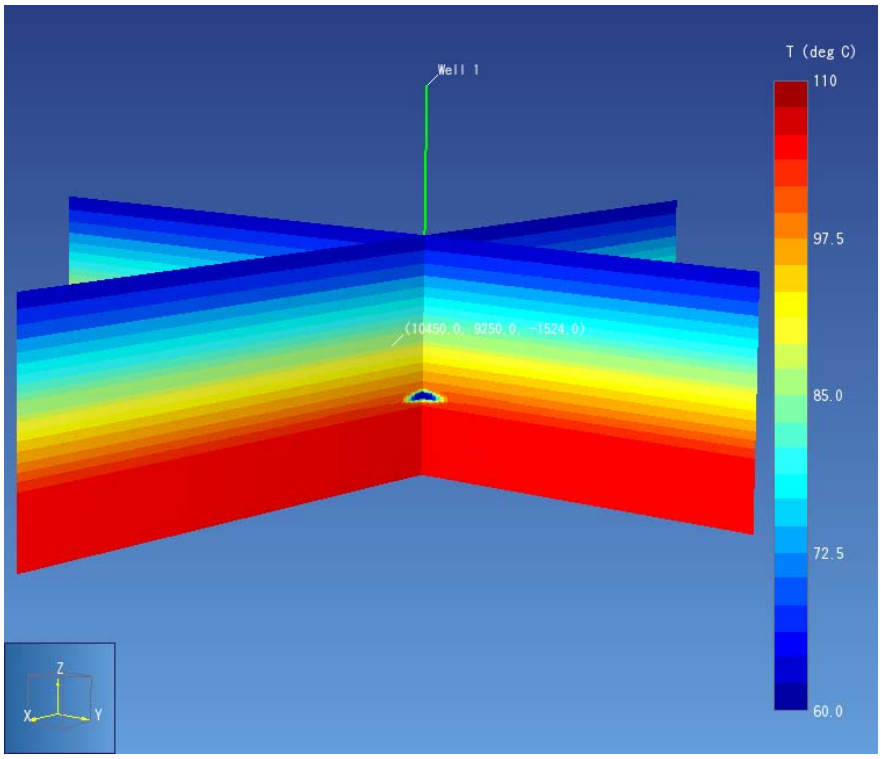

Figure 46: Temperature distribution after 10 years of injection for Pliocene model non-isothermal case -- SS Block 107 field

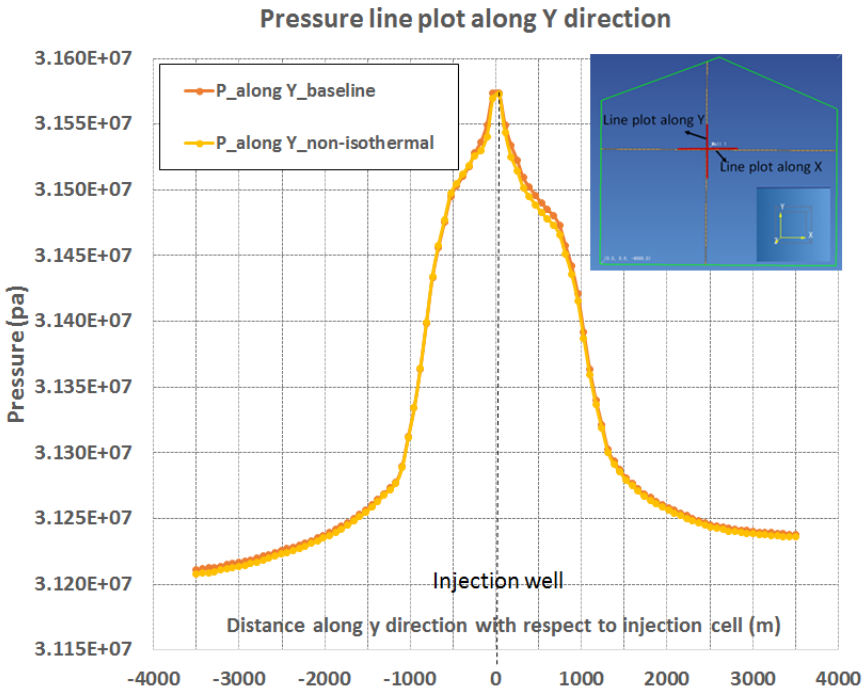

Figure 47: Pressure distribution line plot along Y direction for Pliocene model at the end of 10 years injection -- SS Block 107 field

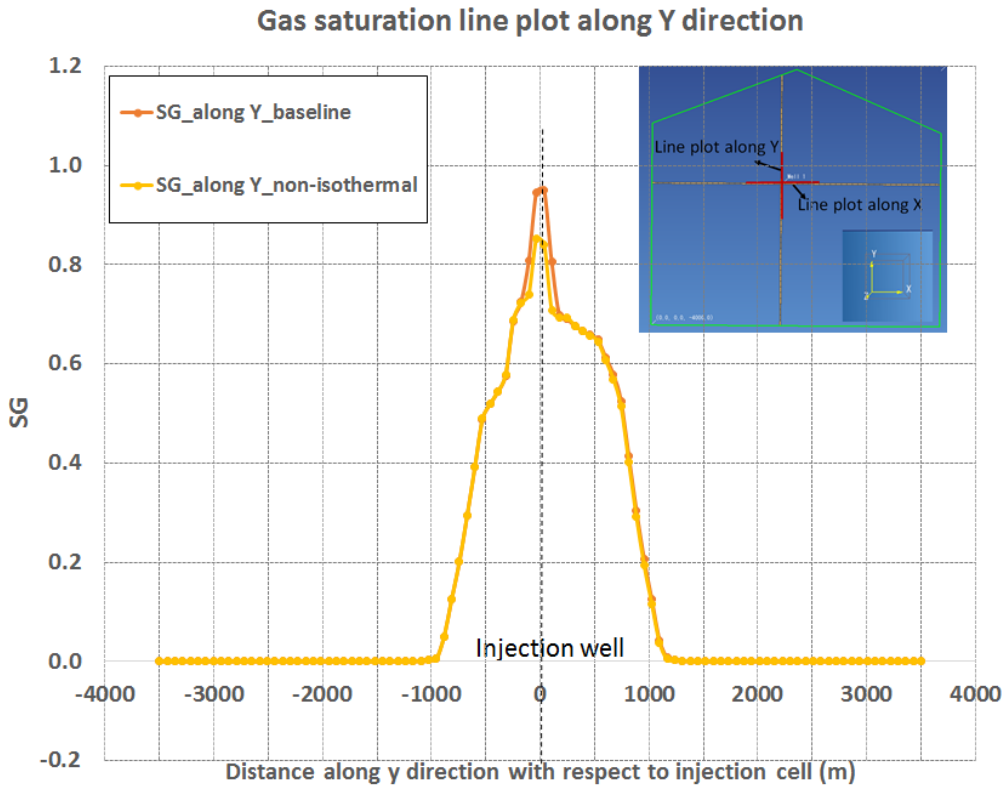

Figure 48: Gas distribution line plot along Y direction for Pliocene model at the end of 10 years injection-- SS Block 107 field

5.1.2.1.7 No capillary pressure case (107_P_sim06) result

No core data regarding the capillary pressure curve for the Ship shoal 107 area is found from the literature review. The capillary pressure curves used in the baseline case are based on the data found for other rocks in different areas. To evaluate the effect of capillary pressure effect on CO2 sequestration, a sensitivity of no capillary pressure case (107_P_sim 06) was run in this study for the worst case scenarios of capturing the CO_2 in the reservoirs.

Figure 49 presents the result of gas saturation after 30 years of injection and after another 30 years of observation. Figure 50 shows the result of CO_2 migration front from top view after 30 years of observation and after another 30 years of observation. The result suggests that when no capillary pressure was used in the simulation, the CO_2 will migrate upward to the depth of -2,500 m or -8,202 ft SSL (650 m or 2132 ft above the injection point) after 30 years of injection. The CO_2 will further migrate to almost the top of the model at the depth of -1675 m or -5495 ft SSL (1480 m or 4855 ft above the injection point). This suggests that the capillary pressure curve play an important role in CO_2 sequestration. For an accurate estimation, a laboratory core analysis to get the capillary pressure curve for this field is necessary.

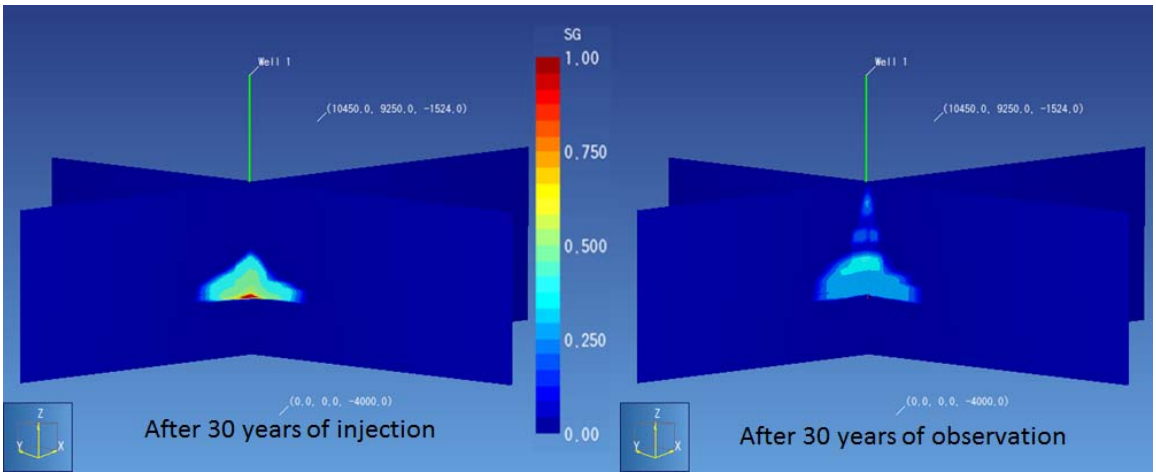

Figure 49: Comparison of gas saturation distribution at year 30 of injection (left) and after 30 years of observation (right) for no capillary pressure case (107_P_sim06) - Pliocene Model in -- SS Block 107 field

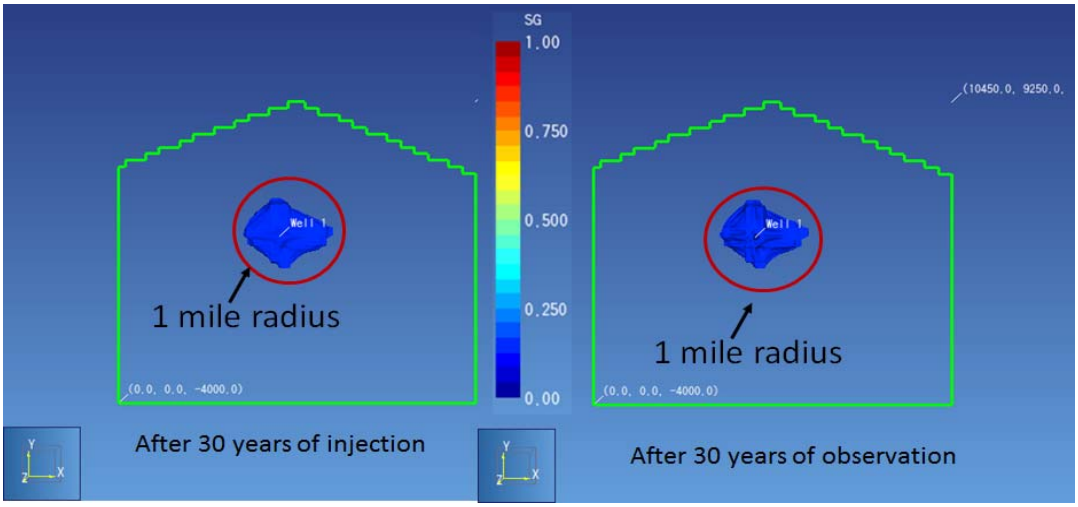

Figure 50: CO2 plume migration front from top view for no capillary pressure case (107_P_sim06) after 30 years injection (left) and after 30 years observation (right) for Pliocene Model – SS Block 107 field

5.1.2.1.8 Pressure profiles comparison

Figure 51 and Figure 52 indicate the comparison of pressure profiles across the injection well through the middle of the injection interval (=-3175 m or 10,416 ft), at in-situ conditions and after 30 years of injection, for the five isothermal scenarios. The pressure change profiles are very similar for all the cases including 107_P_sim01, 107_P_sim02, 107_P_sim03, 107_P_sim04. The maximum pressure increase observed is 0.62 MPa (90 psi) from baseline case (107_P_sim01), which is about 2% increase from in situ pore pressur. As can be seen from the plot, the pressure change for the case with no capillary pressure (107_P_sim06) is less than the other cases. Overall, the pressure change due to the 30 years of CO_2 injection is not significant.

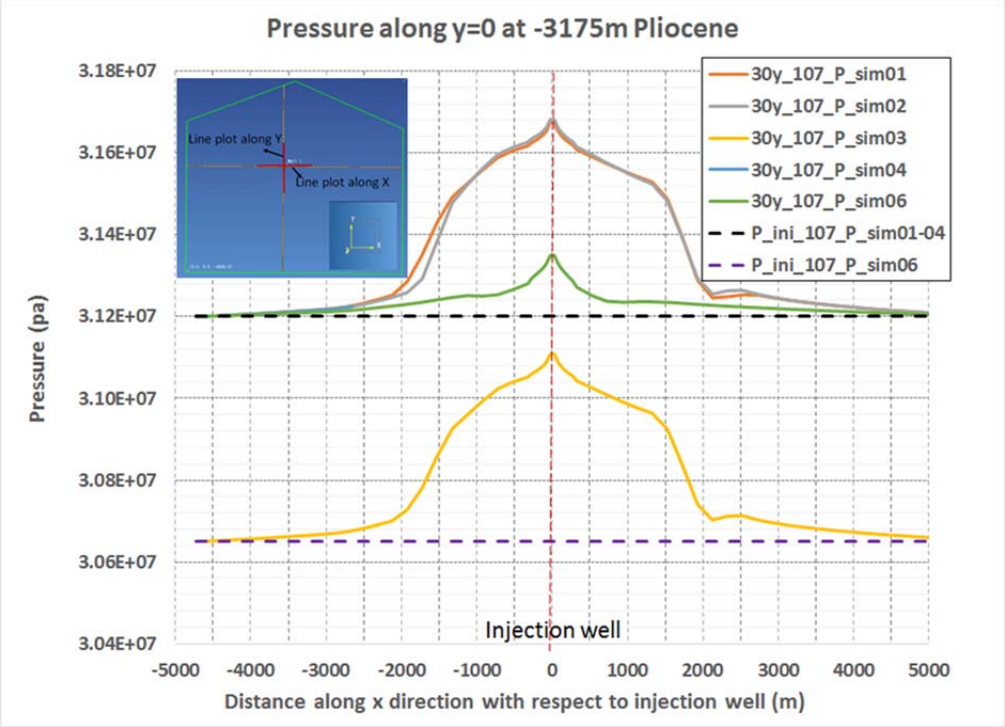

Figure 51: Comprison of pressure profiles across (y=0) injection well through the middle of injection interval, at initial and after 30 years injection into Pliocene model – Ship Shoal Block 107 field

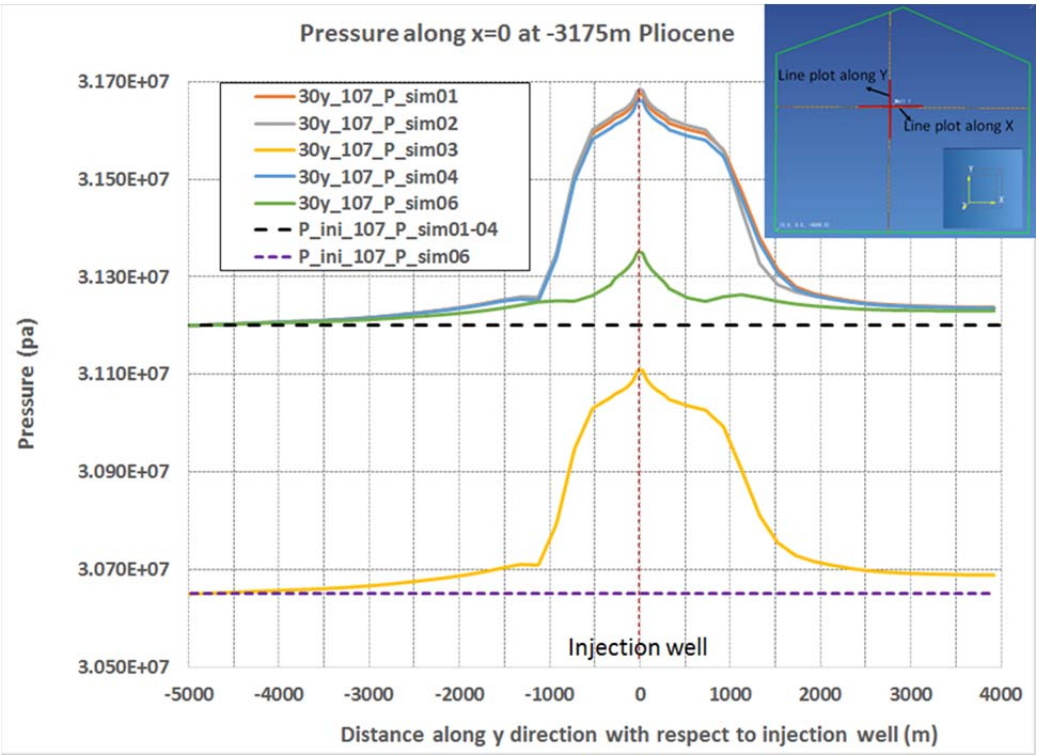

Figure 52: Comprison of pressure profiles across (x=0) injection well through the middle of injection interval, at initial and after 30 years injection into Pliocene model – Ship Shoal Block 107 field

5.1.2.2 Miocene Model Simulation

5.1.2.2.1 Simulation matrix

Five (5) scenarios have been simulated for the Miocene fluid flow model. The following conditions were used for the baseline case:

- Assume an initial reservoir pore pressure gradient of 0.435 psi/ft and initial reservoir temperature gradient of 24 degree/km.
- Assume the salt mass fraction of 0.02148 for the reservoir fluid.
- Assume no initial CO_2 mass fraction in the reservoir,
- Assume initial CH_4 mass fraction of 0.001,
- Simulation is run in isothermal mode,
- Relative permeability for sand is based on the Berea Sandstone lab data.
- An injection rate of 1 million metric tons of CO_2 per year is applied for 30 years
- Additional 30 years of plume migration are modeled after injection ceased
- Capillary pressure was not included
- Upscale all the silt and shale permeability to 10 md

Besides the baseline case (107_M_sim01), different sensitivity scenarios including different permeability for shale and silt formation (107_M_sim02), half injection rate (107_M_sim03), 5 times of injection rate (107_M_sim04), and with capillary pressure (107_M_sim05) effects were also included. The simulation matrix is listed in Table 15 in detail.

Table 15: Simulation Matrix for Miocene Model -- SS Block 107 field

Model	Scenarios	Shale/Silt Permeability	Capillary Pressure	Injection Rate (million ton/y)	Isothermal?	Salt?	PP Gradient (psi/ft)
Miocene	107_M_Sim01 (Baseline)	Set minimum to 10md	No	1	Yes	Yes	0.435
	107_M_Sim02 (Different Permeability for silt and shale)	Use original value from log correlation (around 1 md)	No	1	Yes	Yes	0.435
	107_M_Sim03 (Half injection rate)	Set minimum to 10md	No	0.5	Yes	Yes	0.435
	107_M_Sim04 (5 times injection rate)	Set minimum to 10md	No	5	Yes	Yes	0.435
	107_M_Sim05 (With capillary pressure)	Set minimum to 10md	Yes	1	Yes	Yes	0.435

5.1.2.2.2 Baseline case (107_M_sim01) result

Figure 53 and Figure 54 show the gas saturation distribution results for the baseline case simulation after 30 years injection and after another 30 years observation, respectively. Simulation results show that the injected CO_2 only migrates within a radius of 500 m (1640 ft) in lateral direction over 30 years injection, however, the CO_2 migrates upward to the depth of -3075 m or -10,088 ft (SSL) (about 1000 m or 3280 ft above the injection point). After another 30 years of observation, the CO_2 further migrate upward to the depth of -2575 m or -8448 ft (SSL) (about 1500 m or 4921 ft above the injection point). Figure 55 shows the CO_2 plume lateral migration from top view after 30 years of injection and another 30 years of observation. A maximum of 500 m (1640 ft) in radius in lateral migration is observed from the simulations.

Figure 56 shows the pressure change in the model after 30 years injection. The maximum pressure change of about 60 psi for the whole baseline model is at the top of the CO_2 migration plume. Simulation results also suggest that the injected CO_2 will migrate from the Miocene Formation to the Pliocene Formation after 30 years of injection and another 30 years of observation, but the injected 30 Million tons of CO_2 injected is contained within the Pliocene Formation.

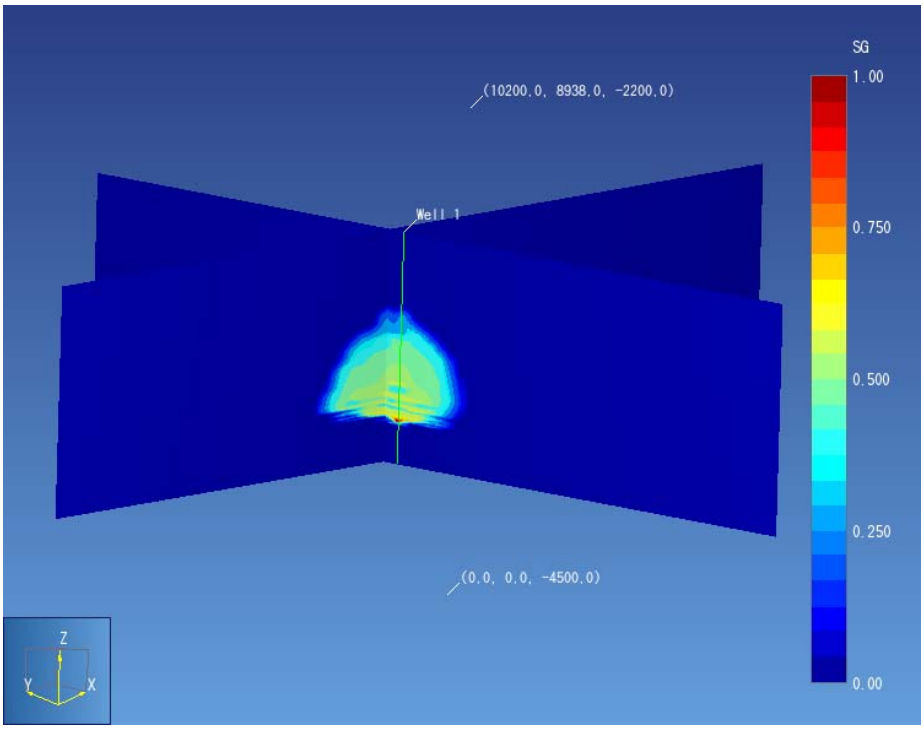

Figure 53: Gas saturation distribution after 30 year injection for baseline case (107_M_sim01)-Miocene Model -- SS Block 107 field

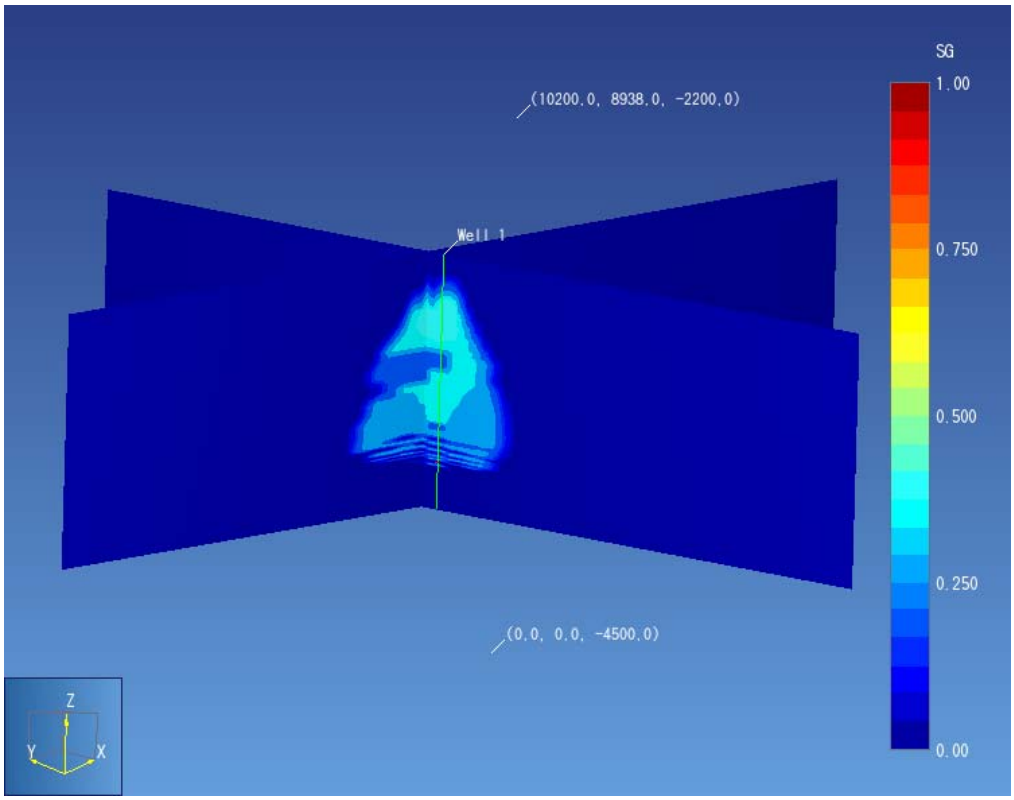

Figure 54: Gas saturation distribution after 30 year observation for baseline case (107_M_sim01)-Miocene Model in SS Block 107 field

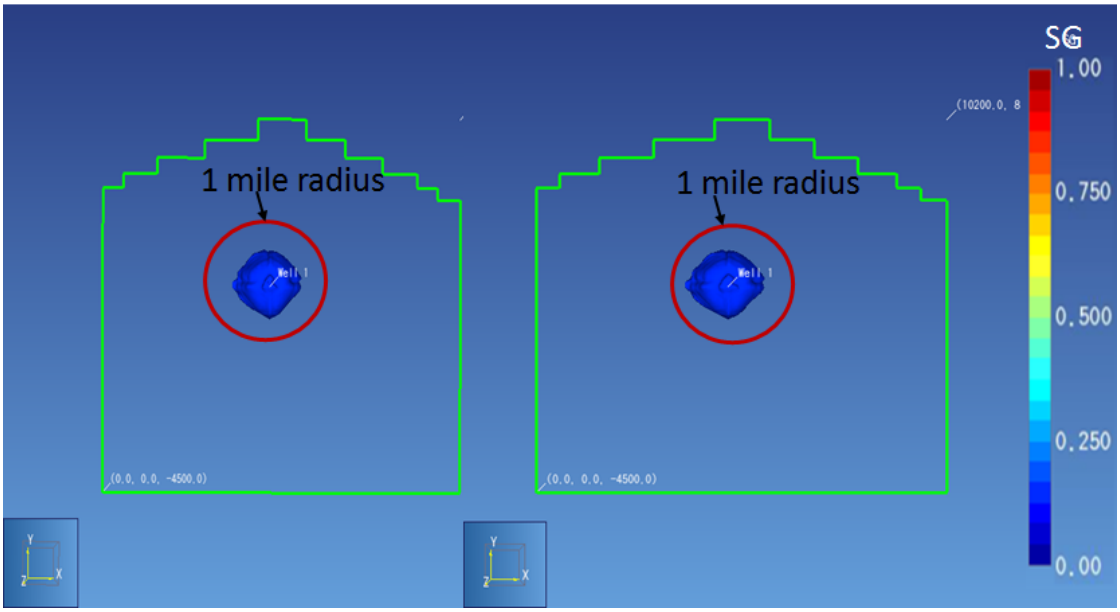

Figure 55: CO2 plume migration front from top view for baseline case after 30 years injection (left) and after 30 years observation (right) for Miocene Model – SS Block 107 field

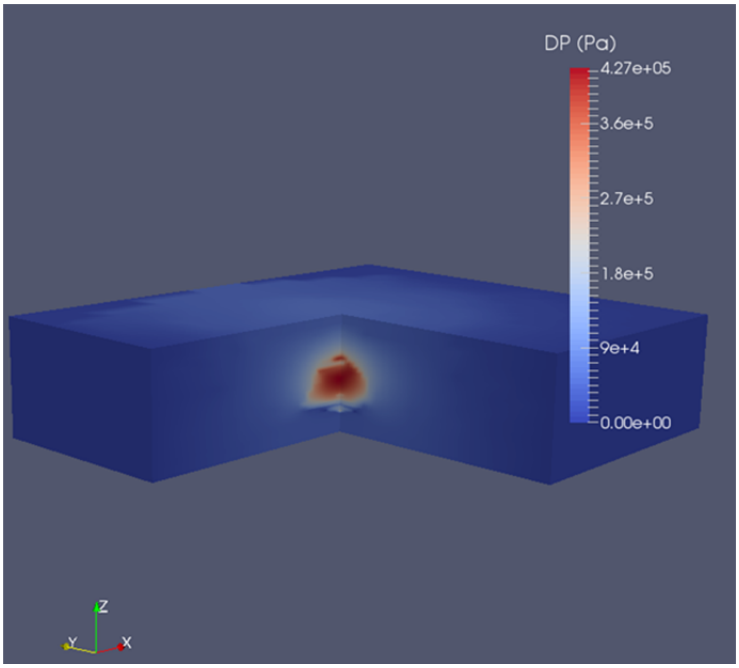

Figure 56: Pore pressure change distribution after 30 year injection for baseline case (107_M_sim01)-Miocene Model in SS Block 107 field

5.1.2.2.3 Different permeability for silt and shale (107_M_sim02) result

Three lithology types (sand, silt, and shale) are defined in our lithology model. Each lithology type has an individual porosity and permeability value as shown in Table 8. The shale and silt permeability for some of the formations obtained from those empirical equation correlating to porosity are low. For a conservative simulation for a worst case scenario of upward migration, we upscale the shale and silt formation permeability from the original value to 10 md. The comparison is shown in Table 16.

From the baseline simulation, we saw that the injected CO_2 will migrate from the Upper Miocene Formation at injection depth of -4075 m (-13,369 ft) to the depth of -3000 m (-9842 ft), into the Pliocene formation, thus a sensitivity analysis using the original permeability value obtained from the correlation was performed.

Table 16: Comparison of permeability used in baseline and original value from correlation SS Block 107 field

	Av. Permeability for Silt (md)		Av. Permeability for Shale (md)	
Formation	Baseline	Original value from correlation (107_M_sim02)	Baseline	Original value from correlation (107_M_sim02)
Top Pliocene	26.8	26.8	18.6	18.6
Tex X	10.0	5.4	10.0	6.9
Top Miocene	10.0	1.2	10.0	1.4
Big A	10.0	1.2	10.0	3.7

Figure 57 shows the CO_2 concentration distribution after 30 years of injection and after another 30 years of observation. The simulation indicates that using the smaller permeability from 10 mD to around 1.4 mD for the overburden shale and silt, the CO_2 plume will be contained within the Miocene. The top of the CO_2 plume for this case is at -3624 m or -11,890 ft (migrate upward about 450 m or 1476 ft from the injection point), which is about 300 meters (984 ft) below the top of Miocene. The gas will migrate laterally about 1609 m or 1 mile radius for this case compared to only 804 m or 0.5 mile radius for the baseline scenario.

The pressure change at the end of 30 years injection is shown in Figure 58. The simulation result shows that the maximum pressure change when using the original permeability from correlation case (107_M_Sim02) is about 74% larger with 742,000 Pa (108 PSI increase at the injection point of -4075 m or -13,369 ft) compared to 427,000 Pa (62 PSI) increase for the baseline case.

The simulation result for the case using the original permeability estimated from the log data correlation suggests that the injected CO_2 will migrate upward about 450 m (1476 ft) from injection point and be contained in the Miocene Formation. It is crucial to get a good understanding of in-situ permeability of those caprock types.

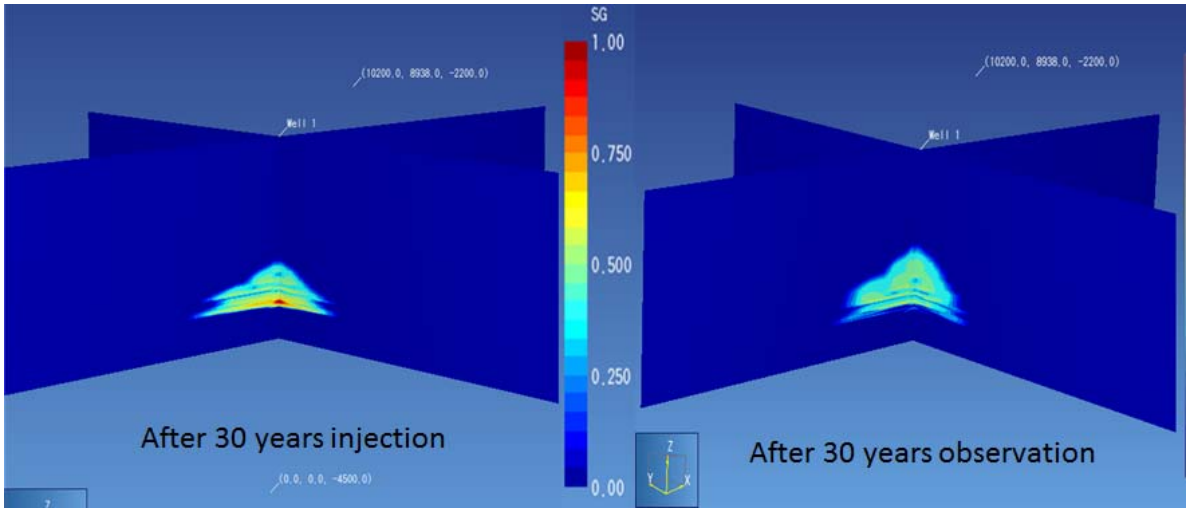

Figure 57: Comparison of CO2 concentration after 30 years of injection (left) and 30 years of observation (right) for Sim02 case for Miocene Model – SS Block 107 field

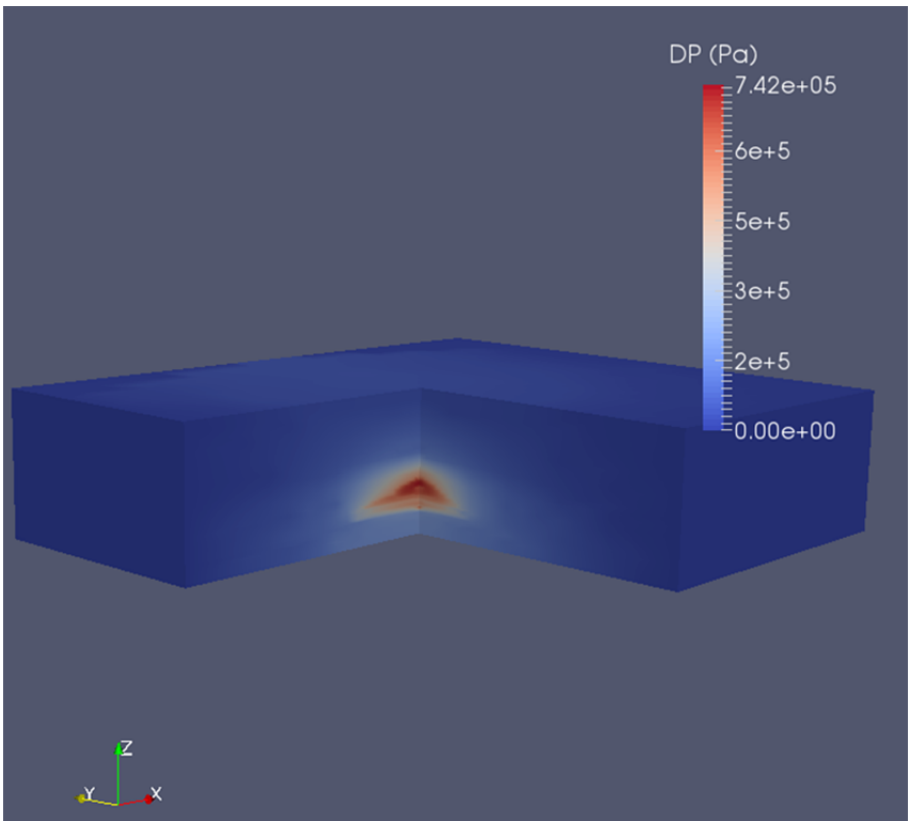

Figure 58: Pore Pressure change distribution after 30 years injection for 107_M_sim02 for Miocene Model – SS Block 107 field

5.1.2.2.4 Half injection case (107_M_sim03) result

Since the CO_2 migrates upwards into the Pliocene Formation for the baseline case, we are interested to investigate how injection rate can affect the CO_2 migration. For this simulation case we reduce the injection rate to half the amount of the baseline simulation, thus 0.5 million metric tons of CO_2 per year and injection for 30 years.

Figure 59 shows the CO_2 distribution after 30 years of injection and another 30 years of observation. Simulation results suggest that the injected CO_2 with injection rate of 0.5 million ton per year will also migrate from the Upper Miocene injection zone (-4075 m or -13,369 ft) to the depth of -3000 m (9842 ft) into the Pliocene Formation. The gas migration is within 643 m or 0.4 mile radius which is less than that of the baseline case (804 m or 0.5 mile).

This sensitivity simulation suggests that the total injected volume (15 million metric tons) of CO_2 over 30 years is contained within the Pliocene Formation.

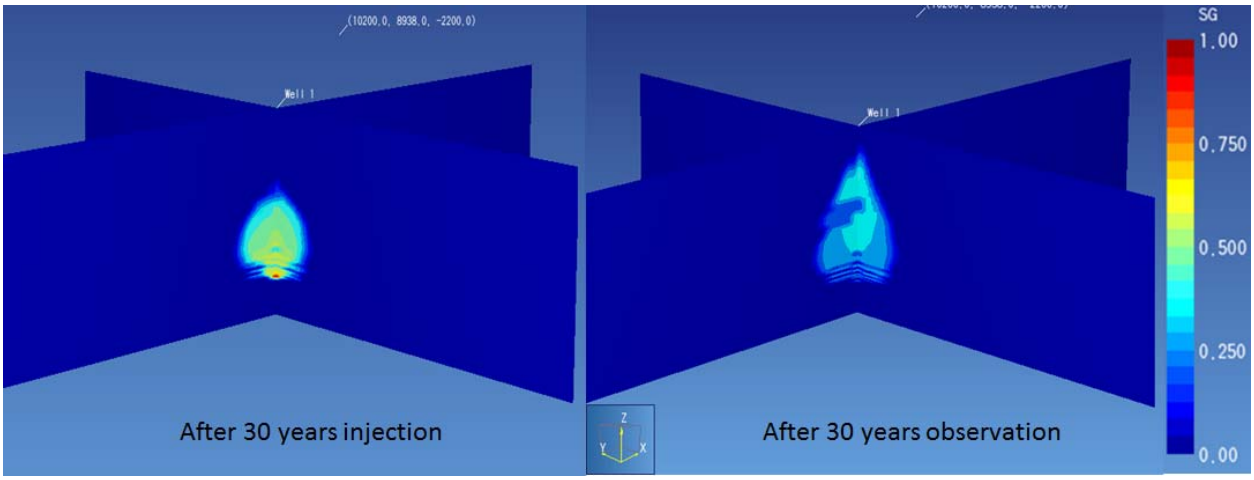

Figure 59: Comparison of CO2 concentration after 30 years of injection (left) and 30 years of observation (right) for half injection rate Sim03 case for Miocene Model – SS Block 107 field

5.1.2.2.5 5 time injection rate case (107_M_sim04) result

From the corresponding geomechanical modeling simulation, we knew the pressure increase after 30 years injection for all cases from the fluid flow simulation is not significant to cause fault slippage. We are interested to know at what pressure and injection rate would cause the fault to slip. For this scenario, we investigate how much pressure increase will be produced by a large injection rate -- 5 times the planned rate at 5 million metric tons CO_2 per year for 30 years of injection.

The pressure change at the end of 30 years injection is shown in Figure 60. The simulation result show that the maximum pressure change for 5 times injection rate case (107_M_sim04) is larger with 1,630,000 Pa (236 psi) increased when compared to baseline case with 427,000 Pa (62 psi) increase.

Figure 61 shows the gas distribution after 30 years of injection and 30 years of observation. The gas migration is about 1609 m or 1 mile radius which is larger than that of the baseline case (804 m or 0.5 mile). After 30 years of injection, the injected CO_2 with injection rate of 5 million ton per year will also migrate from the Upper Miocene injection zone (-4075 m or -13,369 ft) to the depth of -2800 m (-9186 ft) into the Pliocene Formation, however, the result after another 30 years of observation suggests that the CO_2 plume will migrate to the very top of the whole model, meaning it will leak out of the Pliocene Formation and has the potential to migrate further up into the shallower formation.

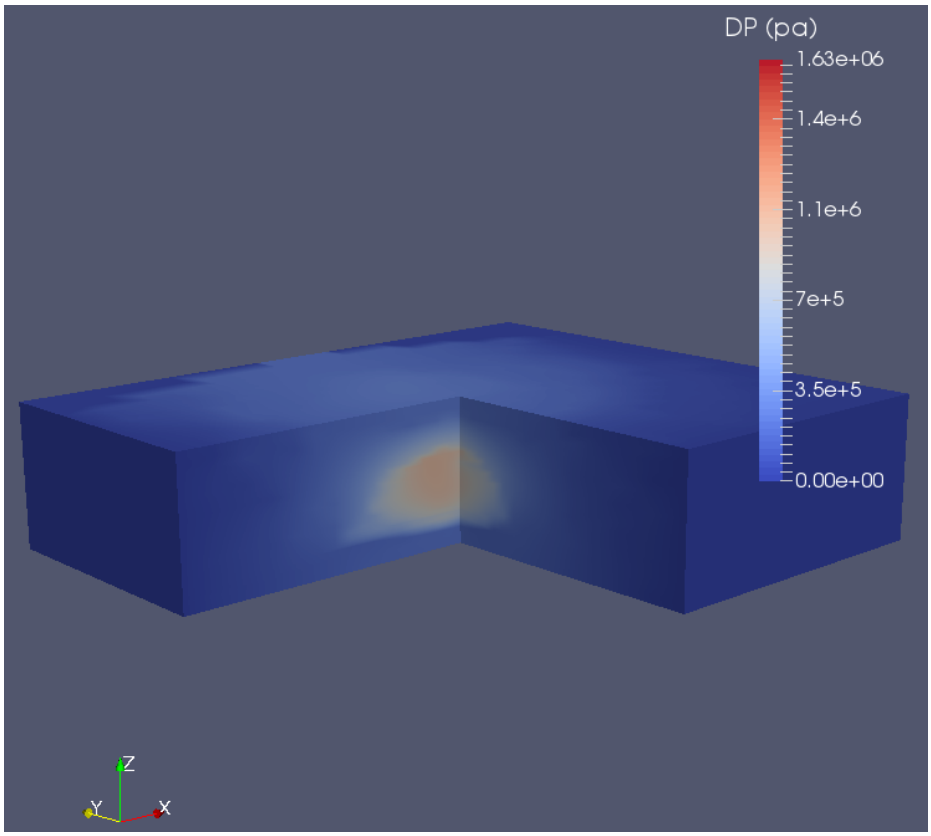

Figure 60: Pore Pressure change for 5 times injection rate case (107_M_Sim05) after 30 years of injection for Miocene model – SS Block 107 field

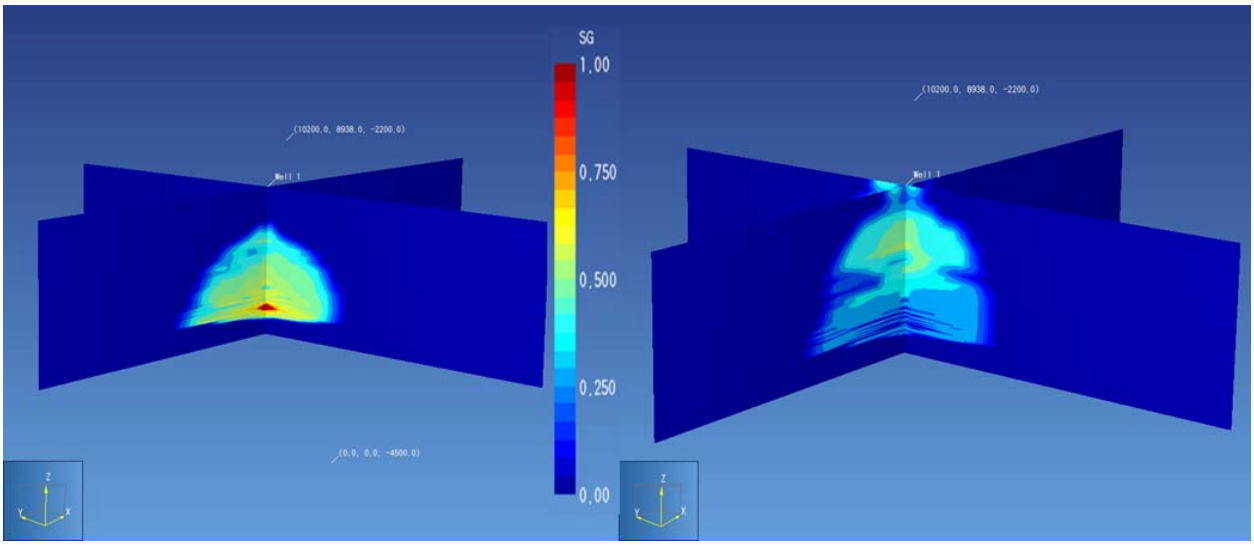

Figure 61: Gas saturation distribution after 30 years injection (left) and after another 30 years of observation (right) for Miocene model– SS Block 107 field

5.1.2.2.6 With capillary pressure case (107_M_sim05) result

Due to a lack of detailed information regarding the capillary pressure curves for different material types in the Ship Shoal Area, no capillary pressure was included in the baseline case simulation for the Miocene model. In this sensitivity simulation, we want to estimate how the capillary pressure affects the CO_2 migration. From the literature review, we found some capillary pressure curves for different type of rocks as shown in Figure 31. Based on similarity of formation porosity, permeability for each rock type, capillary pressure curve for both sand and silt are based on Berea sandstone, and capillary pressure for shale is based on Kimberlina shale.

For this sensitivity simulation, we include the capillary pressure from literature review to the model to evaluate how the capillary pressure effects the CO_2 sequestration.

Figure 62 shows the gas saturation distribution result with capillary pressure case (sim05) after 30 years of injection. The simulation result show that the maximum pressure changes for the case with capillary pressure is 1,810,000 Pa (262 psi) increase compared to baseline case with 427,000 Pa (62 psi) increased.

The CO_2 plume front from top view after 30 years injection and another 30 years observation are shown in Figure 63. The simulation results suggest that with capillary pressure, the CO_2 injected will be contained in the Miocene formation. The CO_2 is contained within 1931 m or 1.2 miles radius from injection point in the lateral direction.

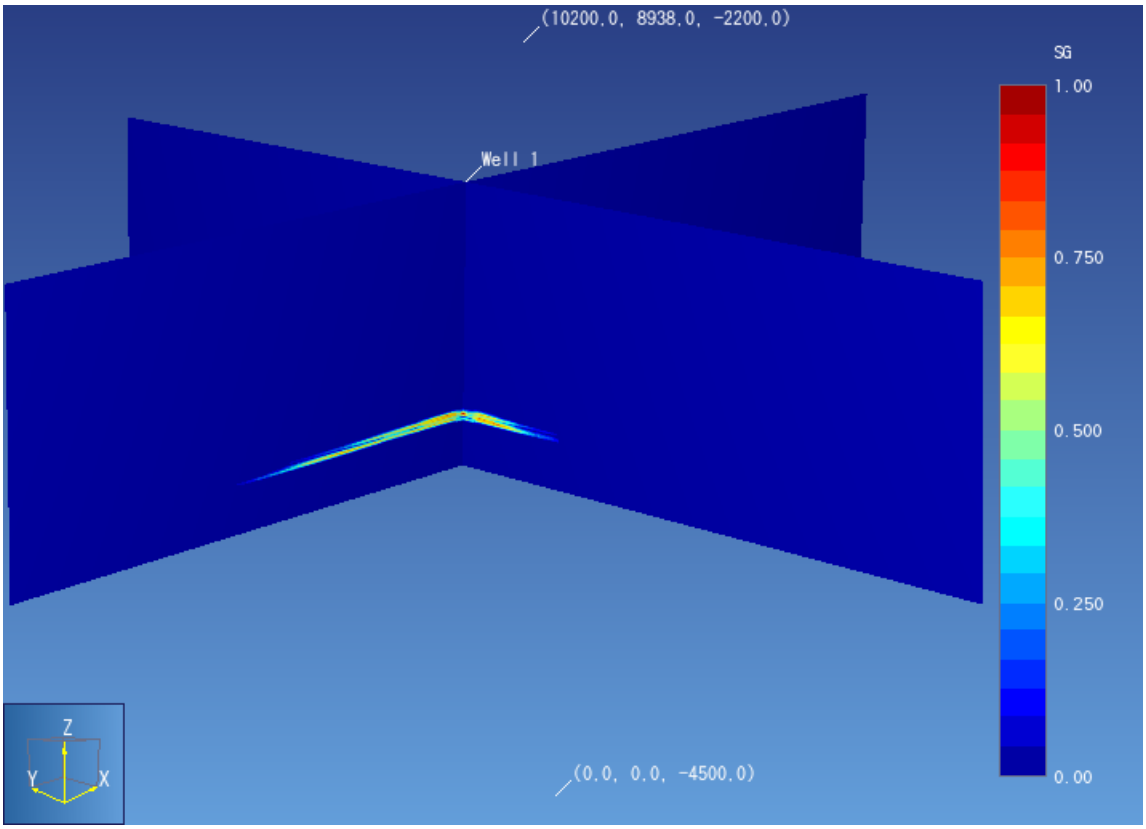

Figure 62: Gas saturation distribution at 30 year of injection for Miocene model with capillary pressure case (107_M_Sim04) – SS Block 107 field

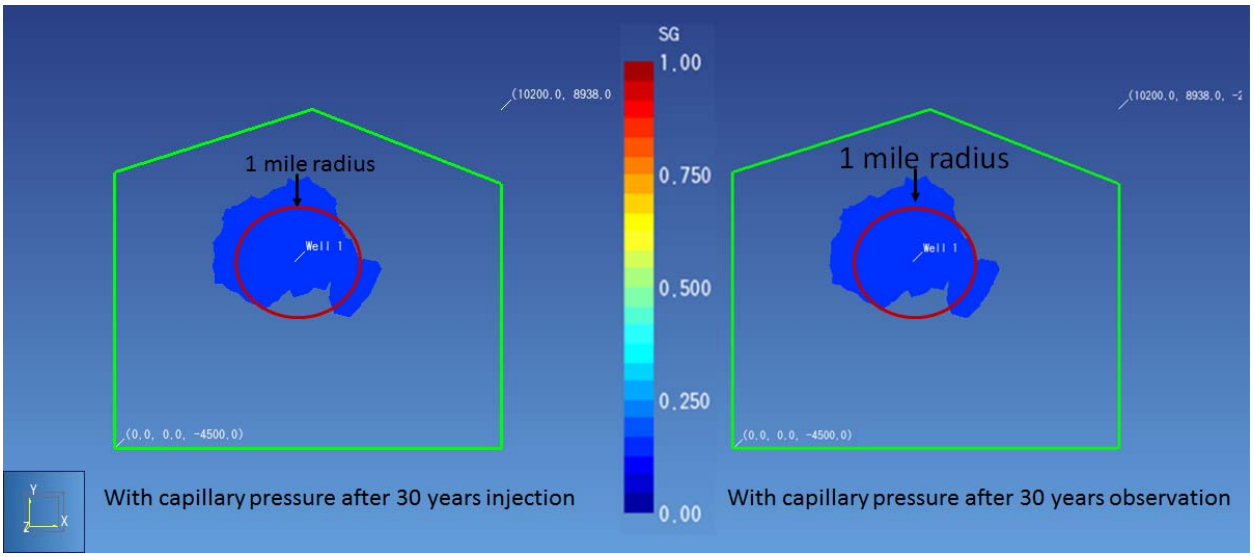

Figure 63: Comparison of CO2 migration front from top view after 30 years of injection (left) and 30 years of observation (right) for the case with capillary pressure (107_M_Sim05) for Miocene Model – SS Block 107 field

5.1.2.2.7 Pressure profiles comparison

Figure 64 and Figure 65 indicate the comparison of pressure profiles across the injection well through the middle of the injection interval (=-4075 m or 13,369 ft), at in-situ conditions and after 30 years of injection for the five scenarios. The maximum pressure increase observed is 1.81 MPa (262 psi) from case 107_M_sim05 when the capillary pressure is included in the simulation. This corresponds to about 4.5% increase from in situ pore pressure; overall, the pressure change due to the 30 years of CO_2 injection is not significant for Miocene model.

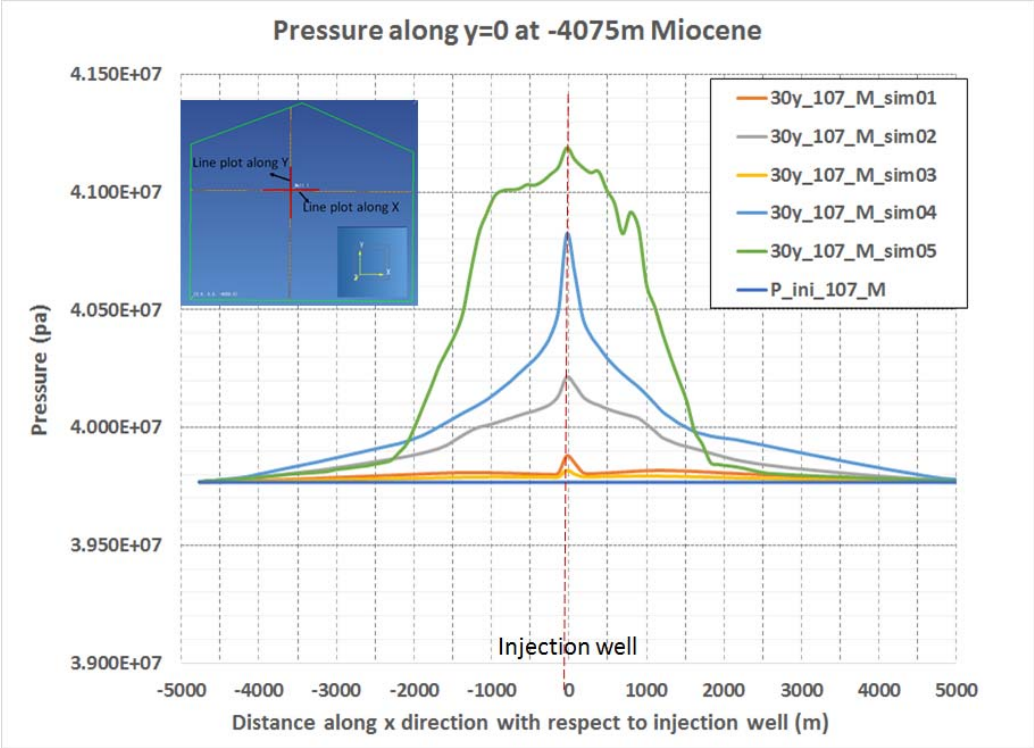

Figure 64: Comprison of pressure profiles across (y=0) injection well through the middle of injection interval, at initial and after 30 years injection into Miocene model – Ship Shoal Block 107 field

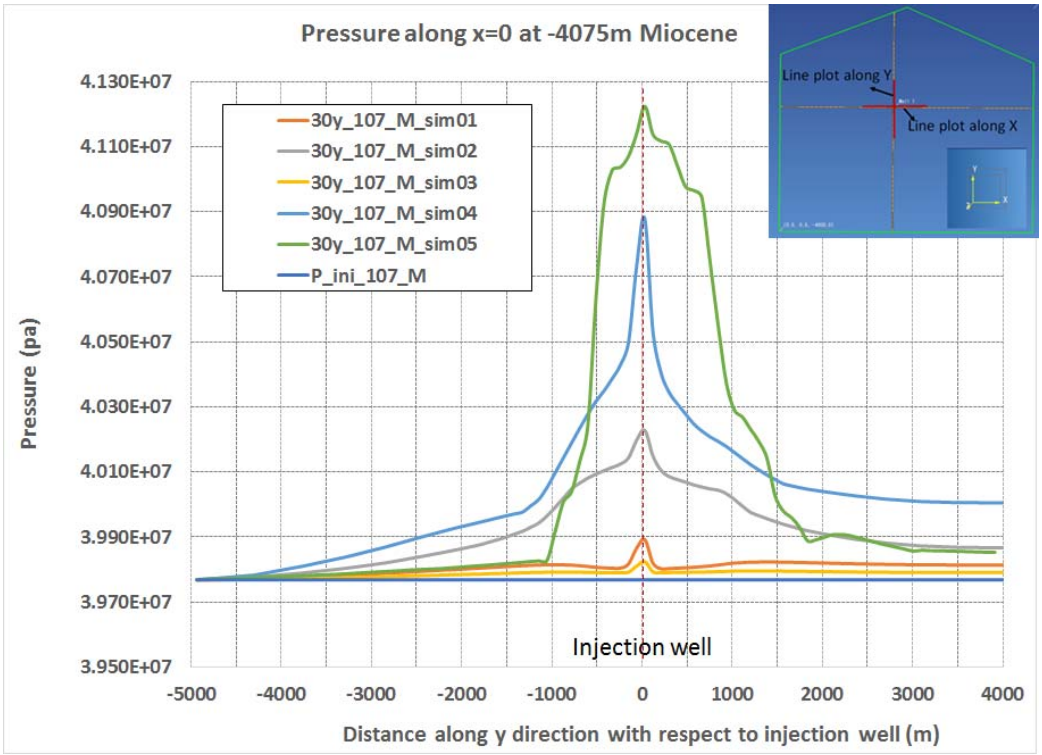

Figure 65: Comprison of pressure profiles across (x=0) injection well through the middle of injection interval, at initial and after 30 years injection into Miocene model – Ship Shoal Block 107 field

5.1.2.3 Summary Result for both Pliocene and Miocene Models

The 30 years observation simulations for all cases were also performed for both Pliocene and Miocene Models. The following Table 17 and Table 18 summarize the simulation results for the Pliocene and Miocene Model, respectively. The results from the different sensitivity analyses indicate that Pliocene and Miocene are good reservoir for the CO_2 sequestration. Most of the cases show that the CO_2 injected will be contained in either the Pliocene or the Miocene Formation. There is only one case with large injection rate (5 million ton per year) for 30 years indicating the potential leak of CO_2 out of the Pliocene Formation. However, this is just an extreme case that was used to evaluate the possible maximum pore pressure that could cause fault slippage and is not for real field practice purpose.

Table 17: SS Block 107 field Fluid Flow- Pliocene Model Summary Results

		Input						Result			
Model	**Scenarios**	**Relative Permeability for Sand**	**Capillary Pressure**	**Injection Rate (million ton/y)**	**Isothermal?**	**Salt?**	**PP Gradient (psi/ft)**	**CO2 Lateral Migration Radius after 30 Years Injection (mile)**	**CO2 Plume Top after 30 Years Injection (m SSL)**	**CO2 Migration after 30 Years of Observation (m SSL)**	**Leaking?**
Pliocene	107_P_Sim01 (Baseline)	Based on Berea Sandstone	Yes	1	Yes	Yes	0.435	1.5	-3115	-3115	Contained
	107_P_Sim02 (Different Relative Permeability for Sand)	Based on Utsira Sandstone	Yes	1	Yes	Yes	0.435	1.4	-3115	-3115	Contained
	107_P_Sim03 (Different PP Gradient)	Based on Berea Sandstone	Yes	1	Yes	Yes	0.3	1.4	-3115	-3115	Contained
	107_P_Sim04 (No Salt)	Based on Berea Sandstone	Yes	1	Yes	No	0.435	1.5	-3115	-3115	Contained
	107_P_Sim05 (Non-isothermal)	Based on Berea Sandstone	Yes	1	No	Yes	0.435	1 mile after 10 years injection	NA	NA	Contained
	107_P_Sim06 (No capillary pressure)	Based on Berea Sandstone	No	1	Yes	Yes	0.435	1	-2500	-1675	Contained

Table 18: SS Block 107 field Fluid Flow- Miocene Model Summary Results

		Input						Result			
Model	**Scenarios**	**Shale/Silt Permeability**	**Capillary Pressure**	**Injection Rate (million ton/y)**	**Isothermal?**	**Salt?**	**PP Gradient (psi/ft)**	**CO2 Lateral Migration Radius after 30 Years Injection (mile)**	**CO2 Plume Top after 30 Years Injection (m SSL)**	**CO2 Plume Top after 30 Years of Observation (m SSL)**	**Leaking?**
Miocene	107_M_Sim01 (Baseline)	Set minimum to 10md	No	1	Yes	Yes	0.435	0.5	-3075	-2575	Contained in Pliocene
	107_M_Sim02 (Different Permeability for silt and shale)	Use original value from log correlation (around 1 md)	No	1	Yes	Yes	0.435	1	-3625	-3415	Contained in Miocene
	107_M_Sim03 (Half injection rate)	Set minimum to 10md	No	0.5	Yes	Yes	0.435	0.4	-3075	-2595	Contained in Pliocene
	107_M_Sim04 (5 times injection rate)	Set minimum to 10md	No	5	Yes	Yes	0.435	1	-2800	Above -2500	Leaking outside Pliocene
	107_M_Sim05 (With capillary pressure)	Set minimum to 10md	Yes	1	Yes	Yes	0.435	1.2	-3975	-3975	Contained in Miocene

5.2 Ship Shoal Block 84 Field

5.2.1 Design and Assemble CO_2 injection model

Figure 66 indicates a top view of the geology and fluid flow (ABCDE) model boundary in Ship Shoal Block 84 field. The fluid flow model covers about 6 by 6 miles (10,002 m by 9,347 m) area, with the injection well located in the model center, and the fault serves as a no flow boundary (section AB and AC).

We build two separate fluid flow models to simulate 30 years of CO_2 injection and observation, and run 12 different cases to analyze the influence of formation heterogeneity, injection rate, isothermal and non-isothermal factor on CO_2 injection in the Pliocene and Upper Miocene, respectively.

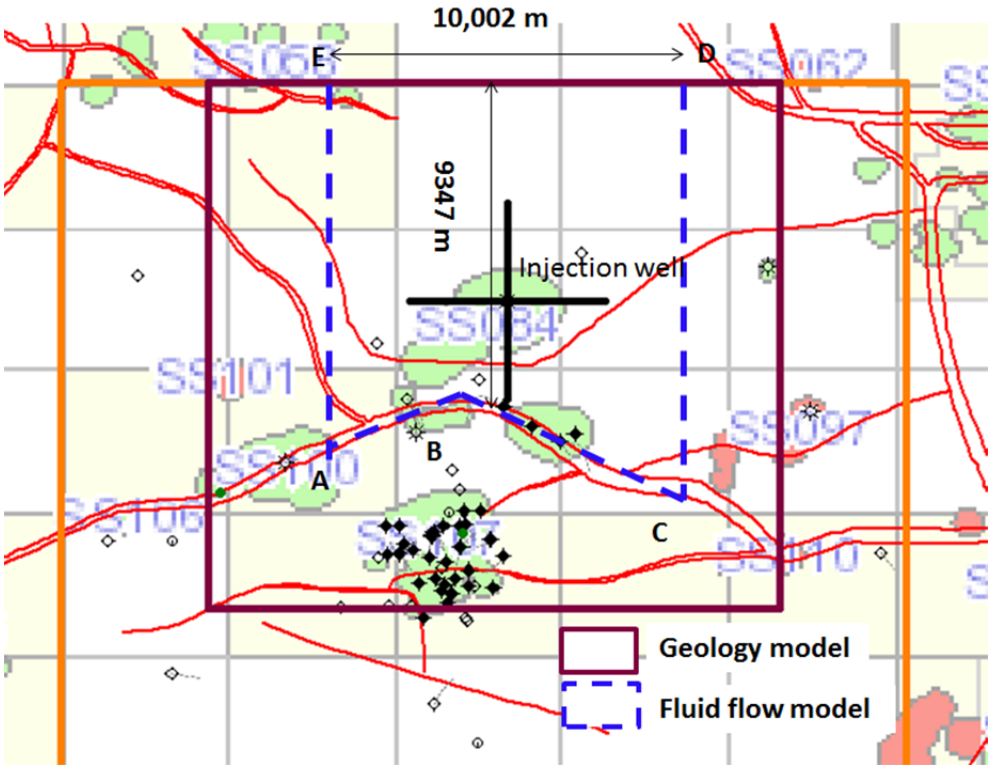

Figure 66: Geology and fluid flow model boundary in SS Block 84 field

5.2.1.1 Material properties

For both Pliocene and Upper Miocene, the input material permeability and porosity values are listed in Table 11 for the baseline case, and the relative permeability and capillary pressure are the same as the baseline case for Ship Shoal Block 107 field (Table 19).

Table 19: Parameters of relative permeability and capillary pressure in TOUGH2

	Relative Perm (Corey's/van Genuchten)				Capillary pressure (van Genuchten)						
	λ	Slr	Sls	Sgr	λ	Slr	1/P0, 1/Pa	Pmax, Pa	Sls	DSL	SIGMAref
sand		0.2		0	0.67	0.11	4.0E-04	1.0E+07	1	0	0
Silt		0.2		0	0.67	0.11	4.0E-04	1.0E+07	1	0	0
Shale	0.9167	0.3	1	0.29	0.412	0.3	1.19E-06	1.0E+09	1	0	0

5.2.1.2 Pliocene Fluid Flow Model Assembly

For Ship Shoal Block 107 field we applied a regular mesh in the fluid flow model. It took a couple of weeks to finish one simulation with 30 years of CO_2 injection. For the CO_2 storage in field 84, we look for a more efficient simulation approach. We take Pliocene, as an example; build the fluid flow model with a regular mesh and a polygonal mesh. We then compare the simulation results and pressure data; our conclusion is that the polygonal mesh (which has less number of elements) has the same accuracy as the regular mesh. It is much more efficient and we have been able to reduce the simulation time from weeks to several hours. Therefore, we will apply polygonal mesh model in the Ship Shoal Block 84 field study.

Similar to Block 107 field, we apply TOUGH2/Petrasim ECO2N module to simulate 30 years of CO_2 injection in the Pliocene formation, at an injection rate of 1 million metric tons CO_2 per year (double injection rate to study injection rate effect).

Figure 67 is the conceptual model for the Pliocene fluid flow model, with the model dimensions and boundary conditions. The model is about 6 by 6 miles (9656 m by 9656 m); the corner points A B C D E are the same corresponding points in Figure 66; and the vertical interval is 9,000 ft (2743 m), with top depth -3,000 ft (-914.4 m SSL) and bottom depth -12,000 ft (-3658 m SSL). The injection well we use is Ship Shoal Block 84_A1, a vertical well at the center of the SS Block 84 field. The model consists of a finer mesh around the injection well (maximum area per cell is 2,500 m^2), and a coarser mesh away from injection well (maximum area per cell is 247,428 m^2). The vertical cell size is 10 m at the injection interval (-9,352 ft to -9,417 ft, or -2,850.5 m to -2,870.5 m), and it gradually increases to the top and bottom of the model (to about 200 m at the upper model boundary). The model has 94,656 cells in total.

The model consists of a no flow boundary condition at the model top, bottom, and fault sections (AB and BC) and constant pressure at the other three sides (W, N, E).

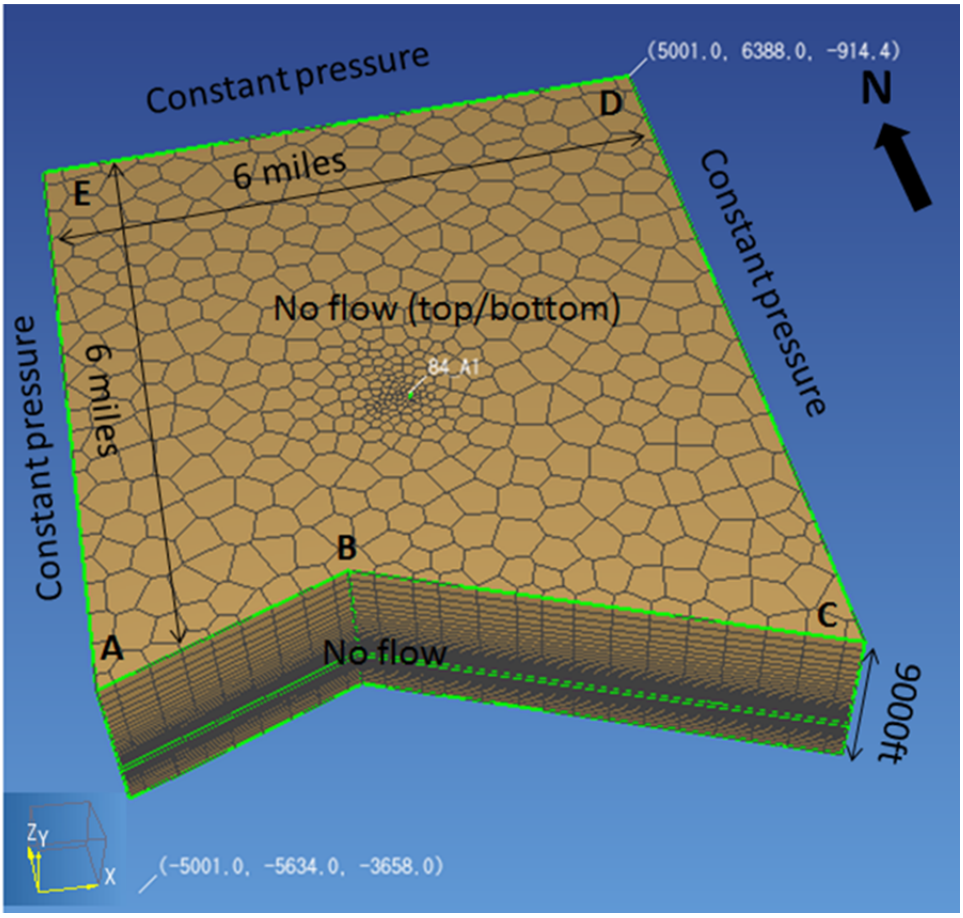

Figure 67: Conceptual model of Pliocene fluid flow model, Ship Shoal Block 84 field

Figure 68 shows the 3D lithology model, and Figure 69 and Figure 70 are the N-S and E-W cross sections of the Pliocene section after mapping from the geological model discussed in Chapter 4 Geologic model development. Combining with the stratigraphy data, we identify the sand, silt, and shale material in each stratigraphy formation, where continuous sand was found.

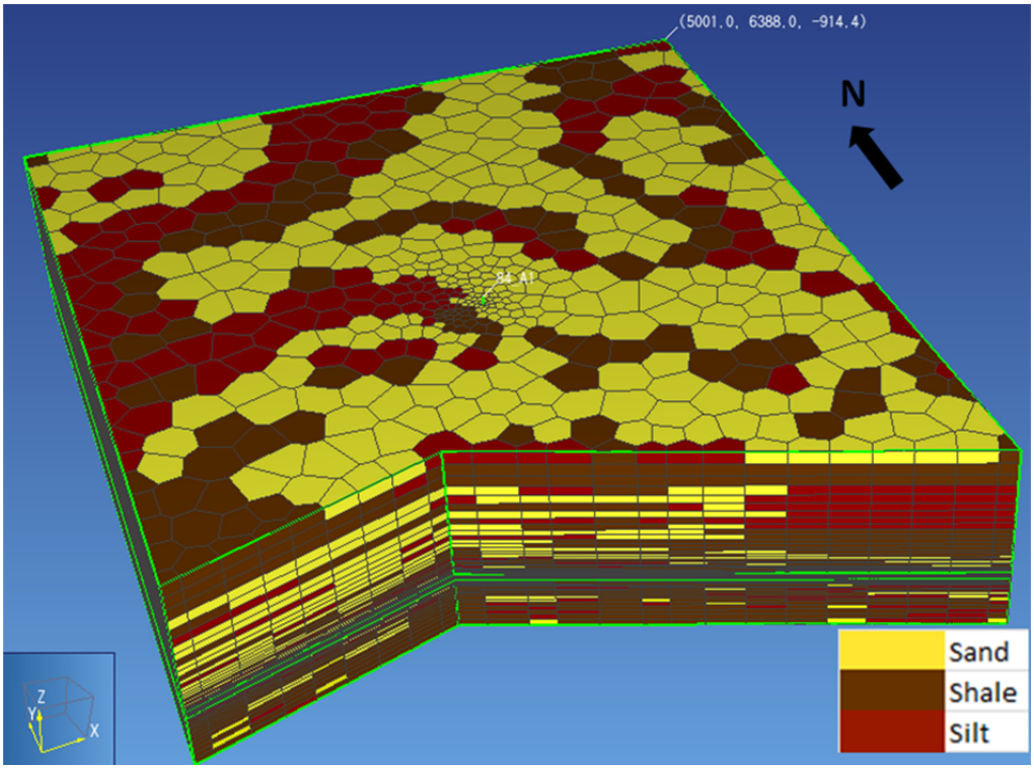

Figure 68: 3D lithology model of Pliocene in Petrasim/TOUGH2 – Ship Shoal Block 84 field

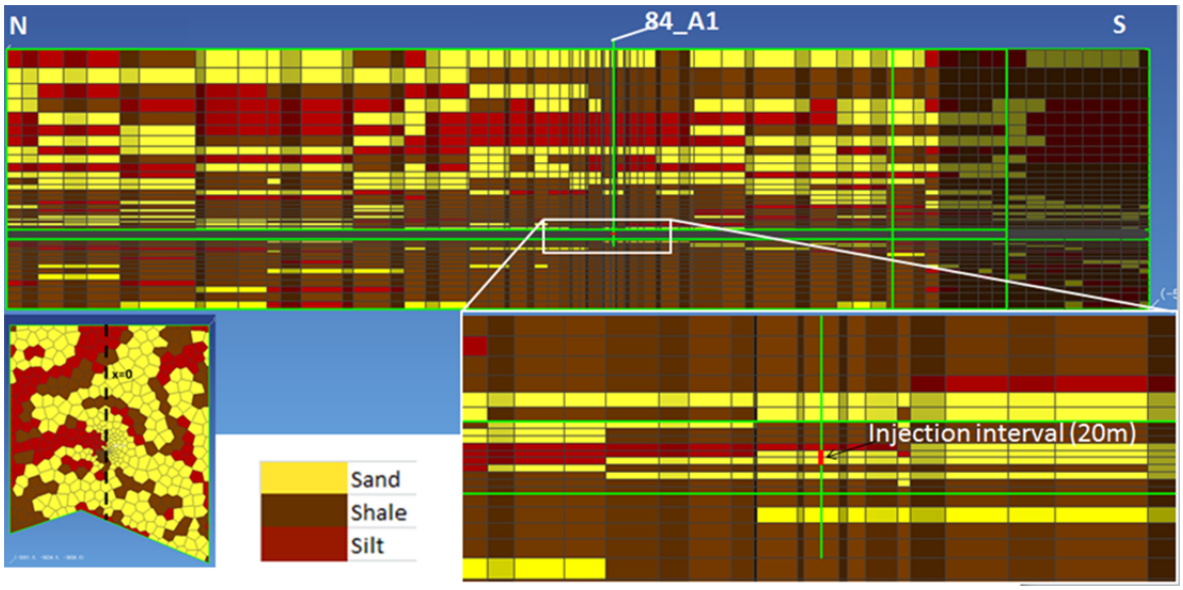

Figure 69: North-South cross section of the Pliocene fluid flow lithologic model mapped– SS Block 84 field

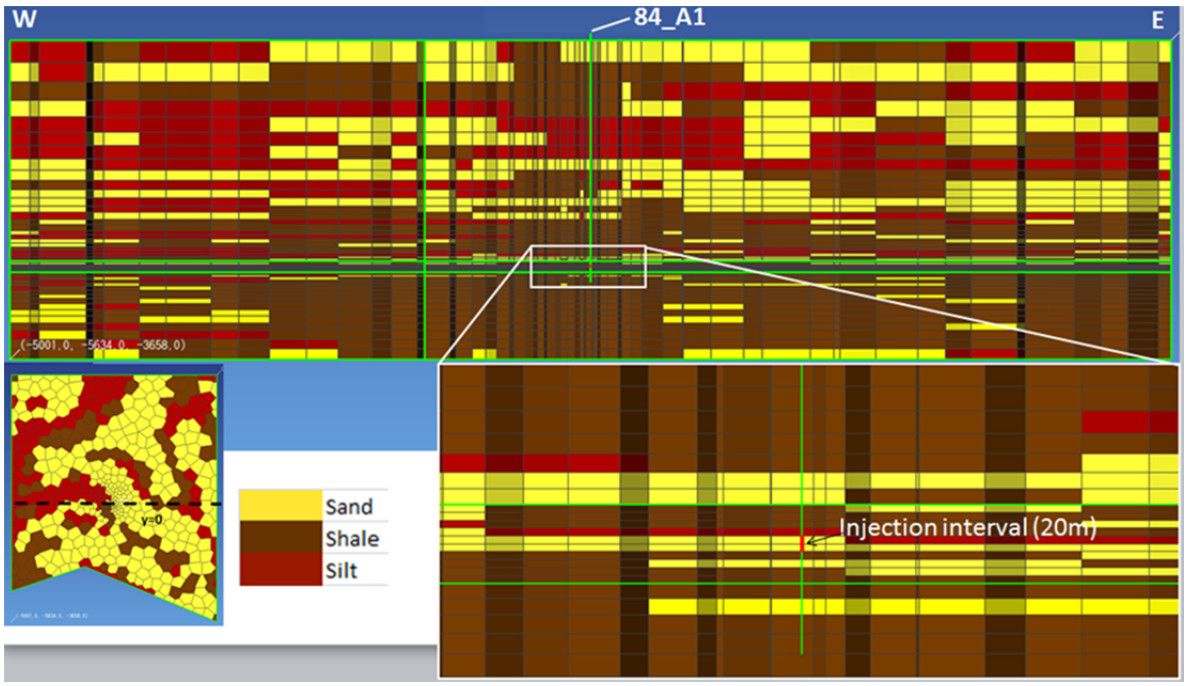

Figure 70: East-West cross section of the Pliocene fluid flow lithologic model mapped– SS Block 84 field

5.2.1.3 Upper Miocene fluid flow model assembly

Similar to fluid flow modeling in Ship Shoal Block 107 field, we apply TOUGH2/ EOS7C module to simulate 30 years of CO2 injection into the Upper Miocene formation, at the injection rate of 1 million tons per year (double injection rate to study injection rate effect).

Figure 71 is the conceptual model of the Upper Miocene fluid flow model, with the model ranges and boundary condition. The model is about 6 miles by 6 miles (9656 m by 9656 m), and the corner points A B C D E are corresponding to the same points as shown in Figure 66, and the vertical interval is 5,000 ft (1524 m), with a top depth at -10,000 ft (-3,048 m SSL) and a bottom depth of -15,000 ft (-4,572 m SSL). The injection well is the same as in the Pliocene model – Ship Shoal Block 84_A1. The model has a finer mesh around the injection well (maximum area 2,500 m^2), and a coarser mesh away from injection well (maximum area 247,428 m^2). The vertical cell size is 10 m at injection interval (-12,524.3 ft to -12,622.7 ft, or -3,817.4 m to -3,847.4 m) - where continuous sand was found.-, and it gradually increases to the top and bottom of the model (to about 150 m or 492 ft at the upper and lower model boundary). The model has a total number of cells of 18,060.

The model applies no flow boundary condition at the model top, bottom, and fault sections (AB and BC), constant pressure at the other three sides (W, N, E).

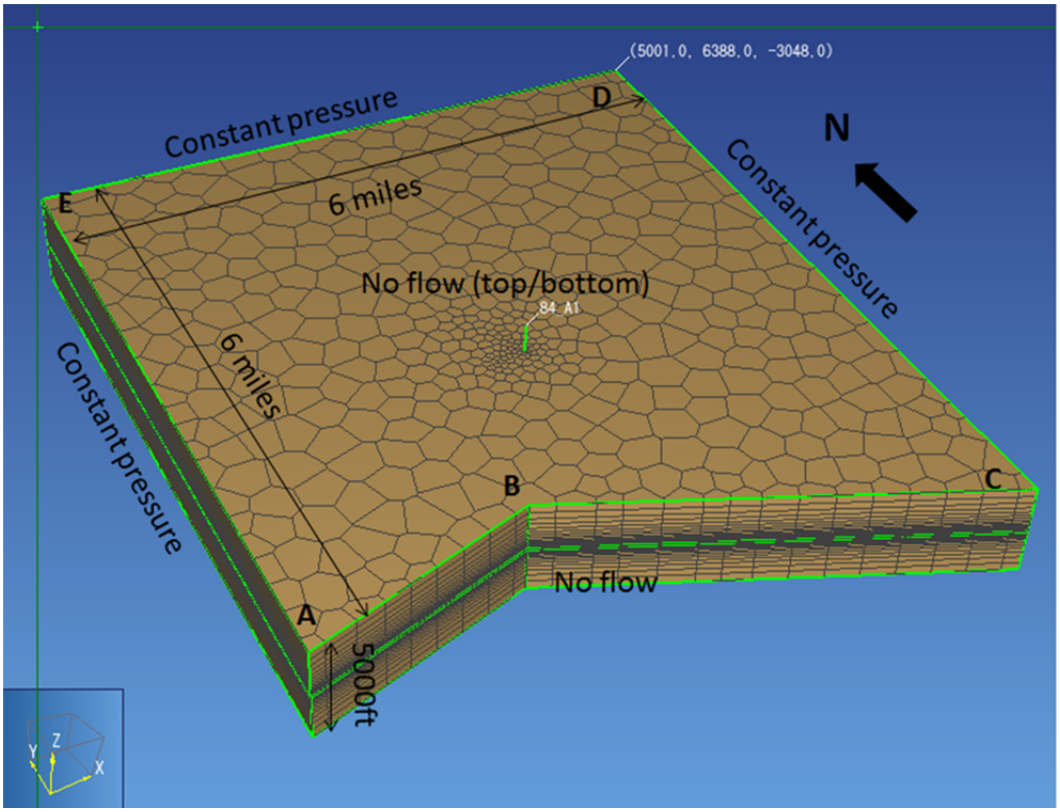

Figure 71: Conceptual model of Upper Miocene fluid flow model, Ship Shoal Block 84 field

Figure 72 shows the 3D lithology model, and Figure 73 and Figure 74 are the N-S and E-W cross sections of Upper Miocene, after data mapping from the geologic model described in Chapter 4 Geologic model development.

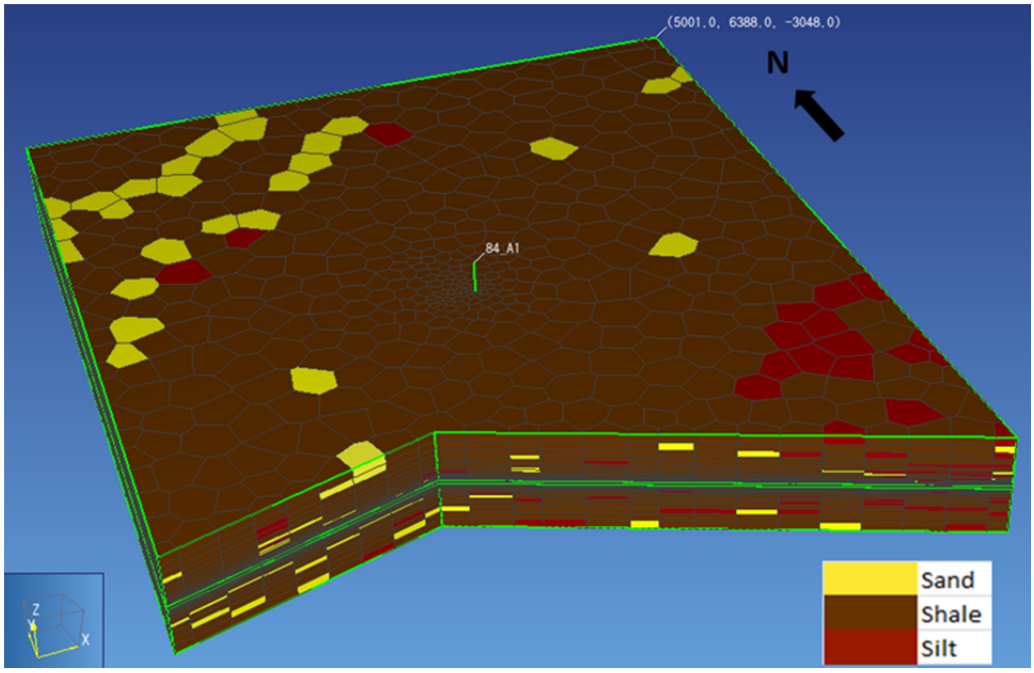

Figure 72: 3D lithology model of the Upper Miocene in TOUGH2 for Ship Shoal Block 84 field

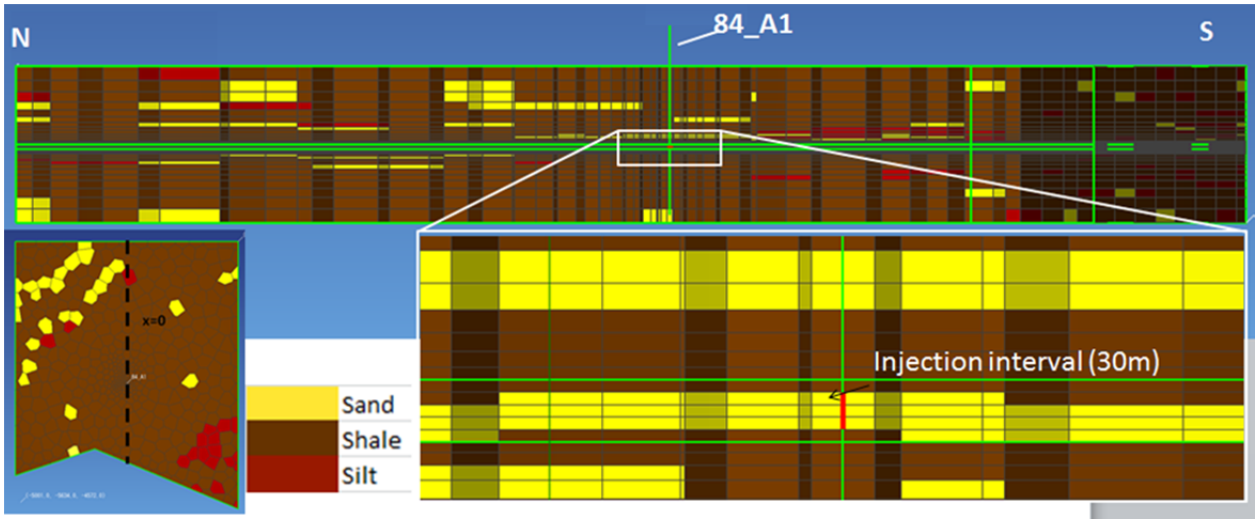

Figure 73: North-South cross-section of the lithology model for Upper Miocene, SS Block 84 field

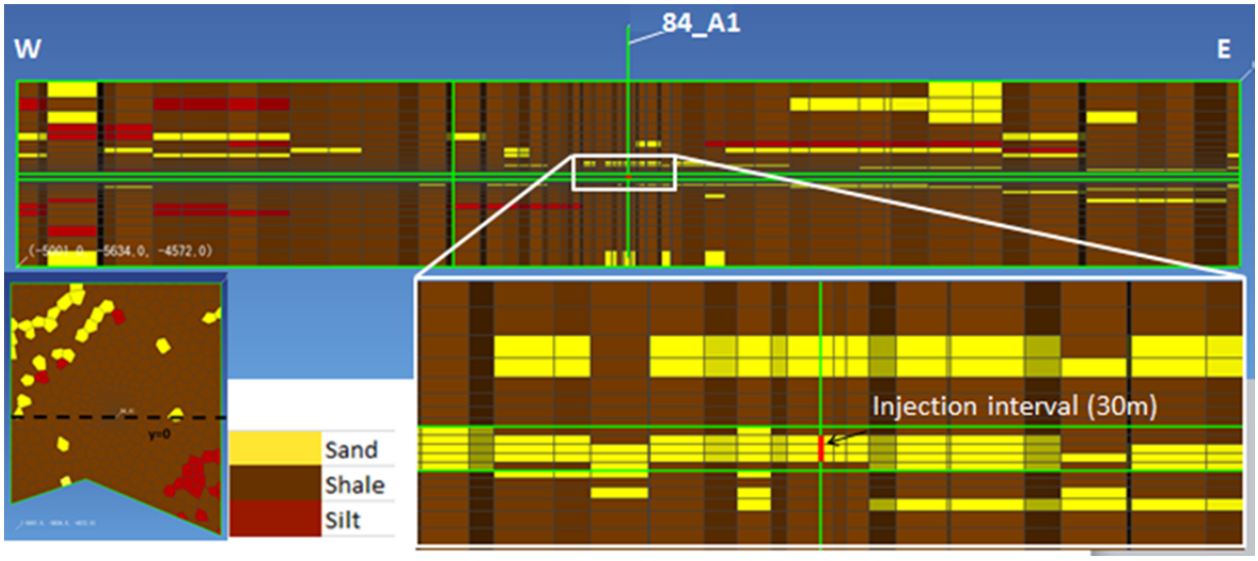

Figure 74: East-West cross-section of the lithology model for Upper Miocene, SS Block 84 field

5.2.2 Simulate varying injection scenarios

5.2.2.1 Pliocene fluid flow simulations

5.2.2.1.1 Simulation matrix

Based upon the baseline case, six isothermal scenarios and six non-isothermal scenarios were simulated to analyze the influence of formation heterogeneity, injection rate, and thermal factor on CO_2 injection. The simulation matrix is indicated in Table 20.

The following conditions were used for the baseline case:

- Assume an initial reservoir pore pressure gradient of 0.435 psi/ft and initial reservoir temperature gradient of 24 degree/km.
- Assume the salt mass fraction of 0.02148 for the reservoir fluid.
- Simulation is run in isothermal mode
- Relative permeability for sand is based on the Berea Sandstone lab data.
- An injection rate of 1 million metric tons of CO_2 per year is applied for 30 years
- Additional 30 years of plume migration are modeled after injection ceased
- 0.001 CH4 mass fraction (for numerical stability)

After running the baseline simulation, all other models are run with reduced porosity in silt and shale. We analyzed and compared the simulation results below.

Table 20: Simulation matrix of Pliocene

field 84-Pliocene-isothermal	permeability & porosity	ratio of Z-perm to XY-perm	capillary pressure	field 84-Pliocene-non-isothermal	permeability & porosity	Z-perm/XY-perm	capillary pressure
84_P_sim01 (baseline)	baseline	½	baseline	84_P_sim07 (baseline)	baseline	½	baseline
84_P_sim02 (reduced porosity)	reduce porosity in silt and shale (1/2 of 84_P_sim01)	½	baseline	84_P_sim08 (half porosity)	reduce porosity in silt and shale (1/2 of 84_P_sim01)	1/10 in shale	baseline
84_P_sim03 (no capillary)	same as 84_P_sim02	½	no	84_P_sim09 (no capillary)	same as 84_P_sim02	½	no
84_P_sim04 (sandy)	silt->sand, based on 84_P_sim02	½	baseline	84_P_sim10 (sandy)	silt->sand, based on 84_P_sim02	1/10 in shale	baseline
84_P_sim05 (shaly)	silt->shale, based on 84_P_sim02	1/2 in sand and silt, 1/10 in shale	reduce P0, Pmax 10 times in shale	84_P_sim11 (shaly)	silt->shale, based on 84_P_sim02	1/10 in shale	reduce P0, Pmax 10 times in shale
84_P_sim06 (double injection rate)	same as 84_P_sim02	1/10 in shale	reduce P0 2 times in shale	84_P_sim12 (double injection rate)	same as 84_P_sim02	1/10 in shale	reduce P0 2 times in shale

For each of the scenarios in Table 20, we simulate CO_2 injection for 30 years, and then shut-in the injection well and let the model run for another 30 years in observation phase. Sim01 to sim05 are injected at the rate of 1 million metric tons CO_2 per year to study the influence of formation heterogeneity on CO_2 injection; while sim06 is injected at the rate of 2 million metric tons CO_2 per year to study injection rate effect. We will analyze and compare the simulation results below.

5.2.2.1.2 Baseline case (84_P_sim01) result

Figure 75 is showing the cross sections of gas saturation of the baseline scenario (84_P_sim01) after 1 year, 15 years, and 30 years CO_2 injection, and after 30 years observation respectively. We can see that CO_2 is contained very well within the injection formation both during injection and observation phase.

Figure 76 indicates the top view of the CO_2 gas plume of the baseline scenario (84_P_sim01) after 30 years injection and another 30 years of observation respectively. The gas plume grows slightly into NW and SE directions during the observation phase, and the gas plume during injection is contained very well within about the 1 mile (1609 m) radius around the injection well, while it goes a little beyond the radius at the southeast corner during observation phase.

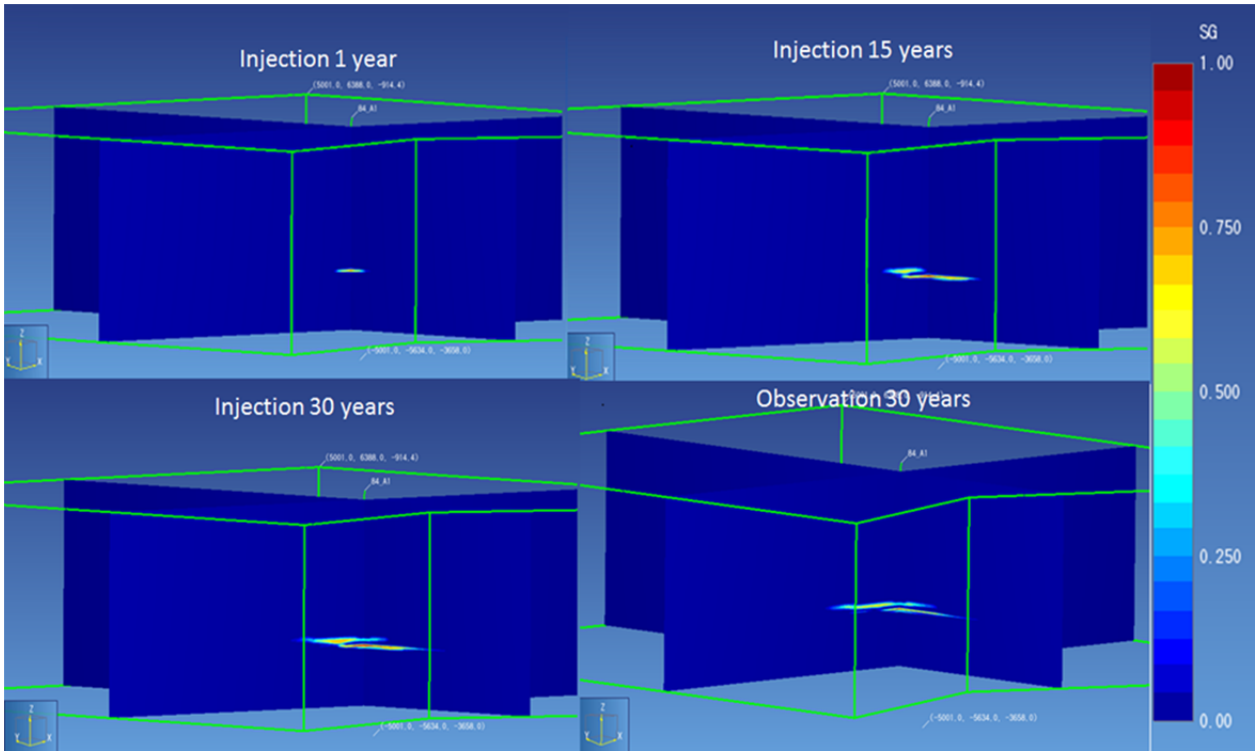

Figure 75: The cross-sections of Gas Saturation after 1, 15, 30 years injection, and 30 years observation, baseline case (84_P_sim01) of Pliocene-isothermal, Ship Shoal Block 84 field

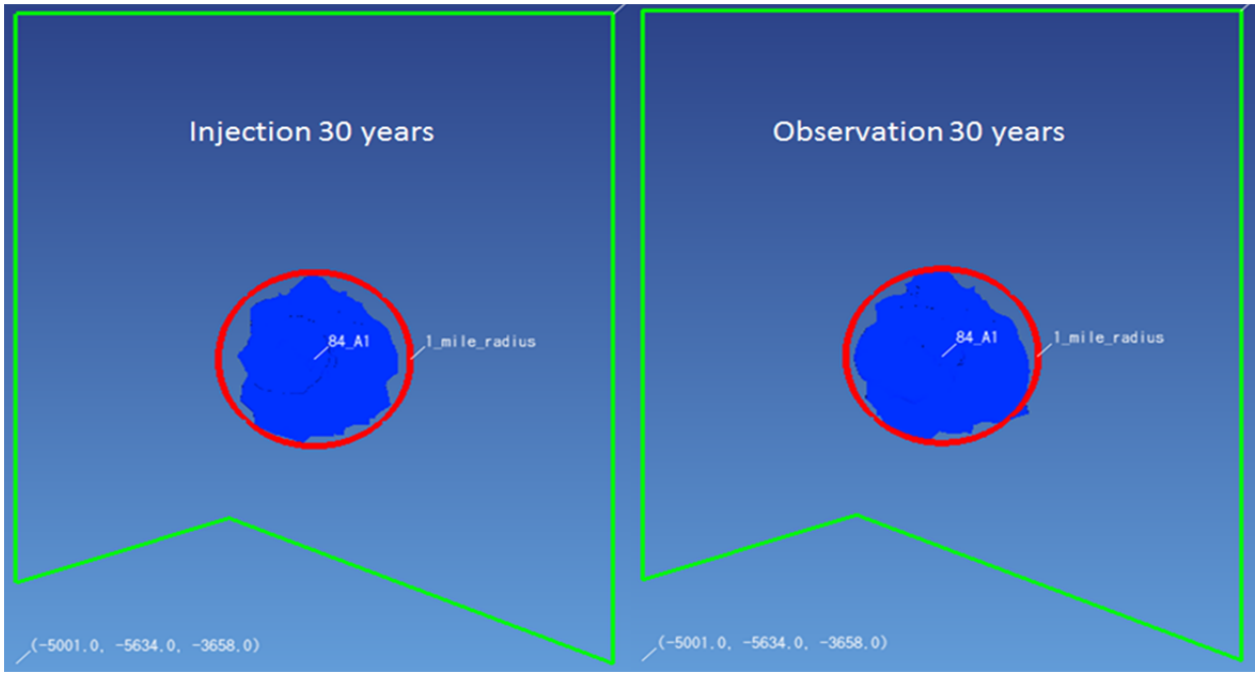

Figure 76: The top view of CO2 Gas plume after 30 years injection, and 30 years observation, baseline case (84_P_sim01) of Pliocene-isothermal, Ship Shoal Block 84 field

5.2.2.1.3 Half porosity (84_P_sim02) result

Considering the heterogeneousness of pore distribution in shale and silt, we reduced half of the porosity in shale and silt based on baseline case, in case 84_P_sim02.

Figure 77 is showing the cross sections of gas saturation of the case 84_P_sim02 after 1 year, 15 years, and 30 years CO2 injection, and after 30 years observation respectively. We can see that, similar to baseline case (84_P_sim01), CO_2 is contained very well within the injection formation both during injection and observation.

Figure 78 indicates the top view of the CO_2 gas plume of the case 84_P_sim02 after 30 years injection and another 30 years of observation respectively. The gas plume grows slightly into all directions except NE during the observation phase, and the gas plume during injection is contained very well within about the 1 mile (1609 m) radius around the injection well, while it goes a little beyond the radius at the corner of west, south-west, and south-east during observation phase.

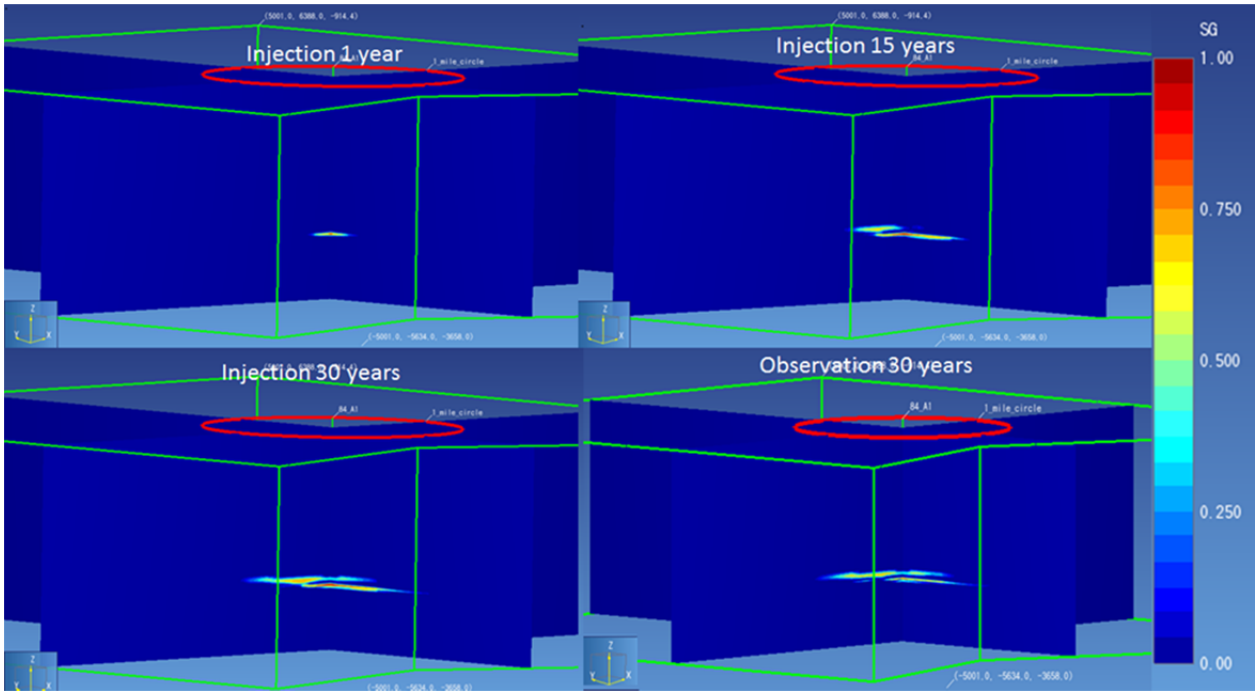

Figure 77: The cross-sections of Gas Saturation after 1, 15, 30 years injection, and 30 years observation, 84_P_sim02 of Pliocene-isothermal, Ship Shoal Block 84 field

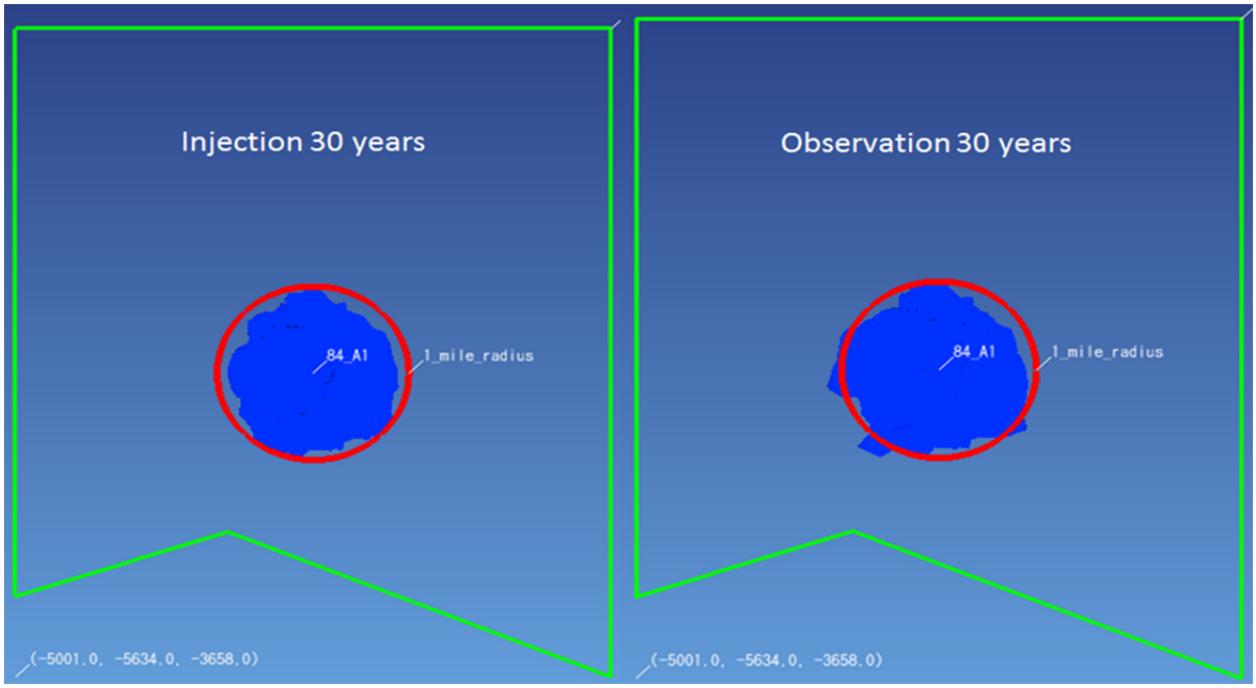

Figure 78: The top view of CO2 Gas plume after 30 years injection, and 30 years observation, 84_P_sim02 of Pliocene-isothermal, Ship Shoal Block 84 field

5.2.2.1.4 No capillary pressure (84_P_sim03) result

To simulate the worst case scenario, we assume there is no capillary pressure in all the formations -- the CO2 can migrate upward to cause leakage, in case 84_P_sim03.

Figure 79 shows the cross sections of gas saturation of the case 84_P_sim03 after 1 year, 15 years, and 30 years CO_2 injection, and after 30 years observation respectively. We can see that CO_2 migrates about 4002ft (1220m) upward from injection interval and is contained during injection, and it continues migrating to model surface and is leaking during observation phase.

Figure 80 indicates the top view of the CO_2 gas plume of the case 84_P_sim03 after 30 years injection and another 30 years of observation respectively. Both are contained very well within about the 1 mile radius around the injection well.

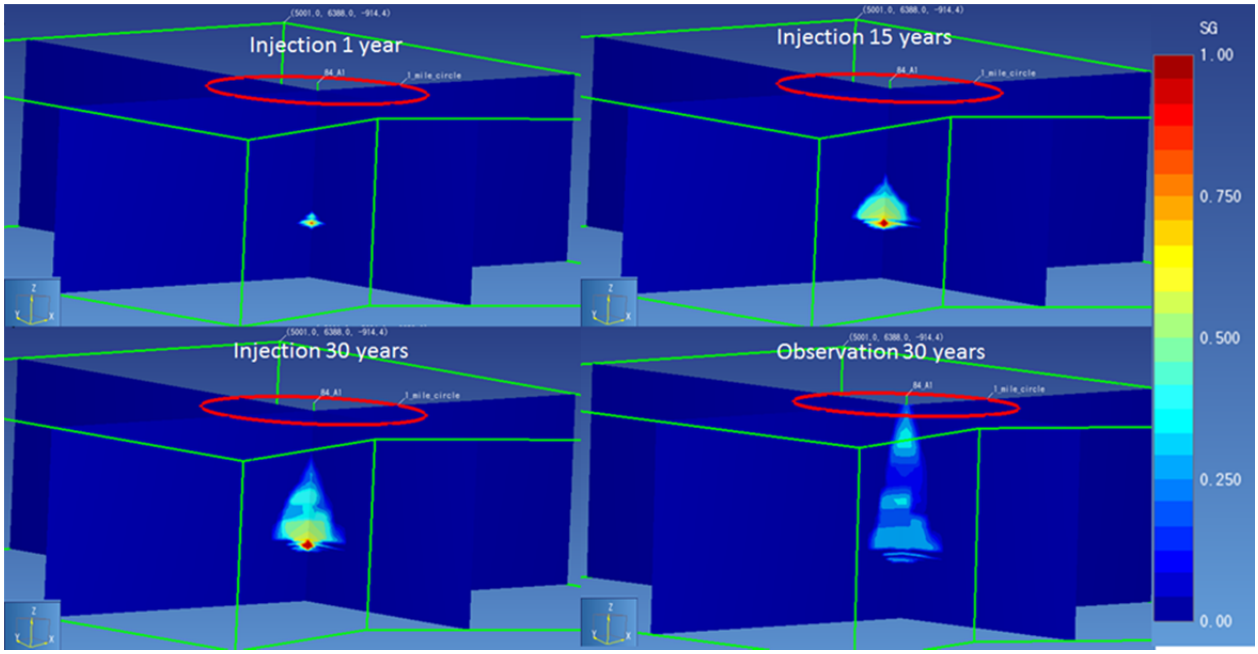

Figure 79: The cross-sections of Gas Saturation after 1, 15, 30 years injection, and 30 years observation, 84_P_sim03 of Pliocene-isothermal, Ship Shoal Block 84 field

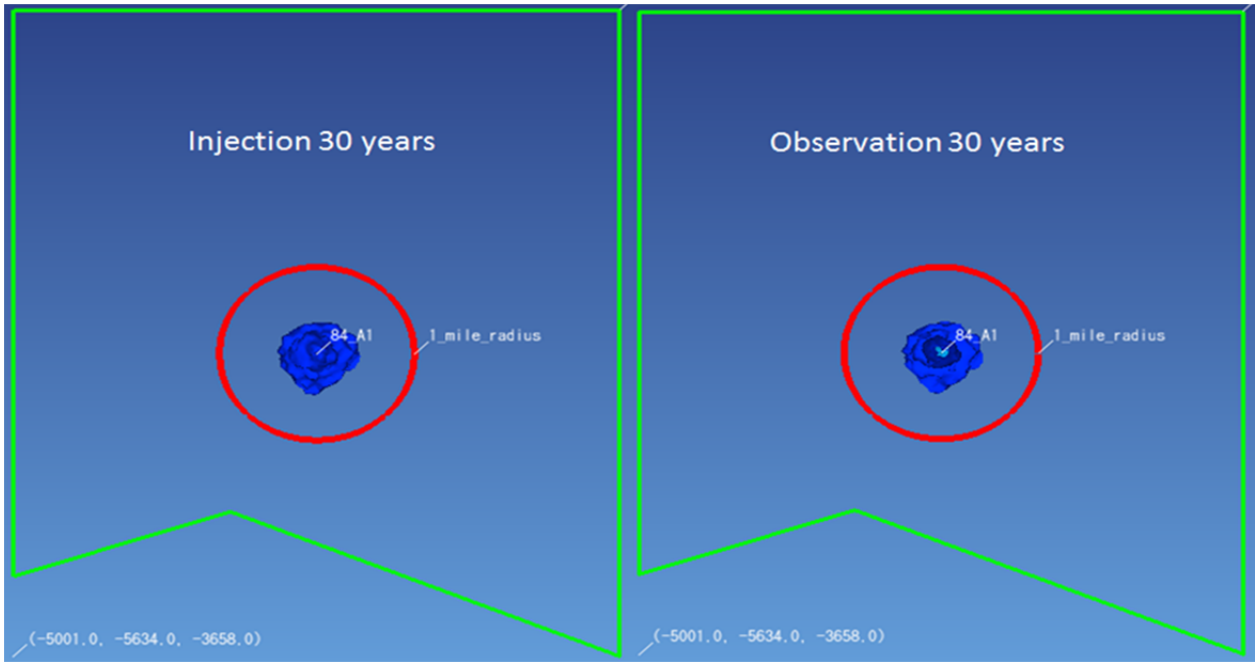

Figure 80: The top view of CO2 Gas plume after 30 years injection, and 30 years observation, 84_P_sim03 of Pliocene-isothermal, SS Block 84 field

5.2.2.1.5 Sandy model (84_P_sim04) result

To study influence of varying geology, we converted formation silt to sand to increase the volume to store CO_2, in case 84_P_sim04.

Figure 81 shows the cross sections of gas saturation of the case 84_P_sim04 after 1 year, 15 years, and 30 years CO2 injection, and after 30 years observation respectively. We can see that, similar to baseline case (84_P_sim01), CO_2 is contained very well within the injection formation both during injection and observation phases.

Figure 82 indicates the top view of the CO_2 gas plume of the case 84_P_sim04 after 30 years injection and another 30 years of observation respectively. The gas plume grows slightly into north, west, and south-east direction during the observation phase, and the gas plume during injection is contained very well within about the 1 mile radius around the injection well, while it goes a little beyond the radius at the western corner during the observation phase.

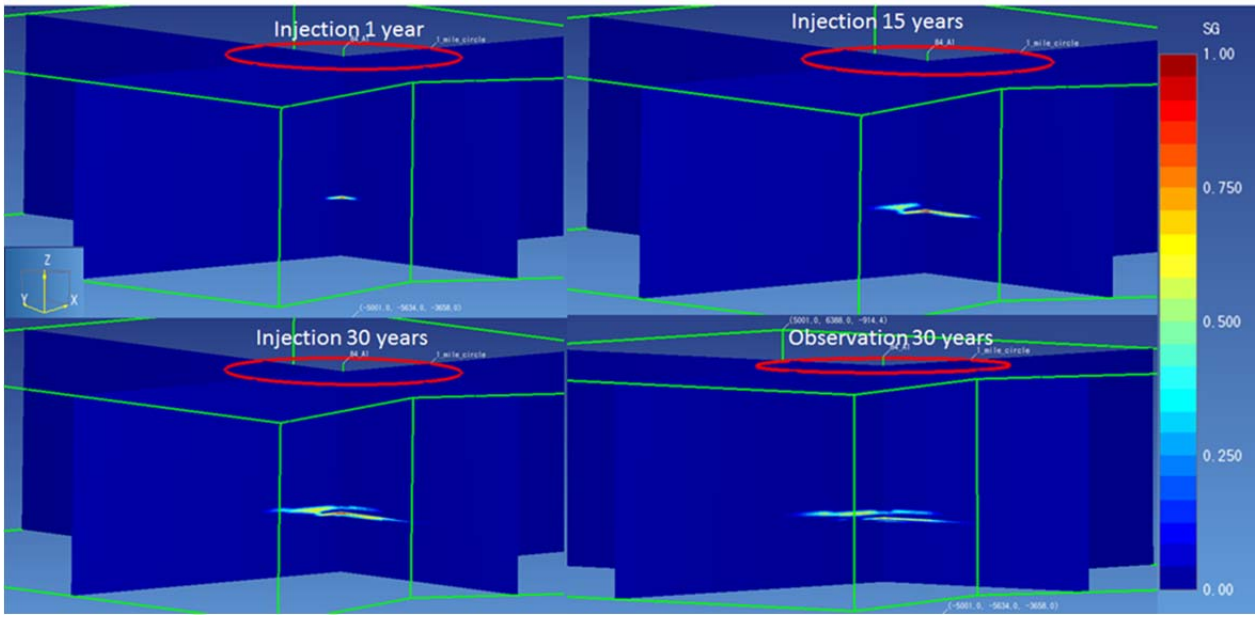

Figure 81: The cross-sections of Gas Saturation after 1, 15, 30 years injection, and 30 years observation, 84_P_sim04 of Pliocene-isothermal, Ship Shoal Block 84 field

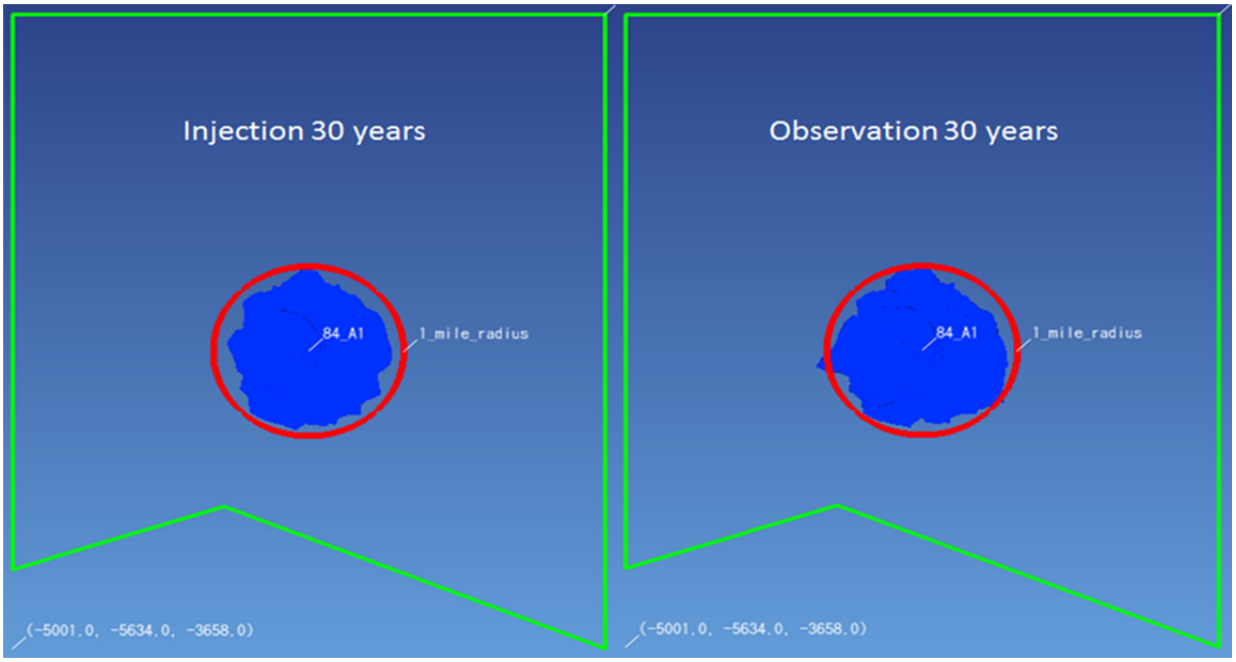

Figure 82: The top view of CO2 Gas plume after 30 years injection, and 30 years observation, 84_P_sim04 of Pliocene-isothermal, Ship Shoal Block 84 field

5.2.2.1.6 Shaly model (84_P_sim05) result

To study the influence of varying geology, we converted lithology silt to shale in case 84_P_sim05.

Figure 83 is showing the cross sections of gas saturation of the case 84_P_sim05 after 1 year, 15 years, and 30 years CO2 injection, and after 30 years observation respectively. We can see that, CO_2 migrates upward about 328ft (100m) from injection interval into the upper sand layer and is contained during injection, and it continues to migrate slightly in these two layers during observation phase.

Figure 84 indicates the top view of the CO_2 gas plume of the case 84_P_sim05 after 30 years injection and another 30 years of observation respectively. The gas plume grows slightly into west and south-east direction during the observation phase, and it goes a little bit beyond the 1 mile radius in the south-west direction during both injection and observation phases.

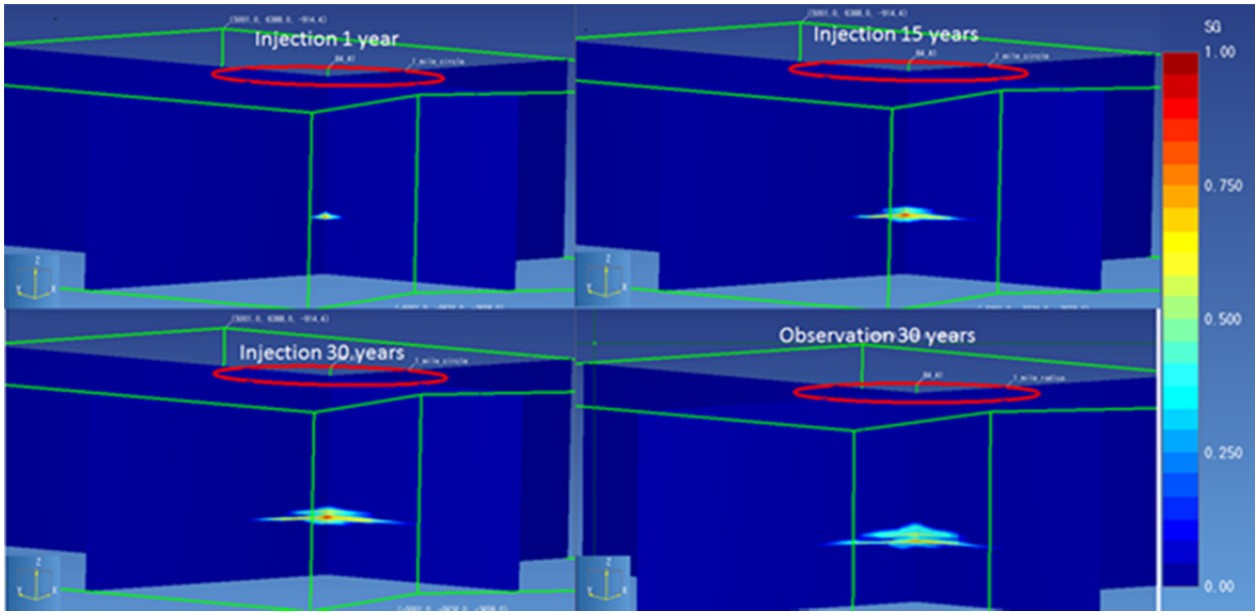

Figure 83: The cross-sections of Gas Saturation after 1, 15, 30 years injection, and 30 years observation, 84_P_sim05 of Pliocene-isothermal, Ship Shoal Block 84 field

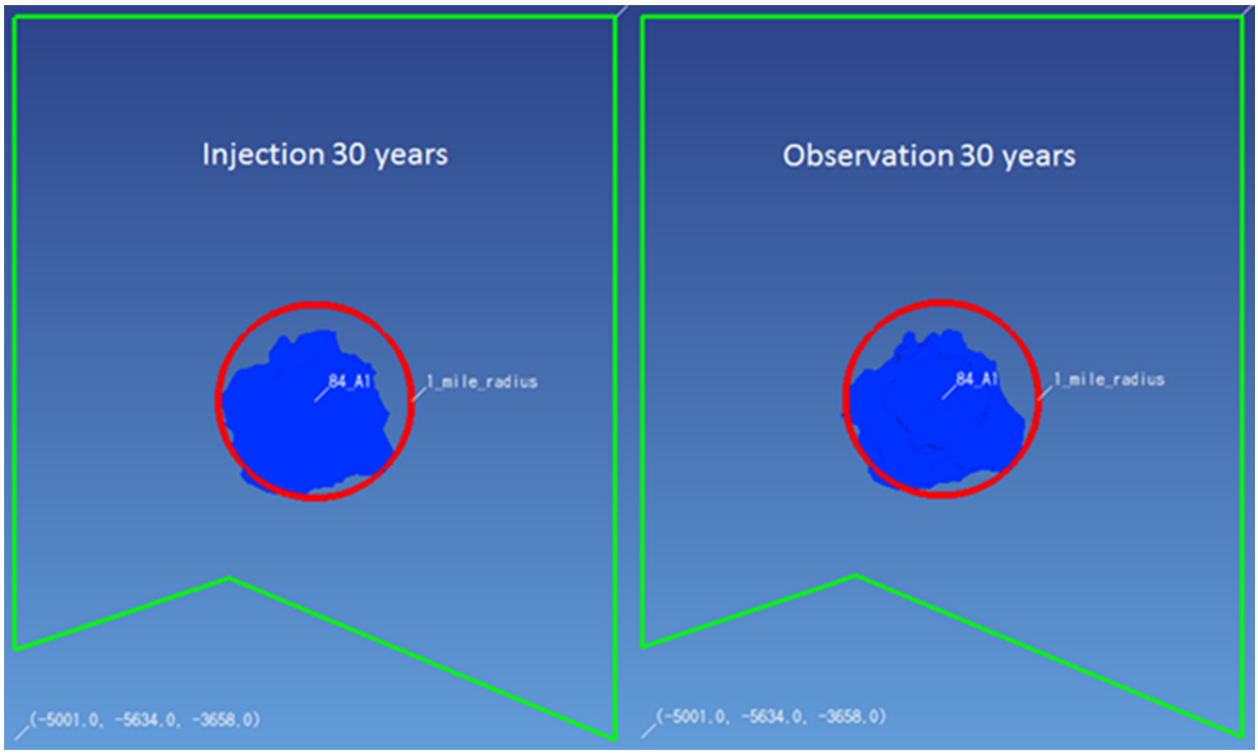

Figure 84: The top view of CO2 Gas plume after 30 years injection, and 30 years observation, 84_P_sim05 of Pliocene-isothermal, Ship Shoal Block 84 field

5.2.2.1.7 Double injection rate (84_P_sim06) result

To study influence of varying injection rate, we doubled the injection from 1million metric ton per year to 2 million metric tons per year, in case 84_P_sim06.

Figure 85 is showing the cross sections of gas saturation of the case 84_P_sim06 after 1 year, 15 years, and 30 years CO2 injection, and after 30 years observation respectively. We can see that, CO_2 migrates upward about 1312ft (400m) from injection interval into the upper sand layer and is contained during injection phase, and it continues to migrate slightly during the observation phase.

Figure 86 indicates the top view of the CO_2 gas plume of the case 84_P_sim06 after 30 years injection and another 30 years of observation respectively. The gas plume grows into north and east direction during the observation phase, and it goes a little bit beyond the 1 mile radius in the south-west direction during both injection and observation phases.

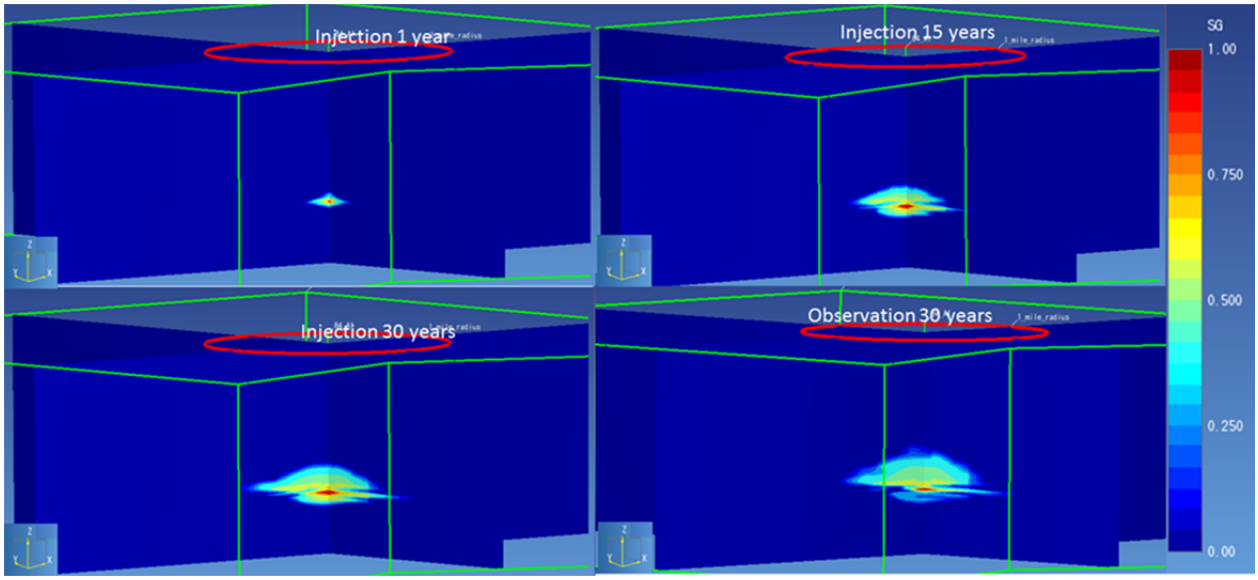

Figure 85: The cross-sections of Gas Saturation after 1, 15, 30 years injection, and 30 years observation, 84_P_sim06 of Pliocene-isothermal, Ship Shoal Block 84 field

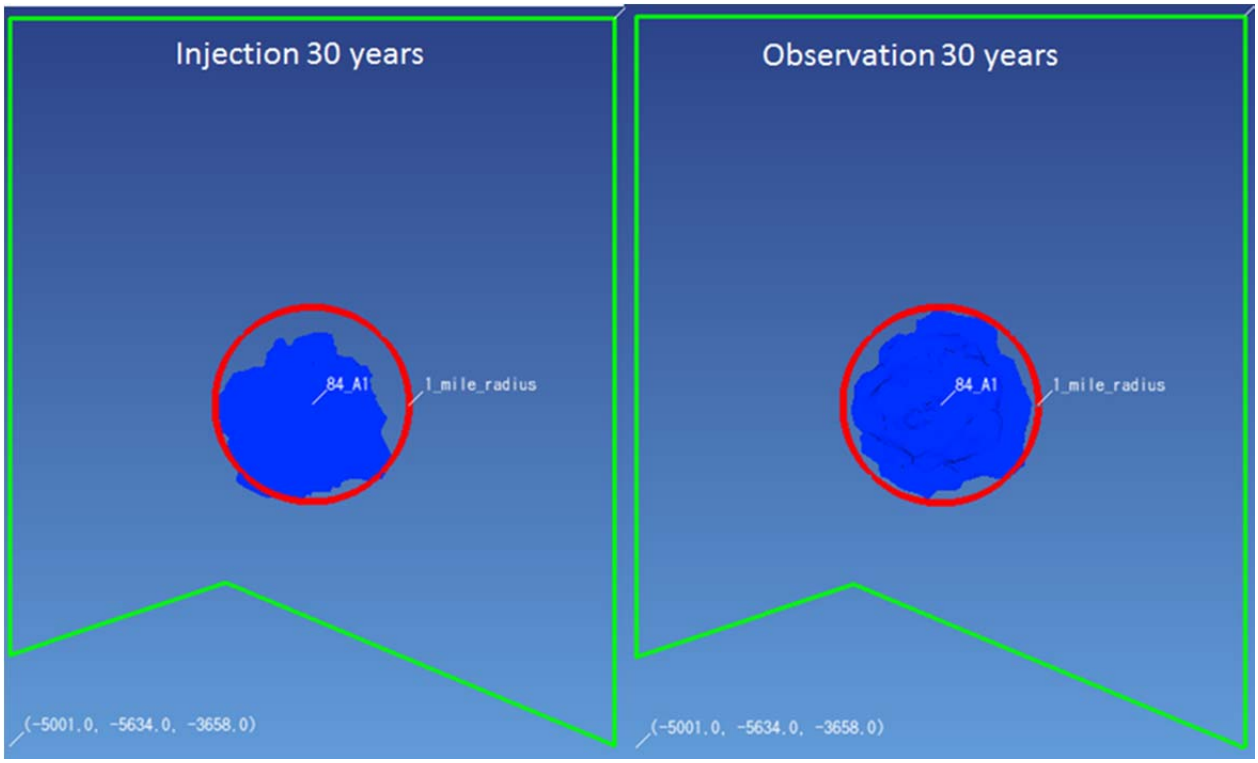

Figure 86: The top view of CO2 Gas plume after 30 years injection, and 30 years observation, 84_P_sim06 of Pliocene-isothermal, Ship Shoal Block 84 field

5.2.2.1.8 Pressure profiles comparison

Figure 87 and Figure 88 indicate the comparison of pressure profiles across the injection well through the middle of the injection interval (=-2860.5m or -9384 ft), at in-situ conditions and after 30 years of injection for the six isothermal scenarios. Maximum delta pressure observed is 1.22 MPa (177 psi) that is about 4.3% from in situ pore pressure. At a 1 mile distance from the injection well the maximum pressure increase observed is 84_P_sim06 (double injection rate), and 84_P_sim03 (contains no capillary pressure) has the lowest pressure after 30 years of constant CO_2 injection. 84_P_sim01, 84_P_sim02 have similar pressure profiles, while the pressure at the injection well is lower in scenario 84_P_sim04 (sandy model) than 84_P_sim05 (contains more shale).

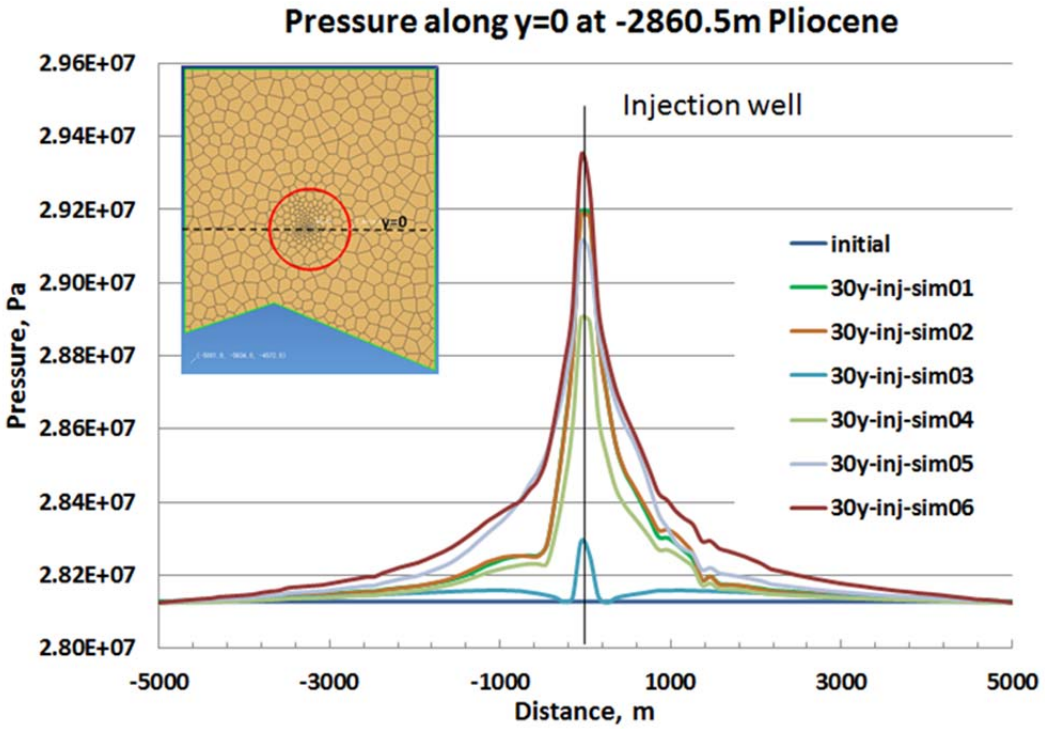

Figure 87: Comprison of pressure profiles across (y=0) injection well through the middle of injection interval, at initial and after 30 years injection into the Pliocene-isothermal – Ship Shoal Block 84 field

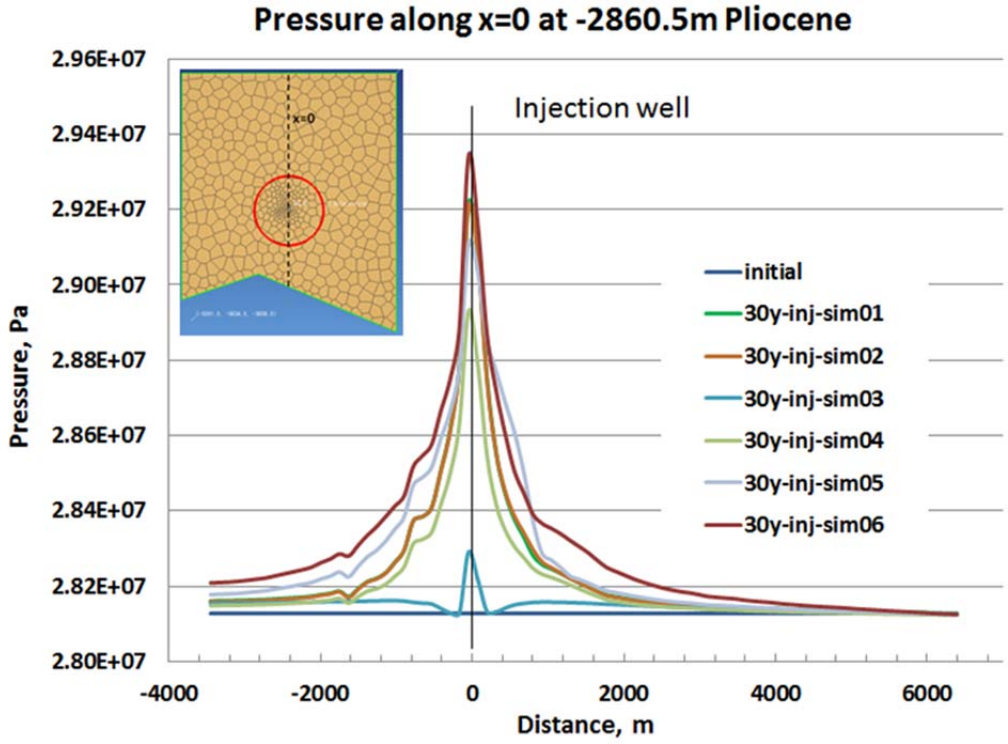

Figure 88: Comprison of pressure profiles across (x=0) injection well through the middle of injection interval, at initial and after 30 years injection into the Pliocene-isothermal – Ship Shoal Block 84 field

5.2.2.1.9 Non-isothermal simulation result

After finishing the six isothermal simulations in Table 20, we ran each of them again with non-isothermal (injection CO_2 at 60 ^{0}C). 84_P_sim07 to 84_P_sim11 are injected at the rate of 1 million metric tons CO_2 per year to study the influence of formation heterogeneity on CO_2 injection; while 84_P_sim12 is injected at the rate of 2 million metric tons CO_2 per year to study injection rate effect.

For all simulations, we can see that the pressure profiles with non-isothermal effect are slightly higher than isothermal around the injection well, and the difference is within 1%. Our analyses and the simulation results are shown in Appendix B.

5.2.2.2 Upper Miocene fluid flow simulations

5.2.2.2.1 Simulation matrix

Based upon the baseline case, six isothermal scenarios and six non-isothermal scenarios were simulated to analyze the influence of formation heterogeneity, injection rate, and thermal factor on CO_2 injection, the simulation matrix is indicated in Table 21.

The following conditions were used for the baseline case:

- Assume an initial reservoir pore pressure gradient of 0.435 psi/ft and initial reservoir temperature gradient of 24 degree/km.
- Assume the salt mass fraction of 0.02148 for the reservoir fluid.
- Simulation is run in isothermal mode
- Relative permeability for sand is based on the Berea Sandstone lab data.
- An injection rate of 1 million metric tons of CO2 per year is applied for 30 years
- Additional 30 years of plume migration are modeled after injection ceased
- 0.001 CH4 mass fraction (for numerical stability)

After running the baseline simulation, all other models are run with reduced porosity in silt and shale.

Table 21: Simulation matrix of Upper Miocene

field 84-Upper Miocene-isothermal	permeability & porosity	ratio of Z-perm to XY-perm	capillary pressure	field 84-Upper Miocene-non-isothermal	permeability & porosity	Z-perm/XY-perm	capillary pressure
84_M_sim01 (baseline)	baseline	½	baseline	84_M_sim07 (baseline)	baseline	1/10 in shale	reduce P0 10 times in shale
84_M_sim02 (reduced porosity)	reduce porosity in silt and shale (1/2 of 84_M_sim01)	1/2 in sand and silt, 1/10 in shale	reduce P0, Pmax 10 times in shale	84_M_sim08 (half porosity)	reduce porosity in silt and shale (1/2 of 84_M_sim01)	1/10 in shale	reduce P0 and Pmax 10 times in shale
84_M_sim03 (no capillary)	same as 84_M_sim02	½	no	84_M_sim09 (no capillary)	same as 84_M_sim02	1/10 in shale	no
84_M_sim04 (sandy)	silt->sand, based on 84_M_sim02	1/2 in sand and silt, 1/10 in shale	reduce P0 10 times, reduce Pmax 100 times in shale	84_M_sim10 (sandy)	silt->sand, based on 84_M_sim02	1/10 in shale	reduce P0 1.5 times in sand, reduce P0 10 times in shale
84_M_sim05 (shaly)	silt->shale, based on 84_M_sim02	1/2 in sand and silt, 1/10 in shale	reduce P0 10 times, reduce Pmax 100 times in shale	84_M_sim11 (shaly)	silt->shale, based on 84_M_sim02	1/10 in shale	reduce P0 10 times, reduce Pmax 100 times in shale
84_M_sim06 (double injection rate)	same as 84_M_sim02	1/5 in shale	reduce P0 10 times, reduce Pmax 100 times in shale	84_M_sim12 (double injection rate)	same as 84_M_sim02	1/5 in shale	reduce P0 10 times, reduce Pmax 100 times in shale

For each of the scenarios in Table 21, we simulate CO_2 injection for 30 years, and then shut-in the injection well and let the model run for another 30 years in the observation phase. Sim01 to sim05 are injected at the rate of 1 million metric tons CO_2 per year to study the influence of formation heterogeneity on CO_2 injection; while sim06 is injected at the rate of 2 million metric tons CO_2 per year to study injection rate effect.

5.2.2.2.2 Baseline case (84_M_sim01) result

Figure 89 shows the cross-sections of gas saturation after 1 year, 15 years, and 30 years CO_2 injection, and another 30 years of observation, of the baseline scenario (84_M_sim01) respectively. We can see that CO_2 is contained very well within the injection formation both during the injection and observation phase in baseline case (84_M_sim01).

Figure 90 indicates the top view of CO_2 gas plume after 30 years injection and 30 years of observation, the baseline scenario (84_M_sim01) respectively. The gas plume grows slightly into all directions except in the south-east during the observation phase, and it is obviously beyond the 1 mile radius circle around the injection well, except in the south-east direction in both injection and observation phases.

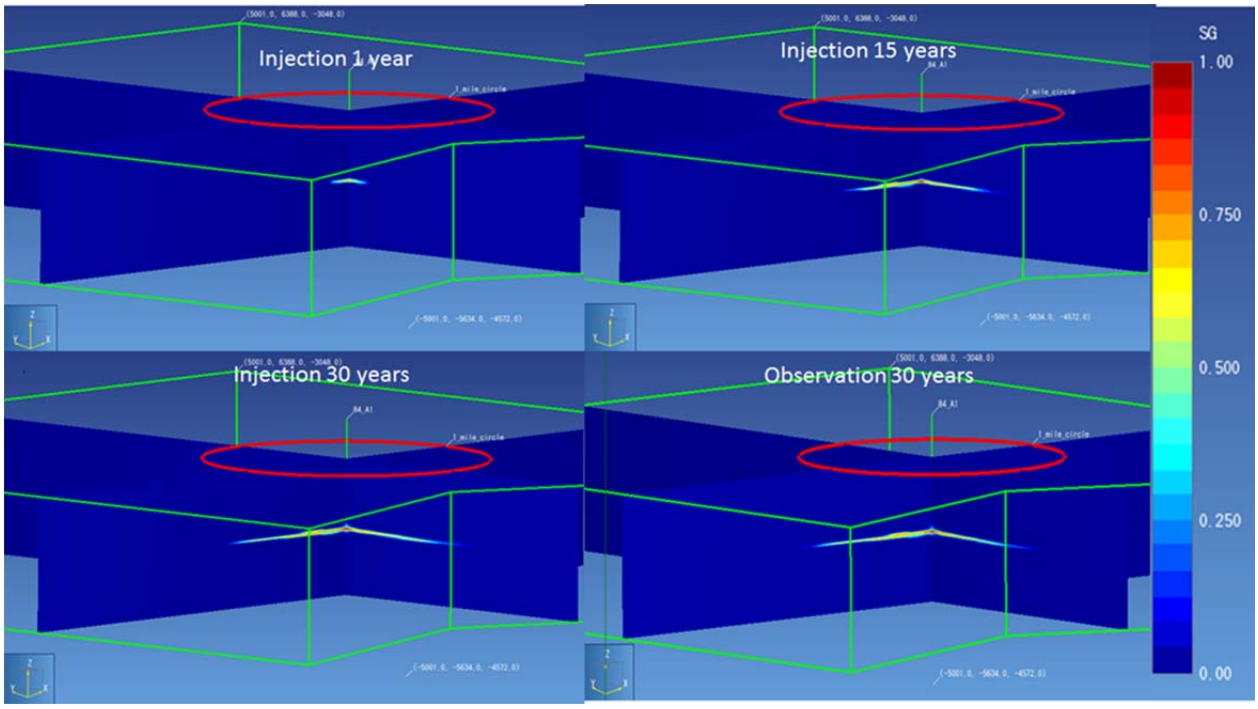

Figure 89: The cross-sections of Gas Saturation after 1, 15, 30 years injection, and 30 years observation, baseline case (84_M_sim01) for Upper Miocene, Ship Shoal Block 84 field

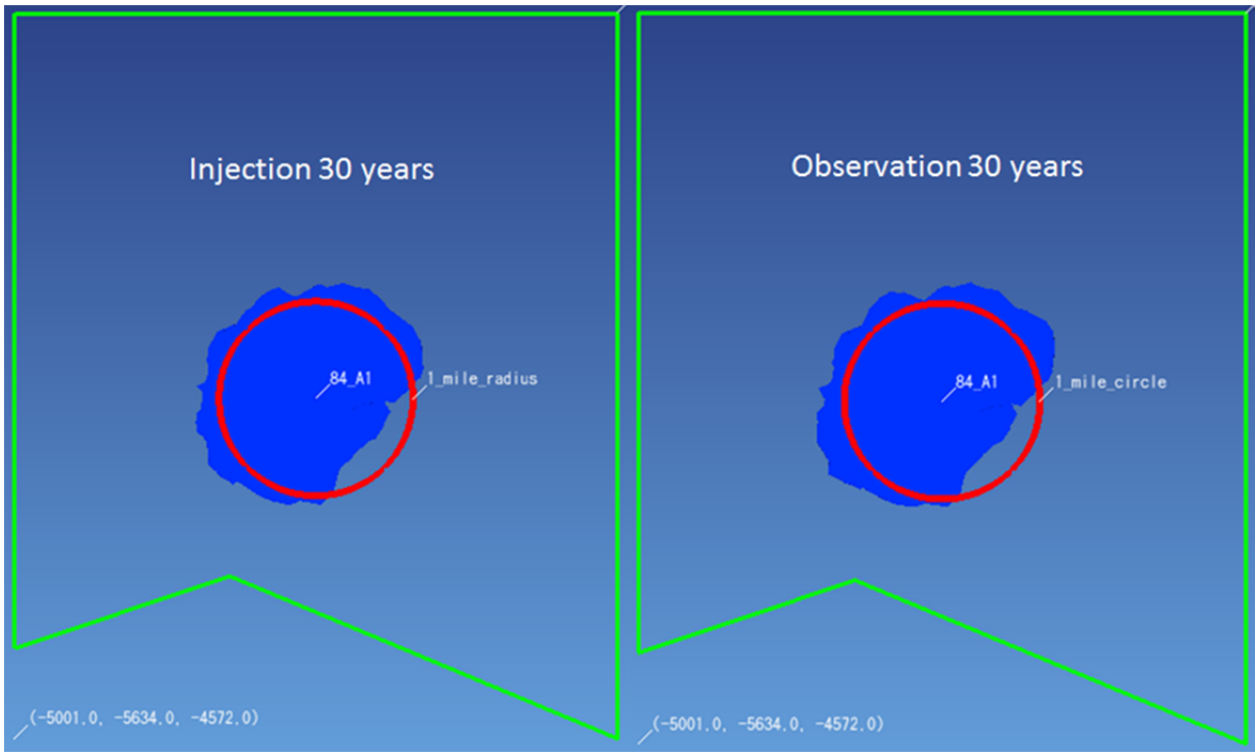

Figure 90: The top view of CO2 Gas plume after 30 years injection, and 30 years observation, baseline case (84_M_sim01) of Upper Miocene, Ship Shoal Block 84 field

5.2.2.2.3 Half porosity (84_M_sim02) result

Considering the heterogeneousness of pore distribution in shale and silt, we reduced half of the porosity in shale and silt based on baseline case, in case 84_M_sim02.

Figure 91 shows the cross-sections of gas saturation after 1 year, 15 years, and 30 years CO_2 injection, and another 30 years of observation, of the scenario 84_M_sim02 respectively. We can see that CO_2 migrates about 500ft (152m) into upper sand formation and is contained both during the injection and observation phases.

Figure 92 indicates the top view of CO_2 gas plume after 30 years injection and 30 years of observation, the scenario 84_M_sim02 respectively. The gas plume after 30 years injection is within the 1 mile radius circle, and it grows slightly into all directions except in the south-east during the injection phase. It is a little bit beyond the 1 mile radius circle around the injection well, except in the south-east direction in the observation phase.

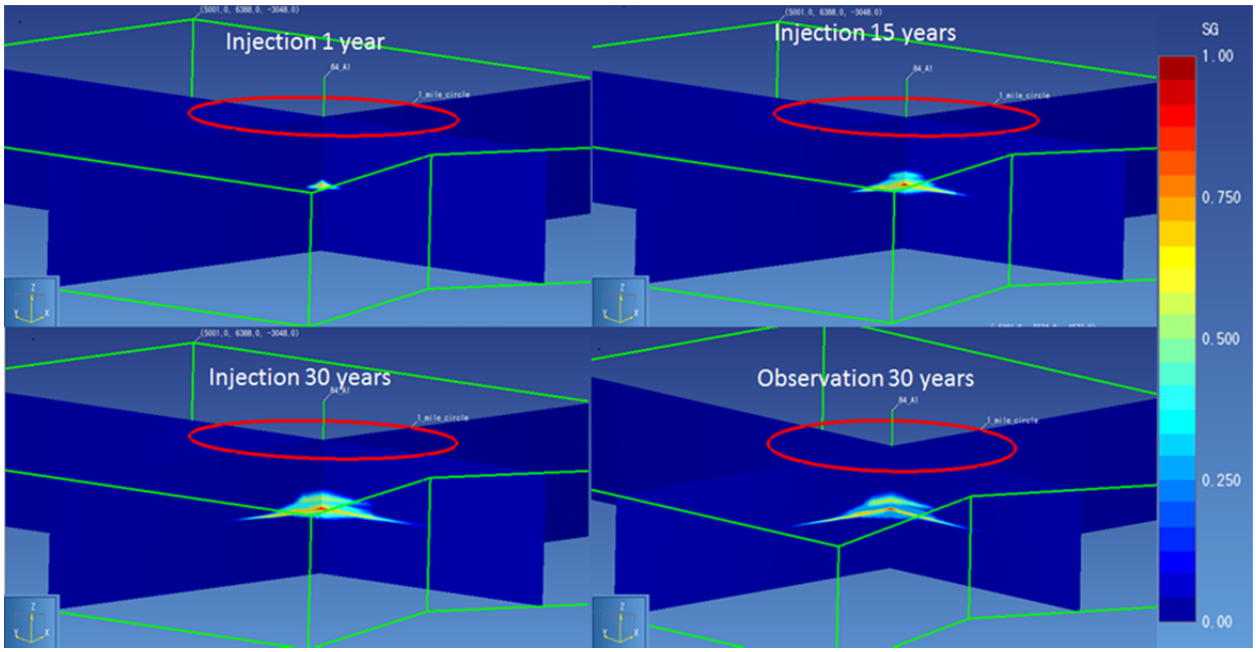

Figure 91: The cross-sections of Gas Saturation after 1, 15, 30 years injection, and 30 years observation, 84_M_sim02 of Upper Miocene, Ship Shoal Block 84 field

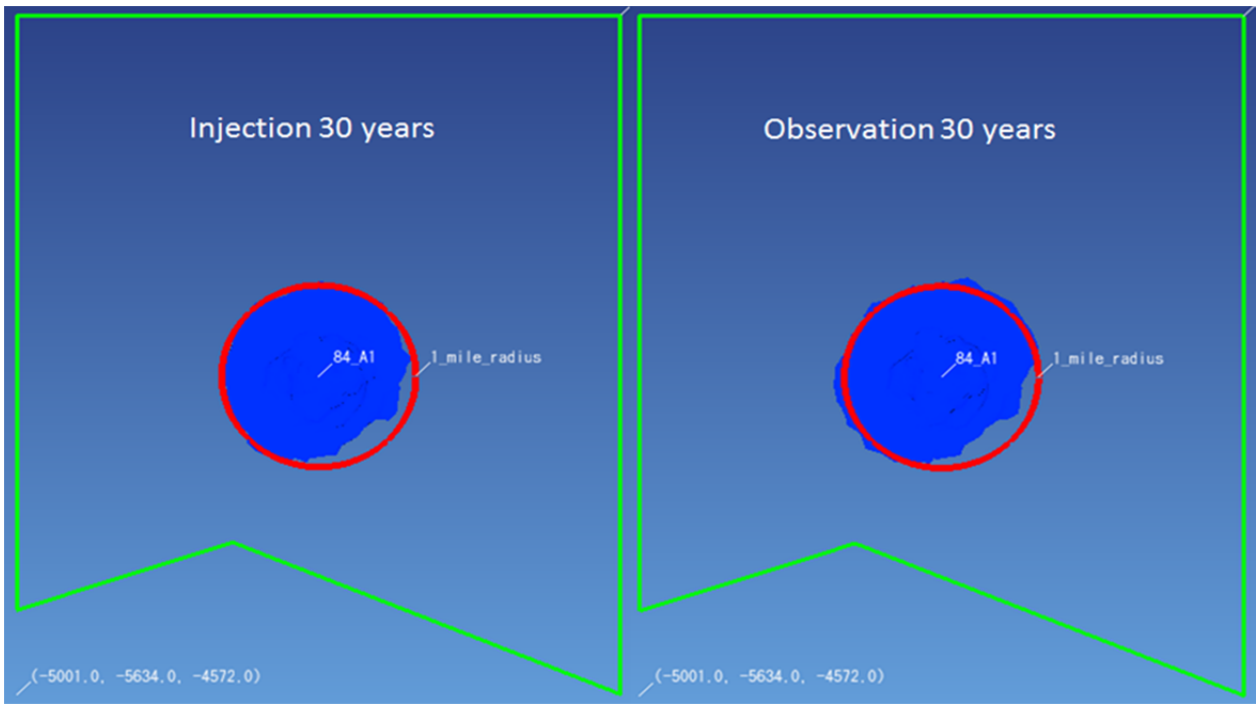

Figure 92: The top view of CO2 Gas plume after 30 years injection, and 30 years observation, 84_M_sim02 of Upper Miocene, Ship Shoal Block 84 field

5.2.2.2.4 No capillary pressure (84_M_sim03) result

To simulate the worst case scenario, we assume there is no capillary pressure in all the formations -- that the CO_2 can easily migrates upward to cause leakage, in case 84_M_sim03.

Figure 93 shows the cross-sections of gas saturation after 1 year, 15 years, 20 years and 30 years CO_2 injection, of the scenario 84_M_sim03 respectively. We can see that the CO_2 gas plume easily migrates upward and causes leakage during injection. We did not simulate the observation phase since leakage already occurred.

Figure 94 indicates the top view of CO_2 gas plume after 30 years injection, the scenario 84_M_sim03 leaks during injection. The gas plume of the critical scenario is within the 1 mile radius circle around the injection well.

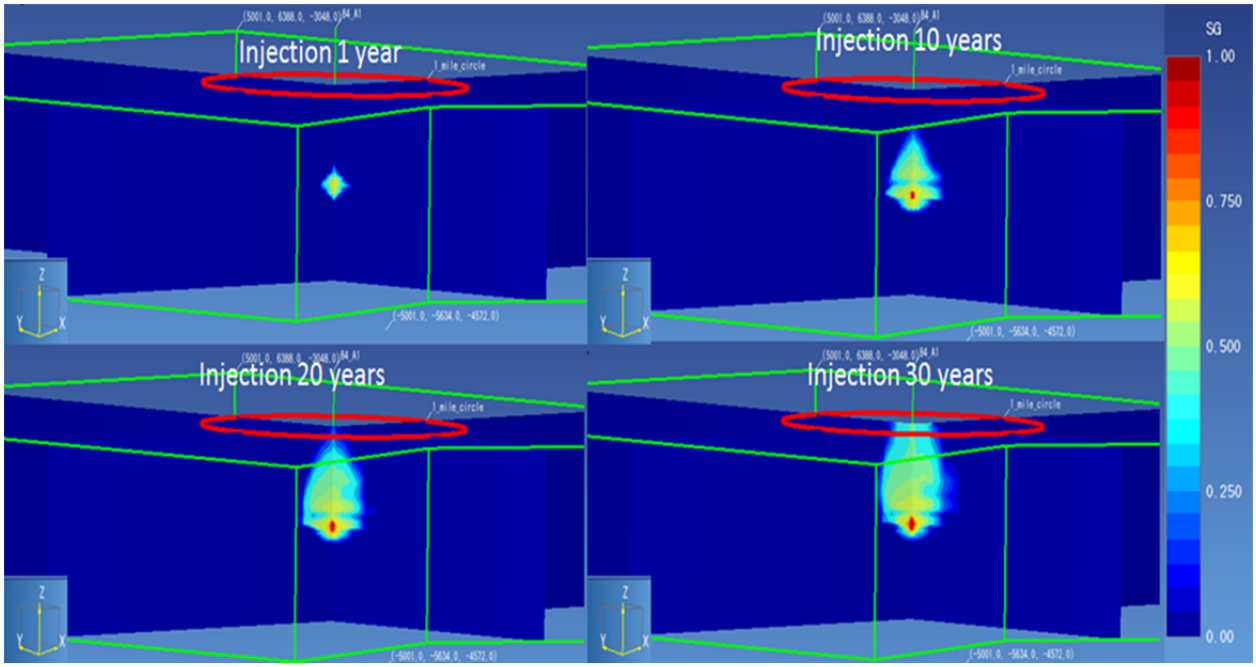

Figure 93: The cross-sections of Gas Saturation after 1, 10, 20, and 30 years injection, 84_M_sim03 of Upper Miocene, Ship Shoal Block 84 field

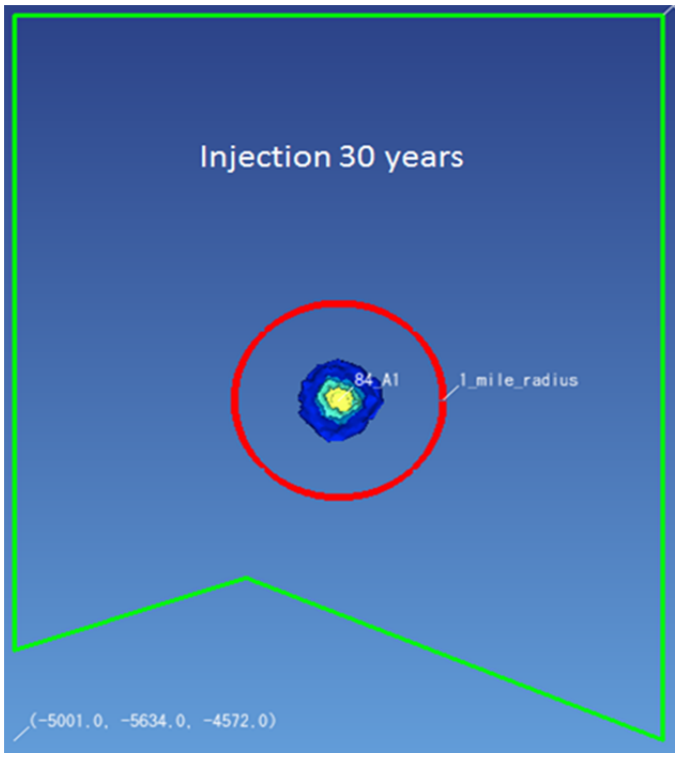

Figure 94: The top view of CO2 Gas plume after 30 years injection, 84_M_sim03 of Upper Miocene, Ship Shoal Block 84 field

5.2.2.2.5 Sandy model (84_M_sim04) result

To study influence of varying geology, we converted lithology silt to sand to increase the volume to store CO_2, in case 84_M_sim04.

Figure 95 shows the cross-sections of gas saturation after 1 year, 15 years, and 30 years CO_2 injection, and another 30 years of observation, of the scenario 84_M_sim04 respectively. We can see that CO_2 migrates about 500ft (152m) to the upper sand formation and is contained both during the injection and observation phases.

Figure 96 indicates the top view of CO_2 gas plume after 30 years injection and 30 years of observation, the scenario 84_M_sim04 respectively. Similar the scenario 84_M_sim02, the gas plume after 30 years injection is within the 1 mile radius circle, and it grows slightly in all directions except south-east during the observation phase; and it is a little bit beyond the 1 mile radius circle around the injection well, except in the south-east direction in the observation phase.

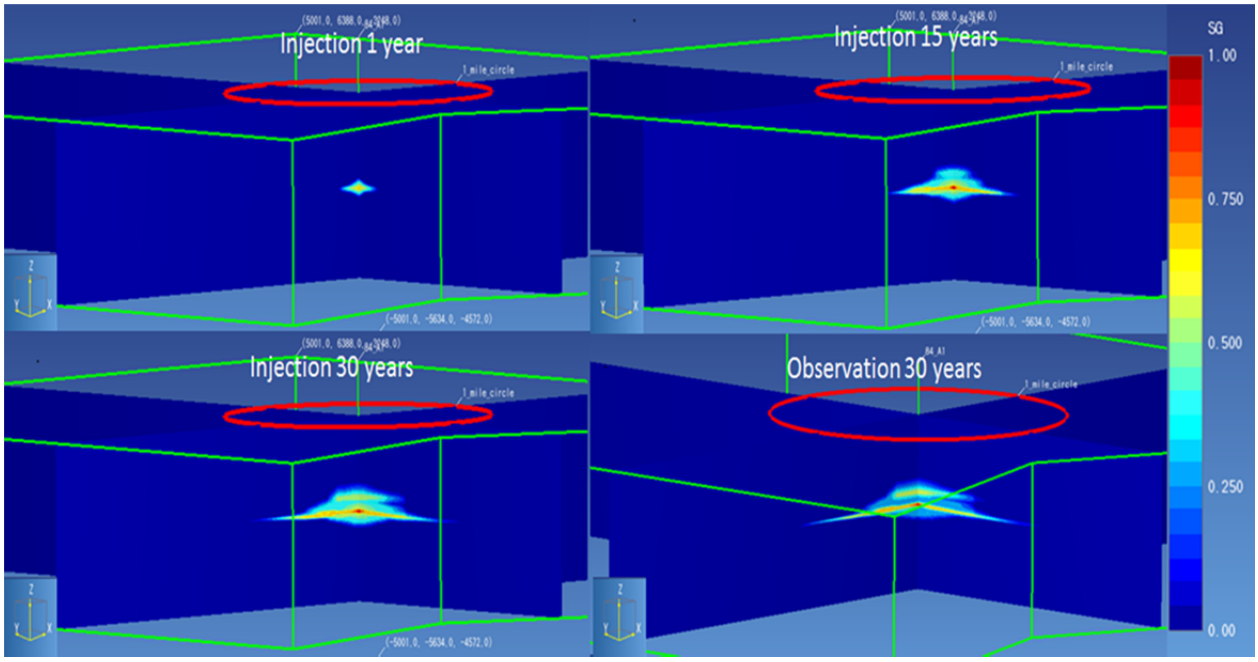

Figure 95: The cross-sections of Gas Saturation after 1, 15, 30 years injection, and 30 years observation, 84_M_sim04 of Upper Miocene, Ship Shoal Block 84 field

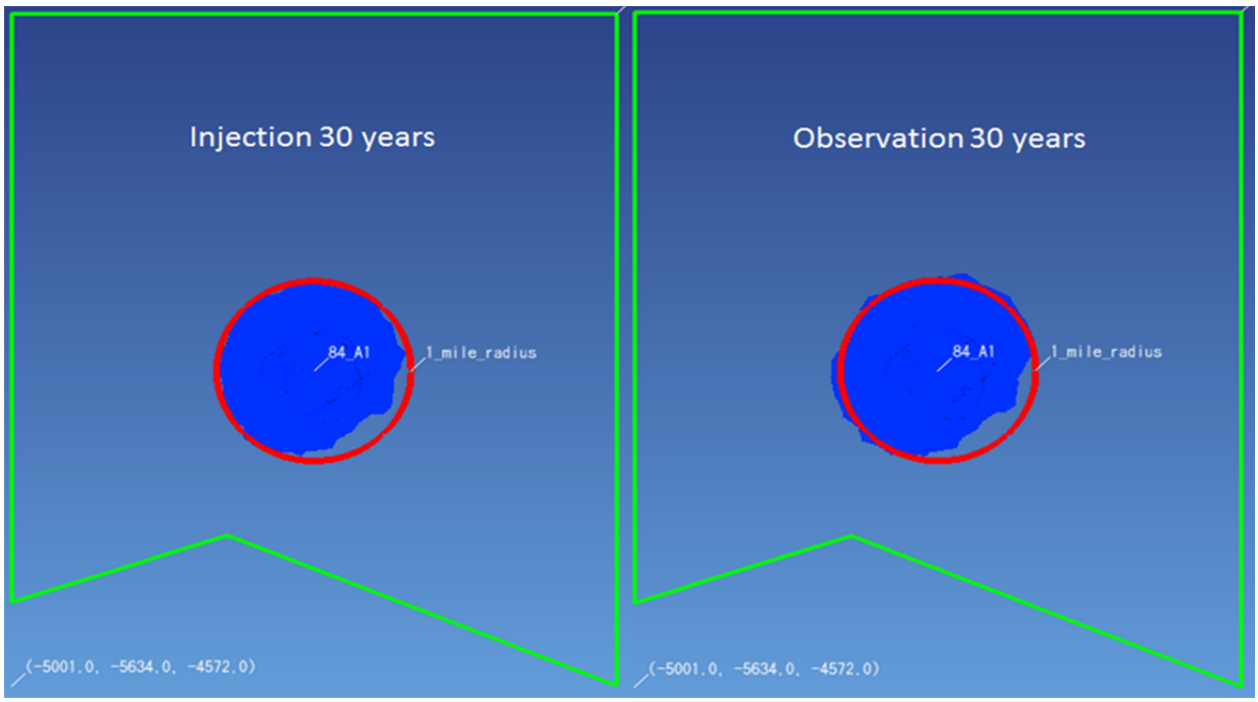

Figure 96: The top view of CO2 Gas plume after 30 years injection, and 30 years observation, 84_M_sim04 of Upper Miocene, Ship Shoal Block 84 field

5.2.2.2.6 Shaly model (84_M_sim05) result

To study the influence of varying geology, we converted lithology silt to shale in case 84_M_sim05.

Figure 97 shows the cross-sections of gas saturation after 1 year, 15 years, and 30 years CO_2 injection, and another 30 years of observation, of the scenario 84_M_sim05 respectively. We can see that CO_2 migrates about 500 ft (152 m) to the upper sand formation and is contained both during the injection and observation phases.

Figure 98 indicates the top view of CO_2 gas plume after 30 years injection and 30 years, of observation, the scenario 84_M_sim05 respectively. Similar the scenario 84_M_sim04, the gas plume after 30 years injection is within the 1 mile radius circle, and it grows slightly in all directions except south-east during the observation phase. It is a little bit beyond the 1 mile radius circle around the injection well, except in the south-east direction in the observation phase.

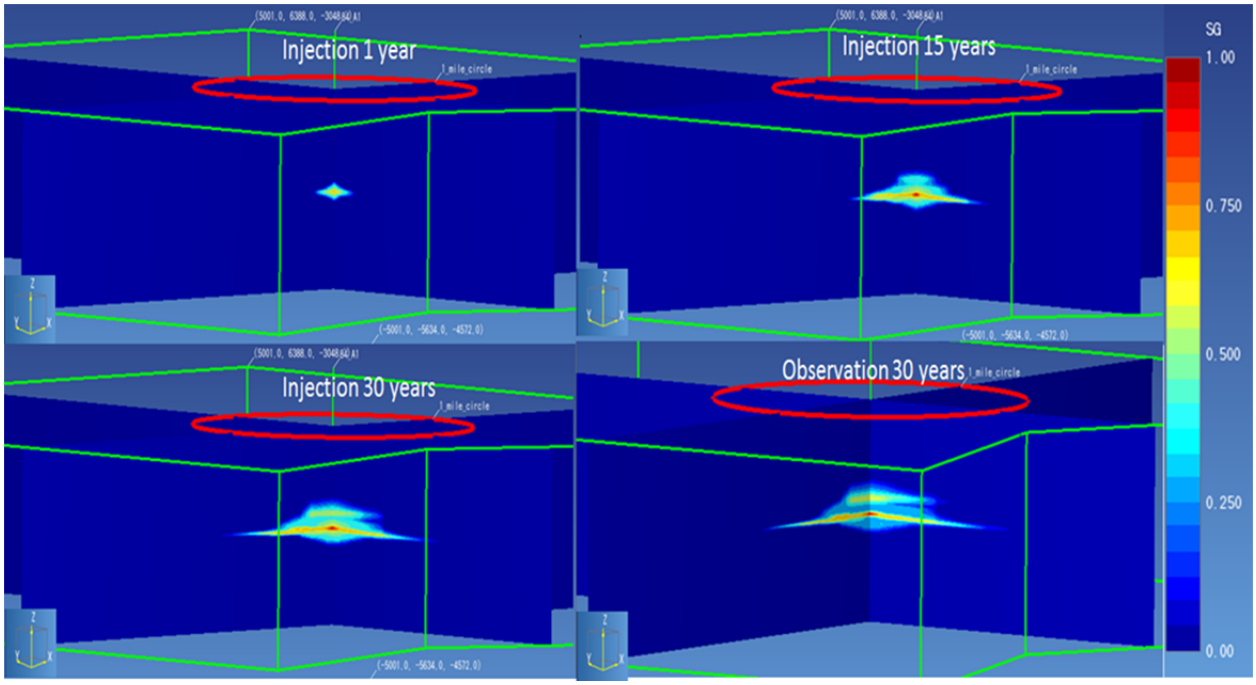

Figure 97: The cross-sections of Gas Saturation after 1, 15, 30 years injection, and 30 years observation, 84_M_sim05 of Upper Miocene, Ship Shoal Block 84 field

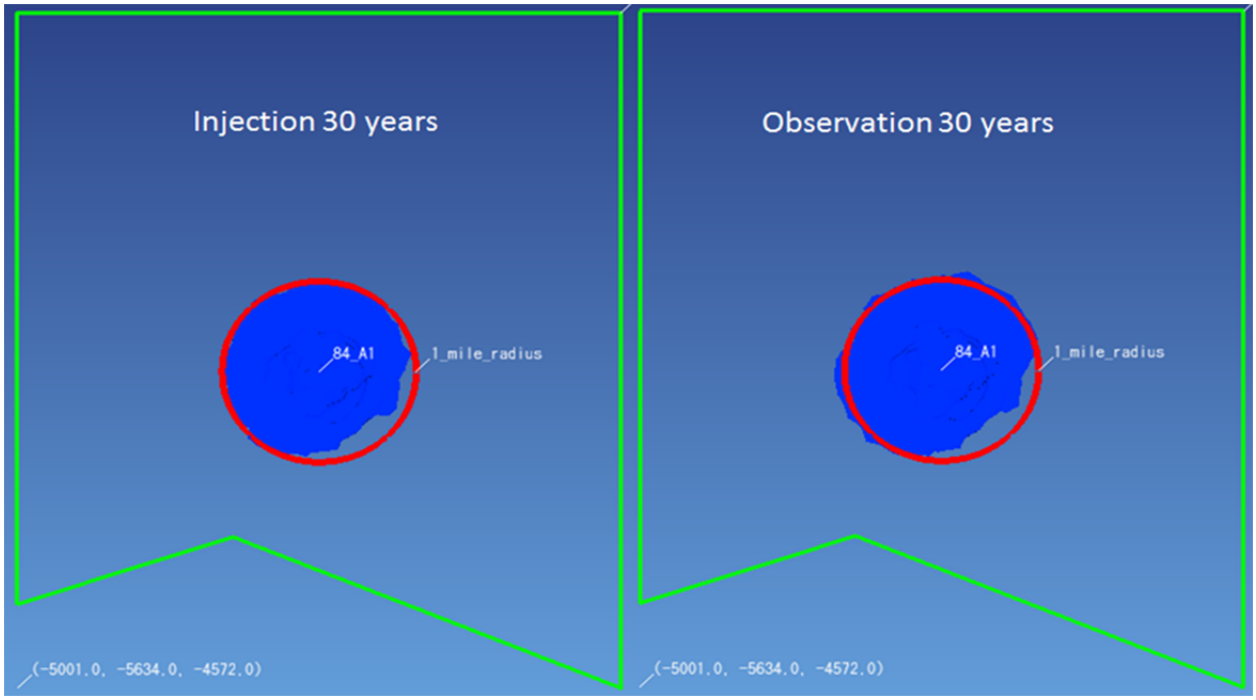

Figure 98: The top view of CO2 Gas plume after 30 years injection, and 30 years observation, 84_M_sim05 of Upper Miocene, Ship Shoal Block 84 field

5.2.2.2.7 Double injection rate (84_M_sim06) result

To study influence of varying injection rate, we doubled the injection from 1million metric ton per year to 2 million metric tons per year, in case 84_M_sim06.

Figure 97 shows the cross-sections of gas saturation after 1 year, 15 years, and 30 years CO_2 injection, and another 30 years of observation, of the scenario 84_M_sim06 respectively. We can see that CO_2 migrates about 1000 ft (305 m) to upper sand formation and is contained during injection, and it continues to migrate further up (1500 ft/457 m) but is still contained during the observation phase.

Figure 98 indicates the top view of CO_2 gas plume after 30 years injection and 30 years of observation, the scenario 84_M_sim06 respectively. The gas plumes are obviously beyond the 1 mile radius circle around the injection well after 30 years injection and observation, except in the south-east direction.

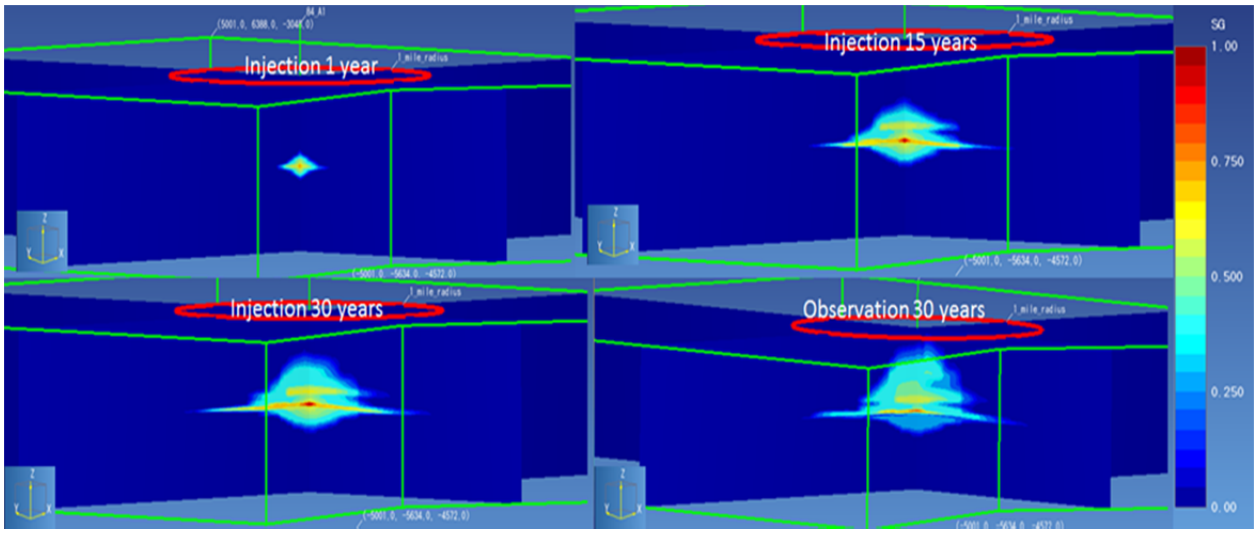

Figure 99: The cross-sections of Gas Saturation after 1, 15, 30 years injection, and 30 years observation, 84_M_sim06 of Miocene-isothermal, Ship Shoal Block 84 field

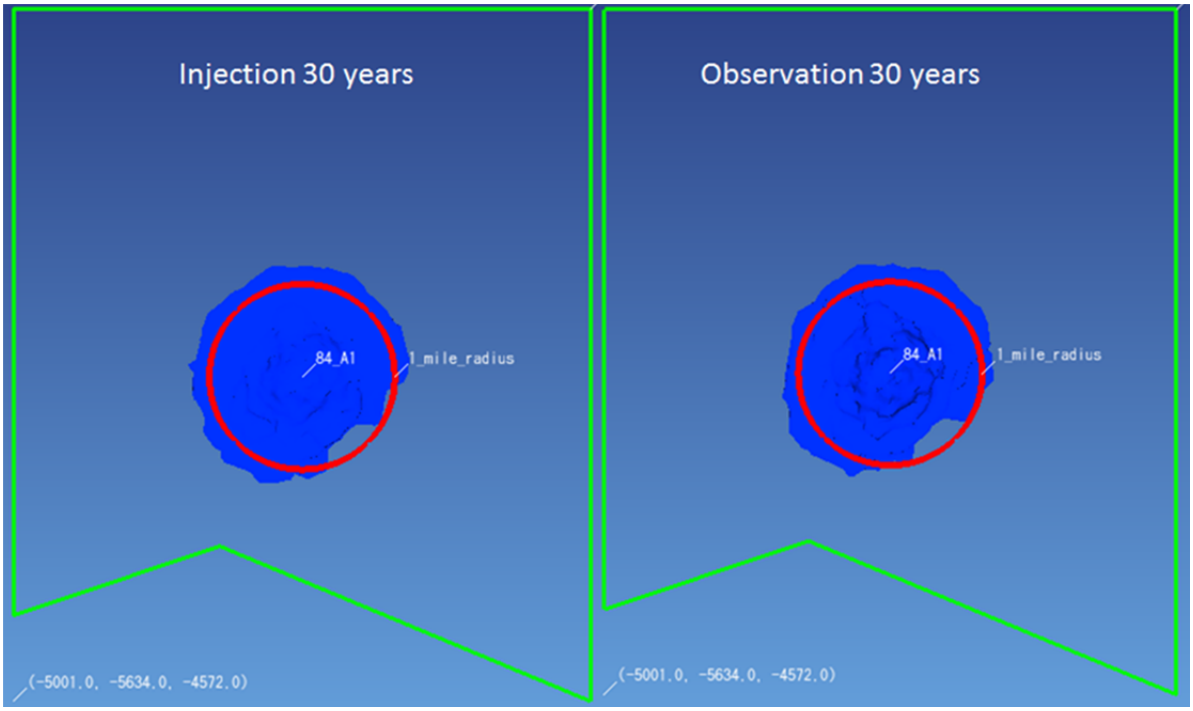

Figure 100: The top view of CO2 Gas plume after 30 years injection, and 30 years observation, 84_M_sim06 of Miocene-isothermal, Ship Shoal Block 84 field

5.2.2.2.8 Pressure profiles comparison

Figure 101 and Figure 102 indicate the comparison of pressure profiles across the injection well through the middle of the injection interval (=-3832.4 m or 12,604 ft), at in-situ conditions and after 30 years of injection, of the six isothermal scenarios. Maximum delta pressure observed is 2.1 MPa (305 psi), that is about 5.6% from in situ pore pressure. At a 1 mile distance from the injection well the maximum pressure increase observed is 84_M_sim06 (double injection rate), and 84_M_sim03 (contains no capillary pressure) has the lowest pressure after 30 years of constant CO_2 injection. 84_M_sim01 has higher pressure profile around injection well; while 84_M_sim02, 84_M_sim04 (sandy model) and 84_M_sim05 (contains more shale) have similar pressure profiles, since Miocene contains less silt, and that it does not make much difference to convert silt to sand or shale in the modeling.

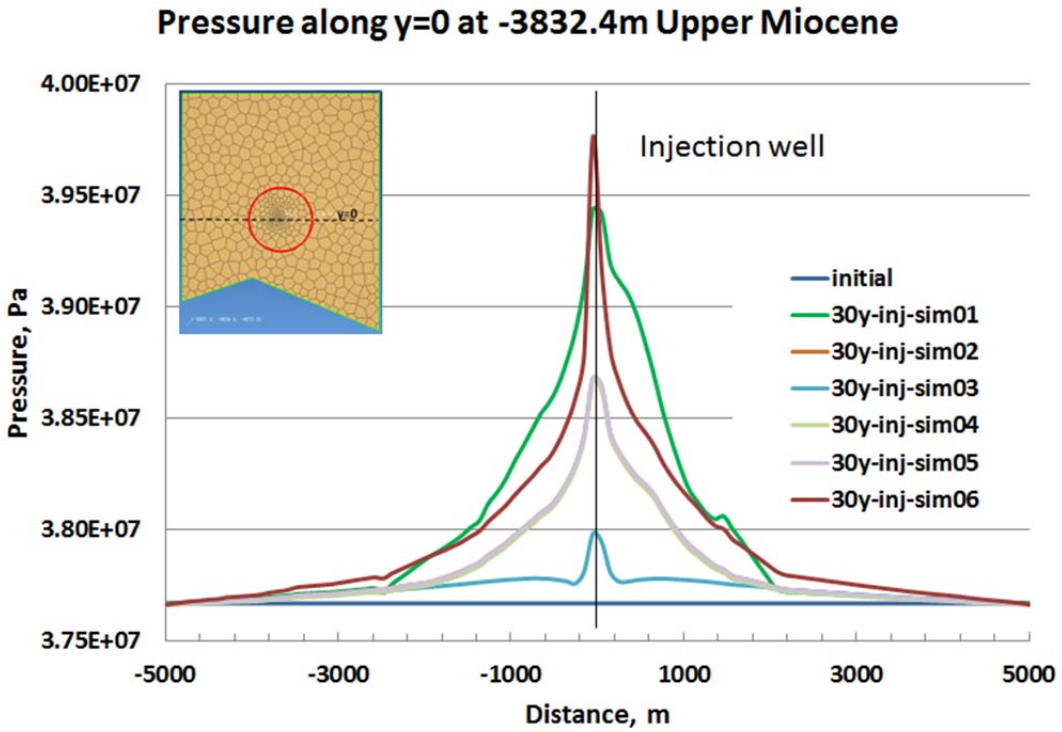

Figure 101: Comprison of pressure profiles across (y=0) injection well through the middle of injection interval, at initial and after 30 years injection into the Miocene-isothermal – Ship Shoal Block 84 field

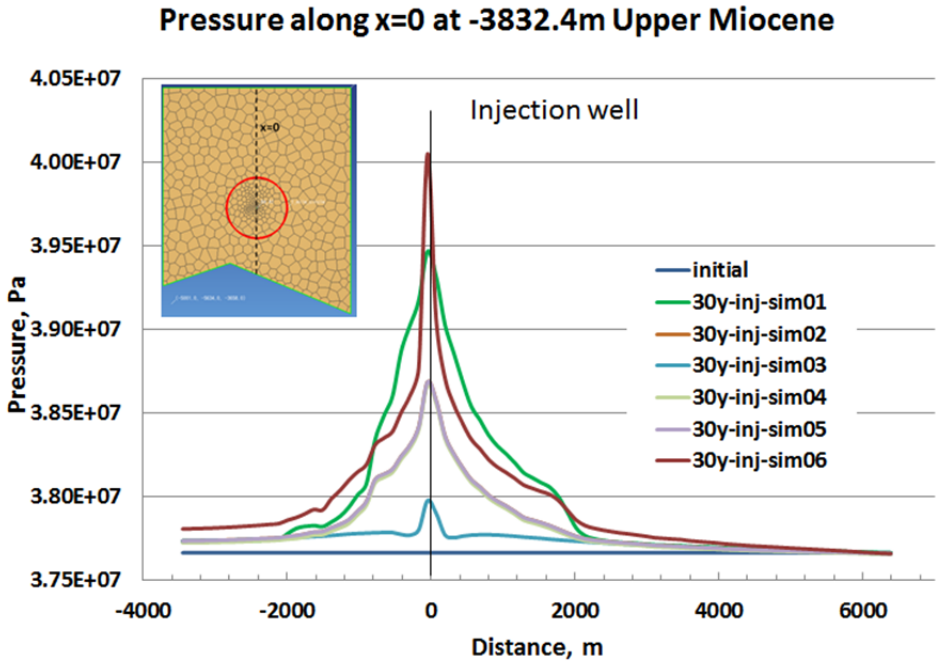

Figure 102: Comparison of pressure profiles across (x=0) injection well through the middle of injection interval, at initial and after 30 years injection into the Miocene-isothermal – Ship Shoal Block 84 field

5.2.2.2.9 Non-isothermal simulation result

Similar to Pliocene scenarios, after finishing all six isothermal simulations in Table 21, we ran each of them again with non-isothermal (injection CO_2 at 60 ^{0}C). 84_M_sim07 to 84_M_sim11 are injected at the rate of 1 million metric tons CO_2 per year to study the influence of formation heterogeneity on CO_2 injection; while 84_M_sim12 is injected at the rate of 2 million metric tons CO_2 per year to study injection rate effect. The 30 years' injection simulations ran smoothly, while all the observation simulations crashed at very early stage. Detailed analysis of this issue showed that numerical instability is given for the calculation of the solubility of CO_2 and CH_4 under the prevailing temperature and pressure conditions (> 350 bar and > 110 ^{0}C) and low amounts of CO_2 and CH_4 in place in certain areas. Since no different plume behavior regarding leakage in the observation phase is observed from the non-isothermal simulations in the Pliocene formation discussed in 5.2.2.1.9 the assumption is made that the behavior in the Miocene formation is similar when taking into account the temperature effect. Future detailed feasibility studies should considered using a different flow and heat simulator model.

We can see that the pressure profiles of the isothermal simulations are slightly higher around the injection well than the simulations taking into account the temperature effect in scenarios 84_M_sim07 and 84_M_sim12, the difference is less than 2%; for the other scenarios, pressure profiles with temperature effect are slightly higher than isothermal simulations, and the difference is about 1%. Results are analyzed and compared in Appendix B.

5.2.2.3 Summary Result for both Pliocene and Miocene Models

For the simulations performed for 30 years of injection at a rate of 1 million metric tons of CO_2 per year and 30 years of observation we observed the following:

For the scenarios injecting into the Pliocene formation, we can see that CO_2 is contained within the injection formation both during injection and observation phase (84_P_sim06 migrates up about 1,300ft (400m) around the wellbore from the injection interval), except in scenario 84_P_sim03. 84_P_sim03 represents the most critical case which assumes no capillary pressure in the sand, silt and shale, and the gas plume easily migrates upward during the injection and causes leakage in the observation phase. The assumption of assuming no capillary pressure is very conservative, thus unlikely to represent the real field conditions.

During the observation phase the gas plumes increase slightly during the observation phase, and they are all contained (or a tiny beyond during observation phase) within the 1 mile radius around the injection well. For the scenarios injecting into the Miocene formation, we can see that CO_2 is contained within the injection formation both during the injection and observation phase in the baseline case (84_M_sim01); CO_2 migrates about 500 ft (152 m) to the upper sand formation and stays contained both during the injection and observation phases in scenarios 84_M_sim02, 84_M_sim04 and 84_M_sim05; CO_2 migrates about 1000 ft (305 m) to the upper sand formation and contained during injection in scenario 84_M_sim06 when the injection rate is doubled, and it migrates further up (1500 ft/457 m) and stays contained during the observation phase; 84_M_Sim03 represents the most critical scenario which again assumes no capillary pressure in sand, silt and shale, and the gas plume easily migrates upward and causes leakage already during the injection phase, thus observation phase was not simulated. For scenario 84_M_sim01 and 84_M_sim06, after 30 years injection and observation both gas plumes are

obviously beyond the 1 mile radius circle around the injection well, except in the south-east direction. For scenario 84_M_sim02, 84_M_sim04 and 84_M_sim05, after 30 years injection the gas plumes are within the 1 mile radius circle, and they are slightly beyond the 1 mile radius after 30 years observation. The gas plume of the critical scenario 84_M_sim03 is within the 1 mile radius circle around injection well.

The summary of the modeling results are presented in Table 22 (isothermal runs) and Table 23 (non-isothermal runs).

Table 22: SS Block 84 field Fluid Flow- isothermal model summary results

field 84-scenarios-isothermal		permeability & porosity	Z-perm/XY-perm	capillary pressure	CO2 Lateral Migration Radius after 30 Years Injection (mile)	30 years' injection	30 years' observation
(baseline)	84_P_sim01	baseline	½	baseline	1	Contained	Contained
	84_M_sim01				1.1	Contained	Contained, fixed
(half porosity)	84_P_sim02	1/2 porosity in silt and shale compared to baseline	½	baseline	1	Contained	Contained
	84_M_sim02		1/10 in shale	lower in shale	1	Contained	Contained
(no capillary)	84_P_sim03	same as sim02	½	no	0.5	Contained	Leakage
	84_M_sim03				0.5	Leakage	
(sandy)	84_P_sim04	based on sim02, silt->sand	½	baseline	1	Contained	Contained
	84_M_sim04		1/10 in shale	lower in shale	1	Contained	Contained
(shaly)	84_P_sim05	based on sim02, silt->shale	1/10 in shale	lower in shale	1	Contained	Contained, fixed
	84_M_sim05		1/10 in shale	lower in shale	1	Contained	Contained
(double injection)	84_P_sim06	based on sim02	1/10 in shale	lower in shale	1	Contained	Contained
	84_M_sim06		1/5 in shale	lower in shale	1.1	Contained	Contained

Table 23: SS Block 84 field Fluid Flow- non-isothermal model summary results

field 84-scenarios-thermal		permeability & porosity	Z-perm/XY-perm	capillary pressure	CO2 Lateral Migration Radius after 30 Years Injection (mile)	30 years' injection	30 years' observation
(baseline)	84_P_sim07	baseline	½	baseline	1	Contained	Contained
	84_M_sim07		1/10 in shale	lower in shale	1	Contained	NA
(half porosity)	84_P_sim08	1/2 porosity in silt and shale compared	1/10 in shale	baseline	1	Contained	Contained
	84_M_sim08		1/10 in shale	lower in shale	1	Contained	NA
(no capillary)	84_P_sim09	same as sim02	½	no	0.5	Contained	Leakage
	84_M_sim09		1/10 in shale		0.7	Contained	NA
(sandy)	84_P_sim10	based on sim02, silt->sand	1/10 in shale	baseline	1	Contained	Contained
	84_M_sim10		1/10 in shale	lower in sand and shale	1	Contained	NA
(shaly)	84_P_sim11	based on sim02, silt->shale	1/10 in shale	lower in shale	1	Contained	Contained
	84_M_sim11		1/10 in shale	lower in shale	1	Contained	NA
(double injection)	84_P_sim12	based on sim02	1/10 in shale	lower in shale	1	Contained	Contained
	84_M_sim12		1/5 in shale	lower in shale	1.2	Contained	NA

5.3 Conclusions

The followings summarize the conclusions for both Miocene and Pliocene simulation from both Block 107 and Block 84:

- The 30 years of CO_2 injection (at a rate of 1 million metric tons CO_2 per year) and 30 years of observation simulations were performed for both Pliocene and Miocene Models in both Block 107 and Block 84 area. Different sensitivity scenarios including reservoir pressure, silt and shale permeability, relative permeability curve, salt effect, temperature effect, injection rate, and capillary pressure effect were also conducted.

- For Block 107, the results from the different sensitivity analyses indicate that Pliocene and Miocene are a good reservoir for the CO_2 sequestration. Most of the cases show that the CO_2 injected will be contained in either the Pliocene or the Miocene Formation. There is only one case with large injection rate (5 million ton per year) for 30 years indicating the potential leak of CO_2 out of the Pliocene Formation. However, this is just an extreme case that was used to evaluate the possible maximum pore pressure that could cause fault slippage and is not for real field practice purpose.
- For Block 84, the results show that almost all of the cases will be contained except for the case assuming no capillary pressure. The gas plume migrates upward during the injection and causes leakage in the observation phase. The assumption of no capillary pressure is very conservative, thus unlikely to represent the real field conditions.
- The reservoir in Block 107 seems to be better than those in Block 84. For the same injection parameters, the pressure increase in Block 84 will be twice as large as that in Block 107. However, the pressure increase in both Blocks does not seem significant. The maximum pressure change among all the scenarios is 5.6% increase compared to the original reservoir pressure.
- Injection into Pliocene tends to spread the plume more laterally in Block 107 compared to Miocene. On the other hand the lateral migration of the plume is very similar in Block 84 for both targets; only for two cases the lateral migration is slightly higher in the Miocene.
- The fluid flow simulation results for Block 107 and Block 84 show a very low risk of CO_2 leakage and a good containment of the injected CO_2 of 30 million metric tons within the 60 years of injection and observation simulated.

6 Geomechanical modeling

6.1 Geomechanics Material Parameters

The main parameters for geomechanical model development are the average bulk (K), shear (G) moduli and average uniaxial compressibility (Cm) for each stratigraphic unit. The Young's Modulus prescribes the magnitude of rock strain in one direction induced by stresses in the same direction. The Poisson's ratio (v) is a measure of the lateral expansion or contraction of the rock induced by stresses in the vertical direction. The material shear strength determines the amount of shear stress that the rock can withstand at a given confining load before failing and the friction angle prescribes how the shear strength increases with confining load.

The most accurate way to estimate rock properties is by direct laboratory measurements on core samples. However, no direct core measurements are available, so electric log data are used to estimate rock mechanical properties. The following estimated geomechanical material parameters for the Miocene and Pliocene formations are used for both Block 107 and 84.

Bulk Modulus:

For bulk modulus estimation, initial Young's modulus (E) was first determined for various stratigraphic formations from Exxon OCS-Block 123 G well-1 sonic and density logs as shown in Figure 103. Since no shear velocity wave logs are available for this well, we have assumed a dynamic Poisson's ratio (v) of 0.35 for the formations. Employing these two properties (E and v), bulk modulus can be calculated, and the resulting values are shown in Table 24.

Shear Modulus:

Similarly, for the shear modulus, the same two quantities are needed: Young's modulus (E) and the Poisson's ratios (v). Employing these two properties the shear modulus (G) can be calculated, and the resulting values are shown in Table 24.

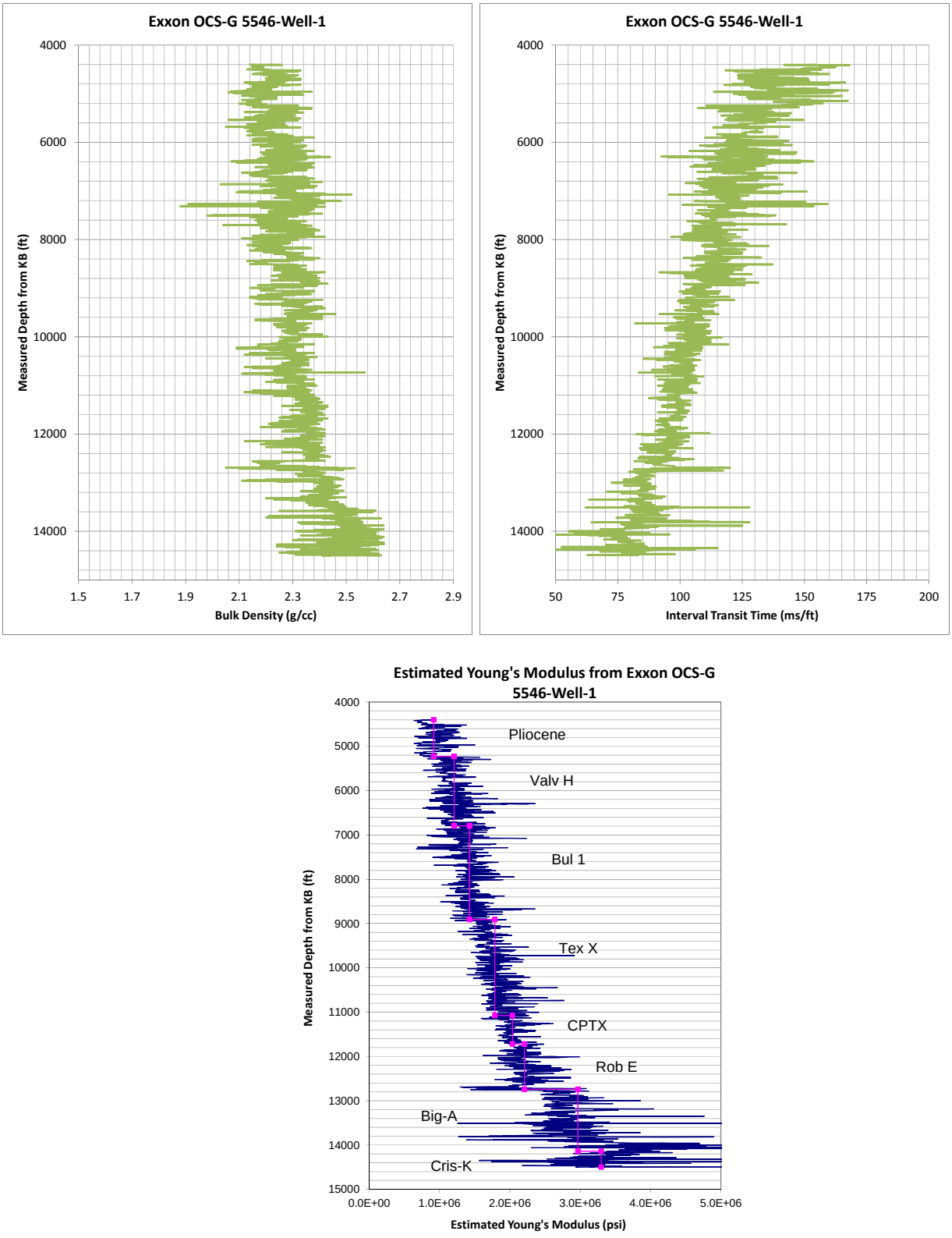

Figure 103: Estimated Dynamic Young's Modulus from Exxon OCS Block 123 G 5546-Well-1 Bulk Density Log (top left) and Sonic Log (top right).

Material properties for the Pliocene layers (Pliocene through CPTX) and Miocene layers (Rob E through Cris-K) are estimated based on velocity and density log data as described above. A summary table for the estimated average dynamic values from Exxon OCS-Block 123 G 5546 well-1 is presented in Table 24.

Table 24: Summary of Estimated Average Dynamic Values of Young's Modulus, Bulk Modulus and Shear Modulus from Exxon OCS-G 5546-Well-1 logs.

Formation	E (psi)	K (psi)	G (psi)
Pliocene	9.18E+05	1.02E+06	3.40E+05
Valv H	1.21E+06	1.34E+06	4.47E+05
Bul 1	1.43E+06	1.59E+06	5.28E+05
Tex X	1.79E+06	1.99E+06	6.62E+05
CPTX	2.04E+06	2.26E+06	7.54E+05
Rob E	2.21E+06	2.45E+06	8.17E+05
Big A	2.97E+06	3.30E+06	1.10E+06
Cris-K	3.30E+06	3.67E+06	1.22E+06

6.2 Ship Shoal Block 107 Field

6.2.1 Geomechanical Model Setup

GeoMechanics Technologies has developed a 3D geomechanical model for Block 107 of the Ship Shoal area, consistent with the geologic model and fluid flow TOUGH2 model boundaries (see Figure 28 and Figure 32). The dimension of the geomechanical model is rectangular with about 10,455 m (34,300 ft) in the easting by 9,205 m (30,200 ft) in northing direction, and from starting depth of about -6mss (20 ft) to about -6,096mss (20,000 ft) depth. The injection well is located near the center of the model (coordinate: 2,239,510 ft, 10,477,740 ft); and the injection zone is in the close proximity (within 500 m or 1640 ft) of three major normal faults as shown in Figure 104. The geomechanical model has approximately 98,000 elements total, with finer mesh near the injection well within the injection intervals. The minimum cell dimensions in the lateral directions are about 60 m by 60 m (196 ft by 196 ft), and the minimum vertical cell dimension is about 50 m near the injection zones. The cell dimensions increase toward the model boundaries, with a maximum cell dimension of approximately 600 m (1968 ft) in the lateral direction and 200 m (656 ft) in the vertical direction. We applied roller boundary conditions on all surfaces except for the top seafloor surface, which is free to move in both vertical and lateral directions. Two injection interval baseline scenarios have been simulated: the base of Pliocene formation and at the upper Miocene formation as identified in the fluid flow model above.

Geomechanical model inputs and results for both base Pliocene injection and upper Miocene injection baseline scenarios are described in the following sections.

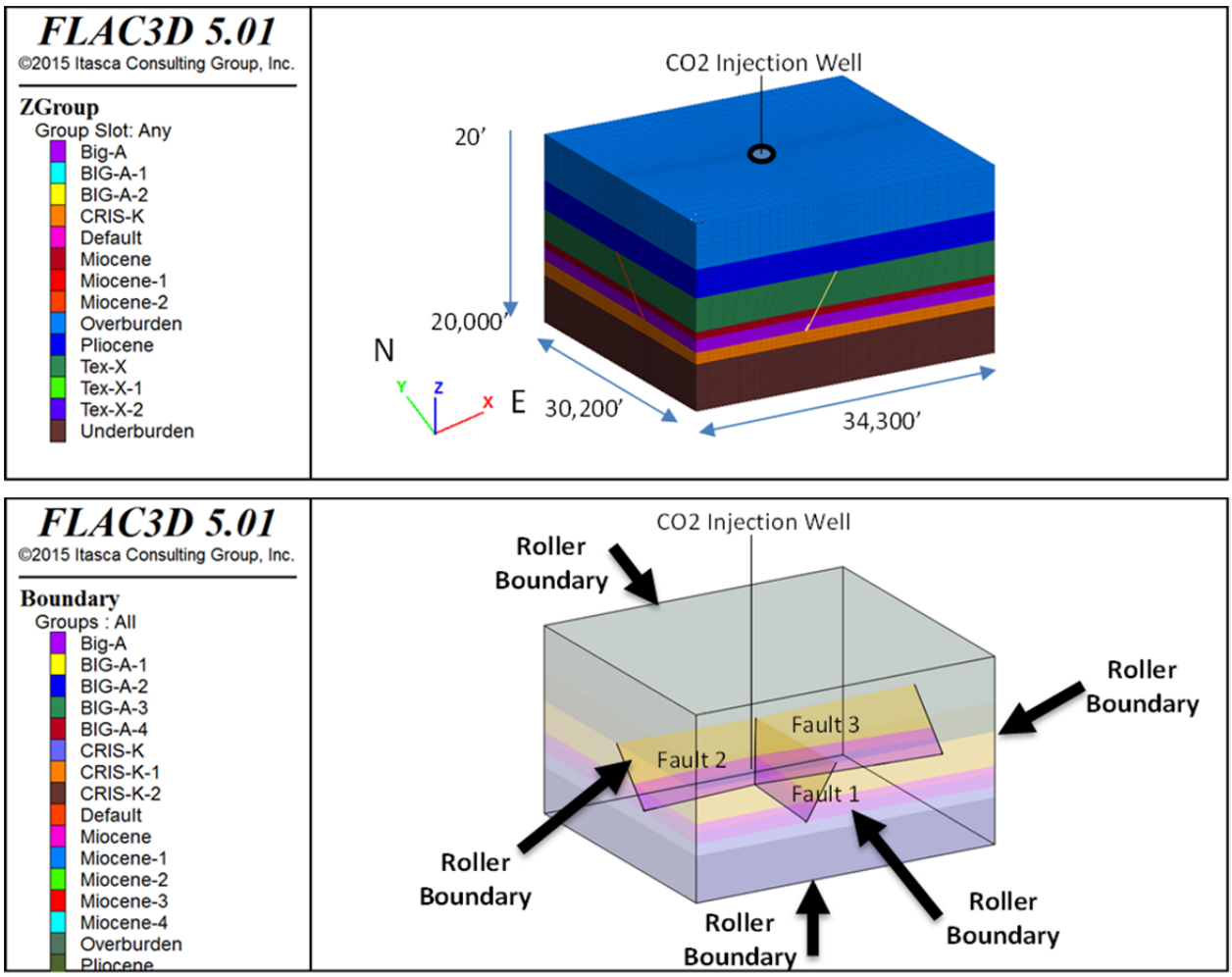

Figure 104: (Top) 3D-Geomechanics model for Ship Shoal area. (Bottom) Three major fault blocks (as labeled within the model) are included near the injection well.

6.2.2 Simulation Matrix

A total of six 3D-geomechanical model simulations are performed for Block 107 base Pliocene and upper Miocene injection scenarios, including potential fault reactivation were evaluated for each injection location. For base Pliocene injection, the baseline scenario (107_P_Sim01) and the largest pressure change scenario (107_P_Sim03) determined from the fluid flow results are selected for geomechanical modeling study. Likewise, for upper Miocene injection, the baseline scenario (107_M_Sim01) and the largest pressure change scenario (107_M_Sim02) determined from the fluid flow results are selected. To evaluate potential fault reactivation, sensitivity analyses are being performed for both the base Pliocene and upper Miocene geomechanical models. Table 25 shows the sensitivity runs of all cases with the description details from the fluid flow models.

Table 25: Geomechanical model simulation matrix for Block 107 base Pliocene and upper Miocene injection scenarios.

Model	Scenarios	PP Gradient (psi/ft)	Shale/Silt Permeability
Pliocene	107_P_Sim01 **(Baseline)**	0.435	Set minimum to 10md
	107_P_Sim03 (Different PP Gradient)	**0.3**	Set minimum to 10md
	107_P_Fault-Reactivation	0.435	Set minimum to 10md
Miocene	107_M_Sim01 **(Baseline)**	0.435	Set minimum to 10md
	107_M_Sim02 (Different Permeability for silt and shale)	0.435	**Use original value from log correlation (around 1 md)**
	107_M_Fault-Reactivation	0.435	Set minimum to 10md

6.2.3 Base Pliocene Geomechanics Model Simulation-01, Baseline

The simulation pressure inputs and induced stress and displacement results for the base Pliocene geomechanical model baseline injection scenario (107_P_Sim01) are described below.

Figure 105 shows the change in pressure distribution across the injection well in N-S and E-W directions, after 30 years of injection. These pressure data are directly imported from the fluid flow model to the geomechanical model. The highest pressure increase is observed near the injection interval, with maximum magnitude of about 5.6E5 Pa (81 psi).

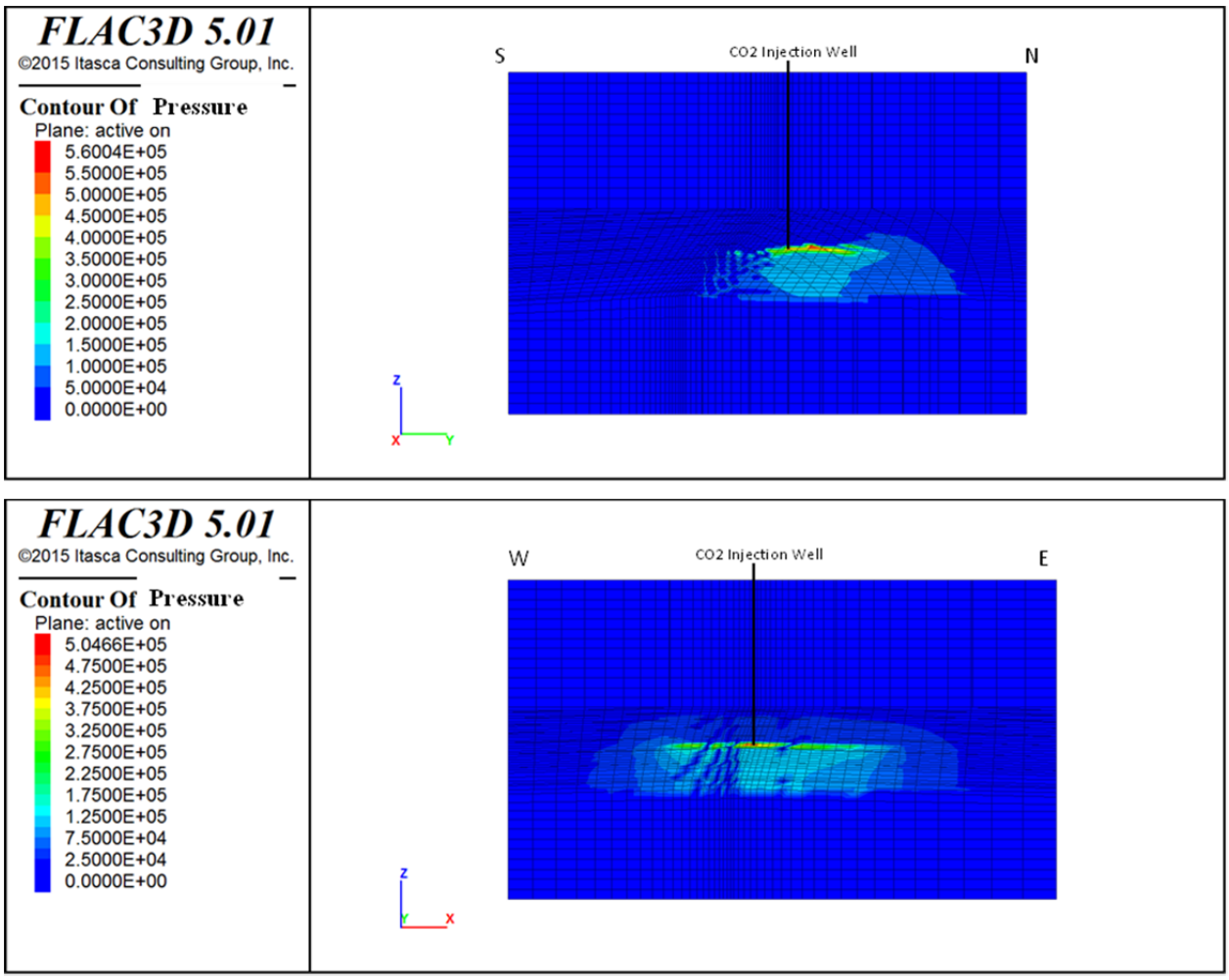

Figure 105: Change in pressure distribution (Pascal) after 30 years of injection in N-S (above) and E-W (below) directions across the injection well (Base Pliocene Injection – Sim01).

Figure 106 presents the contour plots of induced horizontal shear stress across the injection well in N-S direction (Sxz in y-plane) and in E-W direction (Syz in x-plane), respectively; showing the maximum induced shear stresses of about 1.2E4 Pa (< 2 psi), due to the pressure change after 30 years of CO_2 injection.

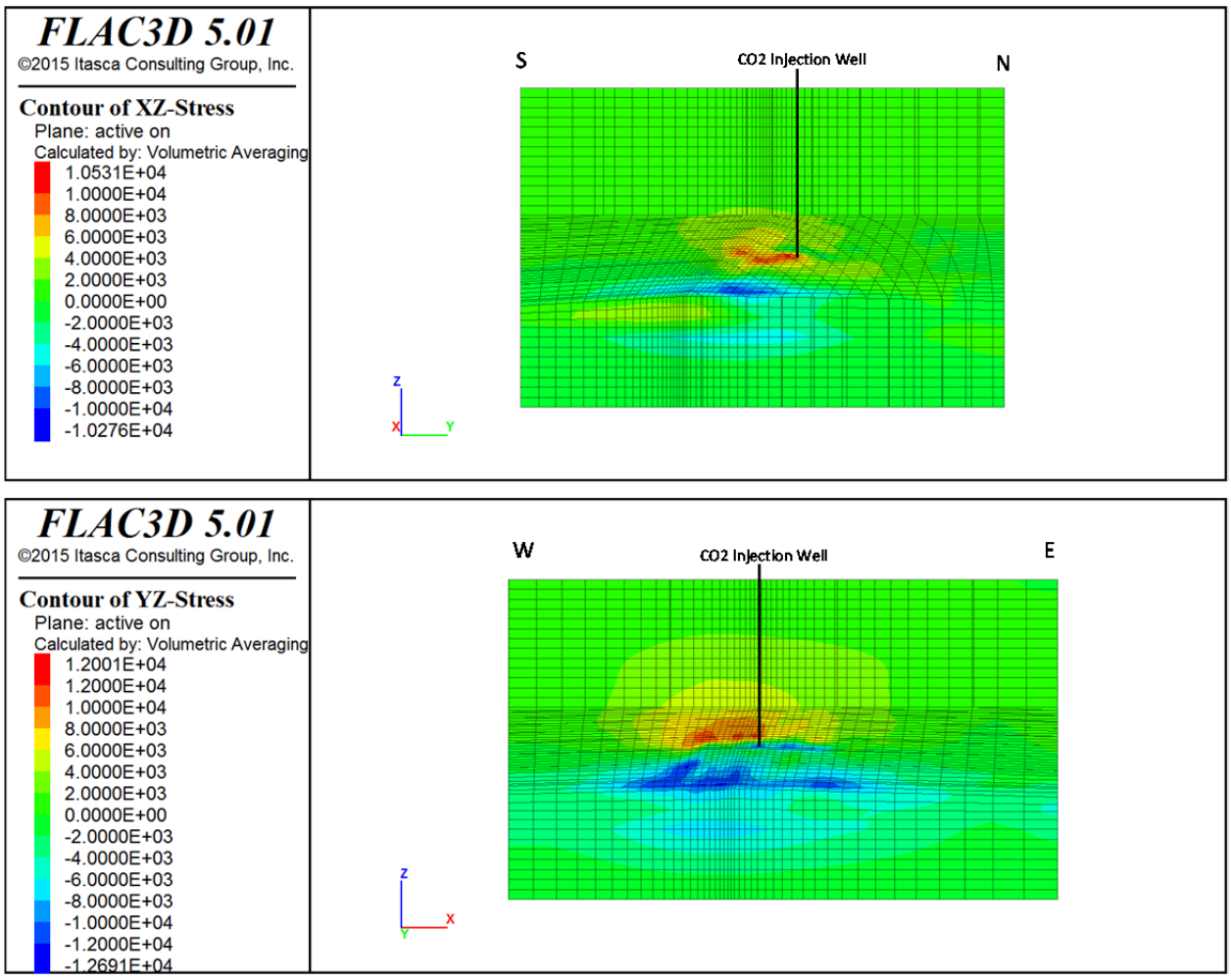

Figure 106: Plot of induced shear stress (Pascal) after 30 years of injection in N-S, (SXZ, above) and E-W (SYZ, below) directions across the injection well (Base Pliocene Injection – Sim01).

Figure 107 shows the resulting induced vertical Z-displacement in isometric view (above) and in cross-section view (below) across the injection well in E-W direction. The maximum surface uplift is toward the north of the injection well, with a maximum value of about 0.49 cm (0.19 in). The center of the maximum surface uplift bowl is spread across in a wide area, at over 3 miles (4.8 km) diameter. The results indicate low to no risks for fault slips or fault reactivation for this injection scenario after 30 years of CO_2 injection and migration with these relatively small induced stresses and strains.

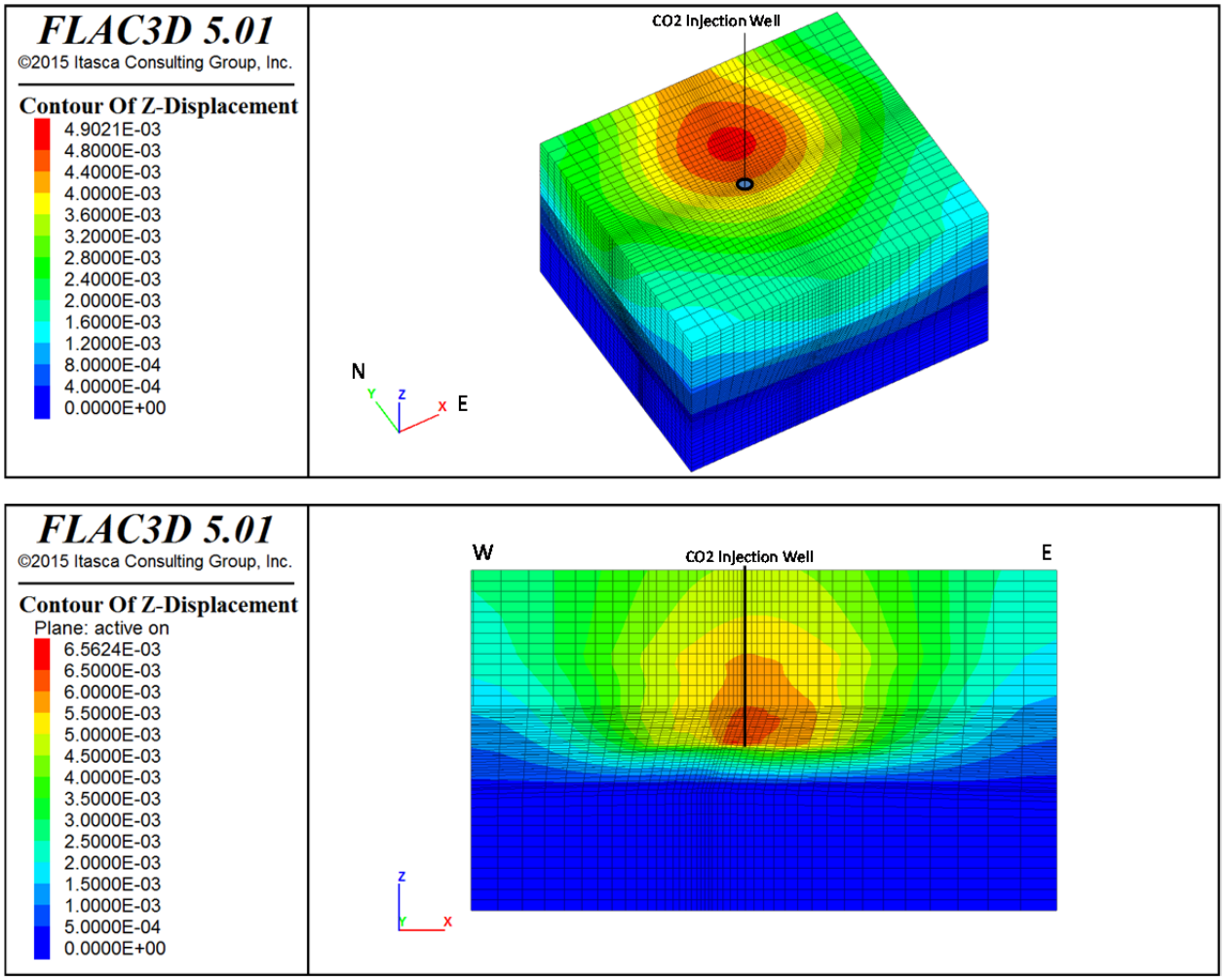

Figure 107: Plot of induced vertical displacement (meter) in 3D-view (above) and in E-W (below) direction across the injection well (Base Pliocene Injection – Sim01).

6.2.4 Upper Miocene Geomechanics Model Simulation-01, Baseline

For the upper Miocene geomechanical model baseline injection scenario, the simulation pressure input and induced stresses and displacement results are described next.

The change in pressure distribution across the injection well in N-S and E-W directions, after 30 years of injection at upper Miocene formation, is shown in Figure 108 below. This pressure data was transferred and used as input from the fluid flow model to the geomechanical model. Similar to the CO_2 migration pattern, the corresponding pressure increased localized area is above the injection interval, with maximum magnitude of about 4.26E5 Pa (62 psi).

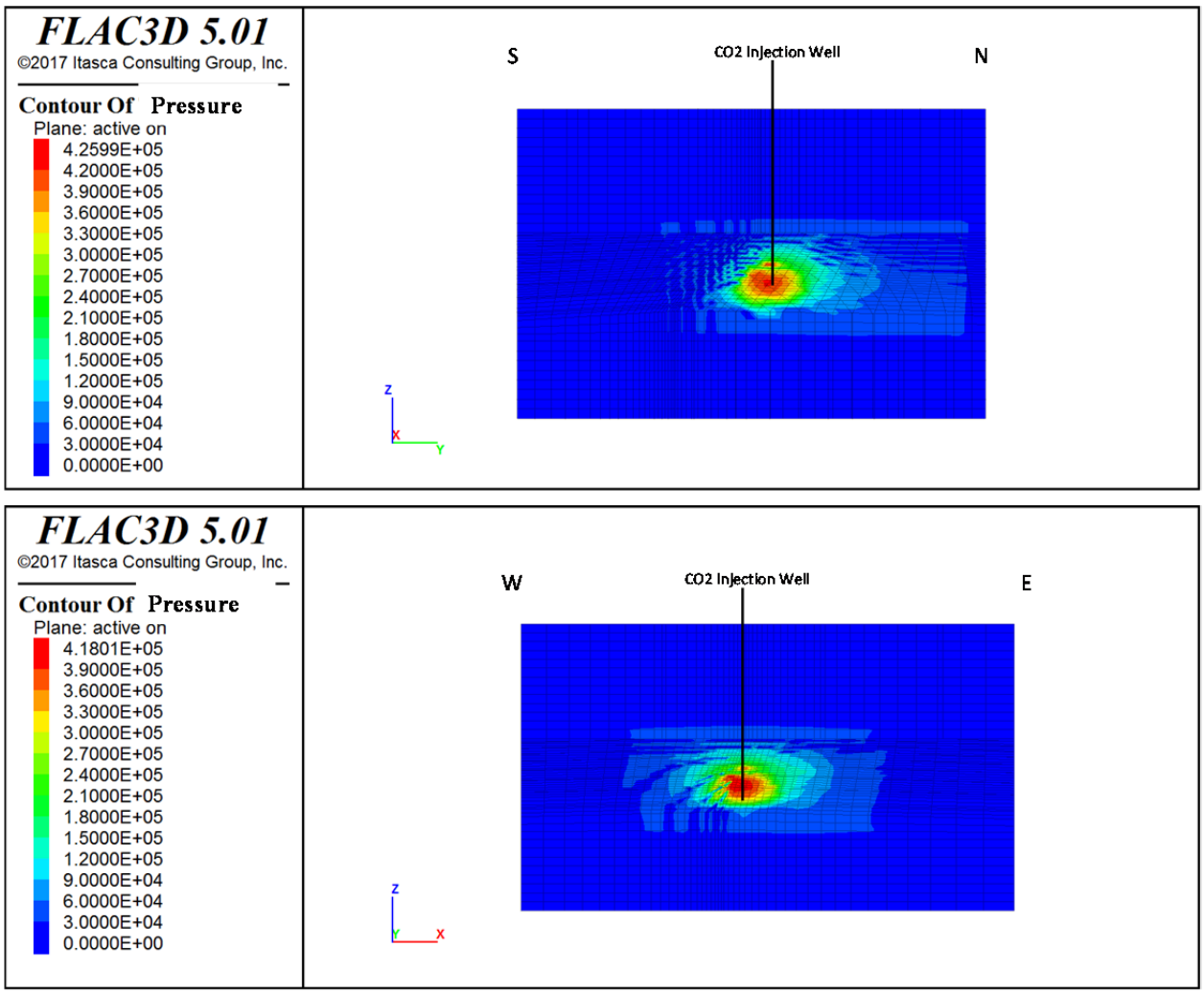

Figure 108: Change in pressure distribution (Pascal) after 30 years of injection in N-S (above) and E-W (below) directions across the injection well (Upper Miocene Injection – Sim01).

Figure 109 presents the contour plots of induced horizontal shear stress across the injection well in the N-S direction (Sxz in y-plane) and the E-W direction (Syz in x-plane), respectively; showing maximum induced shear stresses of about 2.1E4 Pa (~ 3 psi), due to the pressure change after 30 years of CO_2 injection.

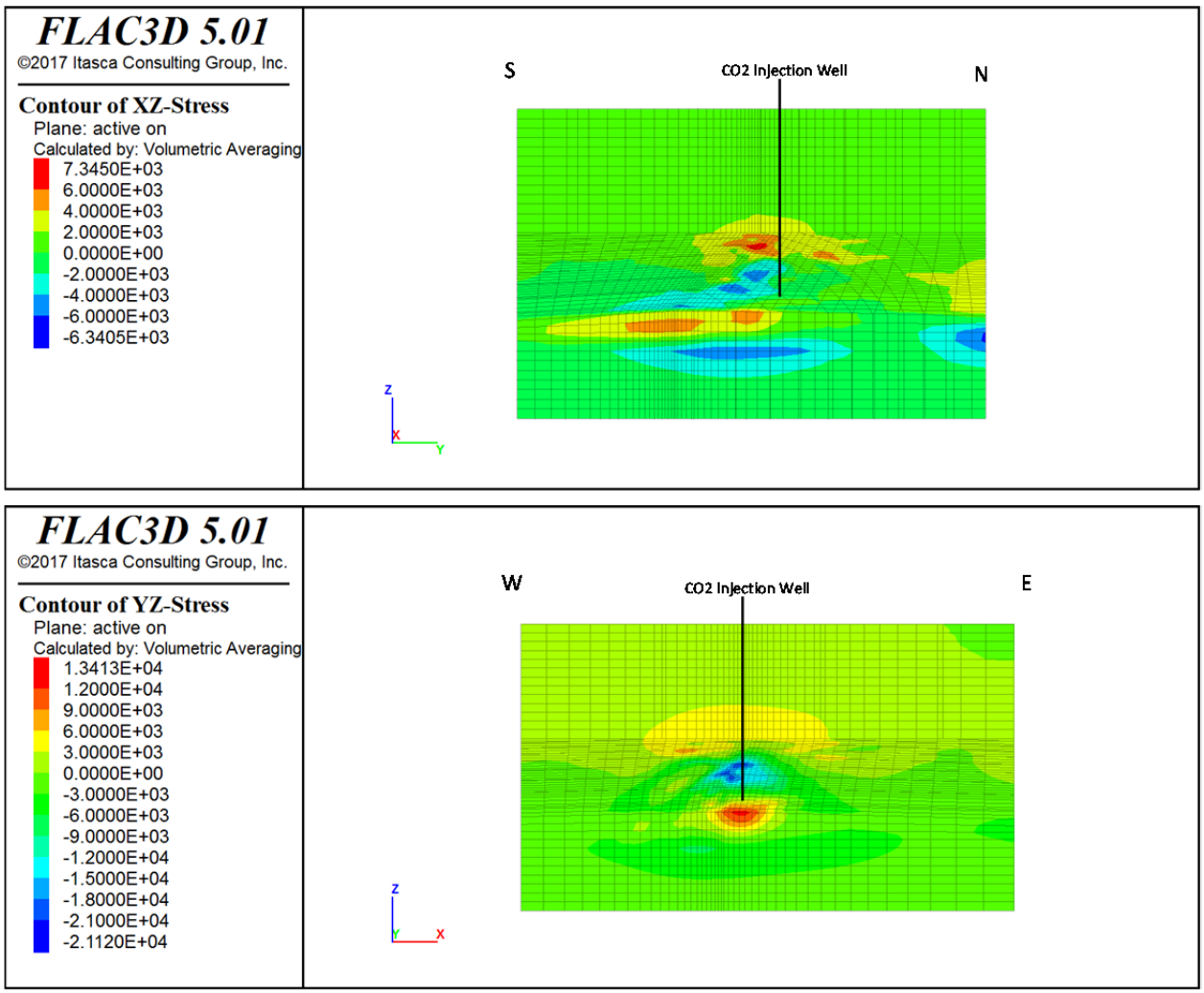

Figure 109: Plot of induced shear stress (in Pascal) after 30 years of injection in N-S, (SXZ, above) and E-W (SYZ, below) directions across the injection well (Upper Miocene Injection – Sim01).

Finally, the resulting induced vertical displacement in isometric view (above) and cross-section view (below) across the injection well in E-W direction is shown in Figure 110. Similar to the upper Pliocene simulation displacement bowl results, the maximum surface uplift is toward the north of the injection well, with a maximum value of about 0.55 cm (0.21 in). The center of the maximum surface uplift bowl is spread across in a wide area, at over 2 miles (3.2 km) diameter. Even with very weak fault mechanical properties assumptions, the results indicate there is very low to no risk of fault slippage or fault reactivation for this upper Miocene injection scenario after 30 years of CO_2 injection and migration with these relatively small induced stresses and strains.

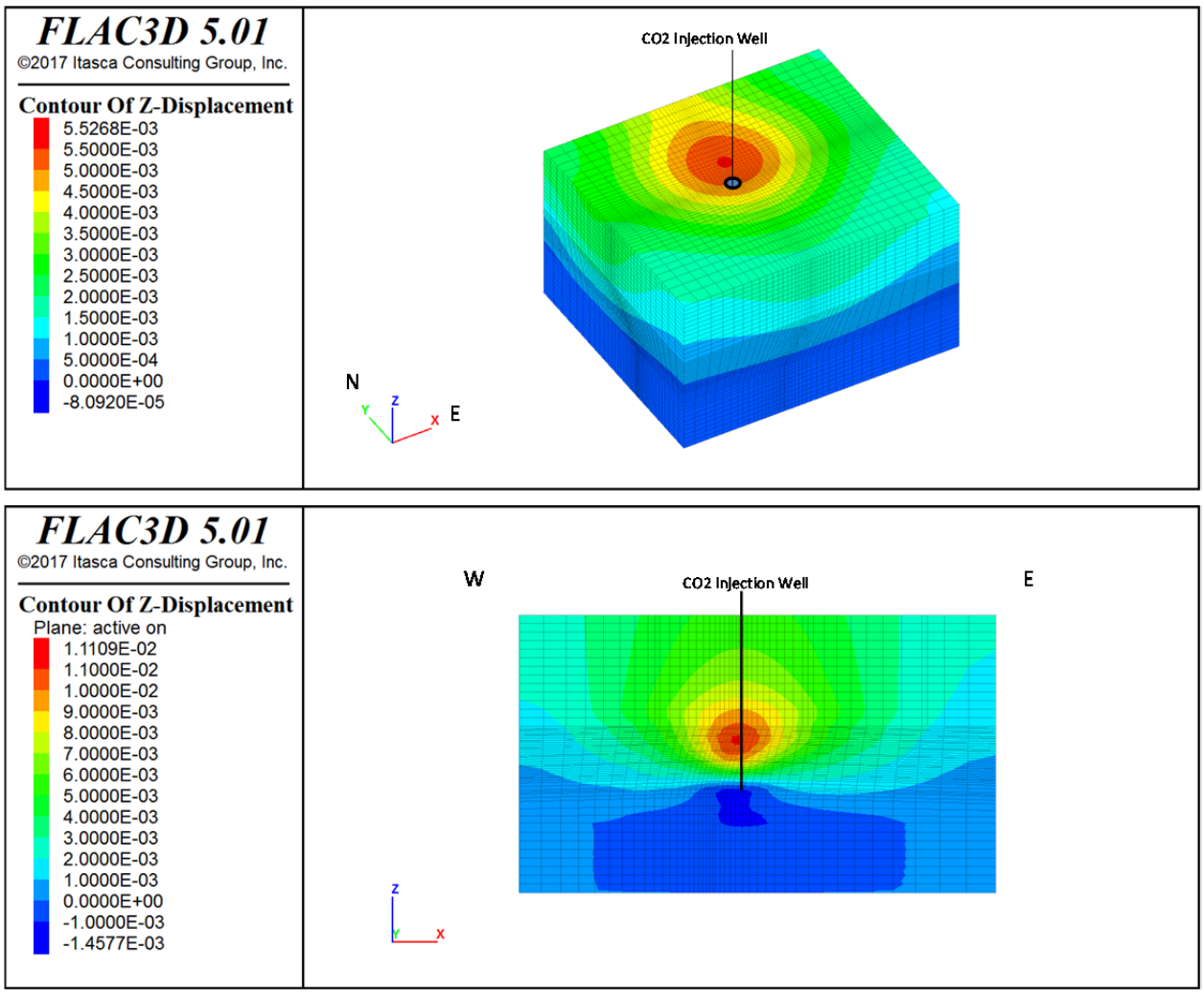

Figure 110: Plot of induced vertical displacement (meter) in 3D-view (above) and in E-W (below) direction across the injection well (Upper Miocene Injection – Sim01).

6.2.5 Pliocene Geomechanics Model Simulation-03, with Different Pore Pressure Gradient)

For one 3D geomechanical model sensitivity study of Block 107, GeoMechanics assumed a reduced or depleted reservoir in-situ pore pressure from 0.435 psi/ft to 0.30 psi/ft. The simulation pressure inputs from fluid flow modeling and the resulting induced stress and displacement for the base Pliocene injection scenario with depleted in-situ reservoir pressure are described below. We continue to investigate induced subsurface stresses and displacements and potential fault reactivation.

As before, pressure data are directly imported from the fluid flow model to the geomechanical model for geomechanical study. Figure 111 shows the change in pressure distribution across the injection well in N-S and E-W directions, after 30 years of injection. The highest pressure increased concentration area is near the injection interval, with maximum

magnitude of about 5.46E5 Pa (79 psi). With this scenario, no significant pressure distribution or absolute magnitude differences from the baseline scenario are evident.

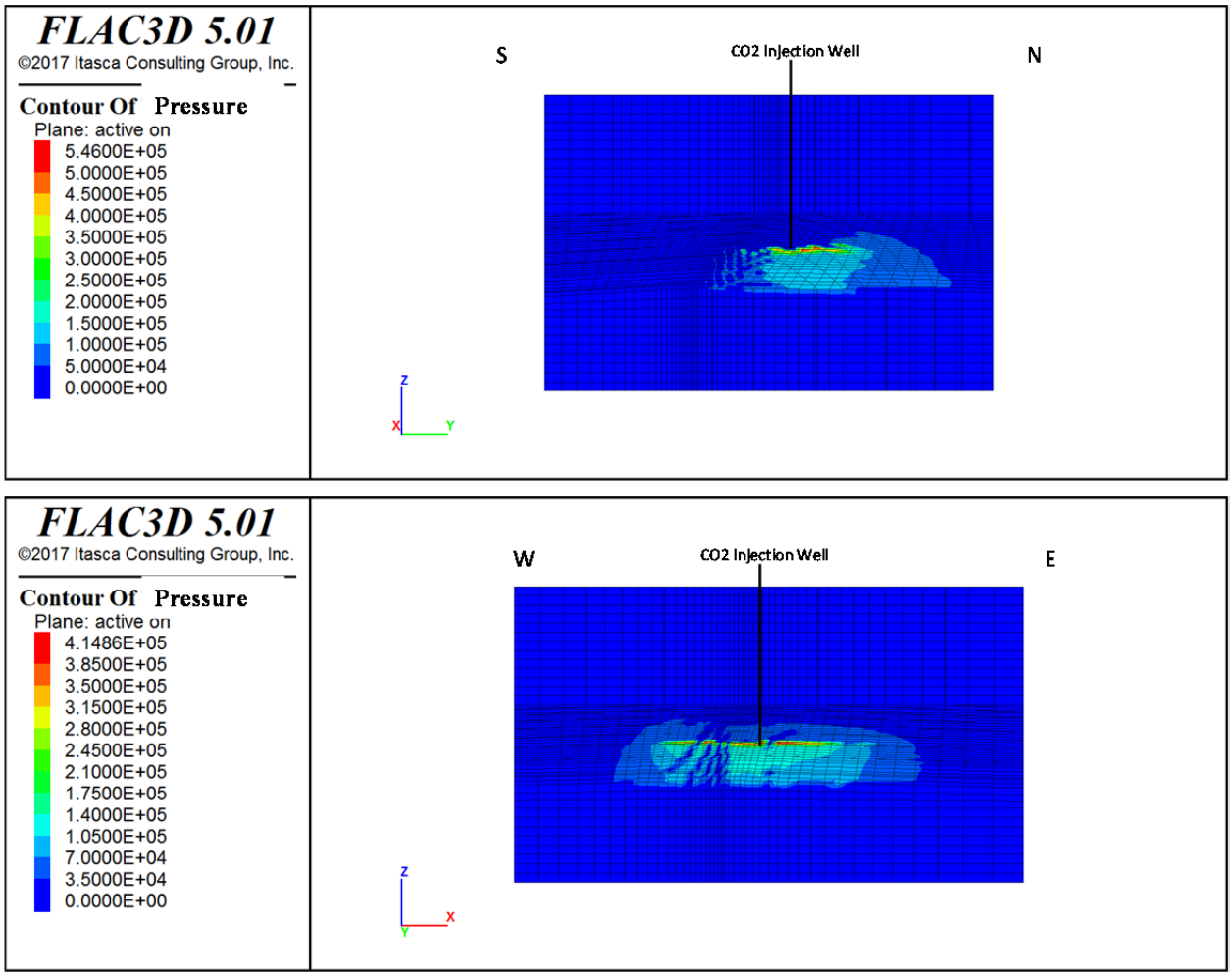

Figure 111: Change in pressure distribution (Pascal) after 30 years of injection in N-S (above) and E-W (below) directions across the injection well (Pliocene injection – Sim03).

Figure 112 presents the contour plots of induced horizontal shear stress across the injection well in the N-S direction (Sxz in y-plane) and in the E-W direction (Syz in x-plane), respectively; showing the maximum induced shear stresses of about 1.35E4 Pa (< 2 psi), due to the pressure change after 30 years of CO_2 injection. This only represents a very small induced shear stress increase (<1 psi) similar to the baseline scenario results.

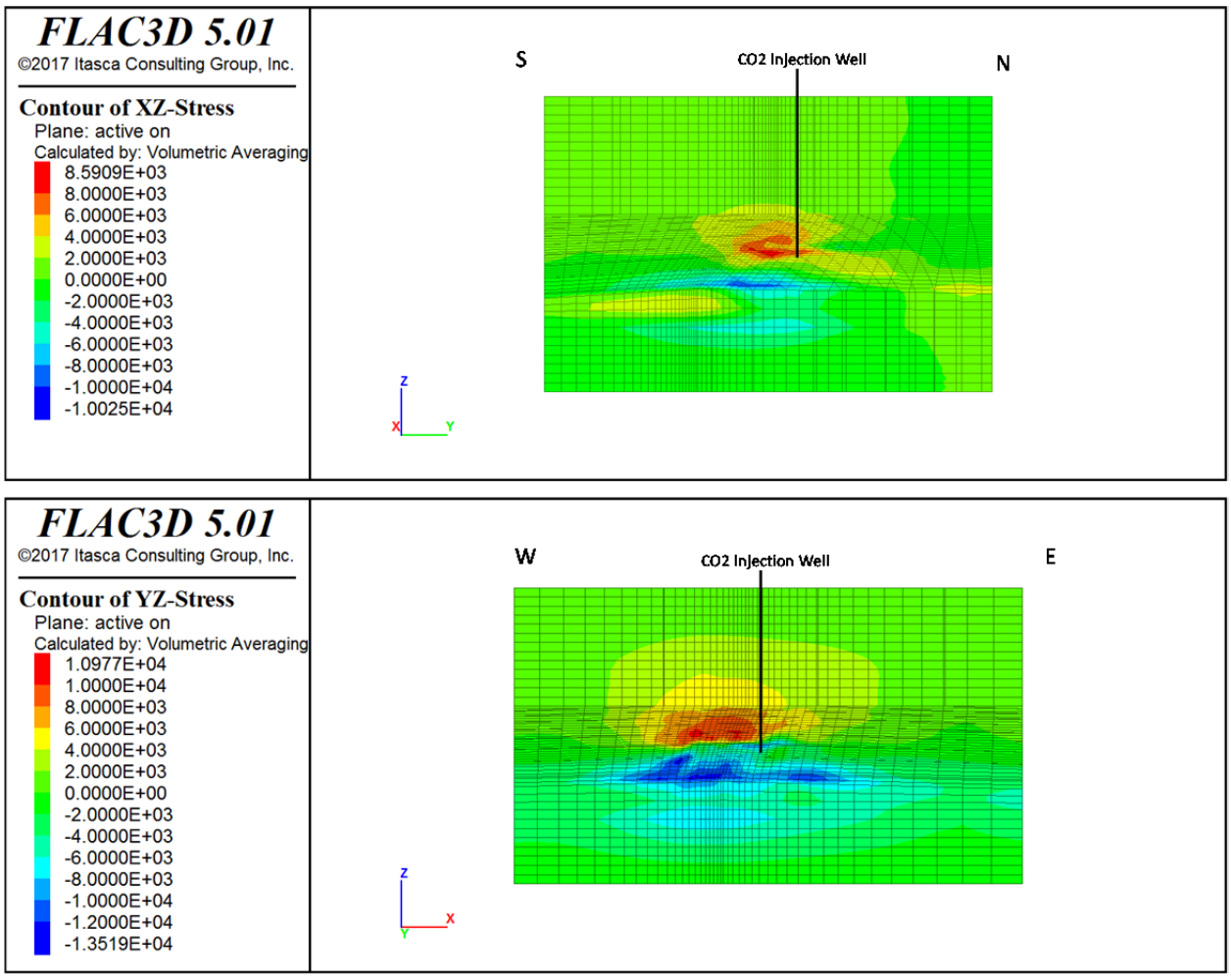

Figure 112: Plot of induced shear stress (Pascal) after 30 years of injection in N-S, (SXZ, above) and E-W (SYZ, below) directions across the injection well (Pliocene injection – Sim03).

Figure 113 shows the resulting induced vertical Z-displacement in (above) isometric view and (below) a cross-section view across the injection well in E-W direction. The maximum surface uplift is toward the north of the injection well, with a maximum value of about 0.58 cm (0.22 in) compared to about 0.49 cm (0.19 in) for the baseline scenario. Similar to the baseline scenario, the center of the maximum surface uplift bowl is spread across in a wide area, at over 3 miles diameter. Again, there are no fault slips or fault reactivation present for this injection scenario after 30 years of CO_2 injection and migration with these relatively small induced stresses and strains.

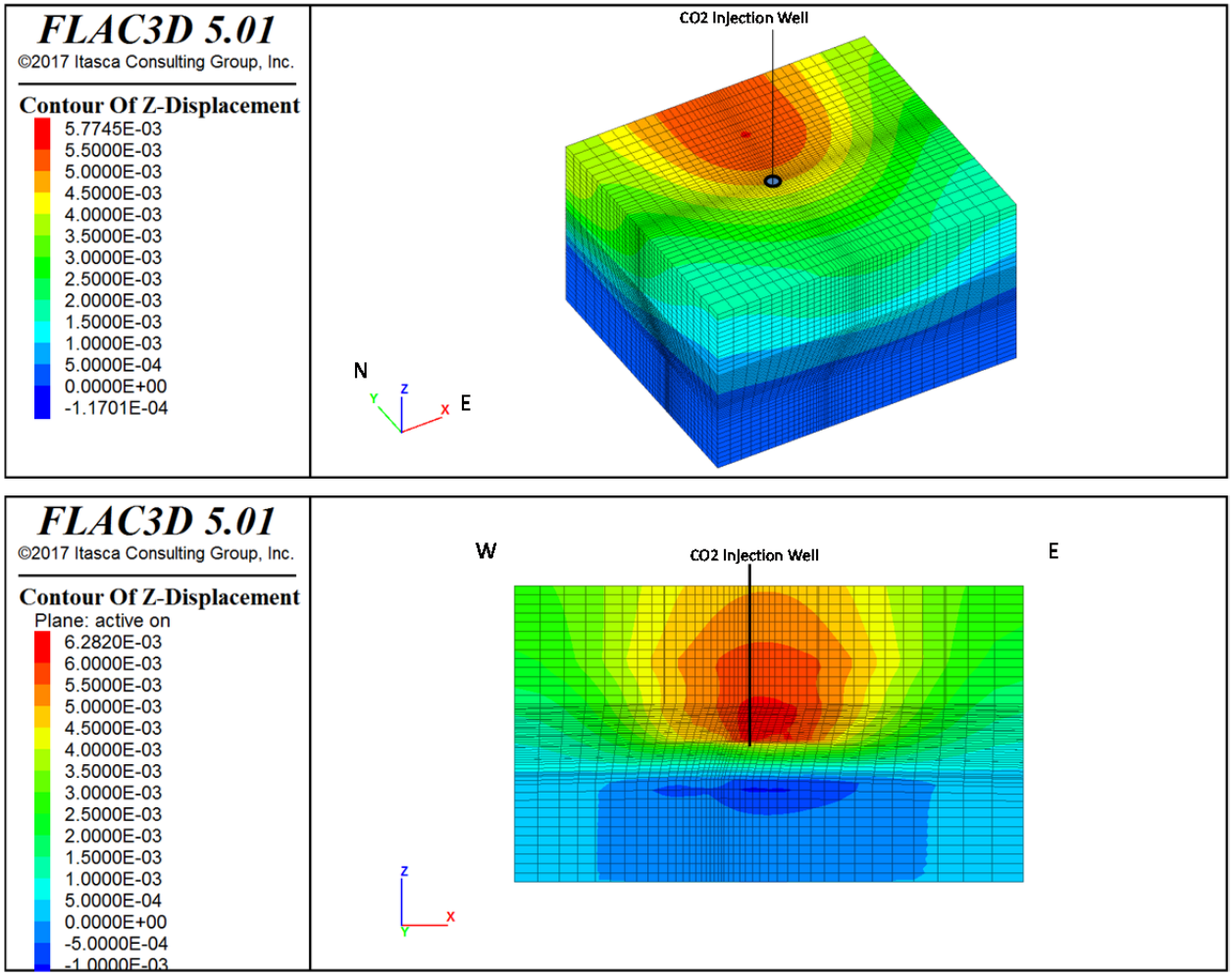

Figure 113: Plot of induced vertical displacement (meter) in 3D-view (above) and in E-W (below) direction across the injection well (Pliocene injection – Sim03).

6.2.6 Upper Miocene Geomechanics Model Simulation-02, with Different Permeability

Sensitivity analysis has also been performed for the upper Miocene geomechanical model injection from the baseline scenario. GeoMechanics have decided to evaluate the geomechanical effects from the simulation-02 (with different permeability for silt and shale) of the fluid flow model, because more pressure distribution differences are observed from the baseline scenario when compare to the other fluid flow sensitivity analyses. The latest simulation pressure input from the Sim-02 fluid flow model and resulting stress and displacement changes are described next.

The change in pressure distribution across the injection well in N-S and E-W directions, after 30 years of injection, is shown in Figure 114 below. This pressure data was transferred and used as input from the fluid flow model to the geomechanical model. Similar to the CO_2 migration pattern, the corresponding pressure increased localized area is above the injection interval, with maximum magnitude of about 7.00E5 Pa (101 psi).

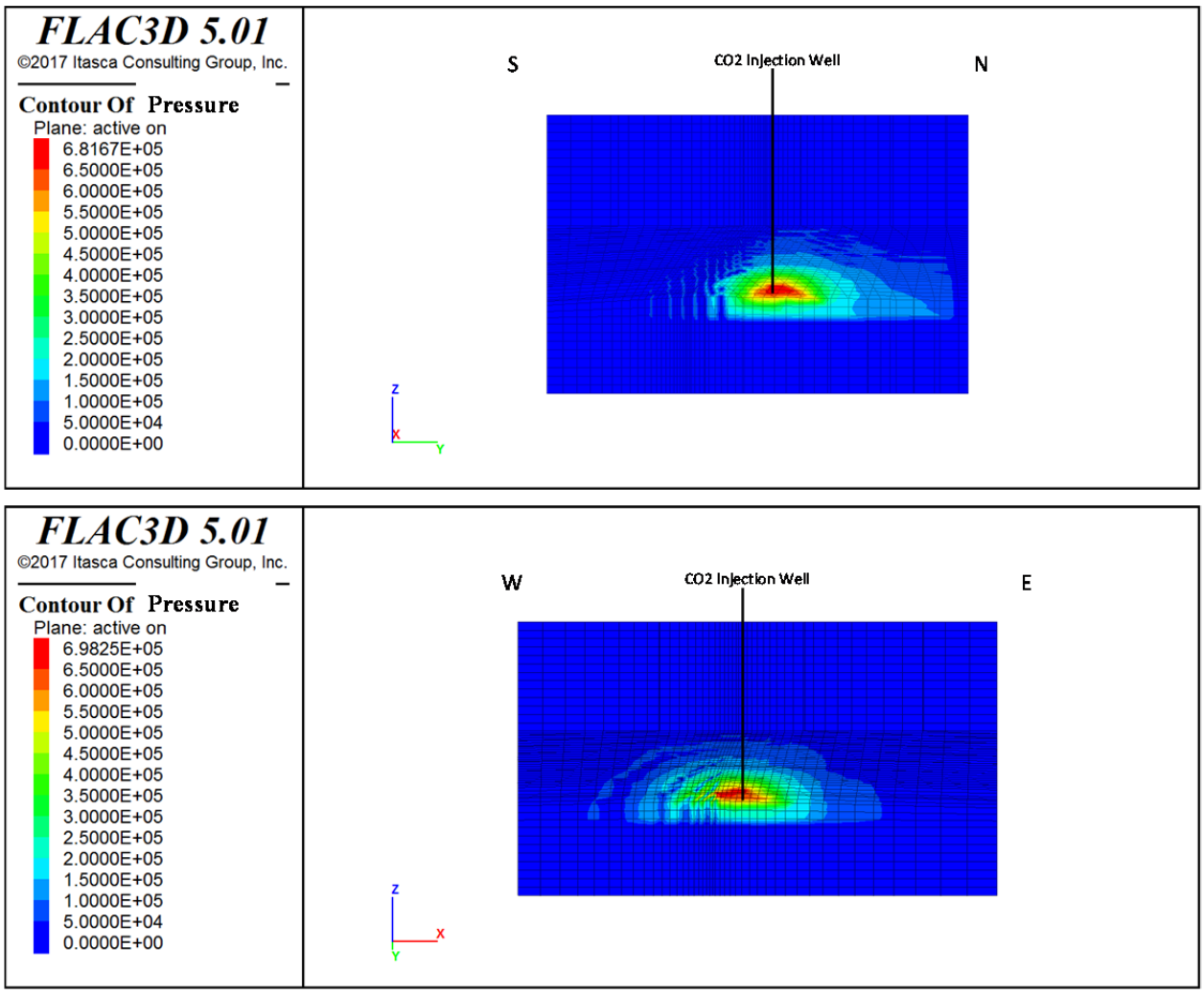

Figure 114: Change in pressure distribution (Pascal) after 30 years of injection in N-S (above) and E-W (below) directions across the injection well (Upper Miocene Injection – Sim02).

Figure 115 presents the contour plots of induced horizontal shear stress across the injection well in the N-S direction (Sxz in y-plane) and the E-W direction (Syz in x-plane), respectively; showing maximum induced shear stresses of about 2.4E4 Pa (~ 3.5 psi), due to the pressure change after 30 years of CO_2 injection.

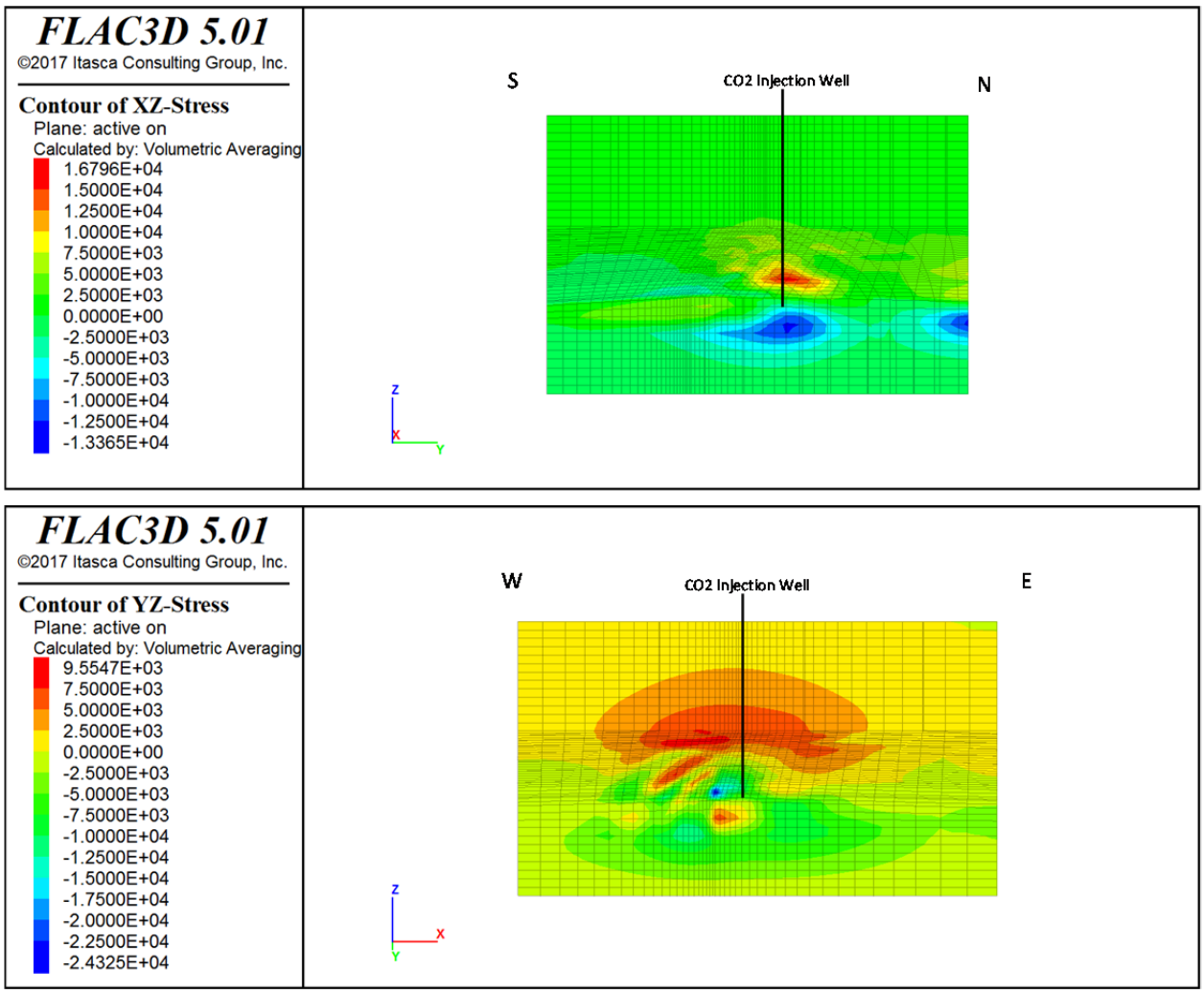

Figure 115: Plot of induced shear stress (in Pascal) after 30 years of injection in N-S, (SXZ, above) and E-W (SYZ, below) directions across the injection well (Upper Miocene Injection – Sim02).

Finally, the resulting induced vertical displacement in isometric view (above) and cross-section view (below) across the injection well in E-W direction is shown in Figure 116. Similar to the upper Pliocene simulation displacement bowl results, the maximum surface uplift is toward the north of the injection well, with a maximum value of about 0.85 cm (0.33 in). The center of the maximum surface uplift bowl is spread across in a wide area, at over 2 miles diameter. Even with very weak fault mechanical properties assumptions, the results indicate there is very low to no risk of fault slippage or fault reactivation for this upper Miocene injection scenario after 30 years of CO_2 injection and migration with these relatively small induced stresses and strains.

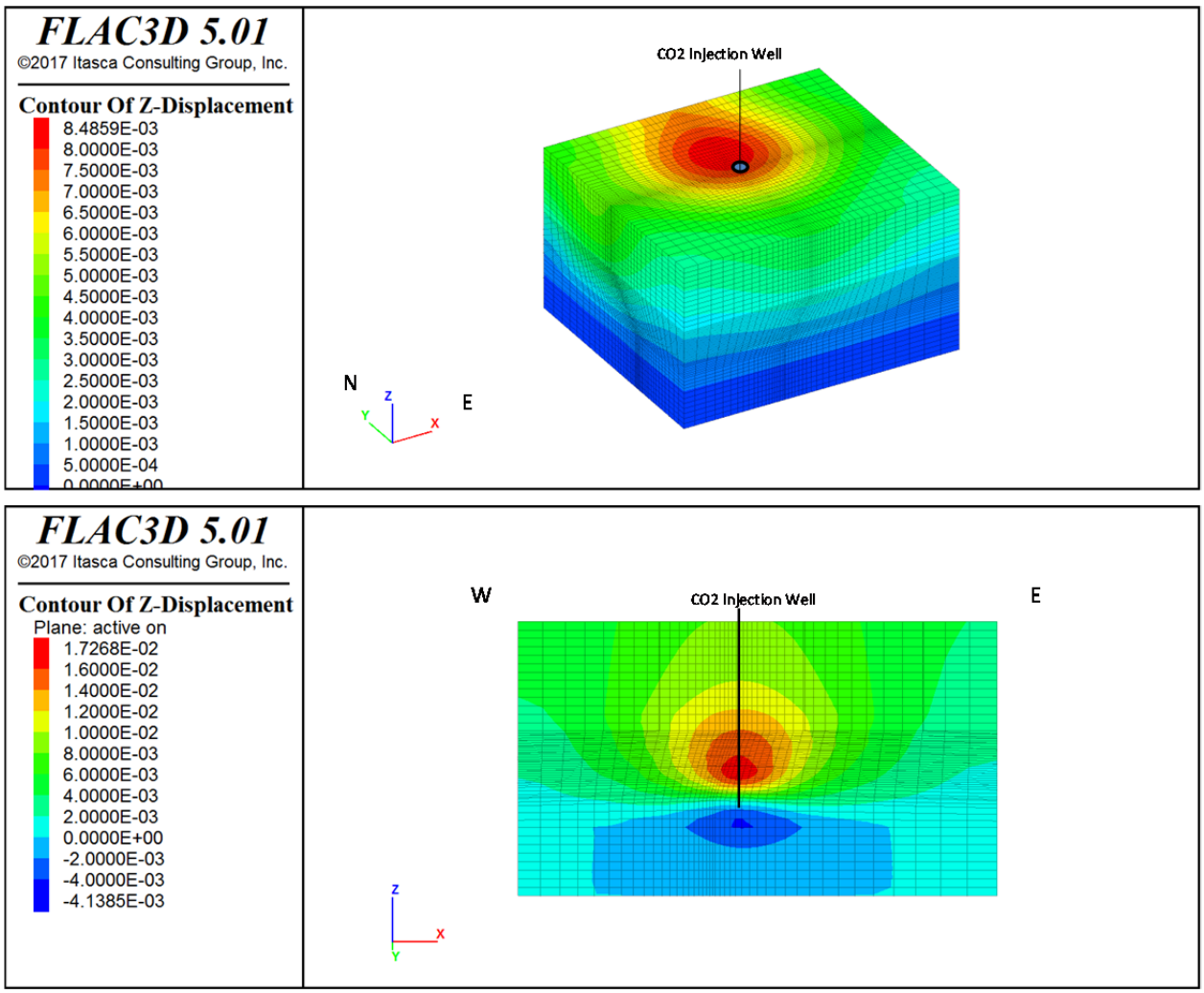

Figure 116: Plot of induced vertical displacement (meter) in 3D-view (above) and in E-W (below) direction across the injection well (Upper Miocene Injection – Sim02).

6.2.7 Upper Miocene Geomechanics Model Simulation - Potential Fault Activation

A sensitivity analysis has been performed for the upper Miocene geomechanical model injection to evaluate potential fault activation if any to the three closes nearby main faults. GeoMechanics Technologies evaluated potential fault activation by incrementally increase the change in pressure until we see initial fault slippage from the Miocene baseline injection scenario (simulation-baseline) of the fluid flow model. Previously, the maximum pressure increased that was observed during the Miocene 30-years injection scenarios, including baseline scenario, are in the range of 480 kPa (70 psi). These relative small pressure increases in the injection zones are insufficient to cause any fault activation or re-activation. Therefore, to study potential fault slips we have artificially increased the pressure change from the baseline scenario. The latest simulations showed that unless the reservoir pressure changes are vastly increased to at least 50 times from about 480 kPa (70 psi) to more than 23 MPa (3,400 psi) then we would observe

potential fault slippage. Therefore, there are very low or no risks of potential fault activation from this CO_2 injection location to the three faults identified.

The increase in total pressure distribution plot with 50 times the baseline scenario across the injection well in E-W directions, after 30 years of injection, is shown in upper Figure 117. The total maximum pressure increase to about 59 MPa from initial reservoir pressure of approximately 36 MPa (difference of 23 MPa) can be seen in the plot. The induced shear stress due to this mocked up pressure increase shows maximum magnitude of about 70 MPa (about 10 kpsi) as presented in the lower Figure 117.

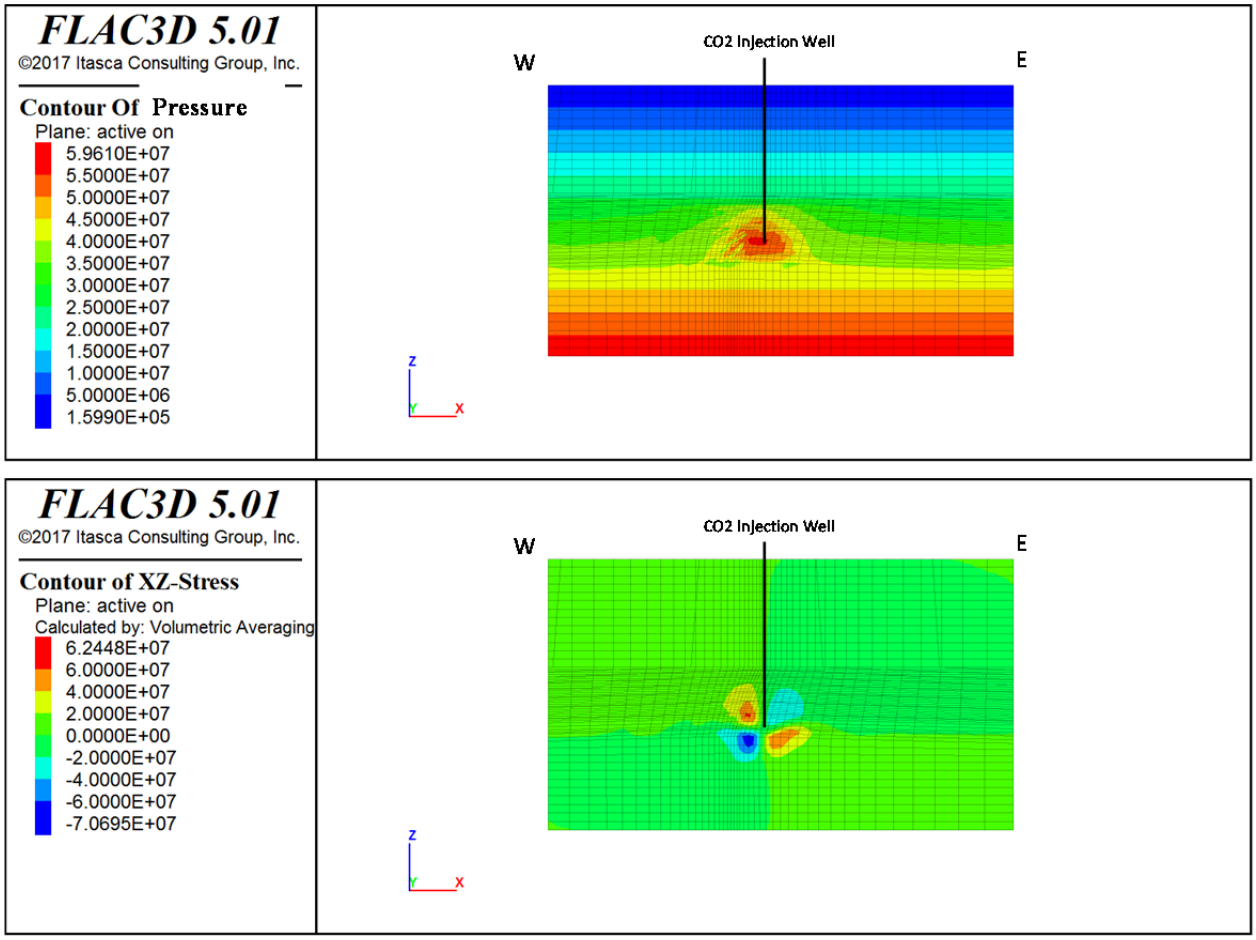

Figure 117: Total pressure distribution (Pascal) in E-W direction across the injection well after 30 years of injection (above), and (below) resulting induced shear stresses (Upper Miocene Injection) – SS Block 107 field. The final pressure distribution assumes 50 times the magnitude of pressure change from baseline scenario to evaluate potential fault slips.

Figure 118 presents the contour plots of the total vertical (Szz) and horizontal stresses (Sxx) across the injection well in the E-W direction, respectively. The maximum total vertical stress is seen to be about 4.97E8 Pa (~ 72 kpsi) and maximum total horizontal stress is about 5.61E8 Pa (~ 81 kpsi), due to the significant pressure change after 30 years of CO_2 injection.

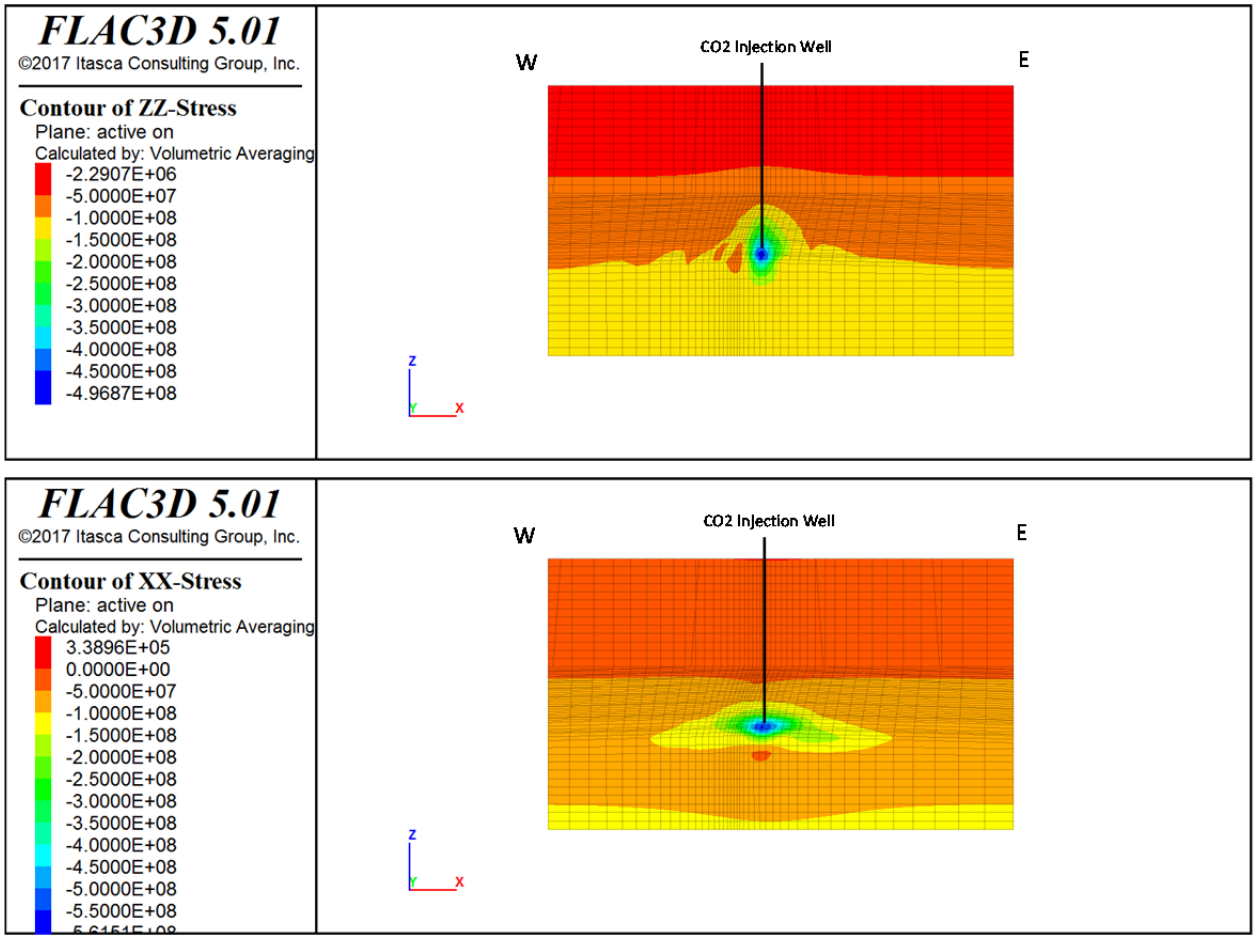

Figure 118: Plot of total vertical and horizontal stresses (Pascal) after 30 years of injection in E-W direction across the injection well, (SZZ, above) and (SXX, below) for SS Block 107 field. The significant increases in reservoir compressional stresses are due to the 50 times the magnitude of pressure change from baseline scenario to evaluate potential fault slips.

Finally, the resulting induced vertical displacement in isometric view (above) and cross-section view (below) across the injection well in E-W direction is shown in Figure 119. Similar in shape to the baseline Miocene simulation displacement bowl results, the maximum surface uplift is toward the north of the injection well, but with a maximum value of about 1.14 m (3.75 ft) compare to 0.85 cm (0.33 in). The center of the maximum surface uplift bowl is spread across in a wide area, at over several miles in diameter. As shown in the lower plot, potential fault re-activation is seen closes to the injection zone if only we assume the injection pressure is increase to over 50 times the magnitude of pressure change from baseline scenario. The results indicate there is very low to low risk of fault slippage or fault reactivation for this upper Miocene significant mocked up injection scenario after 30 years of CO_2 injection and migration.

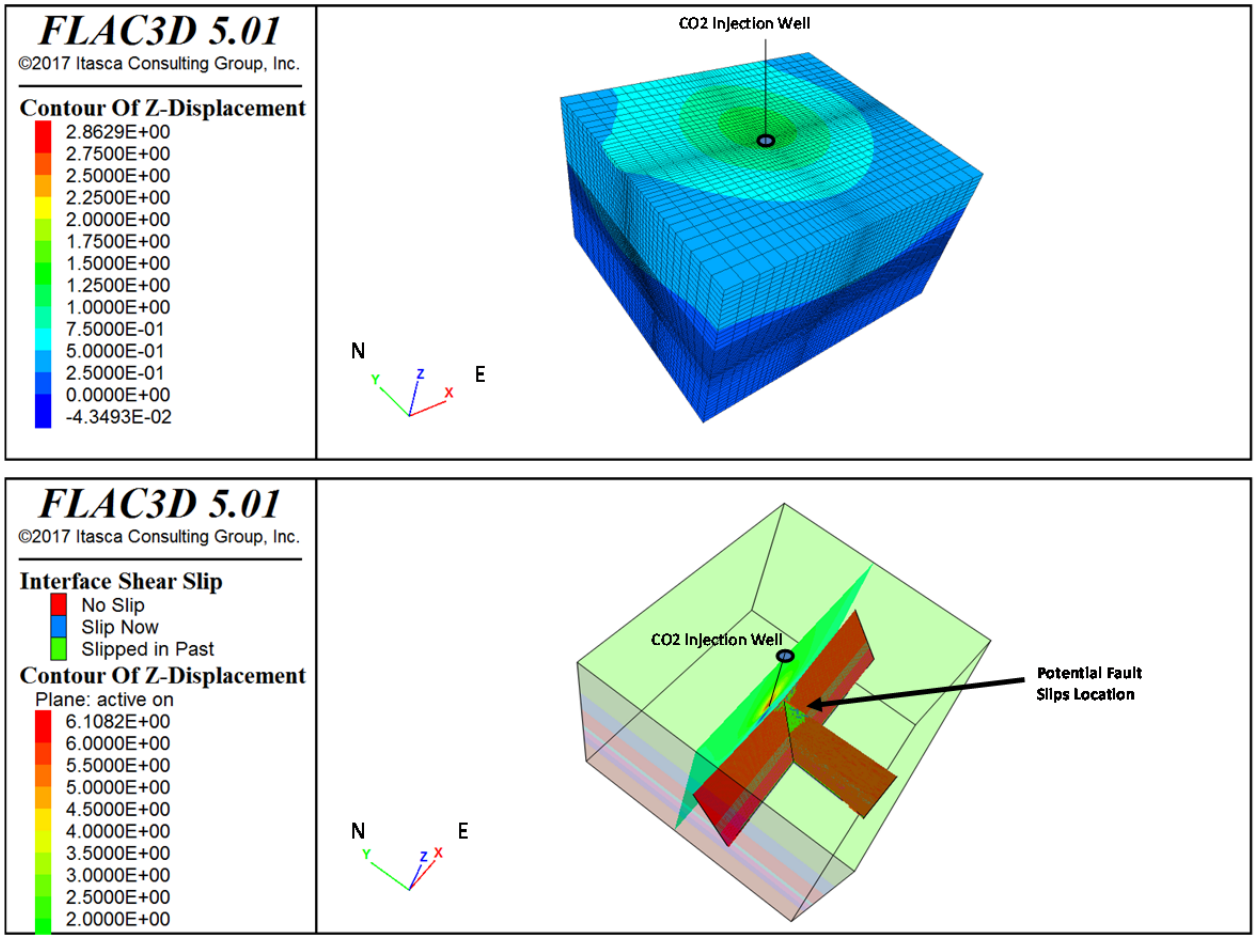

Figure 119: (Above) Plot of induced vertical displacement (meter) in 3D-view, and (below) in cross-section view across the injection well for SS Block 107 field. Potential fault re-activation is seen closes to the injection zone if only we assume the injection pressure is increase to over 50 times the magnitude of pressure change from baseline scenario.

6.2.8 Base Pliocene Geomechanics Model Simulation-Potential Fault Activation

Lastly, another sensitivity analysis is being performed for the base Pliocene geomechanical model injection to evaluate potential fault activation to any of the three closes main faults. Similar to the Miocene injection to evaluate potential fault activation, we incrementally increase the change in pressure from the Pliocene baseline injection scenario (simulation-baseline) of the fluid flow model. Previous maximum pressure increased that was observed during the Pliocene 30-years injection scenarios, including baseline scenario, are in the range of 560 kPa (80 psi). These relative small pressure increases in the injection zones are insufficient to cause any fault activation or re-activation. Therefore, to study potential fault slips we have significantly mocked up the pressure change from the baseline scenario. The latest simulations showed that unless the reservoir pressure changes are vastly increased to at least 50 times 28 MPa (4,000 psi) then we would observe potential fault slippage. Therefore, there are very low or no risks of potential fault activation from this CO_2 injection location to the three faults identified.

The increase in total pressure distribution plot with 50 times the baseline scenario across the injection well in E-W directions, after 30 years of injection, is shown in upper Figure 120. The induced shear stress due to this mocked up pressure increase shows maximum magnitude of about 40 MPa (about 5.8 kpsi) as presented in the lower Figure 120.

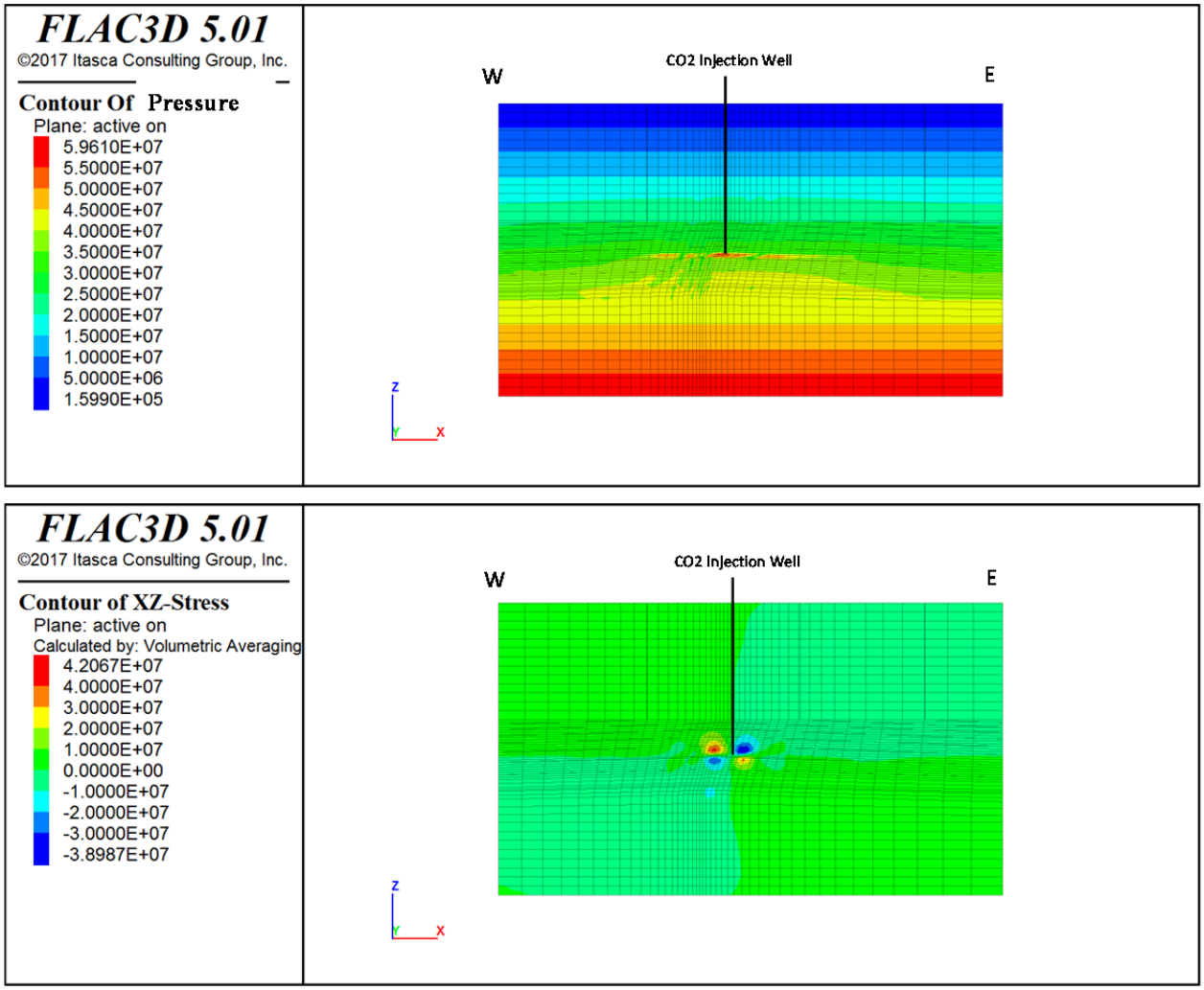

Figure 120: Total pressure distribution (Pascal) in E-W direction across the injection well after 30 years of injection (above), and (below) resulting induced shear stresses (Base Pliocene Injection) – SS Block 107 field. The final pressure distribution assumes 50 times the magnitude of pressure change from baseline scenario to evaluate potential fault slips.

Figure 121 presents the contour plots of the total vertical (Szz) and horizontal stresses (Sxx) across the injection well in the E-W direction, respectively. The maximum total vertical stress is seen to be about 2.36E8 Pa (~ 34 kpsi) and maximum total horizontal stress is about 4.63E8 Pa (~ 67 kpsi), due to the significant pressure change after 30 years of CO_2 injection.

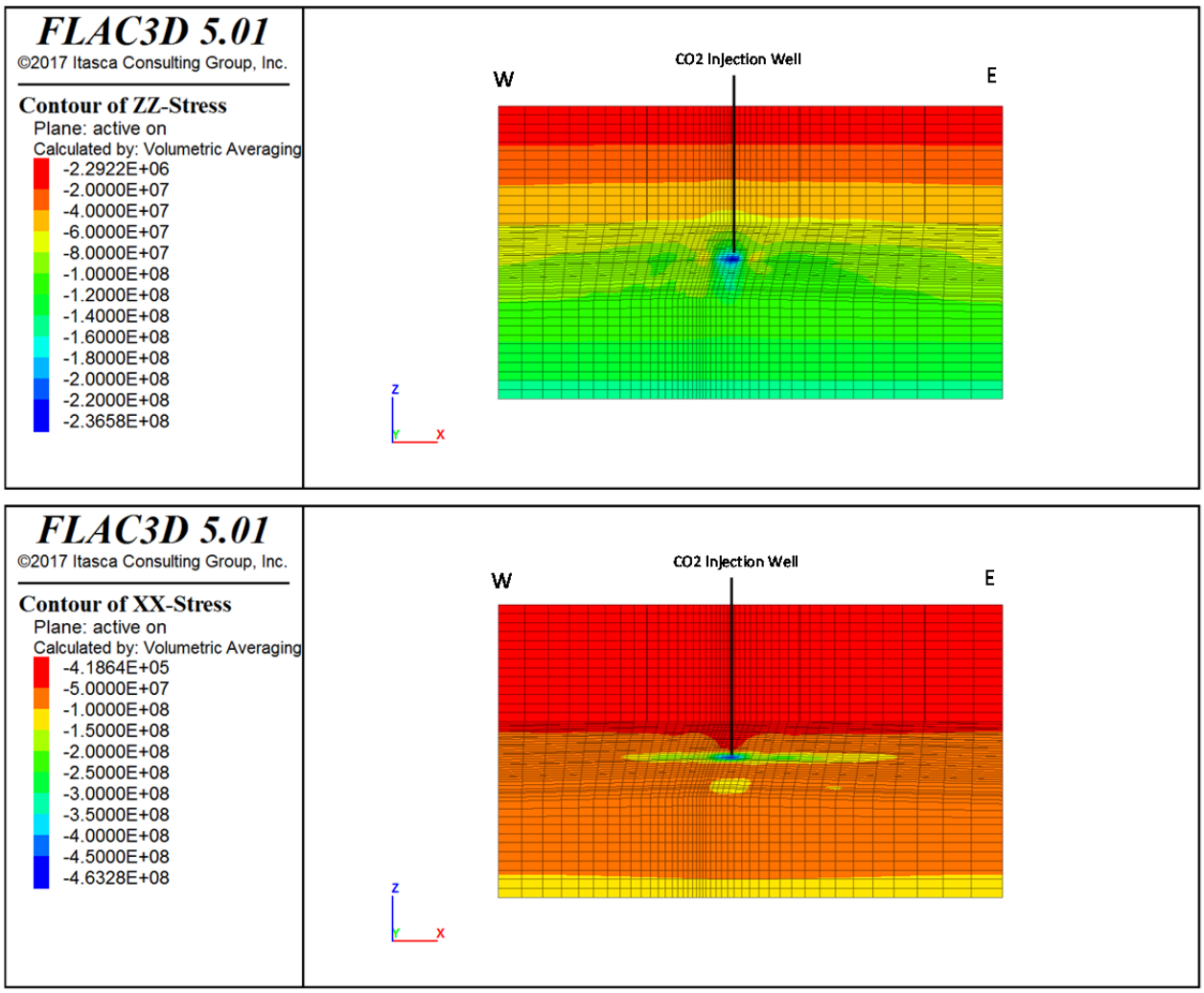

Figure 121: Plot of total vertical and horizontal stresses (Pascal) after 30 years of injection in E-W direction across the injection well, (SZZ, above) and (SXX, below) for SS Block 107 field. The significant increases in reservoir compressional stresses are due to the 50 times the magnitude of pressure change from baseline scenario to evaluate potential fault slips.

Finally, the resulting induced vertical displacement in isometric view (above) and cross-section view (below) across the injection well in E-W direction is shown in Figure 122. Similar in shape to the baseline Pliocene simulation displacement bowl results, the maximum surface uplift is toward the north of the injection well, but with a maximum value of about 1.98 m (6.50 ft) compare to 0.49 cm (0.19 in). The center of the maximum surface uplift bowl is spread across in a wide area, at over several miles in diameter. As shown in the lower plot, potential fault re-activation is seen closes to the injection zone if only we assume the injection pressure is increase to over 50 times the magnitude of pressure change from baseline scenario. The results indicate there is very low to no risk of fault slippage or fault reactivation for this base Pliocene significant mocked up injection scenario after 30 years of CO_2 injection and migration.

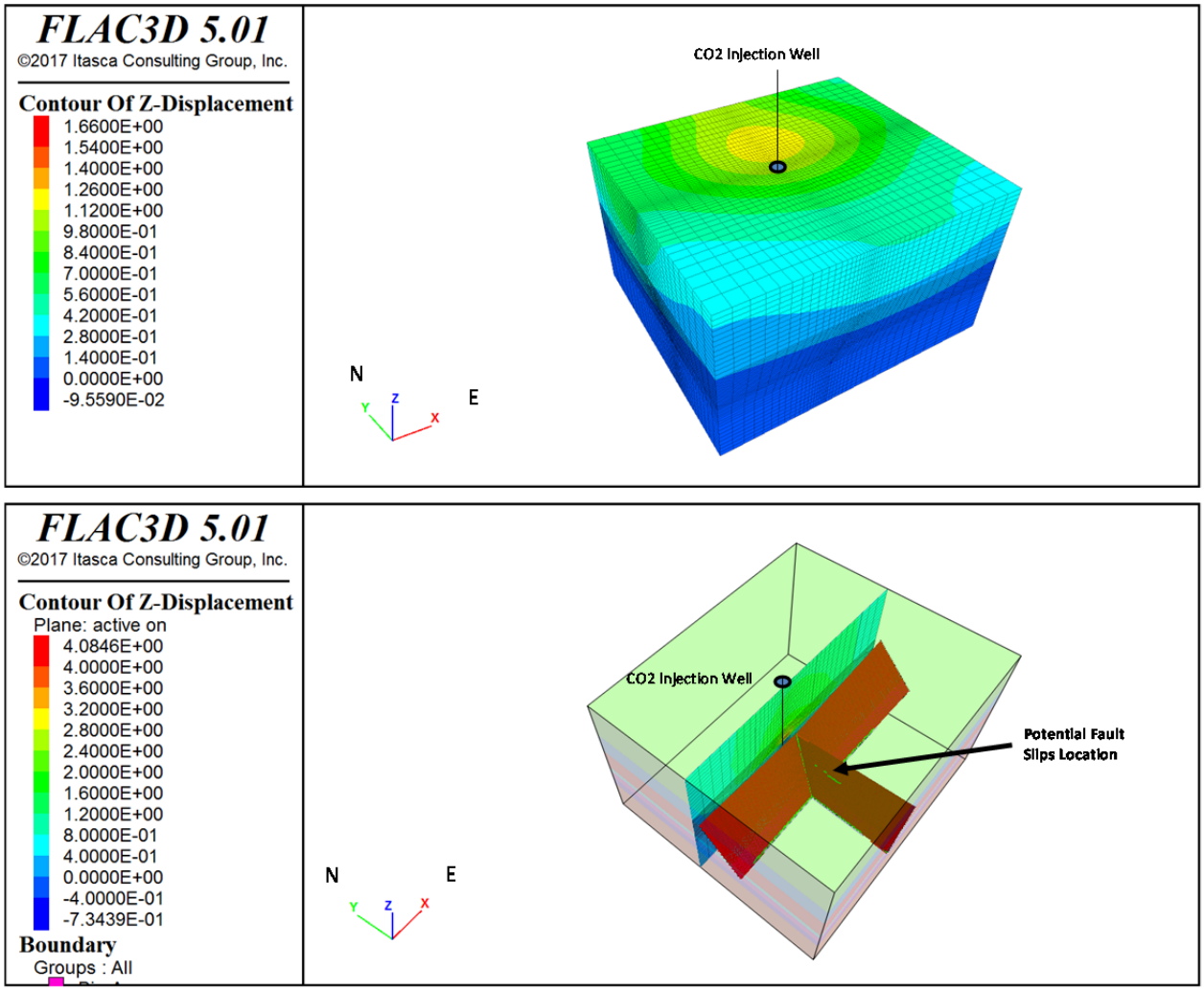

Figure 122: (Above) Plot of induced vertical displacement (meter) in 3D-view, and (below) in cross-section view across the injection well for SS Block 107 field. Potential fault re-activation is seen closes to the injection zone if only we assume the injection pressure is increase to over 50 times the magnitude of pressure change from baseline scenario.

6.3 Ship Shoal Block 84 Field

6.3.1 Geomechanical Model Setup

Based on the geologic model of the Ship Shoal Block 84 field, the top of stratigraphy horizons and the principal southern fault plane were considered to build the 3D geomechanics mesh. The data was carefully analyzed and compared with the 3D geology model to carefully assess its integrity and consistency (Figure 123). Then, a 3D geomechanics mesh was built taking into account the overburden and underburden as given in Figure 124.

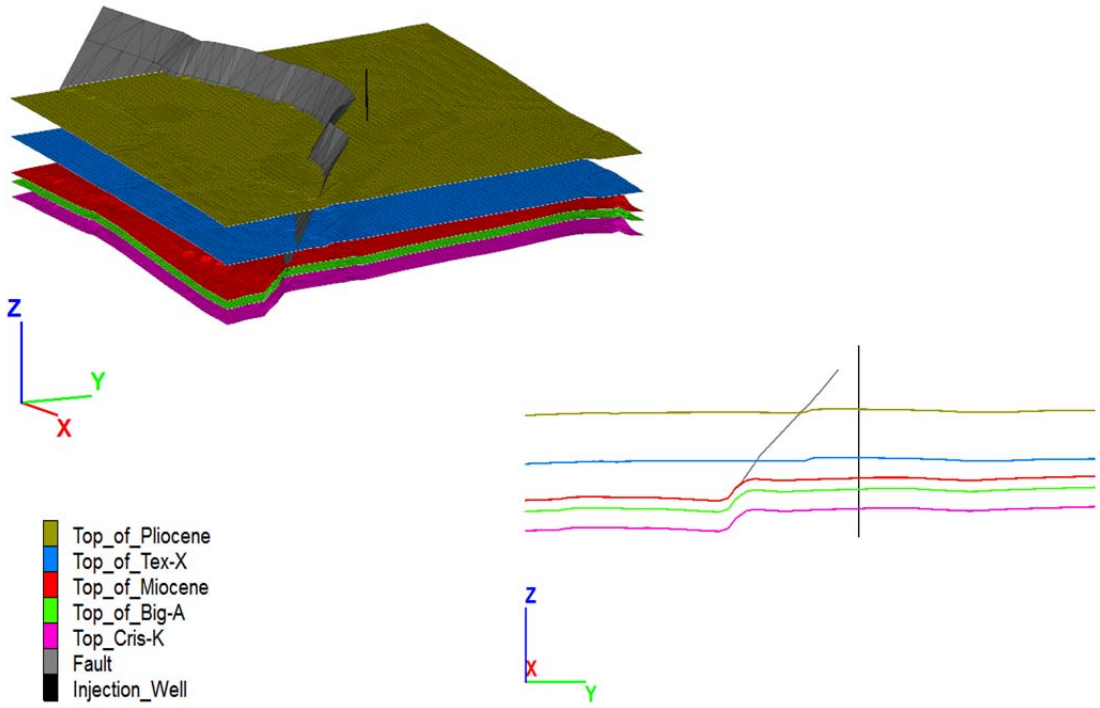

Figure 123: 3D stratigraphy units and N-S cross section for the Ship Shoal Block 84 field

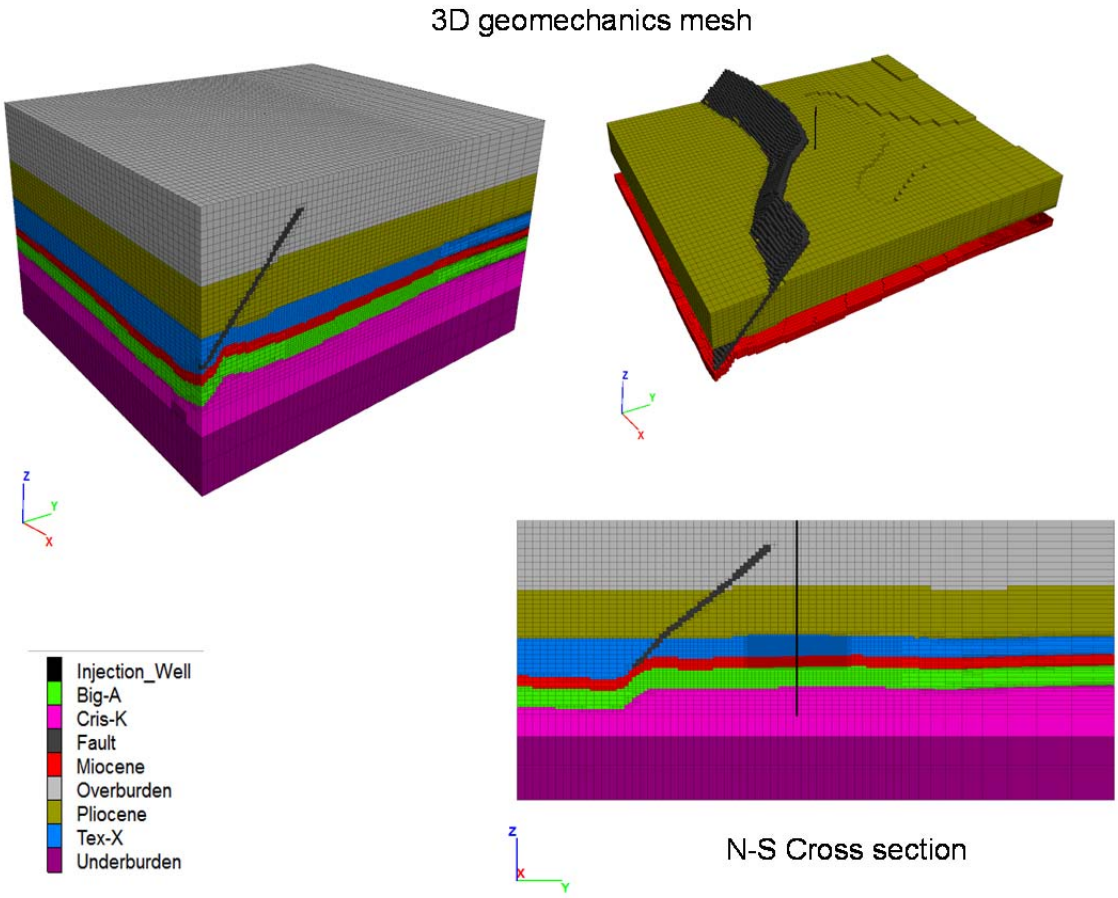

Figure 124: 3D geomechanics mesh and N-S cross section with the stratigraphy units for Ship Shoal Block 84 field

The 3D geomechanics model was assembled in the numerical modeling software FLAC3D with a volume that covers 32,808 ft (10,000 m) by 39,370 ft (12,000 m) by 19,685 ft (6,000 m) as shown in Figure 125. A total number of 1,086,515 elements were defined with higher resolution mesh around the vicinity of the injection well. We applied roller boundary conditions with no lateral movements on *x* and *y* direction, as well as no vertical movement at the bottom. Vertical movements were allowed from the top of the model (Figure 126).

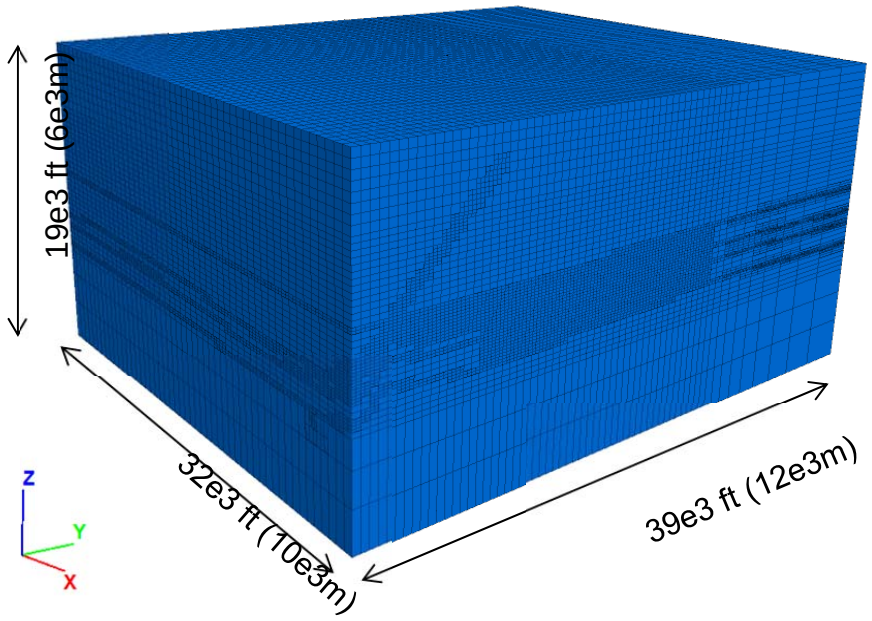

Figure 125: 3D model geometry and dimensions for Ship Shoal 84 field

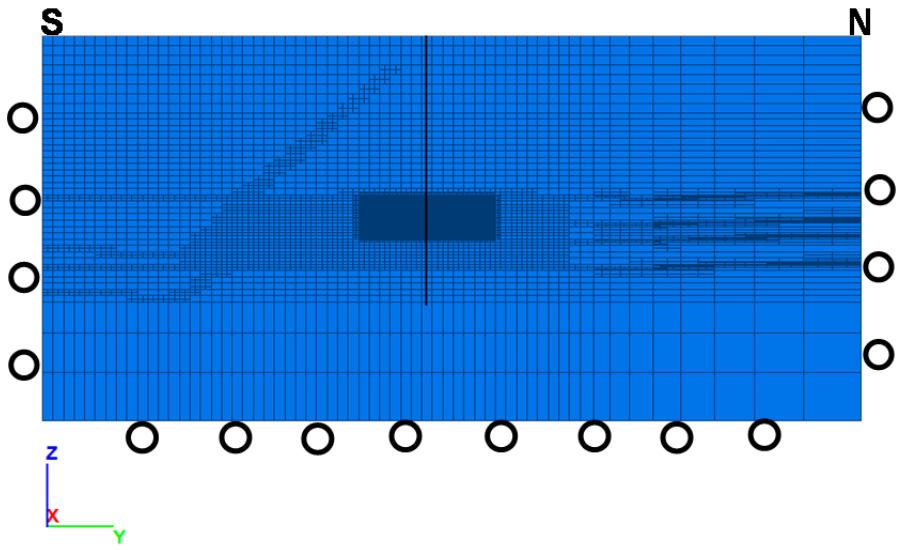

Figure 126: N-S cross section with mesh refinement and boundary conditions for SS Block 84

Based on the CO_2 injection and migration modeling, an induced surface uplift analysis was conducted. The stresses were induced as consequence of pressure changes after 30 years of CO_2 injection at the base Pliocene and upper Miocene. For this geomechanics analysis, the baseline was considered and described below.

6.3.2 Simulation Matrix

Based on the fluid flow model performed in Block 84, a total of 12 simulations for base Pliocene and upper Miocene were respectively conducted to evaluate isothermal and non-isothermal effect. Table 26 shows all the sensitivity cases with the description.

Table 26: Geomechanical model simulation matrix for Ship Shoal Block 84 base Pliocene and upper Miocene injection scenarios.

Temperature Condition	Similation	Description
Isothermal	Sim01	Baseline
	Sim02	Reduced Porosity
	Sim03	No Capillary
	Sim04	Sandy
	Sim05	Shaly
	Sim06	Double Injection Rate
Non-Isothermal	Sim01	Baseline
	Sim02	Reduced Porosity
	Sim03	No Capillary
	Sim04	Sandy
	Sim05	Shaly
	Sim06	Double Injection Rate

6.3.3 Base Pliocene Geomechanics Model Simulation

Analysis of induced vertical displacement caused by pressure and temperature change after 30 years of injection was conducted. 3D view and cross-section view across the injection well in E-W direction are presented from Figure 127 through Figure 130 considering isothermal and non-isothermal effect for baseline and Sim06 scenarios, respectively. These analyses were also conducted by Sim02, Sim03, Sim04 and Sim05 scenarios. All scenarios are summarized in Figure 131 and Figure 132 for isothermal and non-isothermal effect, respectively.

As seen in Figure 131 for the isothermal effect, a maximum surface uplift displacement ranging from 0.004 m (0.4 cm or 0.16 in) to 0.006 m (0.6 cm or 0.23 in) for Sim01, Sim02, Sim03, Sim04 and Sim05 was experienced. Meanwhile, a higher surface displacement around 0.015 m (1.5 cm or 0.59 in) for Sim06 was estimated and expected because the injection rate was doubled. Figure 132 shows a similar trend for the non-isothermal effect for all scenarios. Note that a maximum surface uplift displacement ranging from 0.004 m (0.4 cm or 0.16 in) to 0.0065 m (0.65 cm or 0.25 in) for Sim01, Sim02, Sim03, Sim04 and Sim05 was obtained and a higher surface displacement around 0.016 m (1.6 cm or 0.63 in) for Sim06 was estimated. Overall, a small relative difference of around 5% can be observed between isothermal and non-isothermal effect as shown in Figure 133.

It is also important to point out that these magnitudes indicate low to no risks of a severe surface uplift displacement that can compromise surface facilities or any potential damage after 30 years of injection.

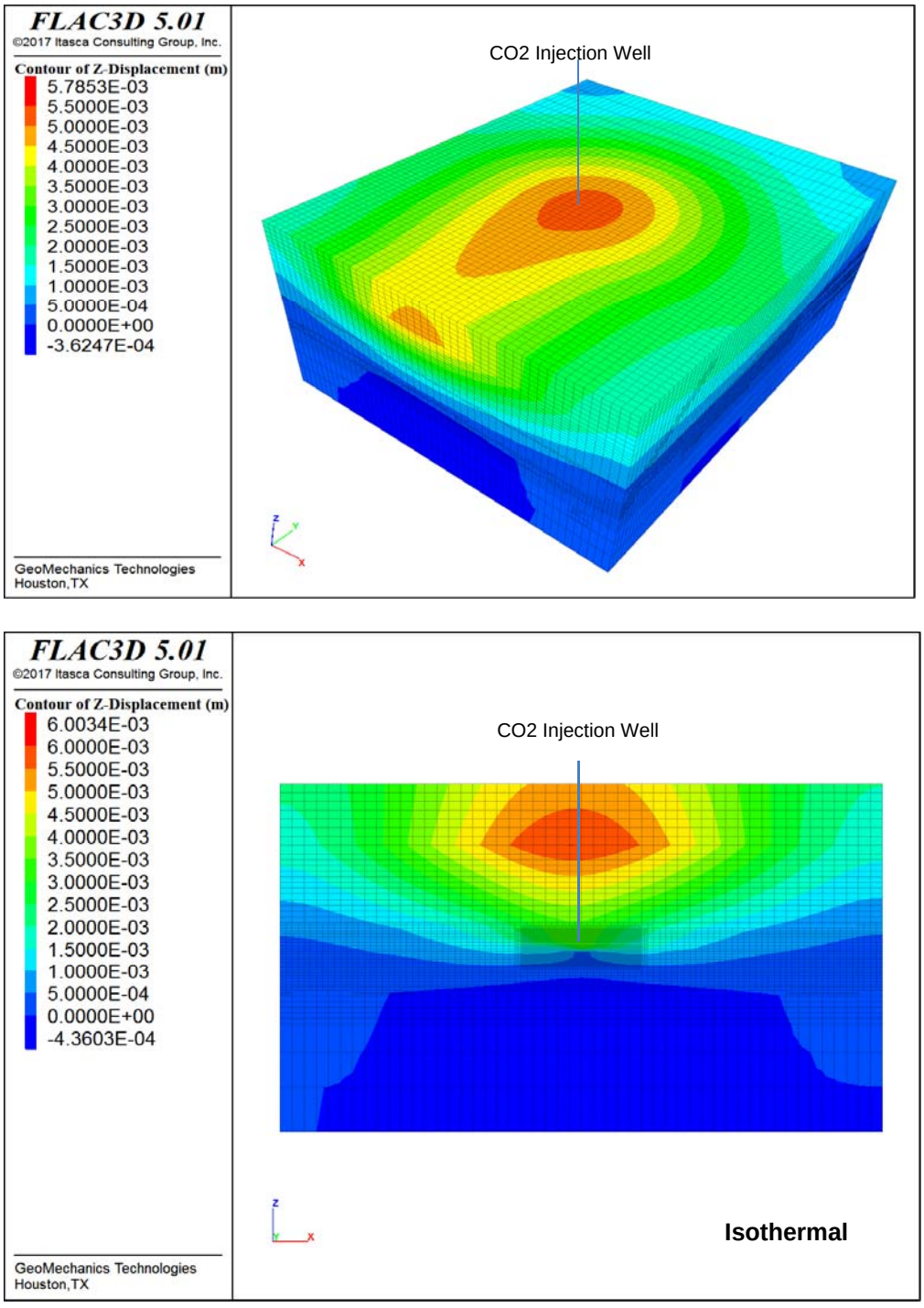

Figure 127: Induced vertical displacement (m) in 3D view (above) and W-E direction (below) across the injection well, isothermal effect, baseline scenario for base of Pliocene, Ship Shoal Block 84 field.

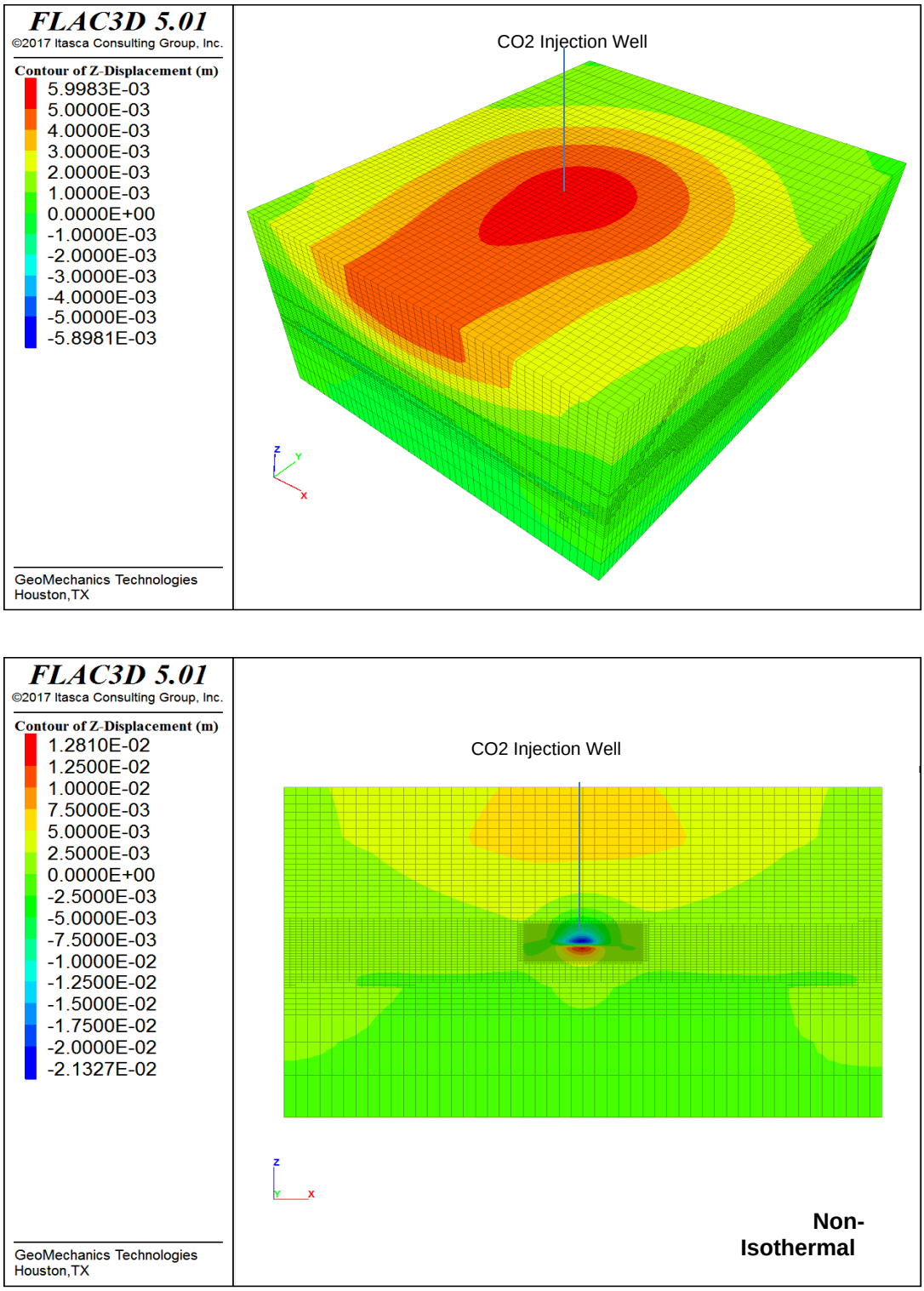

Figure 128: Induced vertical displacement (m) in 3D view (above) and W-E direction (below) across the injection well, non-isothermal effect, baseline scenario for base of Pliocene, Ship Shoal Block 84 field.

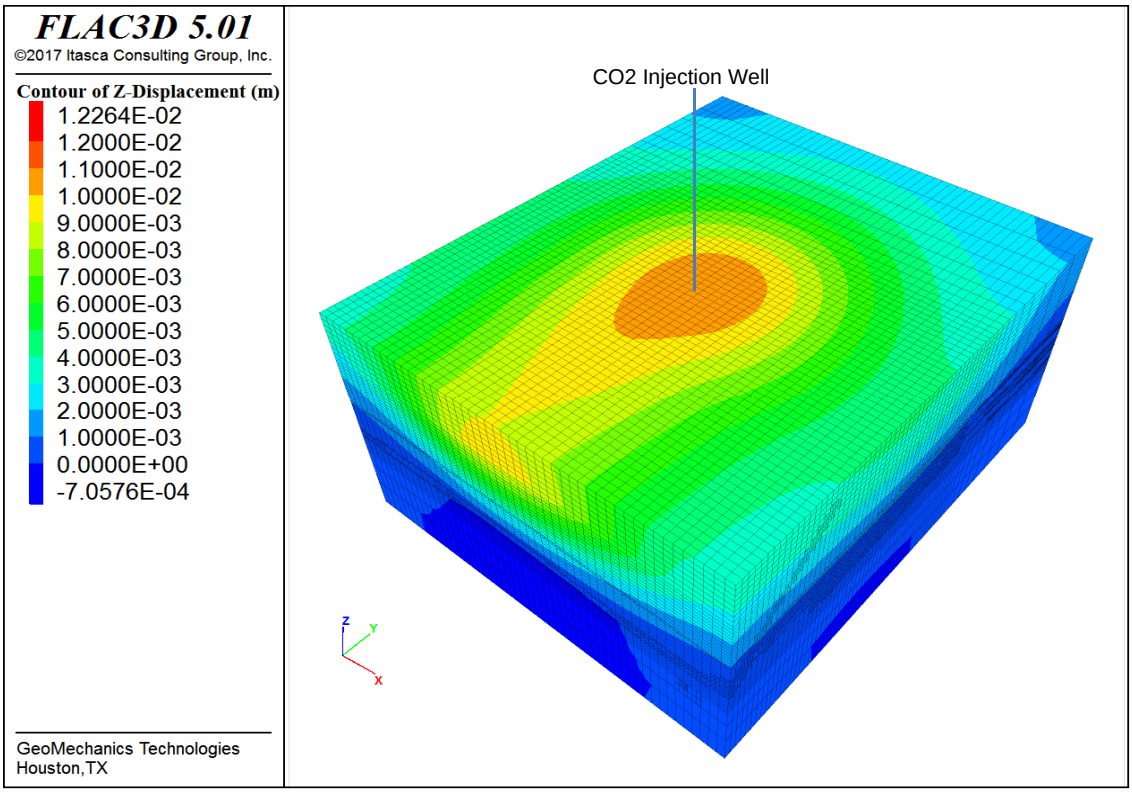

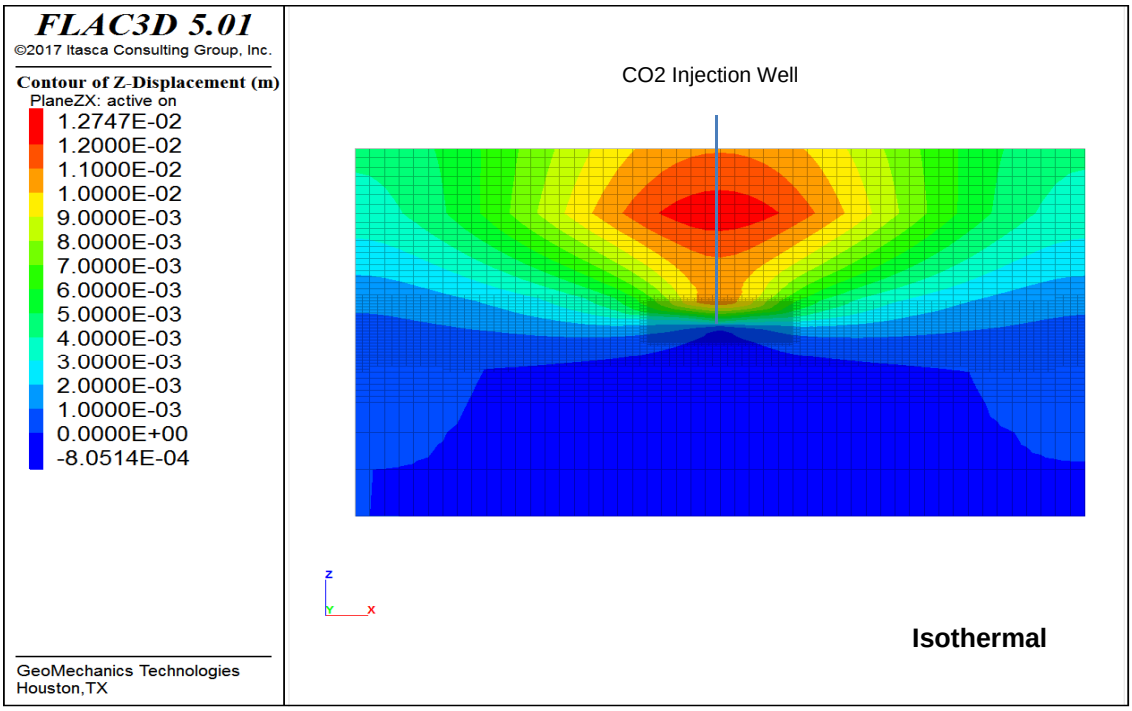

Figure 129: Induced vertical displacement (m) in 3D view (above) and W-E direction (below) across the injection well, isothermal effect, Sim06 scenario for base of Pliocene, Ship Shoal Block 84 field.

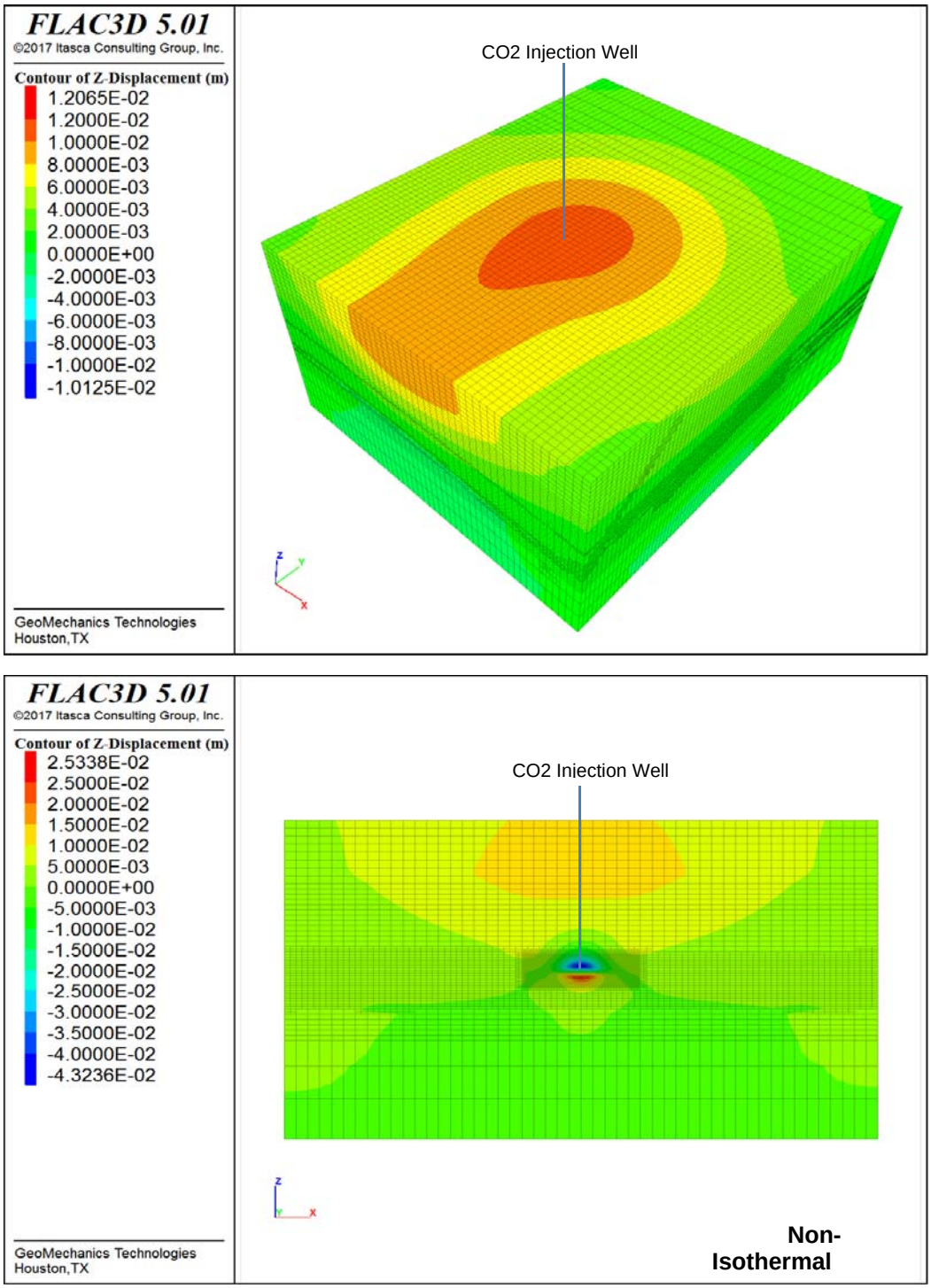

Figure 130: Induced vertical displacement (m) in 3D view (above) and W-E direction (below) across the injection well, non-isothermal effect, Sim06 scenario for base of Pliocene, Ship Shoal Block 84 field.

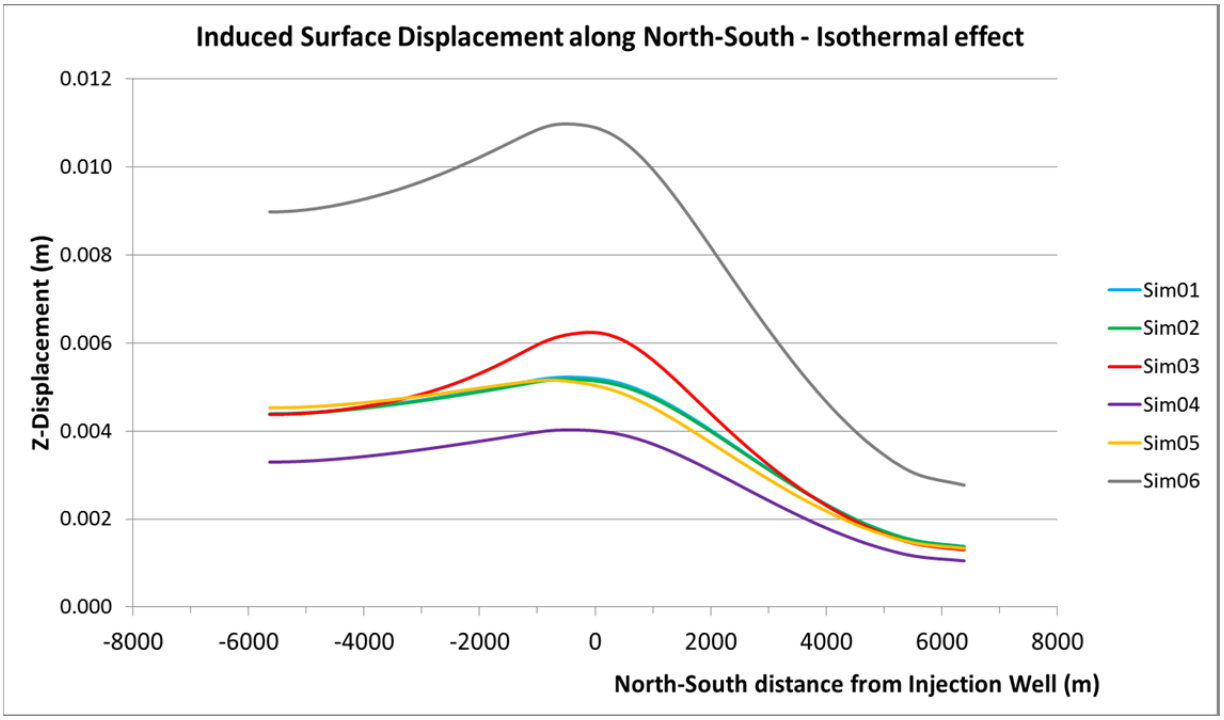

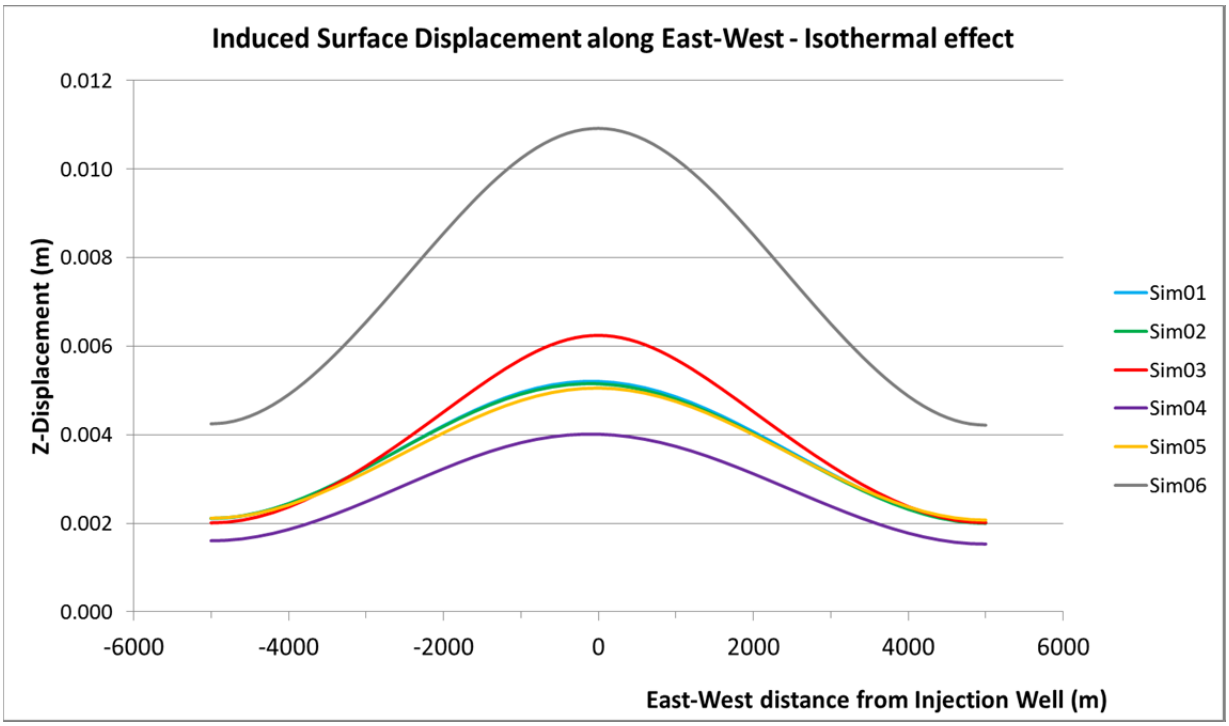

Figure 131: Induced surface displacement (m) in N-S (above) and E-W (below) direction across the injection well, isothermal effect for all scenarios for base Pliocene, Ship Shoal Block 84 field.

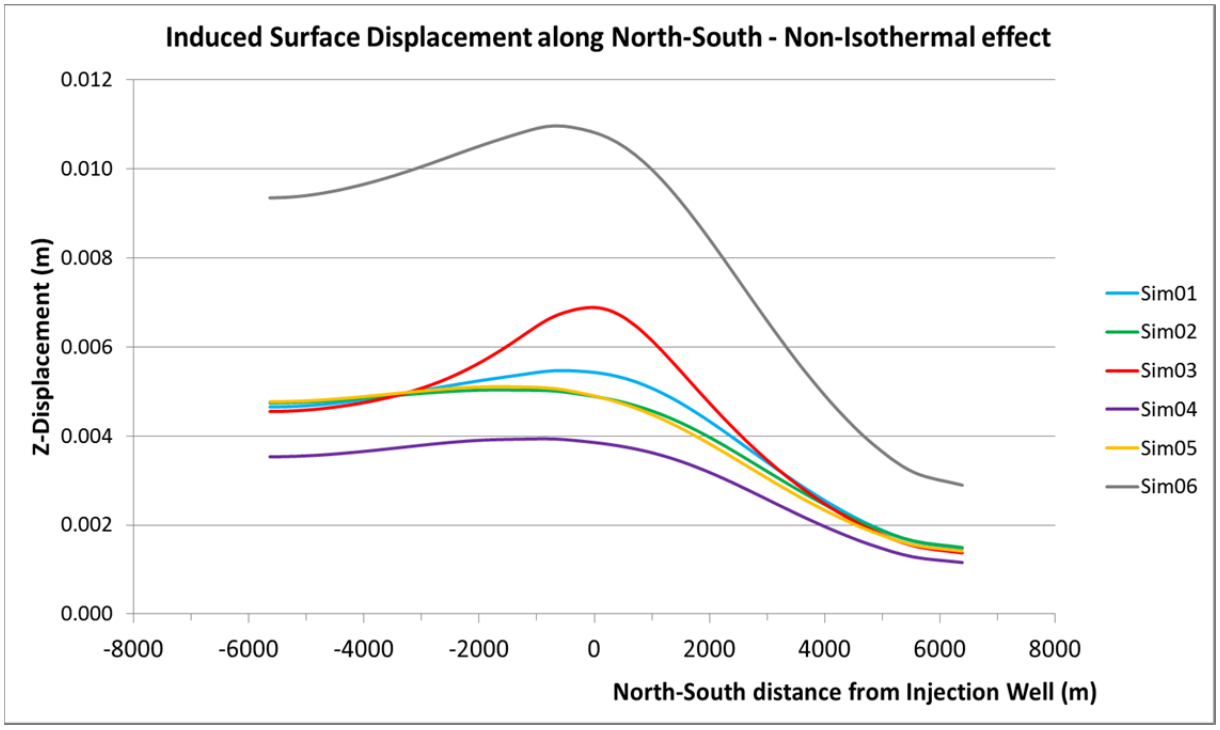

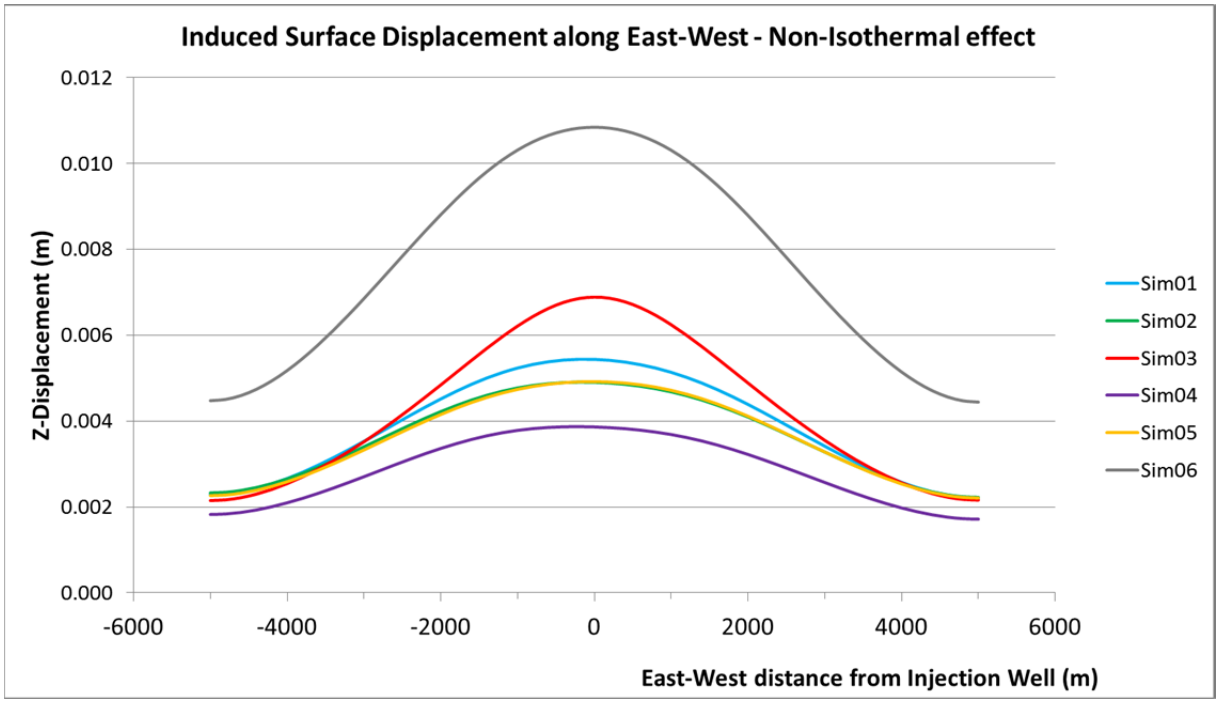

Figure 132: Induced surface displacement (m) in N-S (above) and E-W (below) direction across the injection well, non-isothermal effect for all scenarios for base Pliocene, Ship Shoal Block 84 field.

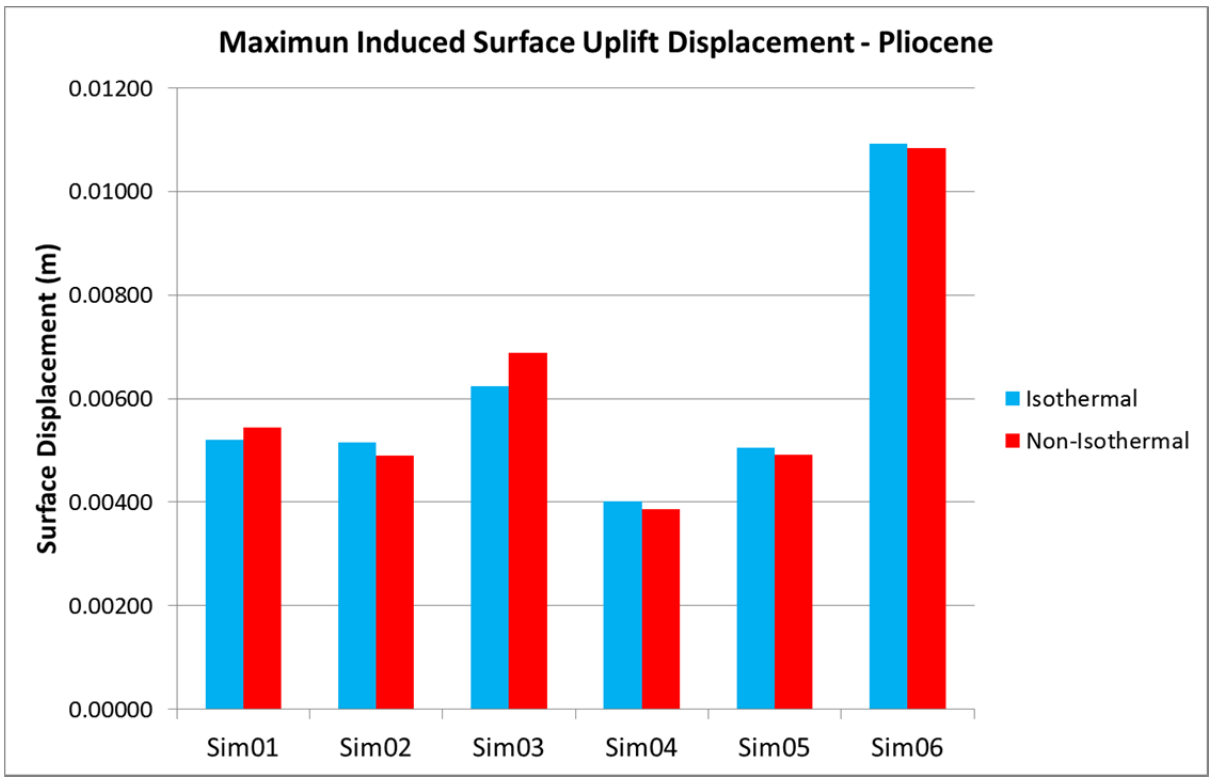

Figure 133: Maximum induced surface displacement (m) for isothermal and non-isothermal effect for all scenarios for base Pliocene, Ship Shoal Block 84 field.

6.3.4 Base Pliocene Geomechanics Model – Potential Fault Activation

Regarding fault reactivation, analysis for potential fault elements failure was performed. From Figure 134 to Figure 137 show the cases for baseline scenario and Sim06 scenario for the original pressure condition and an increment of 3 times, respectively. Note that no element failure was presented along the fault for all cases, even for the most critical Sim06 scenario with 3 times increment of pressure change.

These results can be expected due to the low pressure change of around 2e6 pa (290 psi) as maximum pressure after 30 years of injection and also the long distance of around 3000 m (9840 ft) between the injection point and the fault. Thus, the results indicate low to no risks for fault slips or fault reactivation after 30 years of CO_2 injection and migration with these relatively small pressure change.

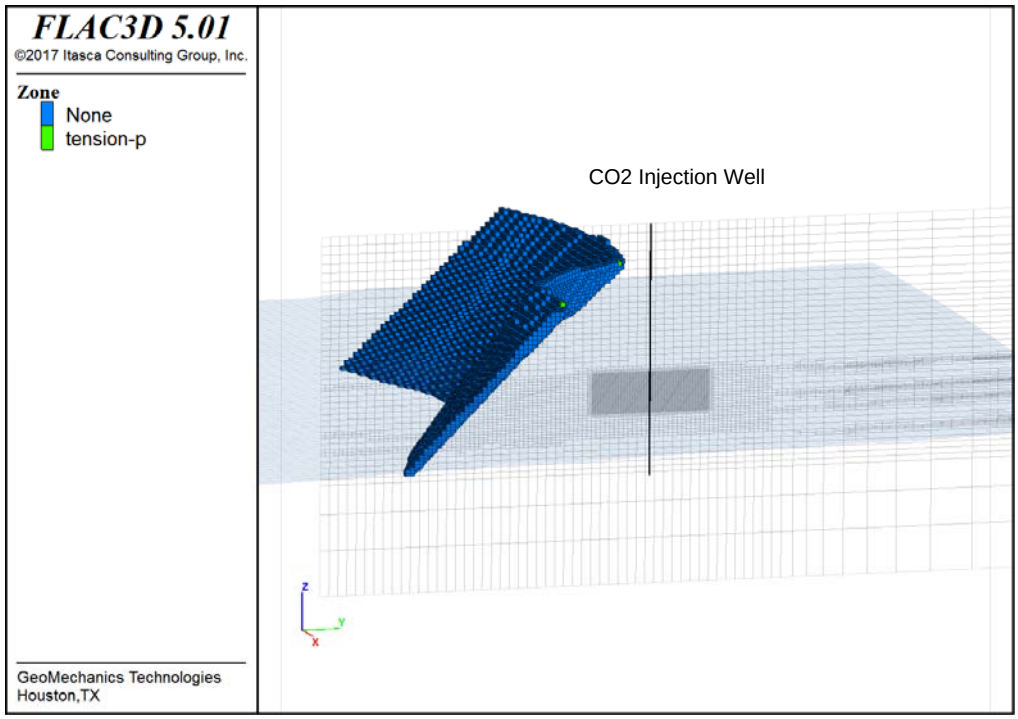

Figure 134: Fault reactivation analysis for baseline scenario, base Pliocene, Ship Shoal Block 84 field.

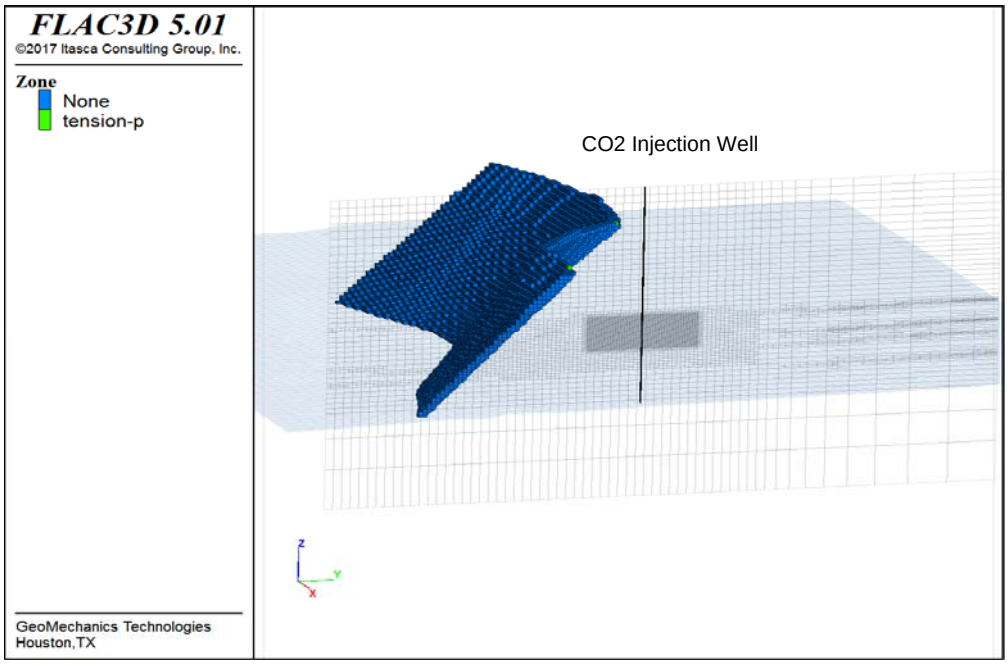

Figure 135: Fault reactivation analysis for baseline scenario with a pressure change increment of 3 times the original pressure, base Pliocene, Ship Shoal Block 84 field.

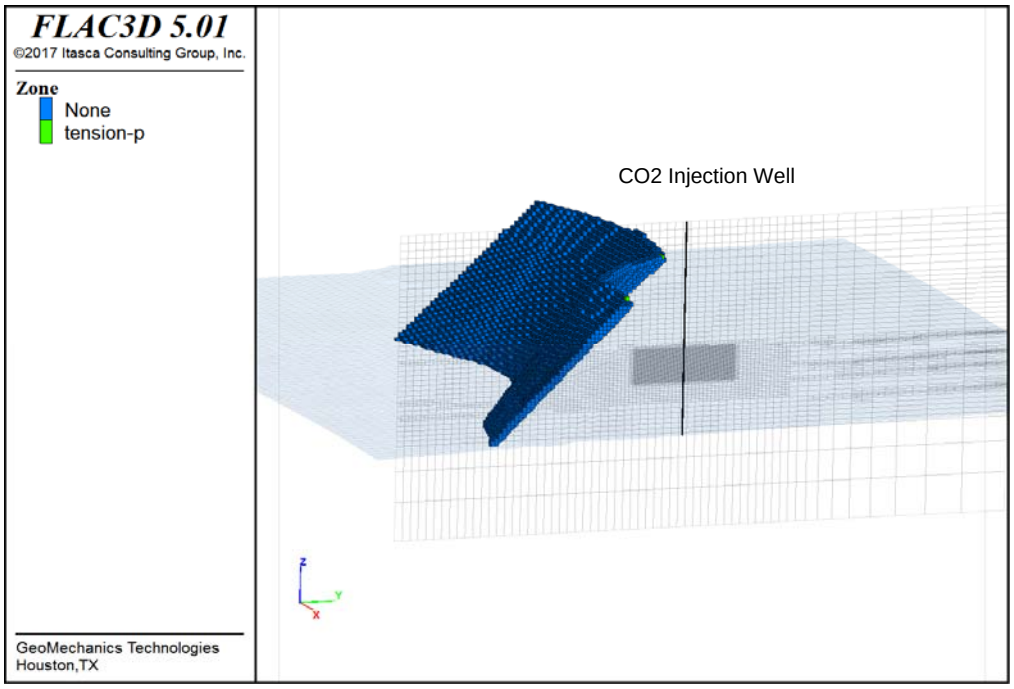

Figure 136: Fault reactivation analysis for Sim06 scenario, base Pliocene, Ship Shoal Block 84 field.

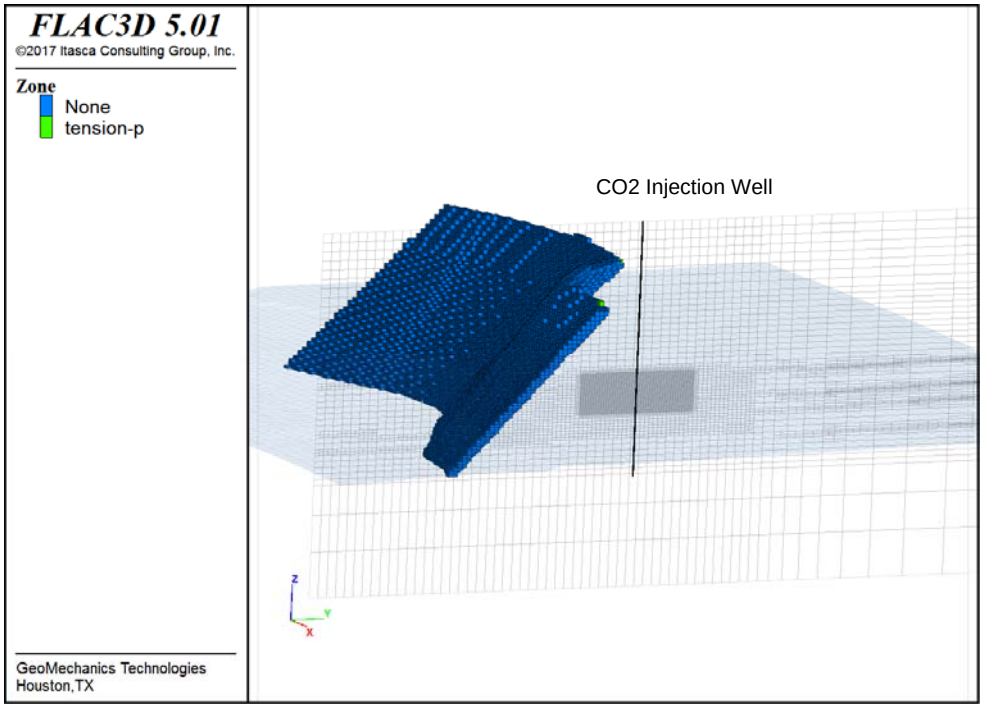

Figure 137: Fault reactivation analysis for Sim06 scenario with a pressure change increment of 3 times the original pressure, base Pliocene, Ship Shoal Block 84 field.

6.3.5 Upper Miocene Geomechanics Model Simulation

For upper Miocene, a similar analysis of induced vertical displacement caused by pressure and temperature change after 30 years of injection was conducted. 3D view and cross-section view across the injection well in E-W direction are presented from Figure 138 through Figure 141 considering isothermal and non-isothermal effect for baseline and Sim06 scenarios, respectively. Similar analyses were also conducted by Sim02, Sim03, Sim04 and Sim05 scenarios and summarized in Figure 142 and Figure 143 for isothermal and non-isothermal effect, respectively.

As seen in Figure 142 for the isothermal effect, a maximum surface uplift displacement ranging from 0.0018 m (0.18 cm or 0.07 in) to 0.0022 m (0.22 cm or 0.08 in) for Sim01, Sim02, Sim03, Sim04 and Sim05 was experienced. Meanwhile, a higher surface displacement around 0.0042 m (0.42 cm or 0.16 in) for Sim06 was estimated and expected because of the injection rate was increased two times in this scenario. Figure 143 shows the results for non-isothermal effect for all scenarios. Note that a maximum surface uplift displacement ranging from 0.0012 m (0.12 cm or 0.04 in) to 0.0013 m (0.13 cm or 0.05 in) for Sim01, Sim02, Sim03, Sim04 and Sim05 was obtained and a higher surface displacement around 0.0025 m (0.25 cm or 0.09 in) for Sim06 was estimated. In general, around 30 % of difference can be observed between isothermal and non-isothermal effect as shown in Figure 144.

Compared with base of Pliocene, a higher temperature effect was obtained for upper Miocene. The temperature change lead to a formation contraction across the injection point and as consequence, lower surface uplift displacement was developed.

In general, it is also important to highlight that these relative small magnitudes indicate low to no risks of a severe surface uplift displacement that can compromise any surface facilities or potential damage after 30 years of CO_2 injection.

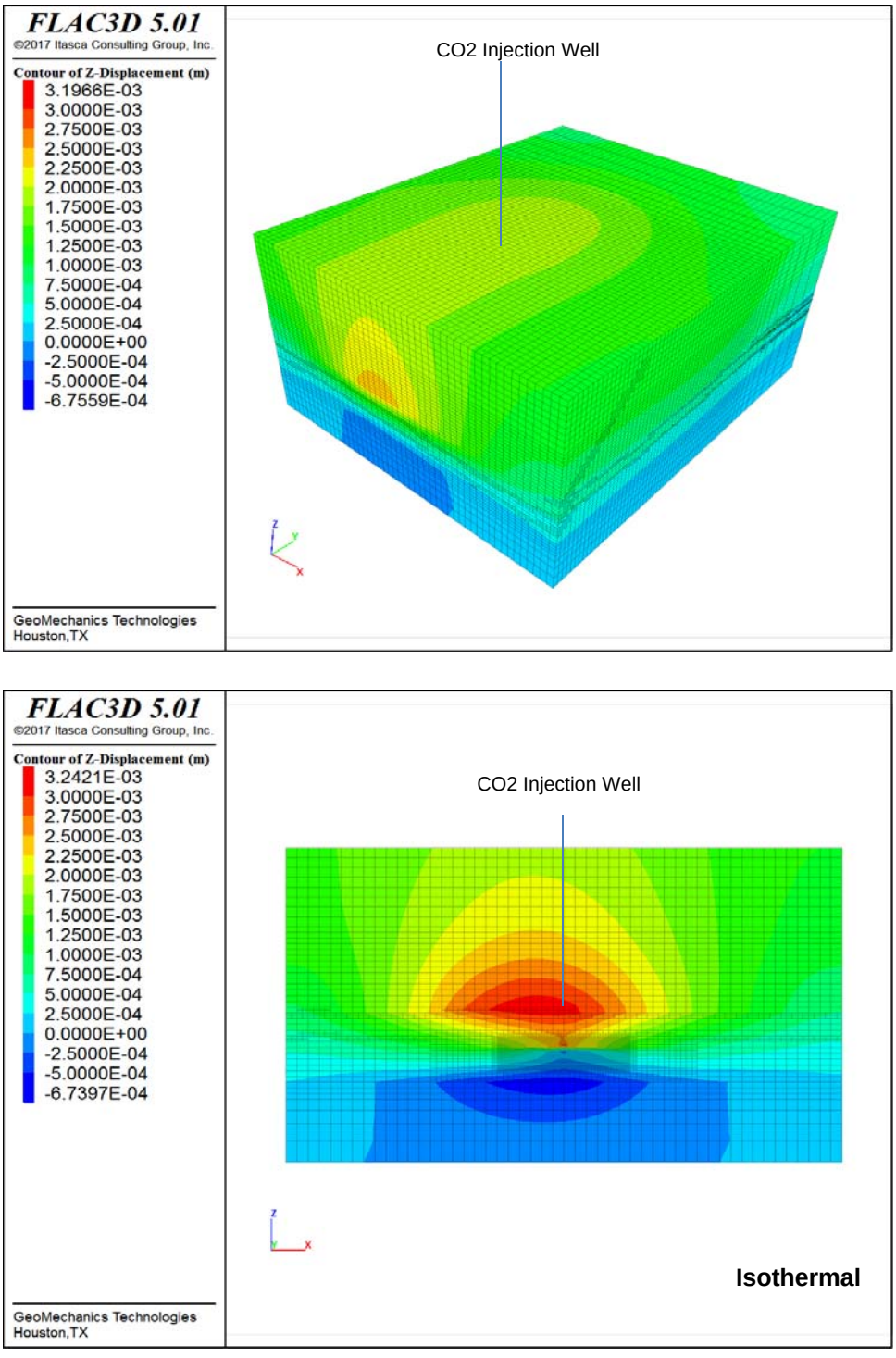

Figure 138: Induced vertical displacement (m) in 3D view (above) and W-E direction (below) across the injection well, isothermal effect, baseline scenario for upper Miocene, Ship Shoal Block 84 field.

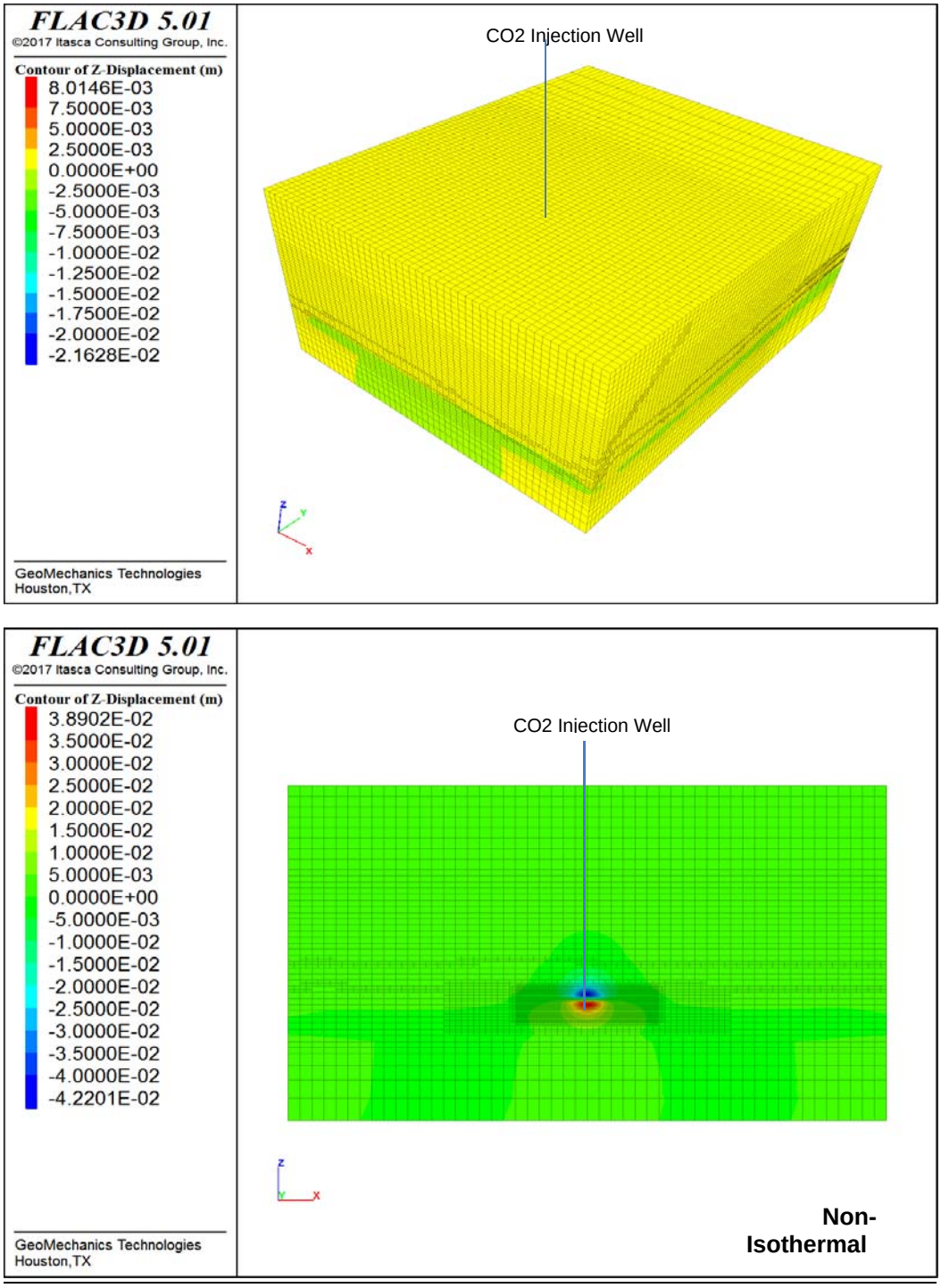

Figure 139: Induced vertical displacement (m) in 3D view (above) and W-E direction (below) across the injection well, non-isothermal effect, baseline scenario for upper Miocene, Ship Shoal Block 84 field.

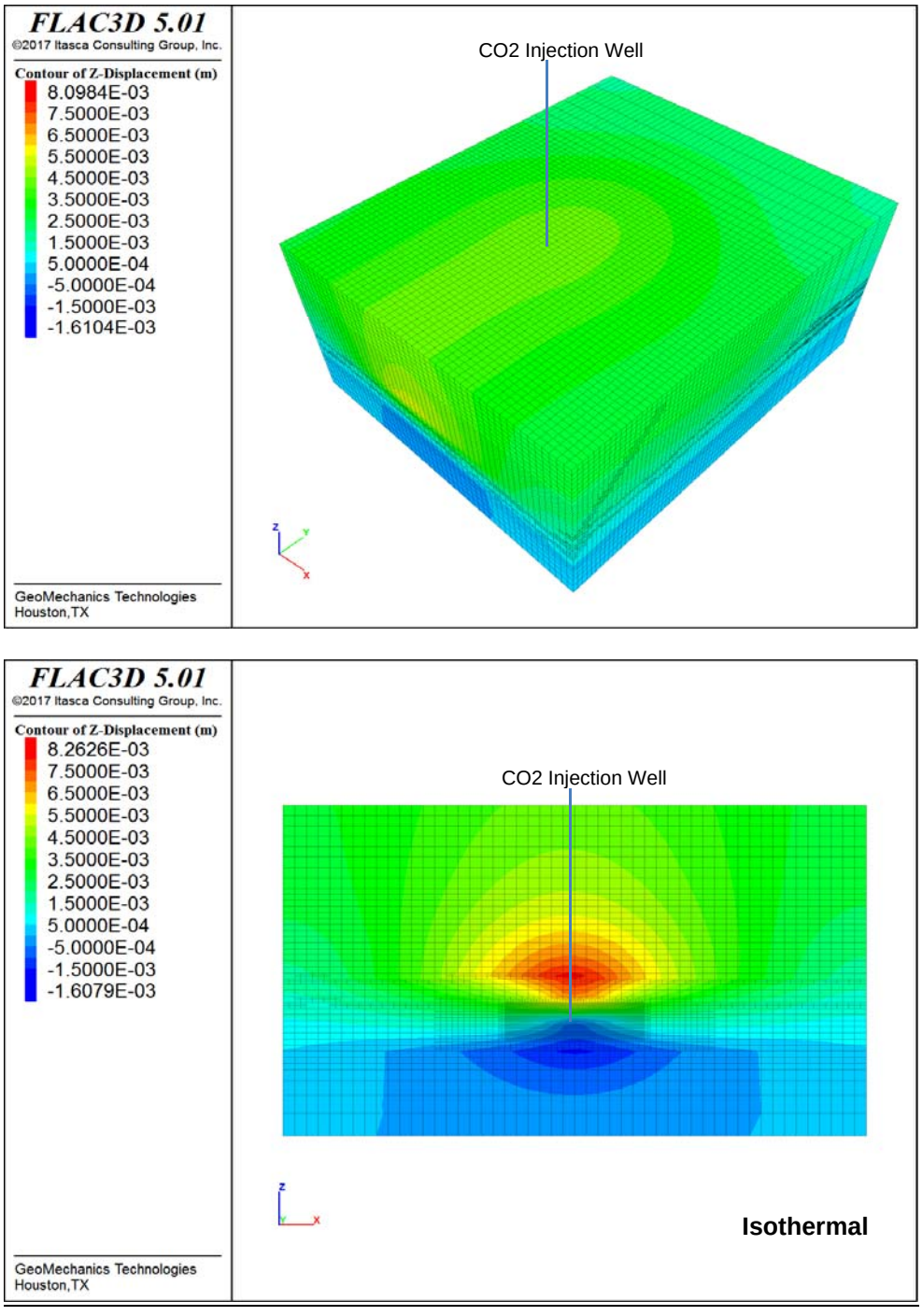

Figure 140: Induced vertical displacement (m) in 3D view (above) and W-E direction (below) across the injection well, isothermal effect, Sim06 scenario for upper Miocene, Ship Shoal Block 84 field.

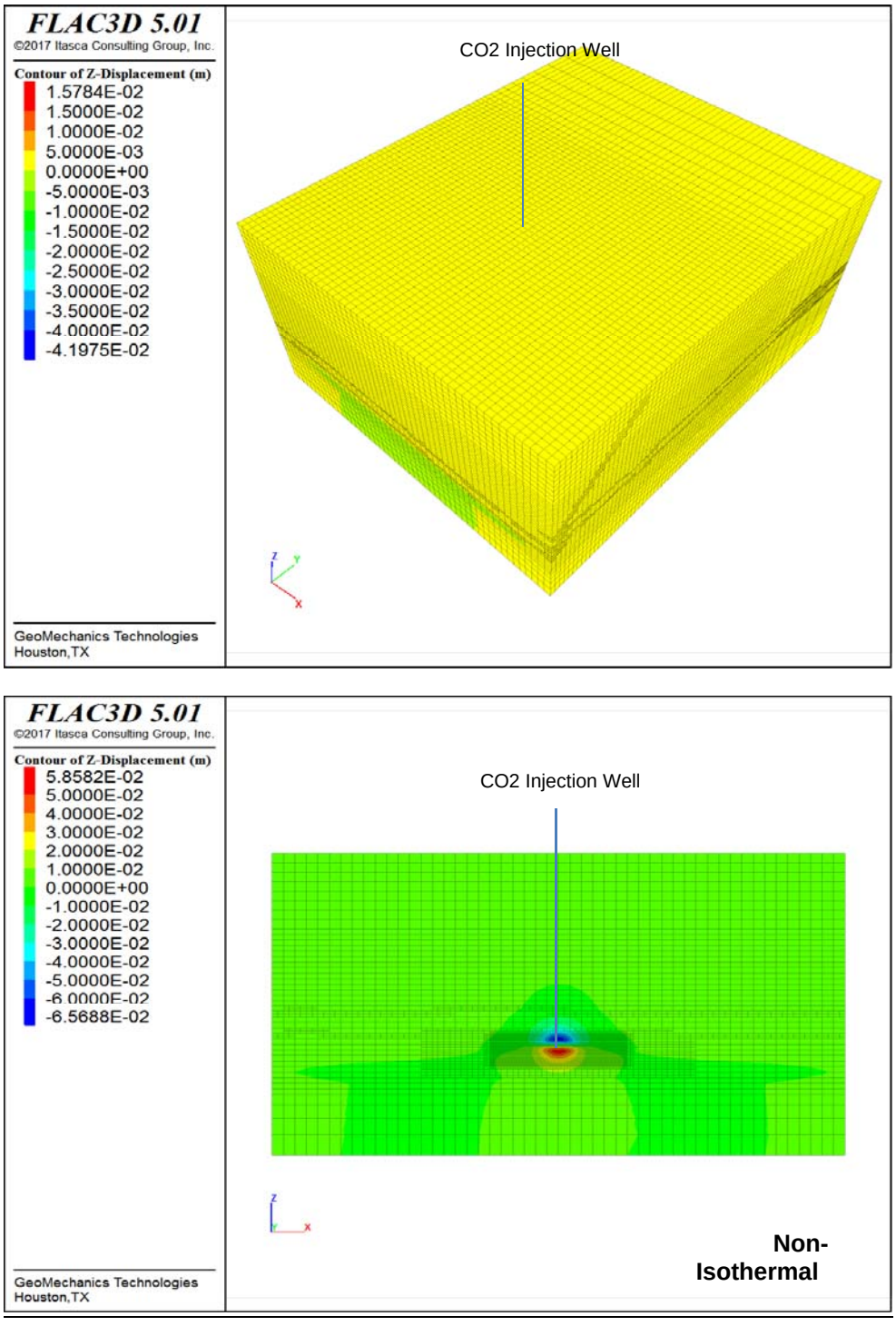

Figure 141: Induced vertical displacement (m) in 3D view (above) and W-E direction (below) across the injection well, non-isothermal effect, Sim06 scenario for upper Miocene, Ship Shoal Block 84 field.

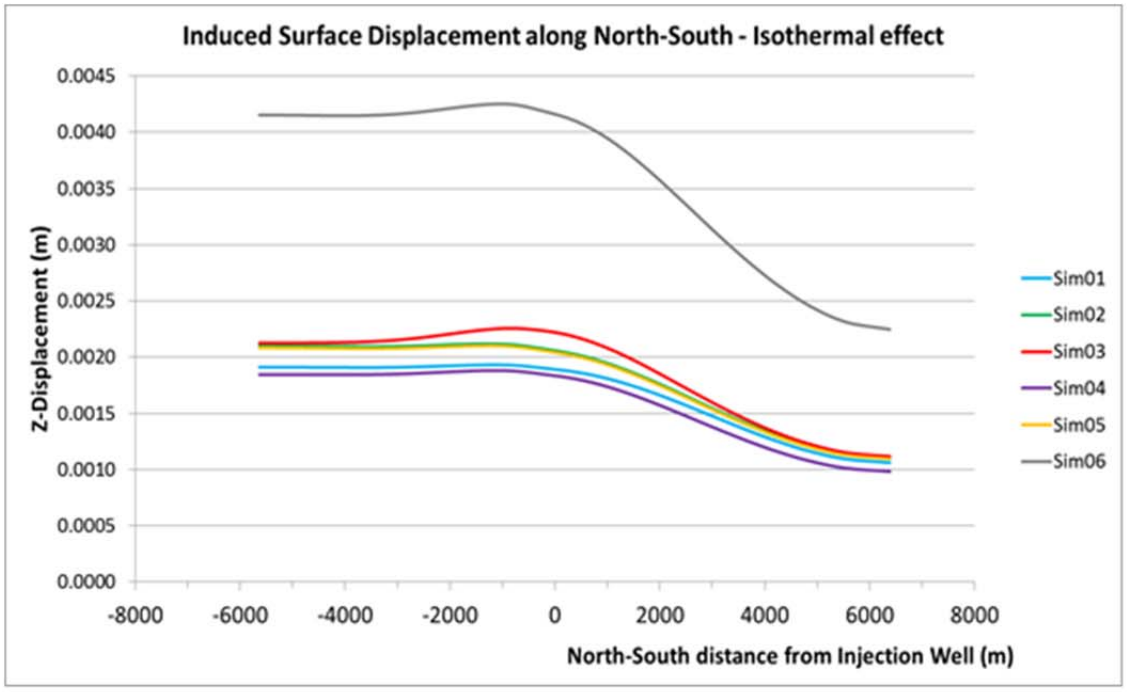

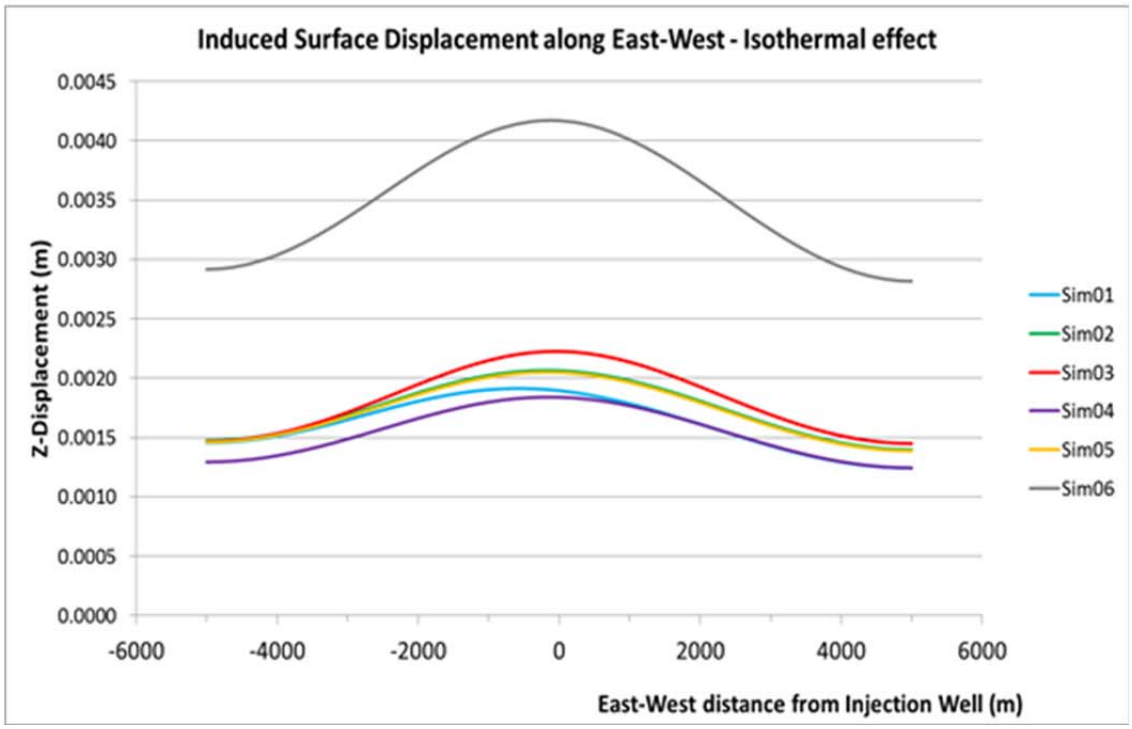

Figure 142: Induced surface displacement (m) in N-S (above) and E-W (below) direction across the injection well, isothermal effect for all scenarios for upper Miocene, Ship Shoal Block 84 field.

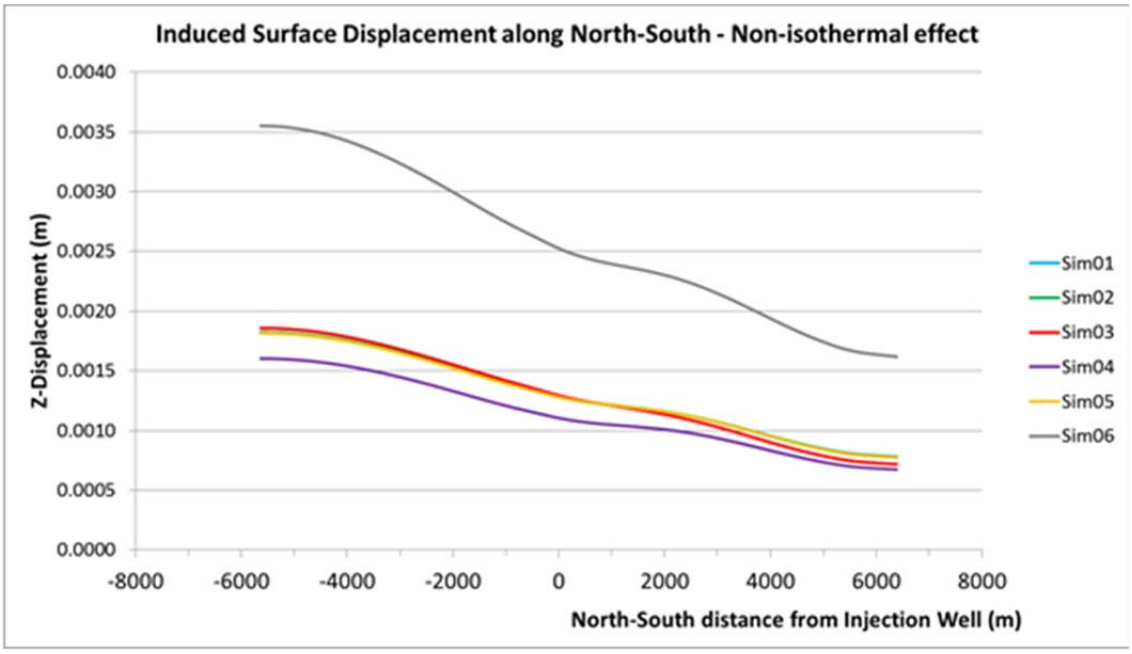

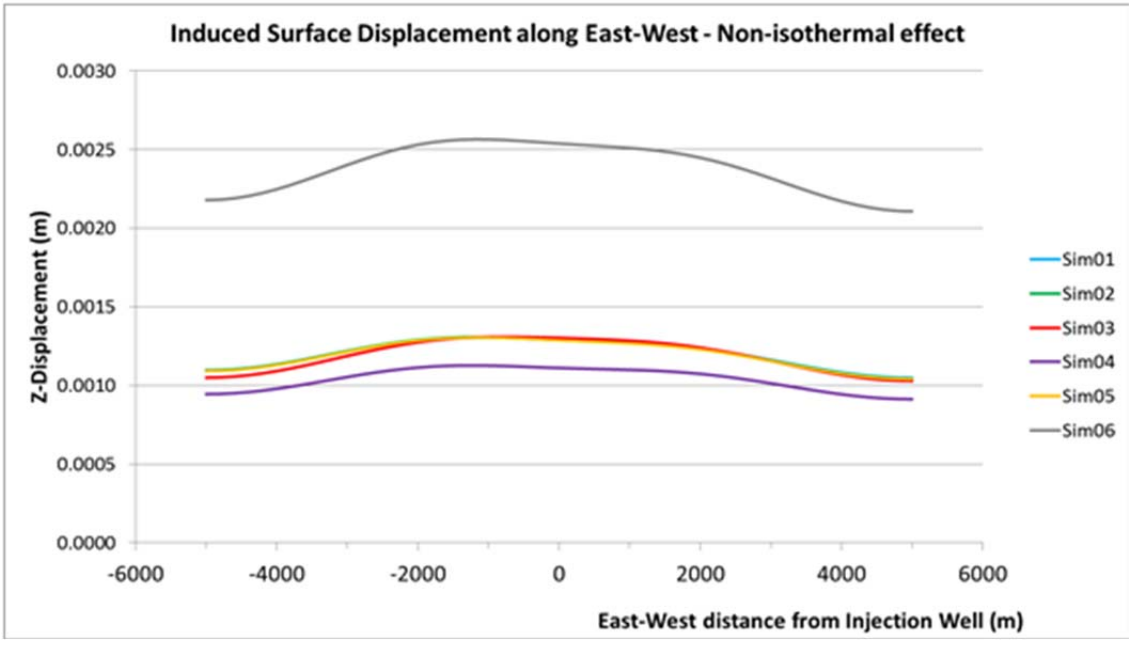

Figure 143: Induced surface displacement (m) in N-S (above) and E-W (below) direction across the injection well, non-isothermal effect for all scenarios for upper Miocene, Ship Shoal 84 Block field.

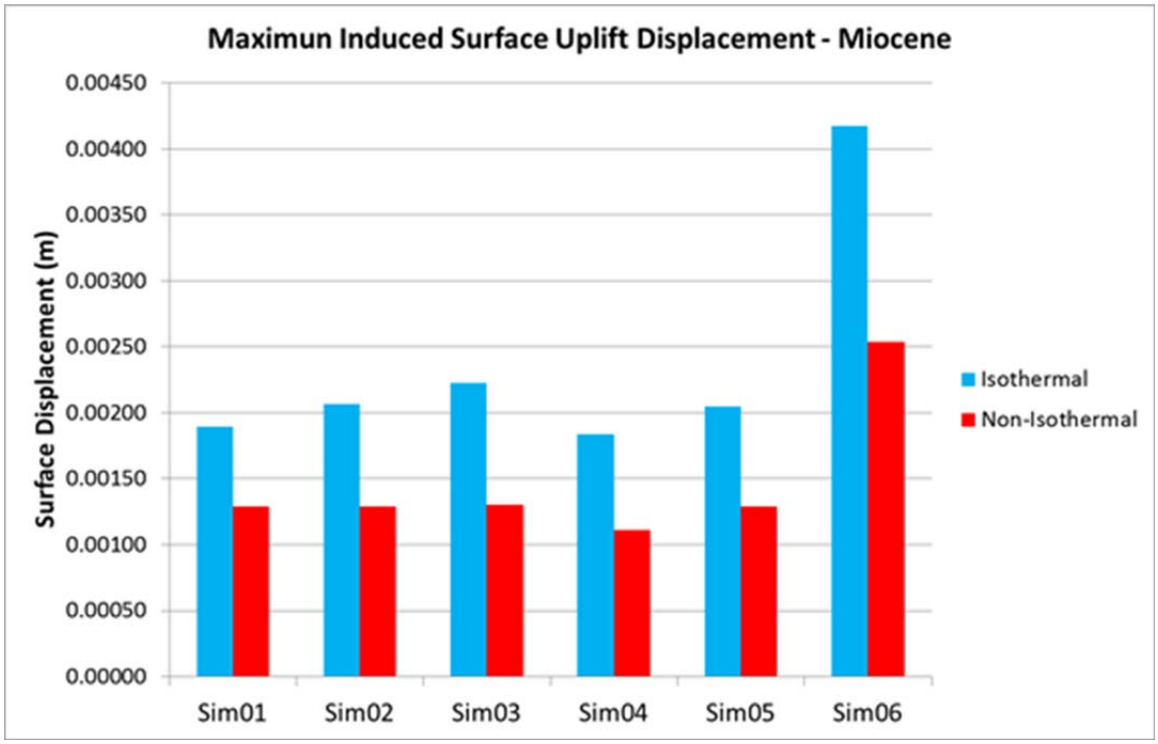

Figure 144: Maximum induced surface displacement (m) for isothermal and non-isothermal effect for all scenarios for upper Miocene, Ship Shoal Block 84 field.

6.3.6 Upper Miocene Geomechanics Model – Potential Fault Activation

For the fault reactivation assessment, potential fault element failures were analyzed. Figure 145 through Figure 148 present the cases for baseline scenario and Sim06 scenario for the original pressure condition and an increment of 3 times, respectively. As seen, no failure was observed along the fault for all cases, even for the most critical Sim06 scenario with an increment of 3 times the original pressure.

After analyze the pressure change imposed after 30 years of CO_2 injection and the distance between the injection point and the fault, these results can be expected due to the low pressure change of around 2.5e6 pa (360 psi) as maximum pressure and also the long distance of around 3500 m (11,480 ft) between the injection point and the fault. Thus, the results indicate low to no risks for fault slips or fault reactivation after 30 years of CO_2 injection and migration with these relatively small pressure change.

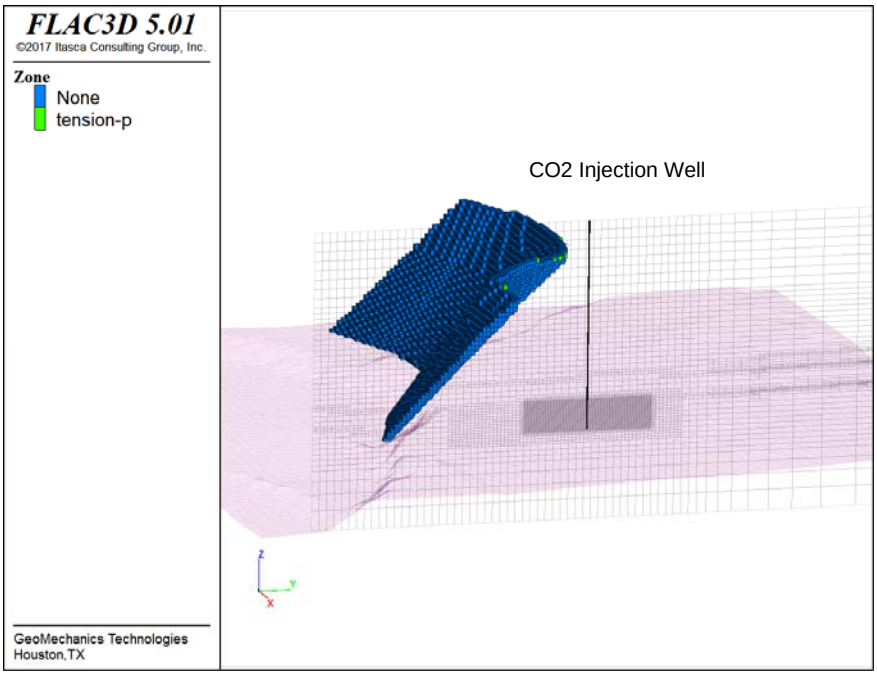

Figure 145: Fault reactivation analysis for baseline scenario, upper Miocene, Ship Shoal Block 84 field.

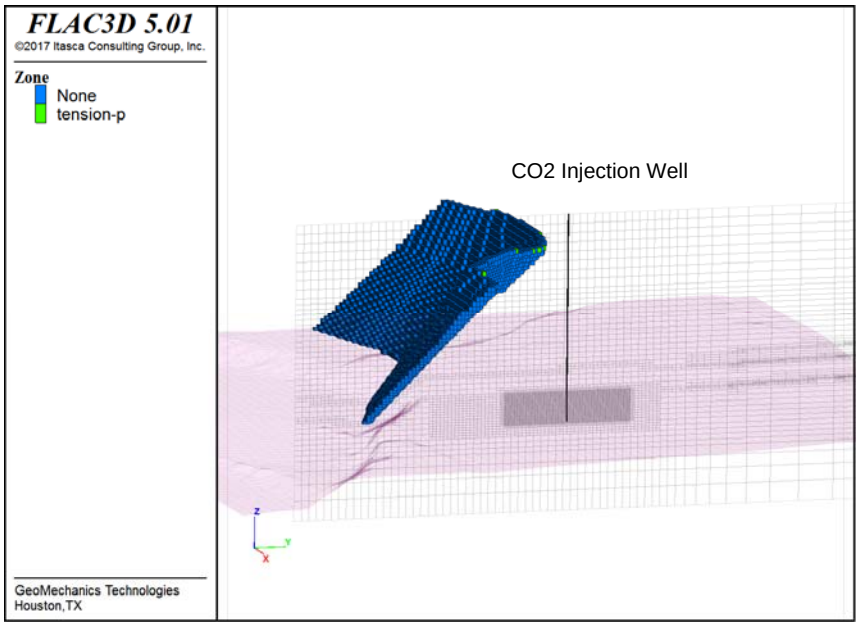

Figure 146: Fault reactivation analysis for baseline scenario with a pressure change increment of 3 times the original pressure, upper Miocene, Ship Shoal Block 84 field.

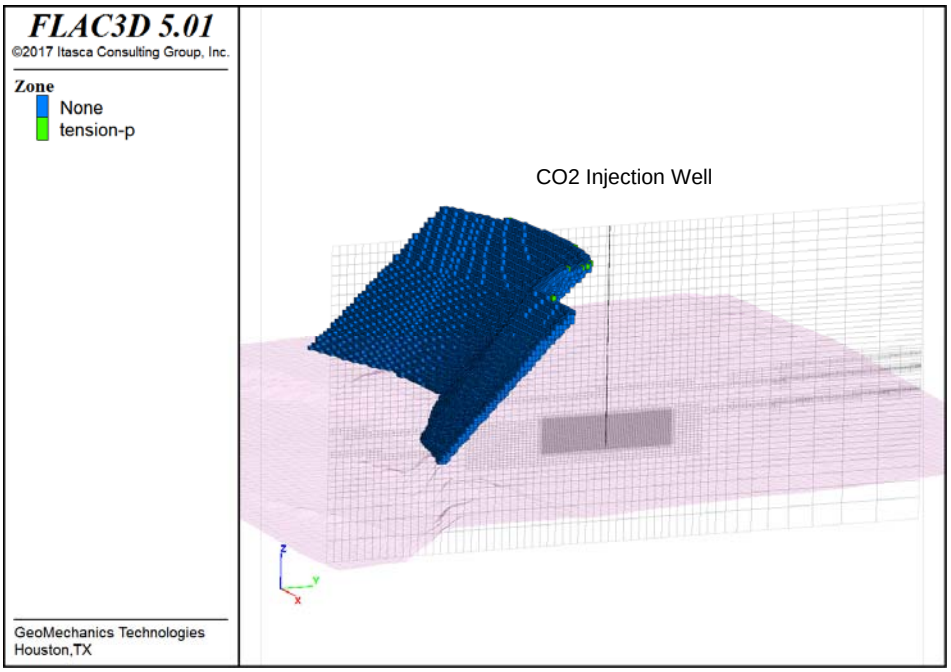

Figure 147: Fault reactivation analysis for Sim06 scenario with original pressure condition, upper Miocene, Ship Shoal Block 84 field.

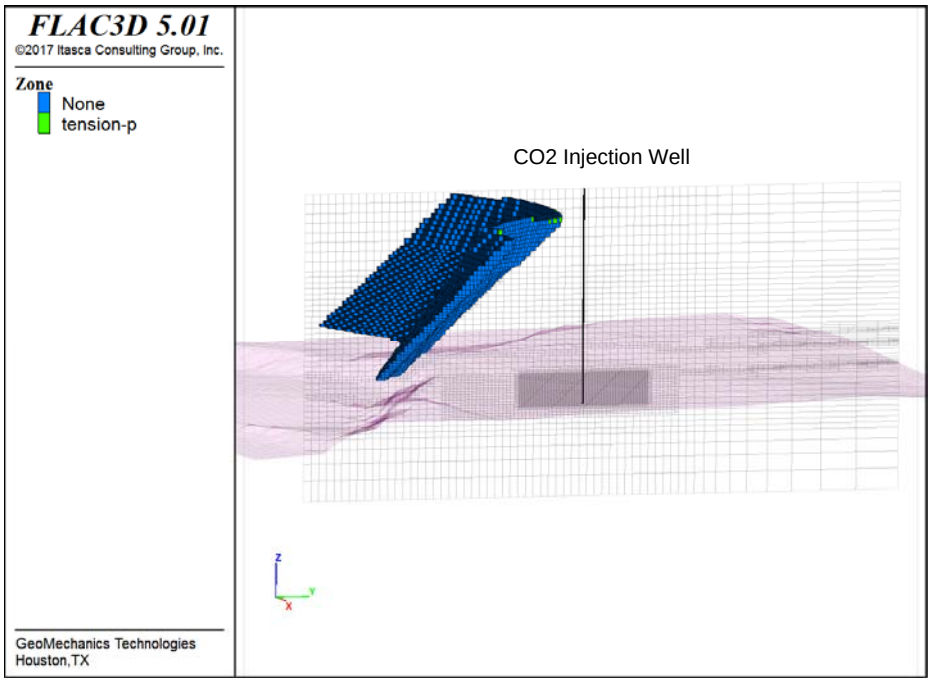

Figure 148: Fault reactivation analysis for Sim06 scenario with a pressure change increment of 3 times the original pressure, upper Miocene, Ship Shoal Block 84 field.

6.4 Conclusions

Block 107 main conclusion are summarize as follows:

GeoMechanics Technologies has developed a 3D geomechanical model for Block 107 of the Ship Shoal area to evaluate induced surface deformation and potential fault reactivation after 30 years CO_2 injection at base of Pliocene and at upper Miocene injection locations. A total of six simulation scenarios were performed.

For base Pliocene injection scenarios, maximum surface uplift is toward the north of the injection well, with a maximum value of about 0.58cm or 0.22 in (worst case scenario – 107_P_Sim03) compared to about 0.49 cm (0.19 in) for the baseline scenario (107_P_Sim01). Similarly for the upper Miocene injection scenarios, maximum surface uplift is toward the north of the injection well, with a maximum value of about 0.85 cm or 0.33 in (worst case scenario – 107_M_Sim02) compared to about 0.55 cm (0.21 in) for the baseline scenario (107_M_Sim01). The center of the maximum surface uplift bowl is spread across in a wide area, at over 3 miles (4.82 km) diameter. For all injection scenarios, the maximum induced shear stresses are less than 7.0E4 Pa (10 psi). The results indicate low to no risks for fault slips or fault reactivation after 30 years of CO_2 injection and migration with these relatively small induced stresses and displacements.

Two sensitivity analyses have been performed for the base Pliocene and upper Miocene geomechanical models to evaluate potential fault activation by significantly increased the change in pressures from the baseline scenarios. The simulations showed that unless the reservoir pressure changes are vastly increased to at least 50 times - more than 23 MPa (3,400 psi) then we would observe any potential fault slippage. Therefore, there are very low or no risks of potential fault activation due to CO_2 injection at Ship Shoal area identified.

Block 84 main conclusion are summarize as follows:

Potential risk of fault reactivation and induced vertical surface uplift displacement after 30 years CO_2 injection in base of Pliocene and Upper Miocene in Ship Shoal field 84 were evaluated, including the isothermal and non-isothermal effect as well as different scenarios of injection rate.

Based on the sensitivity analysis conducted for 12 scenarios with isothermal and non-isothermal effect for base of Pliocene and upper Miocene, relatively small surface uplift magnitude lower than 1 cm for the majority of the scenarios and around 1.6 cm for the most critical case with double injection rate was performed. These relative small magnitudes indicate low to no risks of a severe surface uplift displacement that can compromise any surface facilities or potential damage after 30 years of CO_2 injection. The results also indicate low to no risks for fault slips or fault reactivation after 30 years of CO_2 injection and migration with these relatively small pressure change.

7 Risk assessment and characterization

We have evaluated all well history within Ship Shoal Block 84 and 107 fields for proper plug and abandonment and casing requirements. We also developed a Quantitative Risk and Decision Analysis Tool (QRDAT) for assessing potential leakage during CO_2 injection. In addition, we research the area for seismic risk. The sections below document our results.

7.1 Well Cement History

One potentially serious problem associated with injection into mature sedimentary basins is the possible leakage of injected CO_2 through or along existing well bores. These wells may serve as short-circuit pathways for leakage, which may contaminate the shallow groundwater or subsurface zones, and ultimately leak into the atmosphere. Leakage to the sea floor surface through poorly cemented or abandoned wells is also a major concern.

Possible leakage in abandoned or poorly cemented wells depends on the cement completion practice. When wells are adequately plugged and completed, it is assumed they can trap CO_2 at depth effectively; however, large numbers of orphaned or abandoned wells may not be adequately plugged, completed, or cemented, and such wells represent potential leakage points for CO_2 (Ide et al, 2006). Cementation data for all available wellbores (76 wells within Block 107 and 12 wells within Block 84 fields) have been reviewed for any possible migration risks. Please refer to Appendix A for individual well schematic.

7.1.1 Method

We have searched all publically available data sources and ordered the related well history information from the BOEM website. Wells in green indicate safely abandoned wells that appear to have good integrity. Wells in yellow indicate cautionary wells where further research is required. Depending on the depth of the base of fresh water, some of the cautionary wells may be transferred to the green good-integrity column. Criteria for evaluating into moderate integrity wells are:

- Well not cased, but cement plugs in place,
- Well with surface casing cemented only and cement plugs
- Well with casing but not cemented
- Wells with no top plug

7.1.2 Results

The results are as follows:

7.1.2.1 Ship Shoal Block 107 Field

We have evaluated all 76 well histories within Ship Shoal Block 107 field. (We cannot find the well history for Energy XXI 108-7 ST1 well). The completion integrity for most wells is suitable for safe CO_2 sequestration; as most wellbores are either completely or partially cemented behind casing and contain cement plugs. Table 27 is an inventory of all wells within Block 107 field.

Table 27: Ship Shoal Block 107 Well integrity overview

Good Integrity	Moderate Integrity
Chevron 98-1	Stone 99-A2
Stone 99-1	Chevron 99-2
Stone 99-1 ST1	Chevron 99-4
Stone 99-1 ST2	Chevron 99-5
Stone 99-3	Chevron 107-B1
Stone 99-A1	Chevron 107-5
Stone 99-A1 ST1	Energy XXI 108-1
Stone 99-A2ST1	Energy XXI 108-2
Stone 99-E1	Energy XXI 108-3
Stone 99-E2	Energy XXI 108-4 ST1
Chevron 99-1	Energy XXI 108-7
Chevron 99-3	Energy XXI 108-18
Chevron 99-6	Energy XXI 108-20
Chevron 99-7	Energy XXI 108-21
Chevron 99-8	Energy XXI 108-25
BoisDarc 107-1	Energy XXI 108-27
Chevron 107-1	Energy XXI 108-28
Chevron 107-2	Energy XXI 108-35
Chevron 107-3	Energy XXI 108-40
Chevron 107-4	
Chevron 107-6	
Chevron 107-7	
Energy XXI 108-5	
Energy XXI 108-6	
Energy XXI 108-8	
Energy XXI 108-9	
Energy XXI 108-10	
Energy XXI 108-11	
Energy XXI 108-12	
Energy XXI 108-13	
Energy XXI 108-14	
Energy XXI 108-15	
Energy XXI 108-16 ST1	
Energy XXI 108-17	
Energy XXI 108-19	
Energy XXI 108-22	
Energy XXI 108-23	
Energy XXI 108-24	
Energy XXI 108-26	
Energy XXI 108-29	
Energy XXI 108-30	
Energy XXI 108-31	
Energy XXI 108-32	
Energy XXI 108-33	
Energy XXI 108-34	
Energy XXI 108-34ST1	
Energy XXI 108-36	
Energy XXI 108-37	
Energy XXI 108-38	
Energy XXI 108-39	
Energy XXI 108-41	
Energy XXI 108-41ST1	
Energy XXI 108-41ST2	
Energy XXI 108-41ST2BP	
Energy XXI 108-42	
Energy XXI 108-42ST1	
Energy XXI 108-43	

7.1.2.2 Ship Shoal Block 84 Field

We have reviewed the well schematic, and plugged and abandoned cement plug information for all 12 wells within Ship Shoal Block 84 Field. Current well schematics and cement plug plots for all wells are shown in Appendix A. Table 28 below is a summary of the integrity of these wells.

Table 28: Ship Shoal Block 84 Well Integrity

Good Integrity	Moderate Integrity
Tana 83-1	BP 84-5
Peregrine 84-1	BP 84-A1
BP 84-A3	BP 84-A2
BP 84-A5	BP 84-A4
BP 84-A6	Chevron 99-5
BP 84-A7	
Taylor 85-1BP1	

Seven of the twelve wells appear to have good integrity, with cement seals and plugs in place. Casing was cut and removed for Tana 83-1 (below 3993ft) and Peregrine 84-1 (below 4480ft) wells. Both wells have top cement plugs and cemented surface and intermediate casing impeding the upward migration of CO_2 through these two wellbores.

Moderate integrity is given to wells with questionable abandonment and/or incomplete information. For example, wells BP 84-A1 and BP 84-A4 do not have top plug information, while BP 84-A2 and BP 84-5 only have pre-drilled cement and casing information. Chevron 99-5 appears to only have cement coverage to 4961 ft.

Based on the Plug and Abandon practice of BP on their A platform, we believe BP 84-A1, BP 84-A2, BP 84-A4 and BP 84-5 should have proper top cement plugs, even though the last casing would not be installed for dry wells -- BP 84-A4 and BP 84-5.

7.2 Quantitative Risk and Decision Analysis

We have developed a Quantitative Risk & Decision Analysis Tool (QRDAT) for caprock integrity evaluation, with the aim of assessing the potential for leakage during CO_2 injection. For this purpose we have established a set of parameters (risk factors) that influence the likelihood of caprock failure. We established order of magnitude value ranges for each parameter, which, when applied to particular geologic and operational settings, enable quantification of risk and offer a means by which to compare potential and active storage sites.

We consider three primary leakage mechanisms. These are tensile fracturing of the caprock, fault activation, and well damage. The set of risk factors can be divided into three main groups:

1. Mechanical state of the storage system, which includes stresses, pressures and faults;

2. Caprock and storage zone system, including reservoir and caprock geometry and properties; and
3. Operations, which include the status of the wells and injection practices.

The process of applying QRDAT for caprock integrity evaluation has been discussed in detail in GeoMechanics Technologies' *Development of Improved Caprock Integrity and Risk Assessment Techniques* (2014), a report submitted to the DOE for a different grant and project (DE-FE0009168), and will not be repeated here.

7.2.1 Ship Shoal Block 107 Field

The QRDAT generated mechanical state risk, caprock and storage zone risk, and operations risk for Ship Shoal Block 107 Field are shown in Table 29 through Table 31. The scores generated for the Pliocene and Miocene Ship Shoal Block 107 Field are similar. The total QRDAT score generated for Ship Shoal Block 107 Field for the Pliocene is 750, and for the Miocene is 768. Please see 7.2.3 Comparison to different Storage Sites for comparison.

Table 29: Mechanical state risk factors in risk assessment tool for Ship Shoal Block 107 Field -- Pliocene

MECHANICAL STATE						
	tens frac		fault reac		well fail	
1. STRESS						
Max P/min princ stress						
a. ≥ 0.75	0	100	0	100	0	100
b. 0.5-0.75	1	10	1	10	1	10
c. ≤ 0.5	0	1	0	1	0	1
Stress regime						
a. Compressional	0	100	0	100	0	100
b. Transform	0	10	0	10	0	10
c. Extensional	1	1	1	1	1	1
Shmin/Sv						
a. < 0.55	0	1	0	100	0	100
b. 0.55-0.65	0	1	0	10	0	10
c. > 0.65	1	1	1	1	1	1
2. PRESSURE						
Desired Max P/Discovery P						
a. ≥ 1.5	0	100	0	100	0	100
b. 1.25-1.5	0	10	0	10	0	10
c. ≤ 1.25	1	1	1	1	1	1
Max P/formation depth						
a. ≥ 0.75	0	100	0	100	0	100
b. 0.625-0.75	0	10	0	10	0	10
c. ≤ 0.625	1	1	1	1	1	1
3. FAULTS						
Fault boundaries						
a. Multiple bounding faults	1	1	1	100	1	100
b. One bounding fault	0	1	0	10	0	10
c. None	0	1	0	1	0	1
Natural seismicity						
a. High	0	100	0	100	0	100
b. Moderate	0	10	0	10	0	10
c. Low	1	1	1	1	1	1
Category Score	16		115		115	
Category Total Score	246					

Table 30: Caprock and storage zone risk factors in risk assessment tool for Ship Shoal Block 107 Field – Pliocene

CAPROCK-STORAGE ZONE SYSTEM						
	tens frac		fault reac		well fail	
4. STORAGE ZONE SPECIFIC						
Lateral extent/storage zone depth						
a. <25	1	100	1	100	1	100
b. 25-100	0	10	0	10	0	10
c. >100	0	1	0	1	0	1
Storage zone thickness/storage zone depth						
a. > 0.5	0	100	0	100	0	1
b. 0.1-0.5	0	10	0	10	0	1
c. < 0.1	1	1	1	1	1	1
5. CAPROCK SPECIFIC						
Caprock heterogeneity						
a. Significant	0	100	0	100	0	1
b. Moderate	0	10	0	10	0	1
c. Low	1	1	1	1	1	1
Caprock strength						
a. Weak	0	100	0	100	0	100
b. Moderate	0	10	0	10	0	10
c. Strong	1	1	1	1	1	1
Caprock thickness						
a. ≤ 10 ft	0	100	0	100	0	1
b. 10-100 ft	0	10	0	10	0	1
c. ≥ 100 ft	1	1	1	1	1	1
Caprock lateral extent/caprock thickness						
a. <25	0	100	0	100	0	100
b. 25-100	1	10	1	10	1	10
c. >100	0	1	0	1	0	1
Caprock permeability						
a. k > 1 mD	1	100	1	1	1	1
b. 1E-3 mD ≤ k ≤ 1 mD	0	10	0	1	0	1
c. k < 1E-3 mD	0	1	0	1	0	1
Number of caprocks						
a. Single	0	100	0	100	0	100
b. Double	0	10	0	10	0	10
c. Multiple	1	1	1	1	1	1
Caprock dip						
a. γ ≥ 8°	0	1	0	100	0	1
b. 2°<γ<8°	1	1	1	10	1	1
c. γ ≤ 2°	0	1	0	1	0	1
Category Score	216		126		117	
Category Total Score	459					

Table 31: Operating parameters risk factors in risk assessment tool for Ship Shoal Block 107 Field -- Pliocene

OPERATIONS						
	tens frac		fault reac		well fail	
6. OPERATIONS						
Well density						
a. >15 wells/Km2	0	1	0	1	0	100
b. 5-15 wells/Km2	1	1	1	1	1	10
c. <5 wells/Km2	0	1	0	1	0	1
No. of uncased wells/total no. of wells						
a. >0.6	0	1	0	1	0	100
b. 0.2-0.6	1	1	1	1	1	10
c. <0.2	0	1	0	1	0	1
ΔT between CO2 and storage zone						
a. ≥ 60 ◦C	0	100	0	100	0	1
b. 30 ◦C - 60 ◦C	1	10	1	10	1	1
c. ≤ 30 ◦C	0	1	0	1	0	1
Category Score	12		12		21	
Category Total Score	45					

7.2.2 Ship Shoal Block 84 Field

The QRDAT generated for Ship Shoal Block 84 Field are shown in Table 32 through Table 34. The total QRDAT score generated for Ship Shoal Block 84 field is 750 for the Pliocene and 737 for the Miocene.

Table 32: Mechanical state risk factors in risk assessment tool for Ship Shoal Block 84 Field – Miocene

MECHANICAL STATE						
	tens frac		fault reac		well fail	
1. STRESS						
Max P/min princ stress						
a. ≥ 0.75	0	100	0	100		100
b. 0.5-0.75	1	10	1	10		10
c. ≤ 0.5	0	1	0	1		1
Stress regime						
a. Compressional	0	100	0	100		100
b. Transform	0	10	0	10		10
c. Extensional	1	1	1	1		1
Shmin/Sv						
a. < 0.55	0	1	0	100		100
b. 0.55-0.65	0	1	0	10		10
c. > 0.65	1	1	1	1		1
2. PRESSURE						
Desired Max P/Discovery P						
a. ≥ 1.5	0	100	0	100		100
b. 1.25-1.5	0	10	0	10		10
c. ≤ 1.25	1	1	1	1		1
Max P/formation depth						
a. ≥ 0.75	0	100	0	100	0	100
b. 0.625-0.75	0	10	0	10	0	10
c. ≤ 0.625	1	1	1	1	1	1
3. FAULTS						
Fault boundaries						
a. Multiple bounding faults	1	1	1	100	1	100
b. One bounding fault	0	1	0	10	0	10
c. None	0	1	0	1	0	1
Natural seismicity						
a. High	0	100	0	100	0	100
b. Moderate	0	10	0	10	0	10
c. Low	1	1	1	1	1	1
Category Score	16		115		102	
Category Total Score	233					

Table 33: Caprock and storage zone risk factors in risk assessment tool for Ship Shoal Block 84 Field – Miocene

CAPROCK-STORAGE ZONE SYSTEM						
	tens frac		fault reac		well fail	
4. STORAGE ZONE SPECIFIC						
Lateral extent/storage zone depth						
a. <25	1	100	1	100	1	100
b. 25-100	0	10	0	10	0	10
c. >100	0	1	0	1	0	1
Storage zone thickness/storage zone depth						
a. > 0.5	0	100	0	100	0	1
b. 0.1-0.5	0	10	0	10	0	1
c. < 0.1	1	1	1	1	1	1
5. CAPROCK SPECIFIC						
Caprock heterogeneity						
a. Significant	0	100	0	100	0	1
b. Moderate	1	10	1	10	1	1
c. Low	0	1	0	1	0	1
Caprock strength						
a. Weak	0	100	0	100	0	100
b. Moderate	0	10	0	10	0	10
c. Strong	1	1	1	1	1	1
Caprock thickness						
a. ≤ 10 ft	0	100	0	100	0	1
b. 10-100 ft	0	10	0	10	0	1
c. ≥ 100 ft	1	1	1	1	1	1
Caprock lateral extent/caprock thickness						
a. <25	0	100	0	100	0	100
b. 25-100	1	10	1	10	1	10
c. >100	0	1	0	1	0	1
Caprock permeability						
a. k > 1 mD	1	100	1	1	1	1
b. 1E-3 mD ≤ k ≤ 1 mD	0	10	0	1	0	1
c. k < 1E-3 mD	0	1	0	1	0	1
Number of caprocks						
a. Single	0	100	0	100	0	100
b. Double	0	10	0	10	0	10
c. Multiple	1	1	1	1	1	1
Caprock dip						
a. γ ≥ 8°	0	1	0	100	0	1
b. 2°<γ<8°	0	1	0	10	0	1
c. γ ≤ 2°	1	1	1	1	1	1
Category Score	225		126		117	
Category Total Score	468					

Table 34: Operating parameters risk factors in risk assessment tool for Ship Shoal Block 84 Field -- Miocene

OPERATIONS						
	tens frac		fault reac		well fail	
6. OPERATIONS						
Well density						
a. >15 wells/Km2	0	1	0	1	0	100
b. 5-15 wells/Km2	0	1	0	1	0	10
c. <5 wells/Km2	1	1	1	1	1	1
No. of uncased wells/total no. of wells						
a. >0.6	0	1	0	1	0	100
b. 0.2-0.6	1	1	1	1	1	10
c. <0.2	0	1	0	1	0	1
ΔT between CO2 and storage zone						
a. ≥ 60 ◦C	0	100	0	100	0	1
b. 30 ◦C - 60 ◦C	1	10	1	10	1	1
c. ≤ 30 ◦C	0	1	0	1	0	1
Category Score	12		12		12	
Category Total Score	36					

7.2.3 Comparison to different Storage Sites

The total score generated for Ship Shoal Block 107 and Block 84 Fields by QRDAT is 750 to 768, and 737 to 750, respectively. Next we compared this number to known and potential CO_2 sequestration sites -- Kevin Dome, Loudon, Wilmington Graben, Sleipner, In Salah, and Illinois Industrial CCS, as shown in Table 35 and a graphic presentation in Figure 149 for the three types of risk factors. Table 36 and Figure 150 shows the risk based on failure types.

Ship Shoal Block 84 and 107 fields pose similar risk as the other known CO_2 sequestration sites, but much less than the Wilmington Graben, a site in offshore southern California where we analyzed the Pliocene – Miocene turbidite reservoirs for CO_2 sequestration. Note, we did not recommend using Wilmington Graben for CO_2 sequestration.

Table 35: The relative risk ranking based on 3 types of risk factors

Category	Range	Kevin Dome	Loudon	Wil Graben	Sleipner	In Salah	Illinois Ind CCS	SS 107_Plio	SS 84_Mio
Mechanical state	21-1902	345	660	840	102	390	633	246	233
Caprock-Storage Zone system	27-2007	27	45	972	396	81	99	459	468
Operations	9-405	9	27	27	9	27	117	45	36
TOTAL	57-4314	381	732	1839	507	498	849	750	737

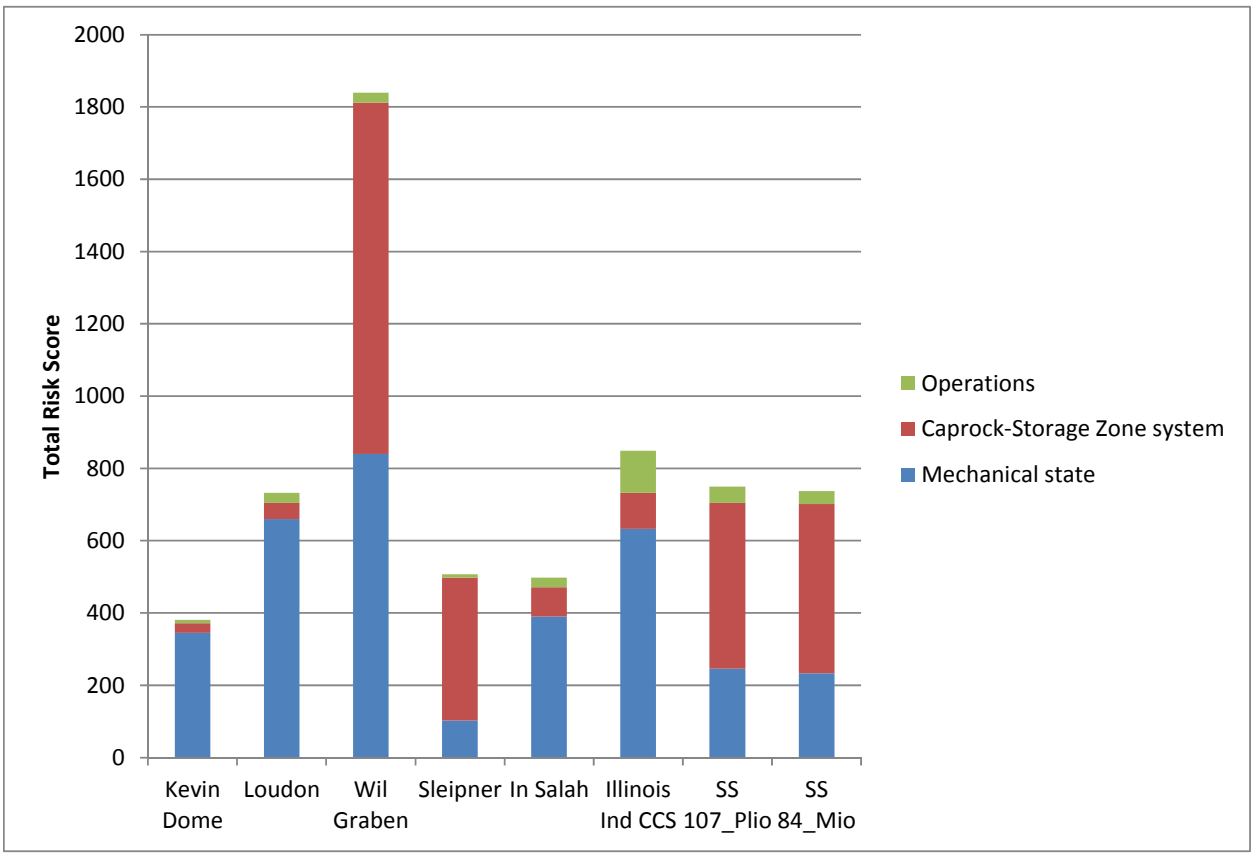

Figure 149: Graphic presentation of risk categories

Table 36: The relative risk ranking based on failure types

Category	Range	Kevin Dome	Loudon	Wilmington Graben	Sleipner	In Salah	Illinois Ind CCS	SS 107_Plio	SS 84_Mio
Tensile fracturing	19-1405	127	235	559	172	163	253	244	253
Fault (re)activation	19-1603	127	244	748	172	172	253	253	253
Wellbore failure	19-1306	127	253	532	163	163	343	253	231
TOTAL	57-4314	381	732	1839	507	498	849	750	737

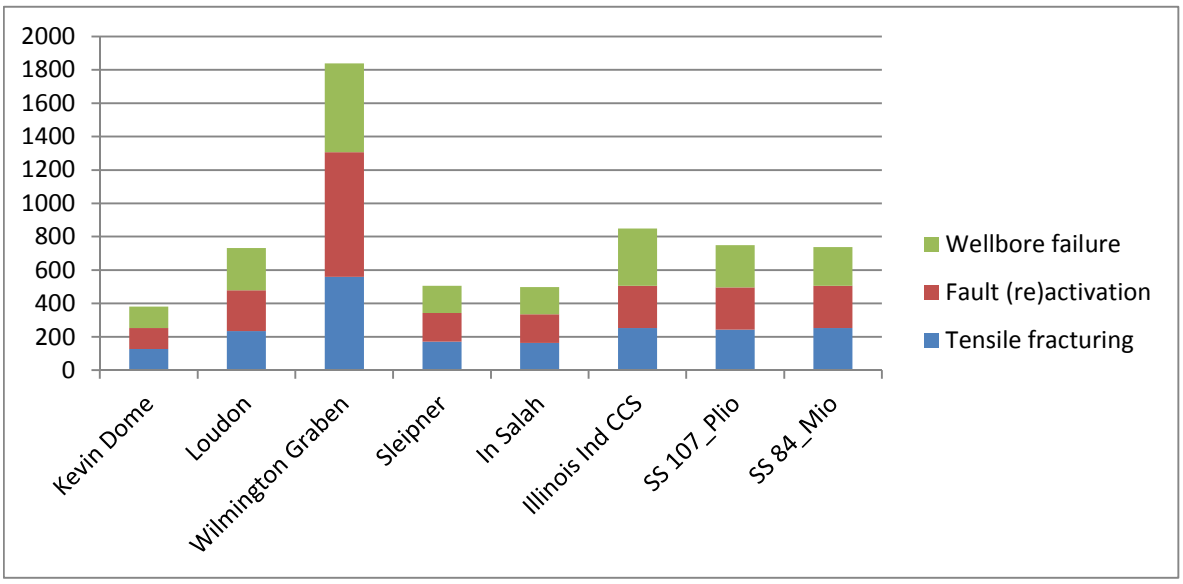

Figure 150: Graphic presentation of failure type

A brief description and background is contained below on the different CO_2 storage sites used in the comparison:

7.2.3.1 Kevin Dome Carbon Storage Project:

Location: Northern Montana, USA

Injection to date: None

This project was managed by the Big Sky Sequestration Partnership (BSCSP). The primary objective of this project was to determine how injected CO_2 chemically reacts with formation rocks and how that affects permanent storage. The project accomplished a very detailed geologic site characterization including seismic surveying, the drilling and coring of two wells, and initial flow and reactive transport modeling. However, this site is no longer considered for large-scale CO2 sequestration because the groundwater lacks sufficient salinity levels at the target injection zone (~4000 ft deep). The project was halted in late 2016/ early 2017.

7.2.3.2 Louden Single-Well Huff 'n' Puff:

Location: Fayette County, Illinois, USA

Injection to Date: 43 tons over summer 2007

This project was managed by the Midwest Geological Sequestration Consortium (MGSC) and was active from 2005 to 2009. The primary objective of this project was to test carbon dioxide huff 'n' puff (HNP) for enhanced oil recovery. This test was performed into a sandstone reservoir at 15,00ft depth. This was a short pilot project to see if CO_2 caused an increase in oil production and if CO_2 would remain sequestered in the target zone. All results were successful.

7.2.3.3 Wilmington Graben:

Location: Offshore Los Angeles, California, USA

Injection to Date: None

The Wilmington Graben project was a CO_2 sequestration characterization project managed by GeoMechanics Technologies (formerly Terralog Technologies). The site was deemed incapable of large-scale storage because flow simulations indicated undesirable vertical CO_2 plume migration through the caprock.

7.2.3.4 Sleipner CO_2 Storage:

Location: Offshore Norway

Injection To Date: 16.5 million tons

The Sleipner project started in 1996 and is a large-scale fully dedicated geologic storage project located offshore Norway. Captured CO_2 is directly injected into an offshore sandstone reservoir. The injection rate is 0.85 million tons of CO_2 per year. To date, 16.5 million tons have been injected.

7.2.3.5 InSalah CO_2 Storage:

Location: Algeria

Injection To Date: 3.8 MT of CO_2 until injection suspended in 2011 due to integrity of the seal.

Injection began in 2004 and continued until 2011 when the project was halted due to potential leakage concerns through the caprock. Injection occurred into the Krechba Formation, located at approximately 6,200 feet deep. The target injection zone is a depleted gas reservoir and is estimated to contain 17 million tons of storage.

7.2.3.6 Illinois Industrial Carbon Capture and Storage

Location: Decatur, Illinois, USA

Injection To Date: 999,215 MT of CO_2 (as Illinois Basin Decatur Project) and 34,626 MT of CO_2 (as Illinois Industrial Carbon Capture and Storage) as of April 26, 2017.

This project initially began as the Illinois Basin Decatur Project, which ran from 2011 to 2014. In April 2017, it became the Illinois Industrial Carbon Capture and Storage project, which is a commercial scale facility that injects CO_2 emissions from an existing corn-to-ethanol plant. This project contains the only two Class VI CO_2 injection wells in the US. Injection occurs into a large saline sandstone aquifer (Mt. Simon Formation) at a depth of 7,000 feet. The site can store approximately one million tons of CO_2 per year.

This project contains a strict monitoring program including shallow groundwater sampling, deep groundwater sampling, well logging, mechanical integrity testing, pressure and

temperature monitoring, CO_2 stream analysis, and geophysical monitoring. Monitoring responsibilities are carried out by Archer Daniels Midland as well as other subcontractors.

7.3 Seismicity Risk

Seismicity in the Gulf of Mexico is relative low. Since 1978, there have been about 10 earthquakes located in the eastern Gulf of Mexico. These earthquakes are mostly small magnitude (3 to 4) events except the two events with magnitudes of 5.3 and 5.9 that occurred during 2006. The small magnitudes of these events are consistent with the absence of tsunamis in the recent historical record of the Gulf coast states (University of Florida website). Earthquake-generated tsunamis generally originate by the sudden vertical movement of a large area of the seafloor during an earthquake. The Gulf of Mexico basin is devoid of subduction zones or potential sources of large reverse faults (Brink, et al., 2009). However, even earthquakes with modest magnitudes (6.0) can produce a tsunami if they occur in the vicinity of unstable sediments deposited on a sloping surface (University of Florida website).

Frohlich (1982), and Brink, et al., (2009) explained the cause of the 5.3 magnitude earthquake occurring on Feb. 10, 2006 in Green Canyon offshore Louisiana, the 5.9 magnitude earthquake on Sept. 10, 2006, the 4.9 magnitude event on July 24, 1978 and other moderate earthquakes in the gulf as related to stresses associated with the downwarping of the lithosphere caused by the accumulation of sediments. University of Florida depicted a schematic showing the possible explanation of the 2006 earthquakes (Figure 151). During the 2005 Katrina hurricane, the Mississippi River sediments deposited in shallow water near the Gulf Coast were redeposited to deeper Gulf waters. Added delta sediments in the deep Gulf increase the load on the underlying Mesozoic oceanic crust of the Gulf, causing it to flex down. Shallow portions of the crust undergo compression during flexure, producing the earthquake on a steeply-dipping fault plane. The fault may have occurred by reactivation of an older Rift sequence fault (University of Florida website).

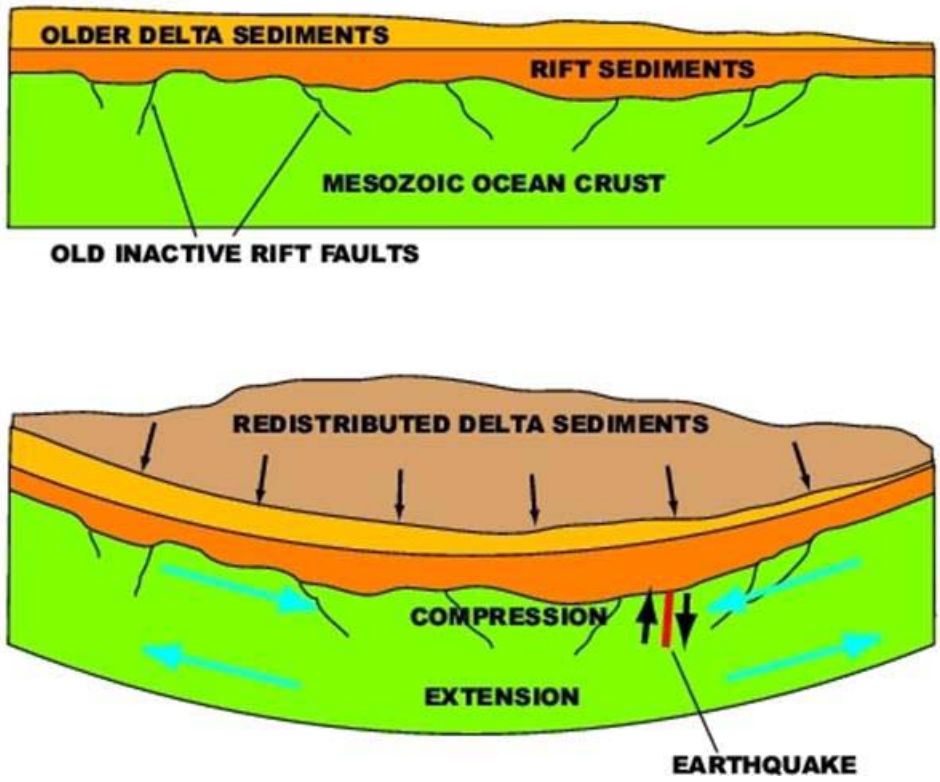

Figure 151: Schematic cross-section showing one possible mechanism for producing the 6.0 magnitude earthquake in GOM

Top: Gulf of Mexico crust and overlying sediments prior to redistribution by hurricane Katrina. Bottom: redeposited of sediments into the deeper Gulf waters. Added delta sediments in the deep Gulf increase the load on the underlying Mesozoic oceanic crust of the Gulf, causing it to flex down

We queried the USGS database from 1800 to present 2017 (USGS database). The earliest recorded earthquake event was the 4.9 magnitude recorded in 1978. Figure 152 shows all the earthquakes in the vicinity of the Ship Shoal studied area. Table 37 lists all the 20 events in the studied area, and color coded according to the magnitude. The 2006 earthquakes are shown in red (5.3 and 5.9 magnitude events). The table also lists the time, location, depth and the data source.

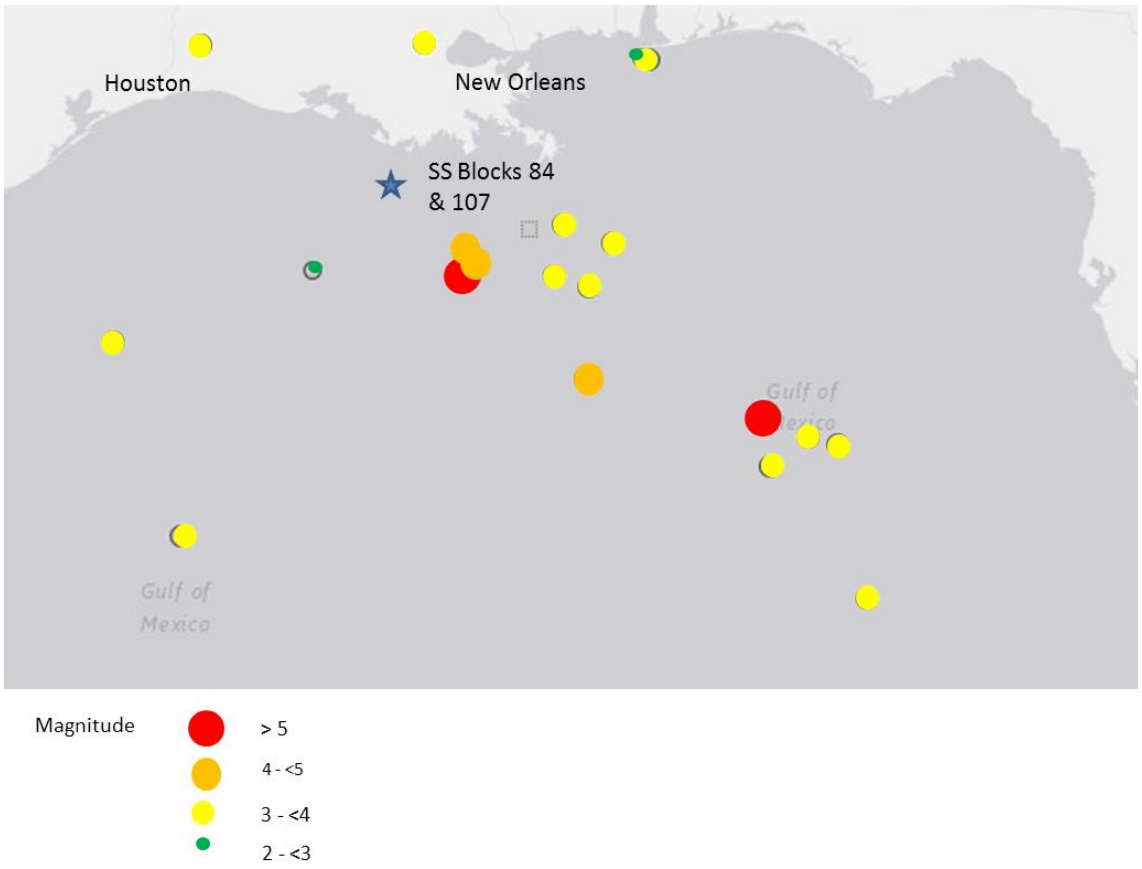

Figure 152: Recorded Earthquakes around Ship Shoal studied area since 1978

Table 37: Recorded Earthquake Events from 1978 to present

time	latitude	longitude	depth	mag	magSource
2013-03-11T15:22:37.220Z	27.875	-92.043	10	2.9	USGS National Earthquake Info Center
2012-11-10T04:24:13.050Z	30.111	-88.097	11	2.6	USGS National Earthquake Info Center
2011-02-18T23:15:31.970Z	30.08	-88.001	5	3.5	USGS National Earthquake Info Center
2006-09-10T14:56:08.160Z	26.319	-86.606	14	5.9	Lamont-Doherty Earth Observation Globe CMT Project
2006-02-10T04:14:22.200Z	27.828	-90.21	5	5.3	USGS National Earthquake Info Center
2005-12-20T00:52:20.510Z	30.258	-90.708	5	3	USGS National Earthquake Info Center
2003-04-13T04:52:53.920Z	26.087	-86.085	10	3.2	USGS National Earthquake Info Center
2002-09-19T14:44:36.150Z	27.822	-89.135	10	3.7	USGS National Earthquake Info Center
2002-05-27T00:28:16.990Z	27.117	-94.442	10	3.8	USGS National Earthquake Info Center
2001-03-16T04:39:07.680Z	28.361	-89.029	10	3.6	USGS National Earthquake Info Center
2000-12-09T06:46:09.120Z	28.027	-90.171	10	4.3	USGS National Earthquake Info Center
1998-07-06T06:54:03.790Z	25.016	-93.633	10	3.4	USGS National Earthquake Info Center
1997-04-18T14:57:35.390Z	25.782	-86.552	33	3.9	USGS National Earthquake Info Center
1994-06-30T01:08:24.220Z	27.911	-90.177	10	4.2	USGS National Earthquake Info Center
1992-09-27T17:02:34.310Z	28.172	-88.438	10	3.6	USGS National Earthquake Info Center
1992-03-31T14:59:39.640Z	26.019	-85.731	5	3.8	USGS National Earthquake Info Center
1986-05-12T04:18:02.470Z	27.7	-88.727	10	3.6	USGS National Earthquake Info Center
1983-10-16T19:40:50.830Z	30.243	-93.393	5	3.8	Oklahoma Geol. Survey
1980-01-10T19:16:19.600Z	24.353	-85.38	10	3.9	USGS National Earthquake Info Center
1978-07-24T08:06:17.600Z	26.729	-88.743	33	4.9	USGS National Earthquake Info Center

7.4 Conclusions

Twelve well bores and 76 well bores for Ship Shoal Block 84 and 107 respectively were reviewed for their cement history. We cannot find any information on Energy XXI 108-7 ST1 well. Most wells (57 out of 76 and 7 out of 12 wells in Ship Shoal Block 107 and 84 respectively) have good integrity. Nineteen and 5 wells (in Ship Shoal Block 107 and 84 respectively) with no top plug, incomplete cement or Plug and Abandonment information are given yellow cautionary indicators. These cautionary wells may provide leakage paths of CO_2 through the well bores to the USDWs.

Using our Quantitative Risk & Decision Analysis Tool (QRDAT) for caprock integrity evaluation, we compared Ship Shoal's risk to that of In Salah, Sleipner, Kevin Dome, Loudon, Illinois Industrial CCS and Wilmington Graben. We found the risk at the Ship Shoal Blocks 84 and 107 fields is comparable to the known CO_2 active sequestration sites, but lower than the Wilmington Graben turbidities offshore California studied site.

The risk of natural seismicity in the Gulf of Mexico is relatively low. Since 1978, there have been about 20 earthquakes located in the Ship Shoal studied area. These earthquakes are mostly small magnitude (3 to 4) events except the two events with magnitudes in the 5.3 and 5.9 occurred during 2006.

8 Analysis of existing Infrastructure of oil and gas for CO_2 transportation

Carbon capture and storage (CCS) is of great interest because of the large amount of CO_2 emitted from the burning of fossil fuels. Carbon capture technologies can potentially remove 80-95% of CO_2 from electric power plant or other industrial source emissions (Parfomak & Folger, 2007). Power plants are the most likely initial candidates for CCS since they are large single point sources that contribute approximately 30% of US CO_2 emitted from the burning of fossil fuels. One common condition for all large-scale CCS is a system for transporting CO_2 from capture sites to storage sites, which requires a dedicated interstate/intrastate pipeline network. Point sources such as power plants – contributing approximately 30% of US CO_2 emitted from the burning of fossil fuels – are of interest for capture sites.

GeoMechanics Technologies has completed a study of the infrastructure assessment associated with CO_2 injection and storage in the Ship Shoal depleted oil and gas reservoirs, in offshore Gulf of Mexico. The various factors evaluated include:

- Top 25 industrial sources of CO_2 emissions near coastal Louisiana,
- Pipeline regulations
- Engineering review and analysis of existing pipeline for CO_2 transport
  - Existing CO_2 pipelines
  - Existing hydrocarbon pipelines
- New pipeline estimated costs

8.1 Top 25 industrial sources of CO_2 emission

Geomechanics Technologies has identified the top 25 CO_2 emitters (sources) in the coastal Louisiana near the Ship Shoal Block 84 and 107 CO_2 storage reservoirs. The CO_2 sources have been separated into 5 categories – power plants, refineries, chemical plants, petroleum and natural gas system, and pulp and paper plants (Table 38).

Figure 154 shows, for example, Big Cajun 2 Power Plant, the top CO_2 emitter in the region, and it produces >10 million tons CO_2 per year (EPA database). The sources and pipelines are all digitized onto an interactive atlas that can be viewed on our website: http://www.geomechanicstech.com/shipshoal.html. (see Figure 153)

Table 38: Top CO2 sources near coastal Louisiana

FACILITY NAME	LATITUDE	LONGITUDE	CITY NAME	COUNTY NAME	PARENT COMPANIES	GHG QUANTITY (METRIC TONS CO2e)	
Big Cajun 2	30.7261	-91.3669	NEW ROADS	Pointe Coupee	ENTERGY CORP (14%);Louisiana Generating, LLC	7,030,778.00	Power Plant
EXXONMOBIL BATON ROUGE REFINERY AND CHEMICAL PLANT	30.484917	-91.17392	BATON ROUGE	EAST BATON ROU	EXXON MOBIL CORP (100%);	4,408,089.00	Refineries
Ninemile Point	29.9472	-90.1458	WESTWEGO	Jefferson	ENTERGY CORP (100%);	4,184,646.00	Power Plant
Marathon Petroleum Company LP	30.09959	-90.648851	Garyville	ST JOHN THE BAF	MARATHON PETROLEUM CO LP (100%);	2,876,827.00	Pet and Nat Gas System
Plaquemine Cogen Facility	30.3215	-91.2392	PLAQUEMINE	Iberville	DOW CHEMICAL (100%);	2,753,237.00	Power Plant
St Charles Operations (Taft/Star) Union Carbide Corp	29.987341	-90.445067	TAFT	SAINT CHARLES	DOW CHEMICAL (100%);	2,328,496.00	Chemical
Norco Manufacturing Complex	30.000723	-90.403768	Norco	SAINT CHARLES	MOTIVA ENTERPRISES LLC (50%);SHELL OIL CO	2,316,202.00	Refineries
The Dow Chemical Company -- Louisiana Operations	30.320903	-91.239015	PLAQUEMINE	IBERVILLE	DOW CHEMICAL (100%);	2,294,212.00	Chemical
CF INDUSTRIES NITROGEN, LLC - DONALDSONVILLE NITROGEN COMP	30.101713	-90.953829	DONALDSONVI	ASCENSION	CF INDUSTRIES HOLDINGS INC (100%);	2,282,933.00	Chemical
OCCIDENTAL CHEMICAL CORPORATION - Taft Facility	29.9861	-90.4575	HAHNVILLE	St. Charles	OCCIDENTAL PETROLEUM CORP (100%);	2,079,692.00	Chemical
Louisiana 1	30.4903	-91.1875	BATON ROUGE	East Baton Rouge	ENTERGY CORP (100%);	1,946,208.00	Power Plant
PHILLIPS 66 CO - ALLIANCE REFINERY	29.68	-89.980833	BELLE CHASSI	PLAQUEMINES	PHILLIPS 66 (100%);	1,305,269.00	Refineries
MOTIVA ENTERPRISES LLC - CONVENT REFINERY	30.10846	-90.89677	CONVENT	ST. JAMES PARIS	MOTIVA ENTERPRISES LLC (100%);	1,261,013.00	Refineries
GEORGIA GULF CHEMICALS & VINYLS LLC	30.265426	-91.18419	PLAQUEMINE	IBERVILLE	AXIALL CORP (100%);	1,236,063.00	Chemical
Carville Energy Center	30.2292	-91.065	Saint Gabriel	Iberville	LS Power Development, LLC (100%);	1,218,056.00	Power Plant
Little Gypsy	30.0033	-90.4611	LAPLACE	Saint Charles	ENTERGY CORP (100%);	1,075,994.00	Power Plant
Michoud	30.0081	-89.9372	NEW ORLEANS	Orleans	ENTERGY CORP (100%);	1,014,605.00	Power Plant
CHALMETTE REFINING LLC - CHALMETTE REFINERY	29.936411	-89.972954	CHALMETTE	SAINT BERNARD	CHALMETTE REFINING LLC (100%);	1,008,664.00	Refineries
Valero Refining - New Orleans, L.L.C.	29.985278	-90.392778	NORCO	ST. CHARLES PAI	VALERO ENERGY CORP (100%);	1,005,968.00	Refineries
GEORGIA-PACIFIC PORT HUDSON OPERATIONS	30.650644	-91.281167	ZACHARY	EAST BATON ROU	KOCH INDUSTRIES INC (100%);	837,551.00	Pulp and Paper
Waterford 1 & 2	29.9994	-90.4758	KILLONA	St. Charles	ENTERGY CORP (100%);	826,737.00	Power Plant
SHELL CHEMICAL CO - GEISMAR PLANT	30.184575	-90.99222	GEISMAR	ASCENSION	SHELL OIL CO (100%);	783,189.00	Chemical
NORANDA ALUMINA LLC	30.0615	-90.6659	GRAMERCY	SAINT JAMES	NORANDA ALUMINUM HOLDING CORP (100%);	777,451.00	Metals
BASF CORP - GEISMAR SITE	30.209725	-91.012892	GEISMAR	ASCENSION	BASF CORP (100%);	720,345.00	Chemical

EPA database 2015 (https://ghgdata.epa.gov/ghgp)

Blue – chemical plant

Orange – power plant

Green – refinery

Purple – pulp and paper plant

Maroon – petroleum and natural gas system

Pink -- Metals

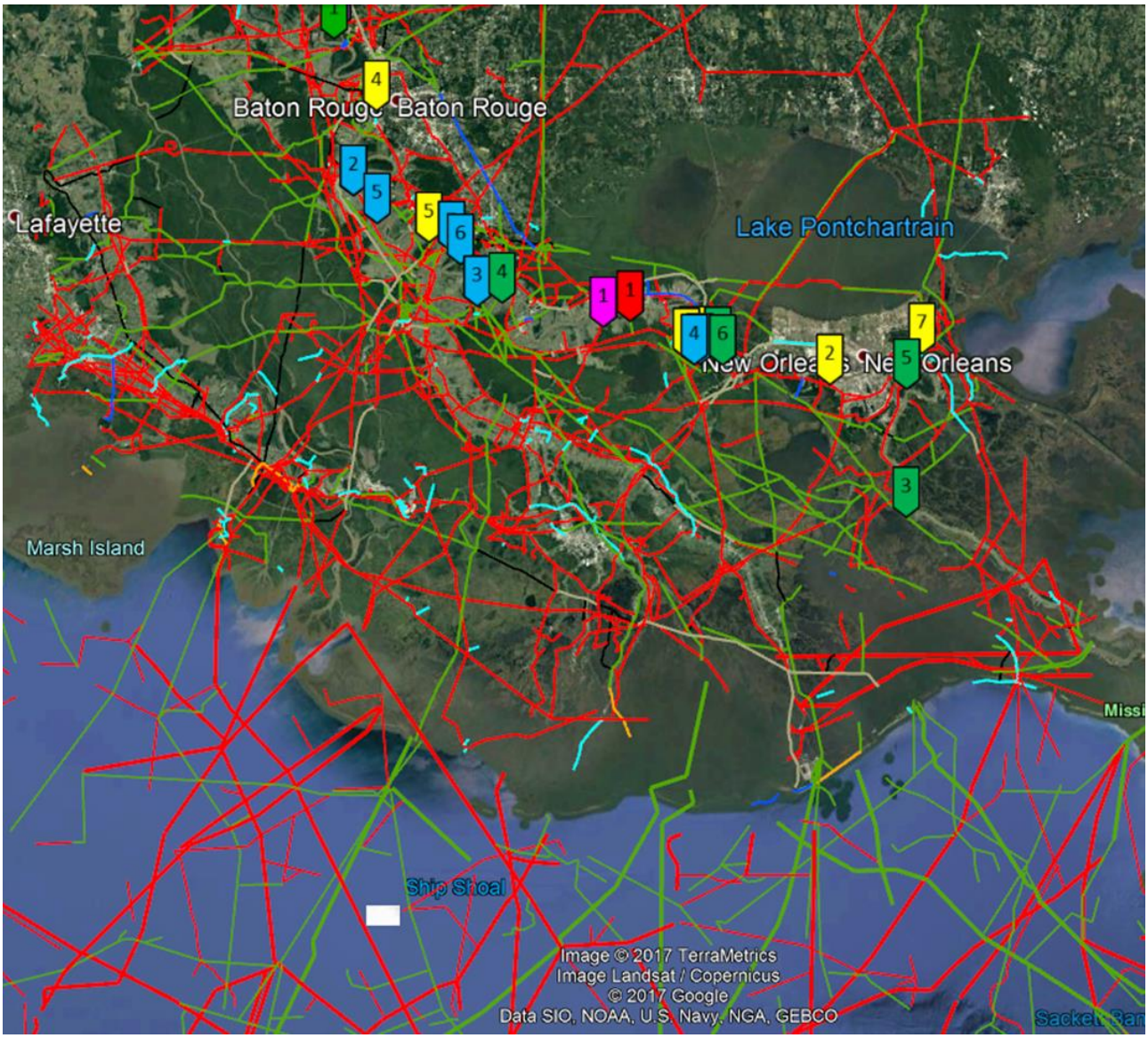

Figure 153: Pipelines and CO_2 emitters in coastal Louisiana

(http://www.geomechanicstech.com/shipshoal.html)

BOEM, EPA database, PHMSA

Green – oil pipeline
Red – gas pipeline
Dark blue – abandoned oil pipeline
Light blue – abandoned gas pipeline
Black – Idled oil pipeline
Silver – Idled gas pipeline
Orange – Retired oil pipeline
Yellow – Retire gas pipeline
White block – location of Ship Shoal 107 Field

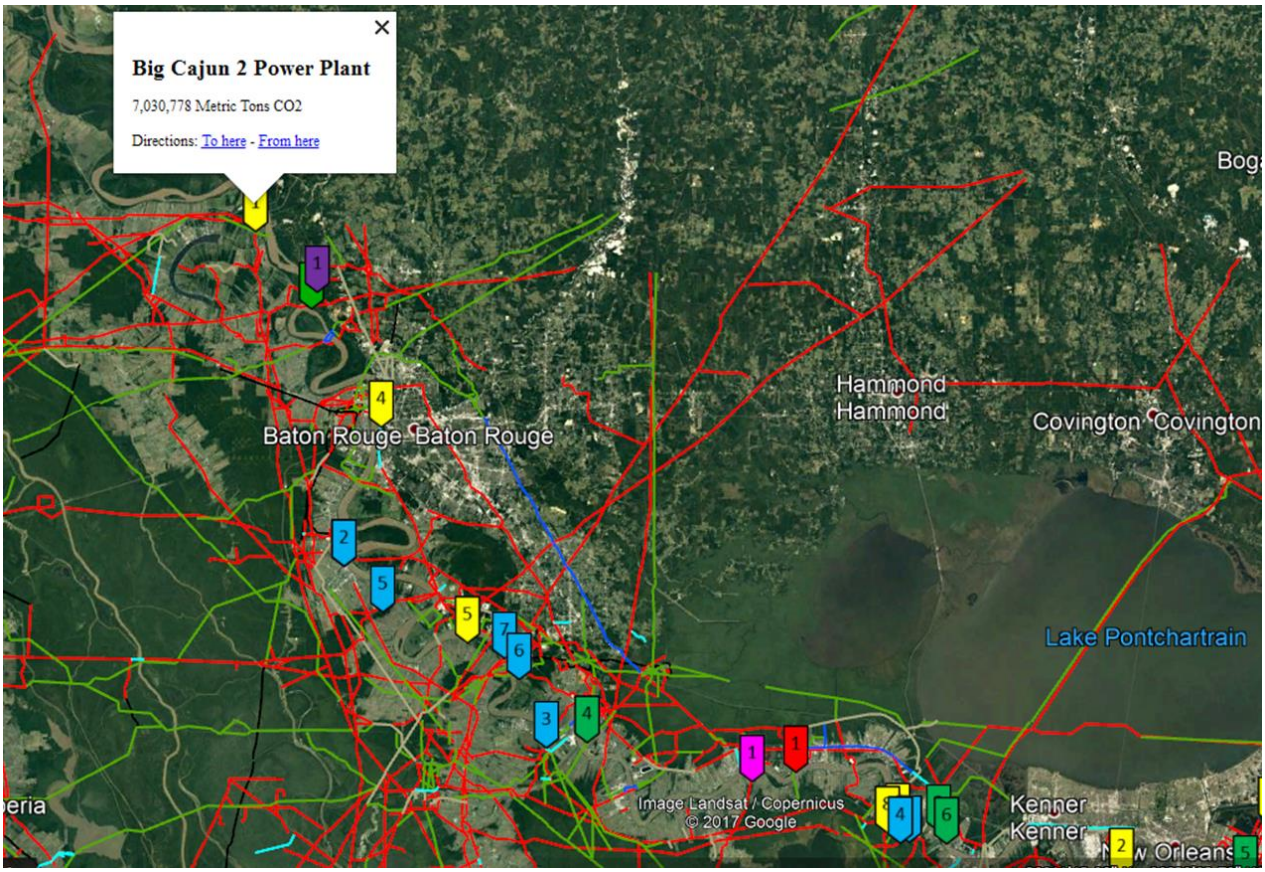

Figure 154: Top Emitter (Big Cajun 2 Power Plant) located north of Baton Rouge

8.2 Pipeline Regulations

The pipeline companies are responsible for the safety of their pipelines. All pipelines are regulated from construction to operation and maintenance. The US Department of Transportation (DOT), Pipelines and Hazardous Materials Safety Administration (PHMSA) issues pipeline safety; construction; operation and maintenance regulations. It also inspects pipeline operators and enforces against violations.

Transmission pipelines are used to transport crude oil and natural gas from their respective gathering systems to refining, processing, or storage facilities. Transmission pipelines also transport refined petroleum products and natural gas to the customers, for use or for further distribution. With very few exceptions, transmission pipelines are dedicated to the transportation of crude oil, refined petroleum products, or natural gas. Gathering lines transport gases and liquids from the rock formations below the surface of the drilling site to the processing site, refineries or transmission line (PHMSA). Below is a schematic from PHMSA showing the distribution network from production to the end users.

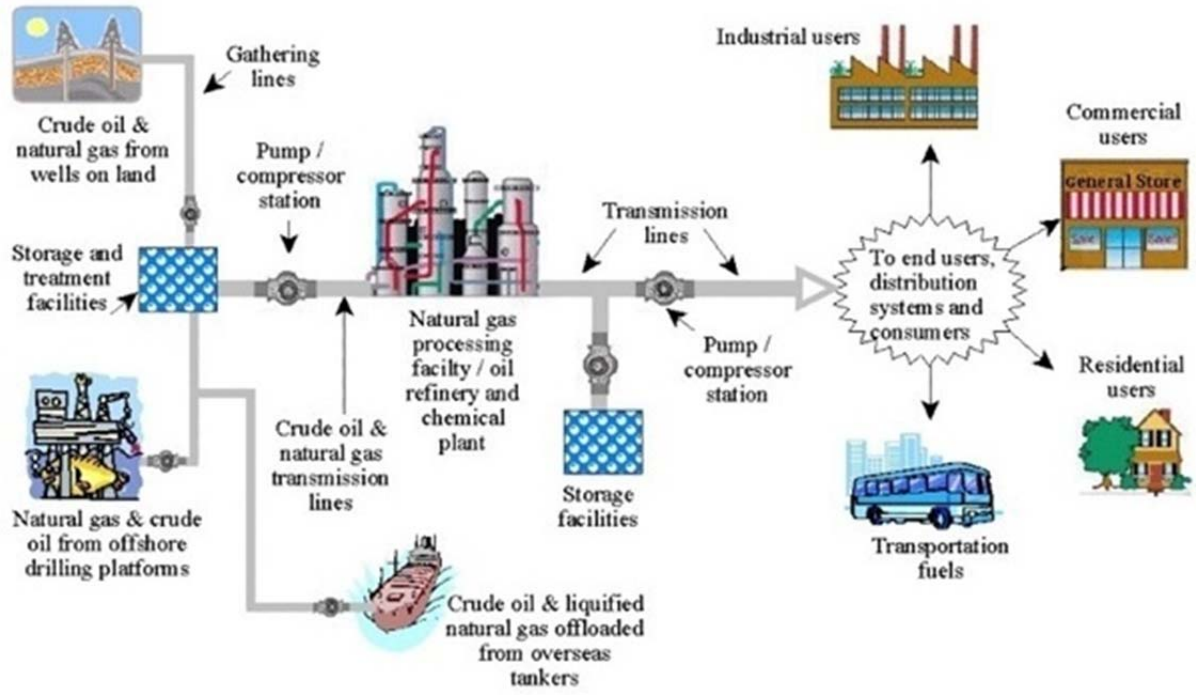

Figure 155: Distribution schematic from production to the end users

https://primis.phmsa.dot.gov/comm/FactSheets/FSTransmissionPipelines.htm

PHMSA regulates both natural gas and hazardous liquid gathering pipelines and transmission pipelines (PHMSA website). However, PHMSA has approved some certified state agencies to exercise interstate inspection authority and/or intrastate inspection and enforcement authority (Pipeline 101). PHMSA also allows some States to issue regulations over intrastate pipelines, as long as they are consistent with the Federal regulations (Pipeline 101). Offshore transmission and gathering pipelines in federal water are regulated by either PHMSA or Bureau of Safety and Environmental Enforcement (BSEE, 2018).

The Federal Energy Regulatory Commission (FERC) regulates the transportation of oil by pipeline in interstate commerce, and approves the siting of, and abandonment of, interstate natural gas facilities, including pipelines, storage and liquefied natural gas (LNG). FERC does not regulate or provide oversight for the construction of oil pipelines; it does not regulate pipeline safety; nor does it regulate pipeline transportation on or across the Outer Continental Shelf (FERC website).

8.3 Engineering Review and Analysis of Existing and New Pipeline and Gas Storage System in the Ship Shoal Area

Transporting CO_2 over long distance is most efficient and economical when the CO_2 is in the dense liquid or supercritical phase above 74 Bar (7.38MPa; IEAGHG 2012). However, it is the industry preference to operate the CO_2 pipeline at > 103 Bar (10.3 MPa) to maintain CO_2 at the supercritical phase and to prevent frictional loss. Figure 156 is a phase diagram for CO_2.

Guidelines in pipeline design, construction, permitting, maintenance, operations, regulations and cost can be found in numerous papers such as IEAGHG (2012, 2014), DNV (2010) and Geomechanics Technologies (2015).

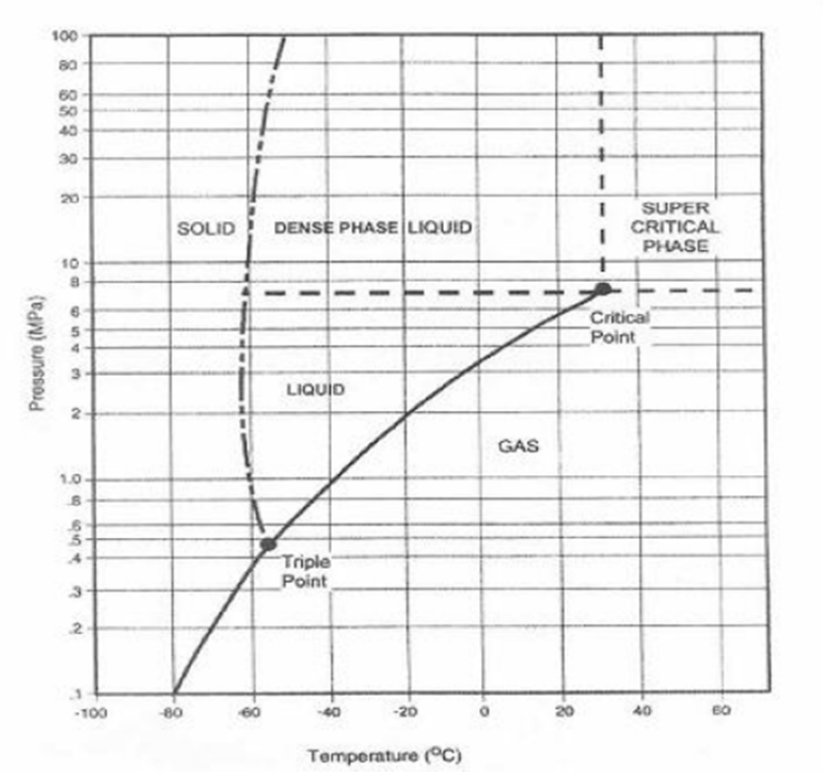

Figure 156: Phase diagram of CO_2

IEAGHG, 2012

8.3.1 Existing CO_2 Pipelines

There are regional CO_2 pipeline networks already operating in the US. Figure 157 below is a map showing the existing CO_2 pipelines across the United States (DOE/NETL, 2015). The construction of a new interstate natural gas pipeline or expansion project takes an average of 3 years from the time of announcement to placement in service; however, it is heavily dependent on whether there are environmental obstacles or public opposing (EIA website).

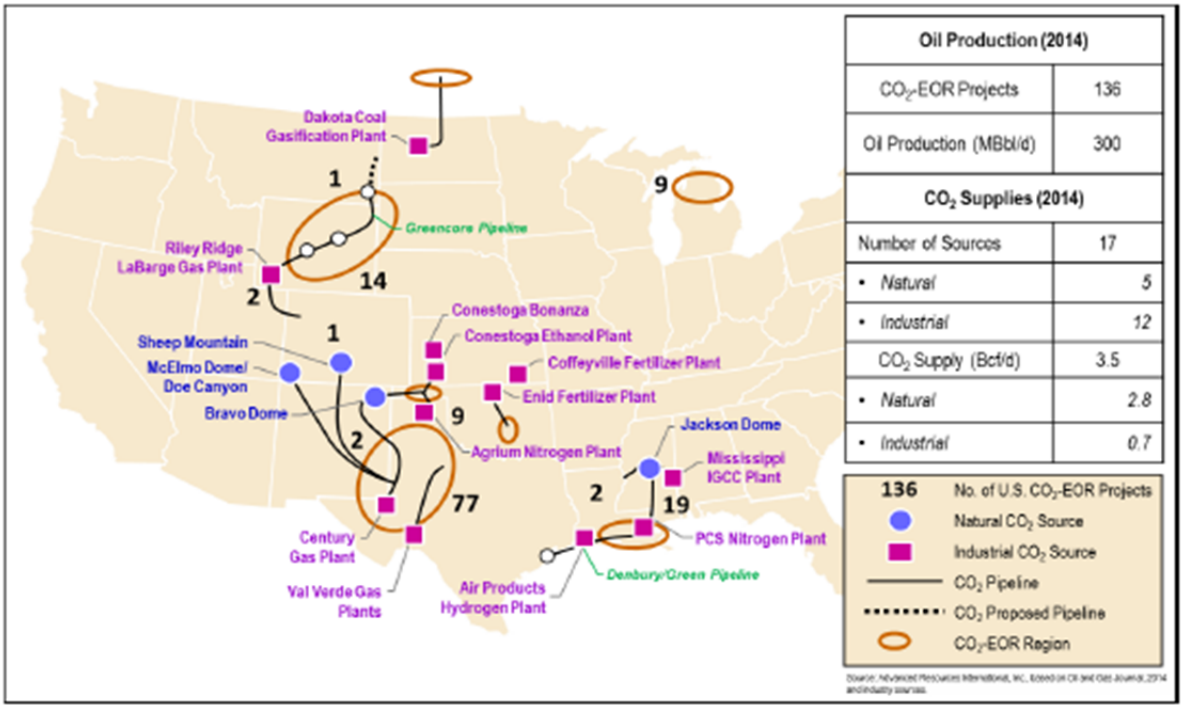

Figure 157: CO_2 – EOR operations and infrastructure

DOE/NETL, 2015

Donald Rehmer (2014) evaluated viable EOR sequestration sites in the Illinois Basin that can serve as nodal points or hubs to expand the CO_2 delivery infrastructure to more distal locations from the emission sources. Model results indicate the inclusion of hubs in the model yields lower transportation cost for CO_2 storage than the point to point infrastructure model. This nodal points or hubs can also be investigated for the Ship Shoal CO_2 sequestration project. In the Gulf Coast, Denbury Onshore LLC owns and operates 740 miles of CO_2 pipelines. The 2 main pipelines connect the natural CO_2 source in Jackson Dome, Mississippi to Denbury's CO_2 EOR project in Mississippi, Louisiana and East Texas as shown in Figure 158 (DOE/NETL, 2015).

The specification for the different pipelines is shown in Table 39. These existing pipelines may be used as hubs to connect to the top CO_2 sources identified, and be transported to the offshore Ship Shoal Block 84 and 107 fields for sequestration.

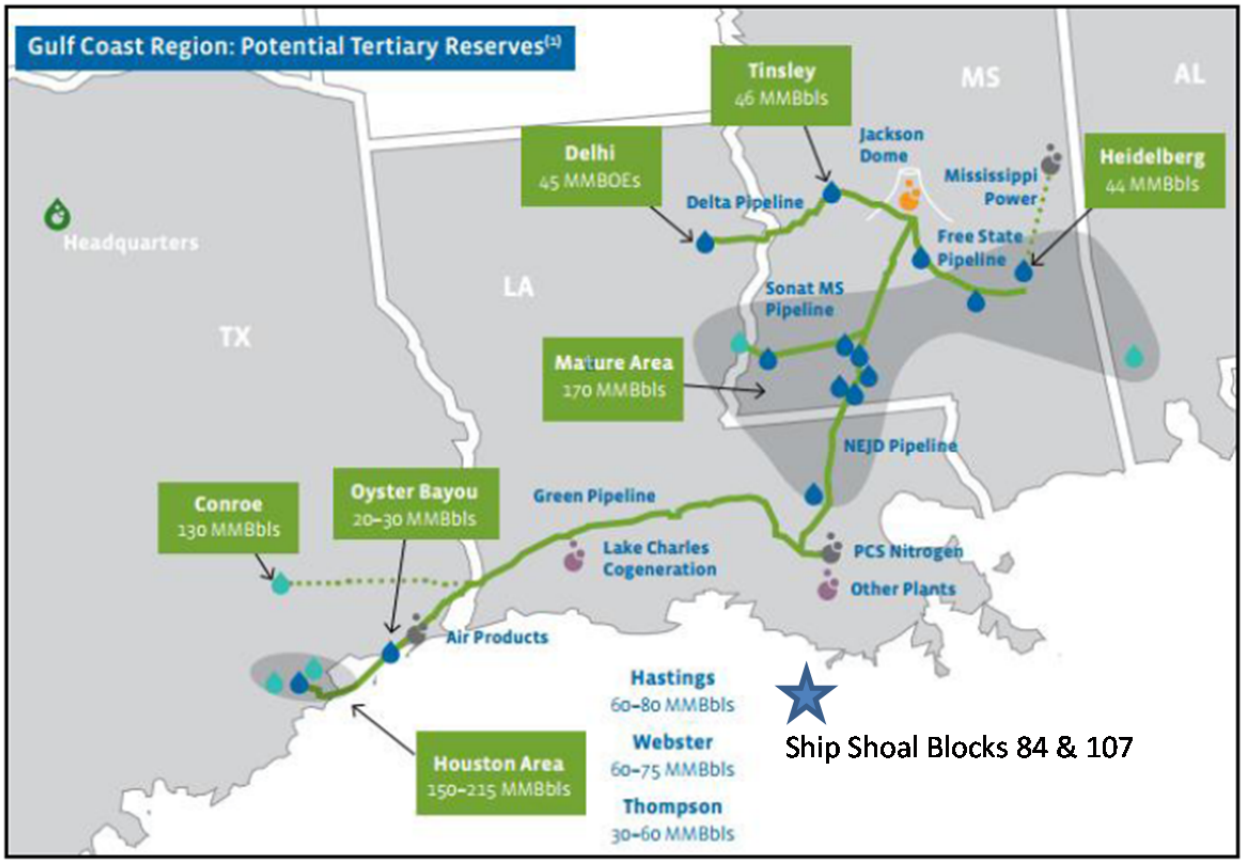

Figure 158: Gulf Coast CO_2 Pipeline infrastructure

DOE/NETL, 2015

Table 39: Denbury Gulf Coast transportation CO_2 pipeline

Scale	Pipeline	Operator	Location	Length (mi)	Diameter (in)	Estimated Flow Capacity (MMcfd)
Large-Scale Trunk-lines	Green Line	Denbury Resources	LA, TX	314	24	930
	Delta	Denbury Resources	MS, LA	108	24	590
	Northeast Jackson Dome (NEJD)	Denbury Resources	MS, LA	183	20	360
Distribution Line	Free State	Denbury Resources	MS	85	20	360
	Sonat	Denbury Resources	MS	50	18	170

DOE/NETL, 2015

8.3.2 Existing Hydrocarbon pipelines

We reviewed pipeline maps from Energy Information Administration (EIA), and Department of Transportation, Pipeline and Hazardous Materials Safety Administration (PHMSA https://pvnpms.phmsa.dot.gov/PublicViewer/) for onshore pipelines, and Bureau of Ocean Energy Management (BOEM) for offshore pipelines. We noticed the onshore pipeline information is sufficiently different between the EIA and PHMSA versions. In addition, PHMSA maps show idled, abandoned and retired pipelines per parish. We decided to use the PHMSA pipeline map. The pipeline maps from different parishes in Louisiana just north of Ship Shoal blocks were digitized and stitched together. Offshore pipeline maps are under the domain of BOEM. The offshore pipelines from BOEM were digitized and plotted using Google Earth. Information such as the pipeline operator and diameter size can be viewed from the interactive map (Figure 159).

Similarly, there are abandoned offshore pipelines. Figure 160 shows the abandoned pipelines in Ship Shoal Block 107 field only. Since there is a mired of abandoned pipelines, we cannot show the abandoned pipelines in the same scale as the operational pipelines. Thus we decided to note that there are abandoned pipelines, and the CO_2 operators should request the specific map from BOEM.

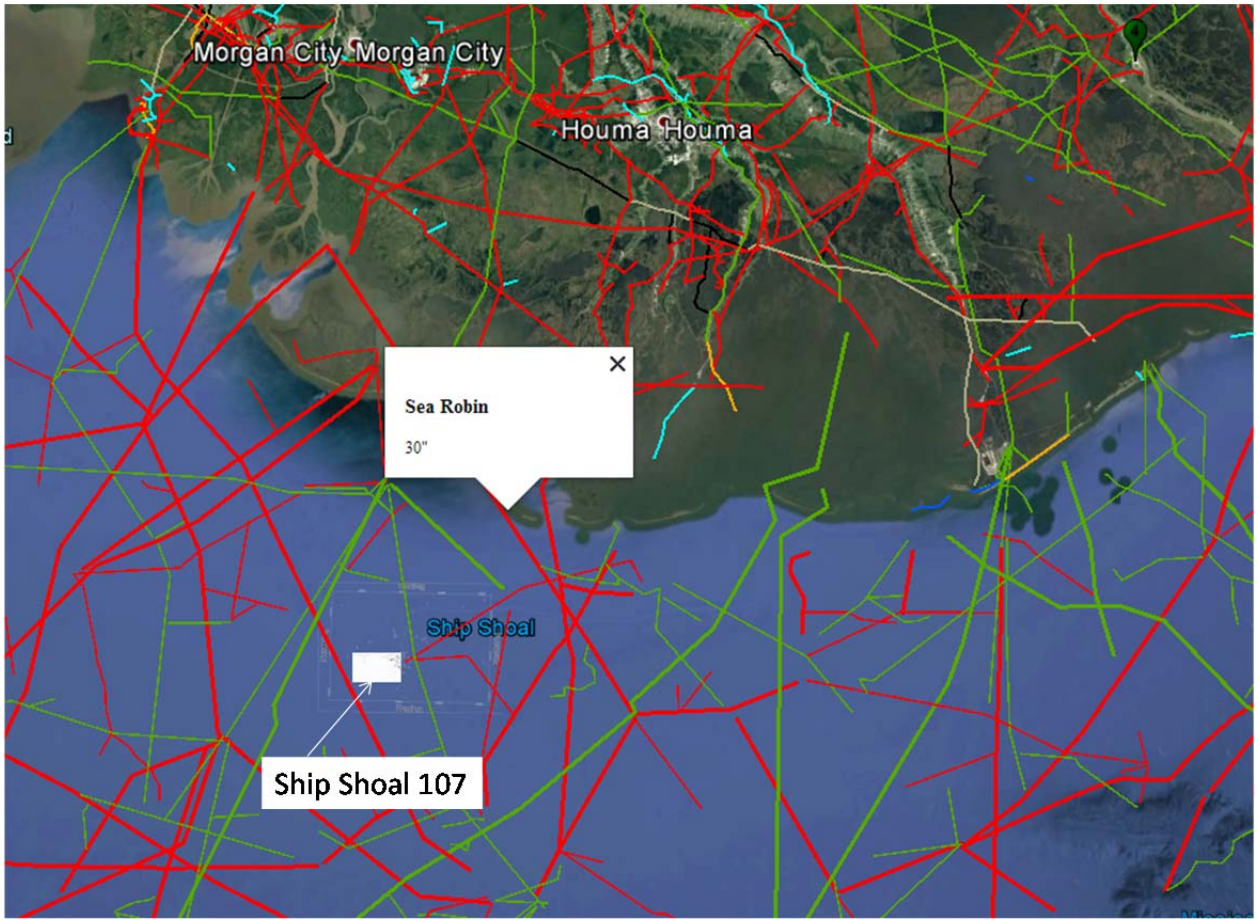

Figure 159: Interactive pipeline map

Offshore:

Heavy lines – > 20" pipeline

Lighter lines -- < 20" pipeline

Red – gas pipeline

Green – oil pipeline

Onshore:

Green – oil pipeline

Dark blue – abandoned oil pipeline

Black – Idled oil pipeline

Orange – Retired oil pipeline

Red – gas pipeline

Light blue – abandoned gas pipeline

Silver – Idled gas pipeline

Yellow – Retire gas pipeline

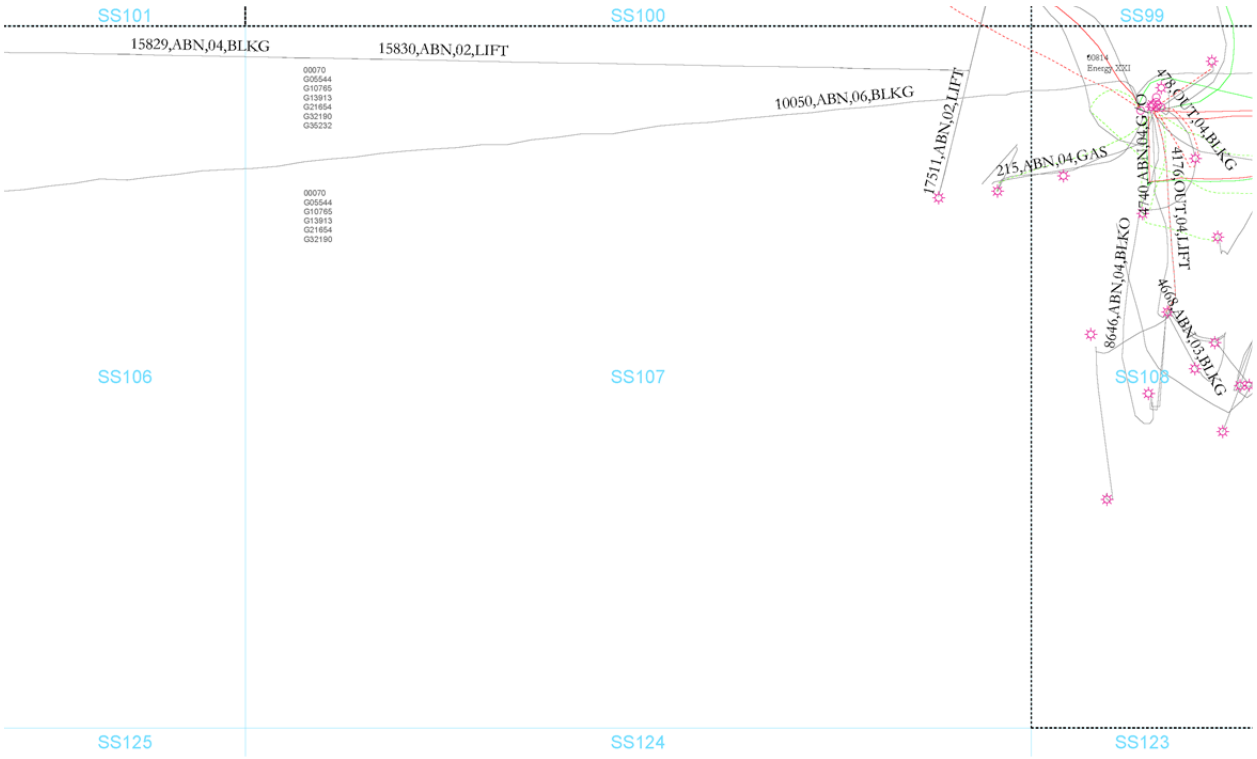

Figure 160: Unused offshore pipeline in Ship Shoal 107 field

BOEM map

8.3.3 Converting Hydrocarbon Pipeline for CO2 Usage

There is no standard specification for maximum pipeline pressures. It is a function of design, materials, testing supported by construction techniques, inspection, records, etc. and is the responsibility of the pipeline operator to correctly determine, maintain and operate within the limits of the pipelines (Lowry, Bill, 2017, DOT -- personal communication). CO_2 pipelines operate at a higher pressure, between 1250 to 2900 psi (Element Energy, 2010); at a much higher pressures than the abandoned oil or gas pipelines may have ever seen even during testing for establishing maximum pressure limits and especially later in service life as field pressures decline (Lowry, Bill, 2017, DOT -- personal communication). CO_2 operators are to comply with USDOT 49 CFR 195 (Transportation of hazardous liquids by pipeline), and USDOT 30CFR Part 550 Subpart J (Pipelines and Pipeline Rights-of-Way).

When converting an idle or abandoned oil or gas pipeline for CO_2 transportation, the design, construction, operation, and maintenance history of the pipeline must be reviewed and, where sufficient historical records are not available, appropriate stress tests must be performed to determine if the pipeline is in satisfactory condition for safe operation. The following regulations must be adhered to -- CFR 195.5 (Conversion to service), CFR 195.111 (Fracture Propagation – material plan and implemented), CFR 195.406 (Maximum operating pressure), Subpart E (pressure testing), CFR 195.413 (Underwater inspection and reburial), CFR 195.420 (valve maintenance), CFR 195.422 (Pipeline repairs), CFR 195.428 (Overpressure protection), Subpart H (Corrosion Control), CFR 195.106 (Internal Design Pressure) and CFR 195.406

(Maximum Operating Pressure), plus review BSEE offshore material, testing, construction and maintenance requirements to maintain lease.

8.4 New CO2 pipeline cost estimate

Average water depth at the Ship Shoal Blocks 84 and 107 is about 6 meters (20 feet); the relative shallow water should reduce the cost for the construction of a new CO_2 pipeline. There are transit corridors nearby. The closest corridor near Ship Shoal connects offshore to onshore pipelines at Cailou Bay where 20" to 36" trunk-lines transport the hydrocarbon produced from the offshore drill sites to the onshore processing plants. Figure 159 shows the 30" gas pipeline and other major pipelines near the Ship Shoal study area. New CO_2 pipelines may be able to be sited from the existing transit corridor.

Analysts commonly develop cost estimates for CO_2 pipelines based on comparable construction costs for natural gas pipelines. NETL (2010) established an equation to estimate several components of the capital cost on CO_2 pipeline. The pipeline cost is broken down into 4 categories:

- Materials
- Labor
- Miscellaneous (including survey, engineering, supervision, contingencies, administration, allowances, overheads and filing fees)
- Right of Way and Damages

In 2002, it cost on average $800,000 per mile (Parfomak and Folger, 2007). Oil and Gas Journal (Sept., 2016) estimated the average cost for the US pipeline constructed between July 1, 2015 to June 30, 2016 have increased to $7.65 million per mile, an increase of 46% from 2015 ($5.2 million per mile). The higher labor cost, and right of way did not offset the lower material and miscellaneous costs. The pipeline construction costs estimated use the data obtained from FERC construction permit filed between July 1, 2015 to June 30, 2016. Table 40 is a table listing the different sizes of the pipelines and the cost per mile for the Gulf Coast States and an average for all the land pipelines. Note the average cost per mile for pipeline costs in the Gulf Coast States ($5,064,046) is about 1/3 cheaper than the average cost for the whole US pipeline.

Table 40: Estimated pipeline costs for Gulf Coast states and all US land projects

Size (inch)	Location	Length (mile)	Material Cost	Labor Cost	Misc Cost	ROW & Damages	Total Cost	$/mile
12	Louisiana-Mississippi	51.78	$ 11,203,427	$320,056,680	$ 21,351,501	$ 1,592,820	$ 66,204,428	$ 1,278,571
30	Louisiana	3	$ 2,897,992	$ 9,874,969	$ 6,991,431	$ 573,560	$ 20,337,952	$ 6,779,317
36	Texas	66	$ 73,543,447	$ 2,012,730	$ 203,846,401	$ 11,539,694	$ 290,942,272	$ 4,408,216
42	Louisiana	42.7	$ 80,000,000	$160,000,000	$ 104,545,279		$ 344,545,279	$ 8,068,976
42	Texas	274	$ 479,138,899	$468,203,355	$ 323,960,732	$ 39,828,080	$ 1,311,131,066	$ 4,785,150
						Gulf Coast	Average $/mile	**$ 5,064,046**
						All Land Project	Average $/mile	**$7,652,901**

FERC construction permits filing July 1, 2015 to June 30, 2015 in Oil and Gas Journal, Sept., 2016

Figure 161 is a pie chart showing the allocation percentage distribution between the 4 categories – materials, Right of Way (ROW) and Damages, Labor and Miscellaneous costs.

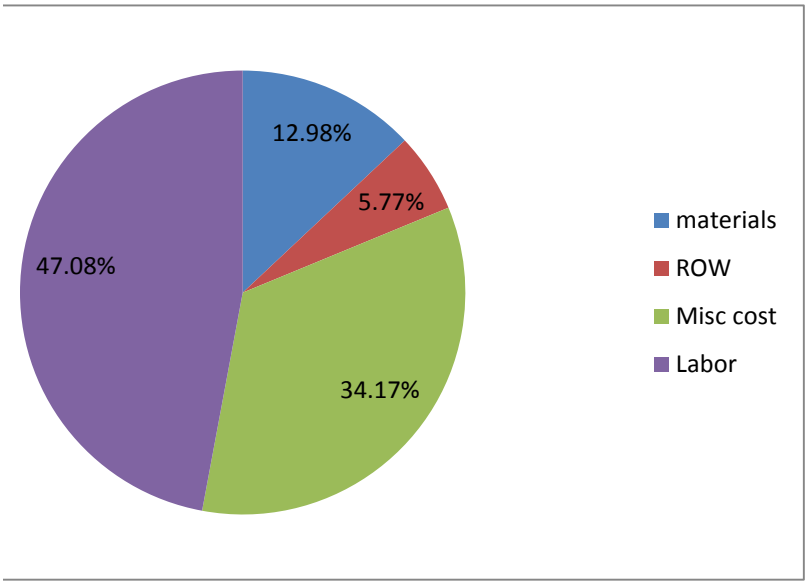

Figure 161: Pipeline construction costs major component estimated

FERC construction permits filing July 1, 2015 to June 30, 2015 in Oil and Gas Journal, Sept.,2016

8.5 Conclusions

Geomechanics Technologies has documented the top 25 CO_2 emission sources within the close proximity of the Ship Shoal Block 84 and 107 fields. All the offshore and onshore pipelines have been digitized and can be viewed in an interactive website. We also performed a feasibility study on the potential for converting existing oil or gas pipelines for CO_2 transport. There are abandoned, idled and retired onshore and offshore pipelines. However, there is no standard specification for maximum pipeline pressures needed for CO_2 transport. It is a function of design, materials, and testing provided; thus it will be the responsibility of the pipeline operator to correctly determine, maintain and operate within the limits of the pipelines. There

are a few transit corridors extending from onshore Louisiana (Cailou Bay) to offshore trunk-lines. The cost for constructing a pipeline has increased about 46% from 2015 to date to an average cost of $5,064,046 per mile.

9 Analysis and Interpretation

We have calculated the resource capacity for each of the oil and gas fields within the northern Ship Shoal area using the NETL approved storage estimation equation. During Phase I of the project, we used the depleted oil and gas reservoir information provided by BOEM to estimate the available volume of the storage resource for each field. After developing a detailed geologic model for Ship Shoal Block 84 and 107 fields during Phase II, we then recalculated the estimated storage capacity for these fields using the available sand volume determined through modeling. The two methods are explained below and have been compared and analyzed.

9.1 Resource capacity estimation based on BOEM oil and gas reservoir data

GeoMechanics Technologies used the NETL approved volumetric equation (Equation 1) to calculate the CO_2 storage resource mass estimate for geologic storage in the oil and gas fields within the northern Ship Shoal area. The CO_2 storage resource mass estimate ($\boldsymbol{G_{CO2}}$) is equal to the product of the total area ($\boldsymbol{A_t}$), gross formation thickness ($\boldsymbol{h_g}$), total porosity ($\boldsymbol{\emptyset}$), CO_2 density ($\boldsymbol{\rho}$) and the storage efficiency factor ($\boldsymbol{E_{saline}}$). A summary spreadsheet including total volume and porosity for each oil and gas reservoir located in the Ship Shoal area was provided by BOEM. We used the most current version of the summary spreadsheet, which had been last updated in 2014 (BOEM, 2014). We estimated CO_2 density based on a nearby regional study provided by Nicholson, 2012. CO_2 fluid density is highly dependent on depth, and therefore we used a density of 0.7 g/cm^3 (43.7 lb/ft^3) for sand reservoirs shallower than 9,000 feet depth and 0.8 g/cm^3 (49.9 lb/ft^3) for reservoirs 9,000 feet and deeper. The efficiency factors used in our calculation were obtained from Goodman et al., 2011 for clastic reservoirs that range from P10 (0.51%), P50 (2.0%), and P90 (5.4%).

$$G_{CO_2} = A_t h_g \emptyset_{tot} \rho E_{saline} \qquad \text{Equation 1}$$

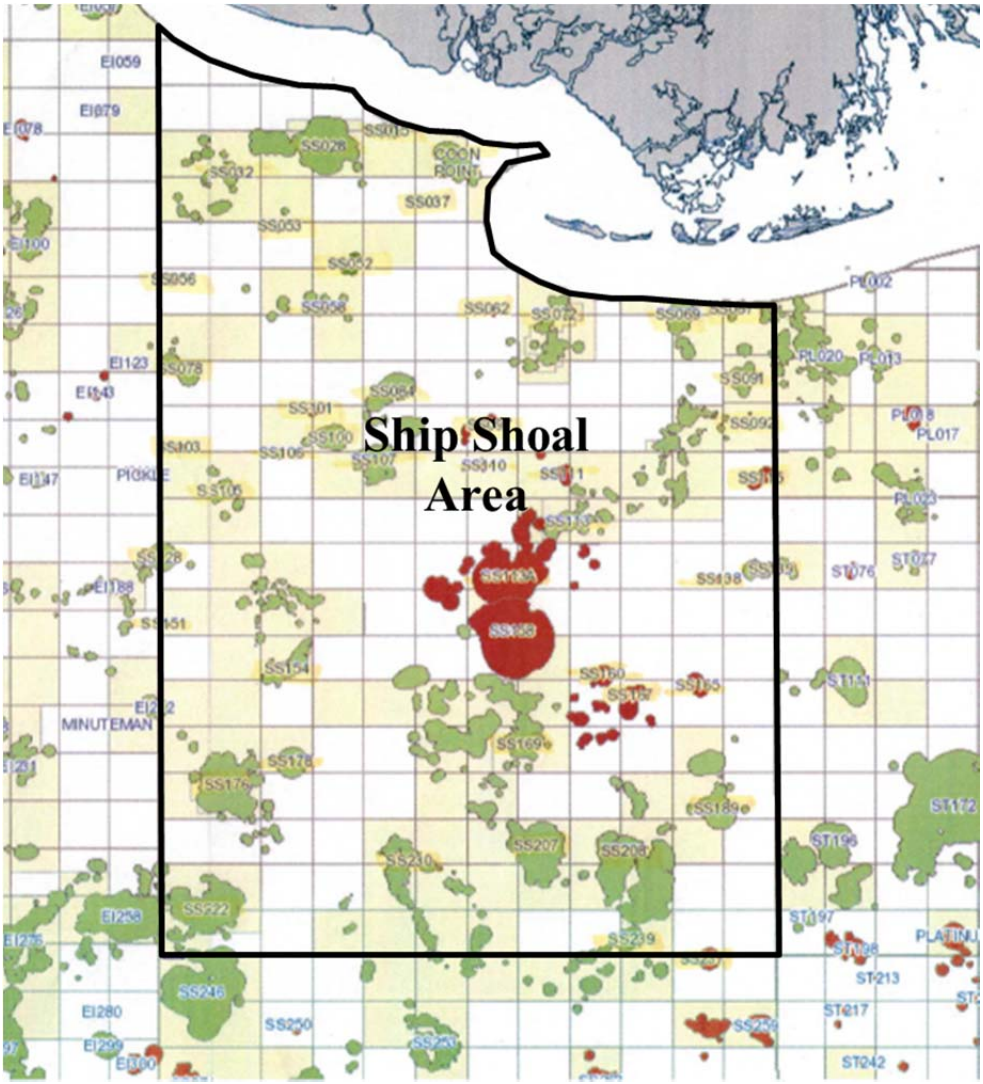

Figure 162: Ship Shoal area showing approximate areas of oil fields (green) and gas fields (red).

Modified from GOMSmart.com, Earth Science Associates.

All 48 fields within the Ship Shoal Area as shown in Figure 162 were evaluated individually for their CO_2 sequestration potential. The figure shows the locations of the oil and gas fields including their approximate areal sizes. The black outline indicates the Ship Shoal area, excluding the fields in the South Ship Shoal area. Table 41 shows the P50 estimation for the CO_2 storage capacity by field. Ship Shoal Block 84 and 107 fields are shown highlighted.

The results of our calculations show that existing oil and gas fields in Northern Ship Shoal have the potential to store:

P10= 12 million tons,

P50= 47 million tons, and

P90= 127 million tons of CO_2.

Table 41: P50 CO2 storage calculation for northern Ship Shoal area

Field Name	Disc Year	Oil Cum (bbl)	Gas Cum (Mcf)	Type	Reserves Oil (bbl)	Reserves Gas (Mcf)	Water Depth	CO2 Storage Capacity (P50)
CP000	1966	7,867,297	357,247,752	Oil/Gas	0	0	9	1206548
SS015	1962	2,828,112	48,544,216	Oil/Gas	341,537	6,079,353	12	220325
SS028	1949	21,367,951	810,458,430	Oil/Gas	69,913	10,034,994	13	5172776
SS032	1947	15,123,335	167,323,035	Oil/Gas	1,691,129	32,381,308	18	786330
SS037	1985	370,850	10,906,158	Oil/Gas	0	0	12	48299
SS052	1987	300,240	1,005,031	Oil	967,078	2,079,207	15	48297
SS053	2006	305,835	4,492,872	Gas	0	0	13	18946
SS056	2005	0	2,217,491	Gas	0	0	20	15993
SS058	1966	3,914,506	29,267,660	Oil/Gas	55,735	3,466,712	19	218247
SS062	1990	54,415	7,172,068	Gas	0	0	28	31598
SS067	1995	4,348,771	19,407,972	Oil/Gas	22,052	16,599	31	102030
SS069	1979	19,893,157	50,052,134	Oil/Gas	4,334,212	28,539,570	29	892734
SS072	1948	25,270,995	244,300,239	Oil/Gas	541,028	3,472,162	30	1384725
SS078	1982	1,279,041	25,541,381	Oil/Gas	121,748	478,714	22	176476
SS084	1976	1,824,522	119,831,052	Oil/Gas	0	0	19	315917
SS091	1979	17,226,193	33,600,218	Oil/Gas	1,378,468	1,617,849	36	163757
SS092	1988	2,040,101	6,726,228	Oil/Gas	0	0	24	36395
SS097	1984	614,360	42,441,917	Gas	524	406,894	25	117752
SS100	1987	6,163,883	87,914,309	Oil/Gas	57,948	2,182	23	341810
SS101	2004	53,218	3,952,433	Gas	0	0	20	29647
SS103	1999	336,643	7,632,240	Gas	0	0	39	26821
SS105	1968	5,265,558	75,970,285	Oil/Gas	988,303	3,474,618	37	256849
SS106	2006	105,796	2,273,617	Oil/Gas	0	0	40	15235
SS107	1957	59,521,205	103,969,633	Oil/Gas	169,177	229,045	23	880529
SS110	2003	230,463	8,586,144	Gas	240,074	2,567,977	29	64801
SS111	1985	994,816	69,338,331	Gas	170,646	10,182,965	39	211400
SS113	1955	126,285,326	490,671,028	Oil/Gas	4,285,149	9,557,113	41	2786688
SS113A	1972	422,250	377,313,229	Gas	247	15809	44	421324
SS115	1974	0	22,821,605	Gas	0	0	54	103850
SS128	1990	3,822,074	18,436,684	Oil/Gas	771,554	5,354,408	58	156338
SS138	2006	249,061	5,302,258	Gas	905	28,907	62	21006
SS139	1957	3,807,674	50,710,360	Oil/Gas	164,747	3,362,321	62	673184
SS151	1997	3,254,904	2,475,923	Oil	99,765	56,846	64	31048
SS154	1955	91,138,066	187,938,866	Oil/Gas	780,950	3,279,303	55	1422156
SS158	1960	516,840	375,383,490	Gas	4,829	2,487,717	45	1894727
SS160	1985	114,112	15,380,865	Gas	0	0	50	56618
SS165	1983	0	2,572,553	Gas	0	0	59	0
SS167	1965	903,338	92,750,991	Gas	0	0	61	436956
SS169	1960	165,143,202	874,182,643	Oil/Gas	4,375,128	17,381,510	63	4719469
SS176	1956	67,533,420	1,290,881,290	Oil/Gas	1,070,918	14,509,677	101	4335761
SS178	1984	15,164,357	20,343,334	Oil/Gas	326,974	20,304,253	88	366185
SS189	1961	2,070,770	266,123,597	Oil/Gas	169,903	16,609,942	70	781405
SS207	1967	109,243,499	465,729,203	Oil/Gas	965,179	5,784,196	103	2549795
SS208	1960	223,423,388	1,369,771,470	Oil/Gas	4,189,132	34,781,167	102	5926975
SS222	1966	70,593,207	841,276,306	Oil/Gas	1,881,476	8,796,292	144	3876352
SS230	1962	134,986,440	407,925,156	Oil/Gas	10,765,302	45,007,918	119	2899539
SS237	1980	243	9,537,068	Gas	0	0	129	0
SS239	1965	16,807,574	227,943,839	Oil/Gas	3,702,802	4,057,125	131	1015604
								47,259,216

Fields SS165 and SS237 are only productive from the Lower Pleistocene, thus not included in the reserve calculation for this study

9.2 Resource capacity estimation based on geologic modeling

Under Task 3, GeoMechanics Technologies developed detailed geologic models for both Ship Shoal Block 84 and 107 fields. Using these models, we determined the statistical distribution of lithology types per field. We then recalculated the estimated storage resource capacity of each field using the NETL approved equation (Equation 1), using the re-evaluated volume of the available sand.

To characterize only the field area, a subsection surrounding the boundary of each hydrocarbon field was extracted from the larger geologic model and used for the statistical analysis (see Figure 163 and Figure 164). The boundary shapes of the fields were obtained from GOMsmart. Field 107 consists of three separate regions, a southern main area and two northern smaller pools located adjacent to a large fault. The statistics of each area was evaluated individually and then combined to provide a total overview of the Ship Shoal Block 107 field.

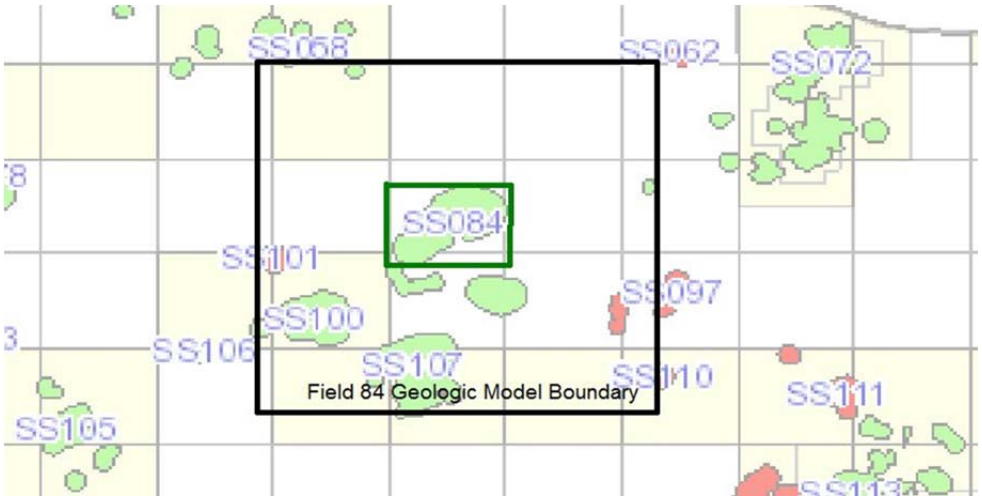

Figure 163: Boundary shown in green of the subsection used for Ship Shoal Block 84 field lithology statistical analysis.

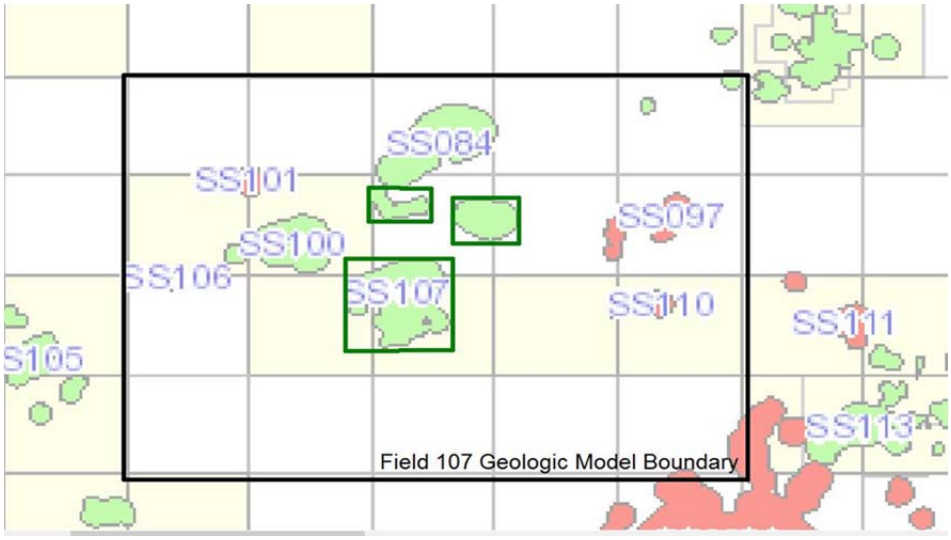

Figure 164: Boundary shown in green of the subsection used for Ship Shoal Block 107 field lithology statistical analysis.

The three sections of Ship Shoal Block 107 field were added together for a total volume analysis.

9.2.1 Ship Shoal Block 84 field

The modeled Pliocene and Miocene formations within the Ship Shoal Block 84 field contain 401,532 voxels, with each voxel measuring 750 x 750 x 10 feet in dimensions – cross sections are shown in Figure 25 and Figure 26 . The volume of each voxel is 5,625,000 cubic feet, for a total modeled Plio-Miocene volume of 2.26E12 cubic feet. Table 42 below displays the lithologic distribution in percentage for the total combined Ship Shoal Block 84. Table 43 shows the calculated volume based on the number of voxels per formation within the field. We observed that the upper Pliocene Valv-H Formation contains a greater percentage of sand than shale and silt, while the other formations contain a greater amount of shale than sand or silt.

Table 42: Lithologic distribution in percentage for the combined Ship Shoal Block 84 field

Percent Distribution	Sand	Shale	Silt
Top Pliocene (Valv-H)	52.03%	18.78%	29.14%
Tex-X	22.48%	53.58%	23.88%
Top Miocene (Bul-1)	8.67%	80.53%	10.48%
Big-A	9.76%	84.77%	5.19%
Cris-K to base of model	12.88%	71.35%	15.78%

Table 43: Volumetric totals generated for different lithologies per formation for Ship Shoal Block 84 field

Volume ft3	Sand	Shale	Silt	Total Voxels
Top Pliocene (Valv-H)	3.52E+11	1.27E+11	1.97E+11	6.75E+11
Tex-X	6.36E+10	1.51E+11	6.75E+10	2.83E+11
Top Miocene (Bul-1)	1.35E+10	1.25E+11	1.63E+10	1.55E+11
Big-A	2.64E+10	2.30E+11	1.41E+10	2.70E+11
Cris-K to base of model	1.13E+11	6.23E+11	1.38E+11	8.74E+11
		TOTAL PLIO/MIO VOLUME		**2.26E+12**

GeoMechanics Technologies used the sand volume to re-calculate the estimated CO_2 storage resource based on the NETL approved volumetric equation (Equation 1). Similar efficiency factors and parameters for porosity and CO_2 fluid density were used. The results of the calculation are shown in Table 44. Table 45 shows the results of the estimated storage resources separated by Pliocene and Miocene epoch. For comparison, Table 46 shows the outcome of the estimated storage resource for SS Block 84 field based on using the depleted reservoir data provided by BOEM. The estimated storage capacity results are greater when using the sand volumes derived through geologic modeling versus the BOEM depleted oil and gas reservoir data. Also, the storage capacity is underestimated for the Pliocene since there are no hydrocarbon reservoirs found within the Pliocene formations.

Table 44: CO_2 storage resource for Ship Shoal Block 84 field based on the NETL calculation using reservoir volumes derived from modeling

Low/P10	(metric tons)	Medium/P50	(metric tons)	High/P90	(metric tons)
Top Pliocene (Valv-H)	1.15E+07	**Top Pliocene (Valv-H)**	4.51E+07	**Top Pliocene (Valv-H)**	1.22E+08
Tex-X	1.81E+06	**Tex-X**	7.10E+06	**Tex-X**	1.92E+07
Top Miocene (Bul-1)	4.14E+05	**Top Miocene (Bul-1)**	1.62E+06	**Top Miocene (Bul-1)**	4.38E+06
Big-A	7.61E+05	**Big-A**	2.98E+06	**Big-A**	8.06E+06
Cris-K to base of model	3.55E+06	**Cris-K to base of model**	1.39E+07	**Cris-K to base of model**	3.76E+07

Table 45: Estimated storage resource for the Pliocene and Miocene for Ship Shoal Block 84 field based on volumes derived from geologic modeling

Low/P10	(metric tons)	Medium/P50	(metric tons)	High/P90	(metric tons)
Pliocene	1.33E+07	Pliocene	5.22E+07	Pliocene	1.41E+08
Miocene	4.72E+06	Miocene	1.85E+07	Miocene	5.00E+07

Table 46: Estimated storage resource for the Miocene for Ship Shoal Block 84 field based on BOEM depleted oil and gas reservoir data

Low/P10	(metric tons)	Medium/P50	(metric tons)	High/P90	(metric tons)
Miocene	8.06E+04	Miocene	3.16E+05	Miocene	8.53E+05

9.2.2 Ship Shoal Block 107 field

The modeled Pliocene and Miocene formations within the Ship Shoal Block 107 field contain 248,184 voxels, with each voxel measuring 750 x 750 x 20 feet in dimensions. The volume of each voxel is 11,250,000 cubic feet, for a total modeled Plio-Miocene volume of 2.79E12 cubic feet. Table 47 below displays the lithologic distribution in percentage for the total combined Ship Shoal Block 107 field. Table 48 shows the calculated volume based on the number of voxels per formation within the field. The upper Pliocene Valv-H Formation contains a greater percentage of sand than shale and silt, while the other formations contain a greater amount of shale than sand or silt.

Table 47: Lithologic distribution in percentage for the combined Ship Shoal Block 107 field

Total Field Percent Distribution	Sand	Shale	Silt
Top Pliocene (Valv-H)	52.49%	29.40%	18.02%
Tex-X	11.55%	77.03%	11.42%
Top Miocene (Bul-1)	5.42%	74.48%	20.10%
Big-A	2.72%	89.78%	7.51%
Cris-K to base of model	8.17%	78.02%	13.81%

Table 48: Volumetric totals generated for different lithologies per formation for Ship Shoal Block 107 field

Volume ft3	Sand	Shale	Silt	Total
Top Pliocene (Valv-H)	4.56E+11	2.56E+11	1.57E+11	8.68E+11
Tex-X	7.65E+10	5.10E+11	7.57E+10	6.62E+11
Top Miocene (Bul-1)	1.19E+10	1.64E+11	4.42E+10	2.20E+11
Big-A	9.56E+09	3.16E+11	2.64E+10	3.52E+11
Cris-K to base of model	5.63E+10	5.37E+11	9.51E+10	6.89E+11
		TOTAL PLIO/MIO VOLUME		2.79E+12

From this information, GeoMechanics Technologies used the volumes of sand to calculate the estimated CO_2 storage resource based on the NETL approved volumetric calculation (Equation 1) using the same efficiency factors, parameters for porosity and CO_2 fluid density. The results are shown in Table 49. Table 50 shows the results of the estimated storage resource separated by Pliocene and Miocene epoch. For comparison, Table 51 shows the estimated CO_2 storage resource calculated using the BOEM depleted oil and gas reservoir data for volume. The estimated storage capacity results are greater when using the sand volumes derived through geologic modeling versus the BOEM depleted oil and gas reservoir data.

Table 49: CO_2 storage resource for Ship Shoal Block 107 field based on the NETL calculation using reservoir volumes derived from modeling

Low/P10	(metric tons)	Medium/P50	(metric tons)	High/P90	(metric tons)
Top Pliocene (Valv-H)	1.34E+07	Top Pliocene (Valv-H)	5.24E+07	Top Pliocene (Valv-H)	1.42E+08
Tex-X	2.24E+06	Tex-X	8.80E+06	Tex-X	2.37E+07
Top Miocene (Bul-1)	3.85E+05	Top Miocene (Bul-1)	1.51E+06	Top Miocene (Bul-1)	4.08E+06
Big-A	2.98E+05	Big-A	1.17E+06	Big-A	3.16E+06
Cris-K to base of model	1.75E+06	Cris-K to base of model	6.88E+06	Cris-K to base of model	1.86E+07

Table 50: Estimated storage resource for the Pliocene and Miocene for Ship Shoal Block 107 field based on volumes derived from geologic modeling

Low/P10	(metric tons)	Medium/P50	(metric tons)	High/P90	(metric tons)
Pliocene	1.56E+07	Pliocene	6.12E+07	Pliocene	1.65E+08
Miocene	2.44E+06	Miocene	9.56E+06	Miocene	2.58E+07

Table 51: Estimated storage resource for the Pliocene and Miocene for Ship Shoal Block 107 field based on BOEM depleted oil and gas reservoir data

Low/P10	(metric tons)	Medium/P50	(metric tons)	High/P90	(metric tons)
Pliocene	1.47E+05	Pliocene	5.78E+05	Pliocene	1.56E+06
Miocene	8.16E+04	Miocene	3.20E+05	Miocene	8.64E+05

9.3 Estimated Resource Comparison and Analysis

The NETL CO_2 storage resource mass estimate (Equation 1) provides a means to approximate the available resource for CO_2 sequestration. We used two common methods to estimate the volume of the potential resource while holding all other variables constant. This resulted in a large difference in resource estimation, as shown in the comparison of Table 45 and Table 46 (SS Block 84 field) as well as for Table 50 and Table 51 (SS Block 107 field). As expected, the estimated storage capacity results are greater when using the sand volumes derived through geologic modeling versus oil and gas reservoir data. The difference is likely due to the depleted oil and gas reservoir information not accounting for the water-flooded sand located below the oil/gas-water contact. It is also not accounting for existing unproductive sand units, as demonstrated by the unaccounted Pliocene resources in SS Block 84 field. Using only the depleted reservoir information, a large quantity of the storage resource is being missed. However, resource calculation using the sand volume obtained through geologic modeling may overestimate the storage capacity as the model accounts for all sand within the formation, not just the interconnected sand.

This discrepancy demonstrates the importance of fluid flow modeling. We have verified that at minimum 30 million tons (over 30 years of injection) can be stored in either the Pliocene or Miocene formations in both fields. For both fields, the Pliocene was estimated to contain a greater storage resource than Miocene formations. This was demonstrated in our fluid flow simulations which repeatedly showed that Pliocene injection would be contained within Pliocene

units, yet injection into the Miocene would spill over into and become sequestered within Pliocene and Miocene units. Therefore, it is important to note that although 30 million tons of CO_2 was shown to be injected and safely sequestered into both formations, this was tested individually and a combined estimated storage resource for the Pliocene and Miocene would be less than 60 million tons of CO_2. Although it may be an overestimation, the results of our fluid flow simulations correlate better with the results of the P50 resource capacity estimation using geologic modeling than the results using the depleted oil and gas reservoir information. Fluid flow modeling can provide an additional method to further test and validate the storage resource estimation calculated by the NETL CO_2 storage resource mass estimate calculation. Although, the model would require further updating once more geologic in-situ information is obtained.

Our findings indicate that the available storage resource of the Ship Shoal area should be much larger than initially estimated under the section: Resource capacity estimation based on BOEM oil and gas reservoir data. Both SS Block 84 and 107 fields demonstrate a substantial difference in resource estimation, of at least one to two orders of magnitude larger than initially estimated. Our results therefore demonstrate that the nearshore Ship Shoal area should be considered an even more prospective location for very large-scale CO_2 sequestration.

9.4 Conclusions

We use the NETL CO_2 storage resource mass estimate to calculate the potential resources for Ship Shoal Block 84 and 107 fields using the depleted oil and gas reservoir volume and sand volume generated from our geologic modeling. Our findings are:

- The estimated storage resource results are greater when using the sand volumes derived through geologic modeling than the oil and gas reservoir data.
- The difference is due to the depleted oil and gas reservoir information not accounting for the water-flooded sand located below the oil/gas-water contact.
- The depleted oil and gas volume calculation does not accounting for existing unproductive sand units; for example, the unaccounted Pliocene resources in SS Block 84 field.
- Resource calculation using the sand volume obtained through geologic modeling overestimate the storage capacity as the model accounts for all sand within the formation, not just the interconnected sand.

It is important to note that for calculating CO_2 storage resource mass estimate, the volume used in the equation should be obtained through geologic modeling and verified through fluid flow simulations rather than dependent on reported oil and gas reservoir volumes. Using the volume of the depleted oil and gas field has been demonstrated to be too conservative an approach for estimating CO_2 storage resource.

10 Conclusions

The Gulf of Mexico is one of the most important regions in the United States for energy resources and infrastructure. Gulf of Mexico federal offshore oil and gas production accounts for 17% of total U.S. crude oil production and 5% of total U.S. gas production (EIA Gulf of Mexico Fact Sheet). This region presents an excellent combination of high need and significant opportunity for large scale geologic storage of CO_2. The Ship Shoal Area is located about 20 miles offshore Louisiana within the Gulf Coast federal waters. Miocene and Pliocene sediments in the Ship Shoal Area are proven to provide excellent and secure traps for oil and gas. The Ship Shoal Area contains a large number of depleted oil and gas fields either currently abandoned, or planned for abandonment by 2025, which may provide very significant potential CO_2 storage capacity.

GeoMechanics Technologies conducted a comprehensive research project to better characterize Neogene sediments in the Ship Shoal Area for high volume CO_2 storage. The research efforts funded by this DOE grant are described below.

The data generated from literature, well data, well log, and formation evaluation were input into Rockwork 16 geologic software to create a detailed geologic model for the Ship Shoal study area. The geologic grids were then fed into TOUGH2, the gas migration model software and FLAC 3D, the geomechanical model software.

A detailed geological model spanning about 24,688 m (81,000 ft) in the x-direction, 21,336 m (70,000) ft in the y-direction, and 4267 m (14,000 ft) in the z-direction was created. A total of 121 wells were input the geologic software program. The 5 structure maps and 5 stratigraphic grids for the Top Pliocene, Textularia X, Top Miocene, Bigenerina A and Cristellaria K were created. The 5 stratigraphic grids were stitched together to form a comprehensive stratigraphic model for the area. We also created a 3D lithologic model for the Ship Shoal study area; lithologies obtained from well logs were used to create the lithologic model. This model is geologically sound and consistent with our interpretation and the regional geology within the Gulf of Mexico.

The fluid flow modeling for both the Miocene and Pliocene simulation from both Block 107 and Block 84 indicated that Pliocene and Miocene are a good reservoir for the CO_2 sequestration. Thirty years of CO_2 injection (at a rate of 1 million metric tons CO_2 per year) and 30 years of observation simulations were run with the fluid flow modeling.

- The fluid flow simulation results for Block 107 and Block 84 show a very low risk of CO_2 leakage and a good containment of the injected CO_2 of 30 million metric tons within the 60 years of injection and observation simulated. Most of the cases show that the CO_2 injected will be contained in either the Pliocene or the Miocene Formation.
- One case (for Block 107) with large injection rate (5 million ton per year) for 30 years indicating the potential leak of CO_2 out of the Pliocene Formation. However, this is just an extreme case that was used to evaluate the possible maximum pore pressure that could cause fault slippage and is not for real field practice purpose.

- One case (for Block 84) where the gas plume migrates upward during the injection and causes leakage in the observation phase when we assume no capillary pressure. The assumption of no capillary pressure is very conservative, thus unlikely to represent the real field conditions.
- The reservoir in Block 107 seems to be better than those in Block 84. For the same injection parameters, the pressure increase in Block 84 will be twice as large as that in Block 107. However, the pressure increase in both Blocks does not seem significant. The maximum pressure change among all the scenarios is 5.6% increase compared to the original reservoir pressure.
- Injection into Pliocene tends to spread the plume more laterally in Block 107 compared to Miocene. On the other hand the lateral migration of the plume is very similar in Block 84 for both targets; only for two cases the lateral migration is slightly higher in the Miocene.
- Different sensitivity scenarios including reservoir pressure, silt and shale permeability, relative permeability curve, salt effect, temperature effect, injection rate, and capillary pressure effect were tested.

GeoMechanics Technologies has developed a 3D geomechanical model for Block 107 and Block 84 of the Ship Shoal area to evaluate induced surface deformation and potential fault reactivation after 30 years CO_2 injection at base of Pliocene and at upper Miocene injection locations.

- A total of 6 simulation scenarios were performed for Block 107. For base Pliocene injection scenarios, maximum surface uplift is toward the north of the injection well, with a maximum value of about 0.58cm or 0.22 in (worst case scenario – 107_P_Sim03) compared to about 0.49 cm (0.19 in) for the baseline scenario (107_P_Sim01). Similarly for the upper Miocene injection scenarios, maximum surface uplift is toward the north of the injection well, with a maximum value of about 0.85 cm or 0.33 in (worst case scenario – 107_M_Sim02) compared to about 0.55 cm (0.21 in) for the baseline scenario (107_M_Sim01). The center of the maximum surface uplift bowl is spread across in a wide area, at over 3 miles (4.82 km) diameter. For all injection scenarios, the maximum induced shear stresses are less than 7.0E4 Pa (10 psi).
- The results for Block 107 indicate low to no risks for fault slips or fault reactivation after 30 years of CO_2 injection and migration with these relatively small induced stresses and displacements.
- Two sensitivity analyses (Block 107) have been performed for the base Pliocene and upper Miocene geomechanical models to evaluate potential fault activation by significantly increased the change in pressures from the baseline scenarios. The simulations showed that unless the reservoir pressure changes are vastly increased to at least 50 times - more than 23 MPa (3,400 psi) then we would observe any potential fault slippage. Therefore, there are very low or no risks of potential fault activation due to CO_2 injection at Ship Shoal area identified.
- A total of 12 scenarios with isothermal and non-isothermal effect were performed for Block 84 for base of Pliocene and upper Miocene. Relatively small surface uplift magnitude lower than 1 cm for the majority of the scenarios and around

1.6 cm for the most critical case with double the injection rate was observed. These relative small magnitudes indicate low to no risks of a severe surface uplift displacement that can compromise any surface facilities or potential damage after 30 years of CO_2 injection. The results also indicate low to no risks for fault slips or fault reactivation after 30 years of CO_2 injection and migration with these relatively small pressure change.

Twelve well bores and 76 well bores for Ship Shoal Block 84 and 107 respectively were reviewed for their cement history. Most wells (57 out of 76 and 7 out of 12 wells in Ship Shoal Block 107 and 84 respectively) have good integrity. Nineteen and 5 wells (in Ship Shoal Block 107 and 84 respectively) with no top plug, incomplete cement or Plug and Abandonment information are given yellow cautionary indicators. These cautionary wells may provide leakage paths of CO_2 through the well bores to the USDWs.

Using our Quantitative Risk & Decision Analysis Tool (QRDAT) for caprock integrity evaluation, we compared Ship Shoal's risk to that of In Salah, Sleipner, Kevin Dome, Loudon, Illinois Industrial CCS and Wilmington Graben. We found the risk at the Ship Shoal Blocks 84 and 107 fields are similar to the known CO_2 active sequestration sites, but lower than the Wilmington Graben turbidities offshore California studied site.

The risk of natural seismicity in the Gulf of Mexico is relatively low. Since 1978, there have been about 20 earthquakes located in the Ship Shoal studied area. These earthquakes are mostly small magnitude (3 to 4) events except the two events with magnitudes in the 5.3 and 5.9 occurred during 2006, which were related to the redistribution of the delta sediments.

Geomechanics Technologies has documented the top 25 CO_2 emission sources within the close proximity of the Ship Shoal Block 84 and 107 fields. All the offshore and onshore pipelines have been digitized and can be viewed in an interactive website (http://www.geomechanicstech.com/shipshoal.html). We also performed a feasibility study on the potential for converting existing oil or gas pipelines for CO_2 transport. There are abandoned, idled and retired onshore and offshore pipelines. However, there is no standard specification for maximum pipeline pressures needed for CO_2 transport. It is a function of design, materials, and testing provided; thus it will be the responsibility of the pipeline operator to correctly determine, maintain and operate within the limits of the pipelines. There are a few transit corridors extending from onshore Louisiana (Cailou Bay) to offshore trunk-lines. The cost for constructing a pipeline has increased about 46% from 2015 to an average cost of $5,064,046 per mile in 2016.

We use the NETL CO_2 storage resource mass estimate to calculate the potential resources for Ship Shoal Block 84 and 107 fields using the depleted oil and gas reservoir volume and sand volume generated from our geologic modeling. It is important to note that for calculating CO_2 storage resource mass estimate, the volume used in the equation should be obtained through geologic modeling and verified through fluid flow simulations rather than dependent on reported oil and gas reservoir volumes.

- The estimated storage resource results are greater when using the sand volumes derived through geologic modeling than the oil and gas reservoir data.
- The difference is due to the depleted oil and gas reservoir information not accounting for the water-flooded sand located below the oil/gas-water contact.

- The depleted oil and gas volume calculation does not accounting for existing unproductive sand units; for example, the unaccounted Pliocene resources in SS Block 84 field.
- Resource calculation using the sand volume obtained through geologic modeling overestimate the storage capacity as the model accounts for all sand within the formation, not just the interconnected sand.

11 References

Bennion, D.B. and S. Bachu: Permeability and Relative Permeability Measurements at Reservoir Conditions for CO2-Water Systems in Ultra Low Permeability Confining Caprocks. SPE International, 2007 (SPE Paper # 106995)

Big Sky Regional Carbon Sequestration Partnership- Kevin Dome Carbon Storage, 2015, https://www.netl.doe.gov/File%20Library/Research/Carbon-Storage/Kevin-Dome-Project.PDF

BOEM, 2014, http://www.data.boem.gov/homepg/data_center/gandg/gandg.asp

BOEM database, www.data.bsee.gov

Brink, et al., 2009, Regional Assessment of Tsunami Potential in the Gulf of Mexico: U.S. Geological Survey Administrative Report.

EIA, Energy Information Administration, http://www.eia.gov/pub/oil_gas/natural_gas/analysis_publications/ngpipeline/develop.html

Det Norske Veritas (DNV), 2010, Design and Operation of CO_2 Pipelines, Recommended Practice, DNV-RP-J202

DOE, 2015, A Review of the CO_2 Pipeline Infrastructure in the US; DOE/NETL-2014/1681

Doughty, C. (2010). Investigation of CO2 plume behavior for a large-scale pilot test of geologic carbon storage in a saline formation. Lawrence Berkeley National Laboratory: Lawrence Berkeley National Laboratory. LBNL Paper LBNL-2243E. Retrieved from:

http://www.escholarship.org/uc/item/94h1d0vg

EPA database, https://ghgdata.epa.gov/ghgp/

Edring, Clint, H., 2008, Long term subsidence and compaction rates: a new model for the Michoud Area, South Louisiana, M Sc. thesis at Louisiana State University and Agricultural and Mechanical College

Element Energy, 2010, CO_2 Pipeline Infrastructure: An Analysis of global challenges and opportunities, Final Report for International Energy Agency for Greenhouse for Greenhouse Gas Program

Enhanced Oil Recovery I: Louden Single Well Huff 'n' Puff, 2009, http://sequestration.org/resources/publish/MGSC_HuffnPuff_Loudon.pdf

Frohlich, Cliff, 1982, Seismicity of the central Gulf of Mexico, Geological Society of America, vol.,10, no.2

Galloway, W.E., 2008, Depositional Evolution of the Gulf of Mexico Sedimentary Basin, in Sedimentary Basins of the World, vol. 5, Chapter 15, Elsevier B.V. Publication

Galloway W.E. et al., 1991, Cenozoic, in Salvador, A. ed., The Gulf of Mexico Basin, Geological Society of America, The Geology of North America, Vol. J. Chapter 11, p. 245-324.

Galloway, W.E., et al., 2009, Regional Controls from Temporal and Spatial Distribution of Continental Slope and Abyssal Plain Reservoir Systems of the Gulf of Mexico Basin, Adapted from poster presentation at AAPG Annual Convention, Denver, Colorado, June 7-10, 2009

Geomechanics Technologies, 2014, Development of Improve Caprock Integrity and Risk Assessment Techniques, DOE Grant No.: De-Fe0009168

Geomechanics Technologies, 2015, Characterization of Pliocene and Miocene Formations in the Wilmington Graben, Offshore Los Angeles, for Large Scale Geologic Storage of CO_2; DOE Grant No: DE-NT0001922.

Goodman, A., Hakala, A., Bromhal, G., Deel, D., Rodosta, T., Frailey, S., Small, M., Allen, D., Romanov, V., Fazio, J., Huerta, N., McIntyre, D., Kutchko, B., Guthrie, G., 2011, U.S. DOE methodology for the development of geologic storage potential for carbon dioxide at the national and regional scale, International Journal of Greenhouse Gas Control, pp. 952-965

Haq, et al., 1987, Chronology of fluctuating sea levels since the Triassic, in Science, vol. 235, p.1156-1166

Ide, S.T., S.J. Fridemann, and H.J. Herog, 2006, CO_2 leakage through existing wells: current technology and regulations, presentedat the 8th International Conference on Greenhouse Gas Control Technologies, Trondheim, Norway, June (2006), available at http://sequestration.mit.edu/pdf/GHGT8_Ide.pdf

IEAGHG, 2012, http://ieaghg.org/docs/General_Docs/IEAGHG_Presentations/3._CO2_Transport_Overview_-_S._Santos_IEAGHG.pdf

IEAGHG, 2014, CO_2 Pipeline Infrastructure, IEAGHG Report 2013/18

IHS database, proprietary information from HIS

Ide, S.T., S.J. Fridemann , and H.J. Herzog, "CO_2 leakage through existing wells: current technology and regulations," presented at the 8th International Conference on Greenhouse Gas Control Technologies, Trondheim, Norway, June (2006), available at http://sequestration.mit.edu/pdf/GHGT8_Ide.pdf

In Salah Fact Sheet: Carbon Dioxide Capture and Storage Project, 2016, https://sequestration.mit.edu/tools/projects/in_salah.html

Kevin Dome Carbon Storage Project- Development Phase, 2017, https://www.globalccsinstitute.com/projects/kevin-dome-large-scale-storage-project

Kevin Dome Project- Duperow Formation, Toole County, Montana, Big Sky Carbon Sequestration Partnership, https://www.netl.doe.gov/File%20Library/Research/Carbon-Storage/Kevin-Dome-Project.PDF

Meckel, T.A., et al., 2013, Offshore CCS in the northern Gulf of Mexico and the significant of regional structural compartmentalization, in Energy Procedia 37, p.4526-4532, published by Elsevier Ltd. www.sciencedirect.com

Mineral Management Service, June 1999, Assessment of Conventionally Recoverable Hydrocarbon Resources of the Gulf of Mexico and Atlantic Outer Continental Shelf, OCS Report MMS 00-0034

Nathan David Moodie, undated: Fundamental Analysis of Relative Permeability and Heterogeneity on Carbon Dioxide Storage and Plume Migration. University of Utah

Nicholson, A., 2012, Empirical analysis of fault seal capacity for CO_2 sequestration, Lower Miocene, Texas Gulf Coast: The University of Texas at Austin, Bureau of Economic Geology, Master;s Thesis, 100p., GCCC Digital Publication Series #12-04.

Oil and Gas Journal, Sept., 2016, Natural gas pipeline profits, construction both up, vol. 1149

Parfomak, P.W., and Folger, P., 2007, Carbon dioxide (CO_2) pipelines for carbon sequestration: emerging policy issues, Congressional Research Service, Library of Congress

Pipeline 101, http://www.pipeline101.com/are-pipelines-safe/who-oversees-pipeline-safety

PHMSA, https://primis.phmsa.dot.gov/comm/FactSheets/FSTransmissionPipelines.htm

PHMSA, http://www.phmsa.dot.gov/portal/site/PHMSA

PHMSA, https://primis.phmsa.dot.gov/comm/FactSheets/FSTransmissionPipelines.htm

PHMSA, https://primis.phmsa.dot.gov/comm/FactSheets/FSOffshorePipelines.htm

PHMSA, https://pvnpms.phmsa.dot.gov/PublicViewer/

Pruess, K., Oldenburg, C., and Moridis, G., 1999, TOUGH2 User's Guide: Earth Sciences Division. Lawrence Berkeley National Laboratory, U. o. C. B.

Rehmer, Donald E., 2014, Mathematical programming model to determine optimal transportation infrastructure for geologic CO_2 storage in the Illinois Basin, Southern Illinois University Carbondale PhD Dissertation

Russel, E.L., 1973, Ship Shoal Block 107 Field, Offshore Louisiana, Chevron Oil Company, pp. 75-79

Salvador, A., 1991, Origin and development of the Gulf of Mexico basin, *in* Salvador, A., ed., The Gulf of Mexico Basin: Boulder, Colorado, Geological Society of America, The Geology of North America, vol. J, p. 389-444.

Sleipner CO2 Storage, 2017, https://www.globalccsinstitute.com/projects/sleipner%C2%A0co2-storage-project

University of Florida website, http://users.clas.ufl.edu/rrusso/florida_eq.html

USGS database, https://earthquake.usgs.gov/earthquakes/search

USGS, 2012, Geologic Framework for the National Assessment of Carbon Dioxide Storage Resources ─ U.S. Gulf Coast, USGS, Open-File Report 2012–1024–H

Wallace, K.J., et al., 2013, Regional CO_2 sequestration capacity assessment for the coastal and offshore Texas Miocene interval, in Greenhouse Gas Sci. Technol., vol. 4, p.53-65.

DOE Grant No: DE-FE-0026041

Office of Fossil Energy

Assessment of CO_2 Storage Resources in Depleted Oil and Gas Fields in the Ship Shoal Area, Gulf of Mexico

Final Report Appendix

DOE-GMT-0026041FA

Dr. Michael S. Bruno (PI)
GeoMechanics Technologies
103 E. Lemon Ave.,
Monrovia, CA 91016
Phone: 626 305-8460
Fax: 626 305-8462

March 14, 2018

DUNS Number: 848908356
Project Period: September 15, 2015 to March 14, 2018

Submitted by Jean Young, Project Manager

jtyoung@geomechanicstech.com

Appendix A: Well Schematics for Ship Shoal Block 84 and 107 Fields

Tana 83-01

Current Wellbore Conditions

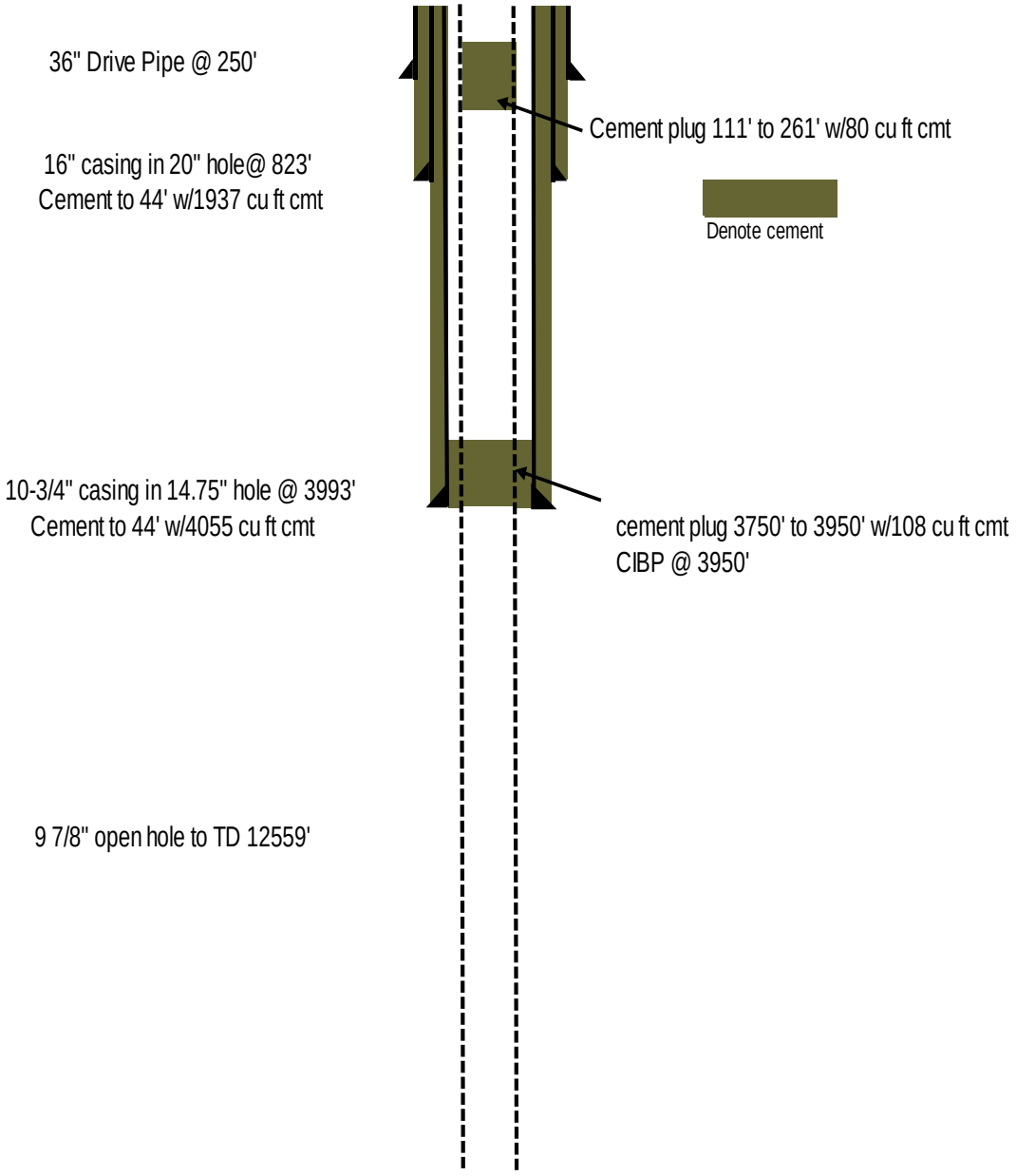

Peregrine 84-01

Current Wellbore Conditions

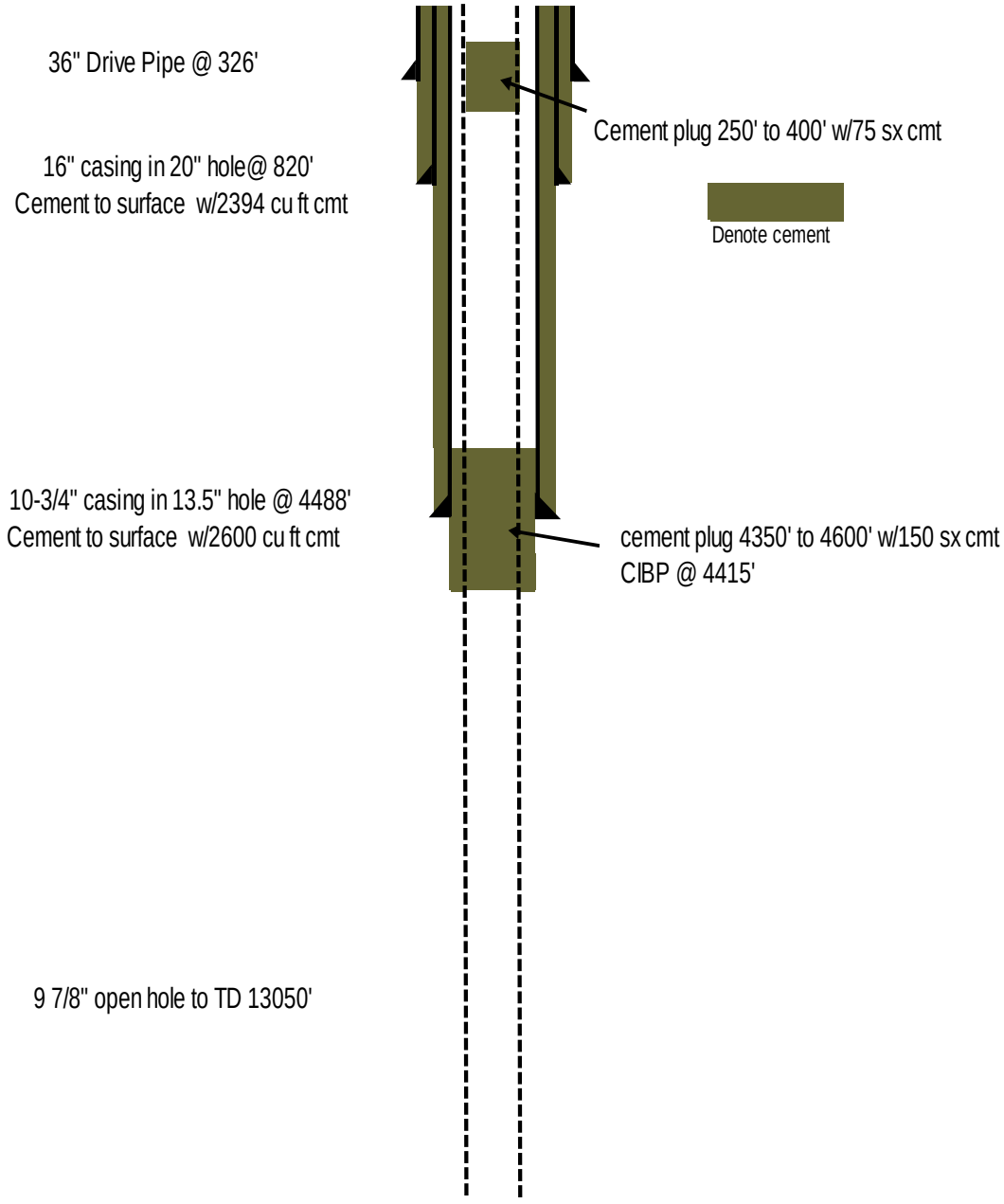

TD 13050' TVD

BP 84 A-1

Current Wellbore Conditions

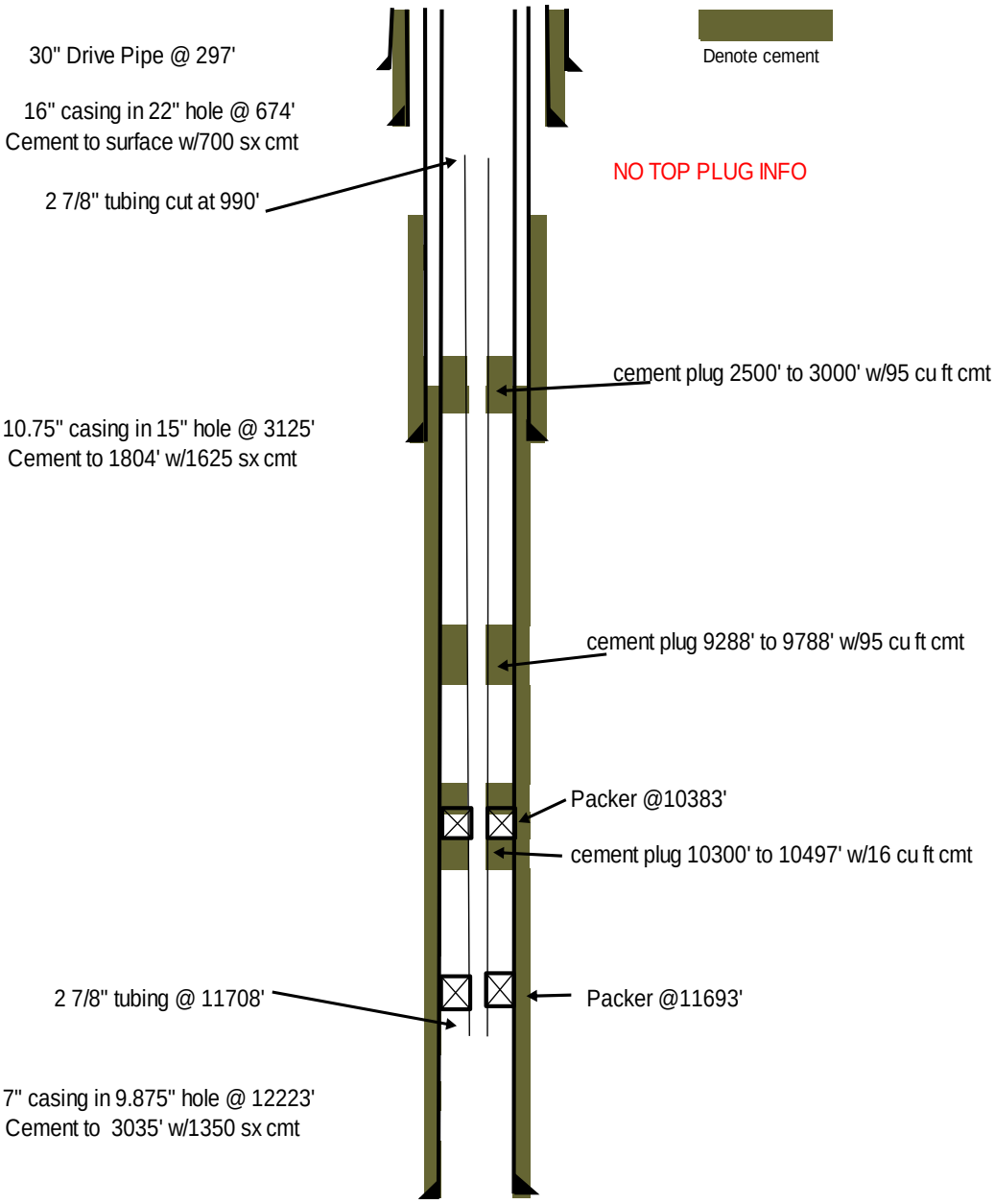

TD 13866' TVD

BP 84 A-2

Proposed Wellbore filed in 1977

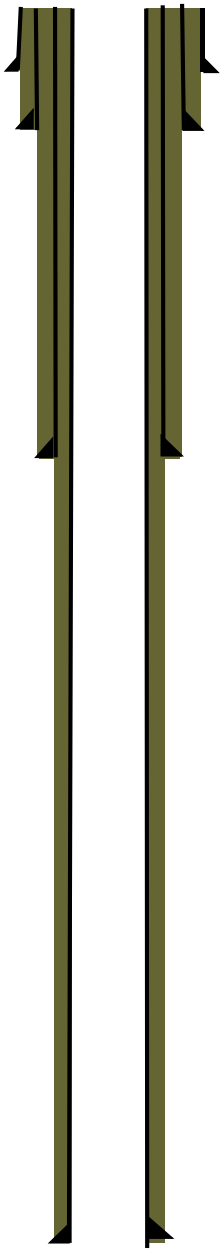

Denote cement

30" Drive Pipe @ 175'

20" casing in 26" hole @ 650'
Cement to surface w/1000 sx cmt

10.75" casing in 15" hole @ 2500'
Cement to surface w/1500 sx cmt

7" casing in 9.5" hole @ 13900'
Cement to surface w/3000 sx cmt

TD 13900' MD
12500' TVD

BP 84 A-3

Current Wellbore Conditions

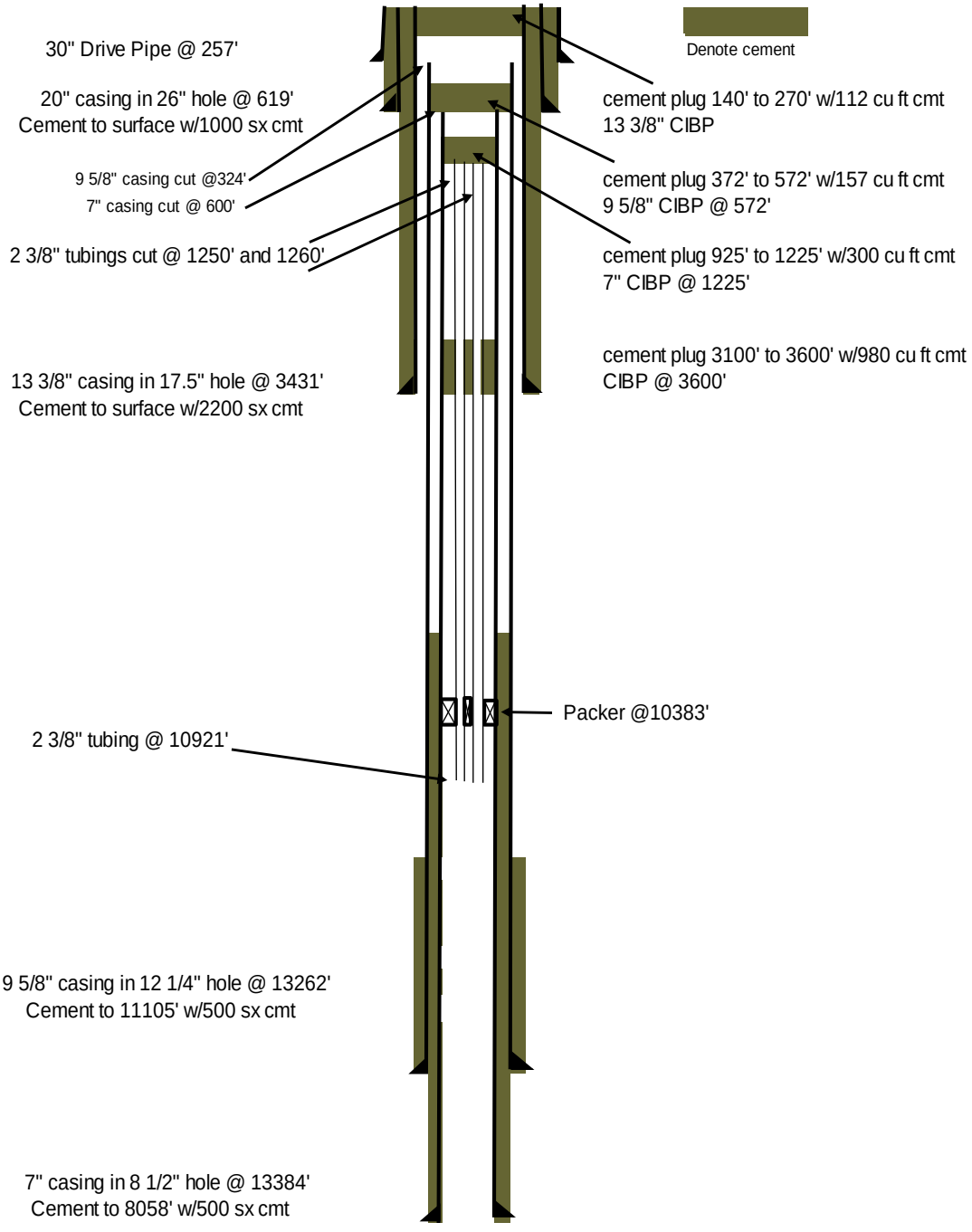

TD 13866' TVD

BP 84 A-4

Current Wellbore Conditions

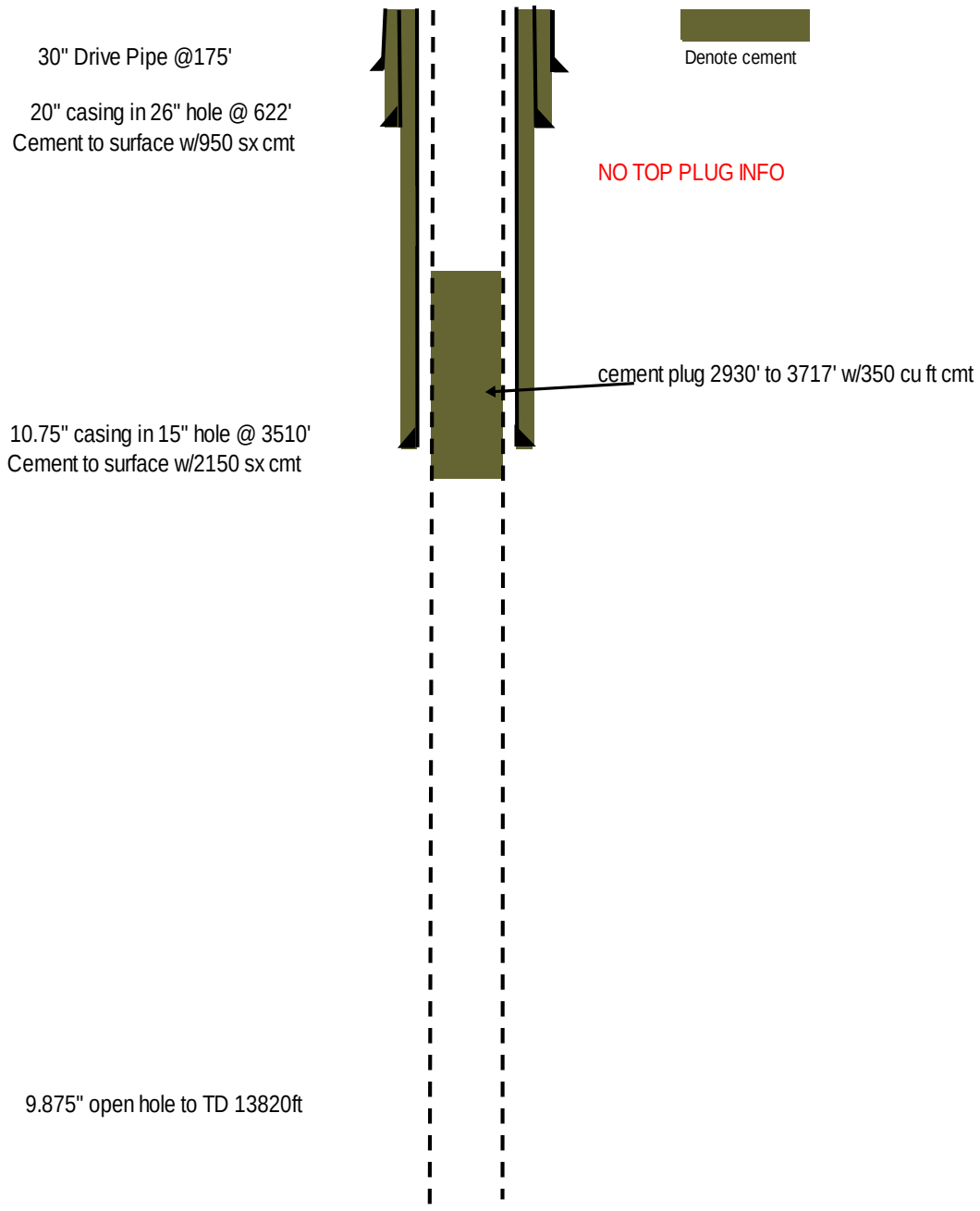

BP 84 A-5

Current Wellbore Conditions

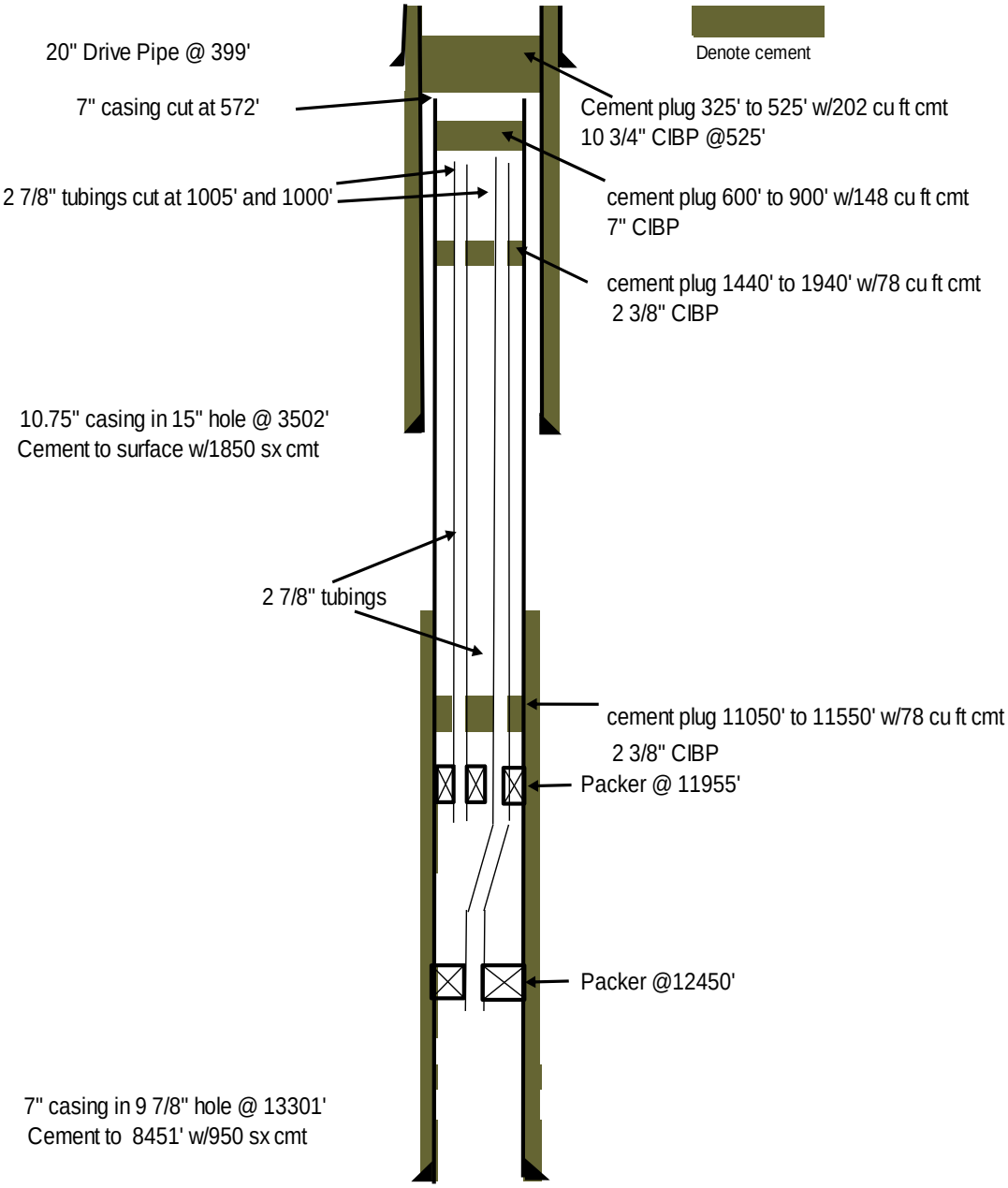

TD 13301' 12969' TVD

BP 84 A-6

Current Wellbore Conditions

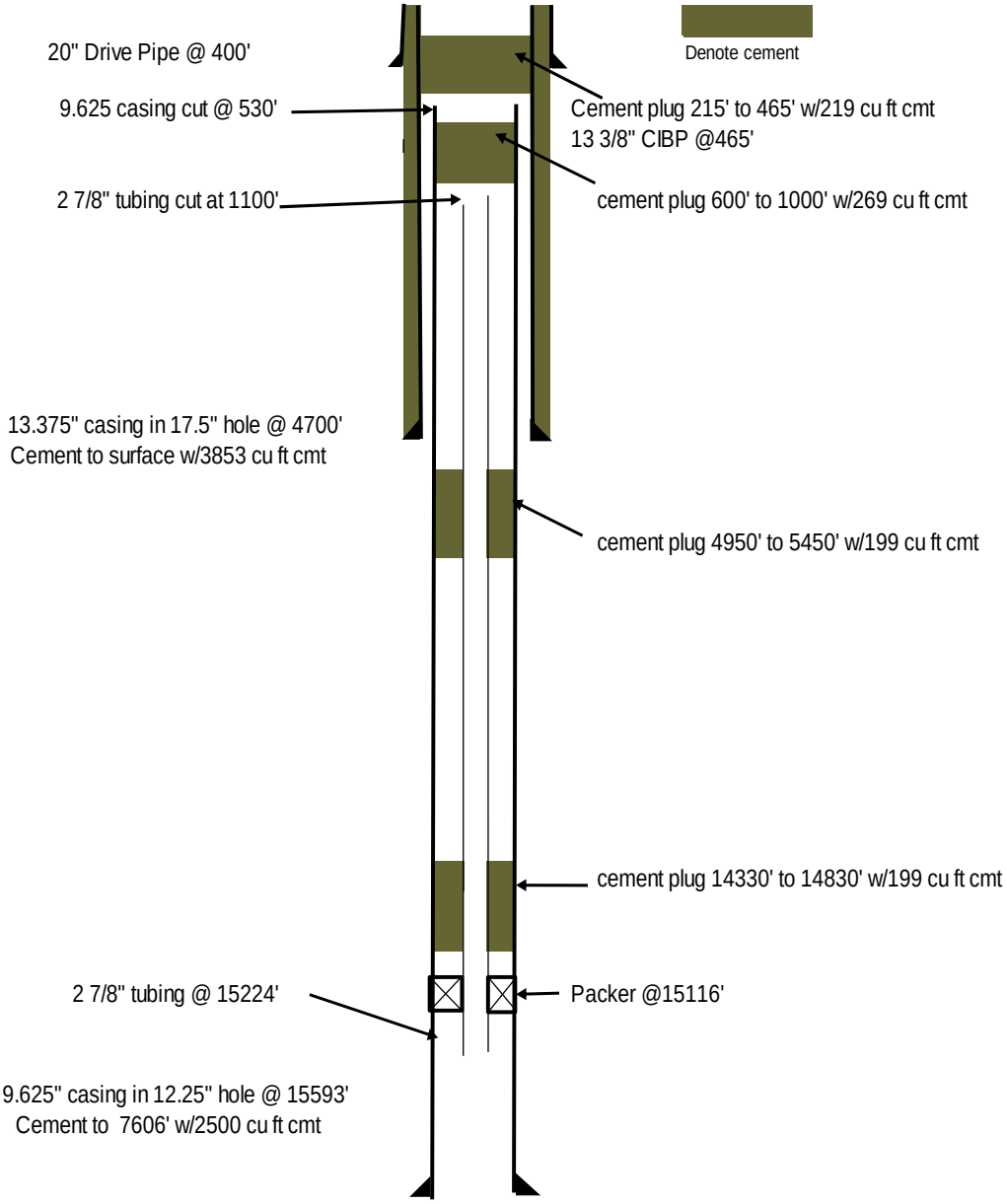

TD 15593' 11850' TVD

BP 84 A-7

Current Wellbore Conditions

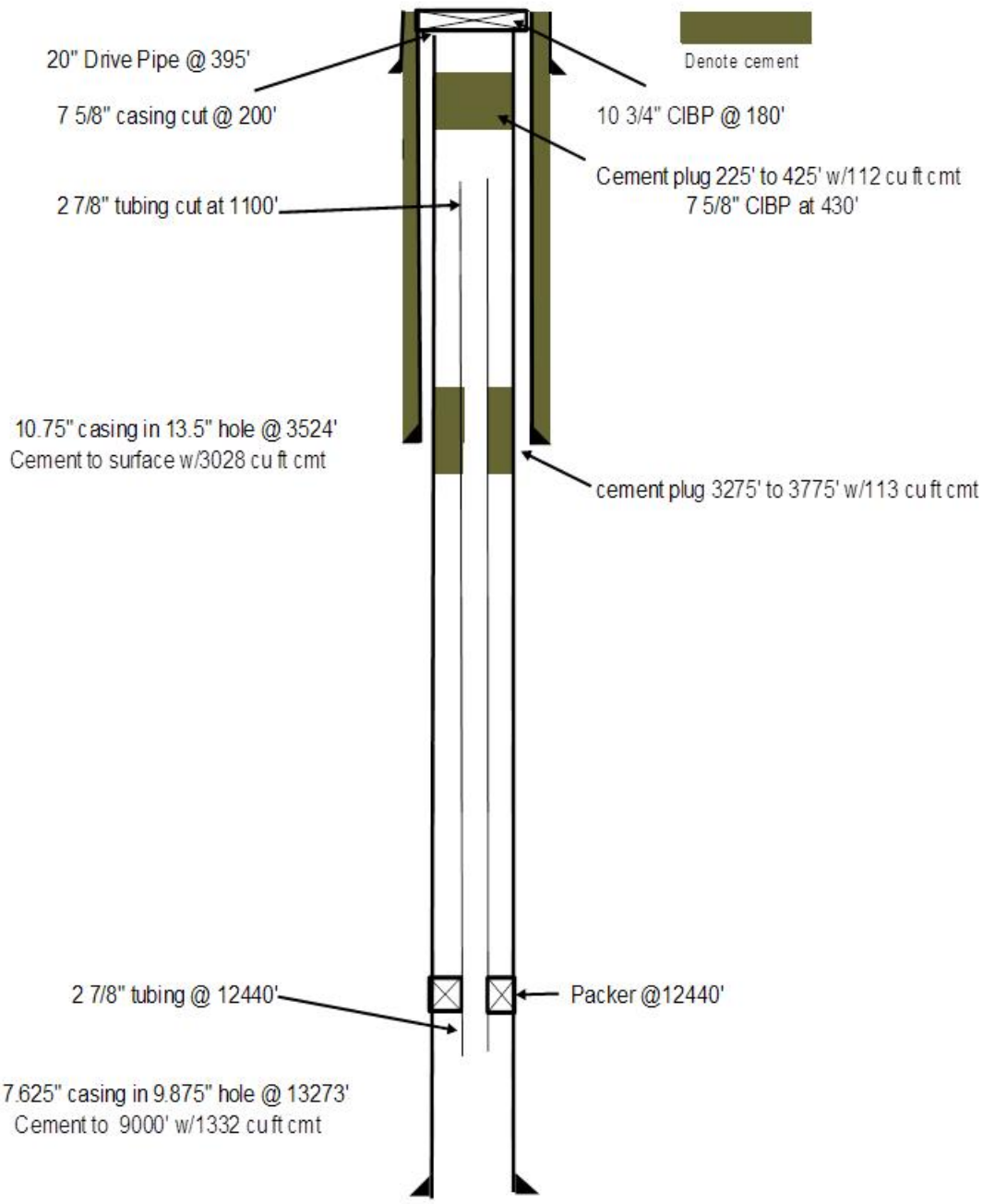

TD 13273' 12935' TVD

BP 84 #5

Proposed Wellbore filed in 1989

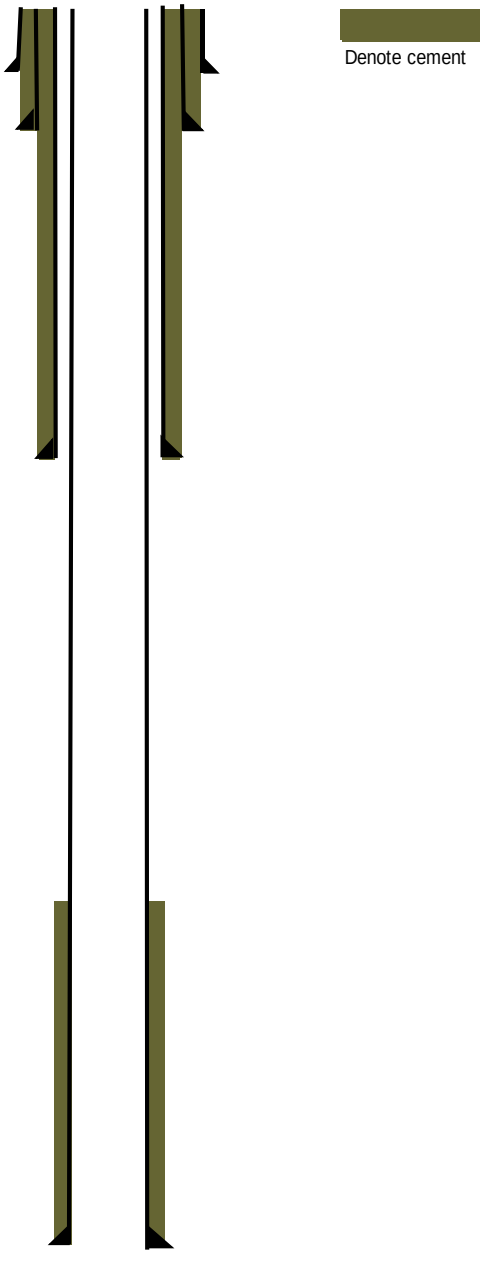

Taylor Energy 85-1 BP1

Current Wellbore Conditions

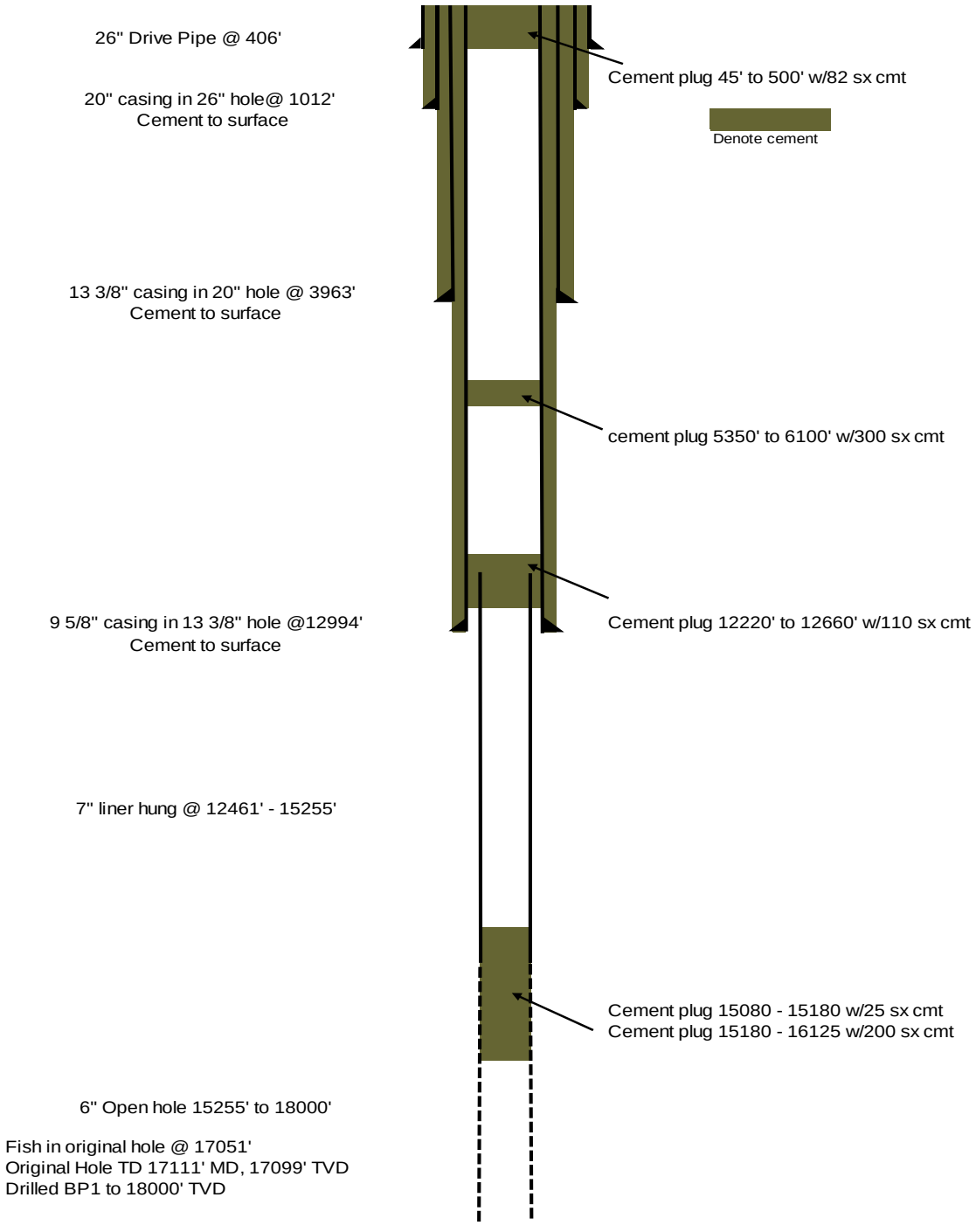

Chevron 98 #1

Current Wellbore Conditions

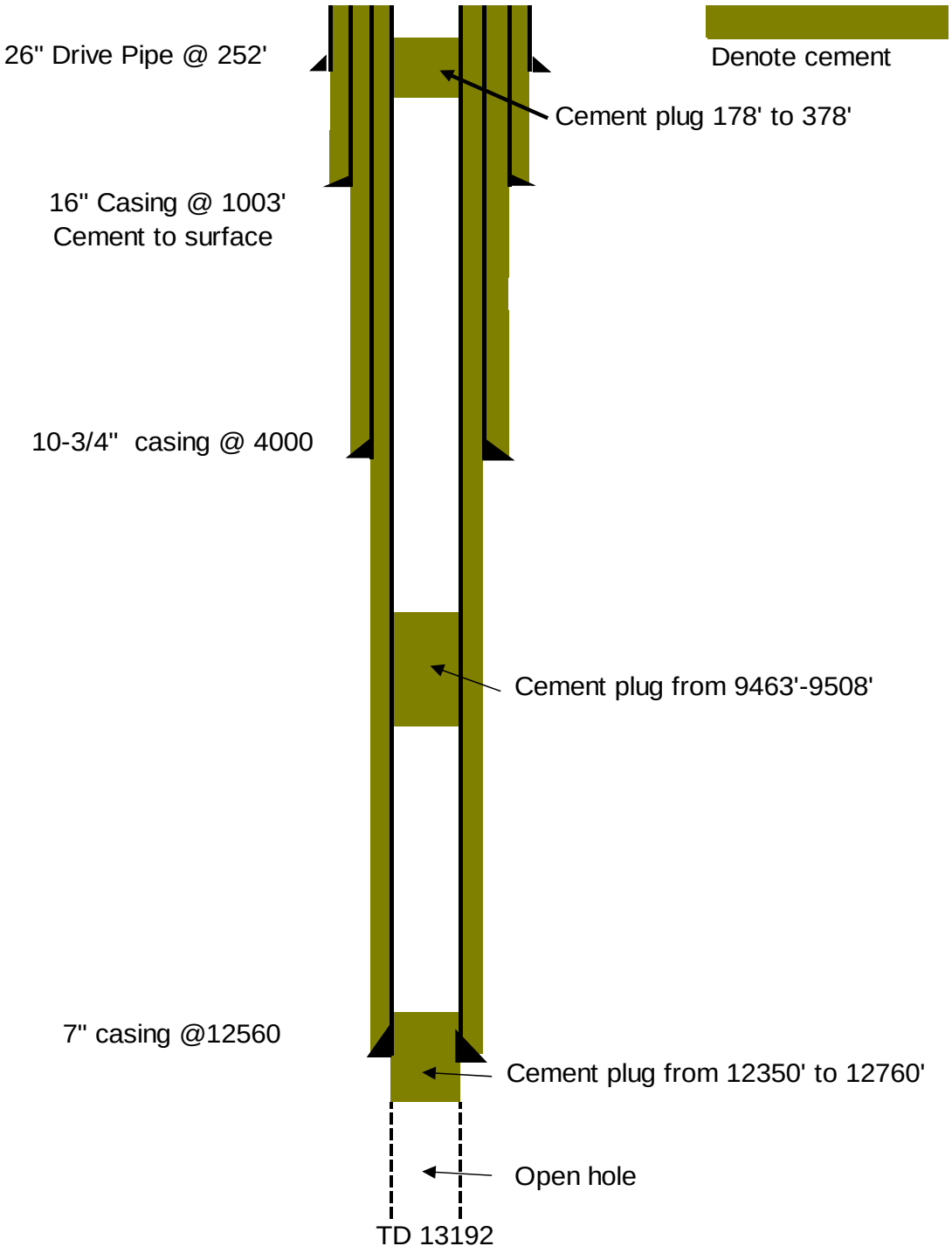

Stone 99-1

Denote cement

Current Wellbore Conditions

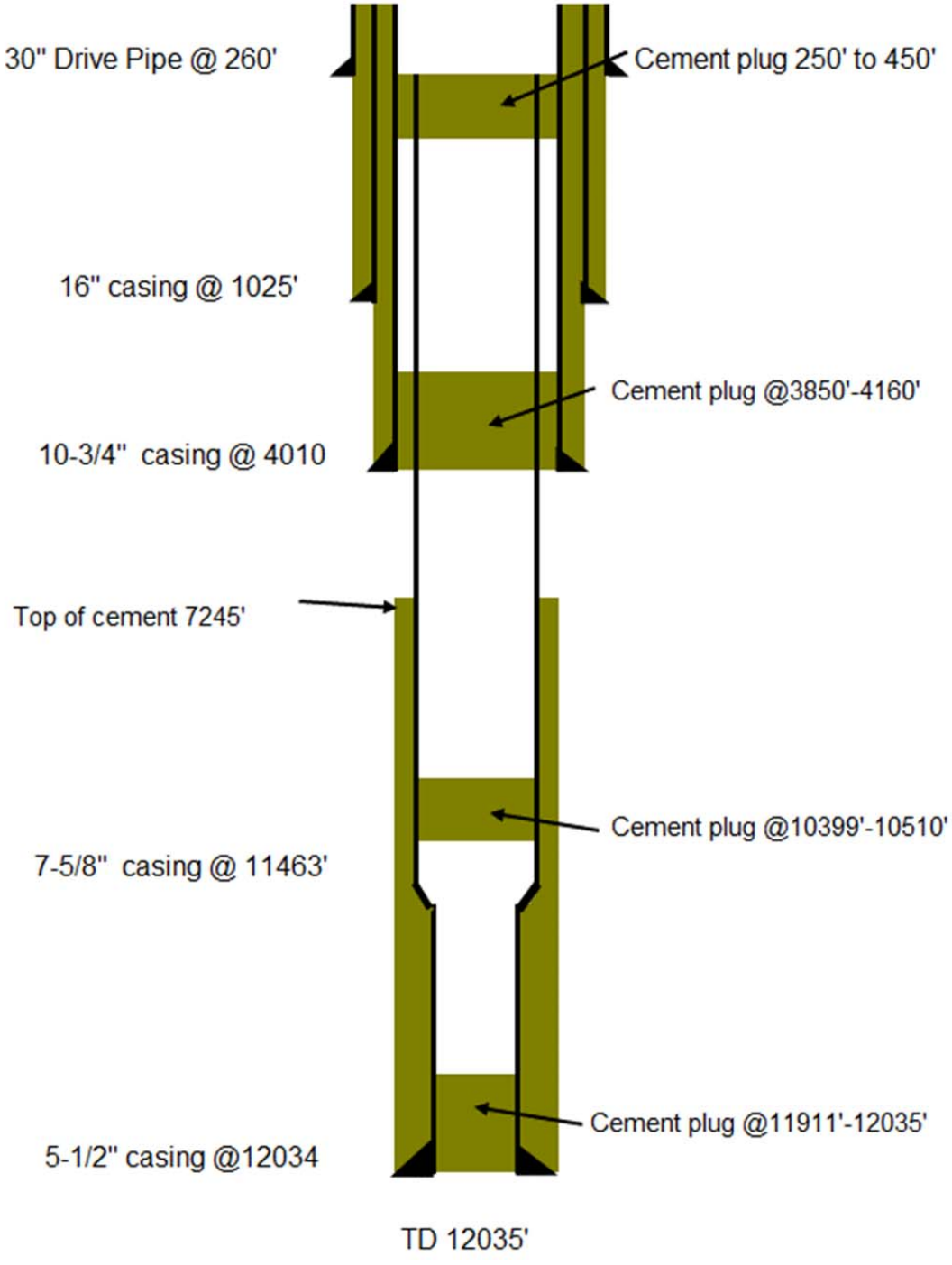

Stone 99-1ST1

Denote cement

Current Wellbore Conditions

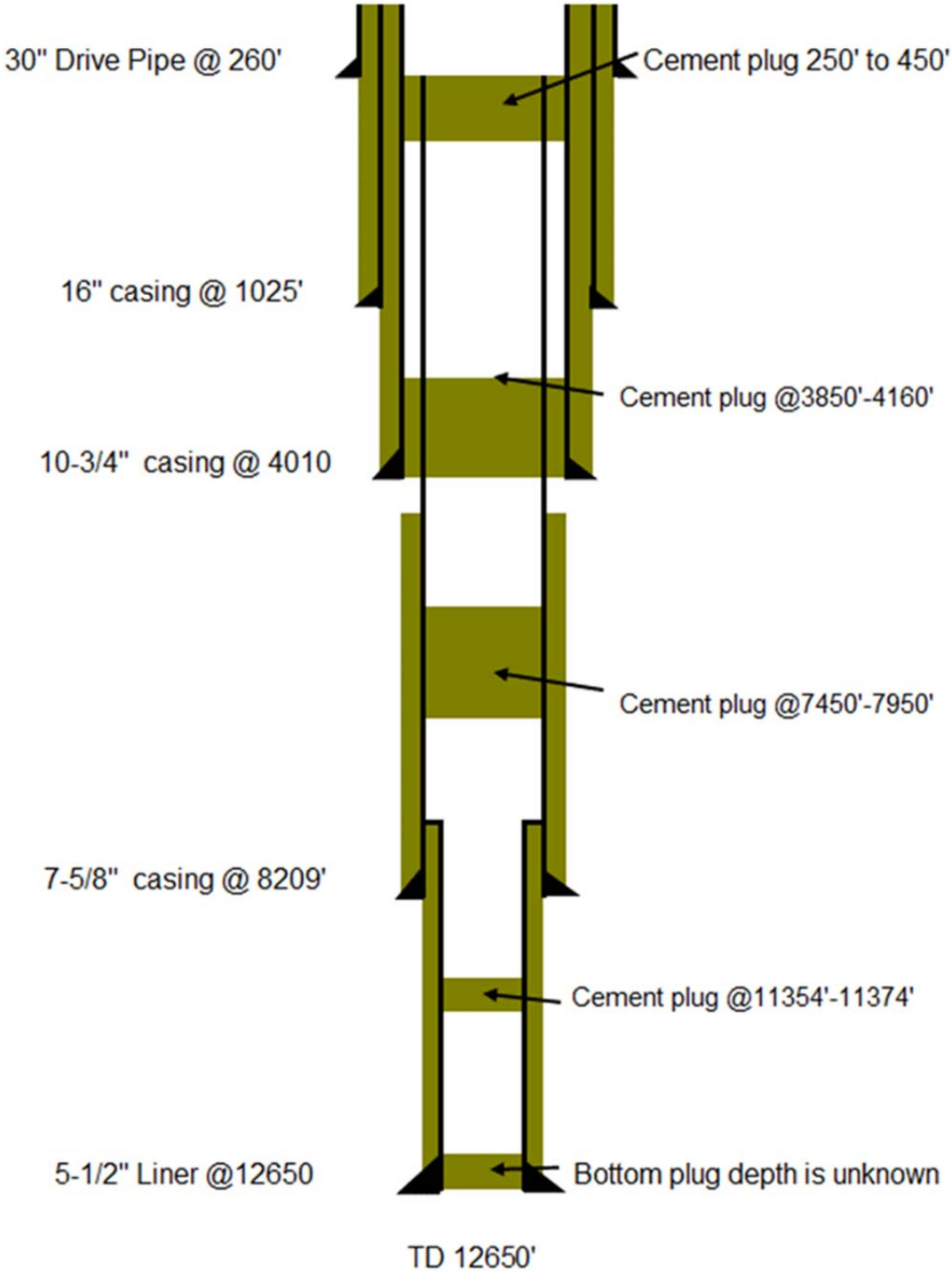

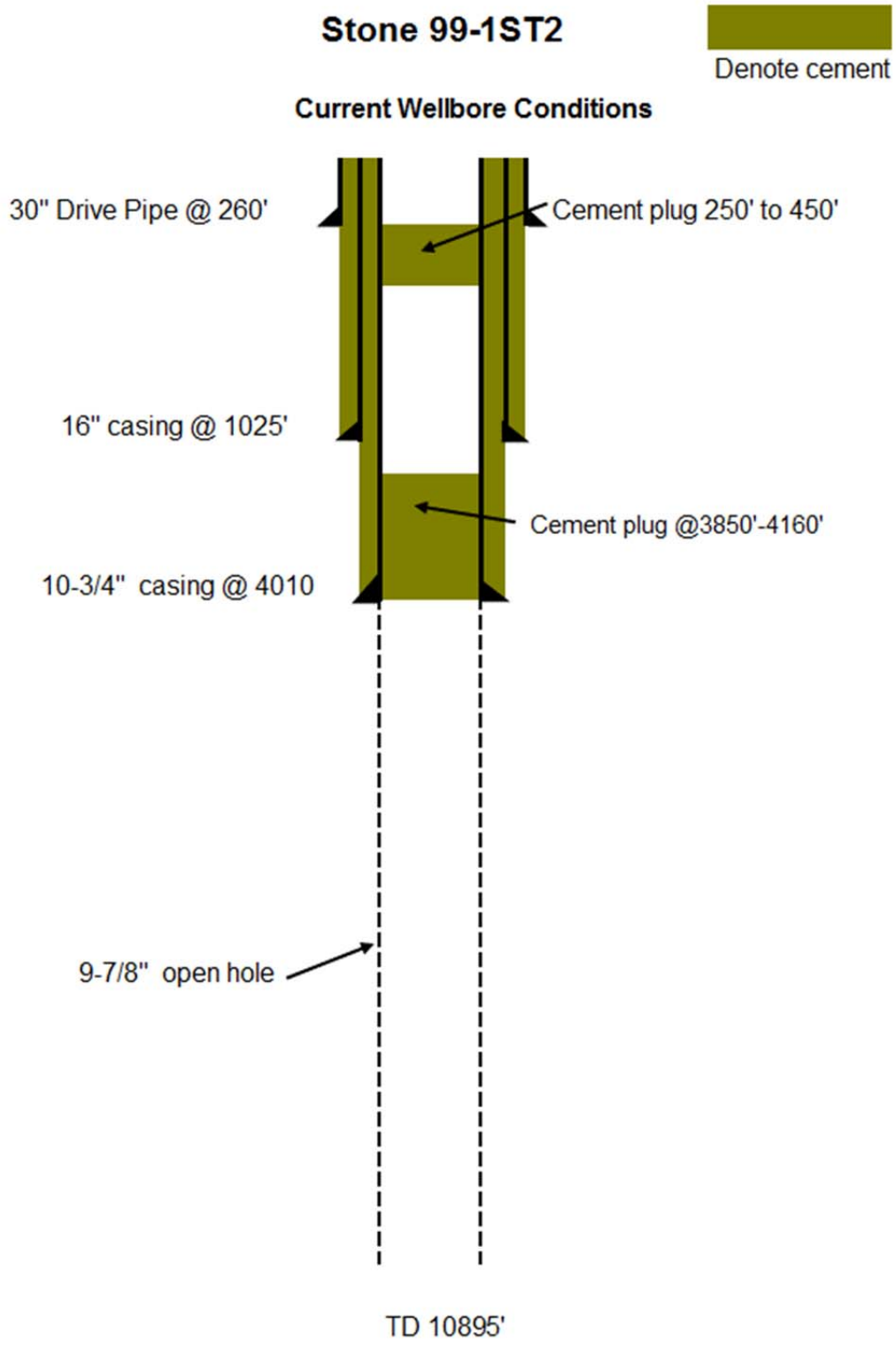

Stone 99-1 ST2 well schematic

Stone 99-3

Current Wellbore Conditions

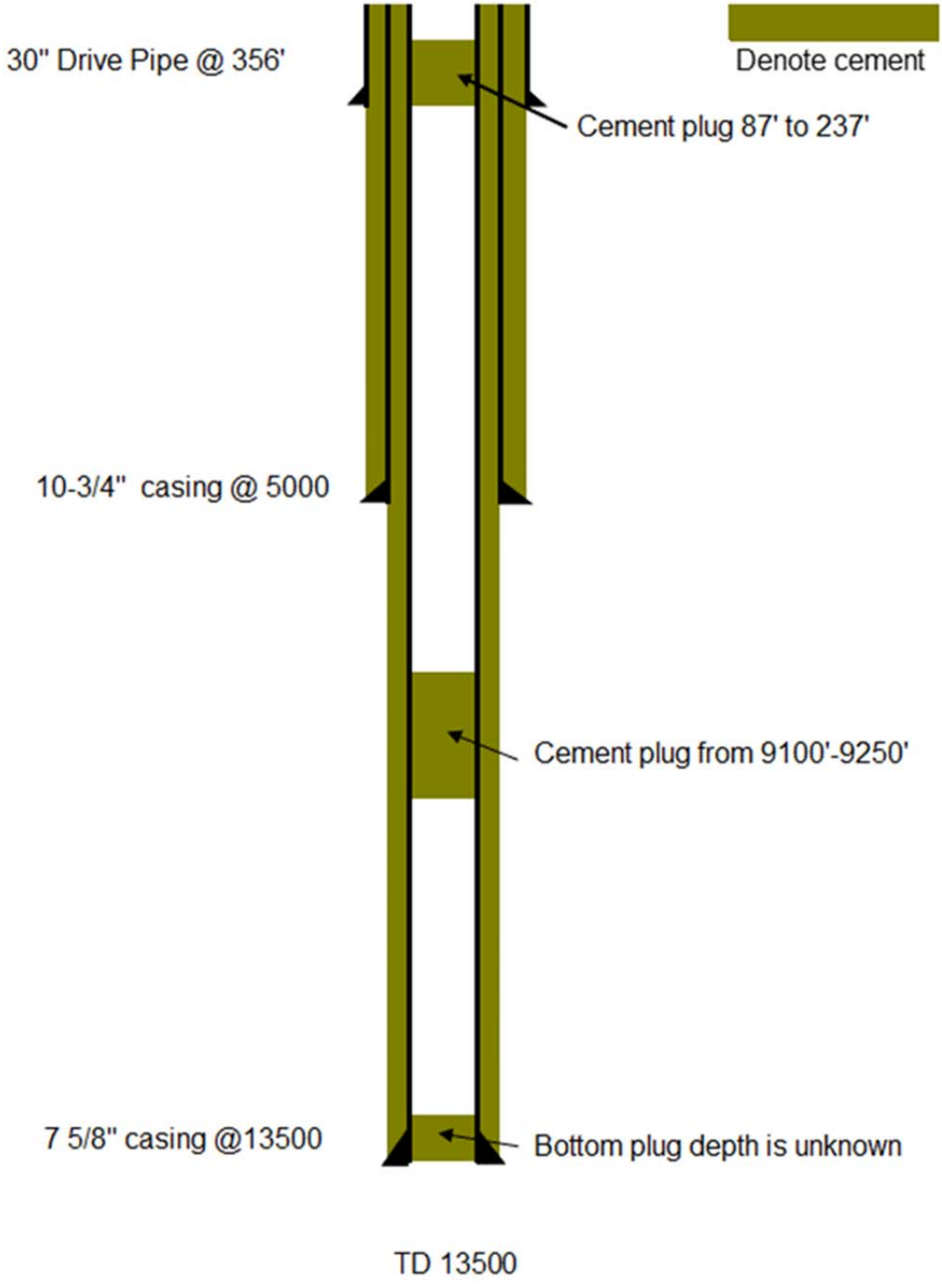

Stone 99-A1

Current Wellbore Conditions

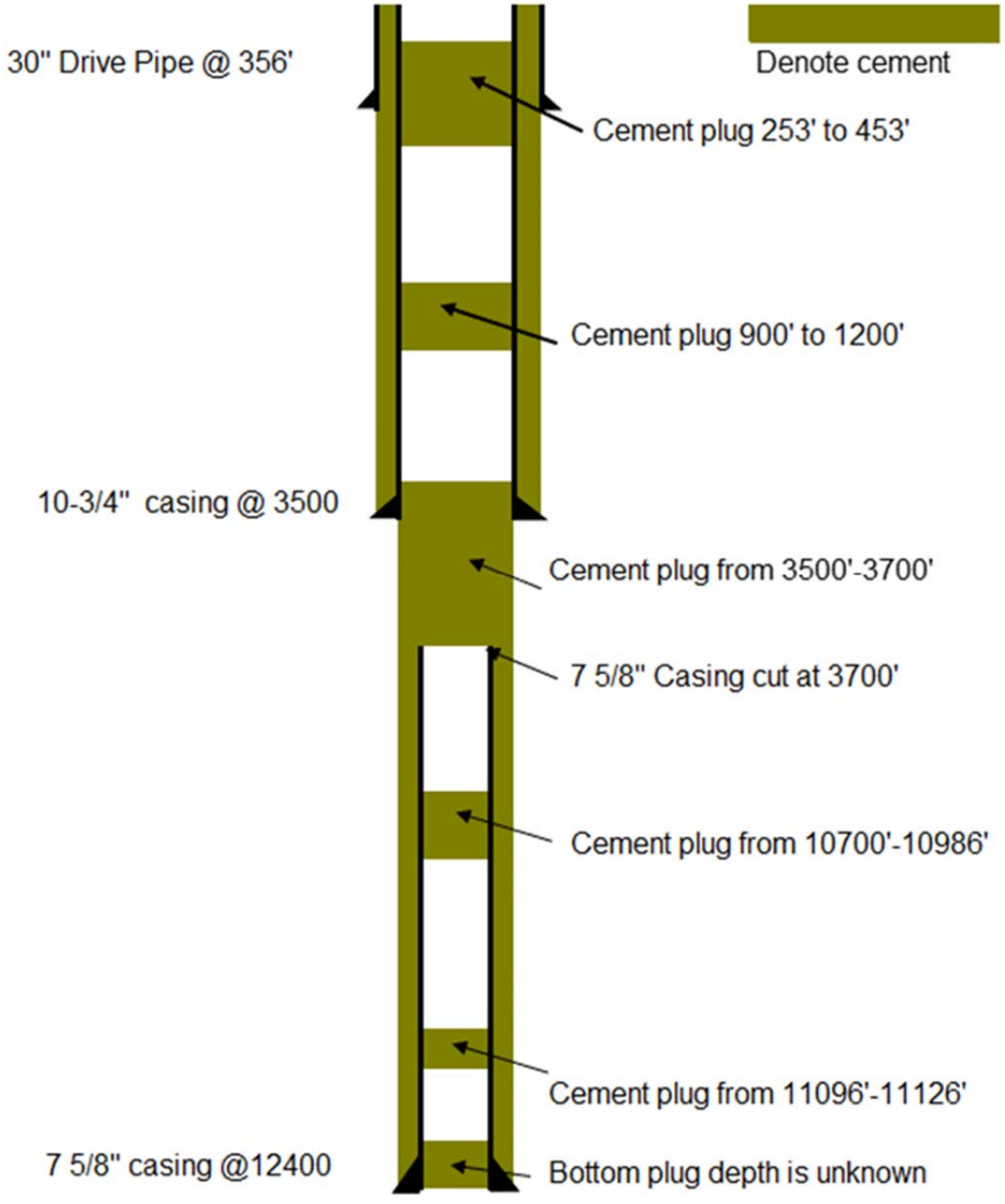

TD 12400

Stone 99-A1ST1

Current Wellbore Conditions

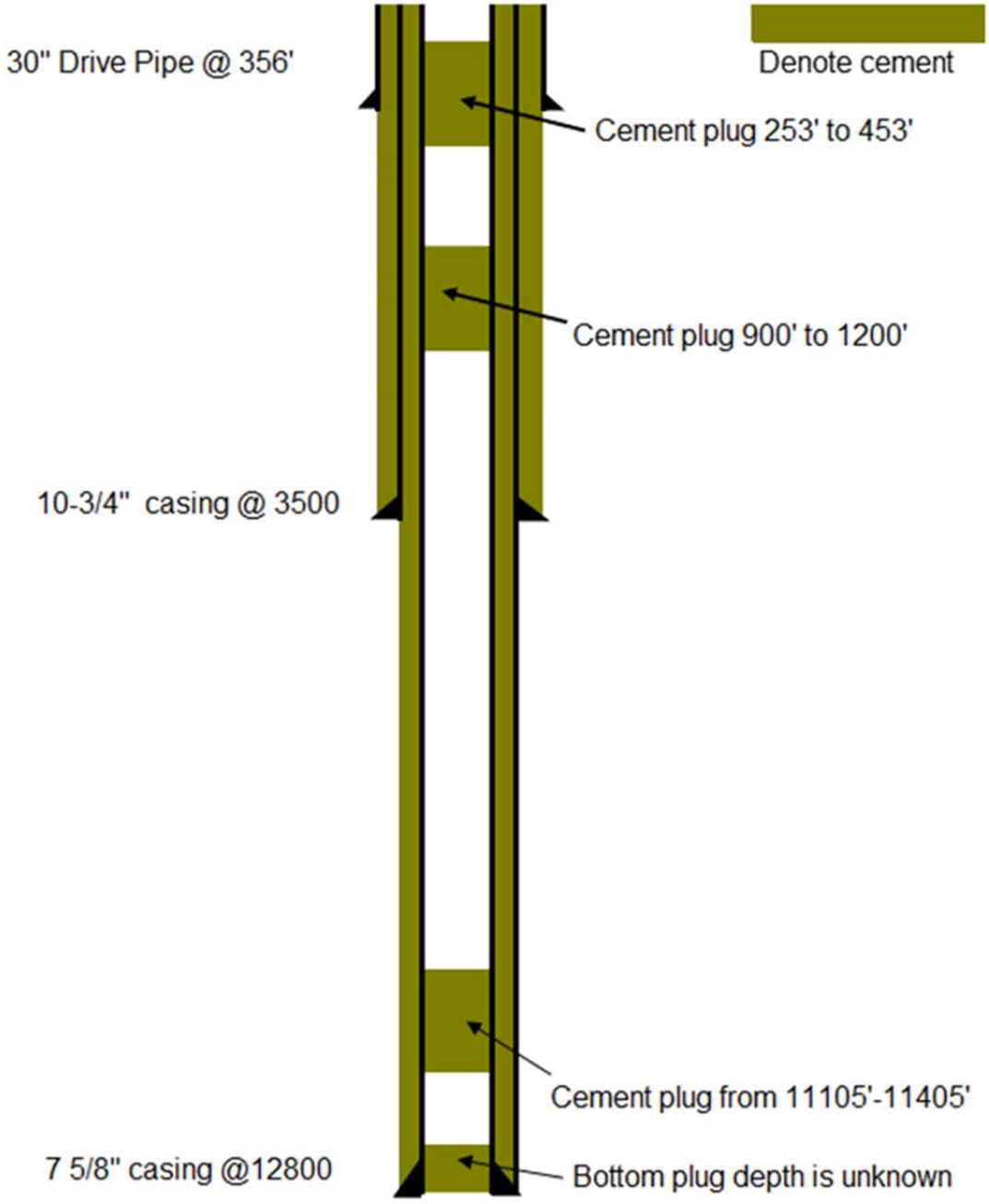

Stone 99-A2

Current Wellbore Conditions

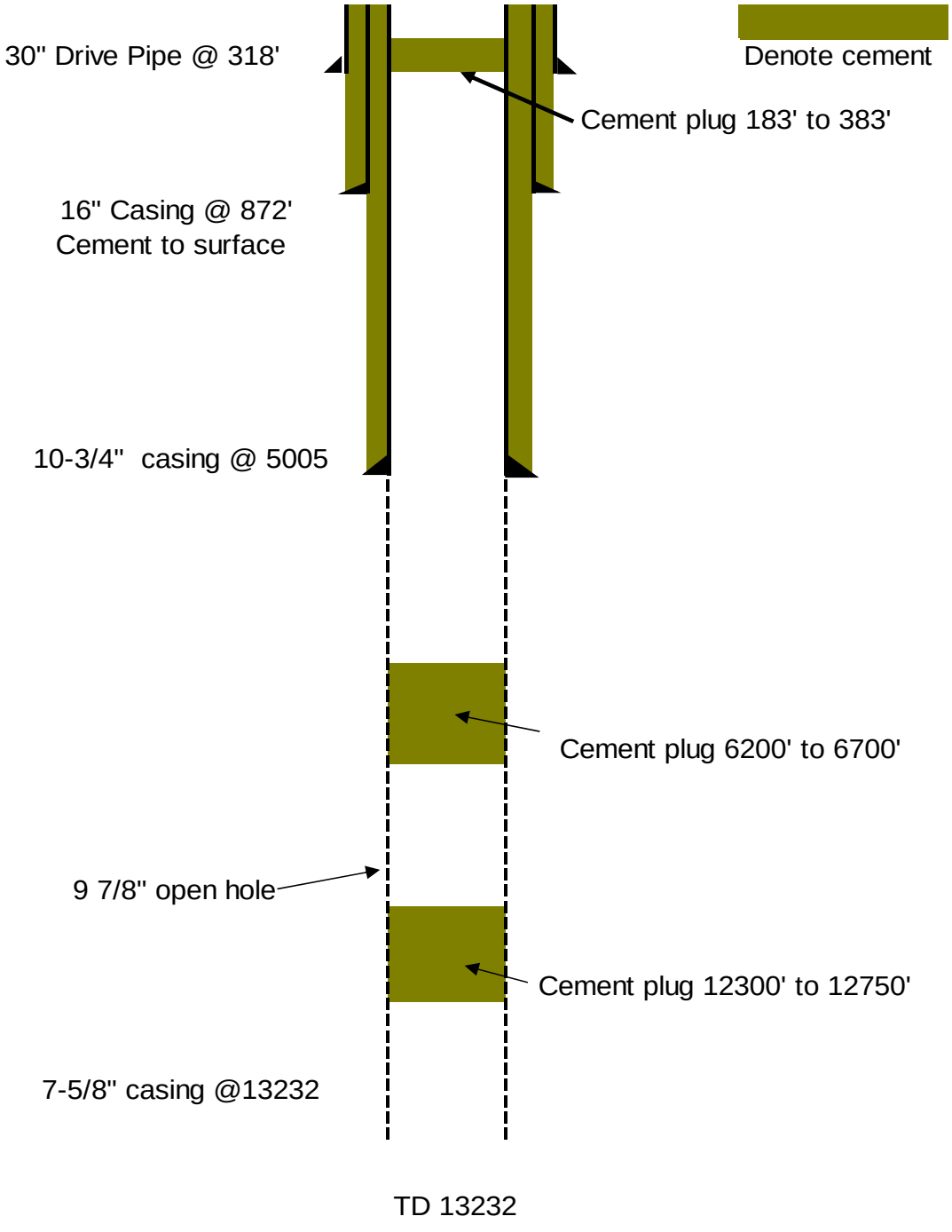

Stone 99-A2-ST1

Current Wellbore Conditions

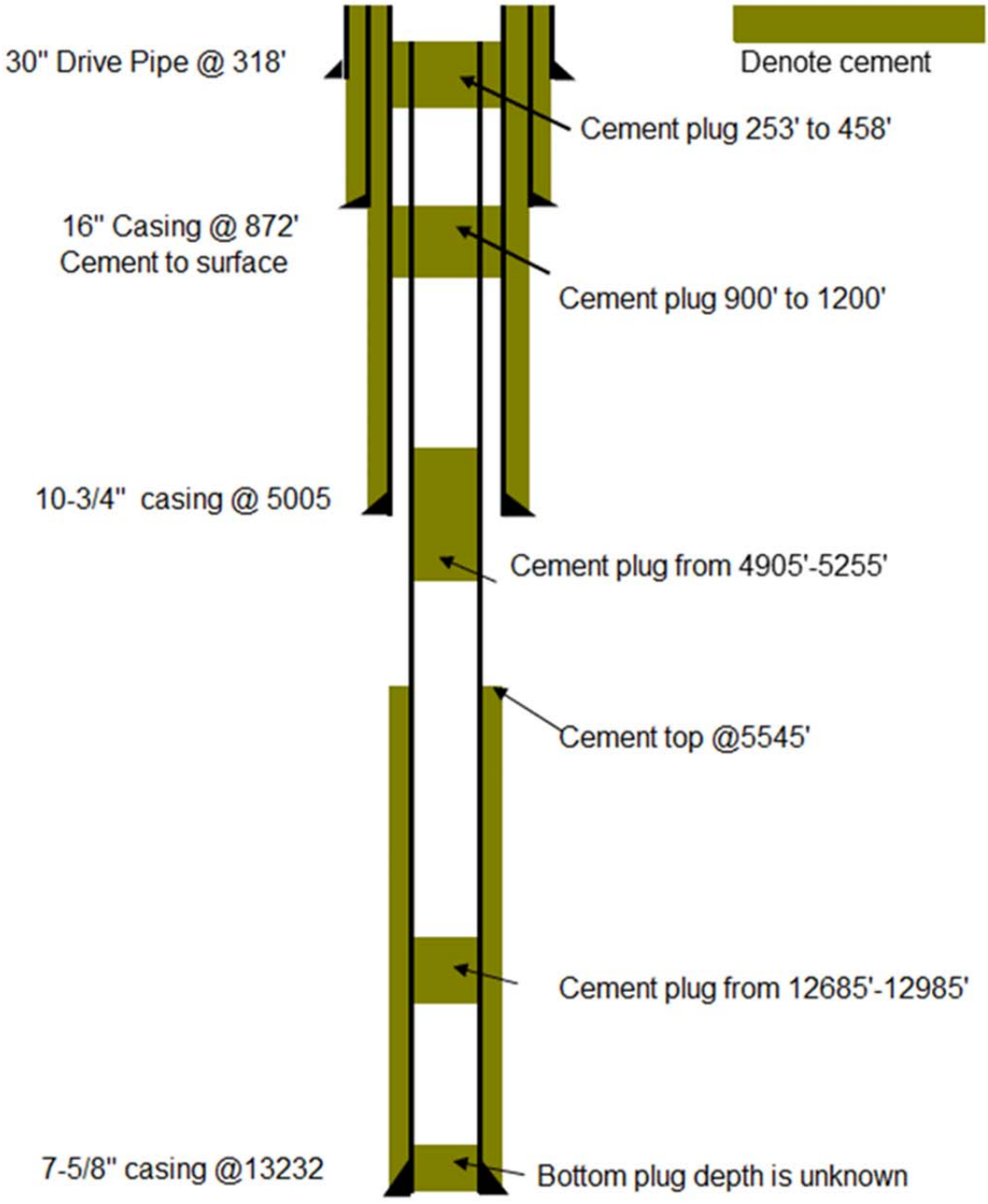

TD 13232

Stone 99-E1

Denote cement

Current Wellbore Conditions

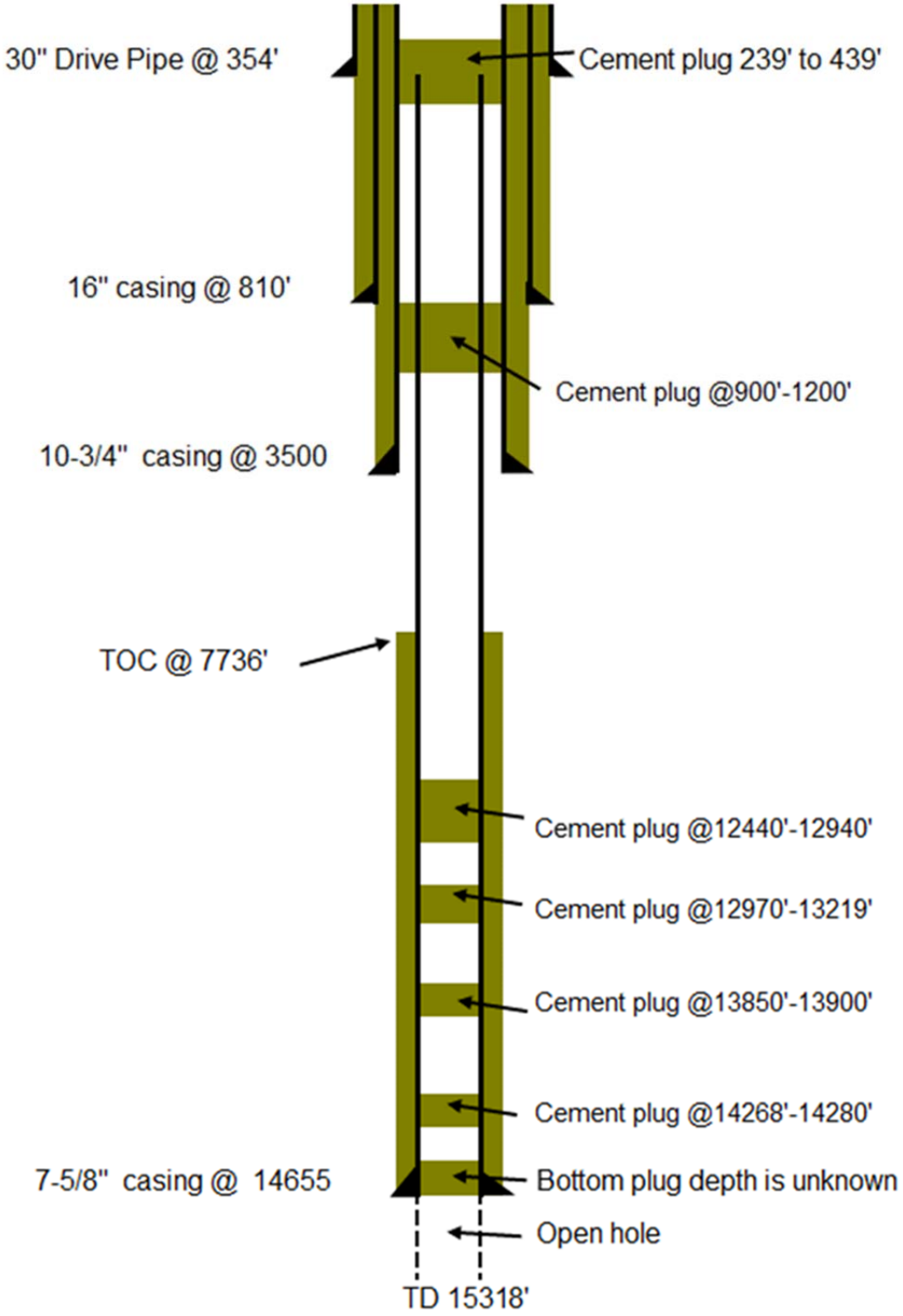

Stone 99-E2

Denote cement

Current Wellbore Conditions

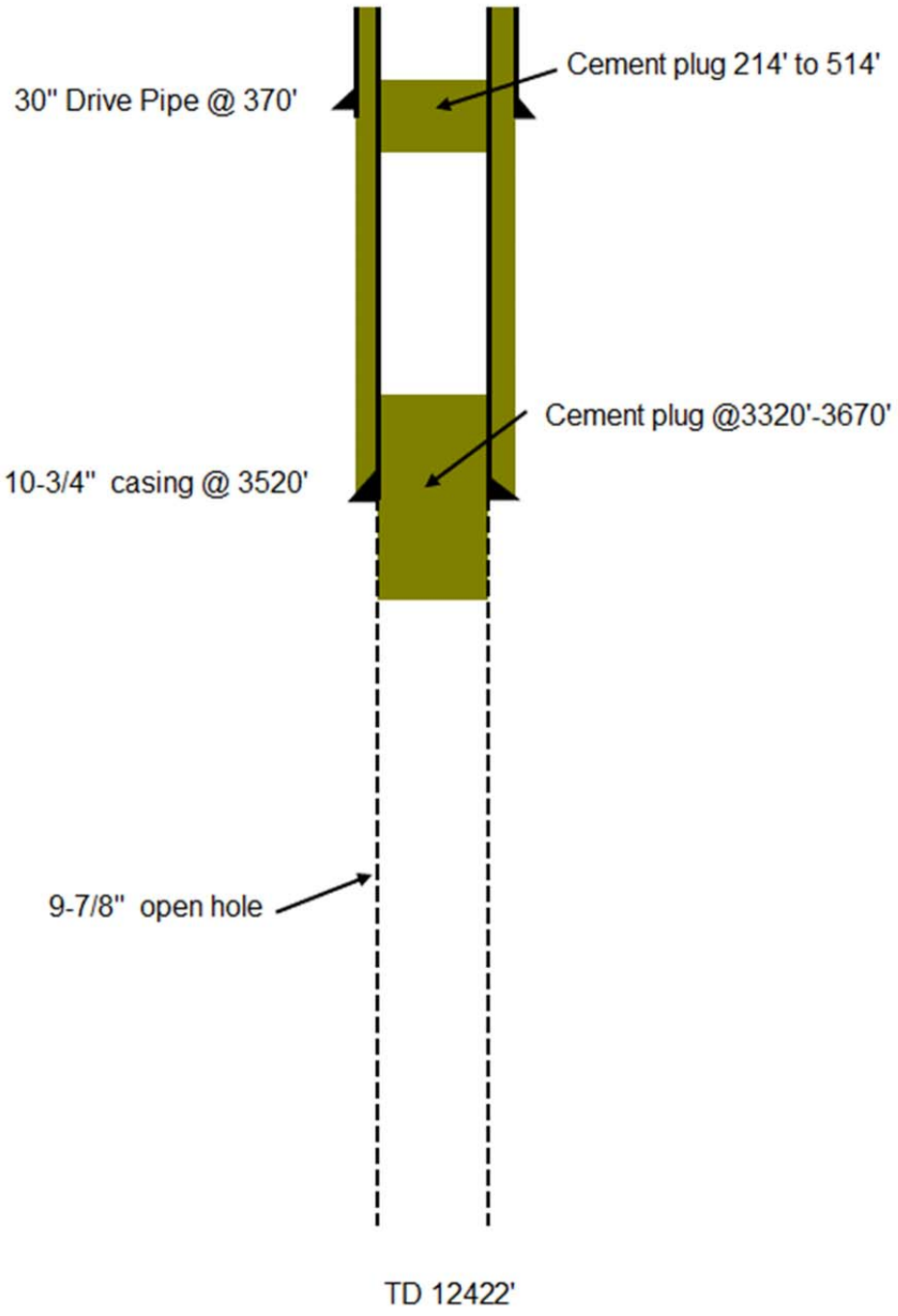

Chevron 99-1

Current Wellbore Conditions

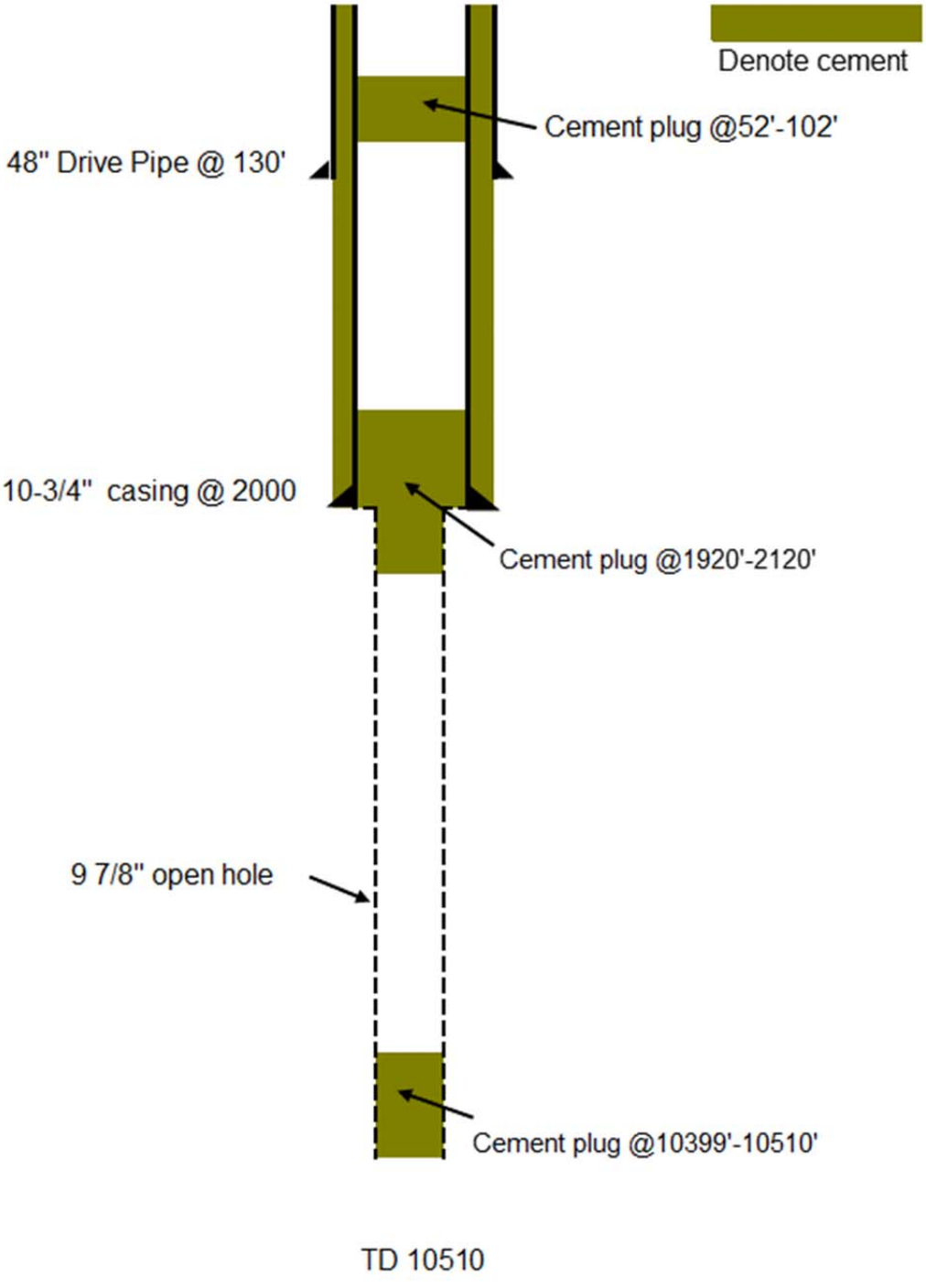

Chevron 99-2

Denote cement

Current Wellbore Conditions

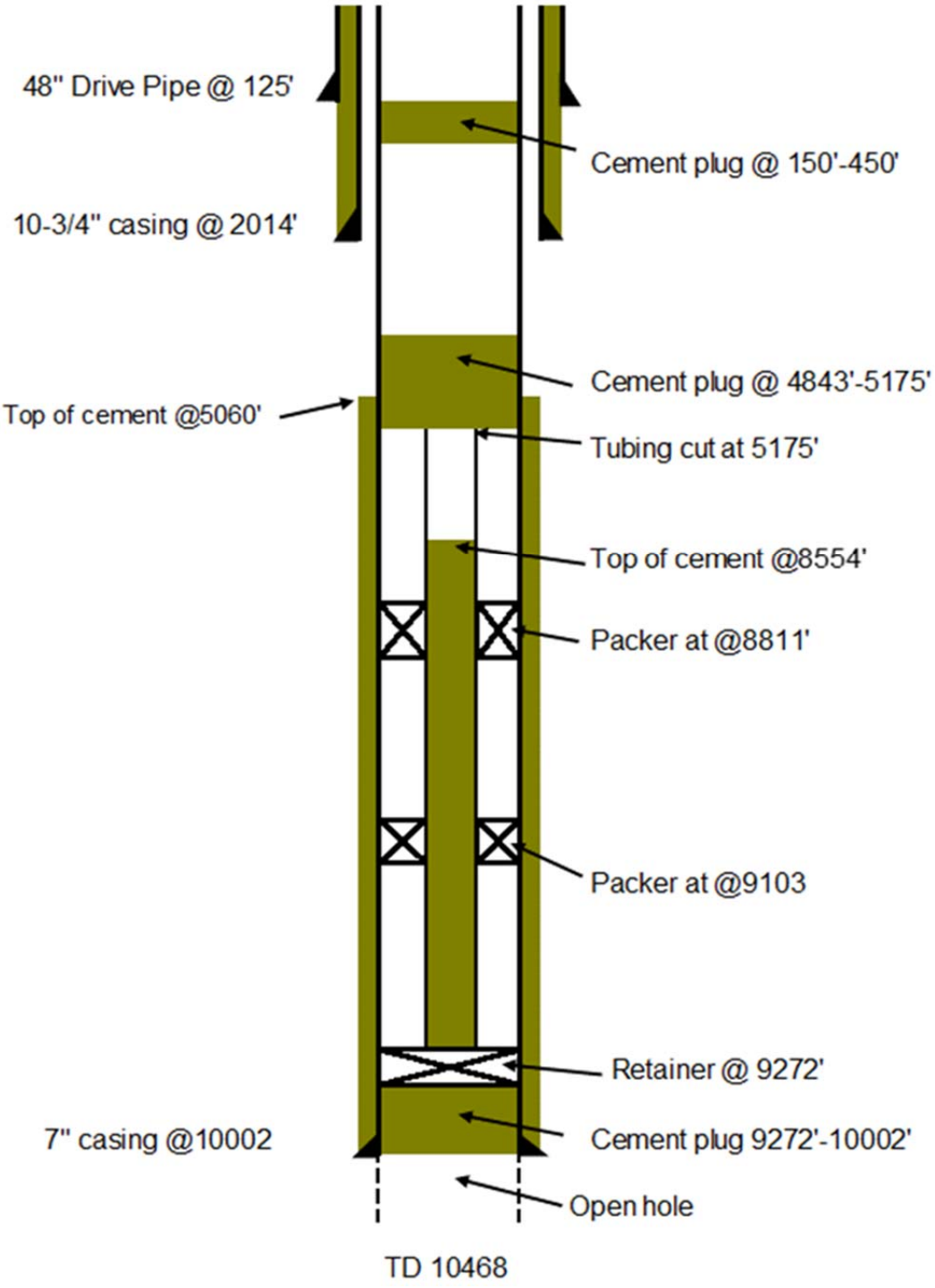

Chevron 99-3

Current Wellbore Conditions

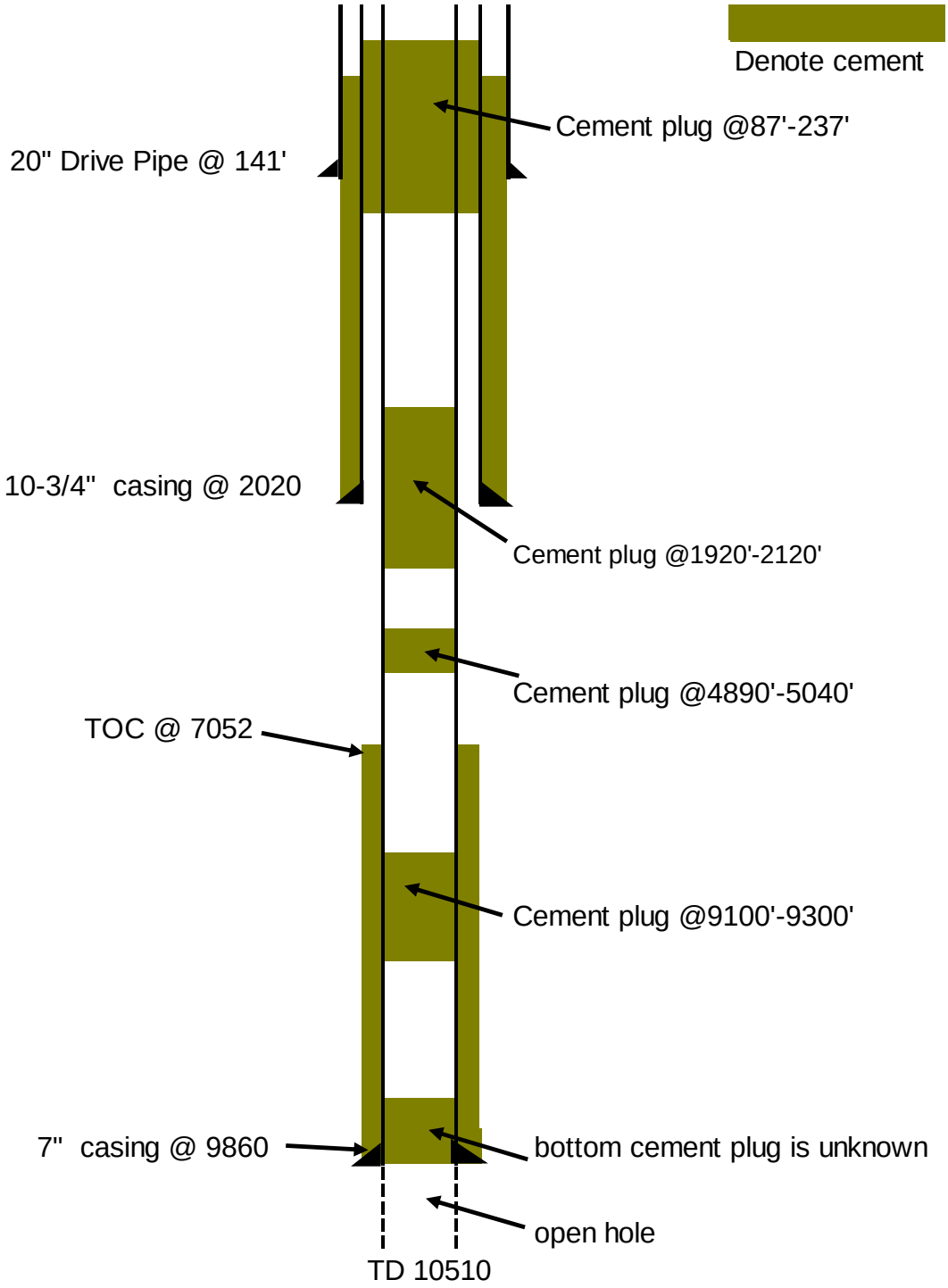

Chevron 99 #4

Current Wellbore Conditions

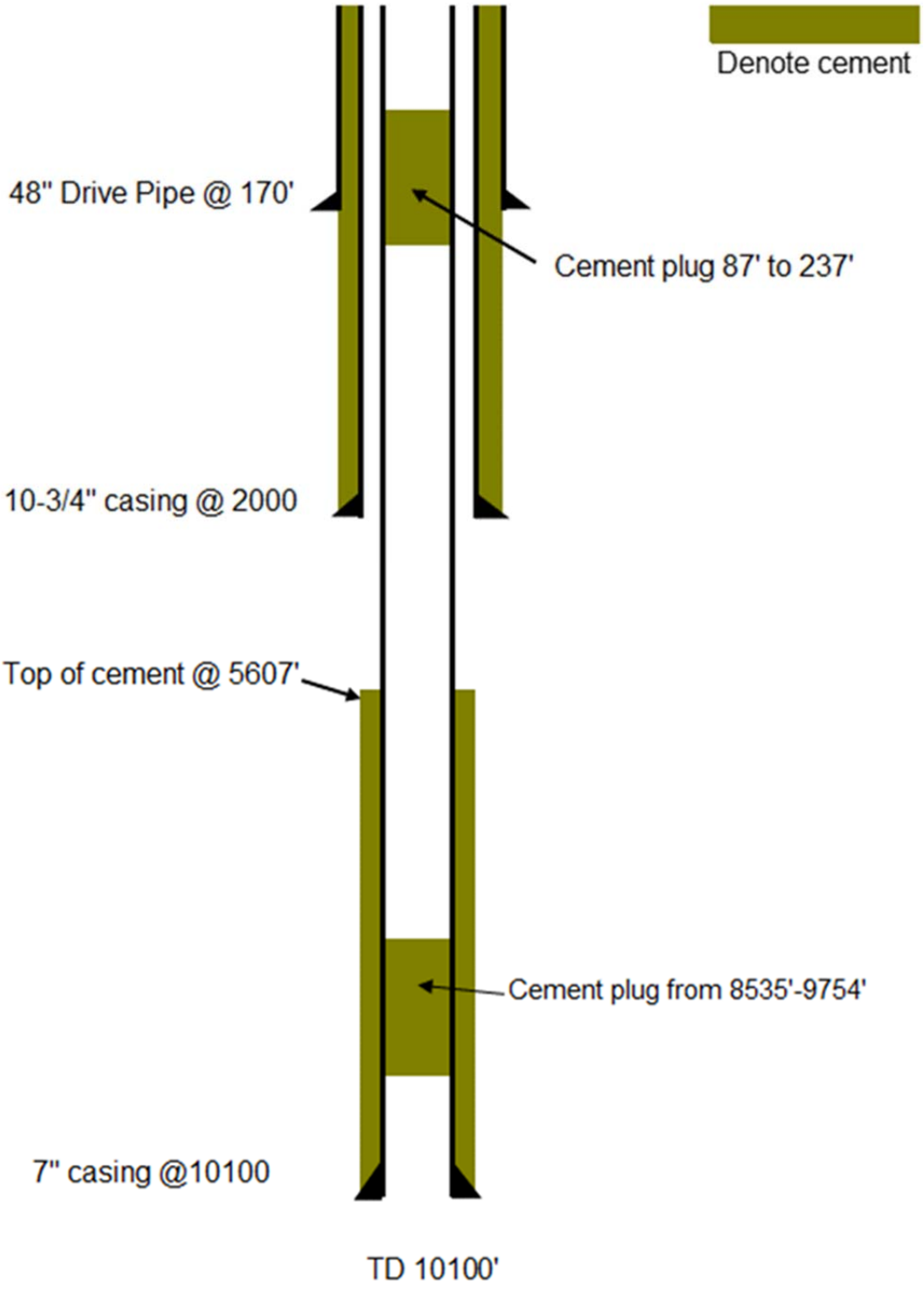

Chevron 99 #5

Current Wellbore Conditions

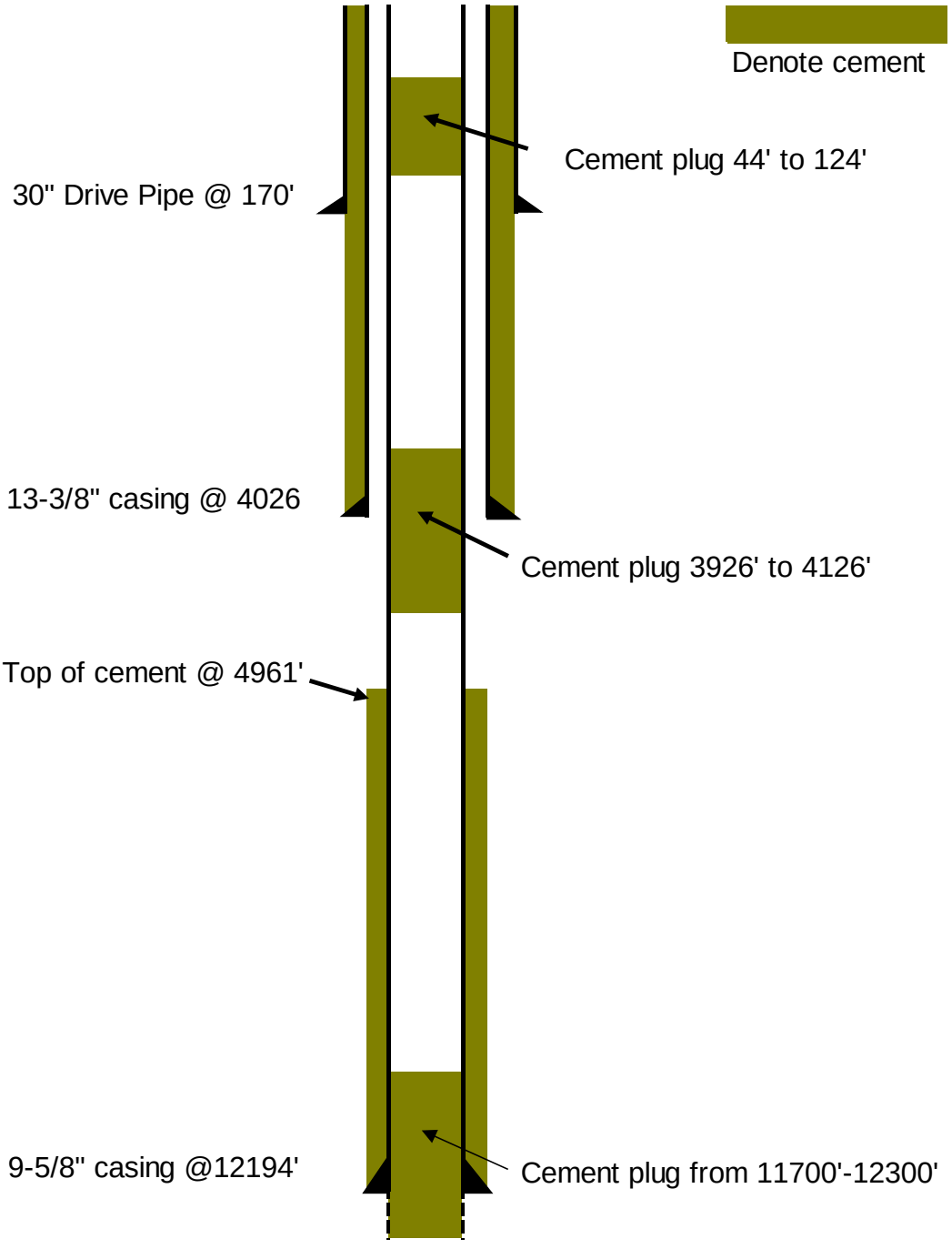

Chevron 99-6

Current Wellbore Conditions

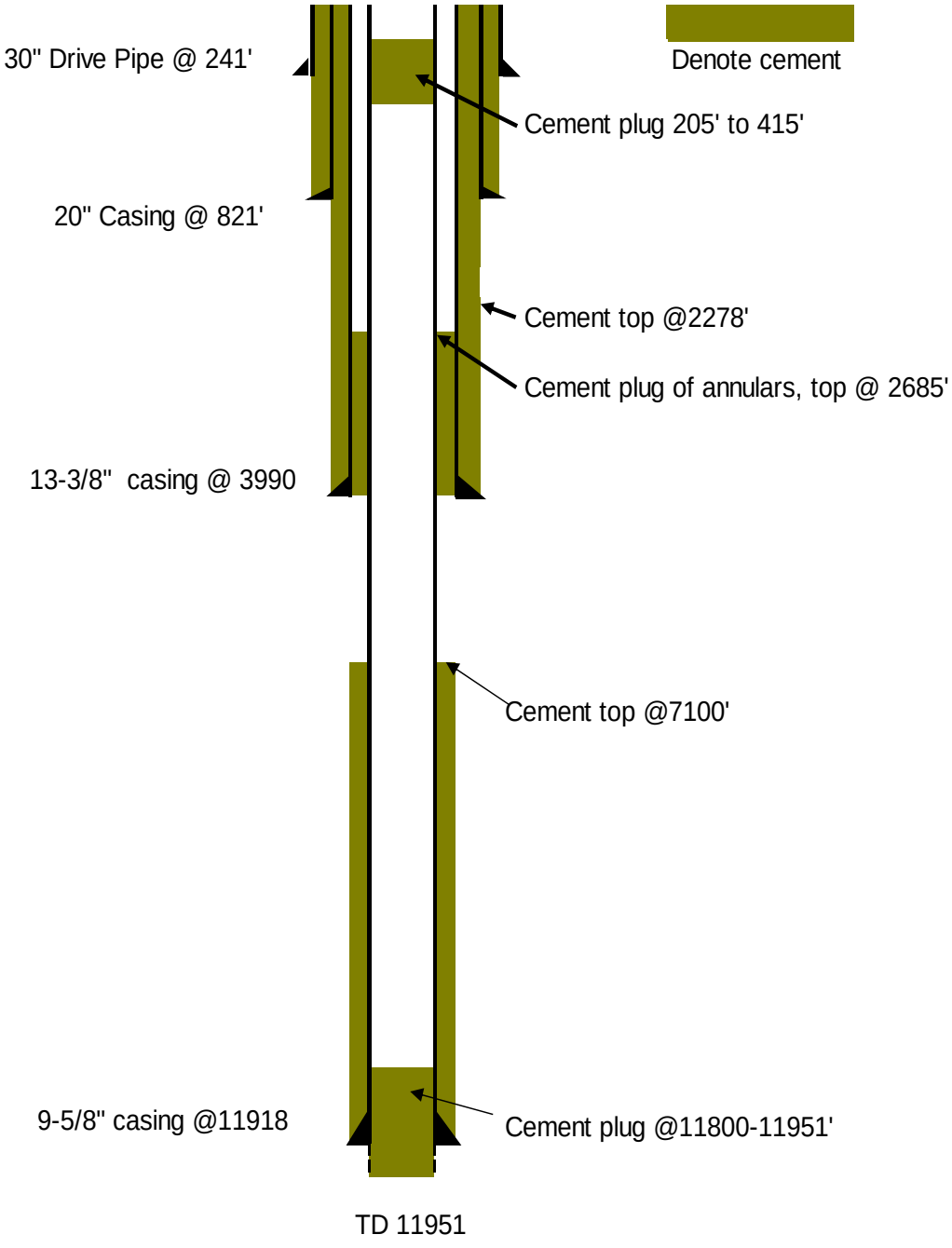

Chevon 99-7

Denote cement

Current Wellbore Conditions

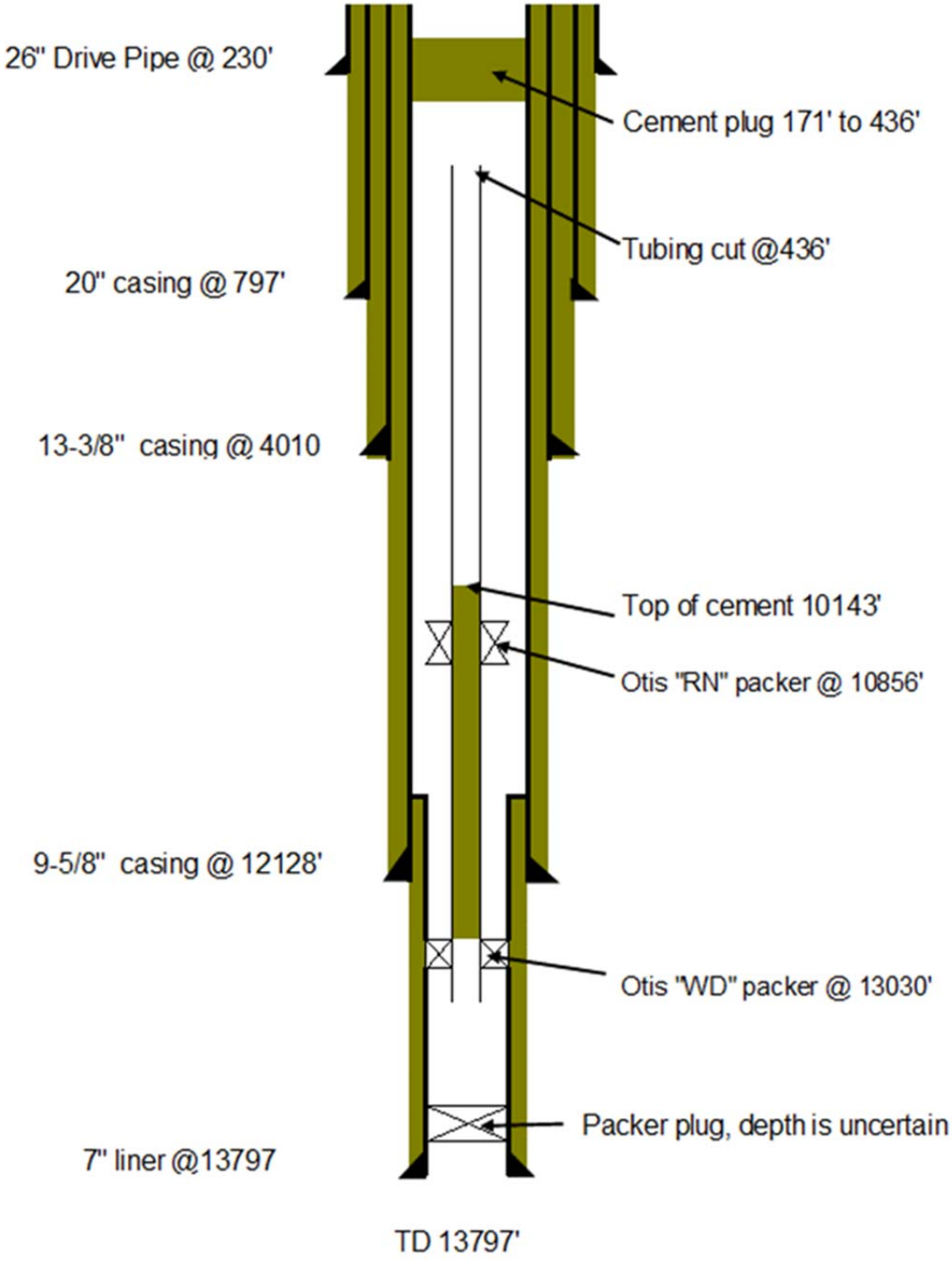

Chevron 99 #8

Current Wellbore Conditions

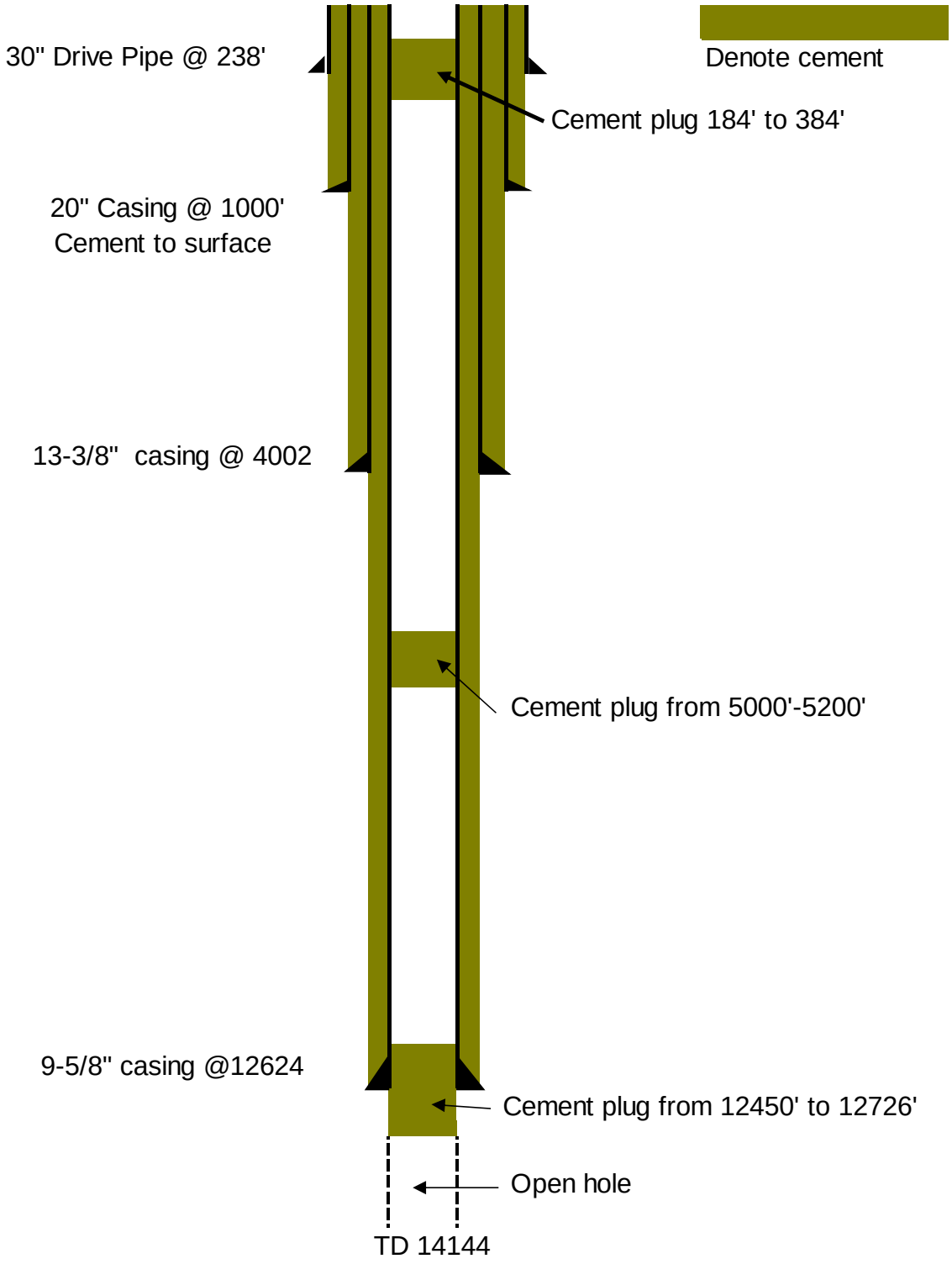

BoisDarc 107 #1

Current Wellbore Conditions

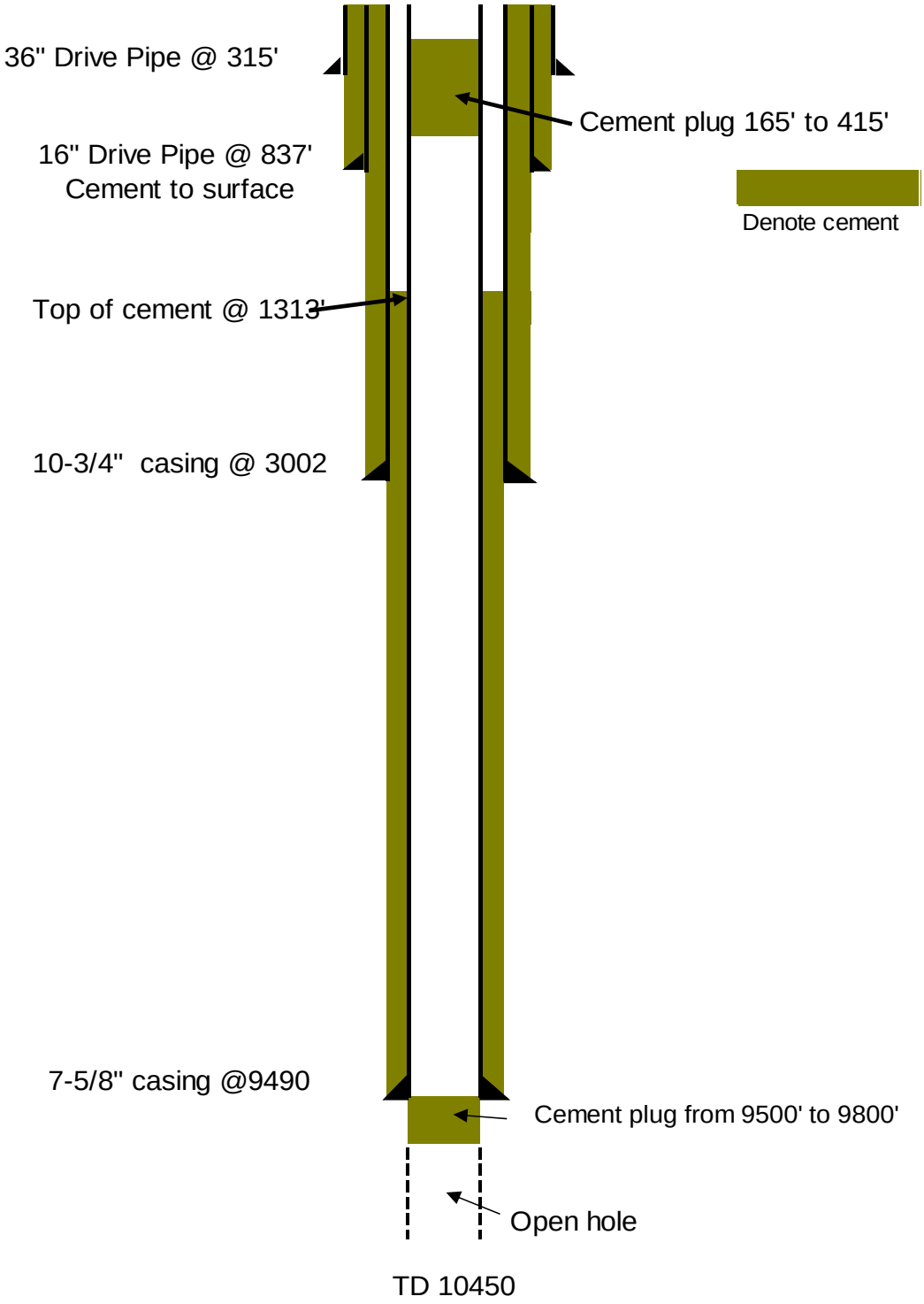

Chevron 107 #1

Current Wellbore Conditions

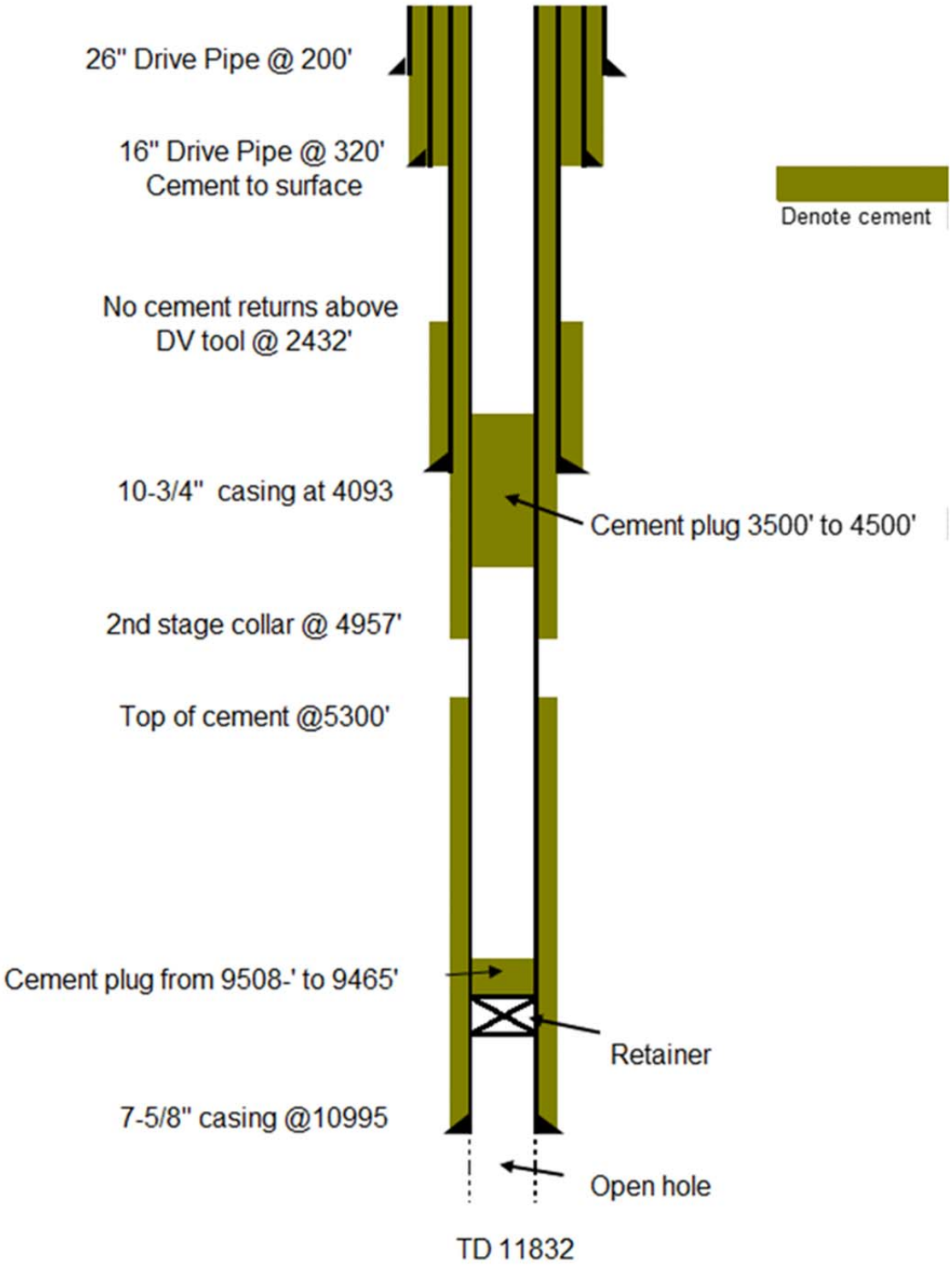

Chevron 107 #2

Current Wellbore Conditions

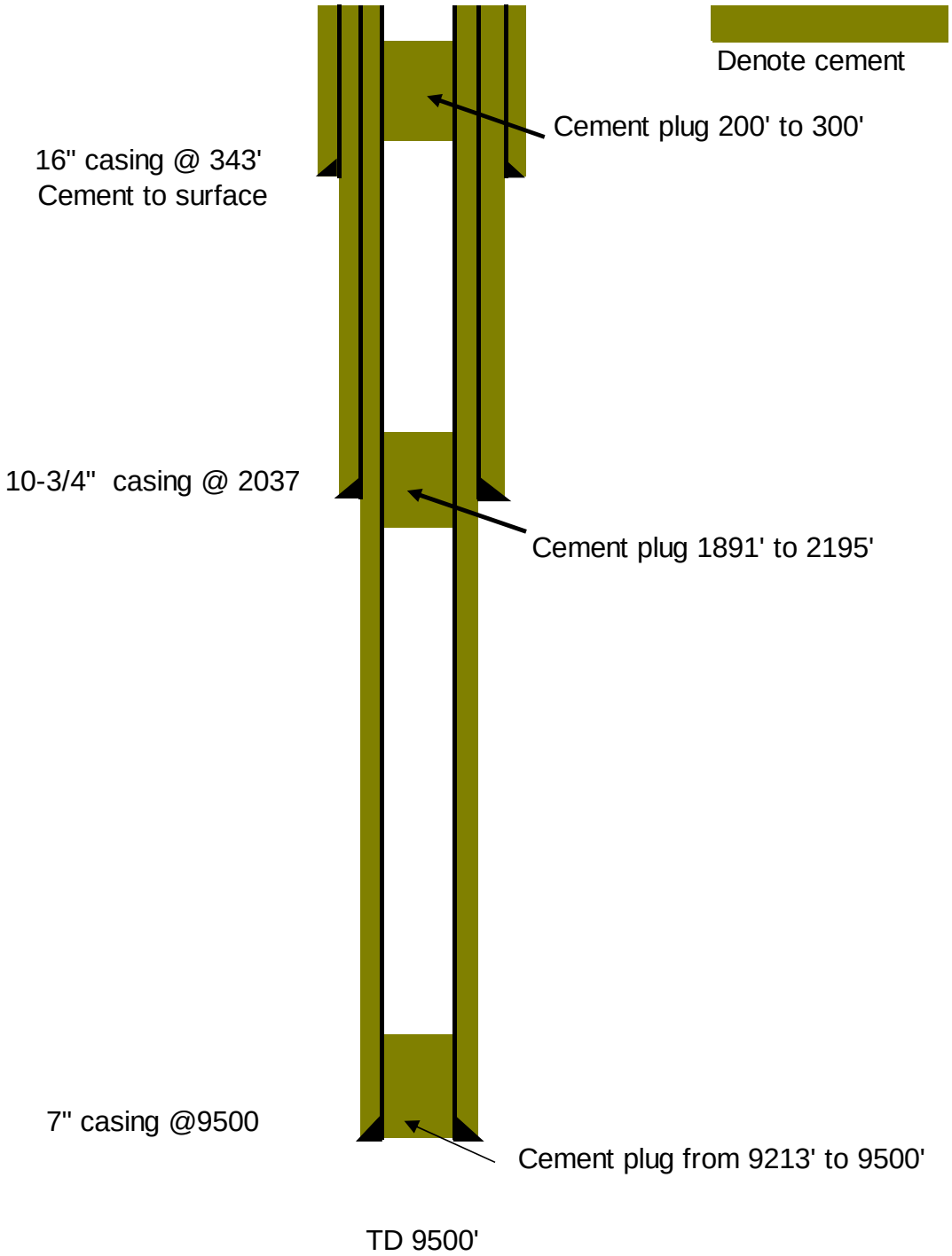

Chevron 107 #3

Current Wellbore Conditions

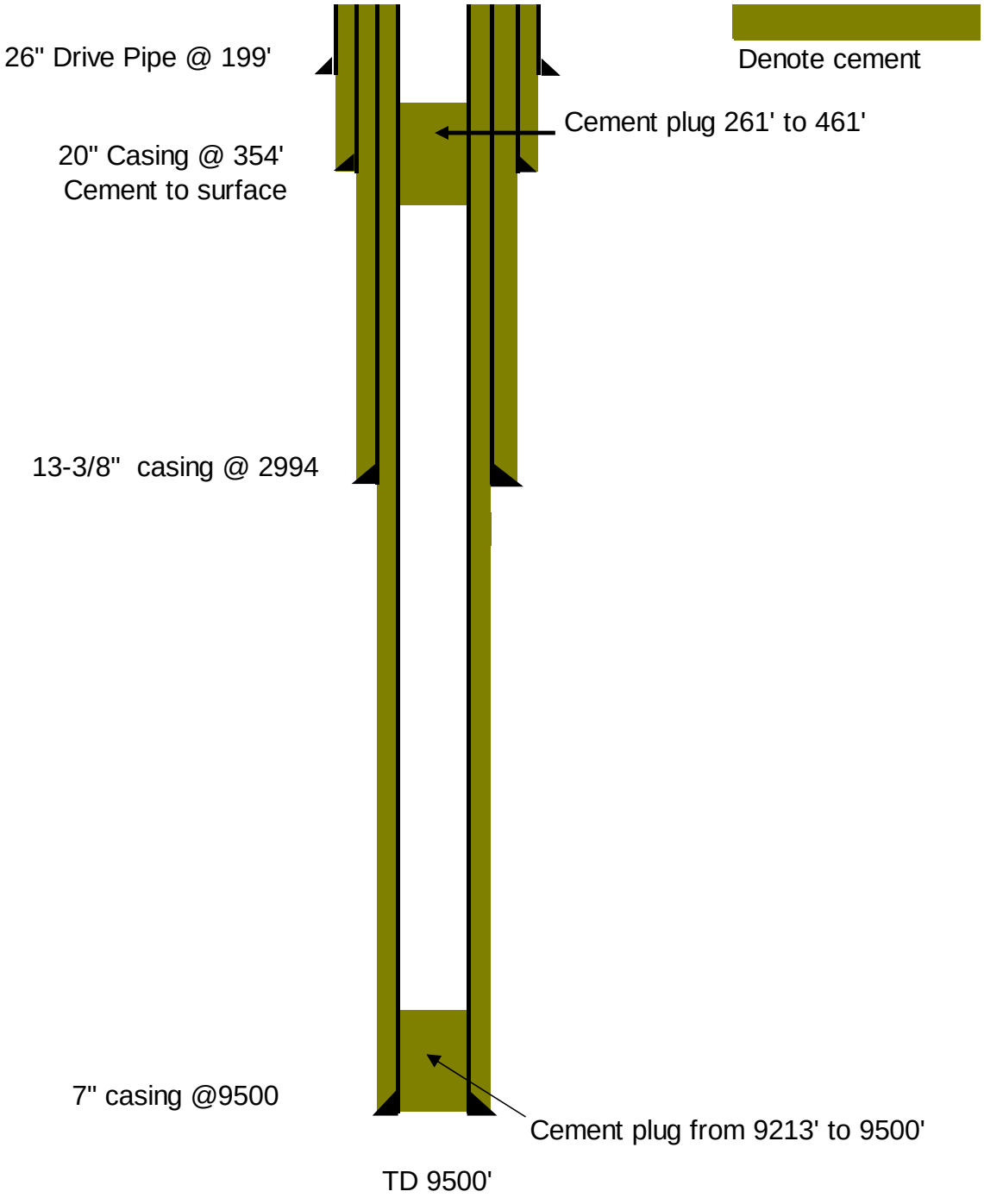

Chevron 107 #4

Denote cement

Current Wellbore Conditions

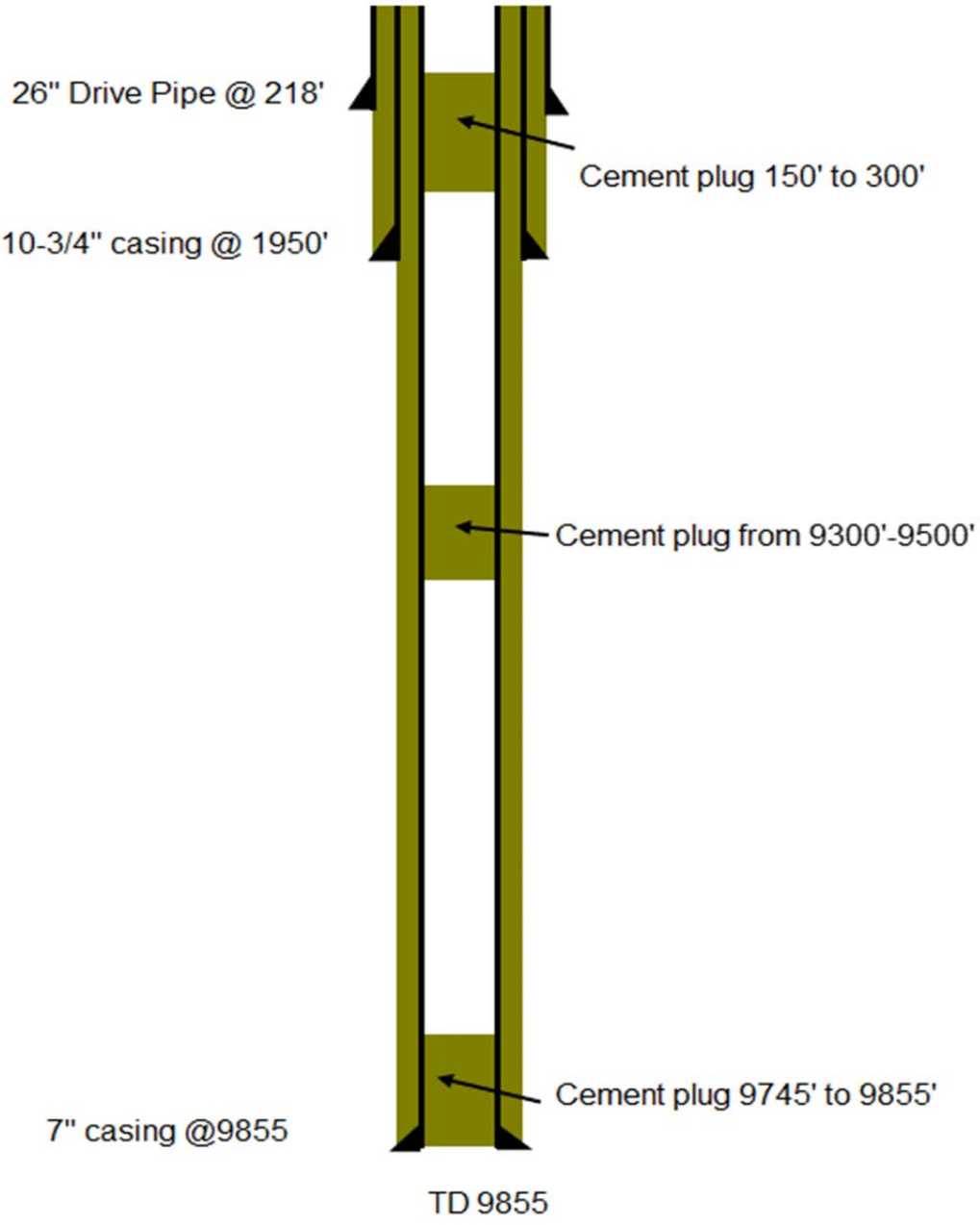

Chevron 107 #5

Denote cement

Current Wellbore Conditions

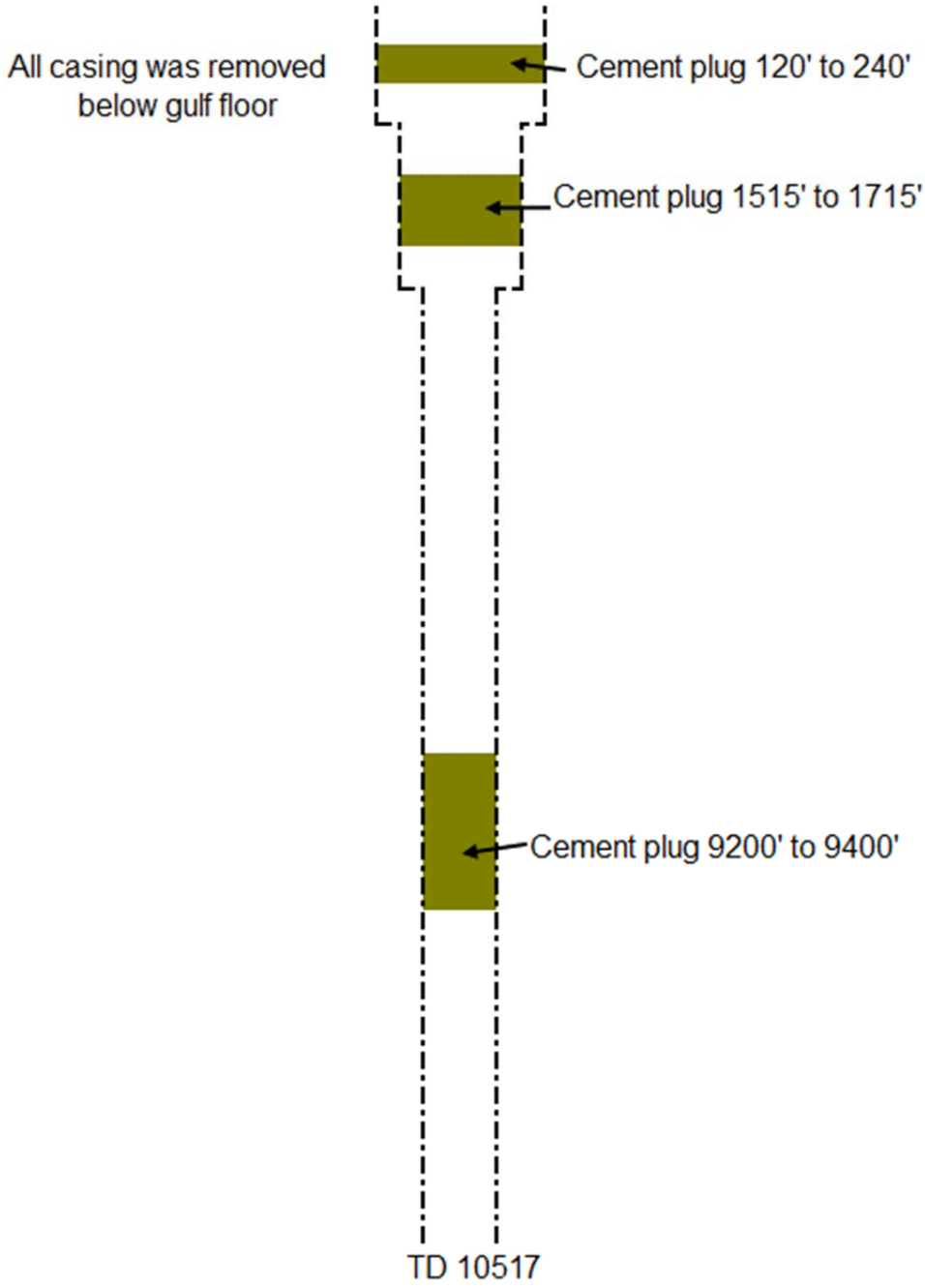

Chevron 107 #6

Denote cement

Current Wellbore Conditions

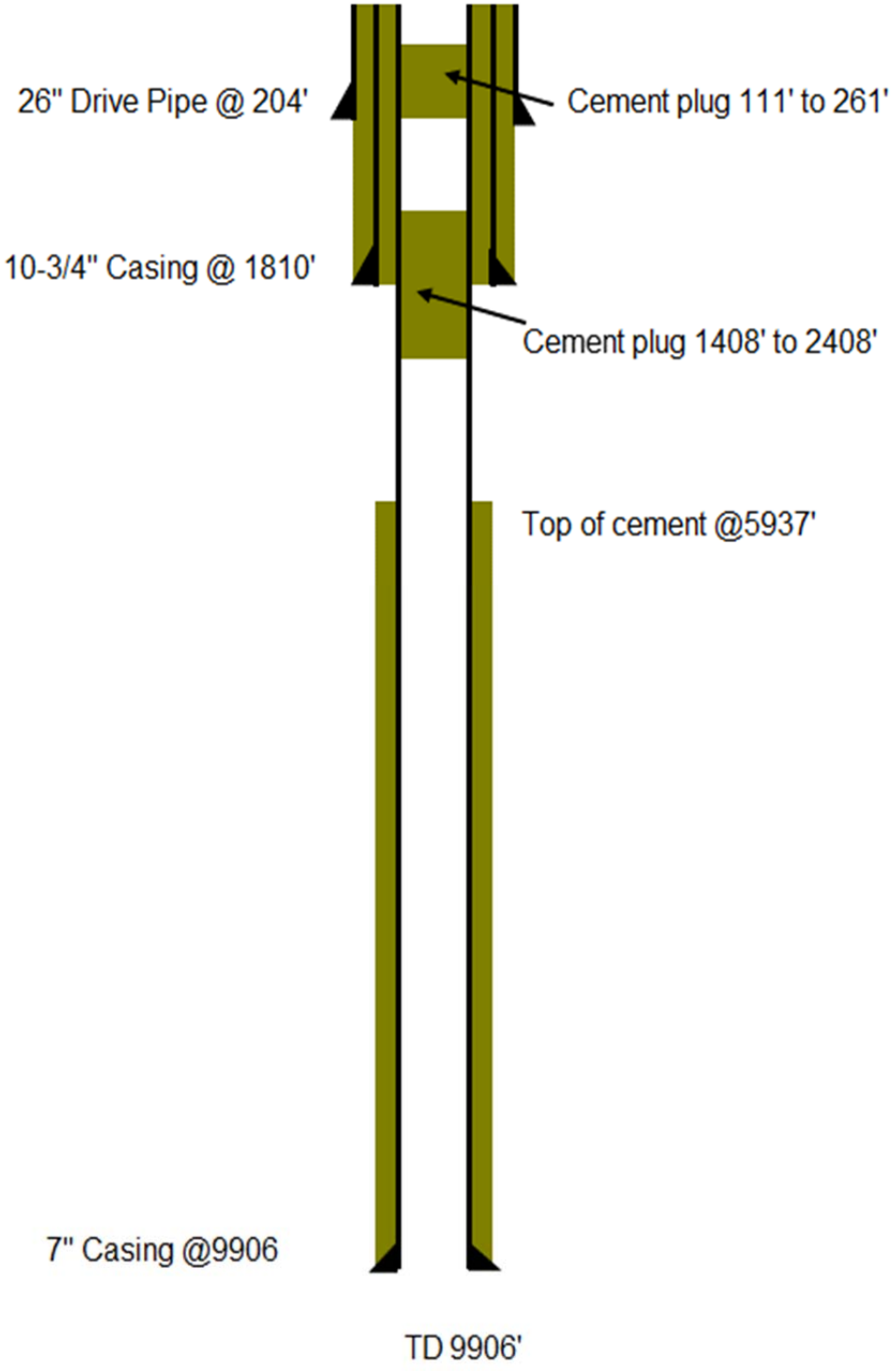

Chevron 107 #7

Current Wellbore Conditions

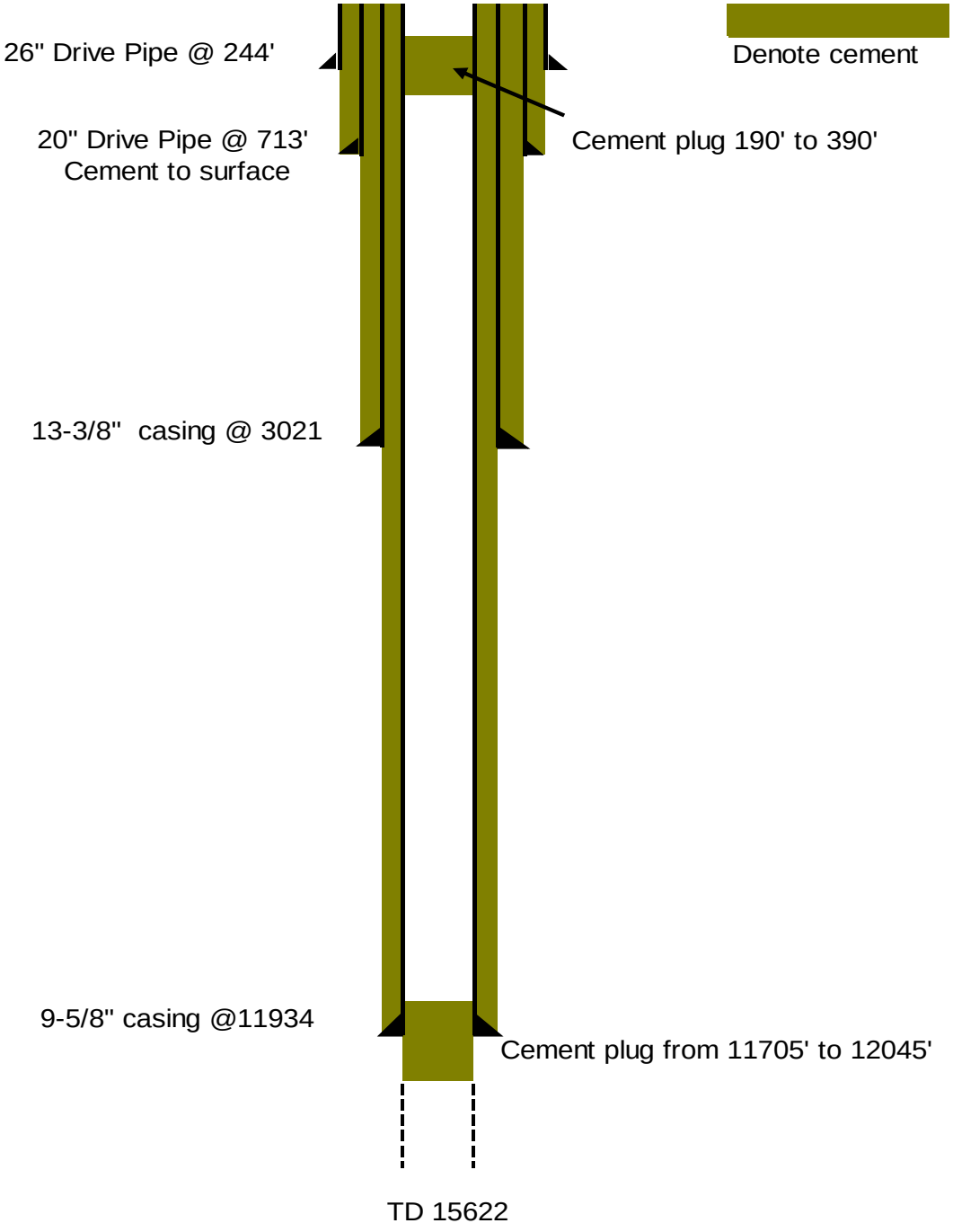

Chevron 107 #B1

Current Wellbore Conditions

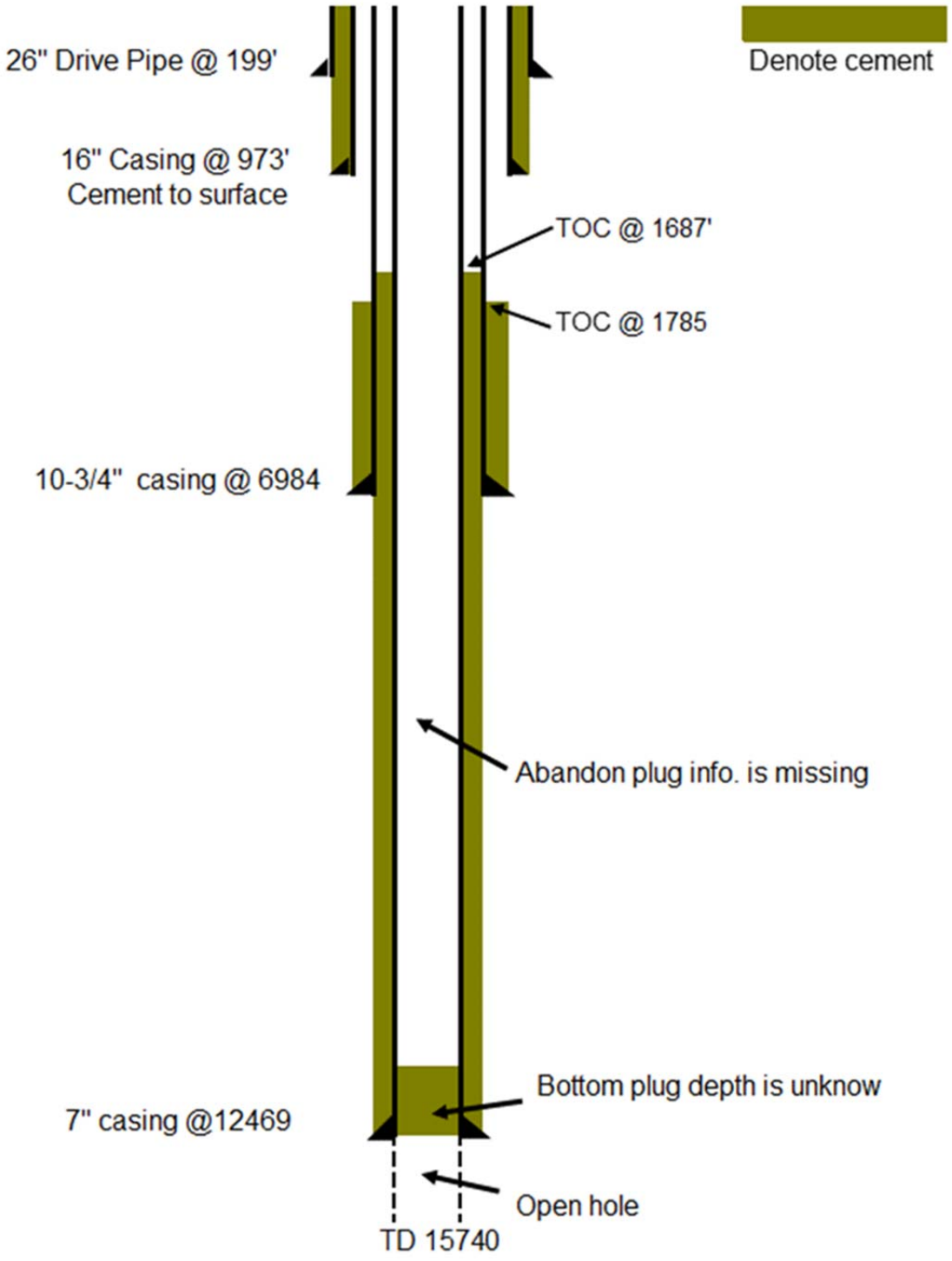

EnergyXXI 108-1

Denote cement

Current Wellbore Conditions

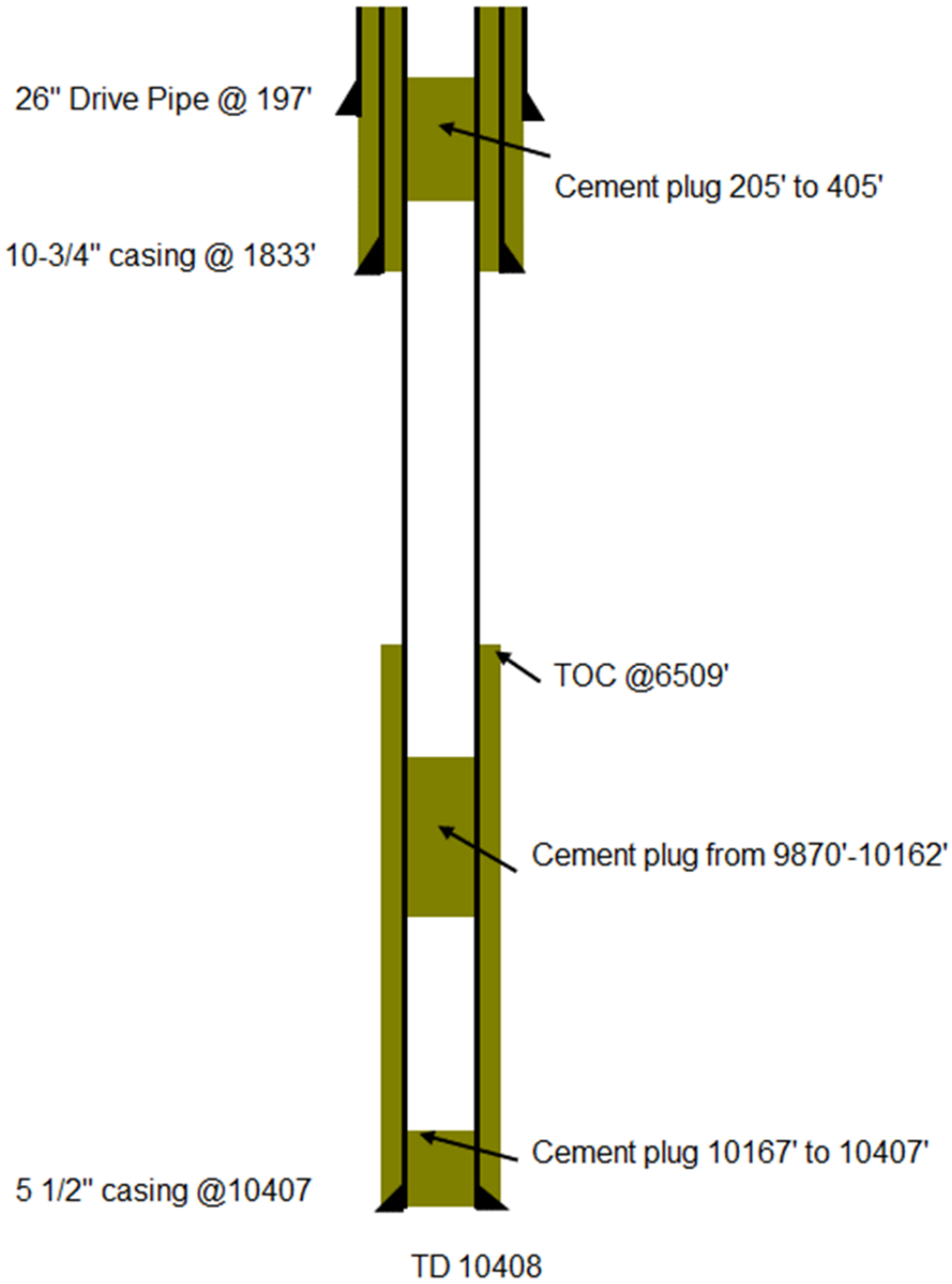

EnergyXXI 108-2

Denote cement

Current Wellbore Conditions

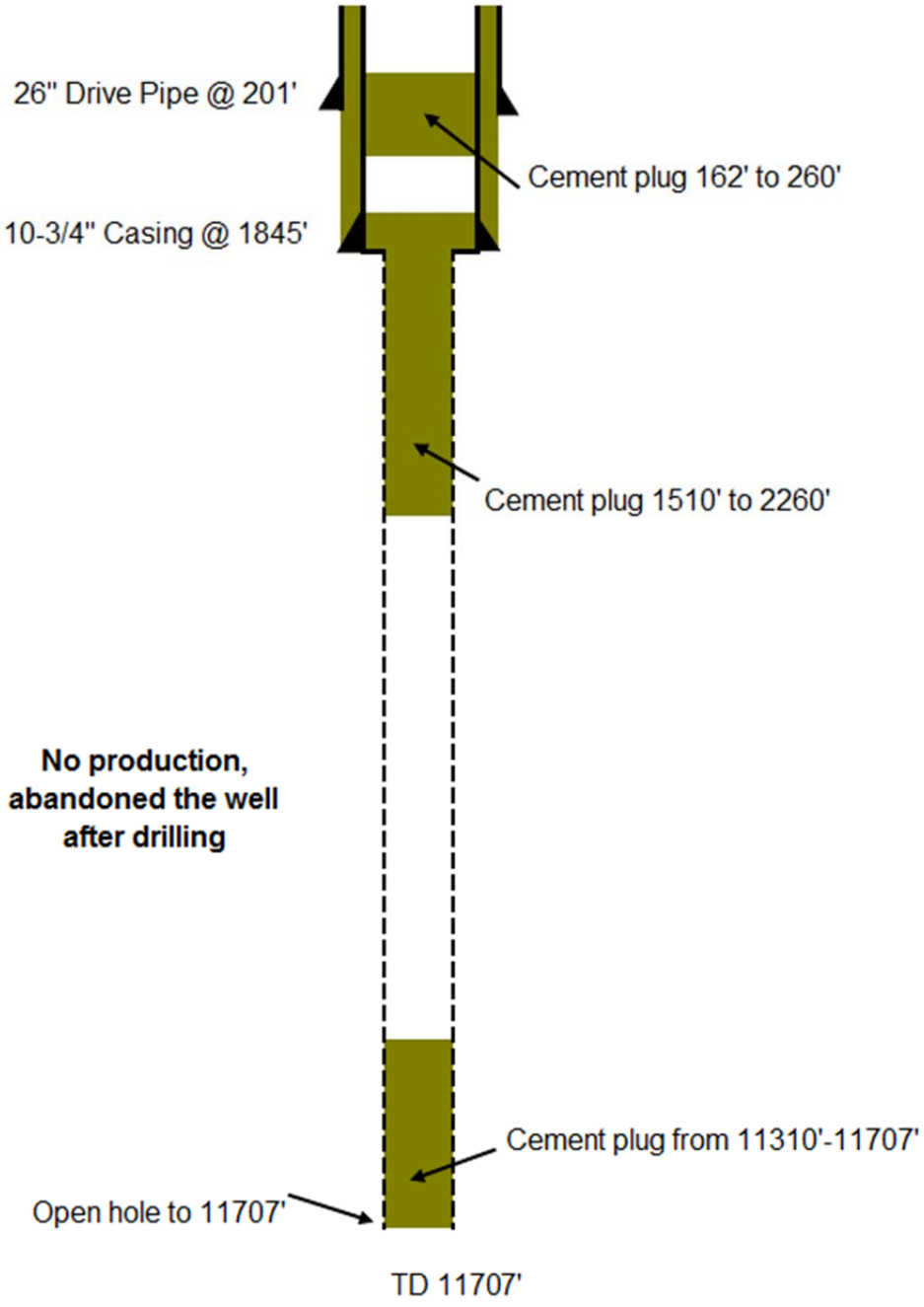

EnergyXXI 108-3

Denote cement

Current Wellbore Conditions

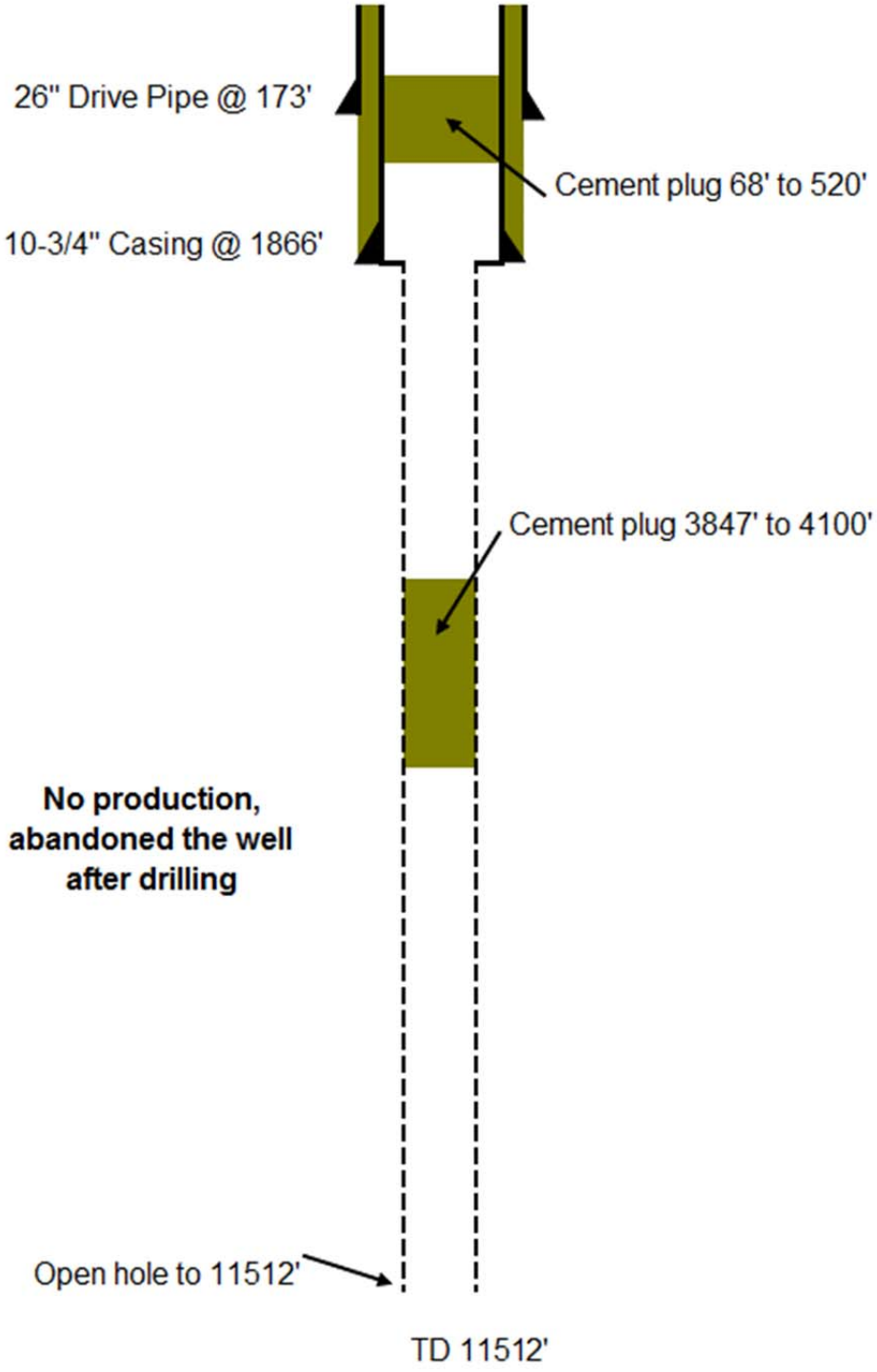

EnergyXXI 108-4 ST1

Denote cement

Current Wellbore Conditions

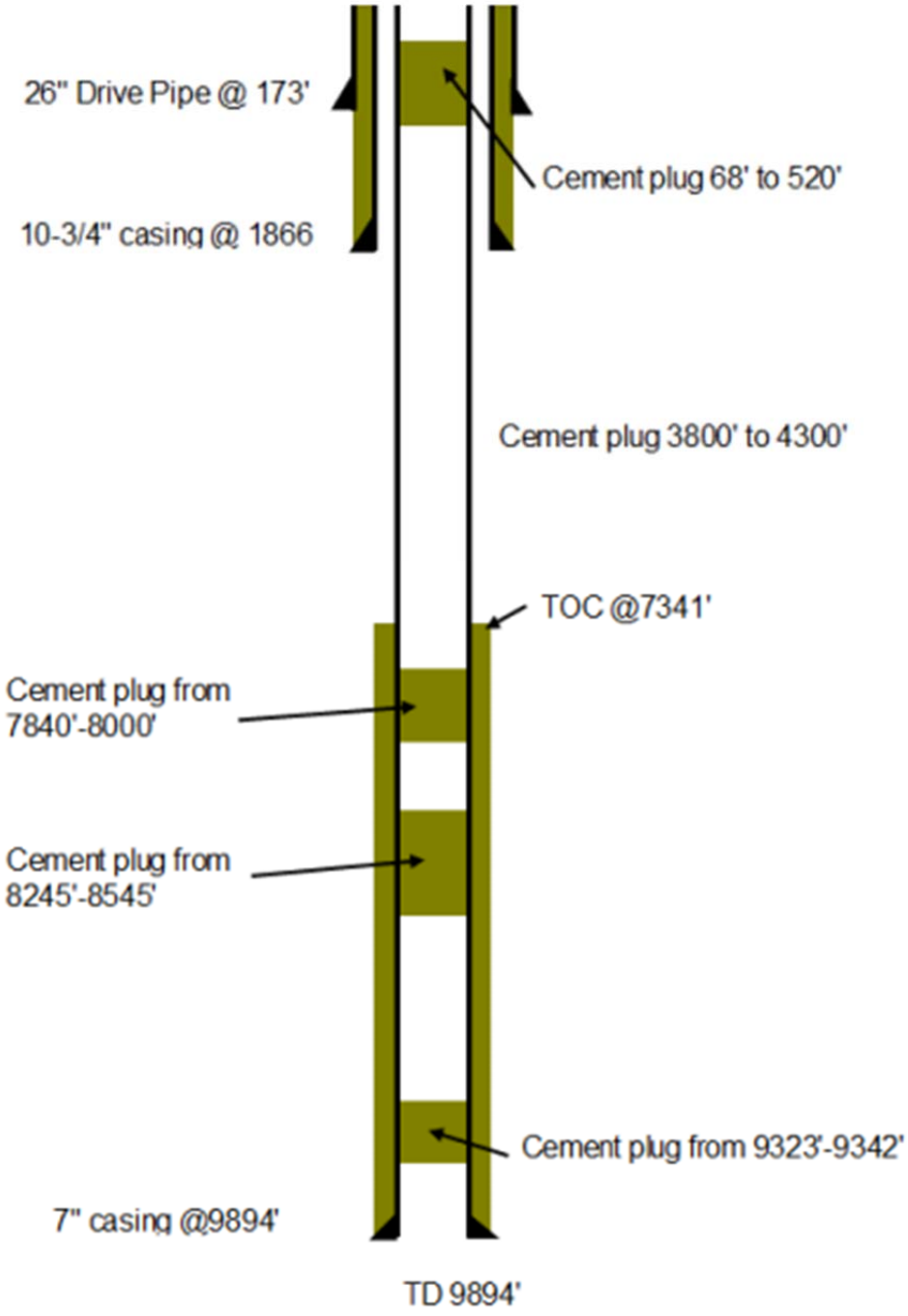

EnergyXXI 108-5

Denote cement

Current Wellbore Conditions

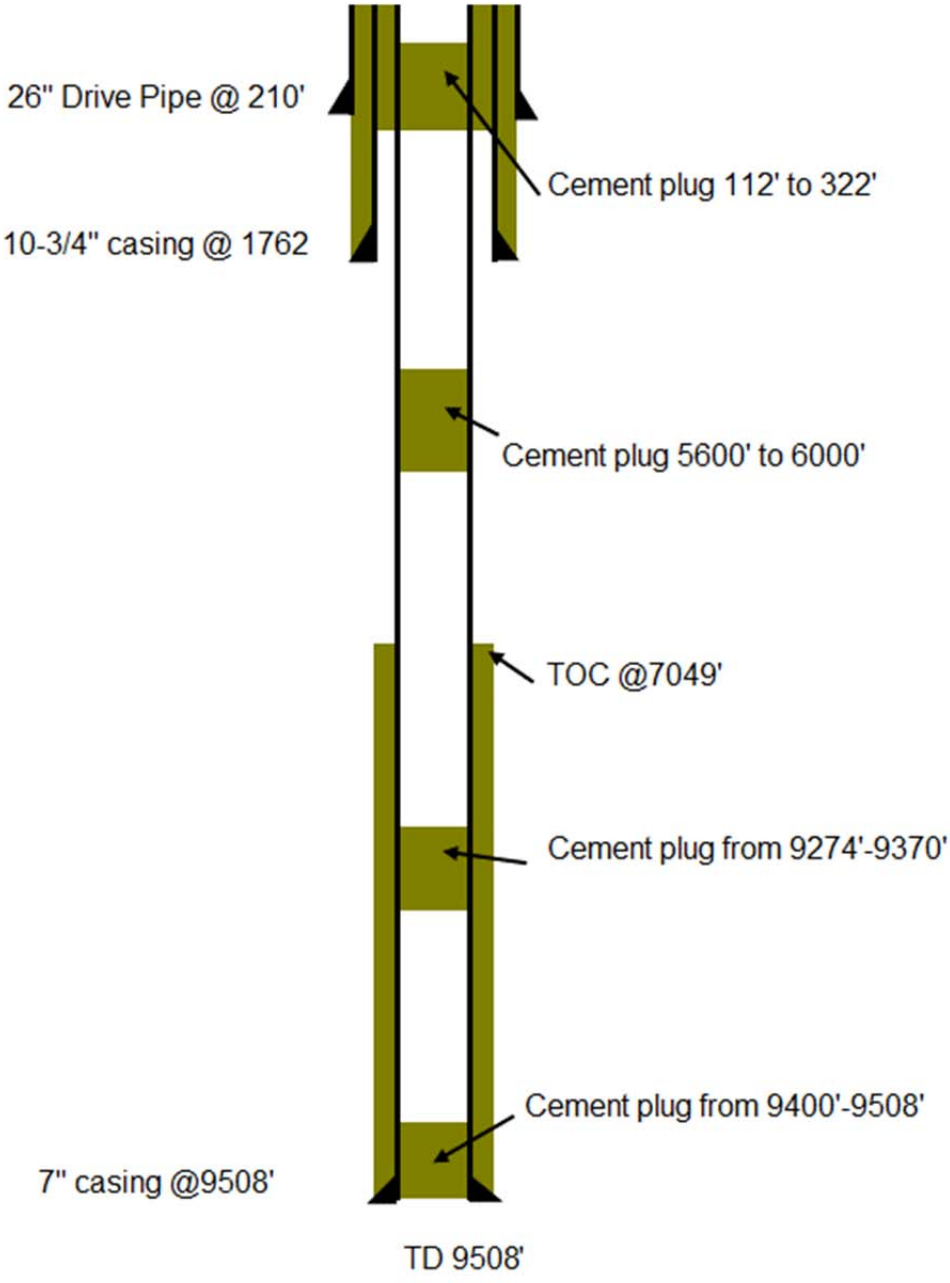

EnergyXXI 108-6

Denote cement

Current Wellbore Conditions

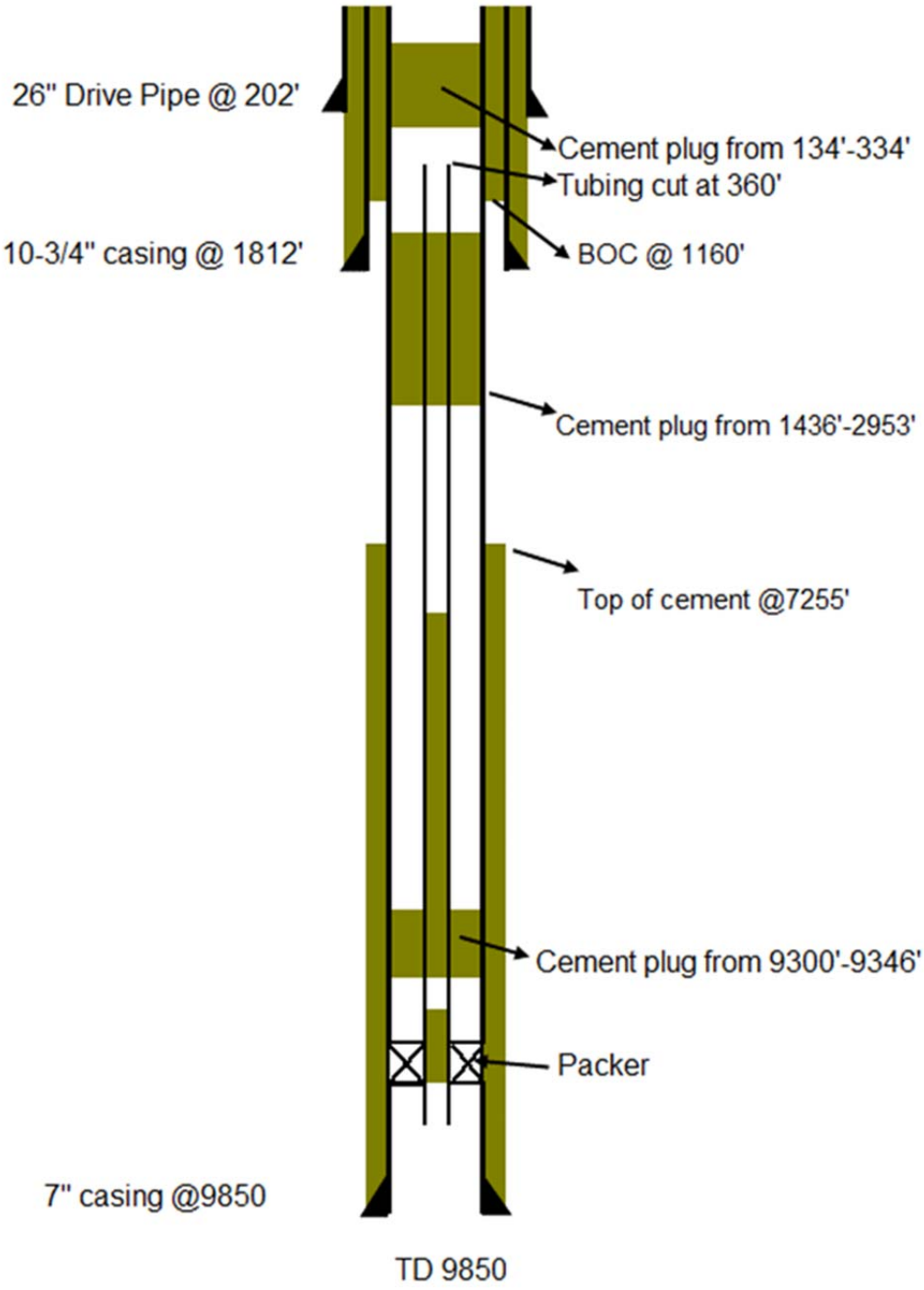

EnergyXXI 108-7

Denote cement

Current Wellbore Conditions

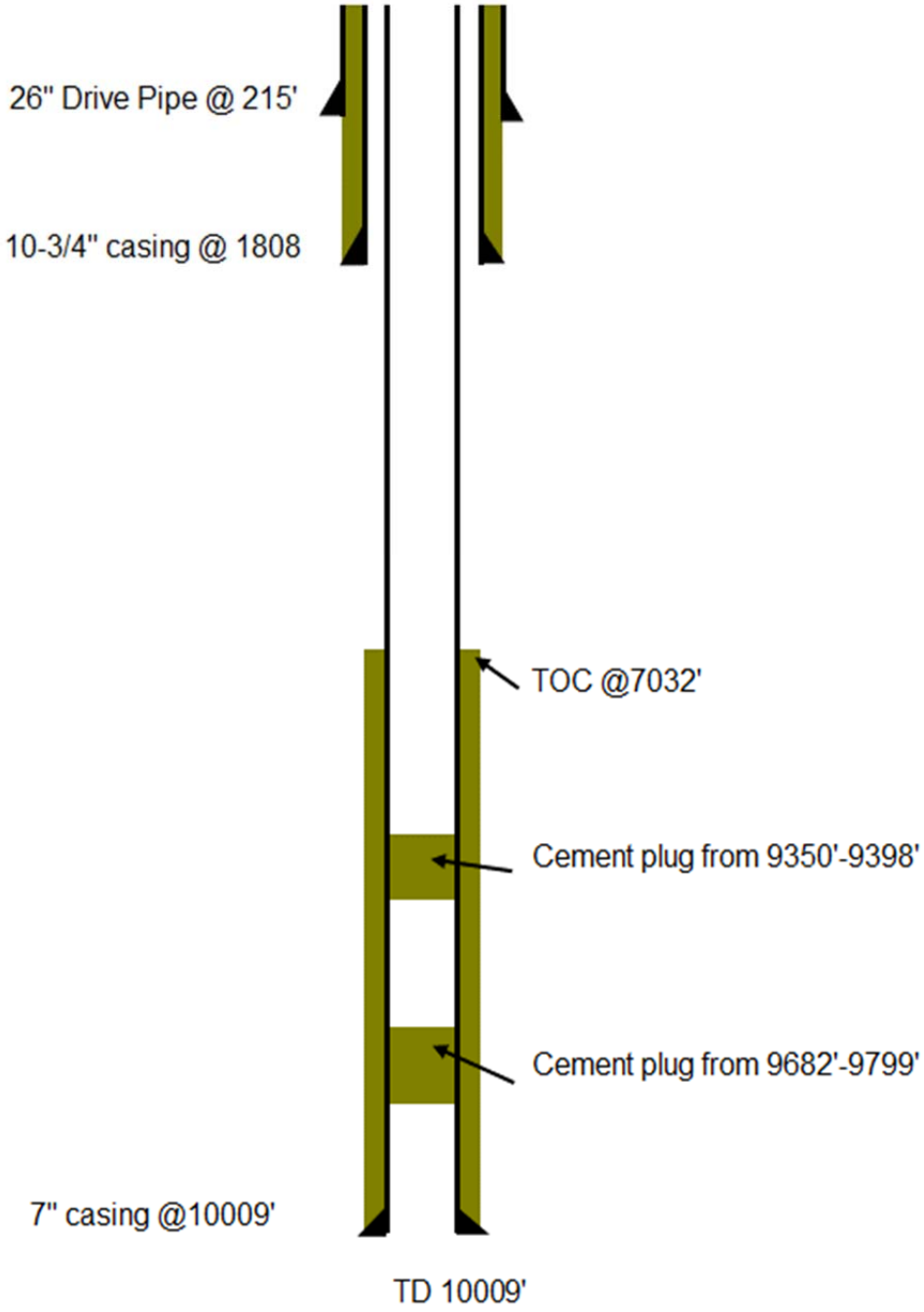

EnergyXXI 108-8

Denote cement

Current Wellbore Conditions

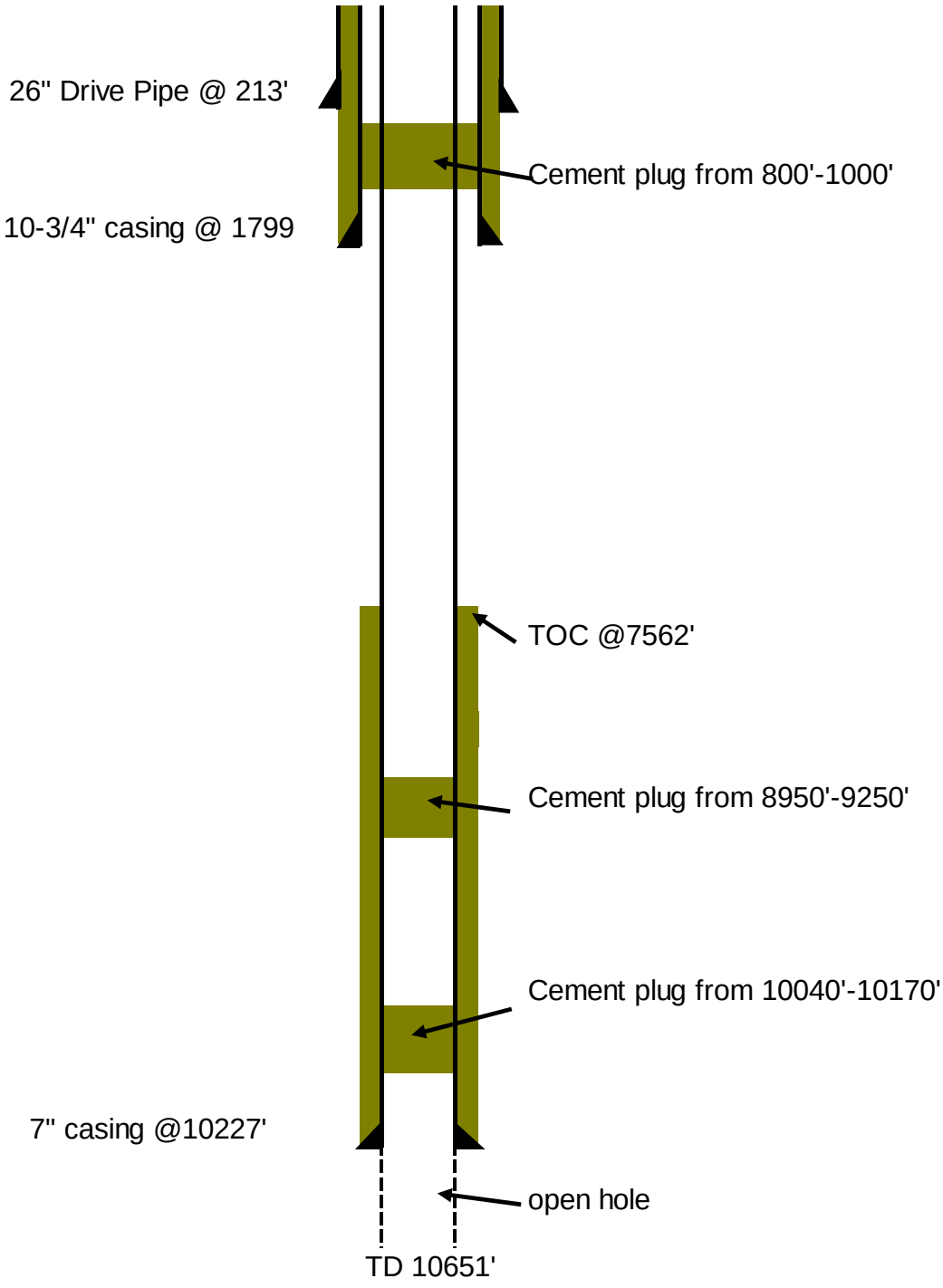

EnergyXXI 108-9

Denote cement

Current Wellbore Conditions

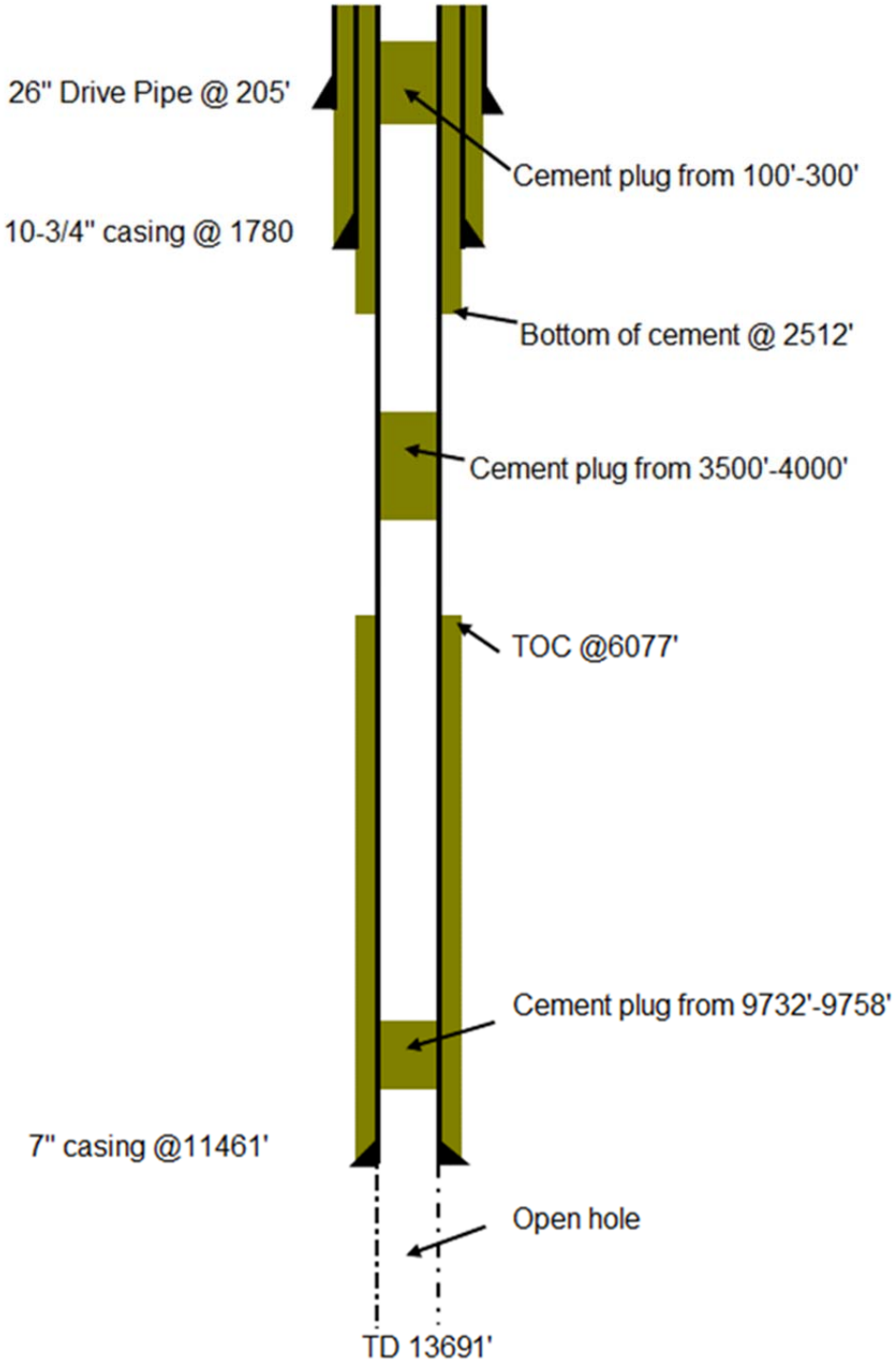

EnergyXXI 108-10

Denote cement

Current Wellbore Conditions

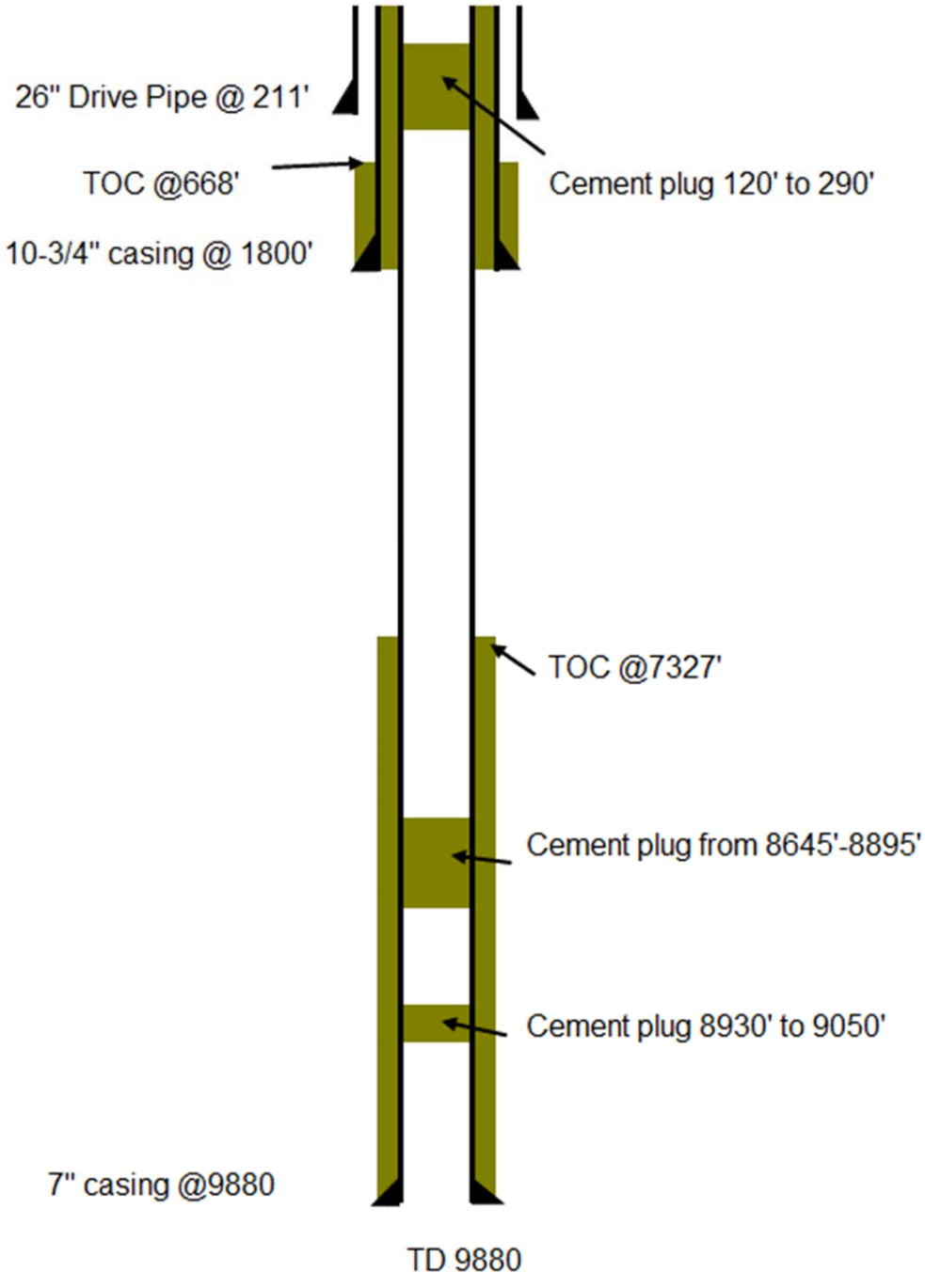

EnergyXXI 108-11

Denote cement

Current Wellbore Conditions

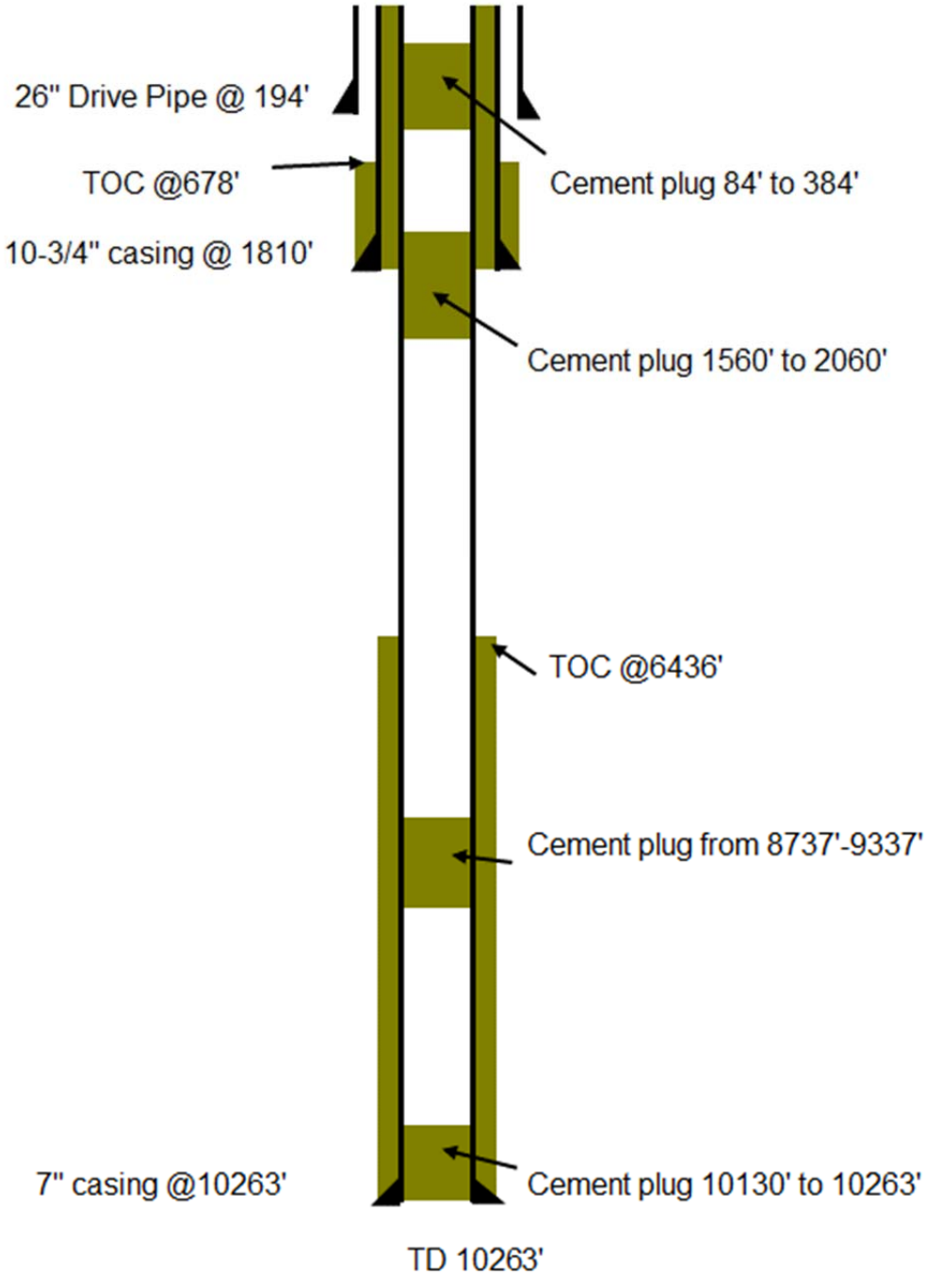

EnergyXXI 108-12

Denote cement

Current Wellbore Conditions

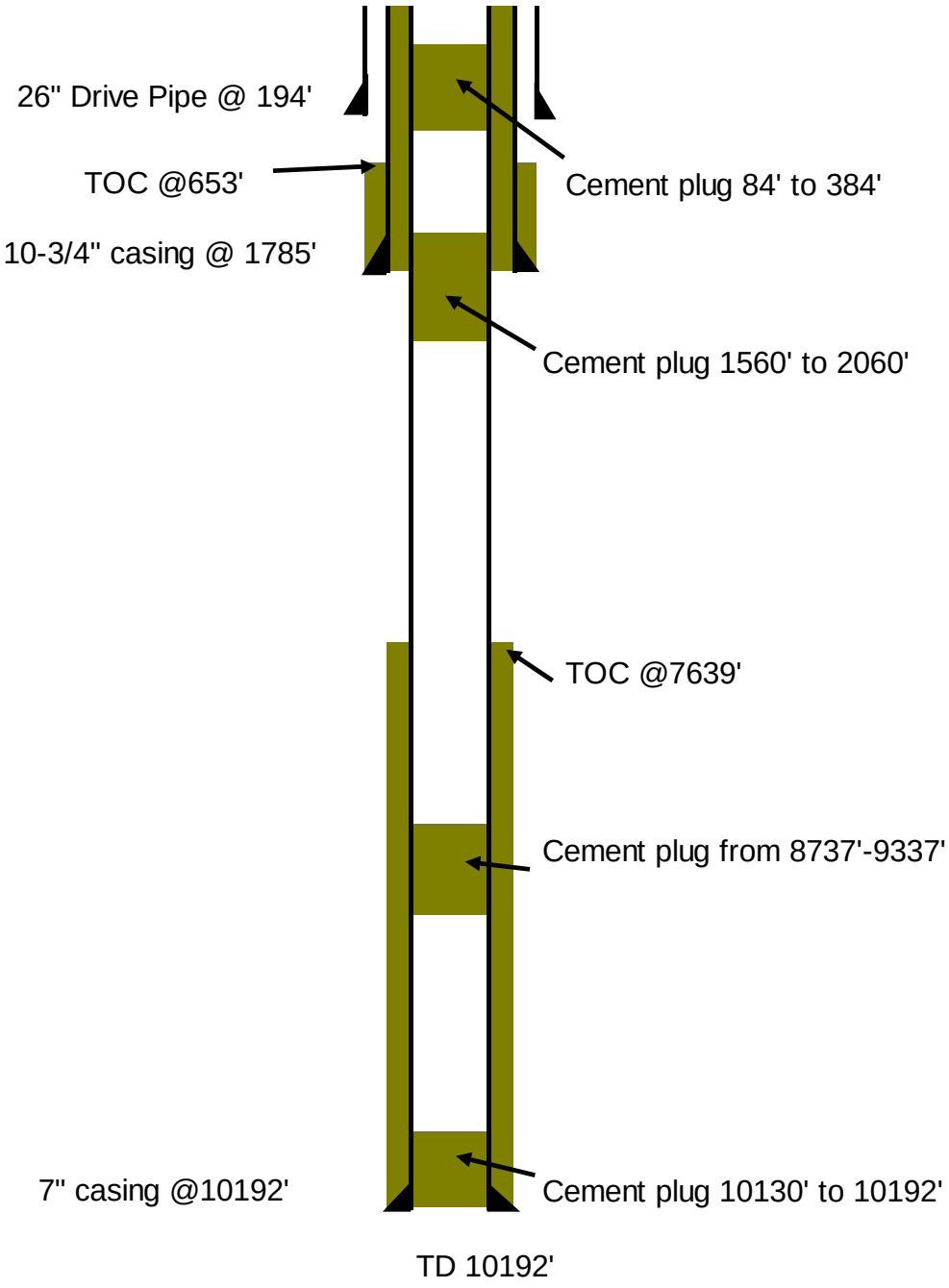

EnergyXXI 108-13

Denote cement

Current Wellbore Conditions

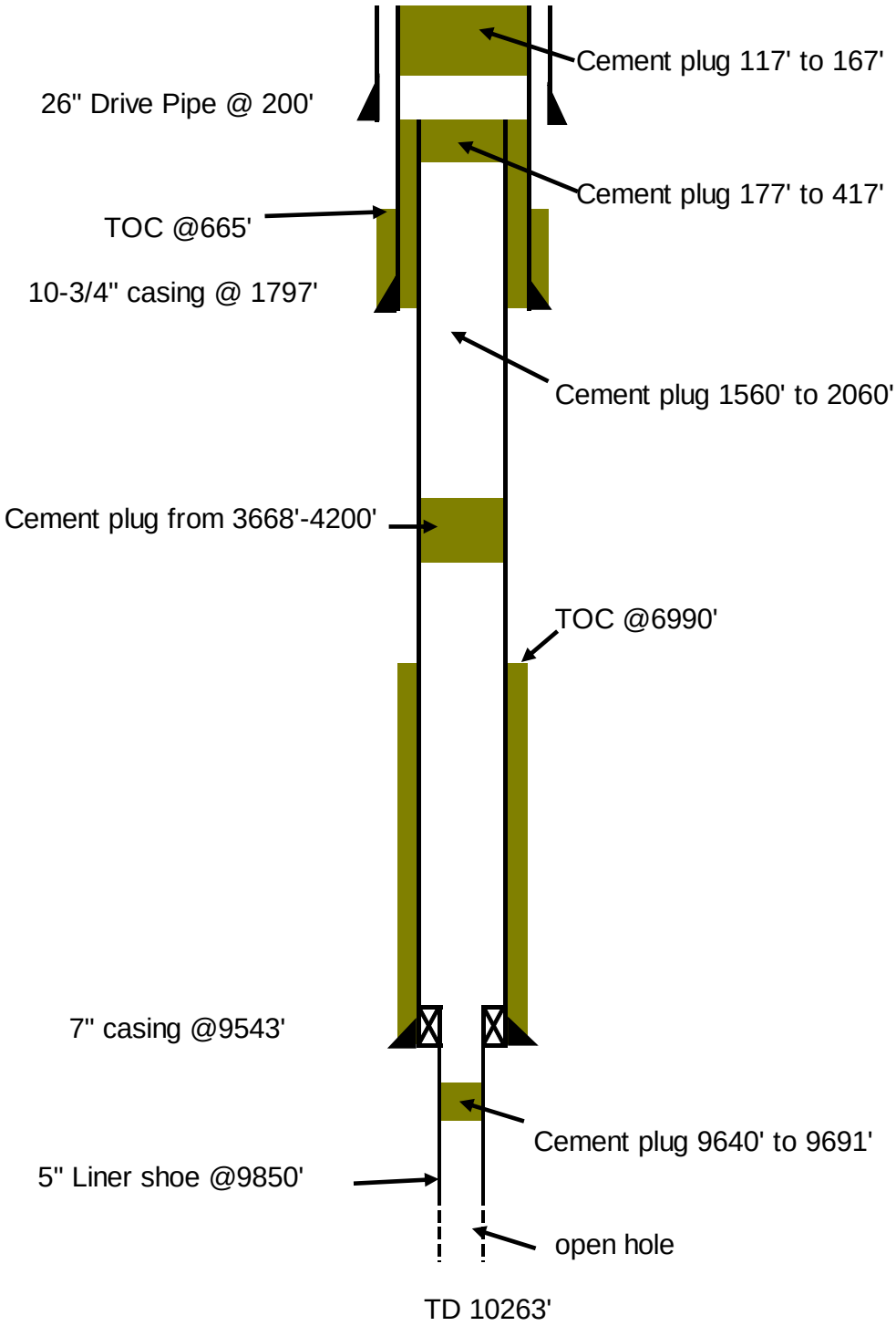

EnergyXXI 108-14

Denote cement

Current Wellbore Conditions

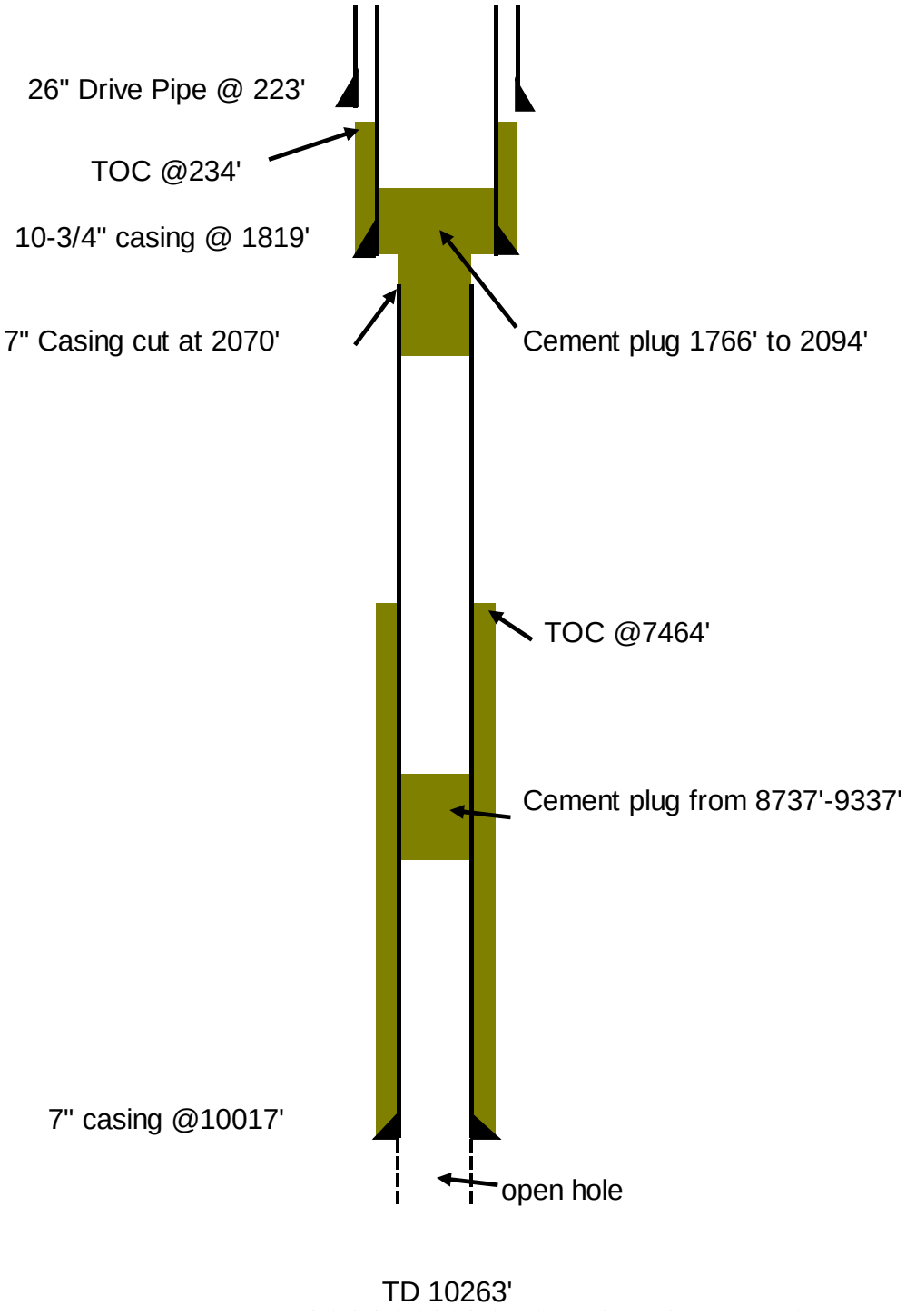

EnergyXXI 108-15

Denote cement

Current Wellbore Conditions

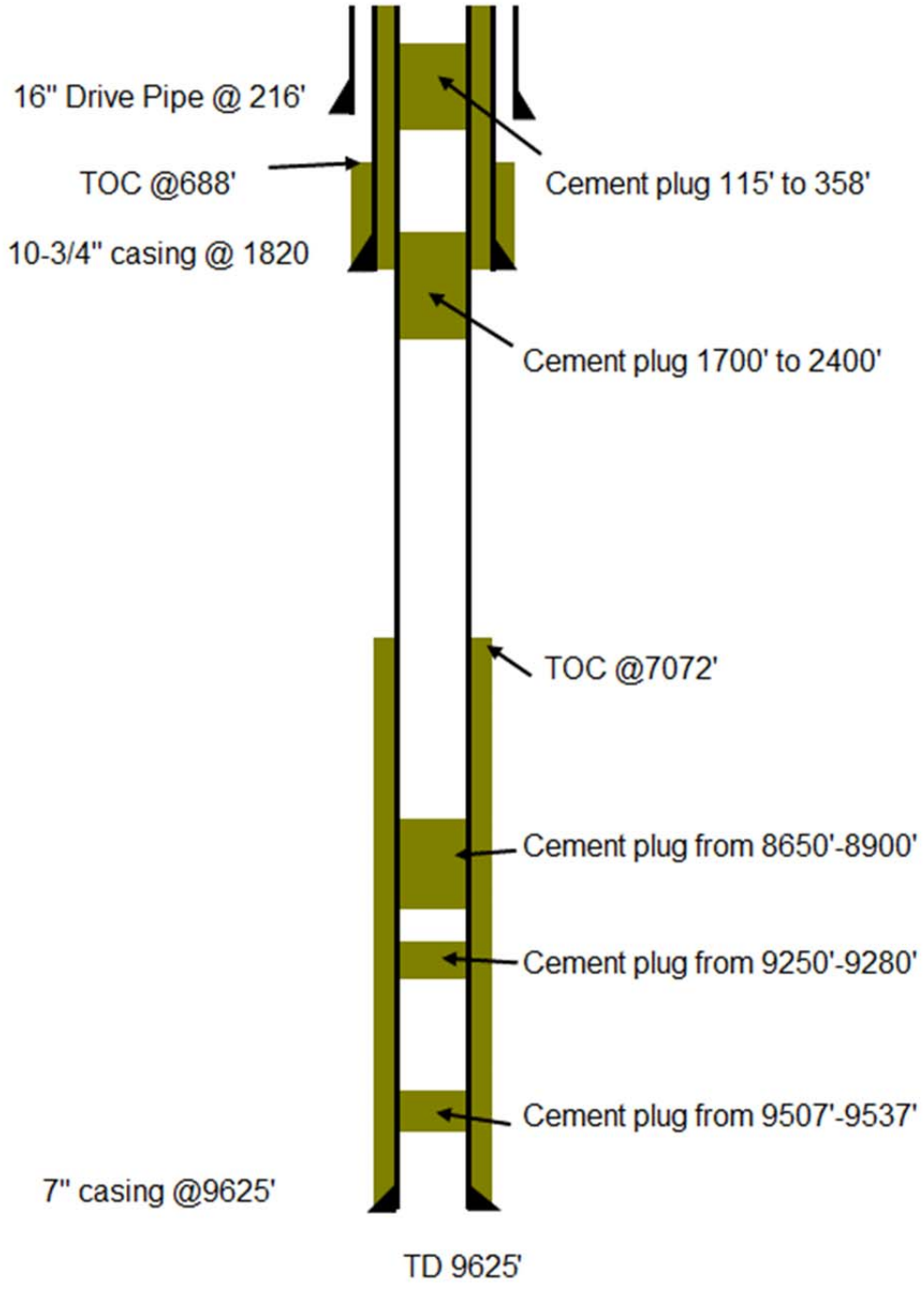

EnergyXXI 108-16ST1

Denote cement

Current Wellbore Conditions

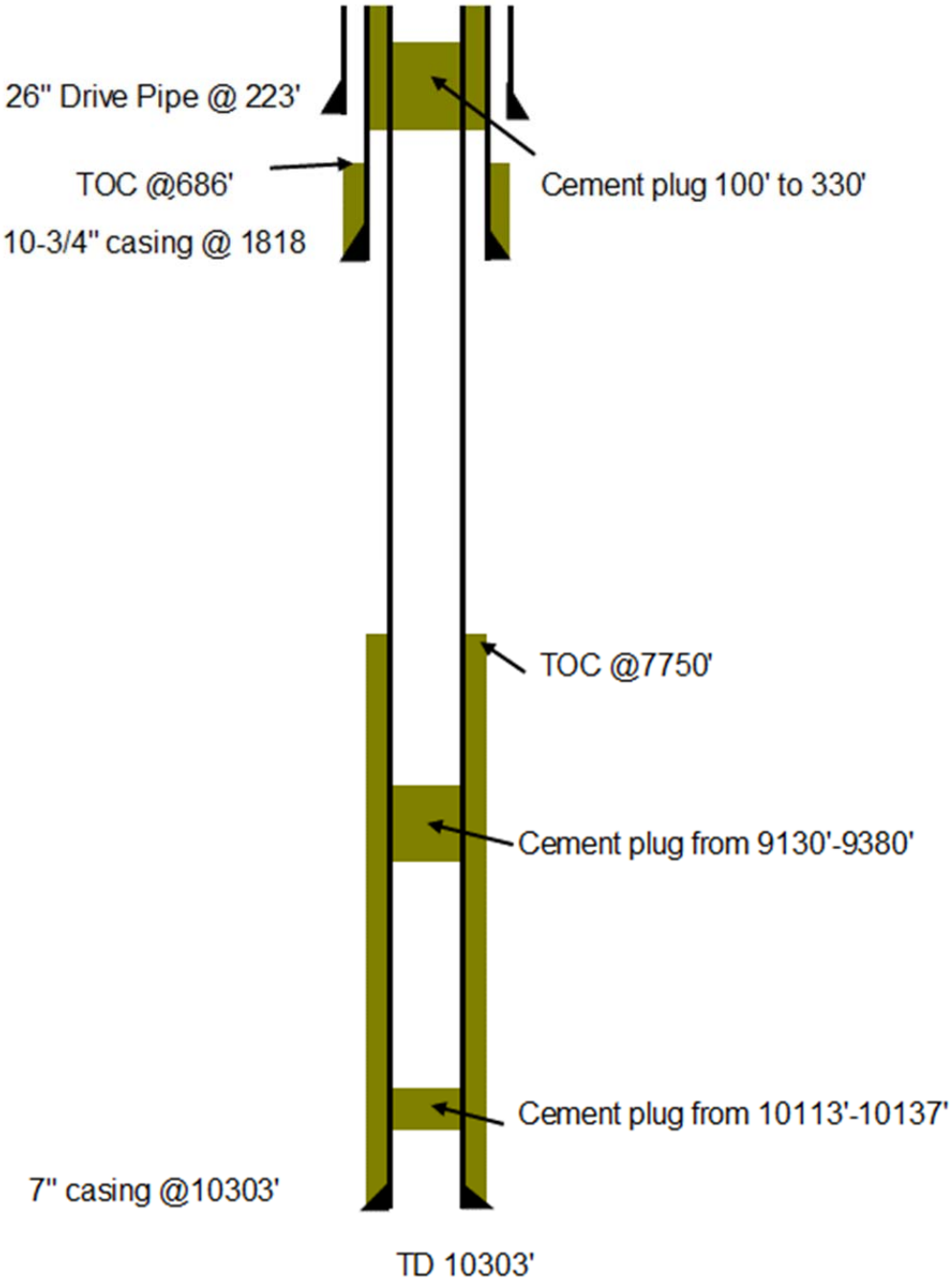

EnergyXXI 108-17

Denote cement

Current Wellbore Conditions

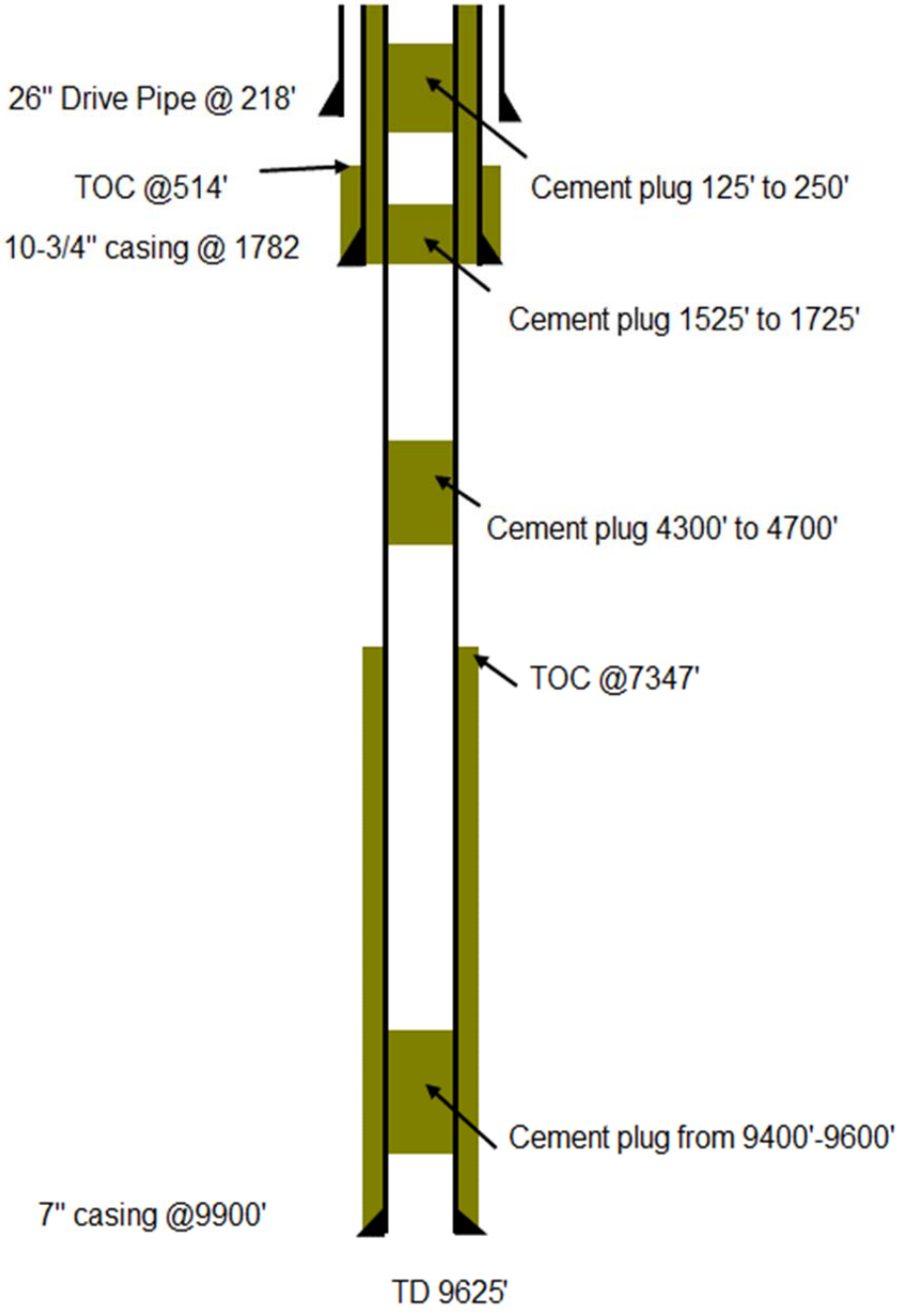

EnergyXXI 108-18

Denote cement

Current Wellbore Conditions

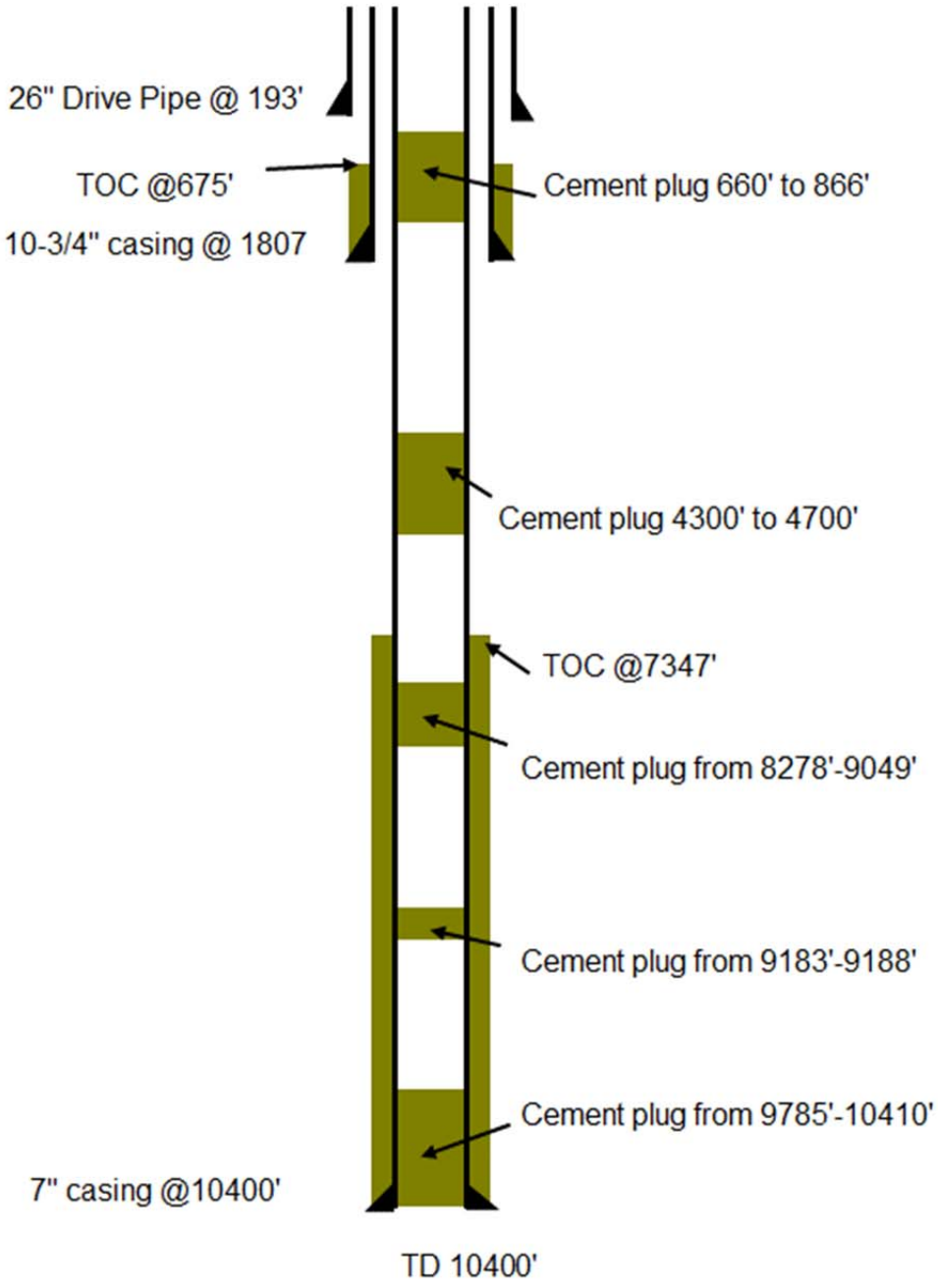

EnergyXXI 108-19

Denote cement

Current Wellbore Conditions

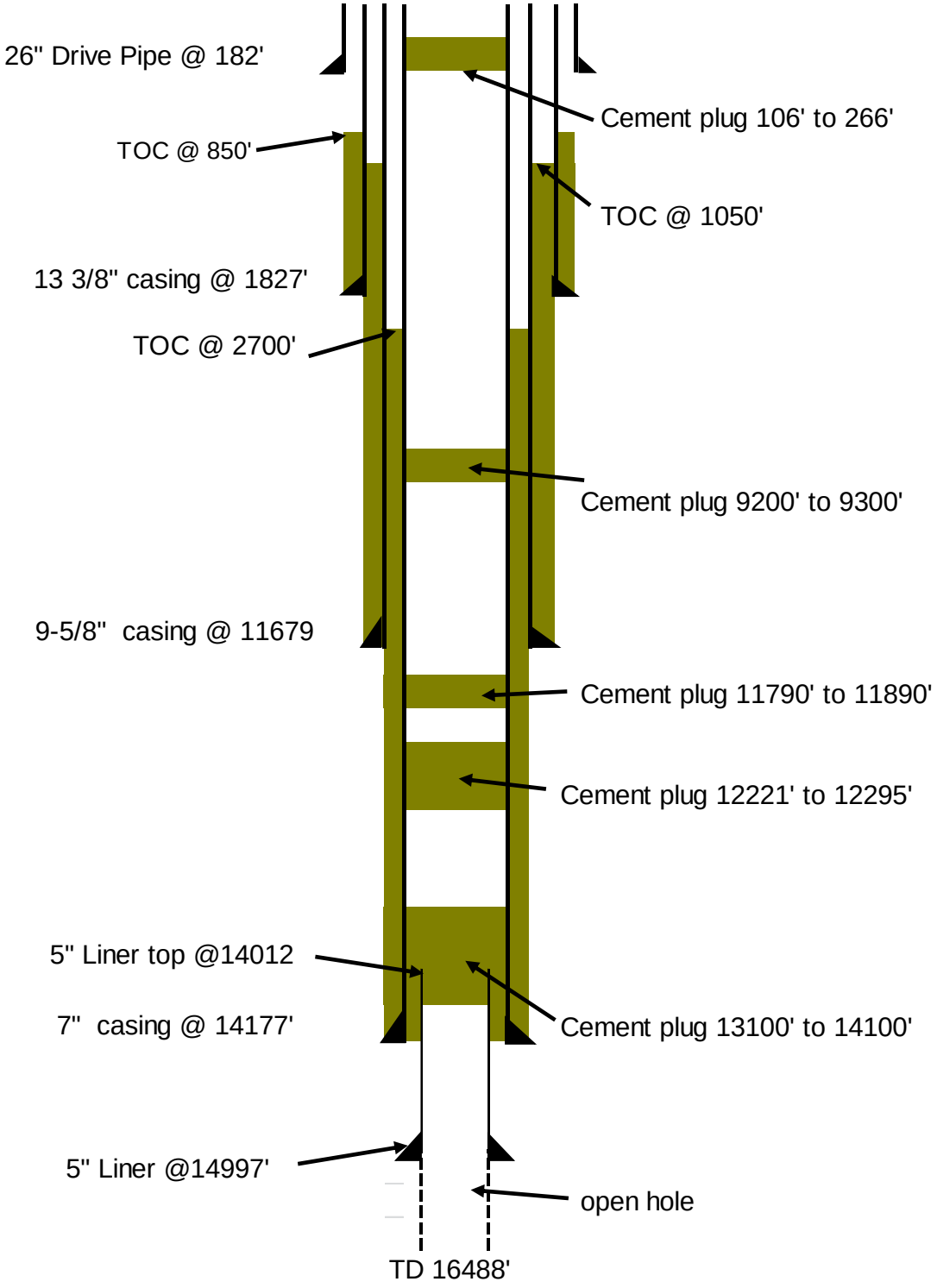

EnergyXXI 108-20

Denote cement

Current Wellbore Conditions

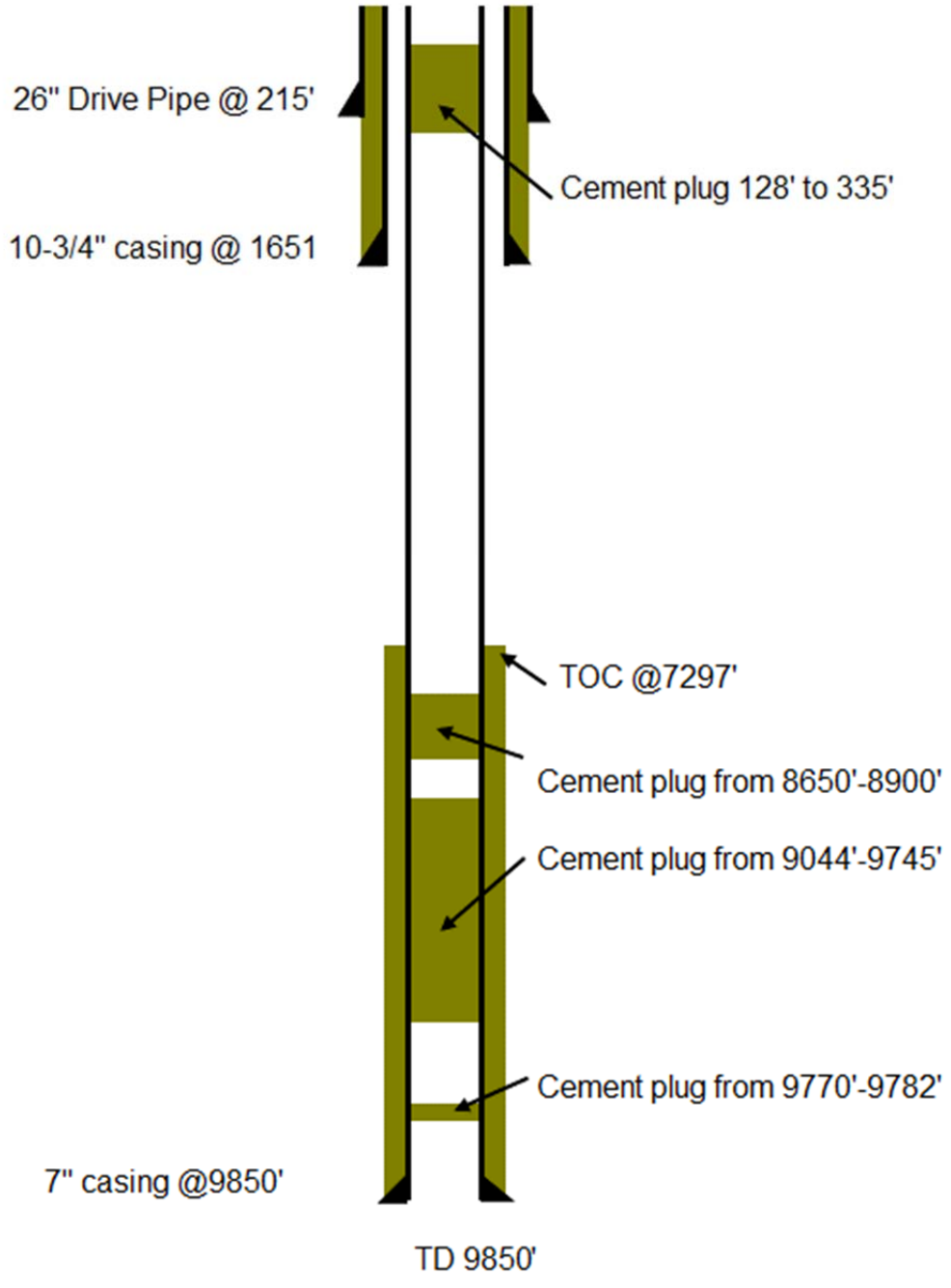

EnergyXXI 108-21

Denote cement

Current Wellbore Conditions

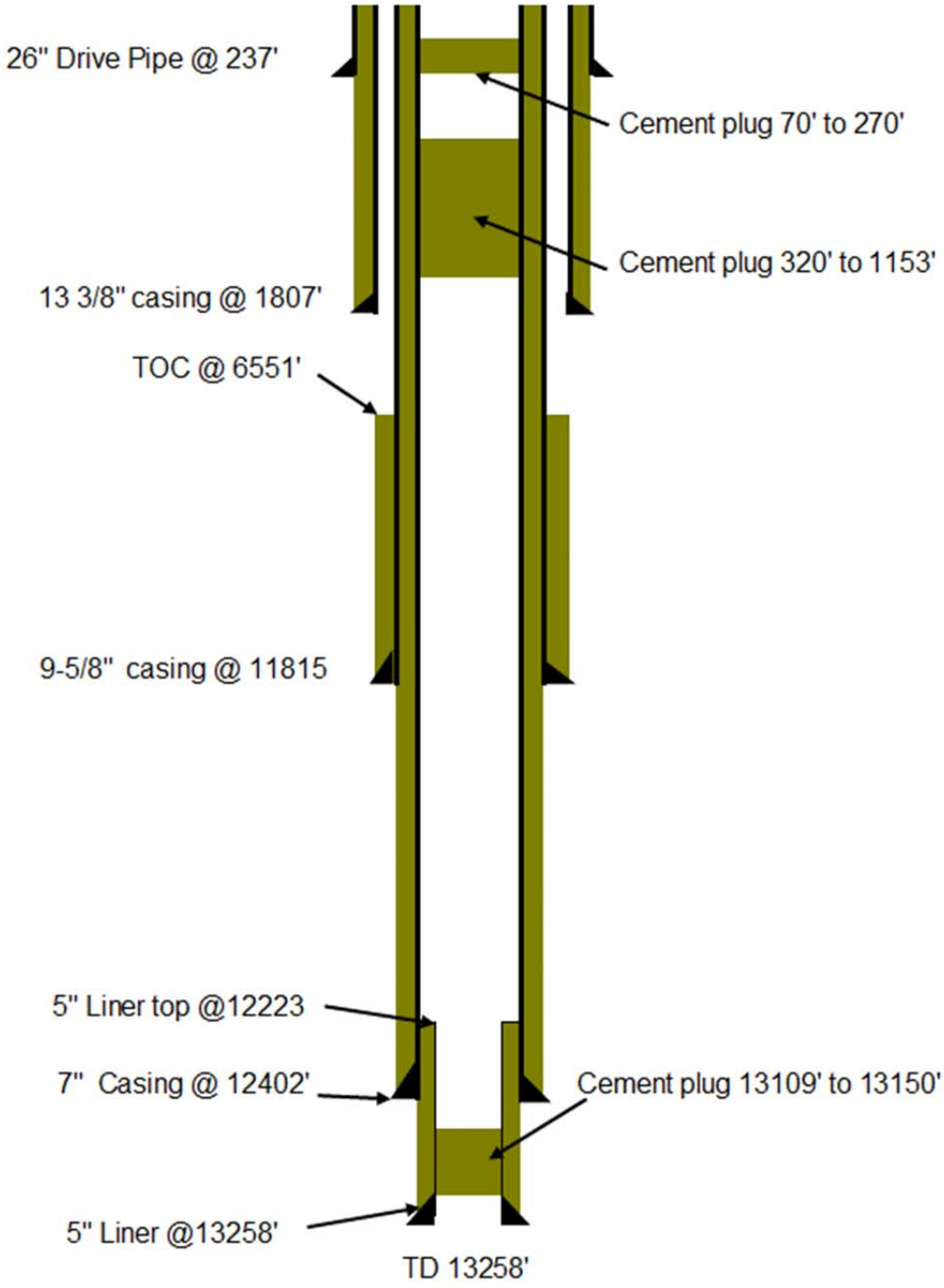

EnergyXXI 108-22

Denote cement

Current Wellbore Conditions

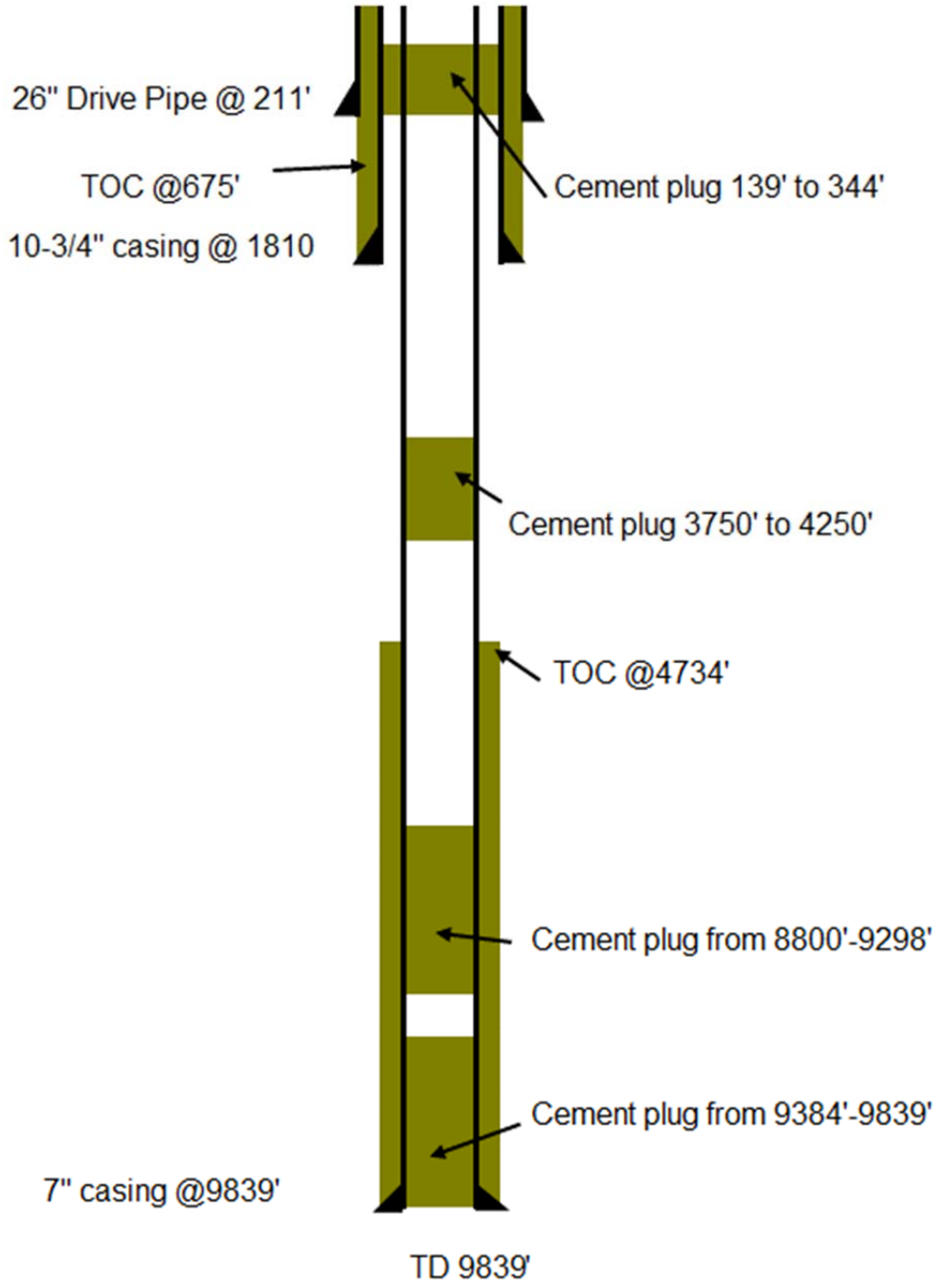

EnergyXXI 108-23

Denote cement

Current Wellbore Conditions

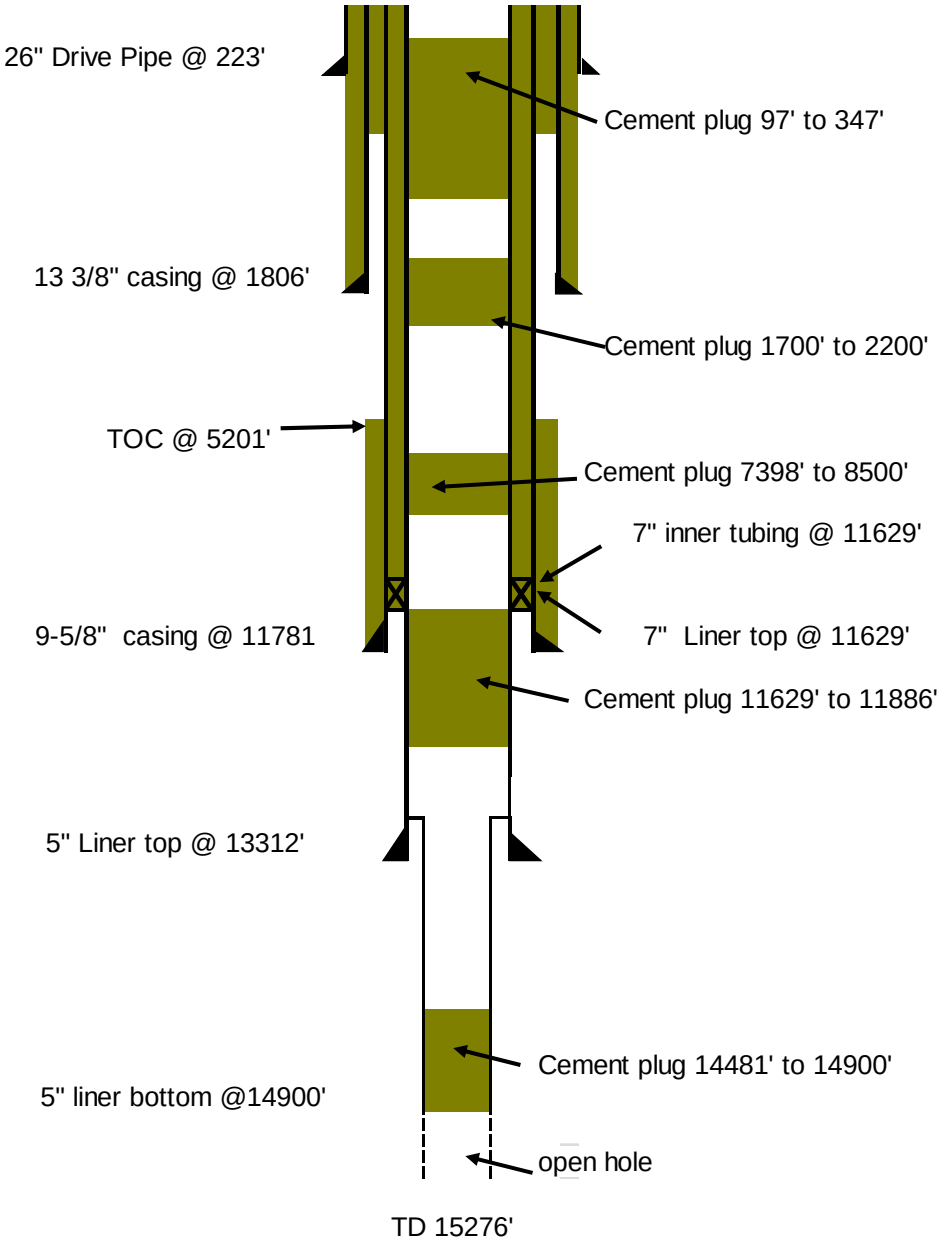

EnergyXXI 108-24

Denote cement

Current Wellbore Conditions

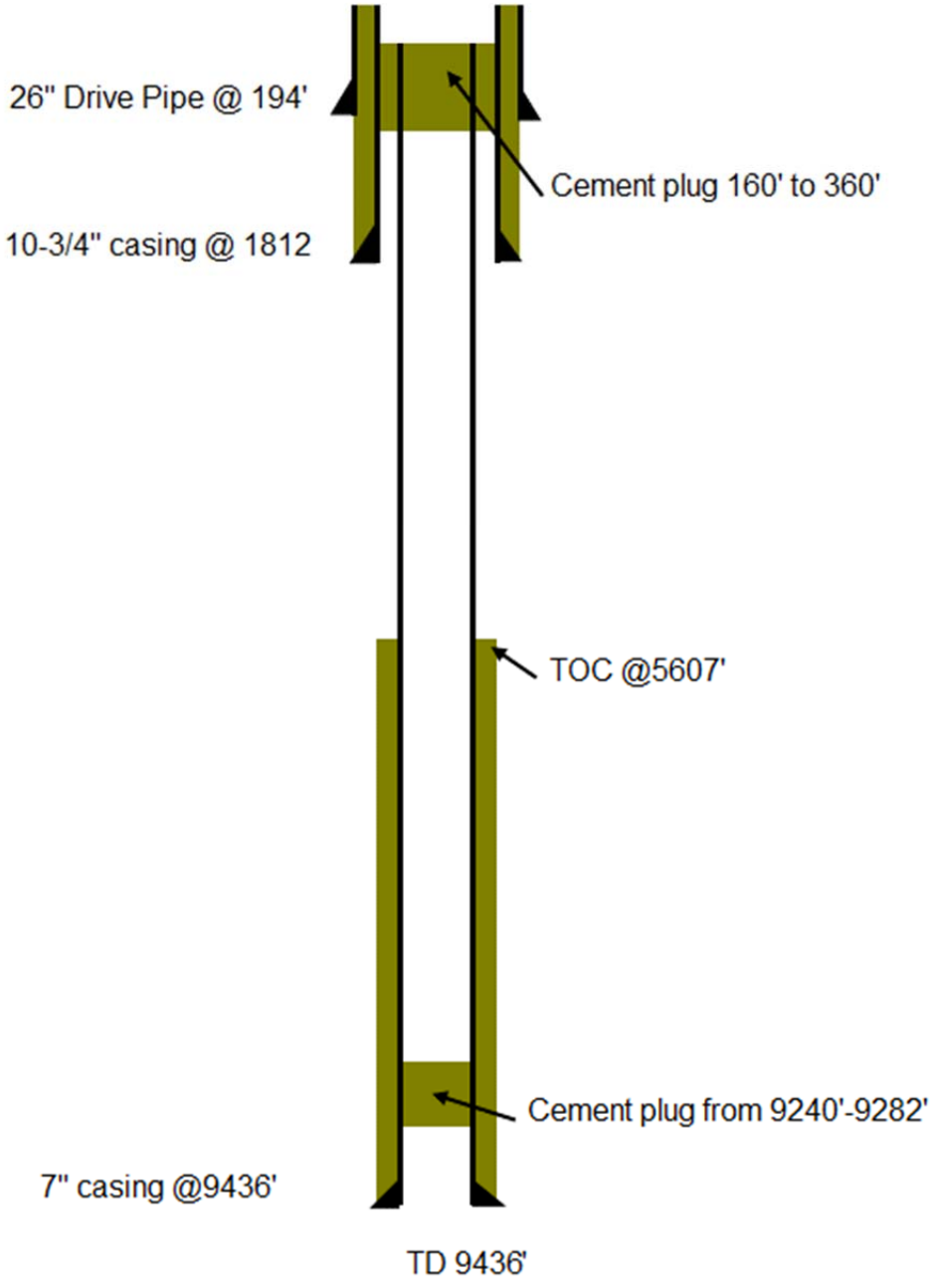

EnergyXXI 108-25

Denote cement

Current Wellbore Conditions

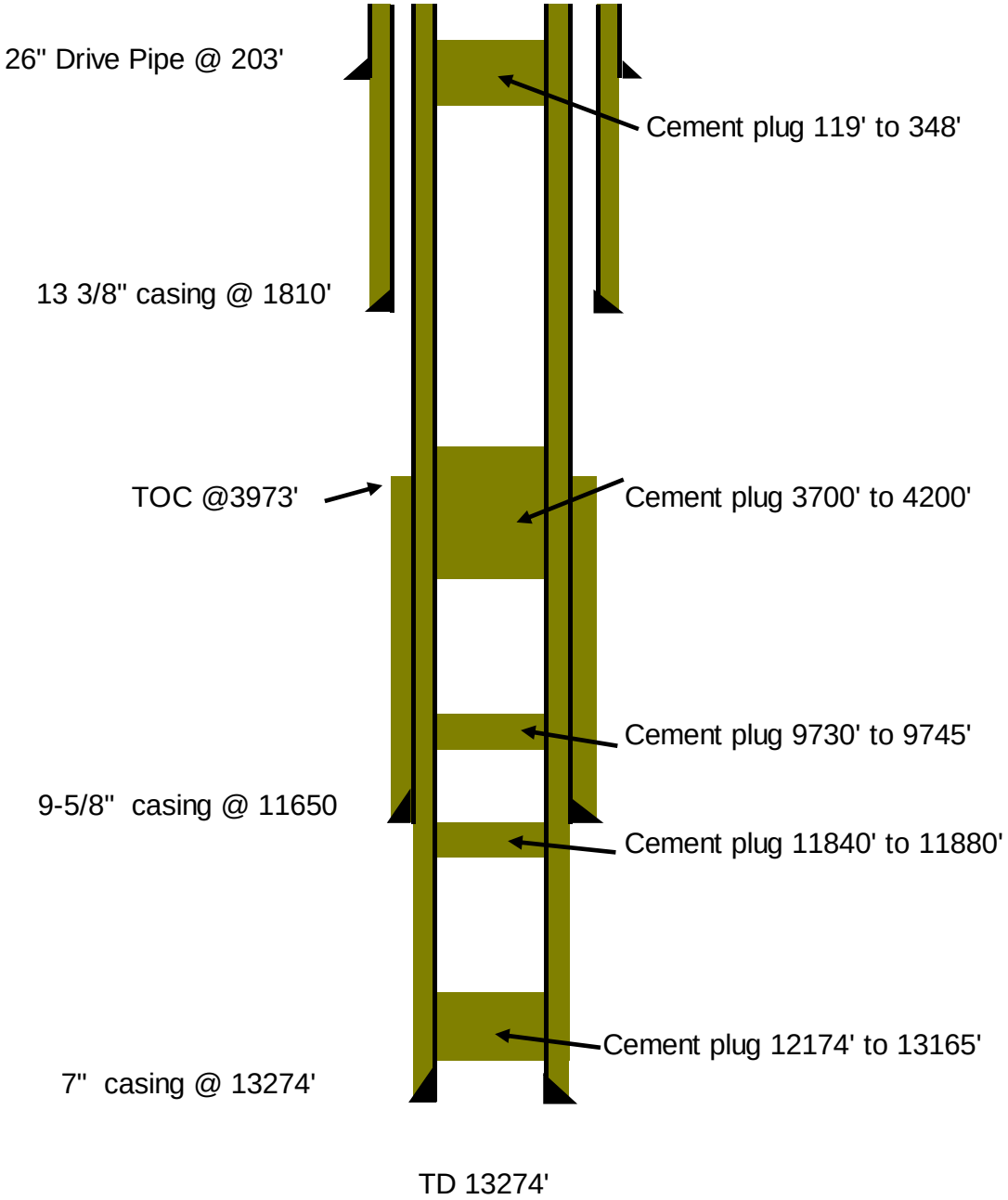

EnergyXXI 108-26

Denote cement

Current Wellbore Conditions

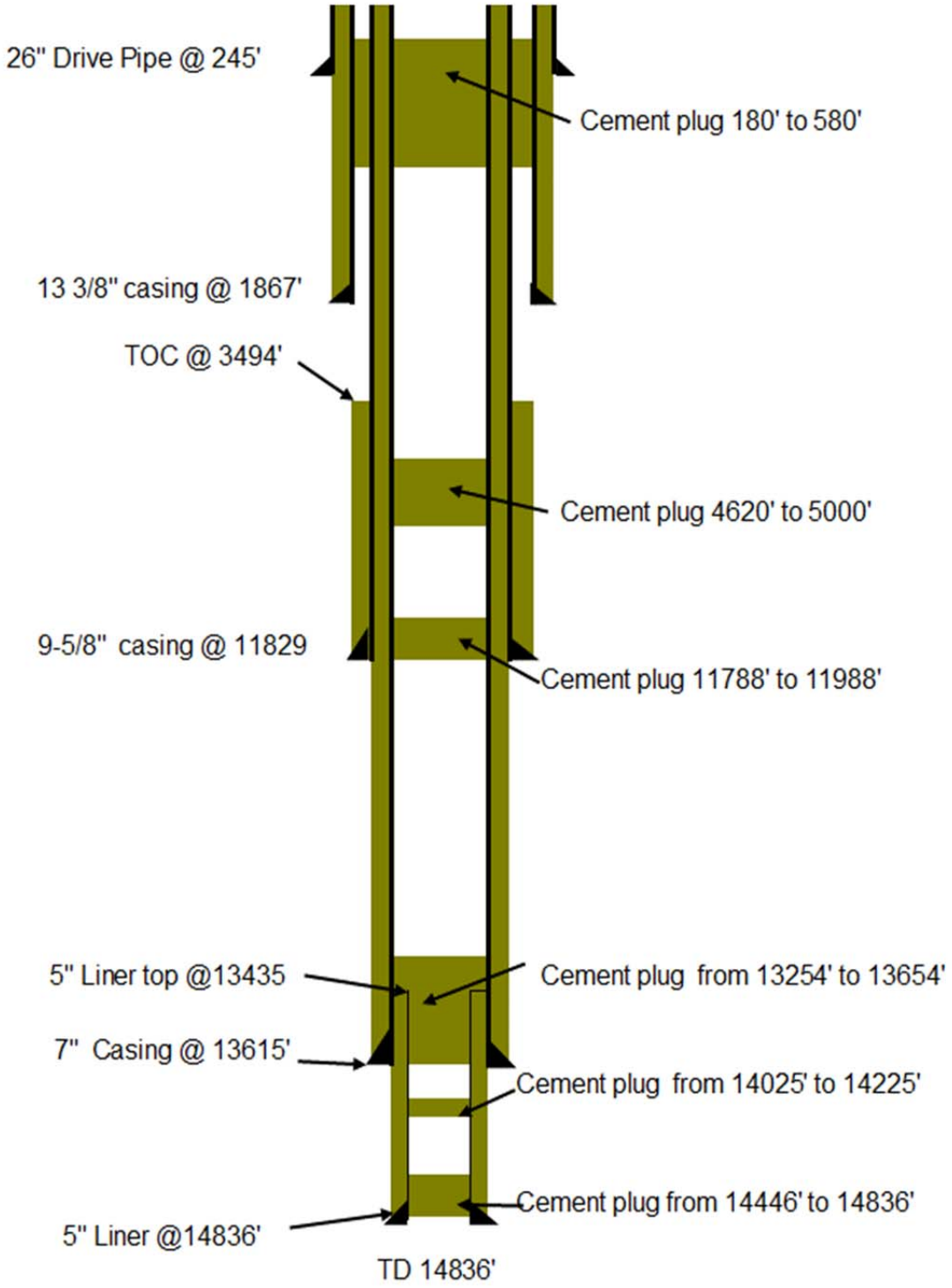

EnergyXXI 108-27

Denote cement

Current Wellbore Conditions

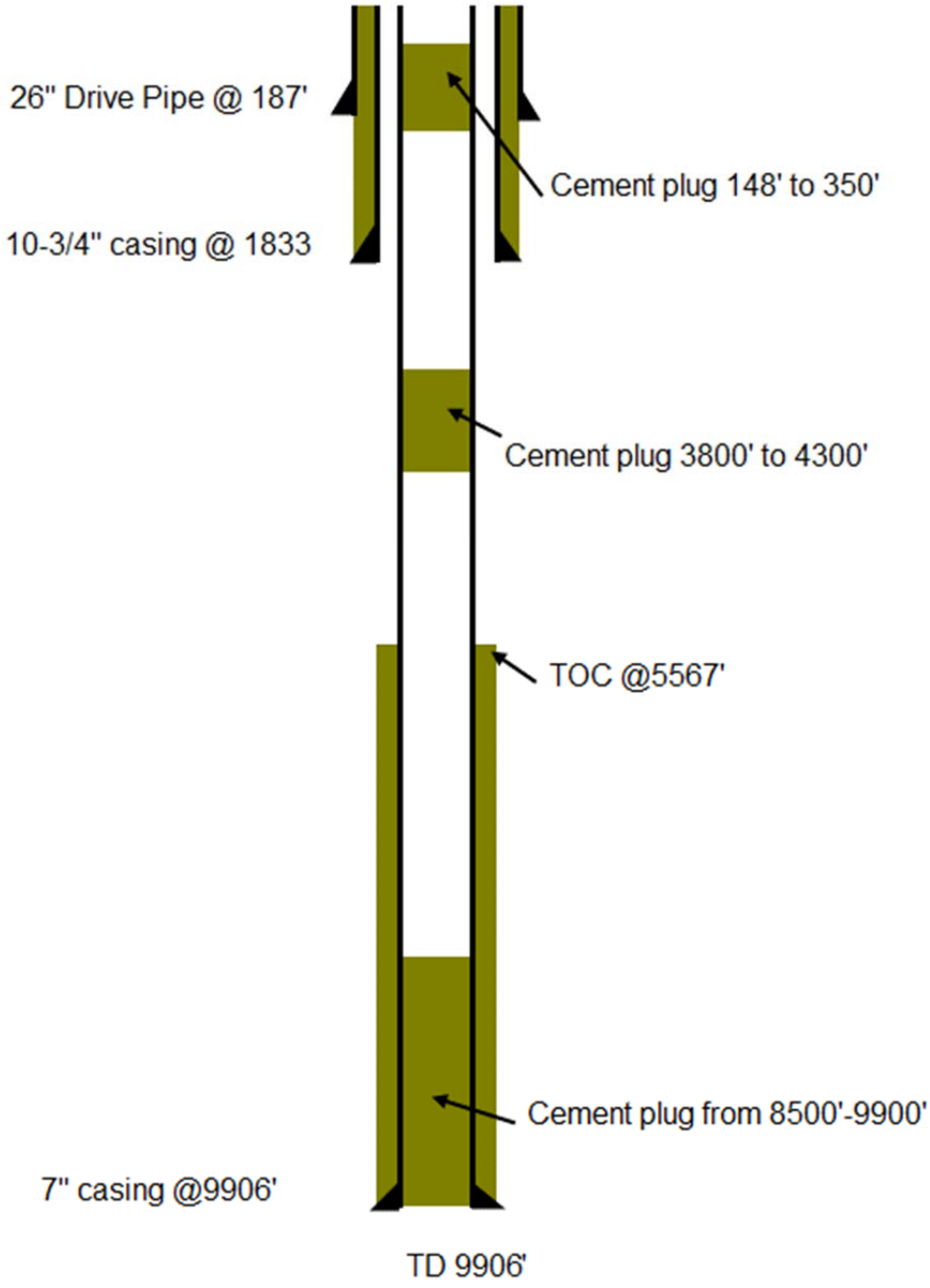

EnergyXXI 108-28

Denote cement

Current Wellbore Conditions

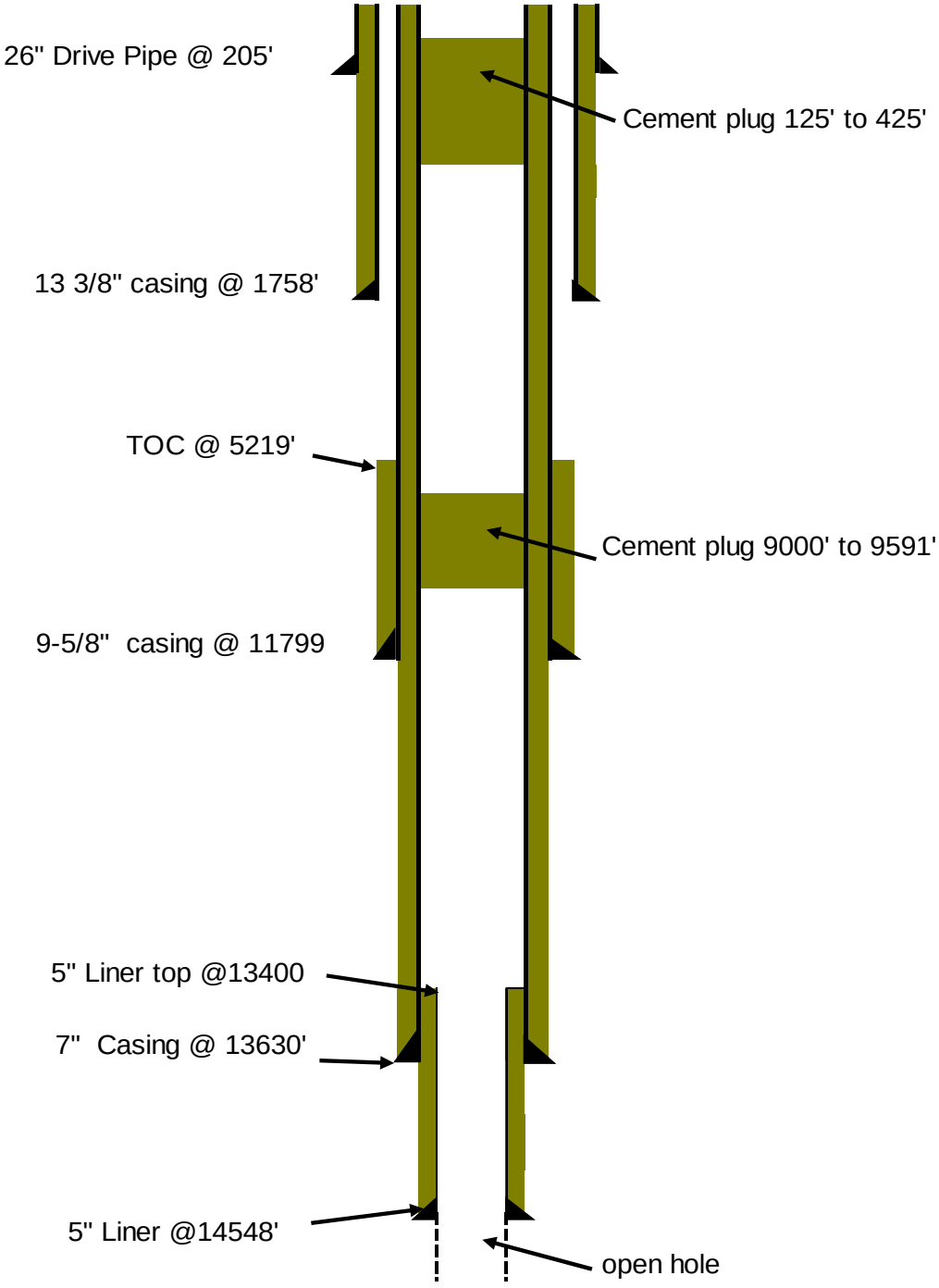

TD 14836'

EnergyXXI 108-29

Denote cement

Current Wellbore Conditions

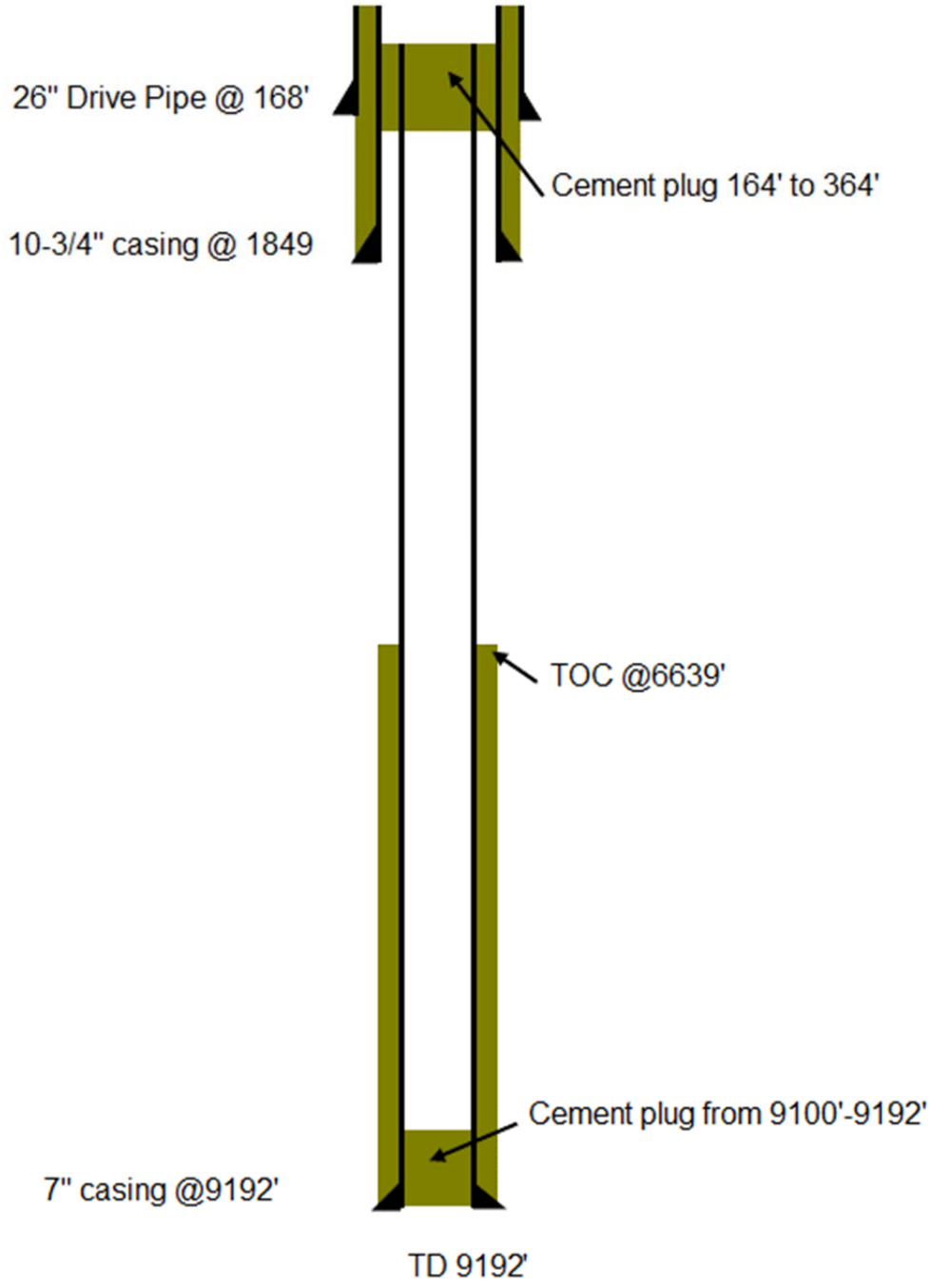

EnergyXXI 108-30

Denote cement

Current Wellbore Conditions

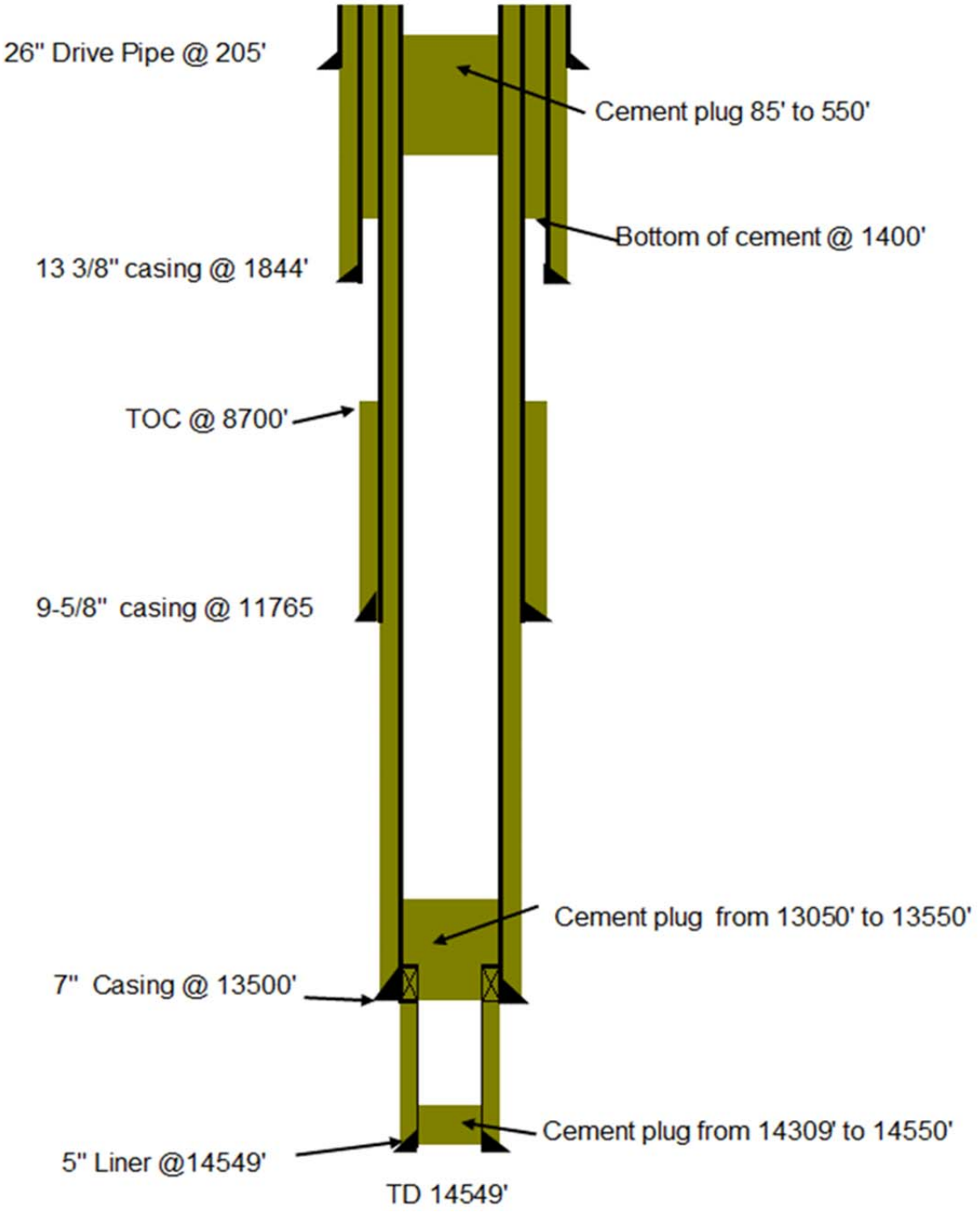

EnergyXXI 108-31

Denote cement

Current Wellbore Conditions

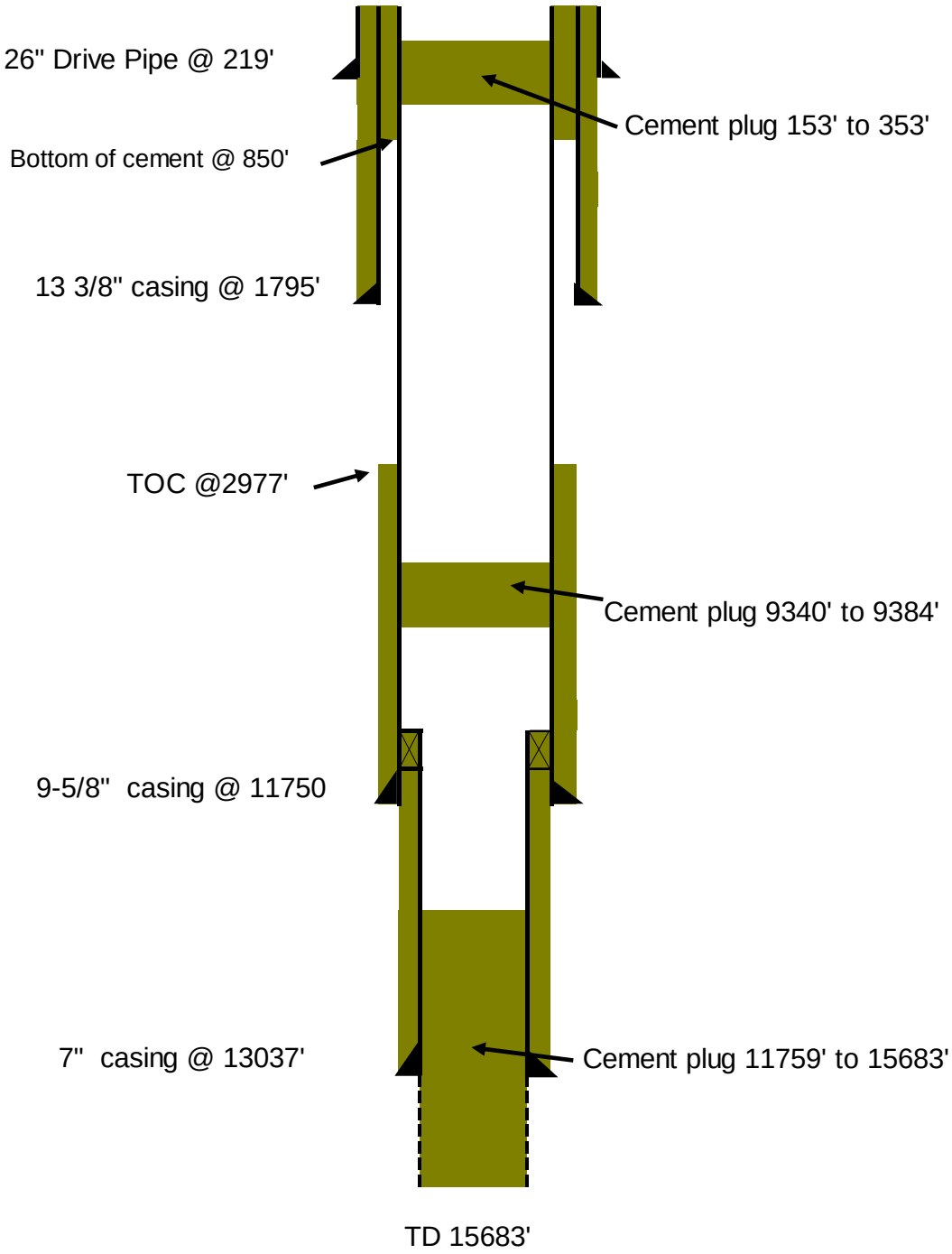

EnergyXXI 108-32

Denote cement

Current Wellbore Conditions

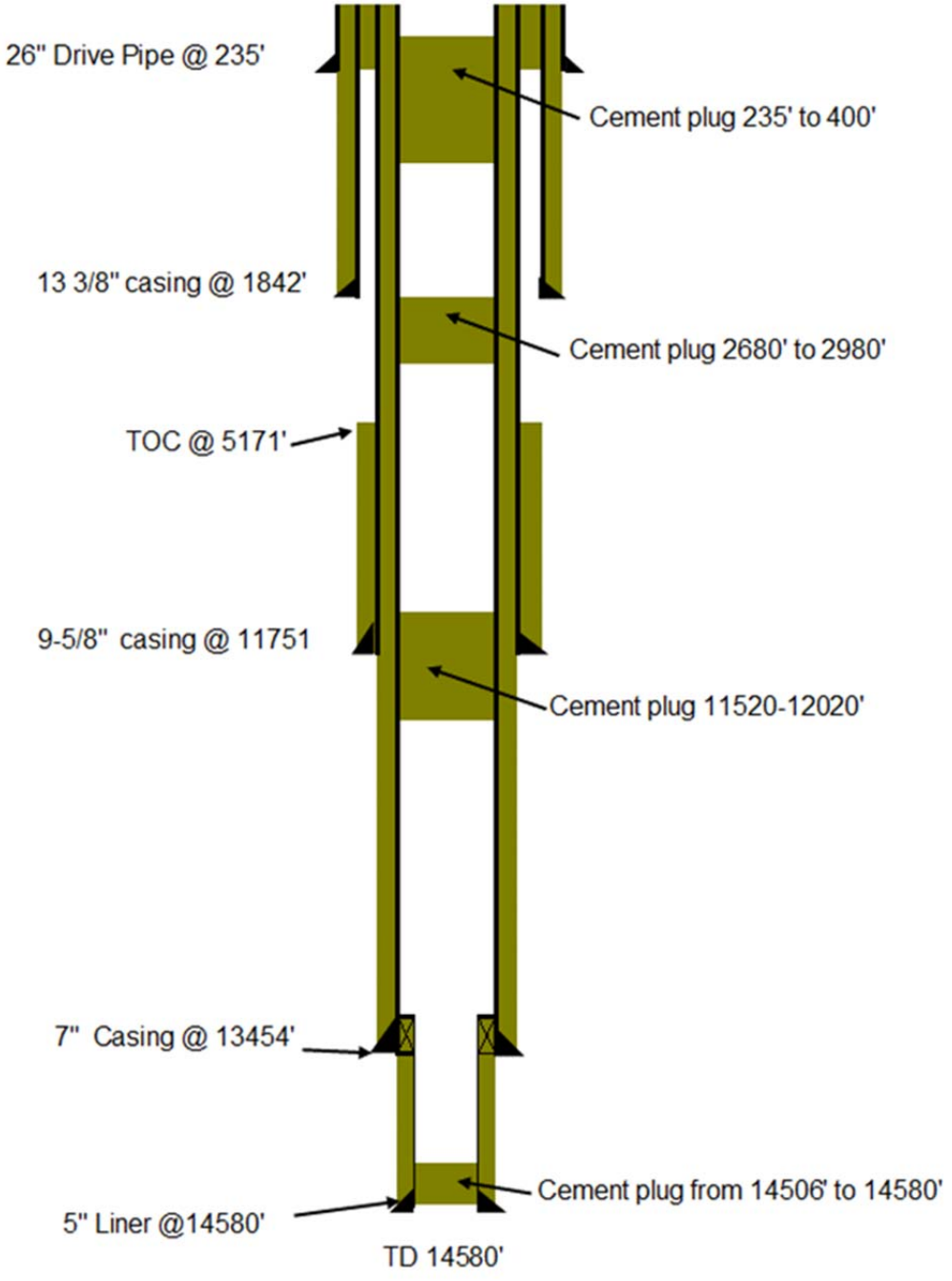

EnergyXXI 108-33

Denote cement

Current Wellbore Conditions

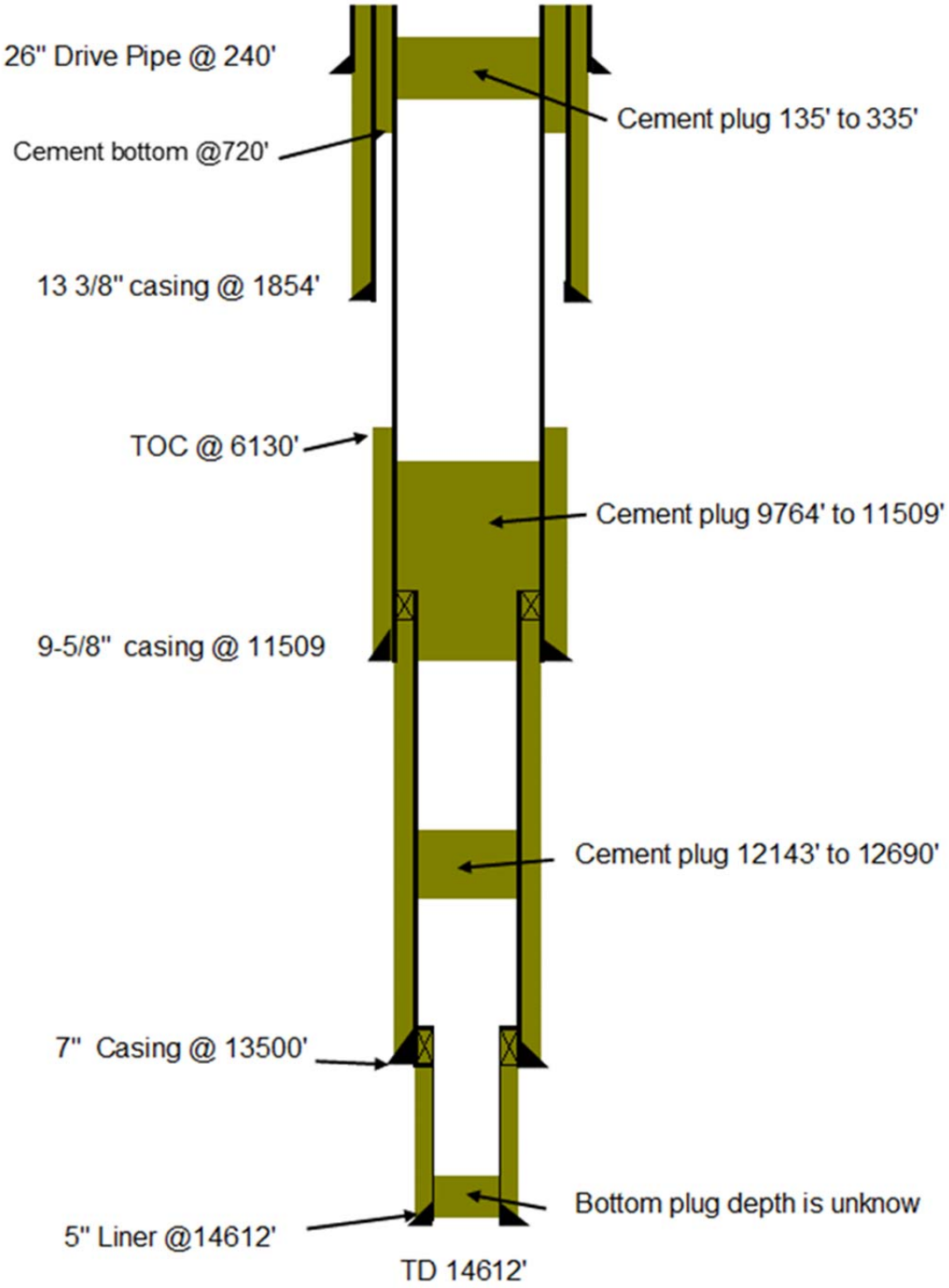

EnergyXXI 108-34

Denote cement

Current Wellbore Conditions

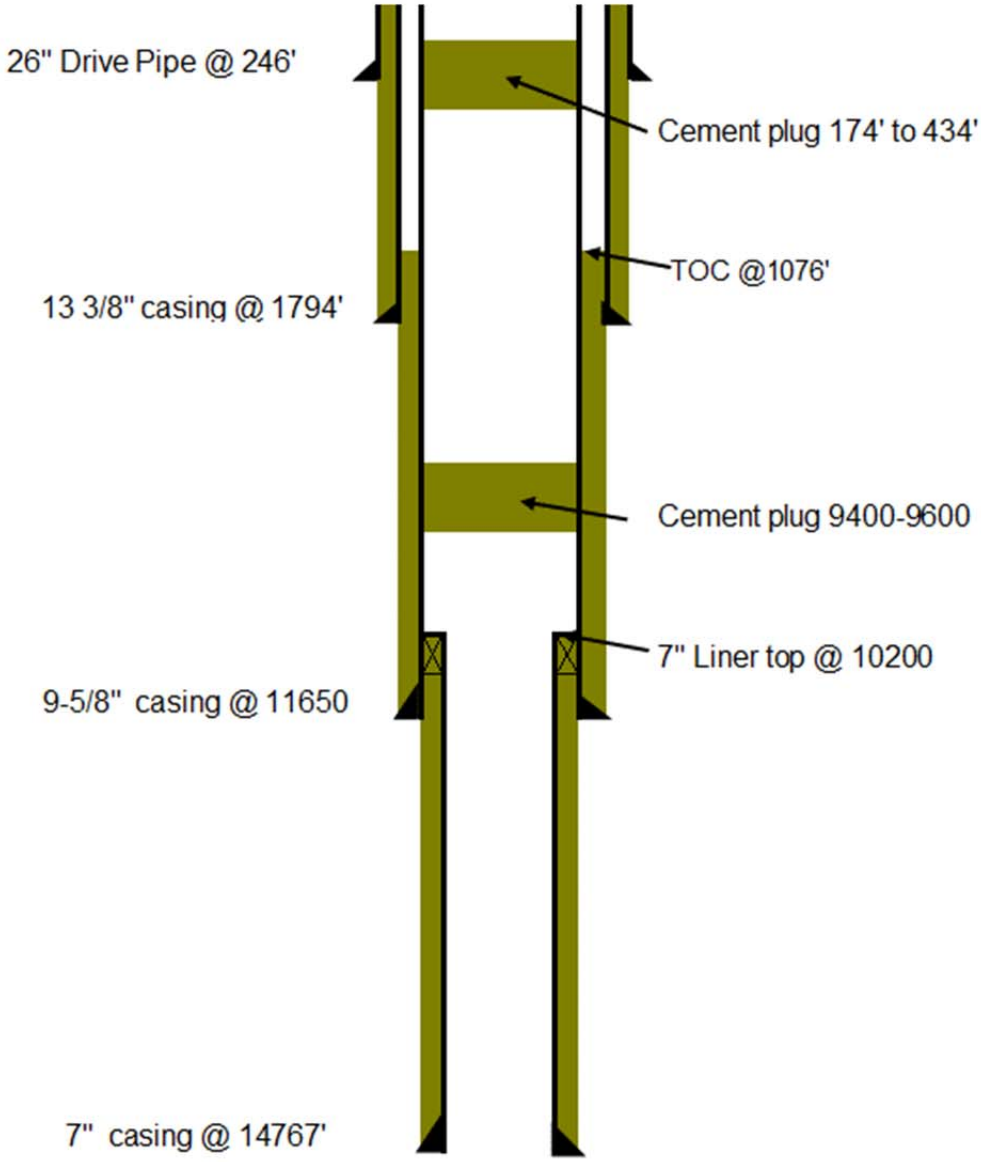

TD 14767'

EnergyXXI 108-34 ST1

Denote cement

Current Wellbore Conditions

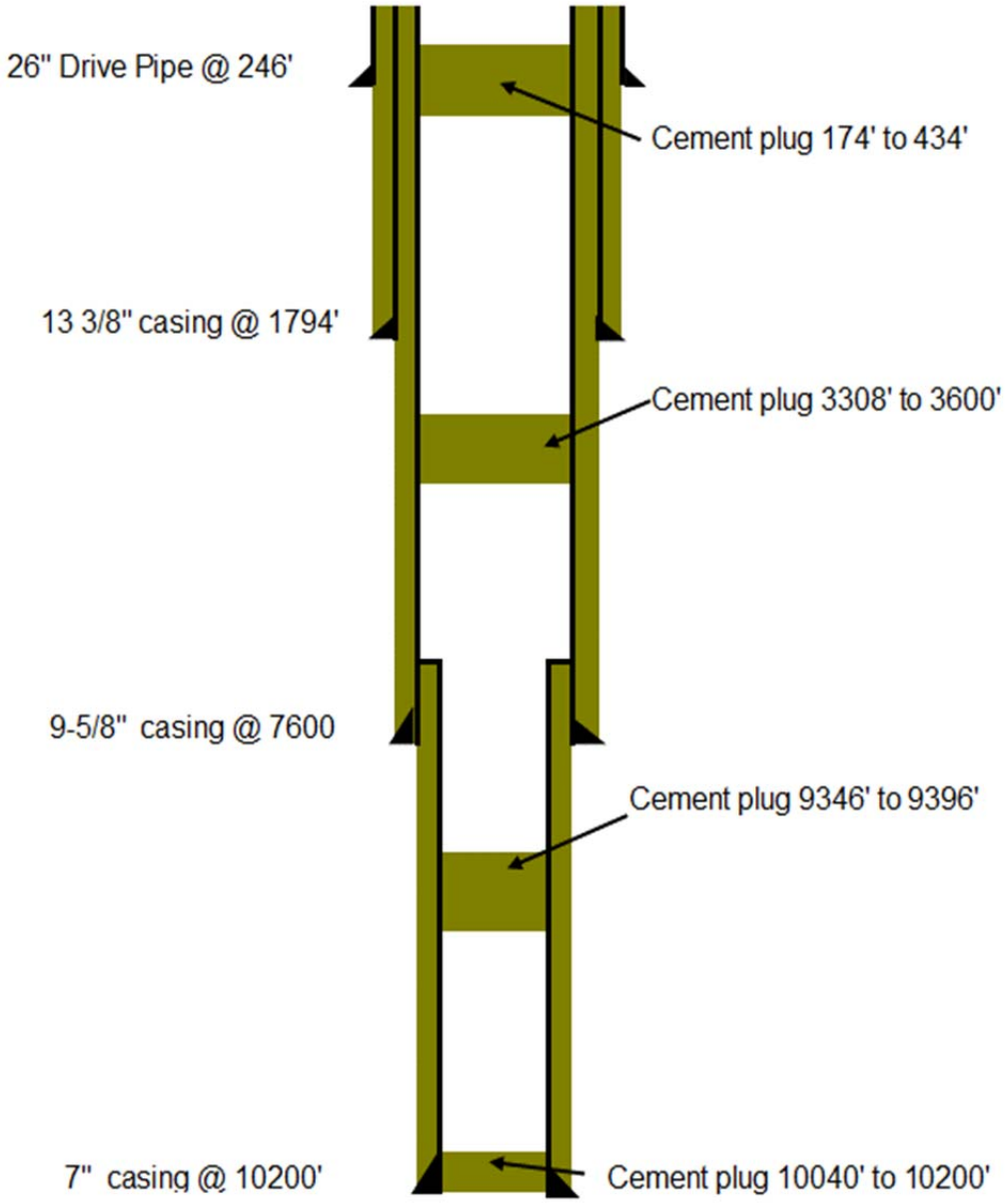

TD 16488'

EnergyXXI 108-35

Denote cement

Current Wellbore Conditions

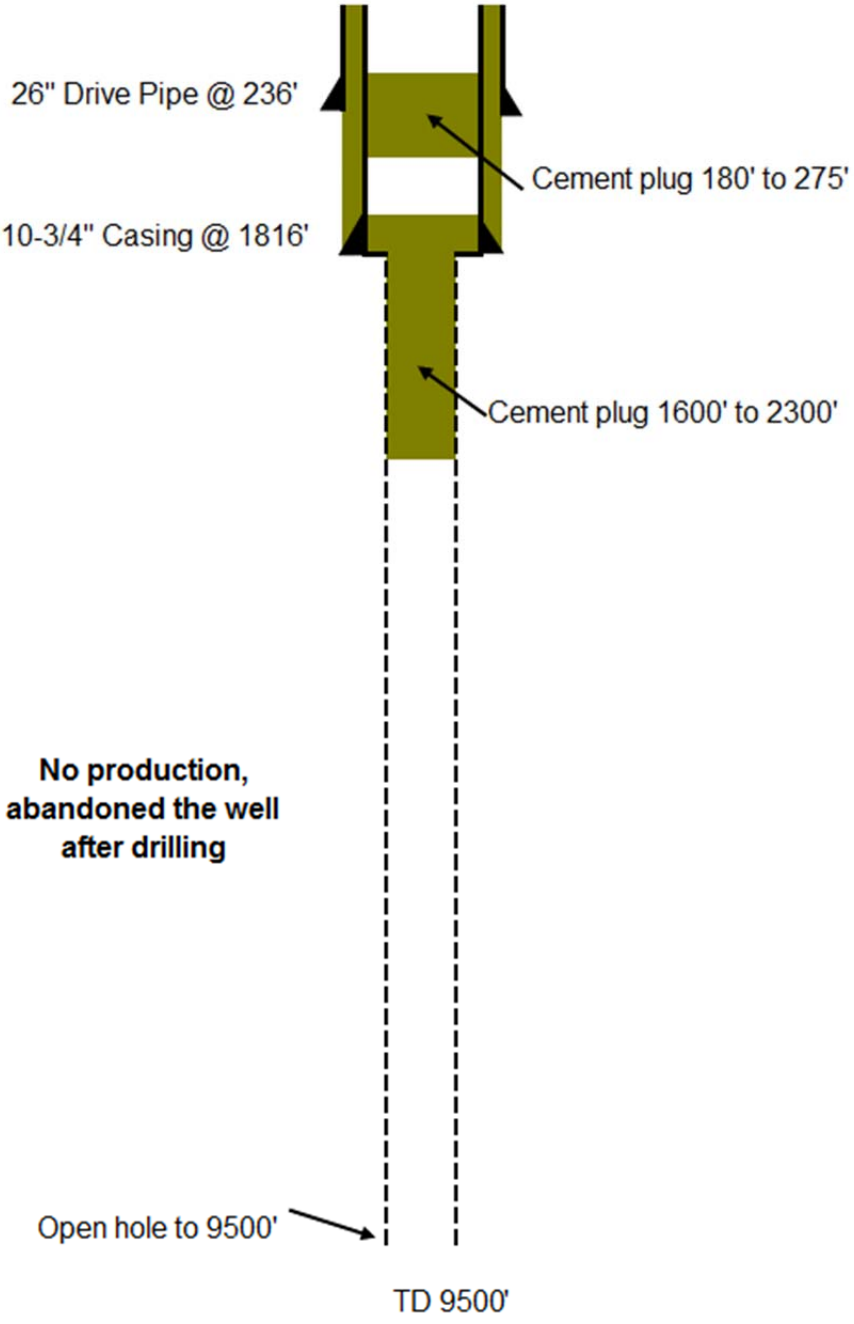

EnergyXXI 108-36

Denote cement

Current Wellbore Conditions

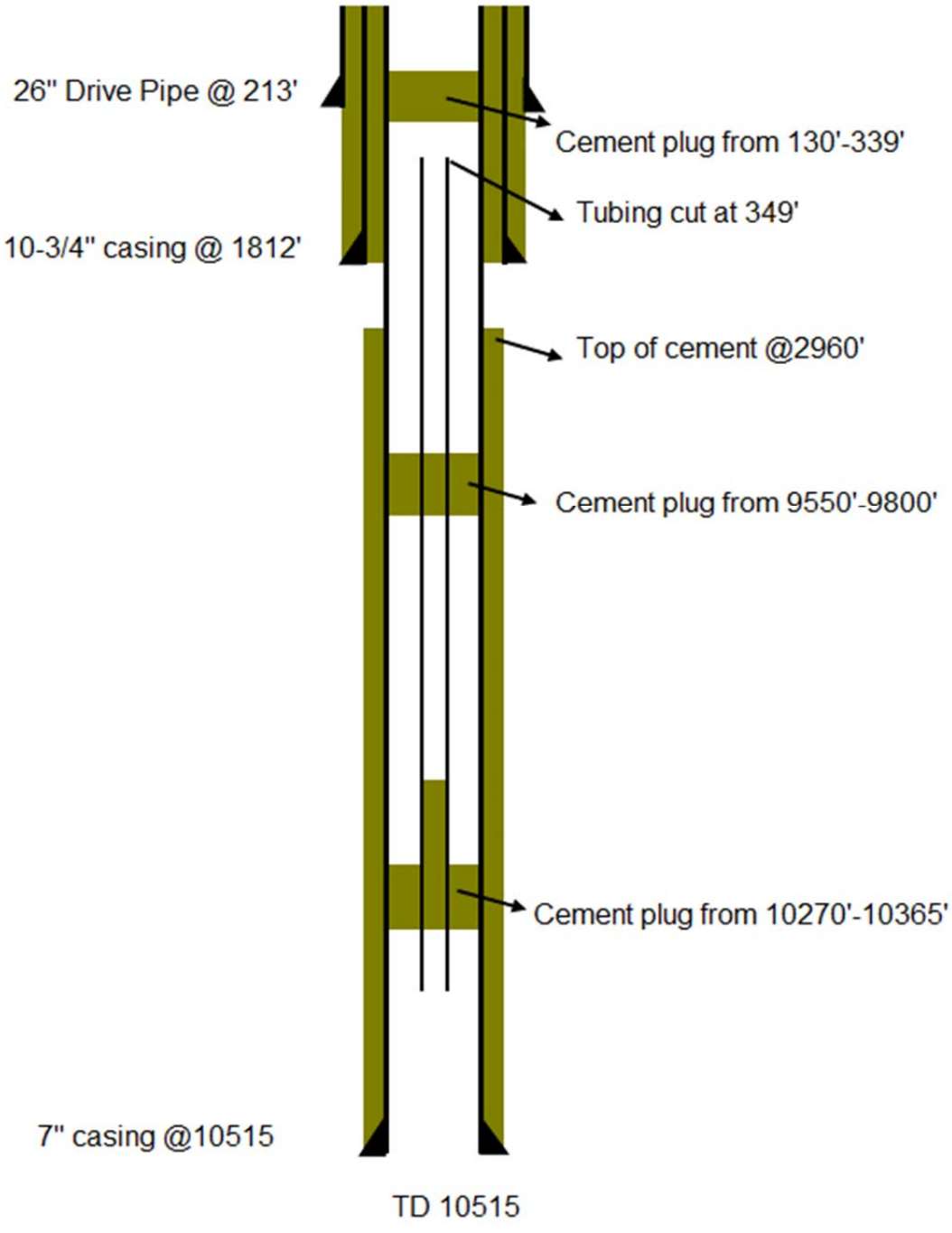

EnergyXXI 108-37

Denote cement

Current Wellbore Conditions

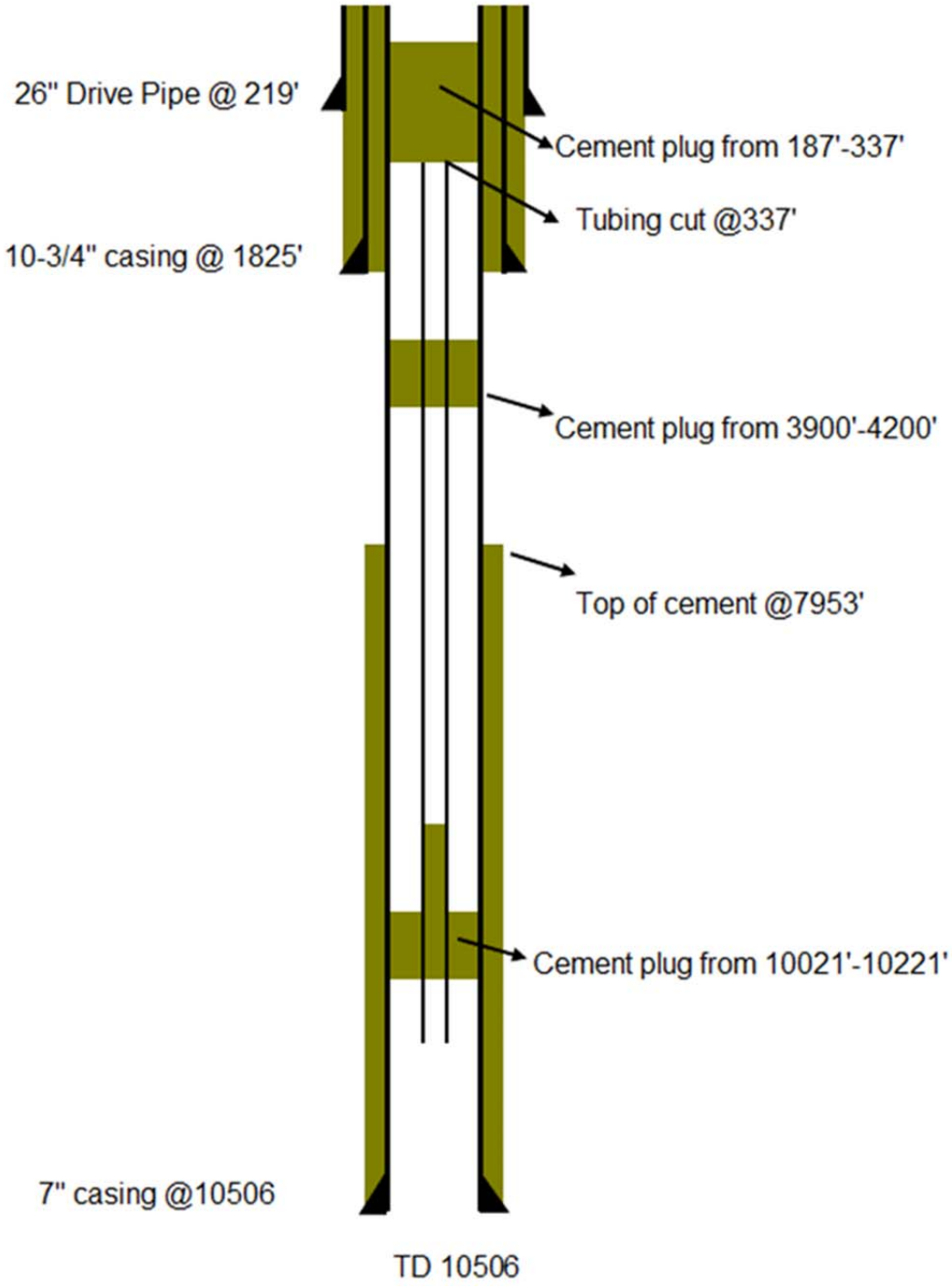

EnergyXXI 108-38

Denote cement

Current Wellbore Conditions

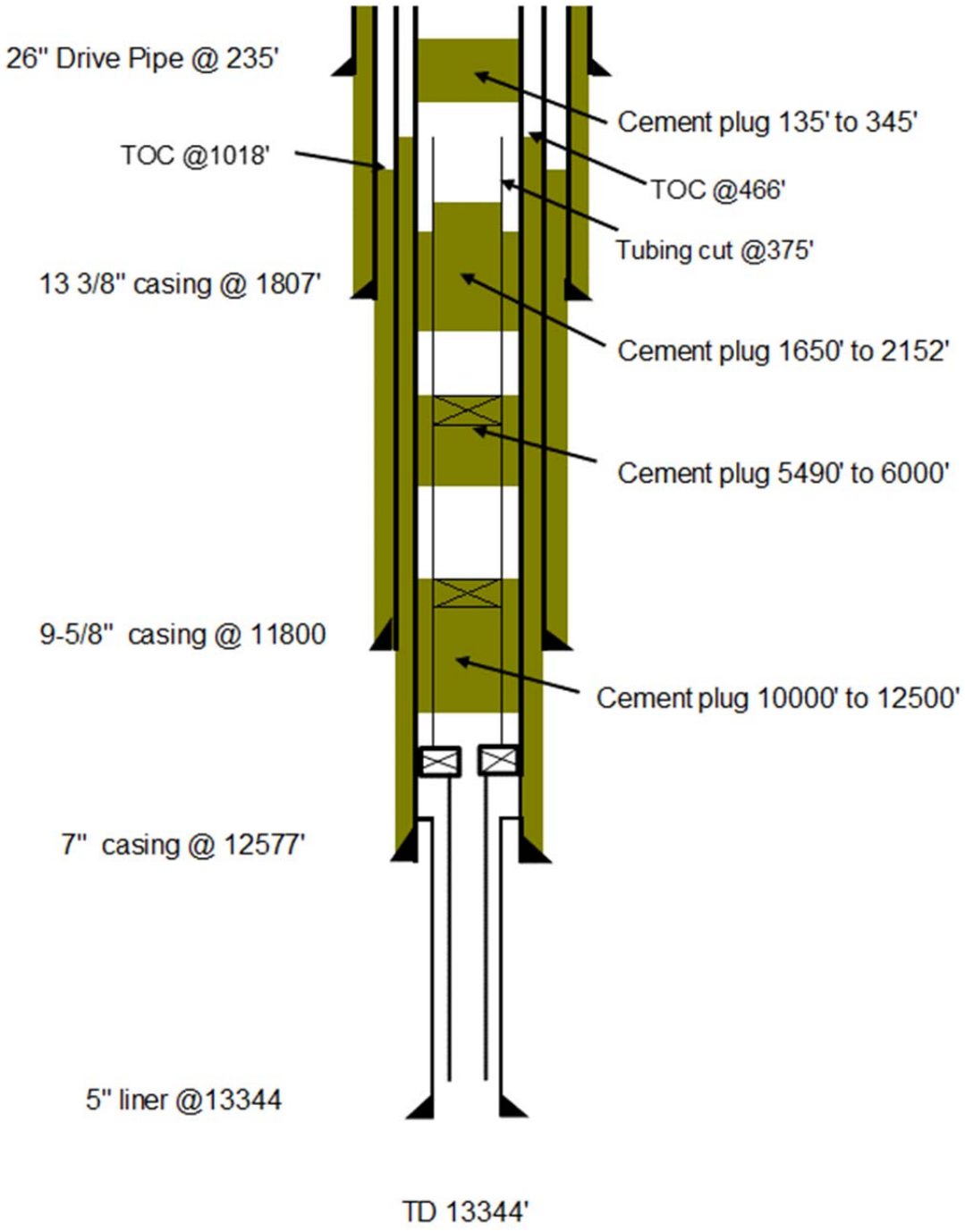

EnergyXXI 108-39

Denote cement

Current Wellbore Conditions

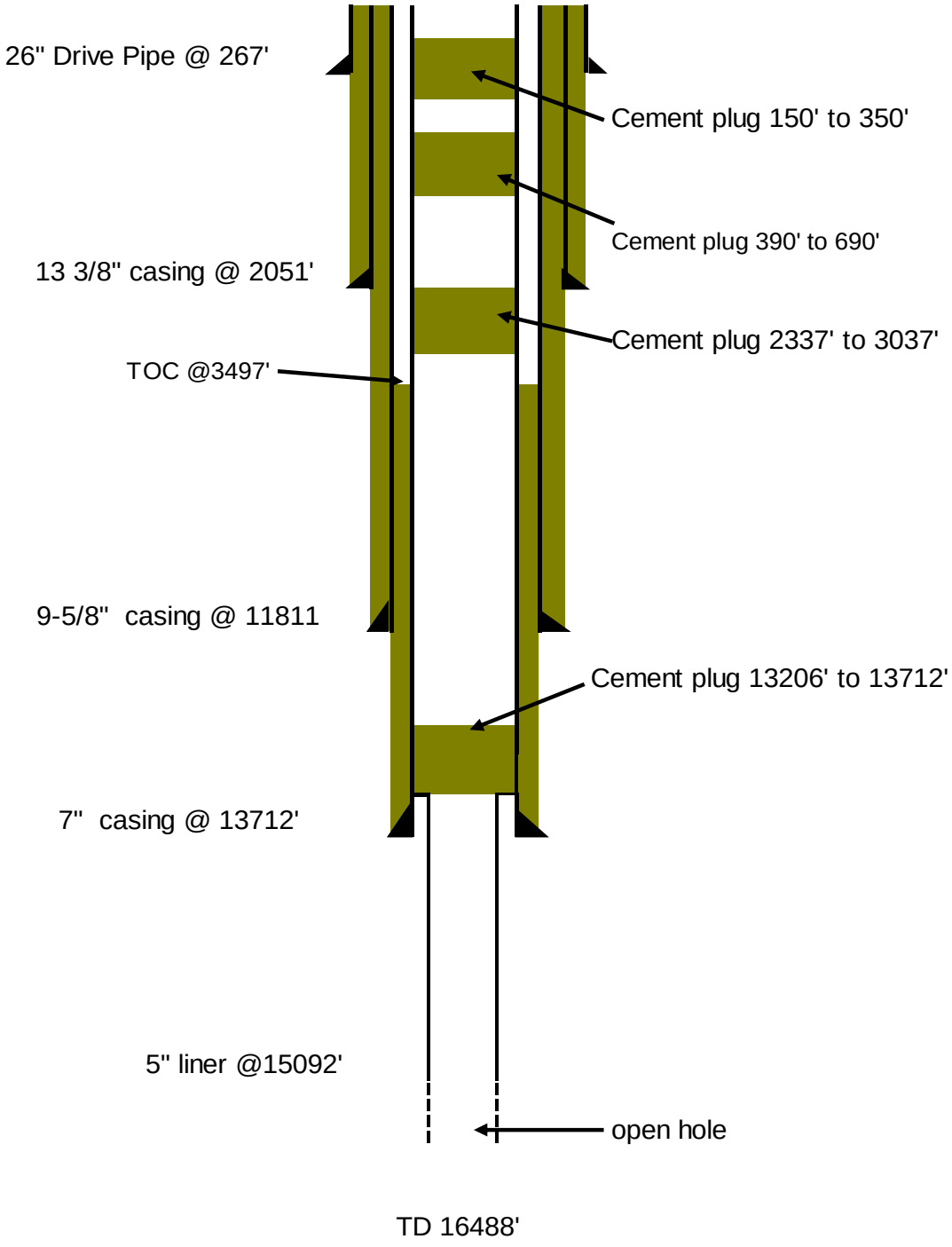

EnergyXXI 108-40

Denote cement

Current Wellbore Conditions

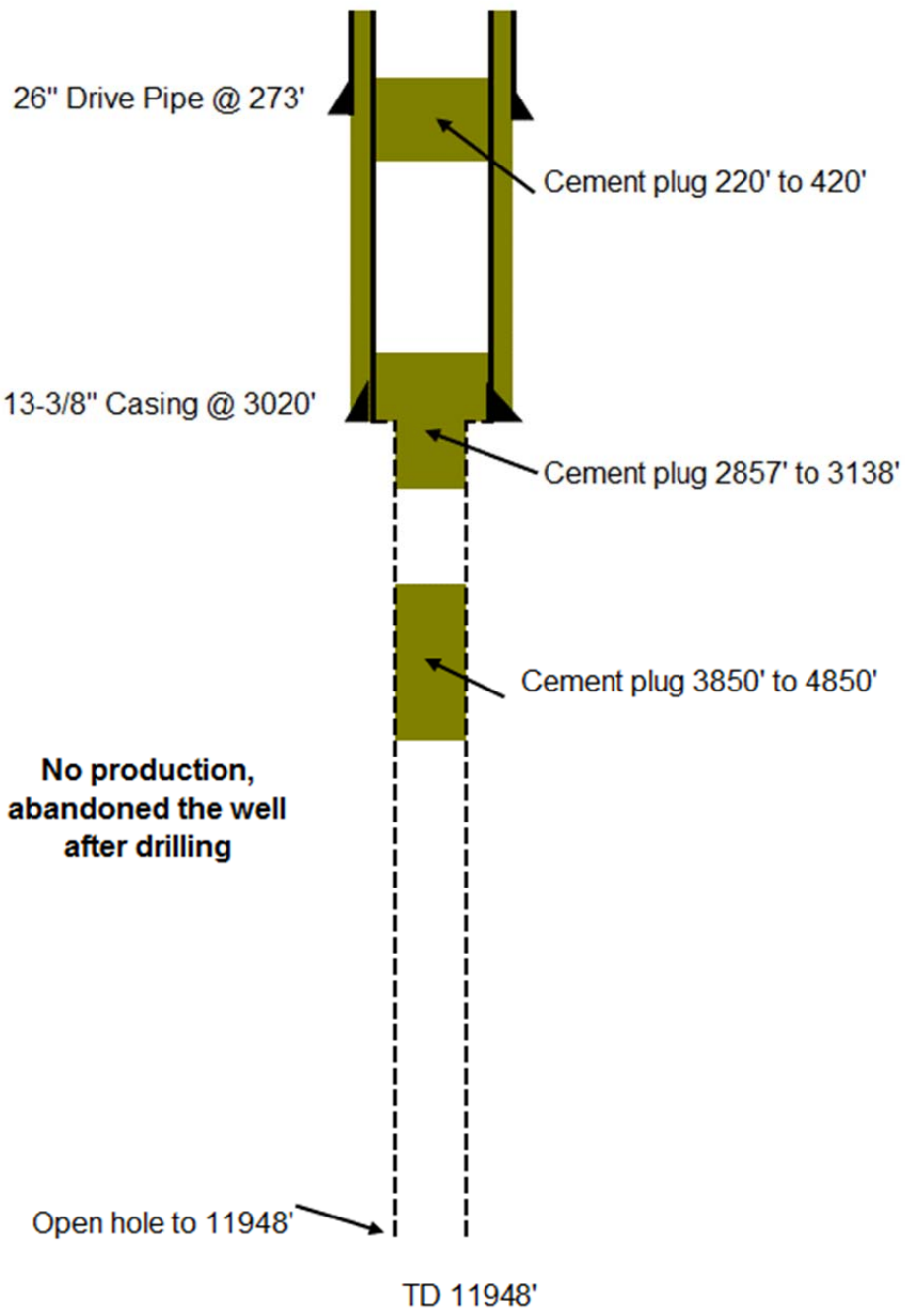

EnergyXXI 108-41

Denote cement

Current Wellbore Conditions

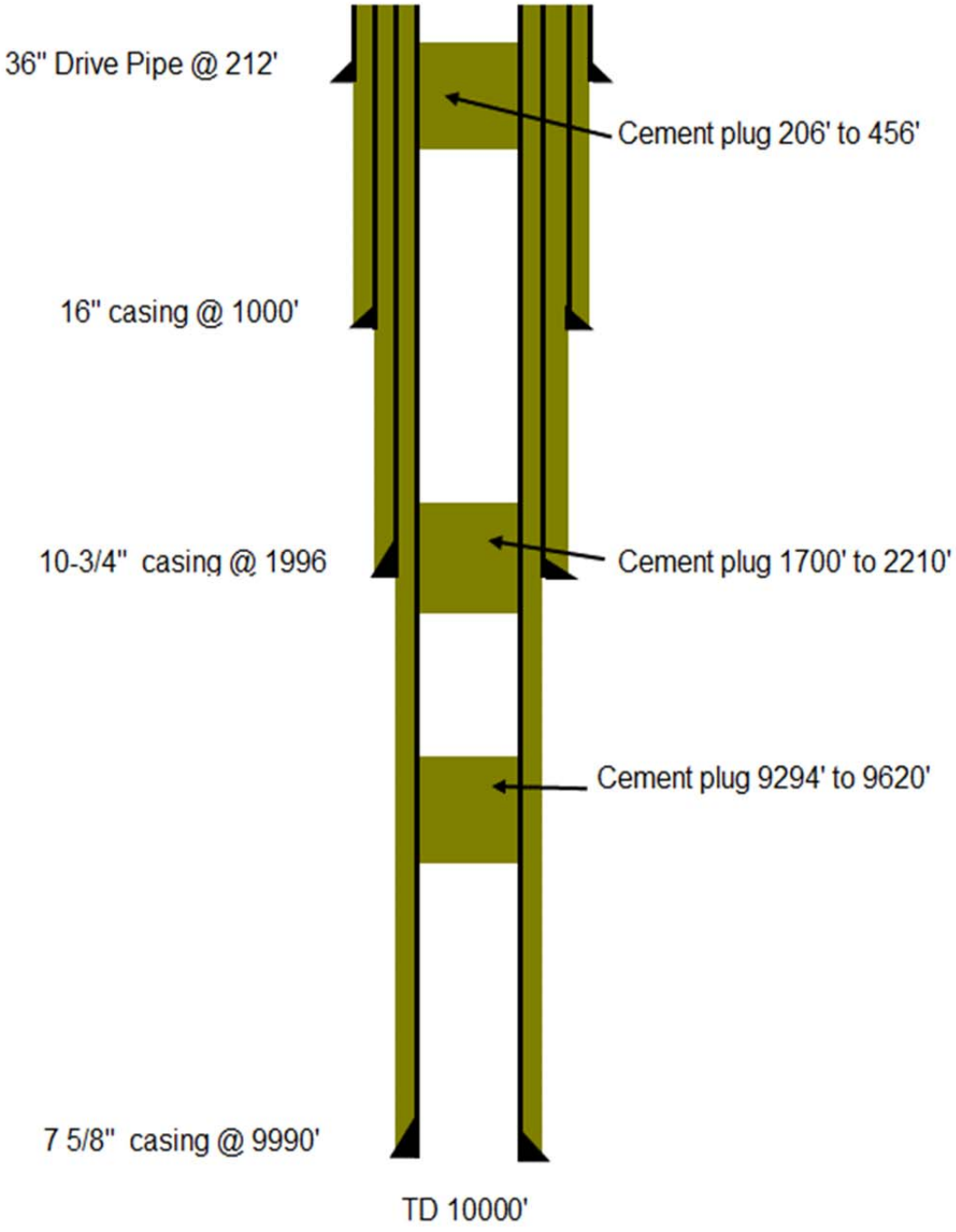

EnergyXXI 108-41 ST1

Denote cement

Current Wellbore Conditions

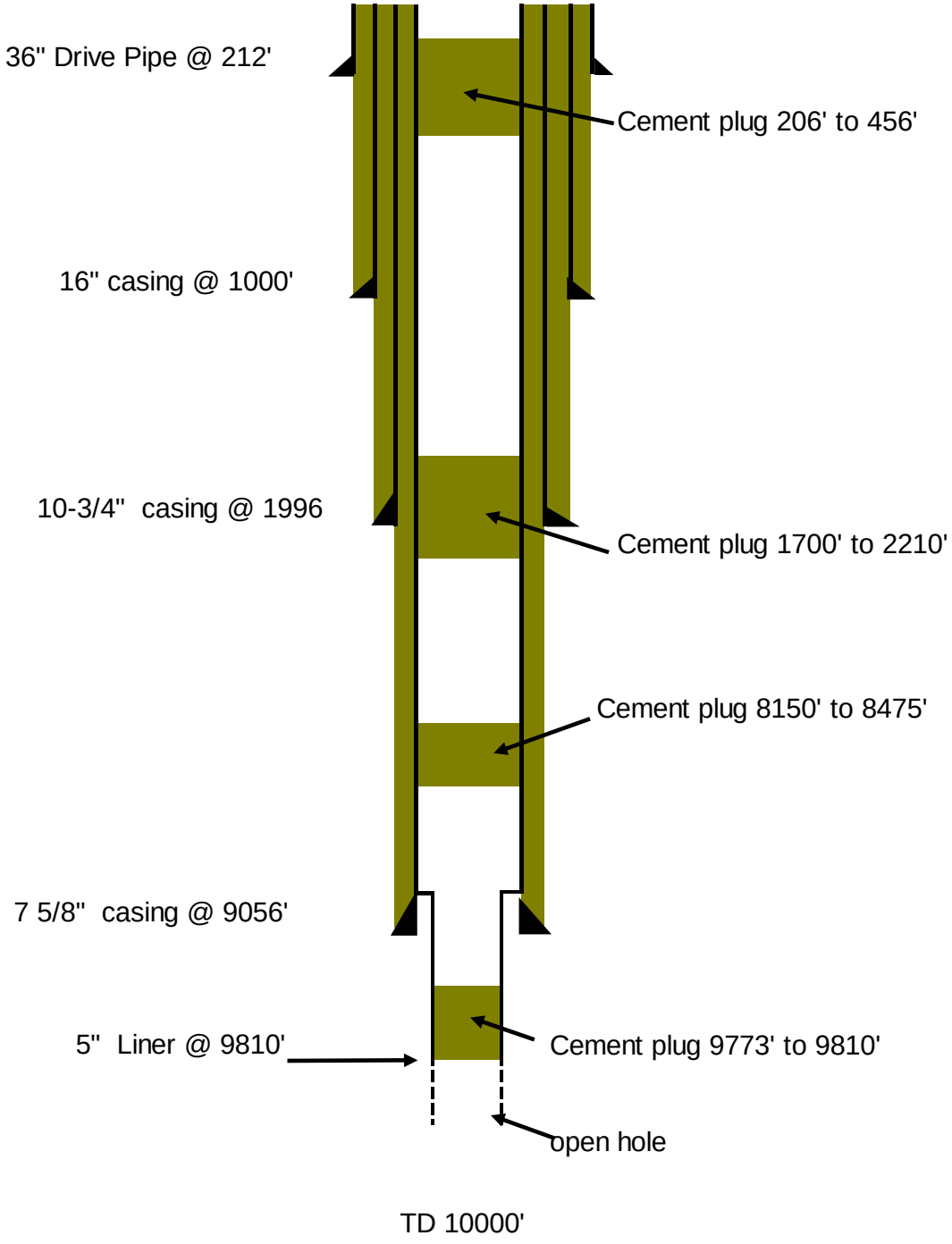

EnergyXXI 108-41 ST2

Denote cement

Current Wellbore Conditions

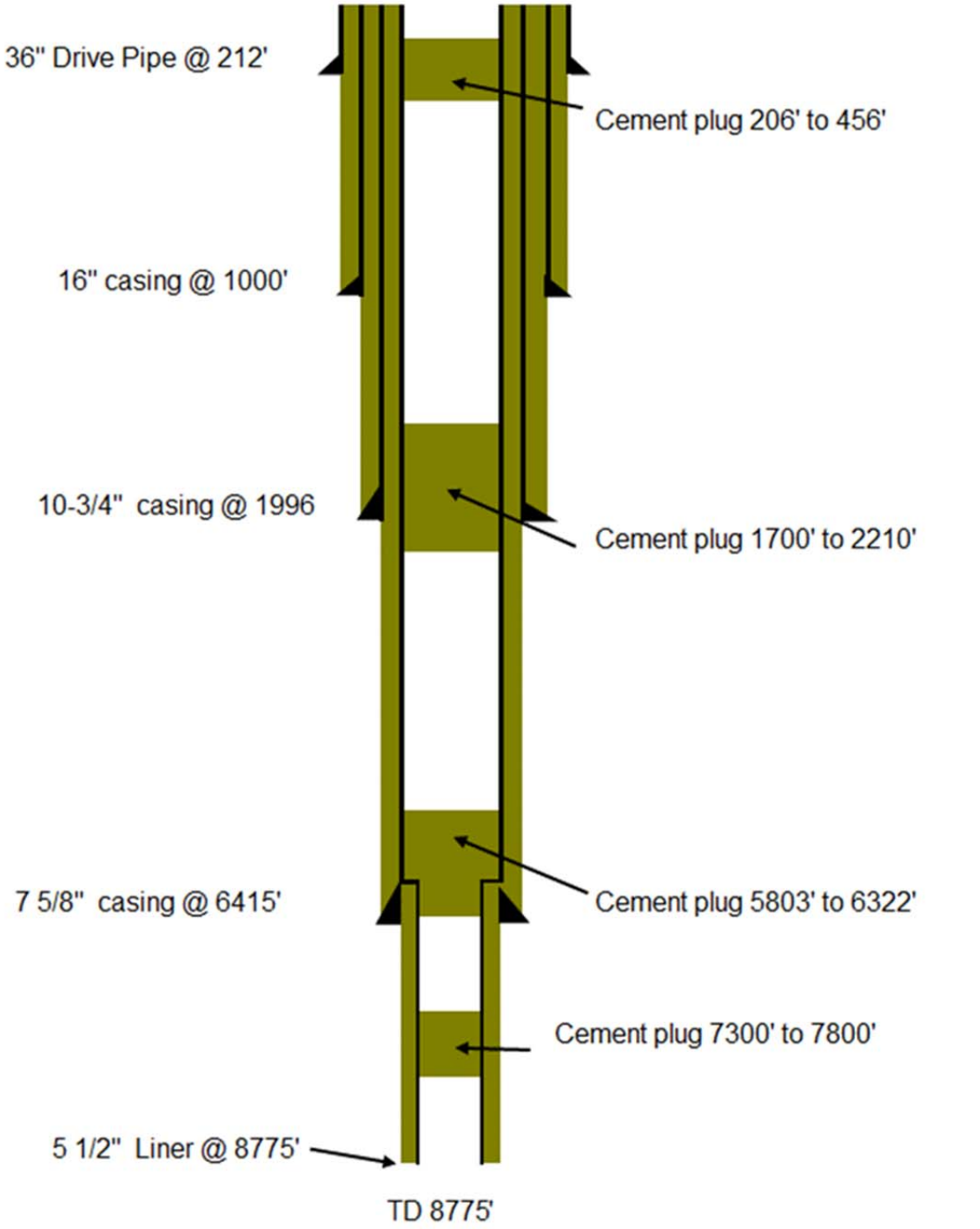

EnergyXXI 108-41 ST2BP1

Denote cement

Current Wellbore Conditions

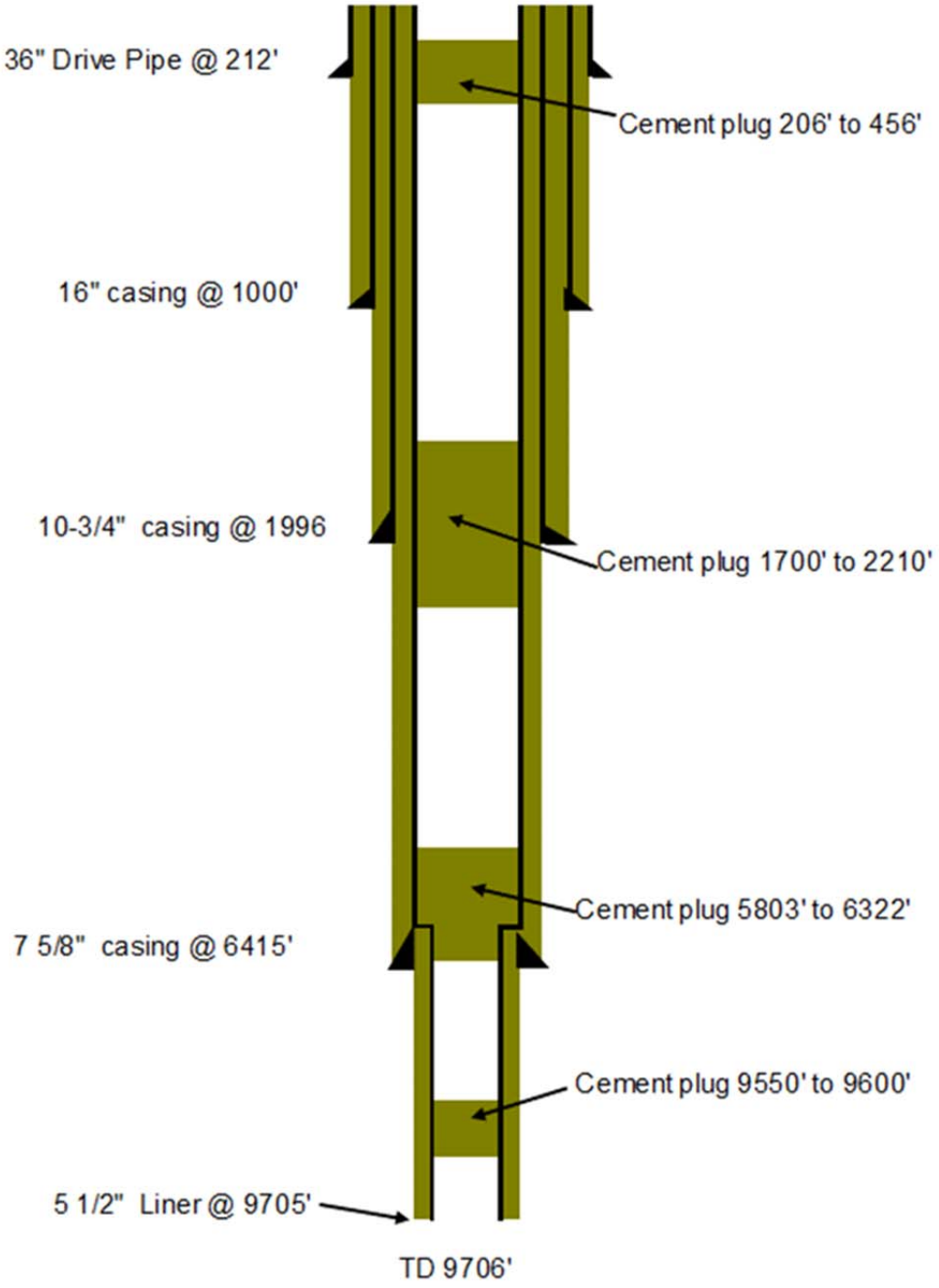

EnergyXXI 108-42

Denote cement

Current Wellbore Conditions

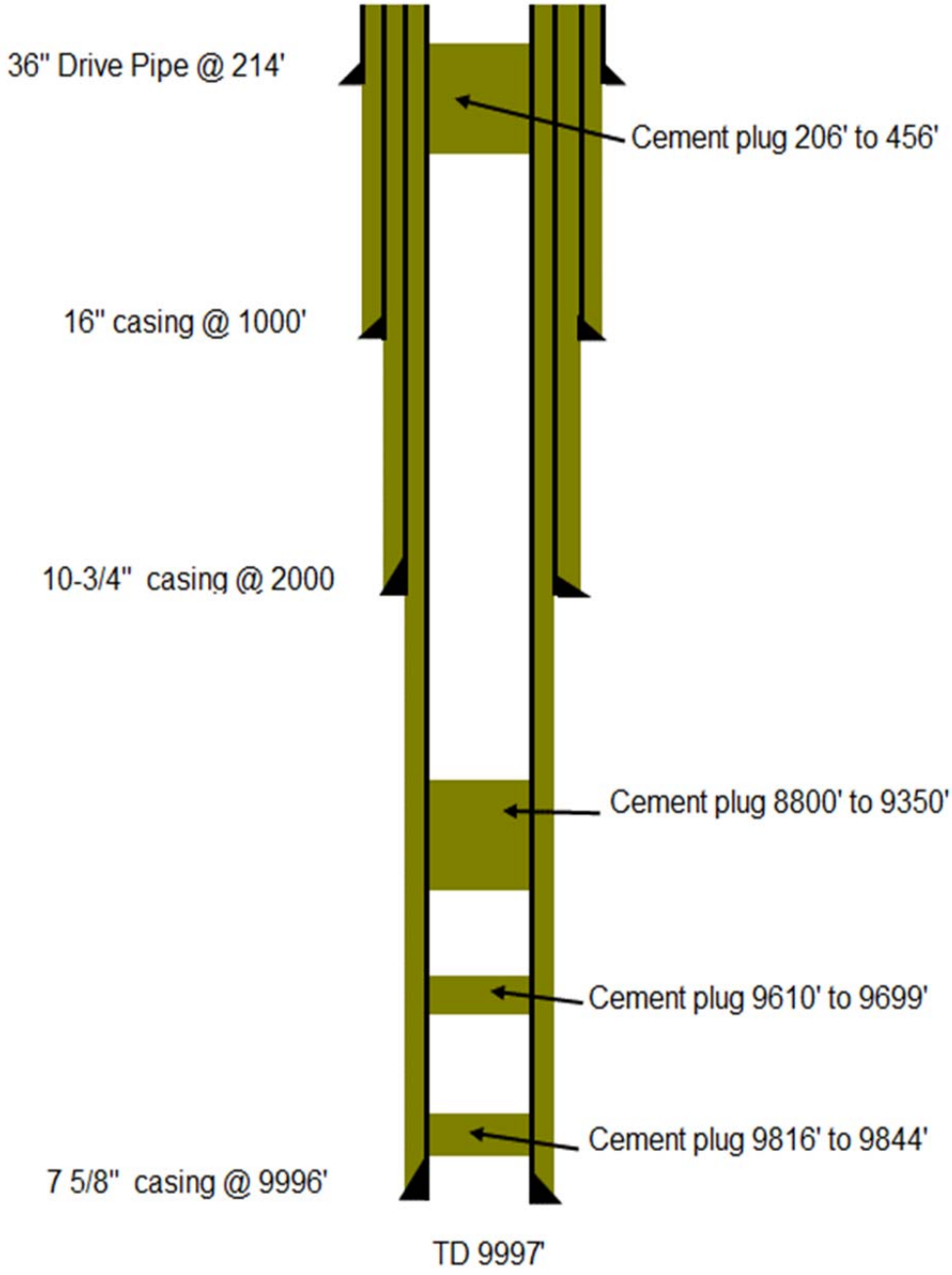

EnergyXXI 108-42 ST1

Denote cement

Current Wellbore Conditions

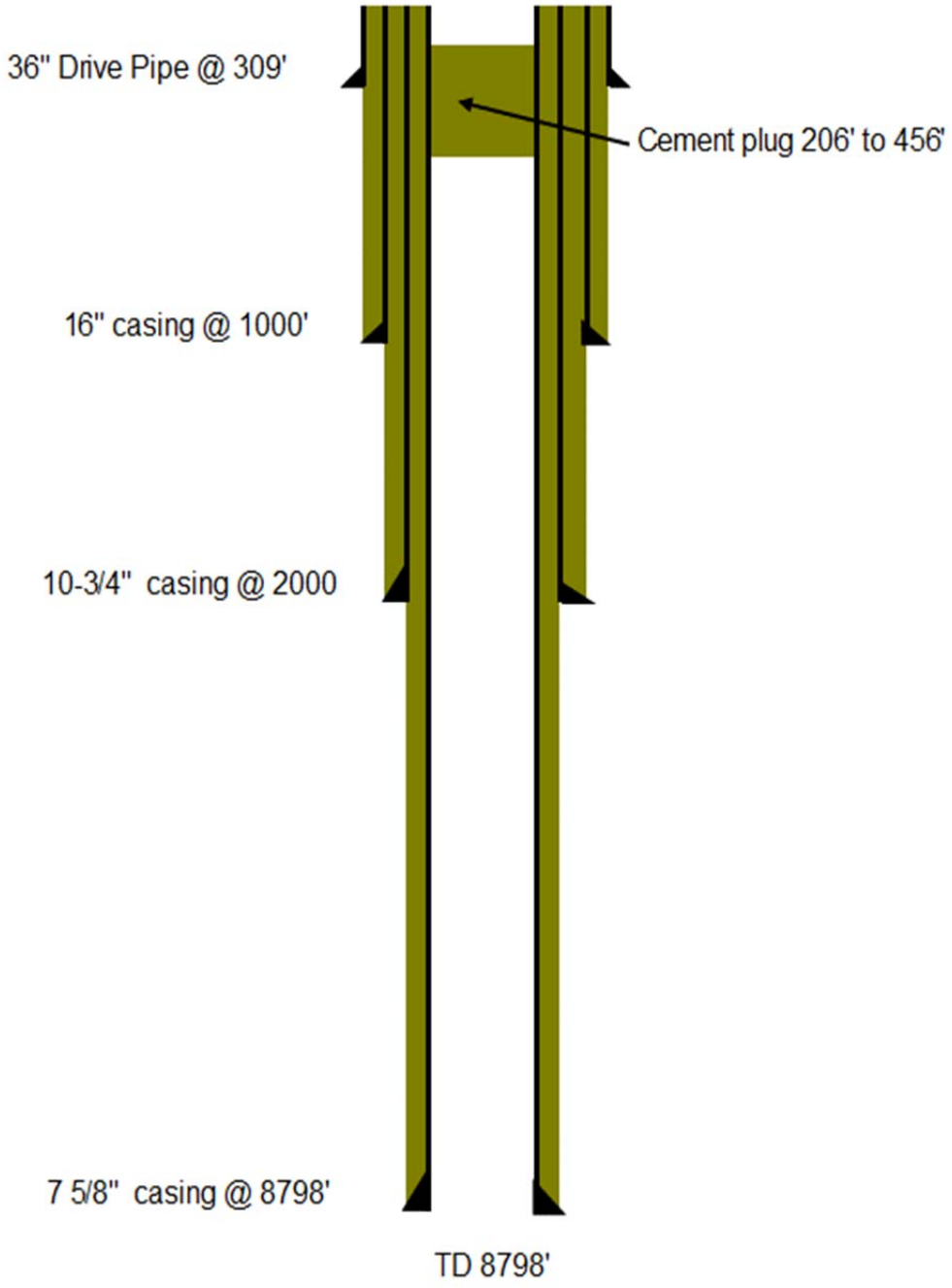

EnergyXXI 108-43

Denote cement

Current Wellbore Conditions

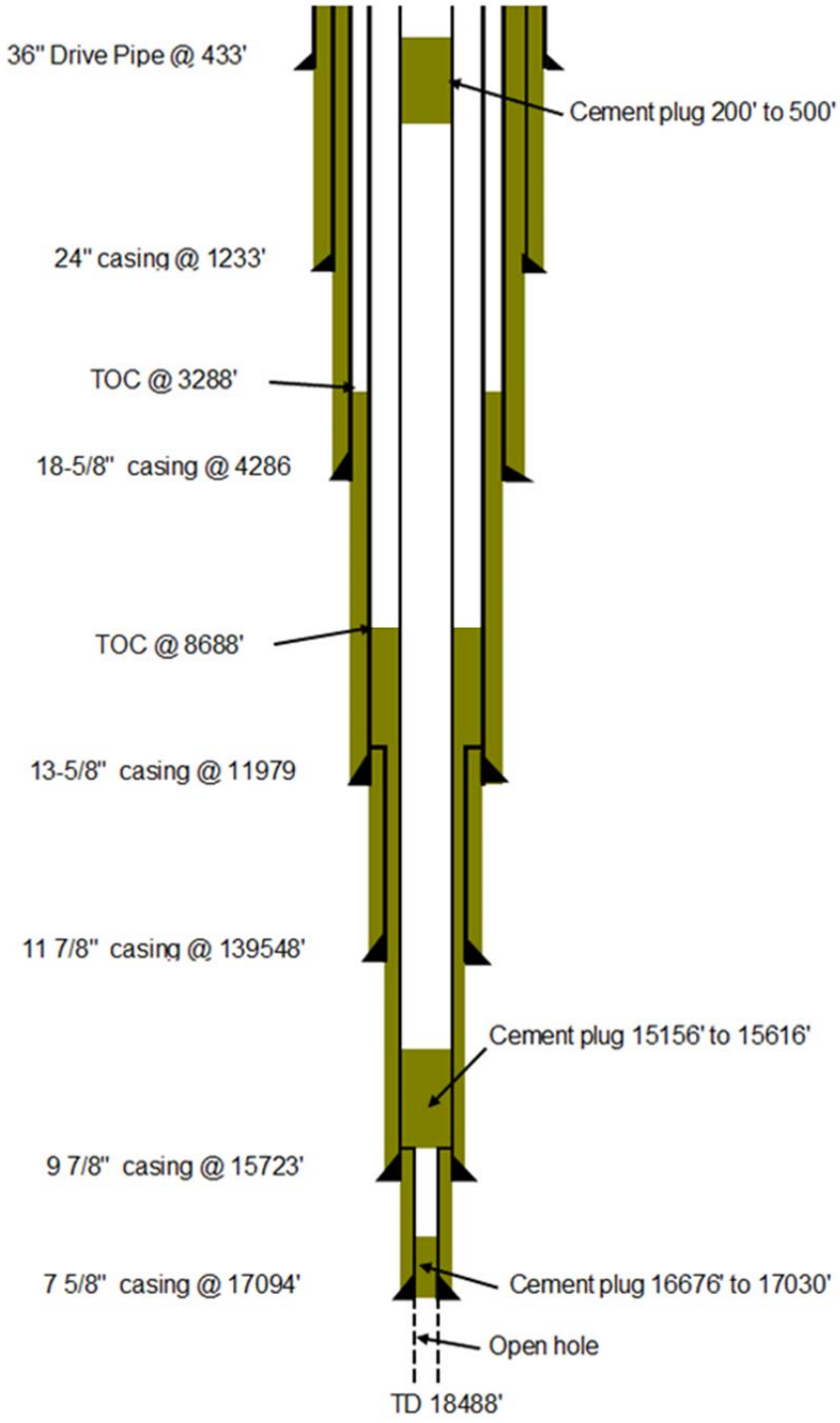

Appendix B: Pliocene Fluid Flow Non-isothermal Simulation Results for Ship Shoal Block 84

1.1 Pliocene Fluid Flow Non-isothermal Simulation results

Figure 1**Error! Reference source not found.**, Figure 4, Figure 7, Figure 10, Figure 13, and Figure 16 are showing the cross sections of gas saturation after 1 year, 15 years, and 30 years CO_2 injection, and after 30 years observation of the six non-isothermal scenarios respectively. We can see that CO_2 is contained within the injection formation both during injection and observation phase, except in scenario 84_P_sim09. 84_P_sim09 representing the most critical case which contains no capillary pressure in the sand, silt and shale, and the gas plume easily migrates upward during the injection and causes leakage in the observation phase.

Figure 2, Figure 5, Figure 8, Figure 11, Figure 14, and Figure 17 are showing the cross sections of temperature after 1 year, 15 years, and 30 years CO_2 injection, and after 30 years observation of the six non-isothermal scenarios respectively. We can see that low temperature plume grows at injection interval during injection as we are injecting CO_2 at 60 ^{0}C, and its temperature increases during observation.

Figure 3, Figure 6, Figure 9, Figure 12, Figure 15, and Figure 18 indicate the top view of the CO_2 gas plume after 30 years injection and another 30 years of observation for the six non-isothermal scenarios. The gas plumes increase slightly during the observation phase, and they are all contained within about the 1 mile radius around the injection well.

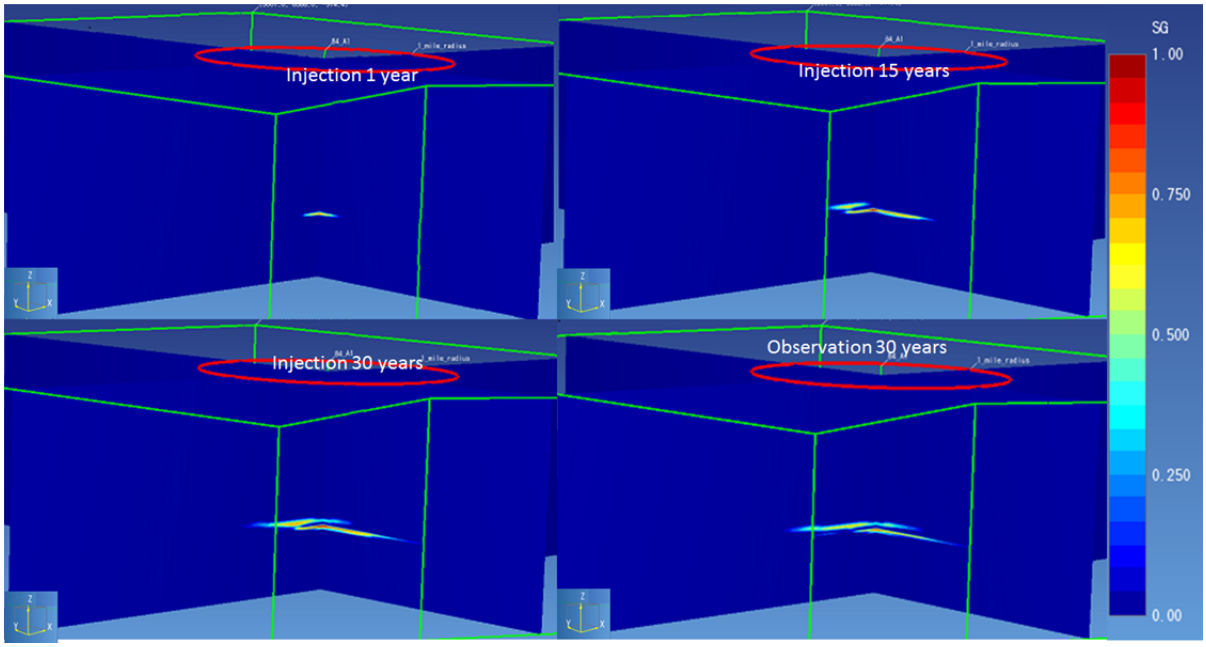

Figure 1 The cross-sections of Gas Saturation after 1, 15, 30 years injection, and 30 years observation, baseline case (84_P_sim07) of Pliocene-non-isothermal, Ship Shoal Block 84 field

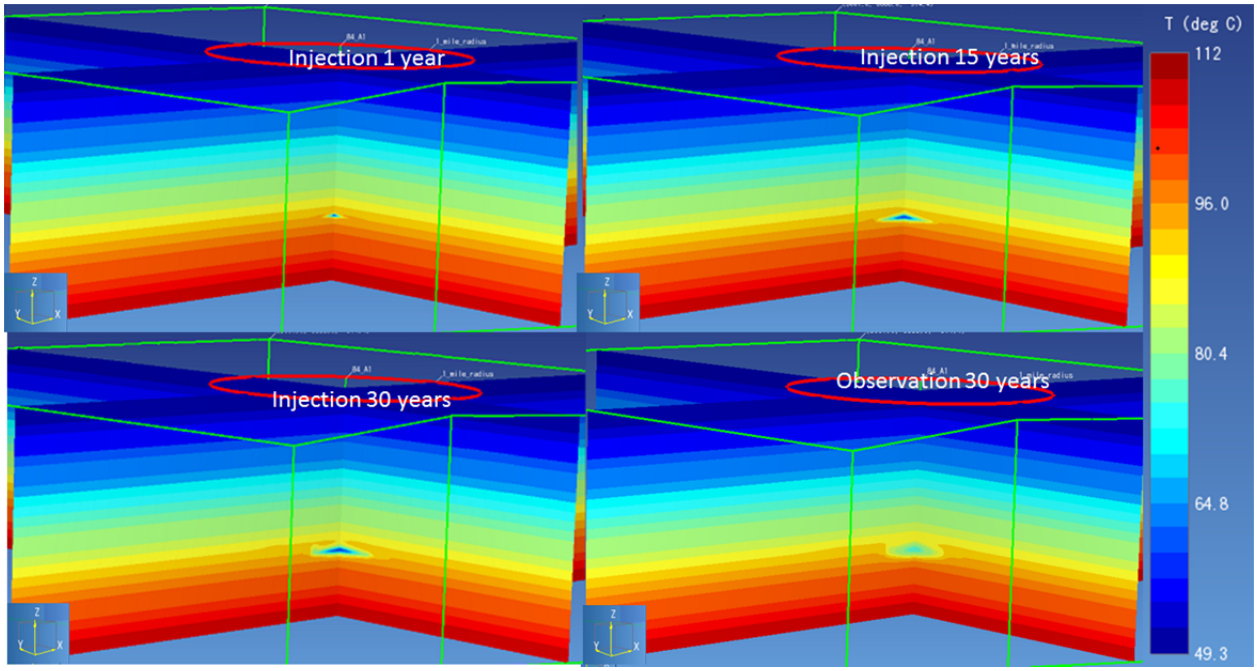

Figure 2 The cross-sections of temperature after 1, 15, 30 years injection, and 30 years observation, baseline case (84_P_sim07) of Pliocene-non-isothermal, Ship Shoal Block 84 field

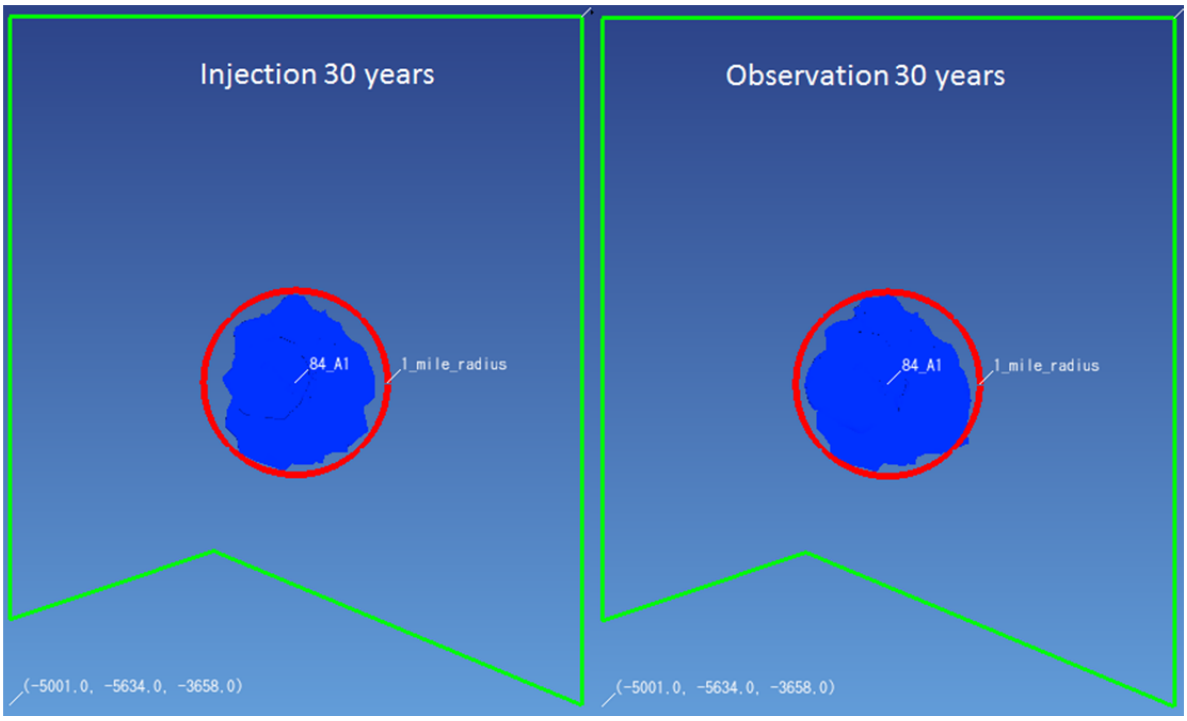

Figure 3 The top view of CO2 Gas plume after 30 years injection, and 30 years observation, baseline case (84_P_sim07) of Pliocene-non-isothermal, Ship Shoal Block 84 field

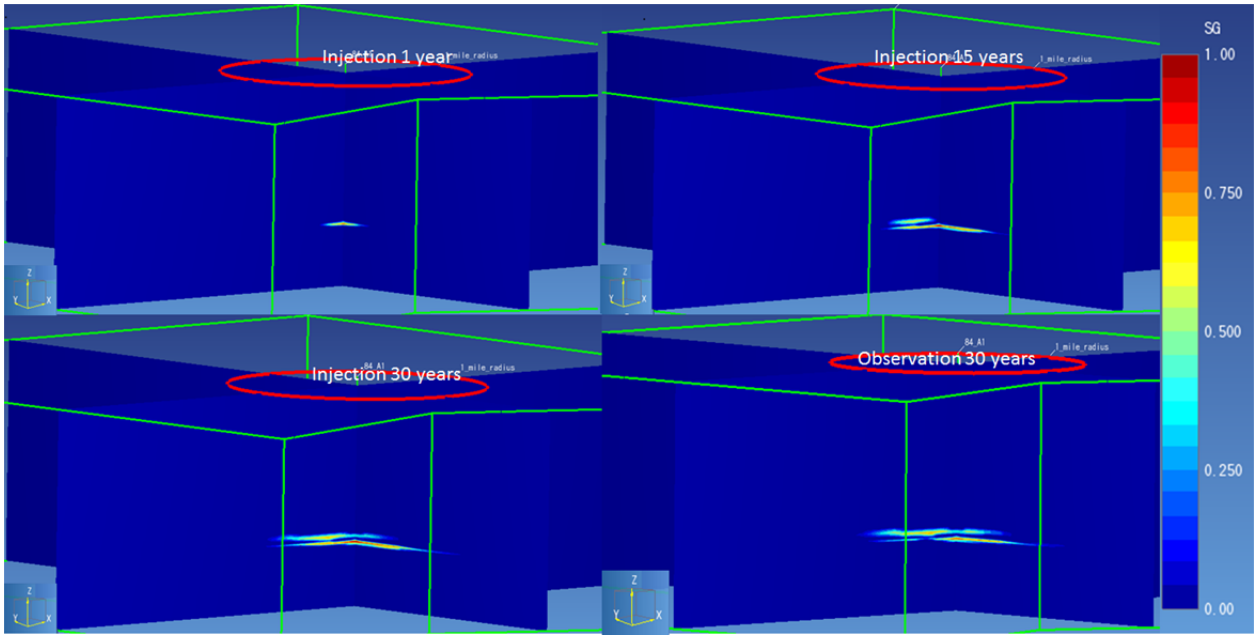

Figure 4 The cross-sections of Gas Saturation after 1, 15, 30 years injection, and 30 years observation (84_P_sim08) of Pliocene-non-isothermal, Ship Shoal Block 84 field

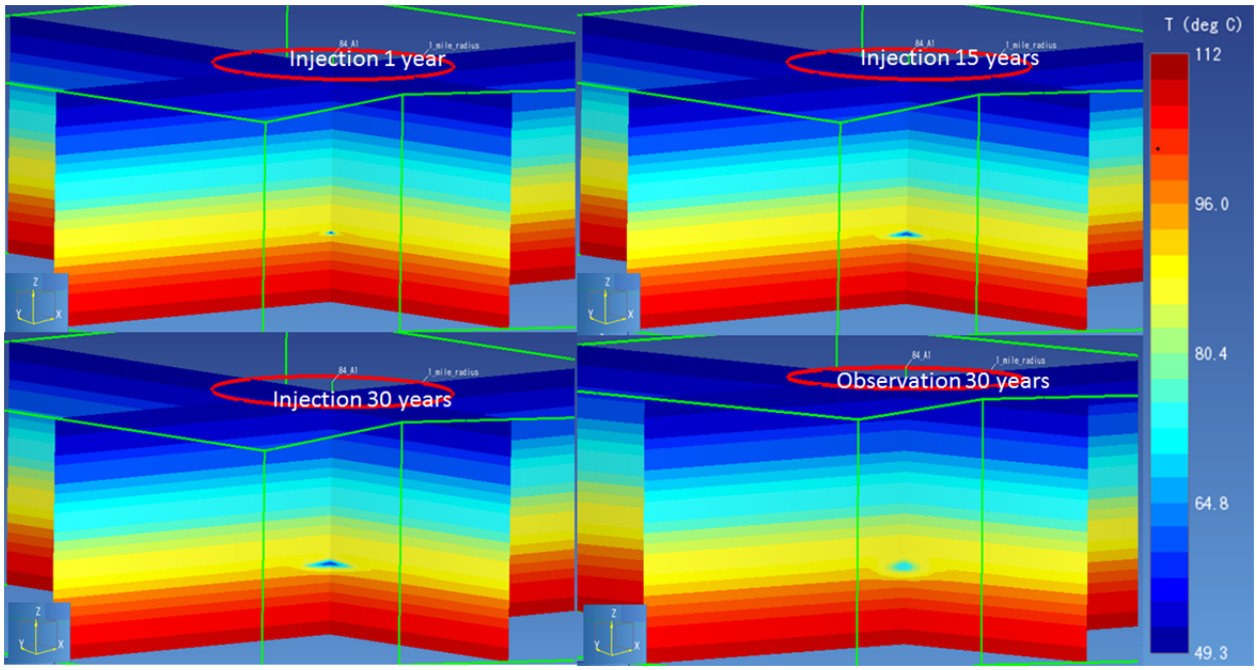

Figure 5 The cross-sections of temperature after 1, 15, 30 years injection, and 30 years observation, (84_P_sim08) of Pliocene-non-isothermal, Ship Shoal Block 84 field

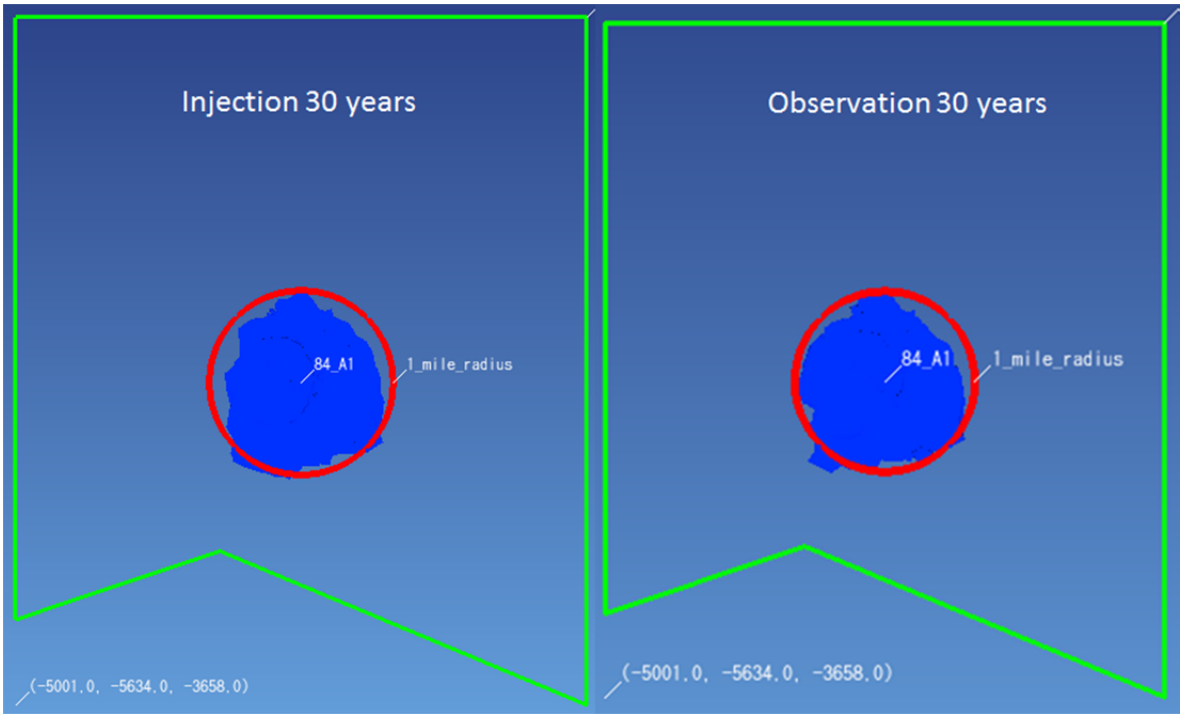

Figure 6 The top view of CO2 Gas plume after 30 years injection, and 30 years observation, (84_P_sim08)of Pliocene-non-isothermal, Ship Shoal Block 84 field

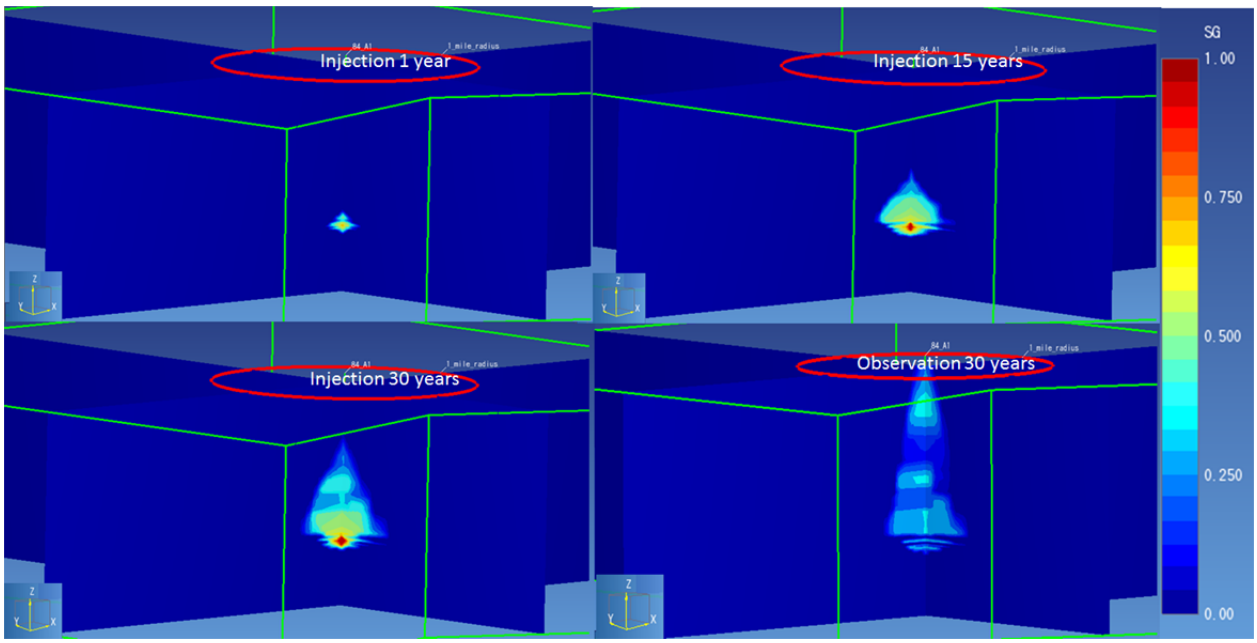

Figure 7 The cross-sections of Gas Saturation after 1, 15, 30 years injection, and 30 years observation, (84_P_sim09) of Pliocene-non-isothermal, Ship Shoal Block 84 field

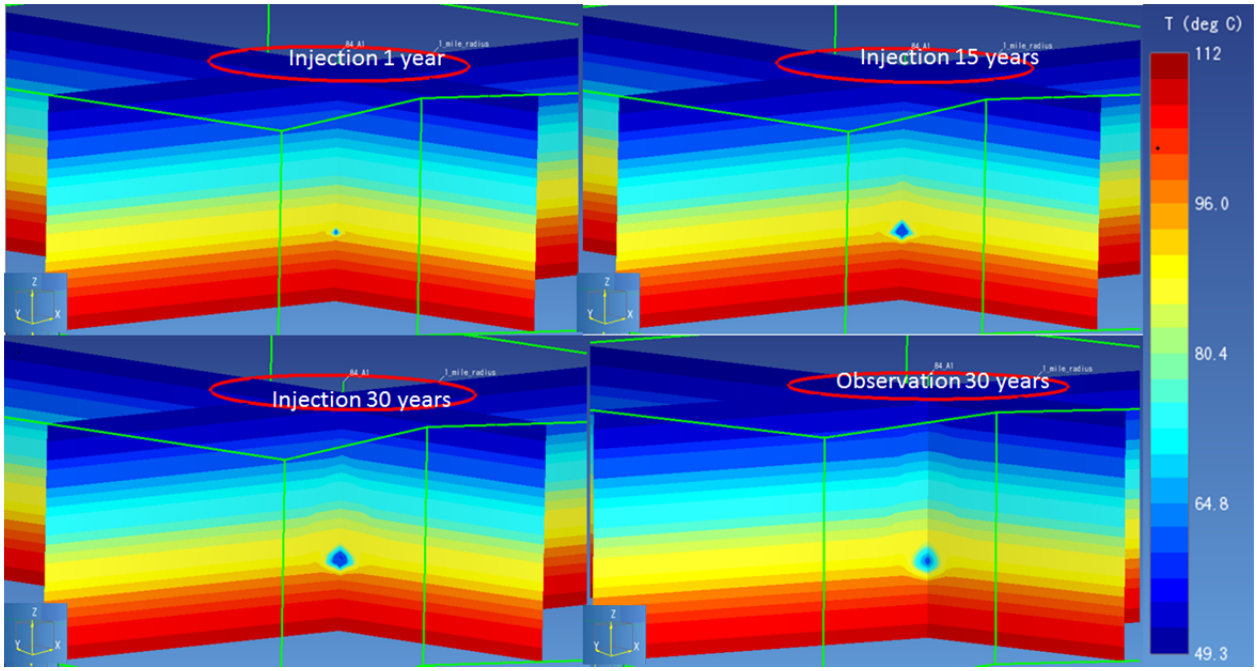

Figure 8 The cross-sections of temperature after 1, 15, 30 years injection, and 30 years observation, (84_P_sim09) of Pliocene-non-isothermal, Ship Shoal Block 84 field

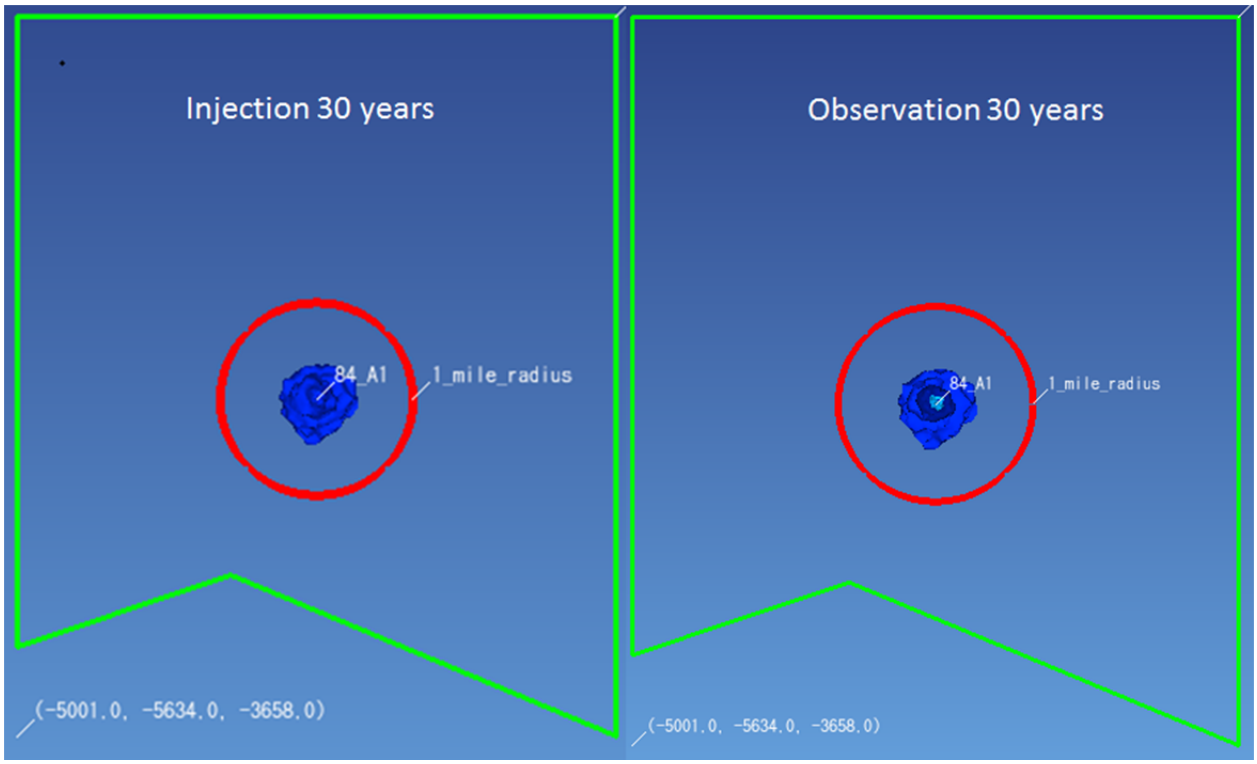

Figure 9 The top view of CO2 Gas plume after 30 years injection, and 30 years observation, (84_P_sim09) of Pliocene-non-isothermal, Ship Shoal Block 84 field

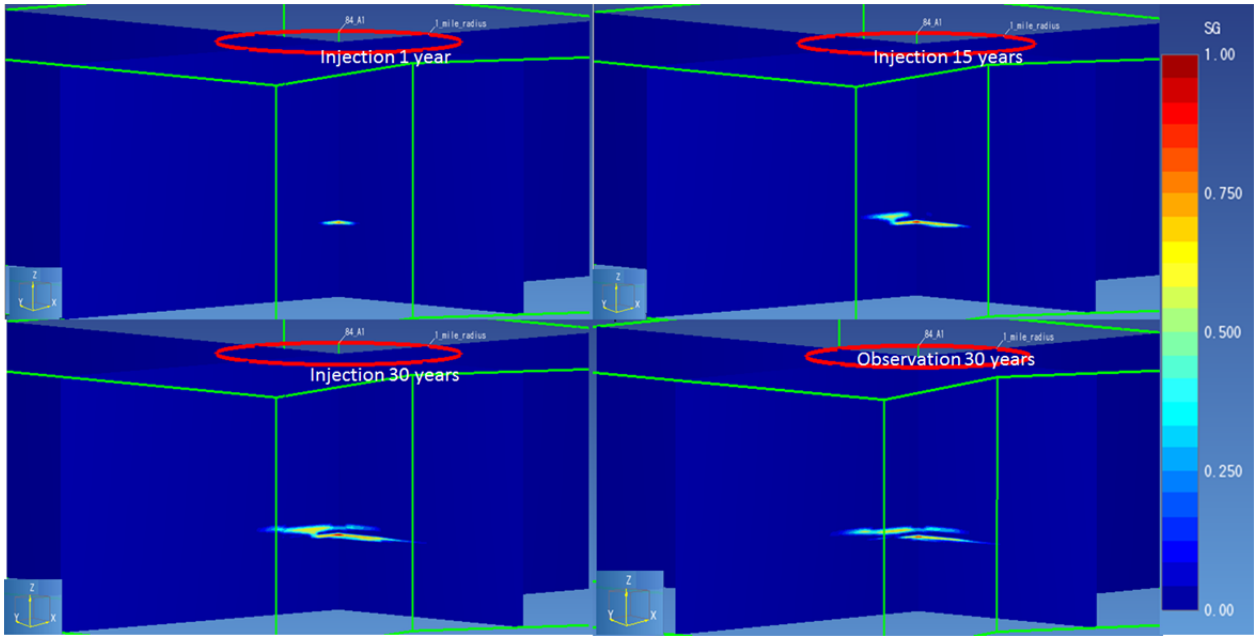

Figure 10 The cross-sections of Gas Saturation after 1, 15, 30 years injection, and 30 years observation, (84_P_sim10) of Pliocene-non-isothermal, Ship Shoal Block 84 field

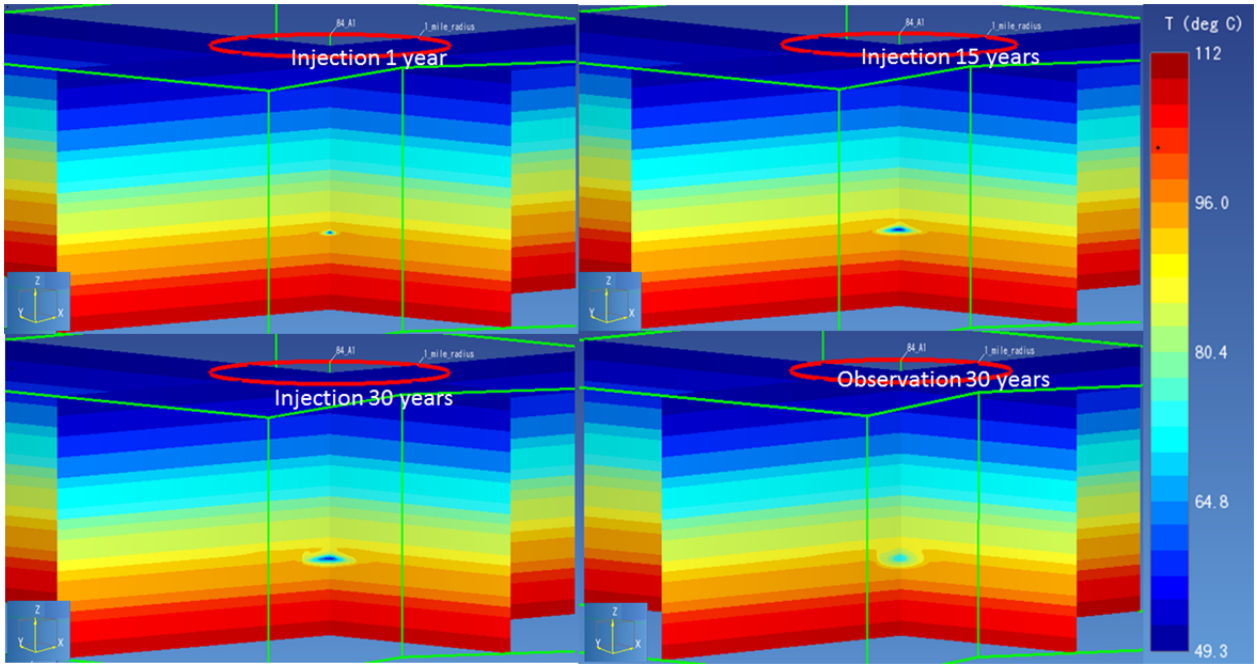

Figure 11 The cross-sections of temperature after 1, 15, 30 years injection, and 30 years observation, (84_P_sim10) of Pliocene-non-isothermal, Ship Shoal Block 84 field

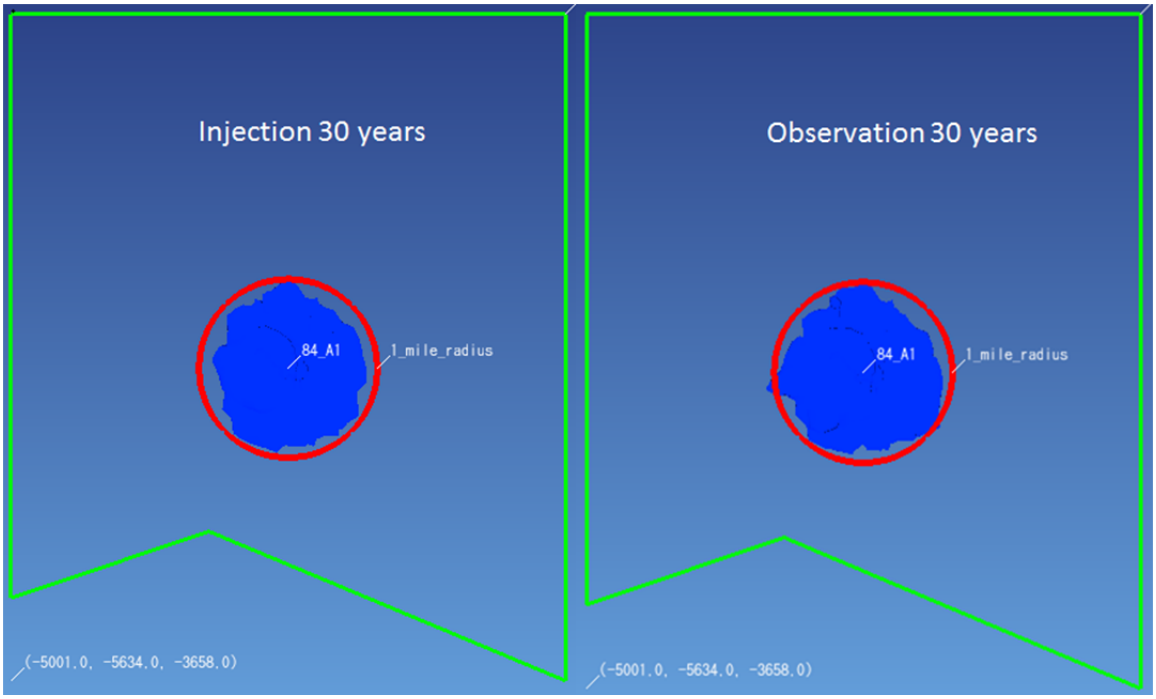

Figure 12 The top view of CO2 Gas plume after 30 years injection, and 30 years observation, (84_P_sim10) of Pliocene-non-isothermal, Ship Shoal Block 84 field

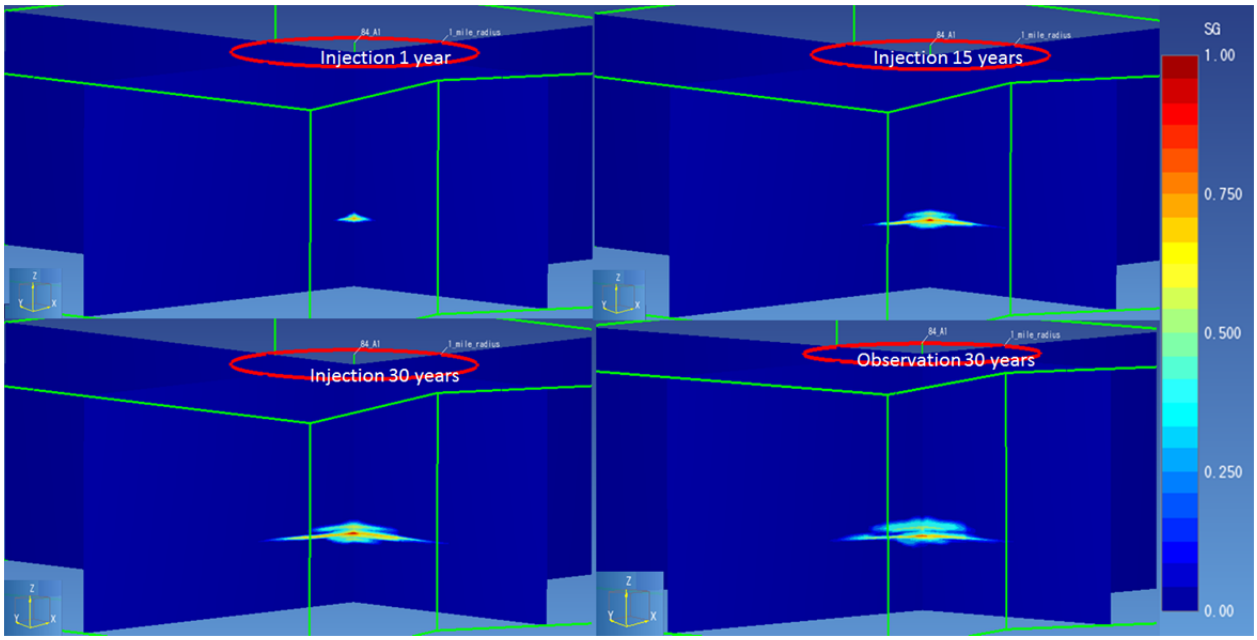

Figure 13 The cross-sections of Gas Saturation after 1, 15, 30 years injection, and 30 years observation, (84_P_sim11) of Pliocene-non-isothermal, Ship Shoal Block 84 field

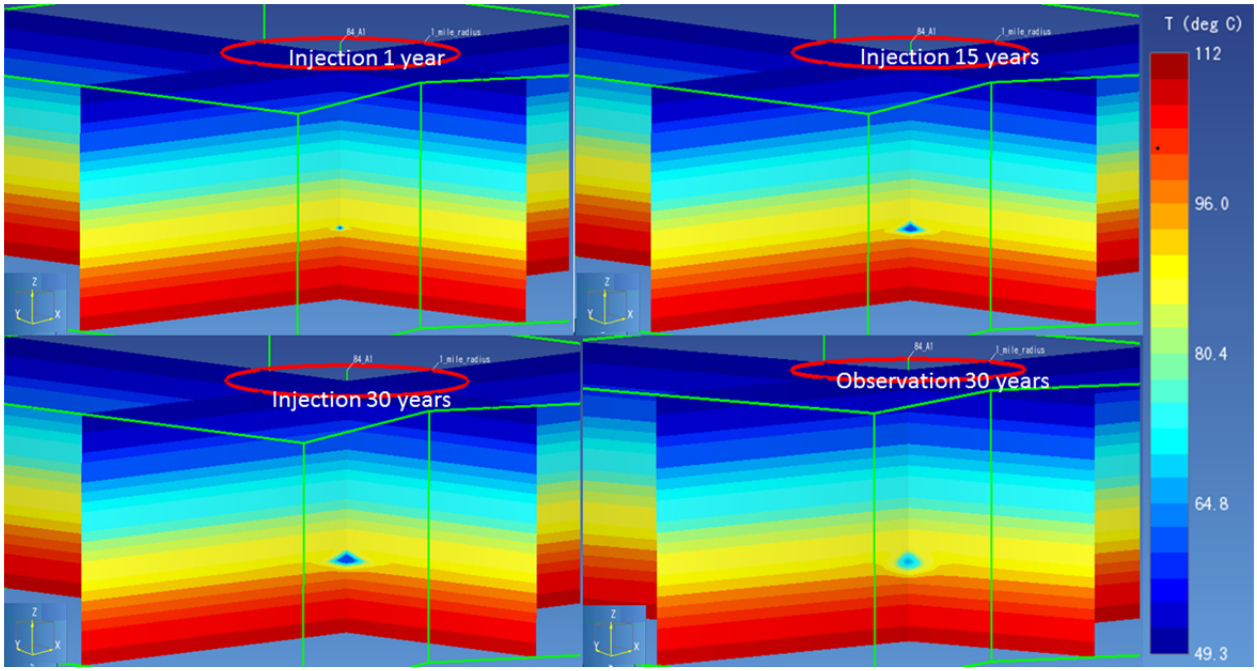

Figure 14 The cross-sections of temperature after 1, 15, 30 years injection, and 30 years observation, (84_P_sim11) of Pliocene-non-isothermal, Ship Shoal Block 84 field

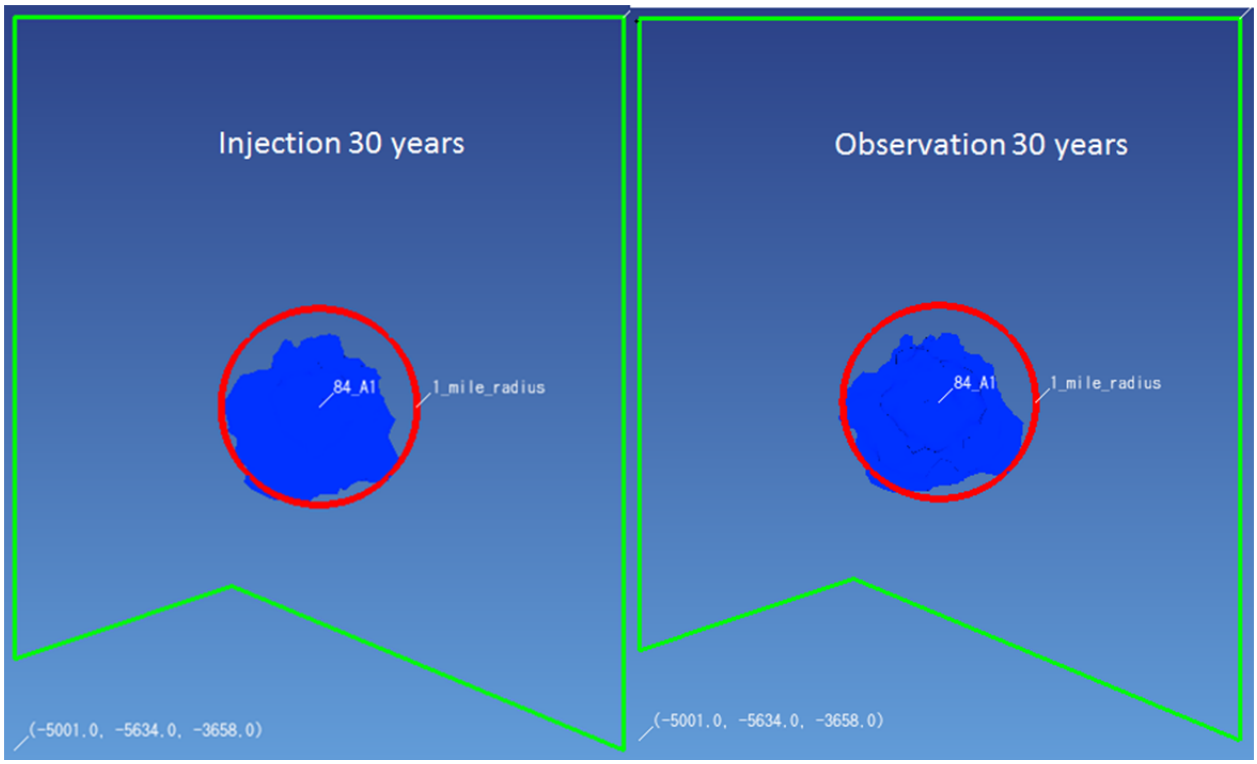

Figure 15 The top view of CO2 Gas plume after 30 years injection, and 30 years observation, (84_P_sim11) of Pliocene-non-isothermal, Ship Shoal Block 84 field

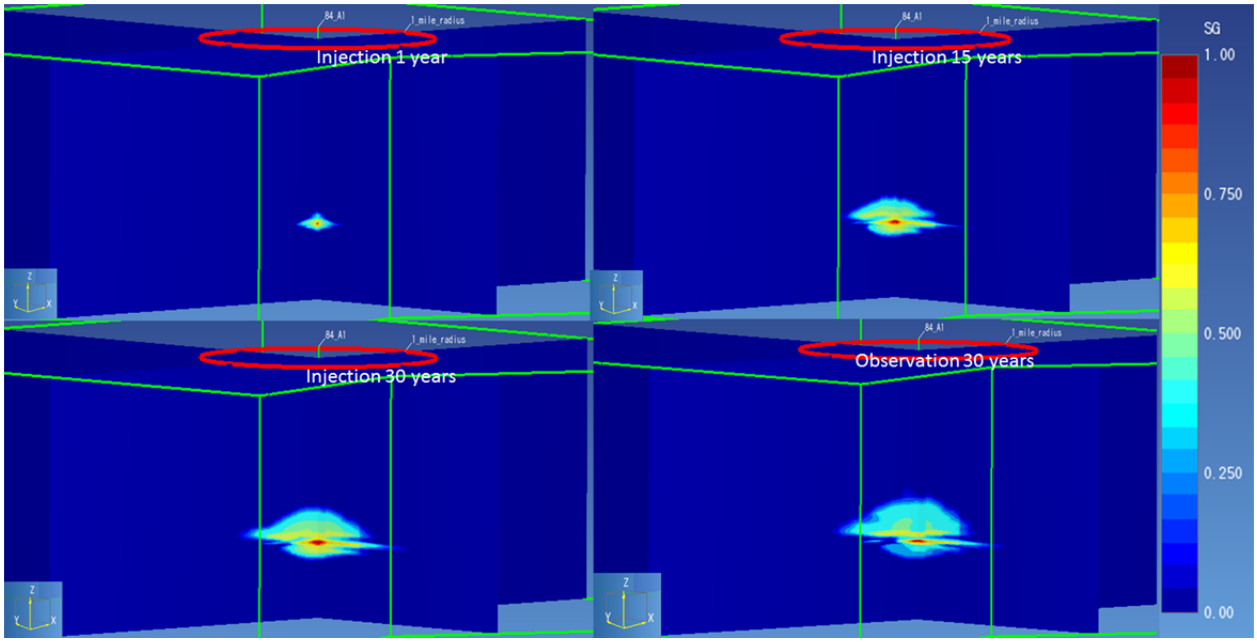

Figure 16 The cross-sections of Gas Saturation after 1, 15, 30 years injection, and 30 years observation, (84_P_sim12) of Pliocene-non-isothermal, Ship Shoal Block 84 field

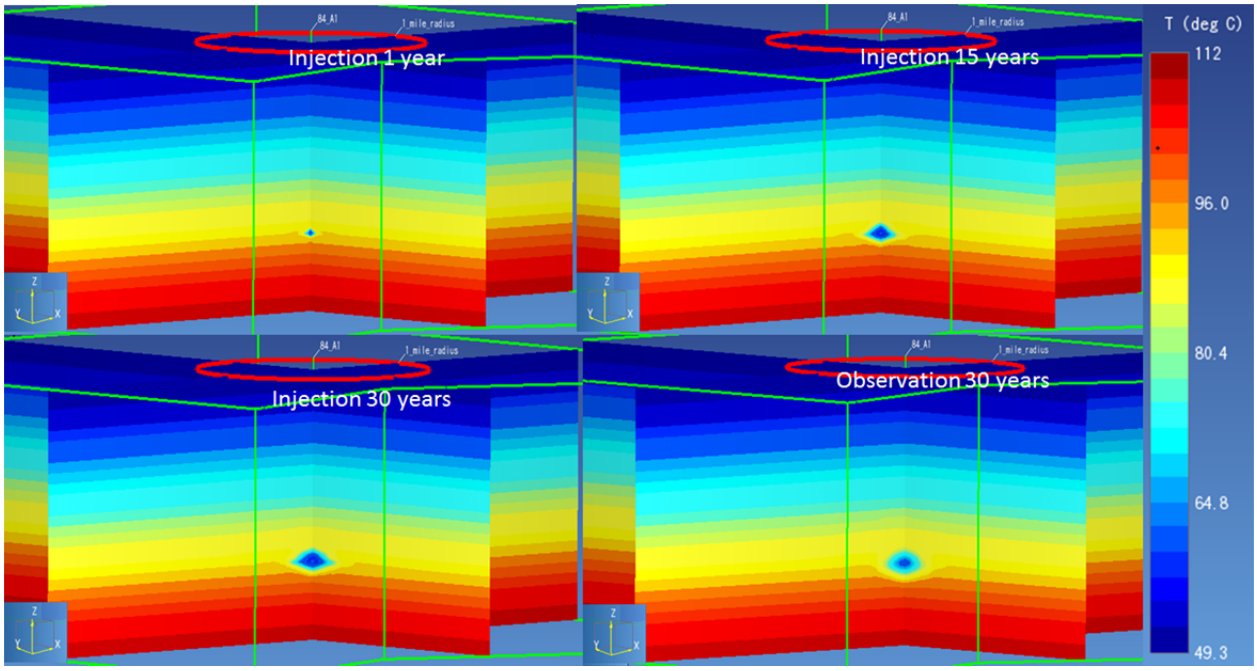

Figure 17 The cross-sections of temperature after 1, 15, 30 years injection, and 30 years observation, (84_P_sim12) of Pliocene-non-isothermal, Ship Shoal Block 84 field

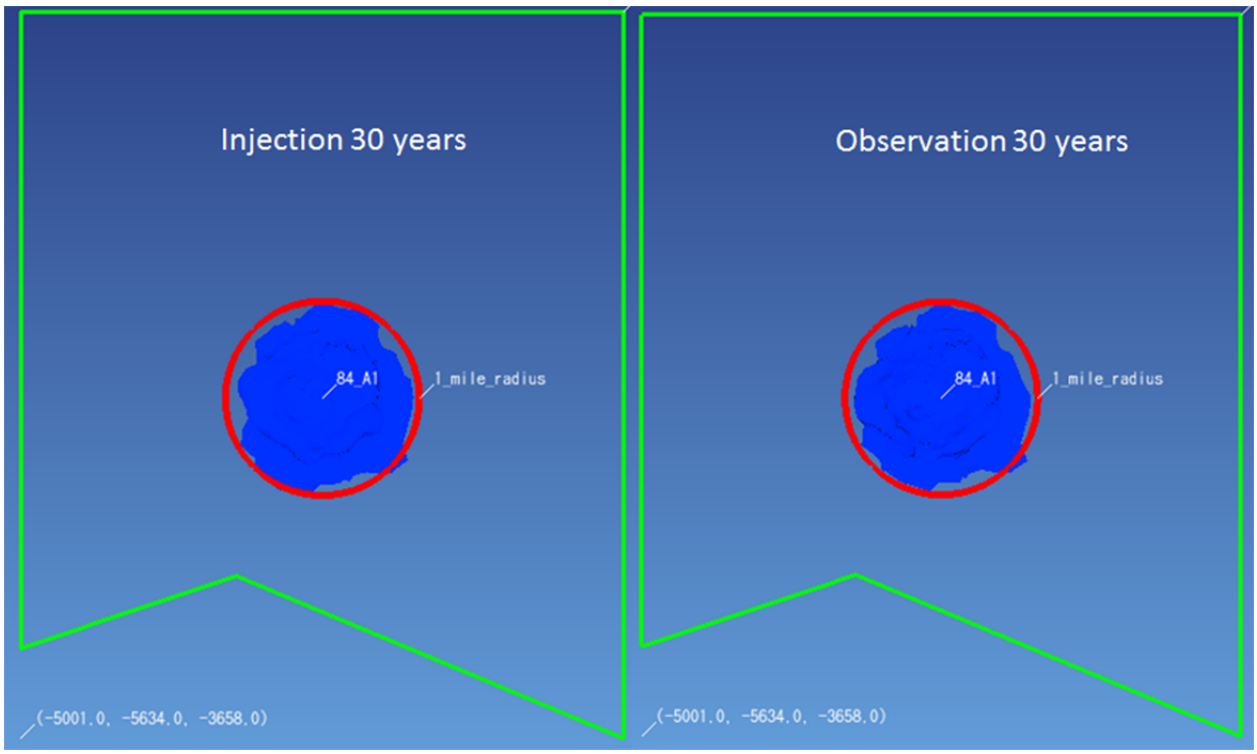

Figure 18 The top view of CO2 Gas plume after 30 years injection, and 30 years observation, (84_P_sim12) of Pliocene-non-isothermal, Ship Shoal Block 84 field

Figure 19 indicates the comparison of pressure profiles across the injection well through the middle of the injection interval (=-2860.5m), at in-situ conditions and after 30 years of injection of the six non-isothermal scenarios. We can see that 84_P_sim12 (double injection rate) reaches higher pressure after 30 years constant rate of CO_2 injection, and 84_P_sim09 (contains no capillary pressure) has the lowest pressure after 30 years of constant CO_2 injection. 84_P_sim08 has higher pressure than 84_P_sim07, while the pressure at the injection well is lower in scenario 84_P_sim10 (sandy model) than 84_P_sim11 (contains more shale).

Figure 20 plots the comparison of temperature profiles across the injection well through the middle of the injection interval (=-2860.5m), at in-situ conditions and after 30 years of injection of the six non-isothermal scenarios. We can see that the temperature fixed at 60 ^{0}C at wellbore for all scenarios during injection, and 84_P_sim12 (double injection rate) has lower temperature profile around injection well after 30 years constant rate of CO_2 injection, and 84_P_sim09 (contains no capillary pressure) has the highest temperature profile around injection

well after 30 years of constant CO_2 injection. 84_P_sim07, 84_P_sim08, 84_P_sim10 and 84_P_sim11 have similar temperature profiles around injection well.

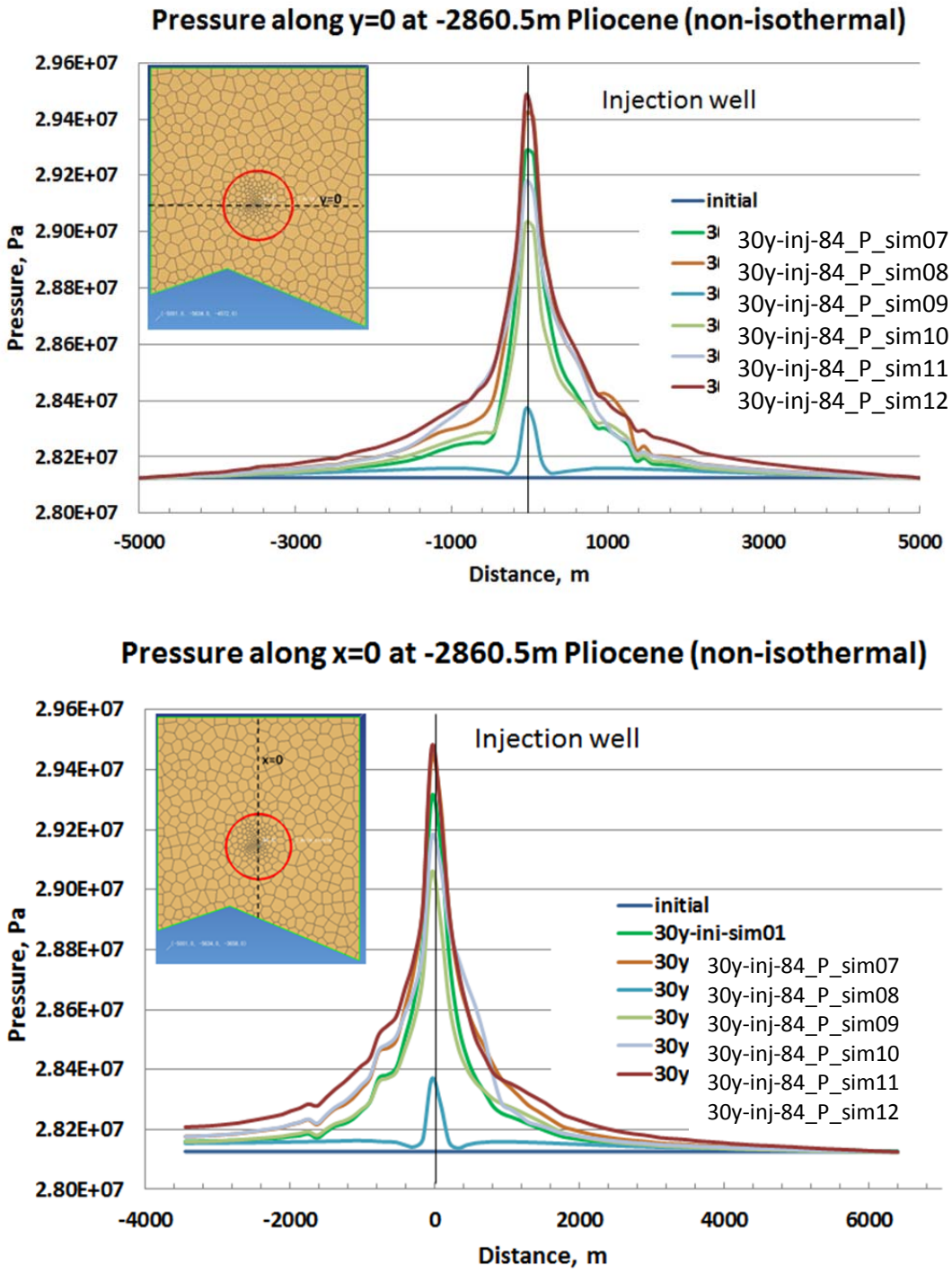

Figure 19 Comprison of pressure profiles across injection well through the middle of injection interval, at initial and after 30 years injection into the Pliocene-non-isothermal – Ship Shoal Block 84 field

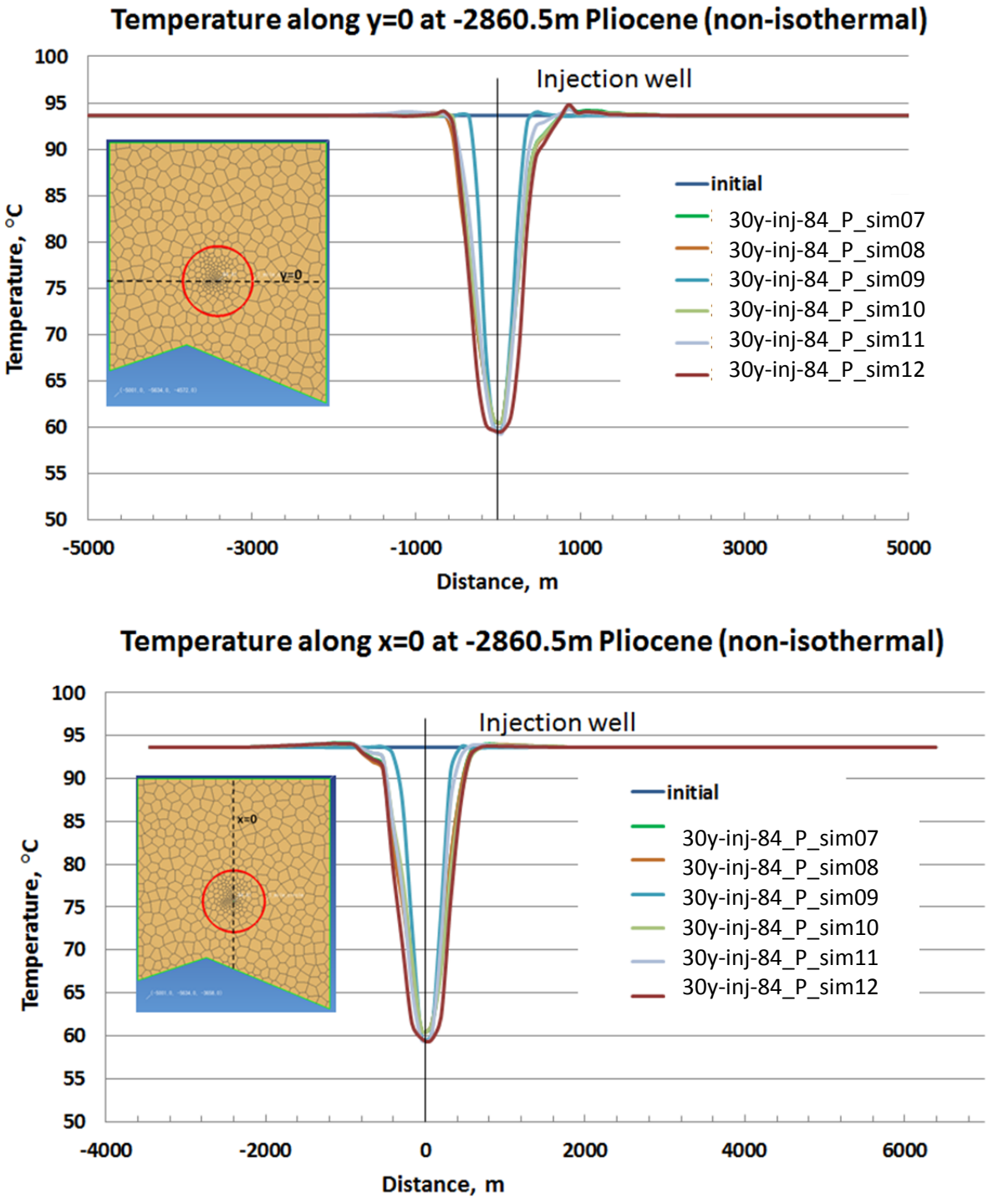

Figure 20 Comprison of temperature profiles across injection well through the middle of injection interval, at initial and after 30 years injection into the Pliocene-non-isothermal – Ship Shoal Block 84 field

Figure 21 to Figure 26 compare the pressure profiles across injection well through middle of injection interval (=-2860.5 m), after 30 years of injection of each scenario respectively, between the isothermal and non-isothermal effects. For all simulations, we can see that the pressure profiles with non-isothermal effect are slightly higher than isothermal around injection well, and the difference is within 1%.

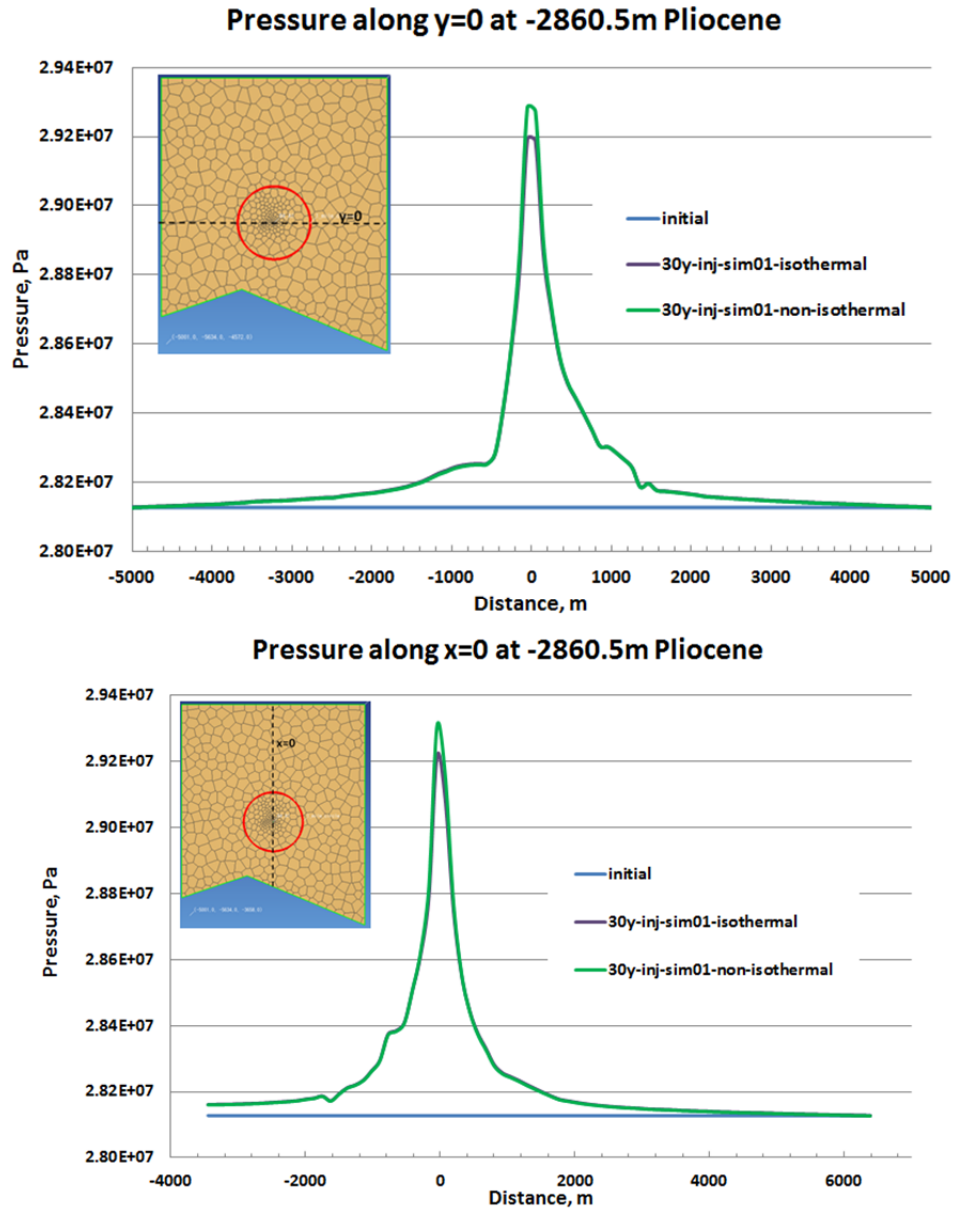

Figure 21: Comprison of pressure profiles across injection well through the middle of injection interval, after 30 years injection into the Pliocene, baseline case (84_P_sim01)-isothermal and non-isothermal (84_P_sim07) – Ship Shoal Block 84 field

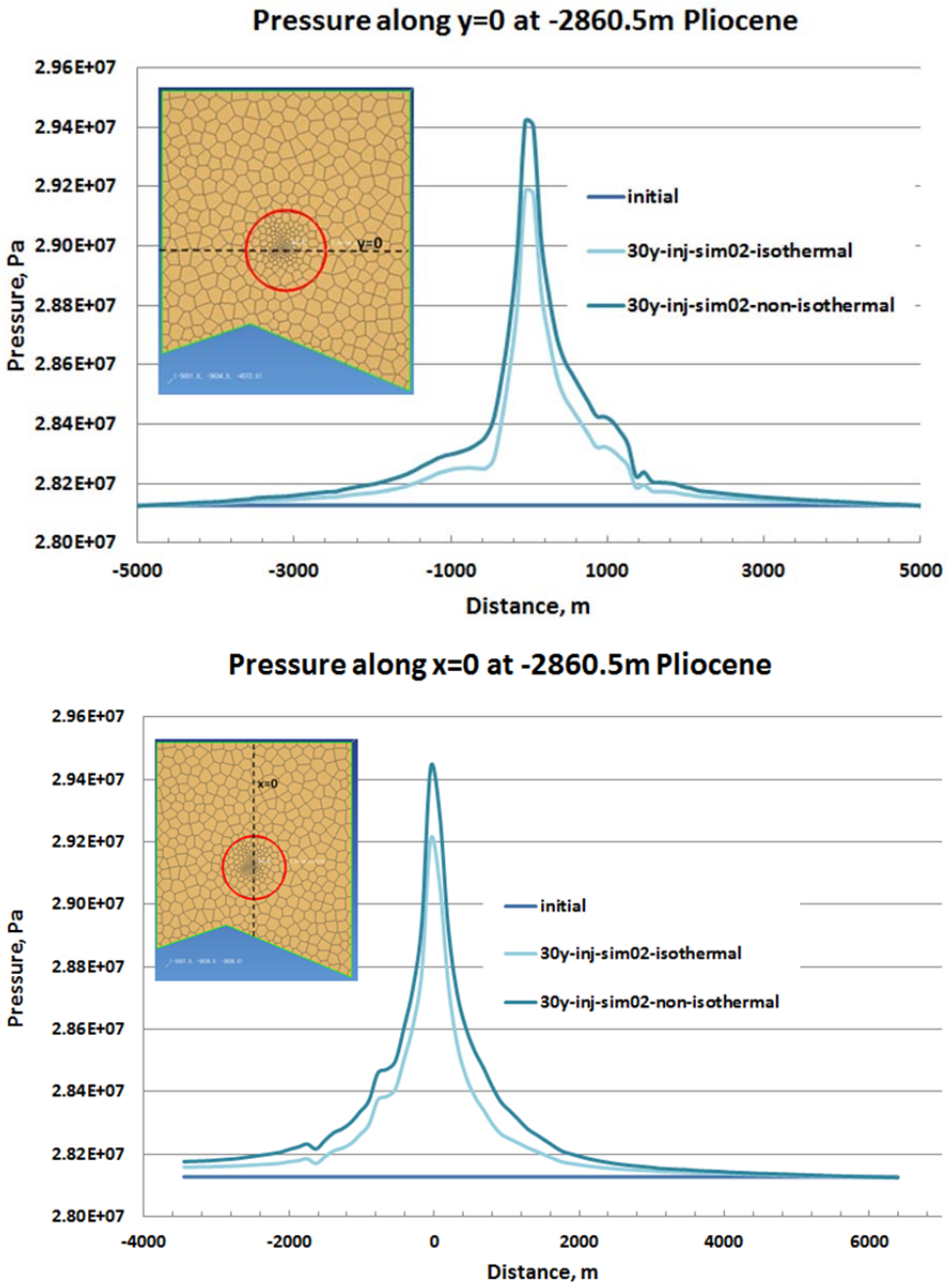

Figure 22 Comprison of pressure profiles across injection well through the middle of injection interval, after 30 years injection into the Pliocene, (84_P_sim02)-isothermal and non-isothermal (84_P_sim08)– Ship Shoal Block 84 field

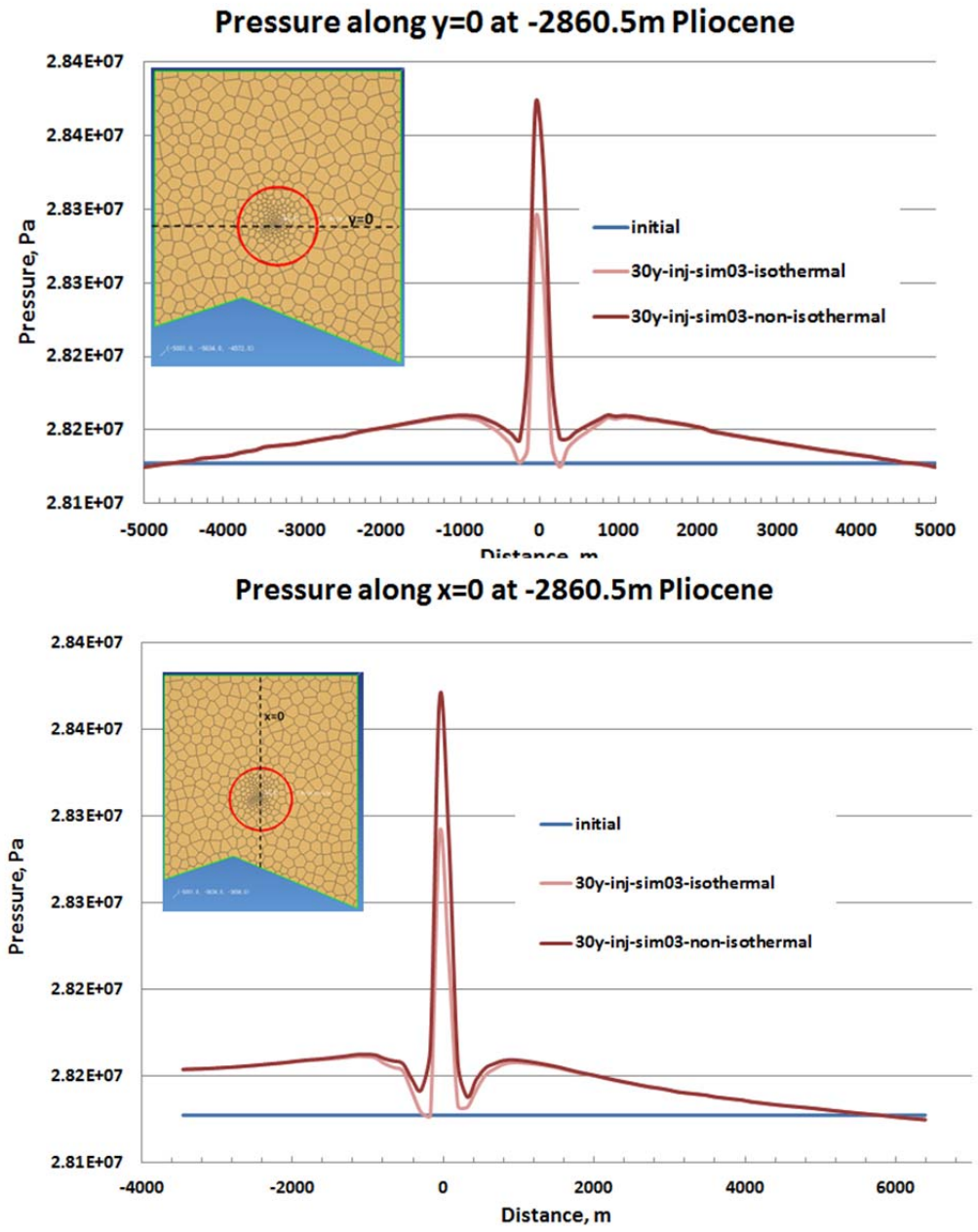

Figure 23 Comprison of pressure profiles across injection well through the middle of injection interval, after 30 years injection into the Pliocene, (84_P_sim03)-isothermal and non-isothermal (84_P_sim09) – Ship Shoal Block 84 field

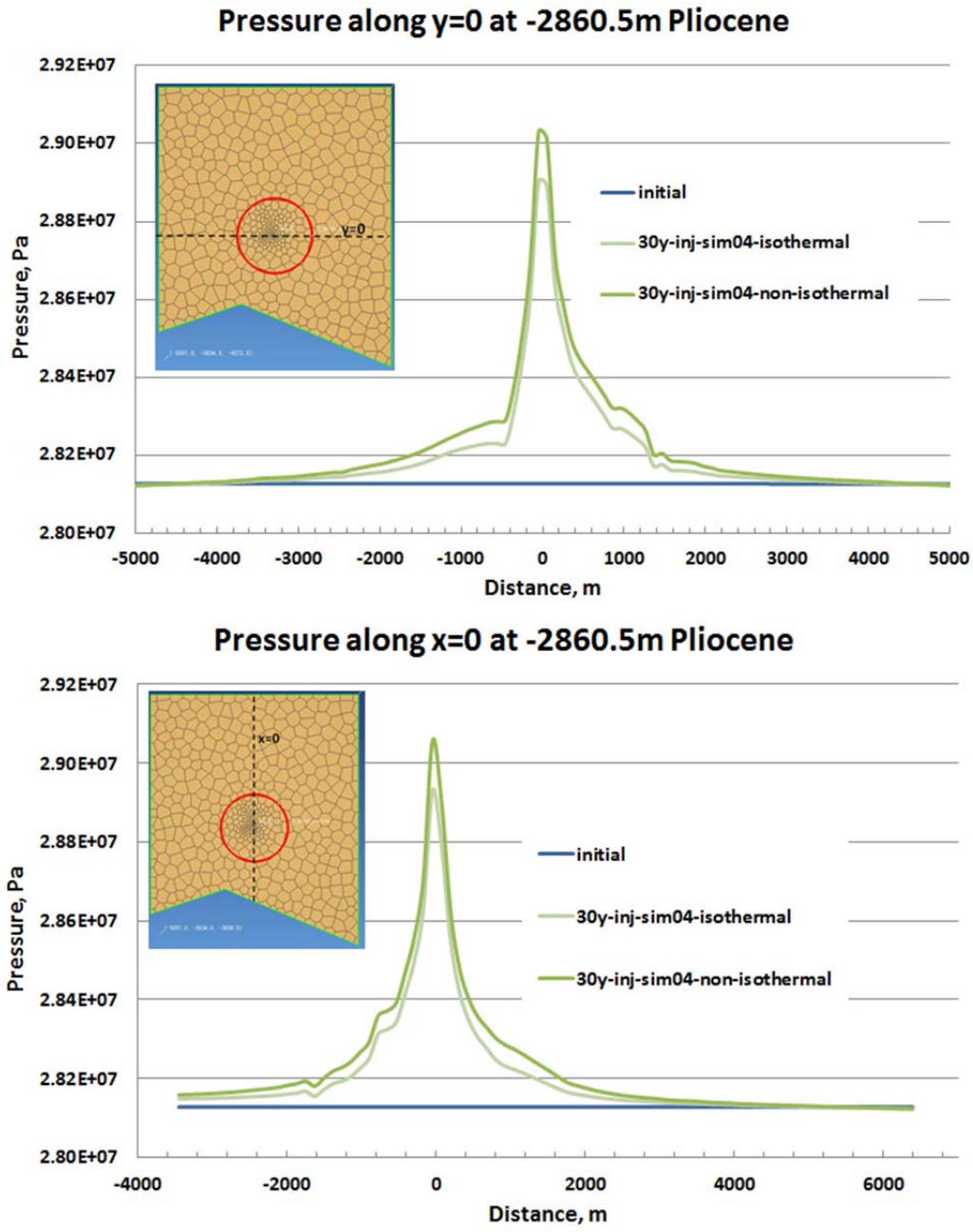

Figure 24 Comprison of pressure profiles across injection well through the middle of injection interval, after 30 years injection into the Pliocene, (84_P_sim04)-isothermal and non-isothermal (84_P_sim10)– Ship Shoal Block 84 field

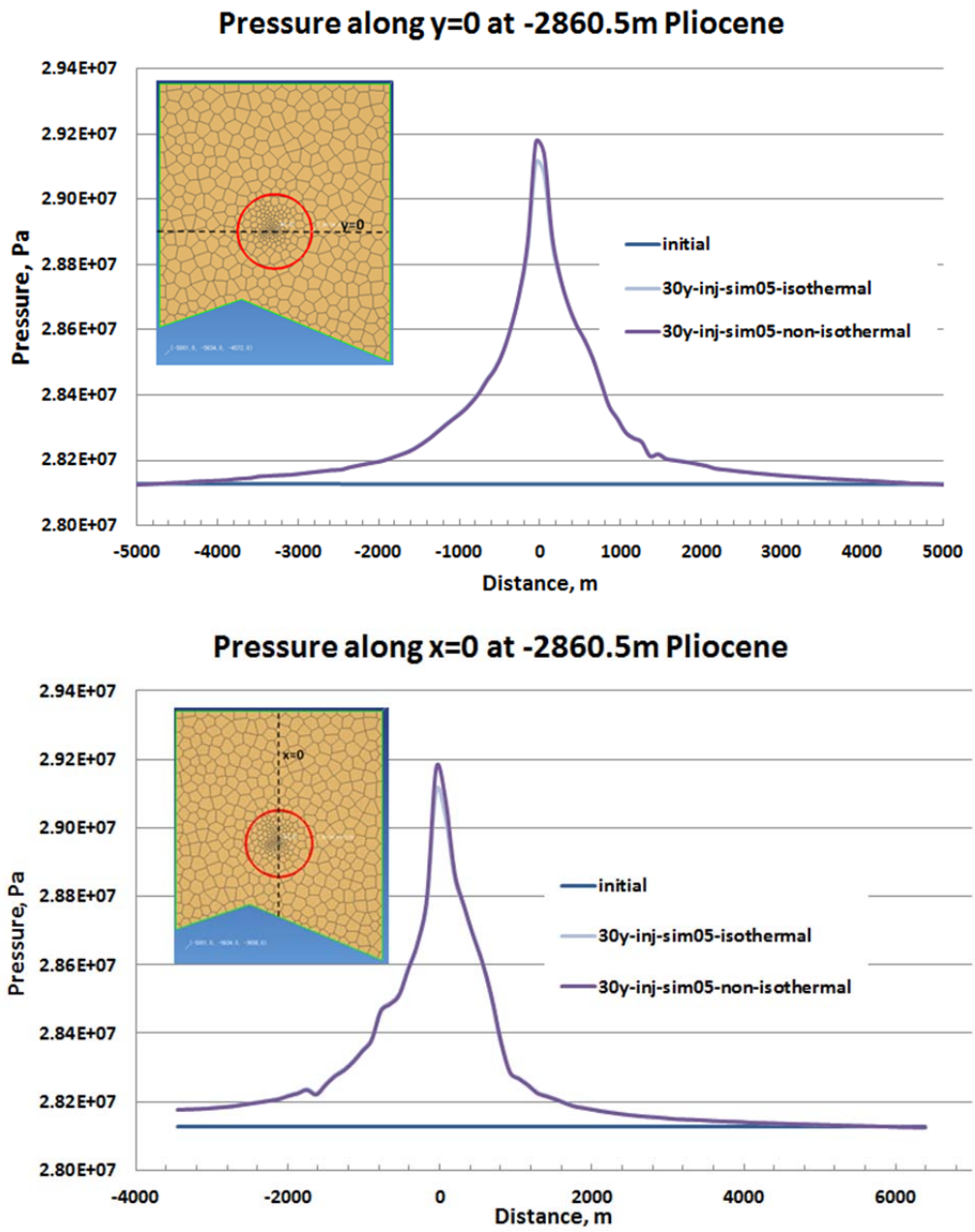

Figure 25 Comprison of pressure profiles across injection well through the middle of injection interval, after 30 years injection into the Pliocene, (84_P_sim05)-isothermal and non-isothermal (84_P_sim11) – Ship Shoal Block 84 field

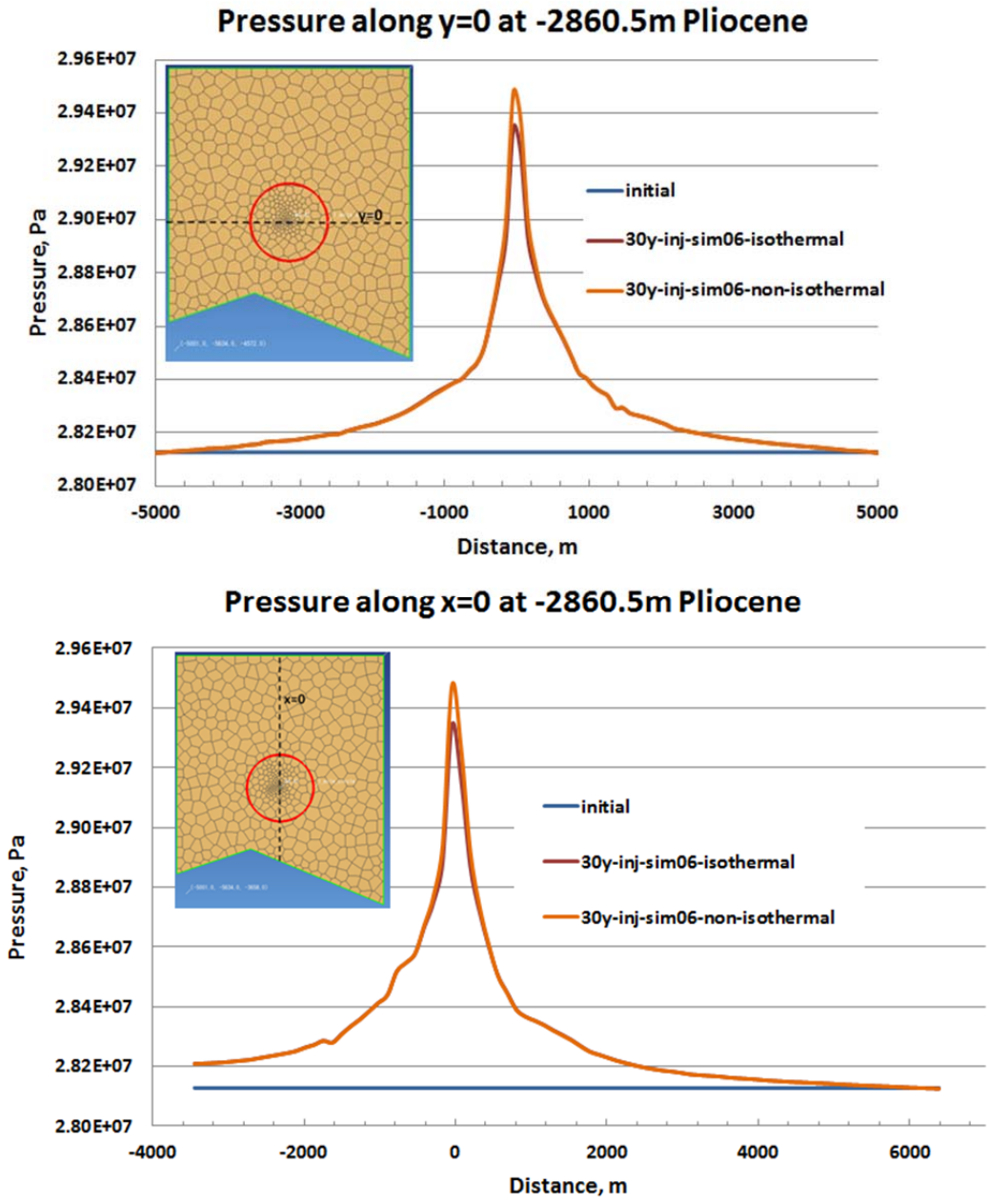

Figure 26 Comprison of pressure profiles across injection well through the middle of injection interval, after 30 years injection into the Pliocene, (84_P_sim06)-isothermal and non-isothermal (84_P_sim12) – Ship Shoal Block 84 field

1.2 Upper Miocene Fluid Flow Non-isothermal Simulation results

Figure 27, Figure 30, Figure 33, Figure 36, Figure 39, and Figure 42 are showing the cross sections of gas saturation after 1 year, 15 years, and 30 years CO_2 injection of the six scenarios

respectively. We can see that CO_2 is contained within the injection formation for 84_M_sim07, 84_M_sim08, 84_M_sim10 and 84_m_sim11 during 30 years' injection, and CO_2 migrates above (about 1000 ft) and below (about 300 to 500 ft) injection interval for scenario 84_M_sim09 (no capillary pressure) and 84_M_sim12 (double injection rate) without leakage. 84_m_sim09 represents the most critical case which contains no capillary pressure in the sand, silt and shale, and the gas plume easily migrates upward during the injection phase.

Figure 28, Figure 31, Figure 34, Figure 37, Figure 40, and Figure 43 are showing the cross sections of temperature after 1 year, 15 years, and 30 years CO_2 injection of the six scenarios respectively. We can see that low temperature plume grows at injection interval similarly for all scenarios as we are injecting CO_2 at 60 ^{0}C, and 84_P_sim12 has slightly larger temperature plume as we doubled the injection.

Figure 29, Figure 32, Figure 35, Figure 38, Figure 41, and Figure 44 indicate the top view of the CO_2 gas plume after 30 years injection for the six scenarios. The gas plumes are all contained within about the 1 mile radius around the injection well, except scenarios 84_M_sim12.

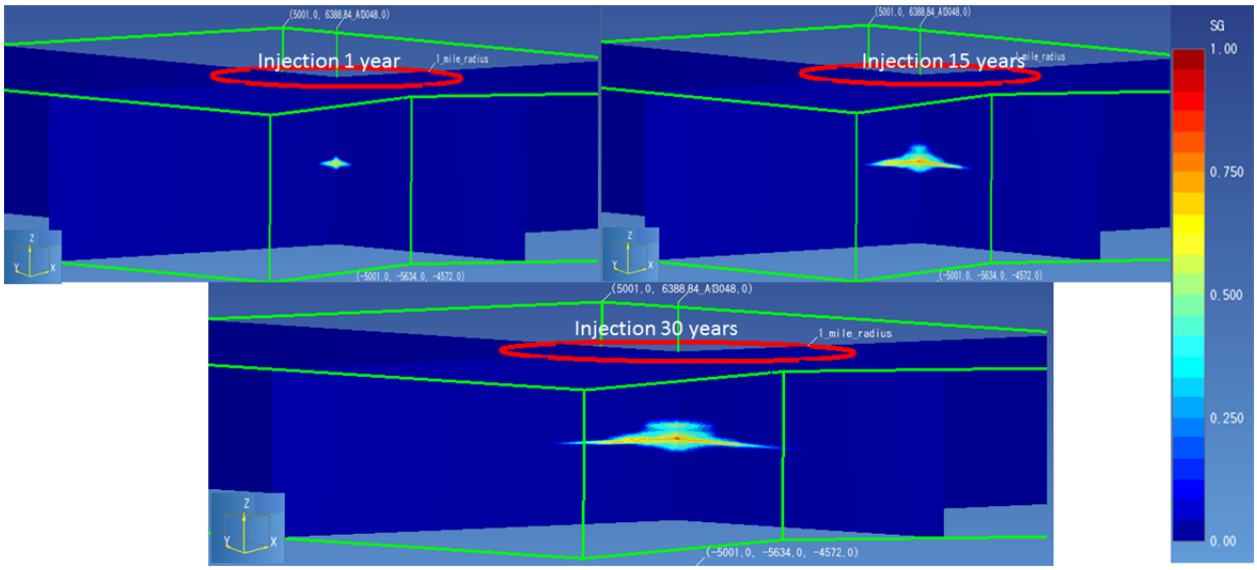

Figure 27: The cross-sections of Gas Saturation after 1, 15, 30 years injection, baseline case (84_M_sim07) of Miocene-non-isothermal, Ship Shoal Block 84 field

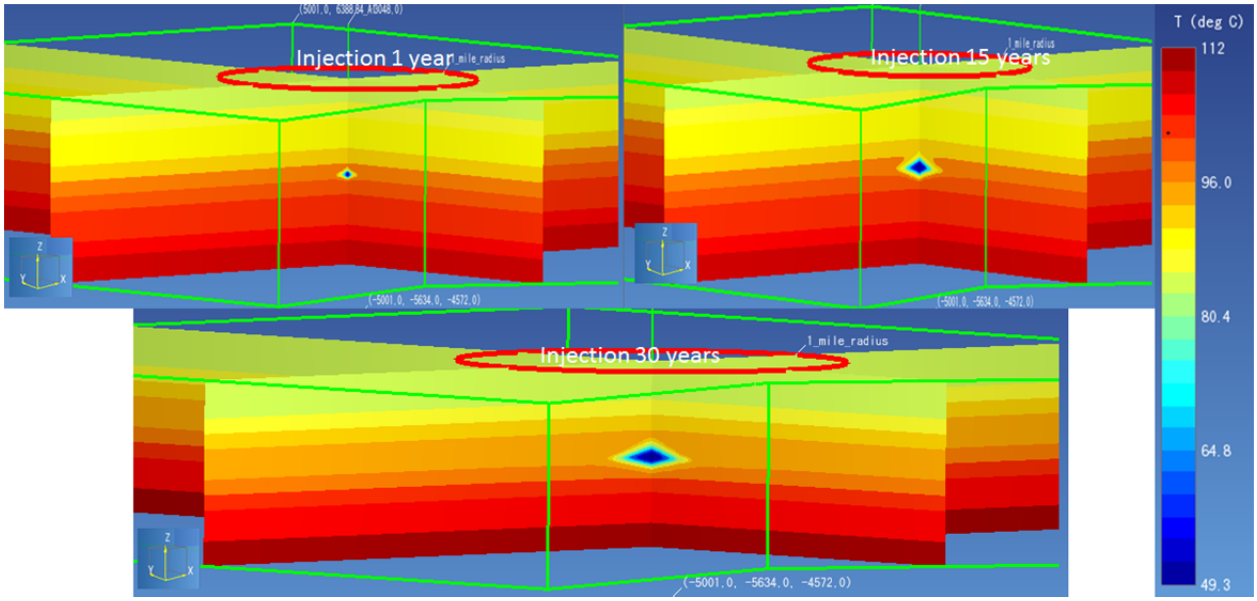

Figure 28: The cross-sections of temperature after 1, 15, 30 years injection, baseline case (84_M_sim07) of Miocene-non-isothermal, Ship Shoal Block 84 field

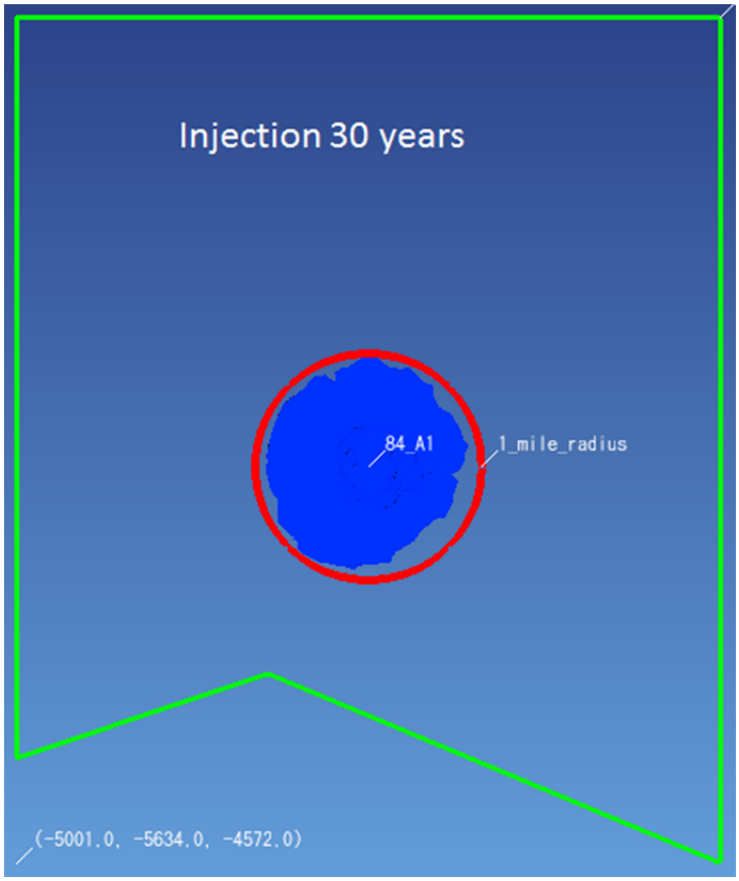

Figure 29: The top view of CO2 Gas plume after 30 years injection, baseline case (84_M_sim07) of Miocene-non- isothermal, Ship Shoal Block 84 field

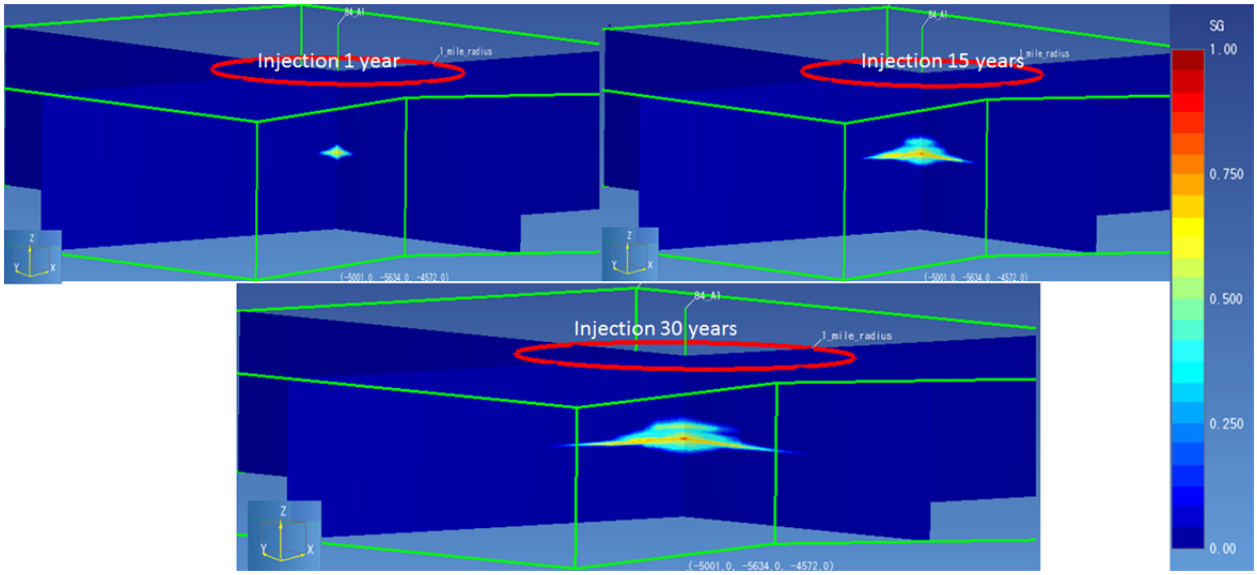

Figure 30: The cross-sections of Gas Saturation after 1, 15, 30 years injection, 84_M_sim08 of Miocene-non-isothermal, Ship Shoal Block 84 field

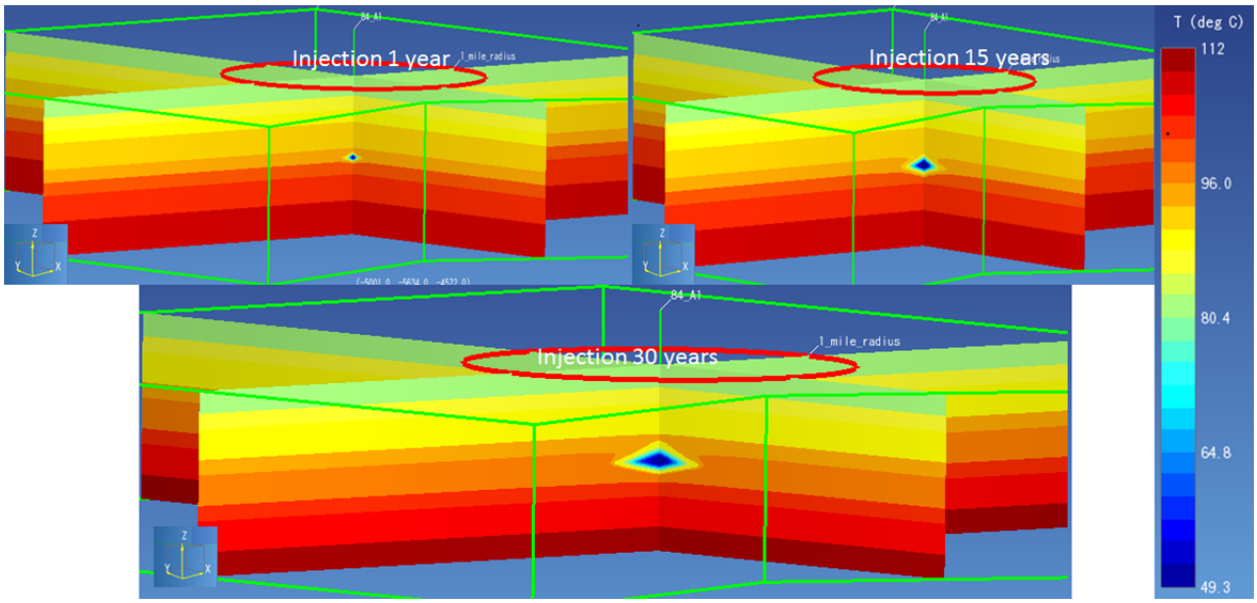

Figure 31 The cross-sections of temperature after 1, 15, 30 years injection, 84_M_sim08 of Miocene-non-isothermal, Ship Shoal Block 84 field

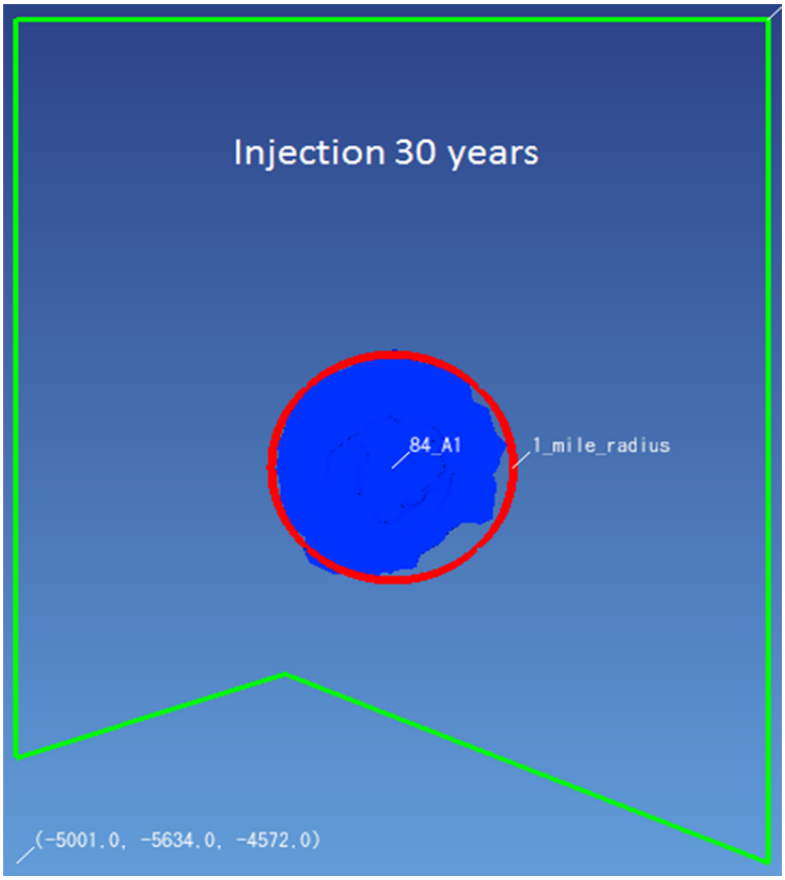

Figure 32 The top view of CO2 Gas plume after 30 years injection, 84_M_sim08 of Miocene-non-isothermal, Ship Shoal Block 84 field

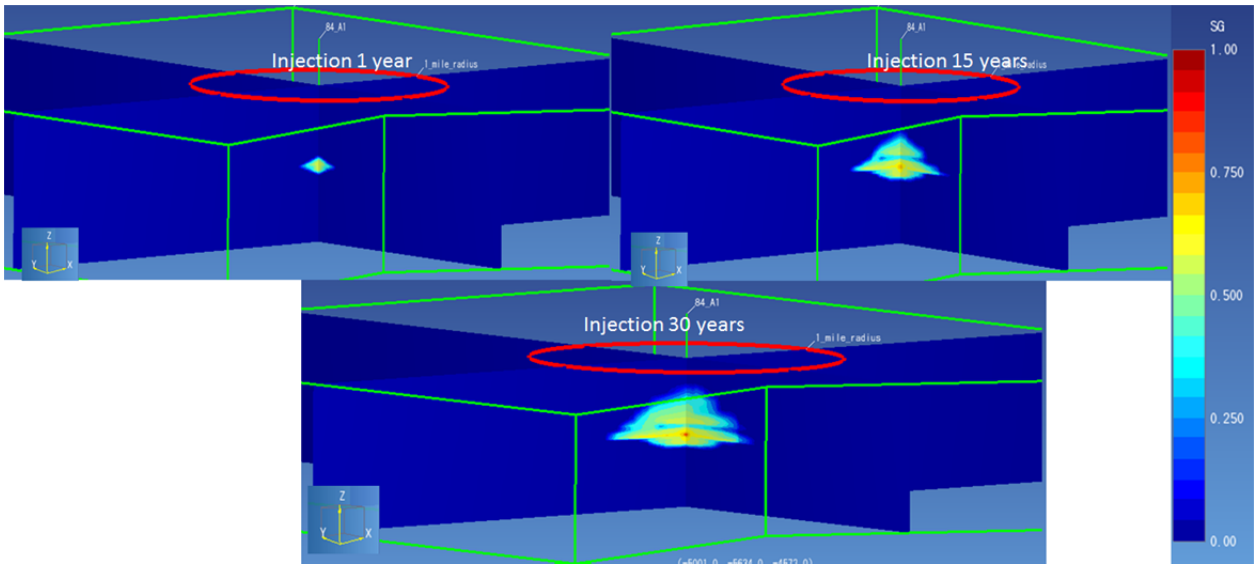

Figure 33 The cross-sections of Gas Saturation after 1, 15, 30 years injection, 84_M_sim09 of Miocene-non-isothermal, Ship Shoal Block 84 field

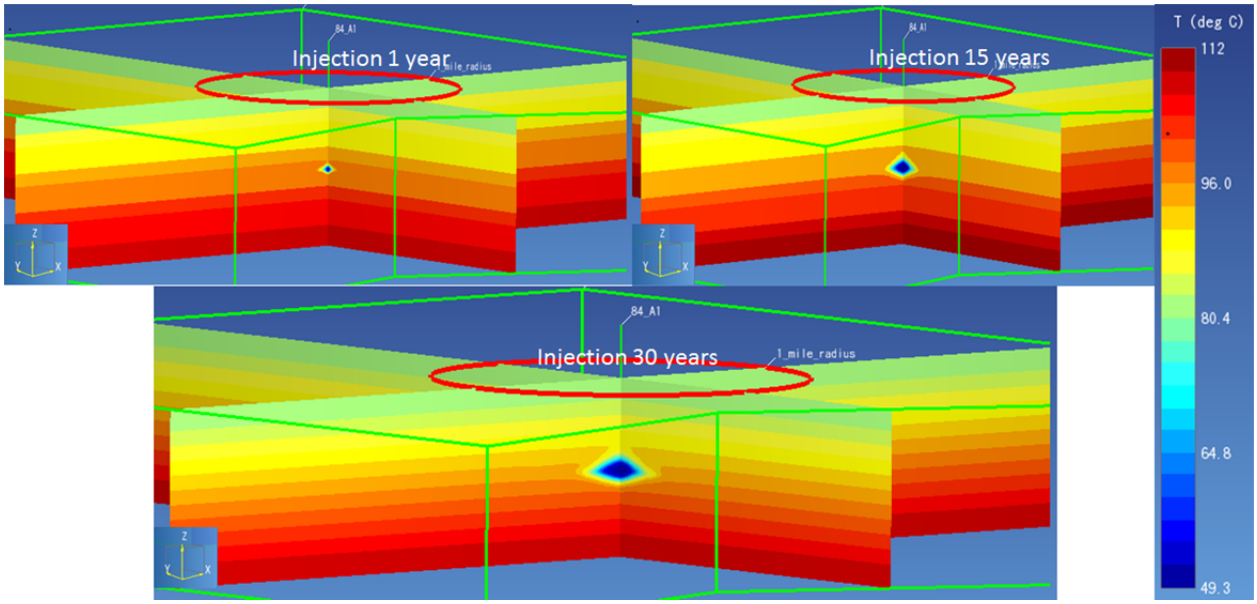

Figure 34 The cross-sections of temperature after 1, 15, 30 years injection, 84_M_sim09 of Miocene-non-isothermal, Ship Shoal Block 84 field

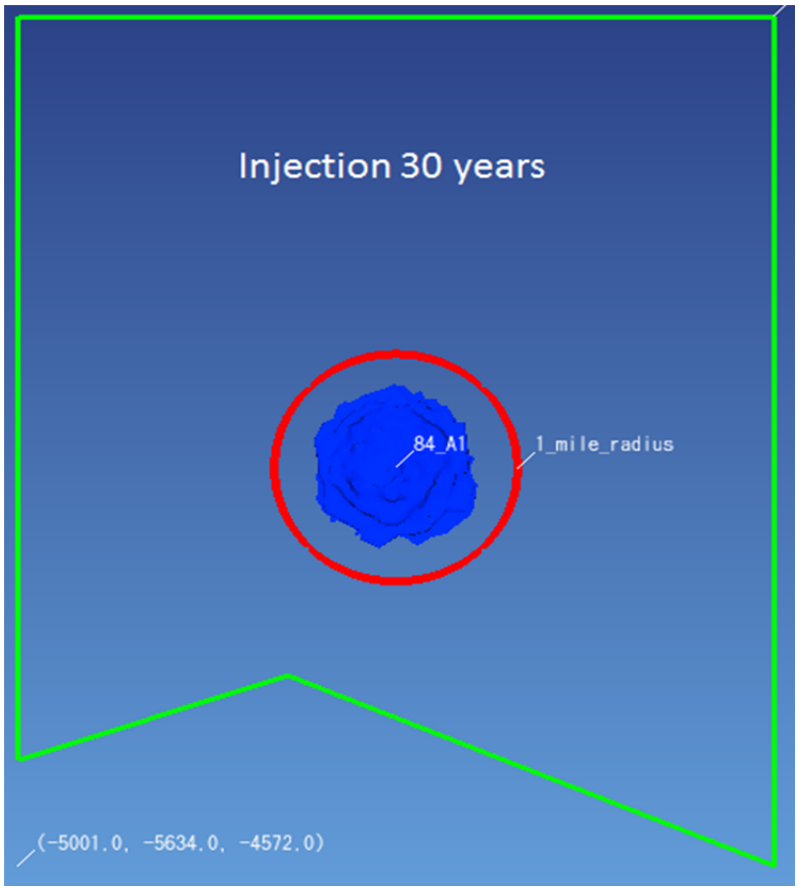

Figure 35 The top view of CO2 Gas plume after 30 years injection, 84_M_sim09 of Miocene-non-isothermal, Ship Shoal Block 84 field

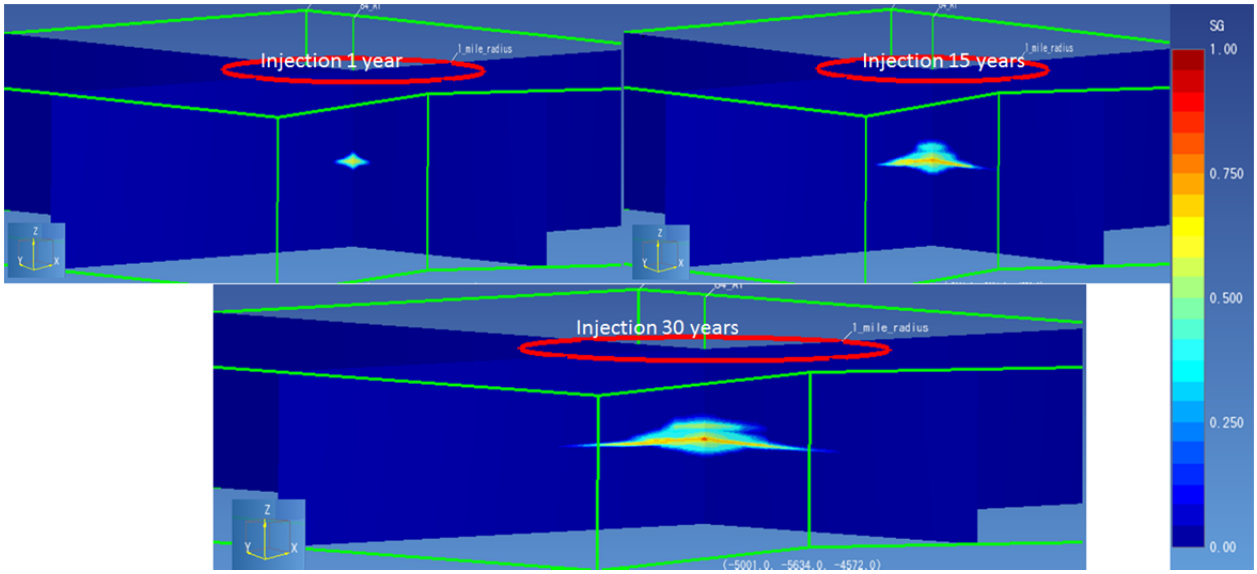

Figure 36 The cross-sections of Gas Saturation after 1, 15, 30 years injection, 84_M_sim10 of Miocene-non-isothermal, Ship Shoal Block 84 field

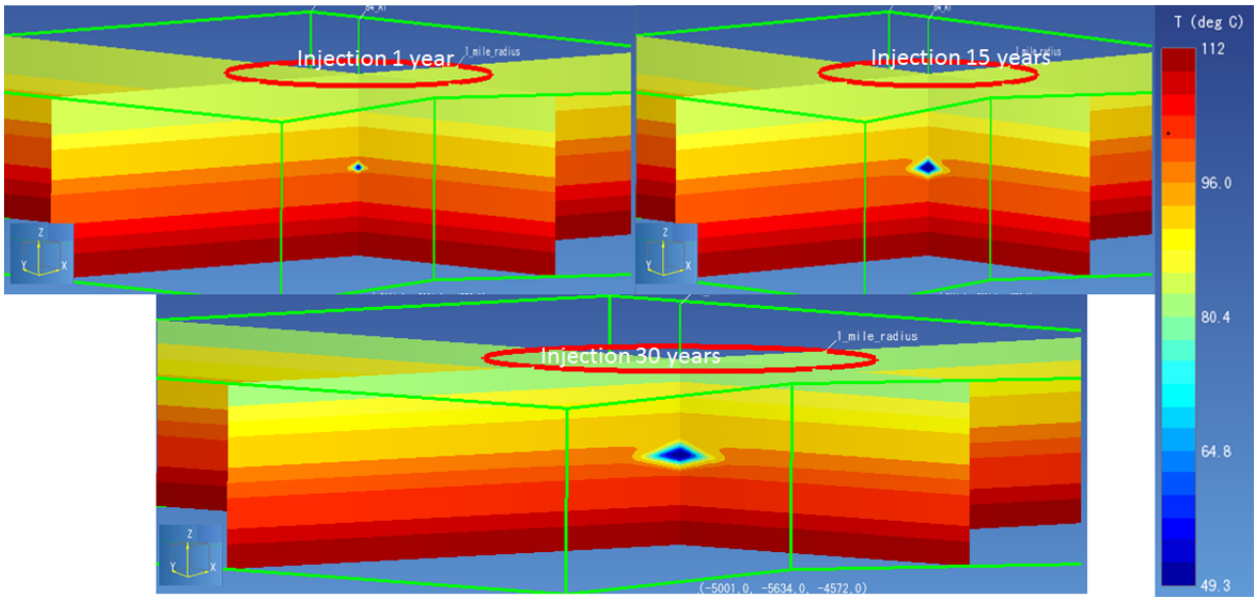

Figure 37 The cross-sections of temperature after 1, 15, 30 years injection, 84_M_sim10 of Miocene-non-isothermal, Ship Shoal Block 84 field

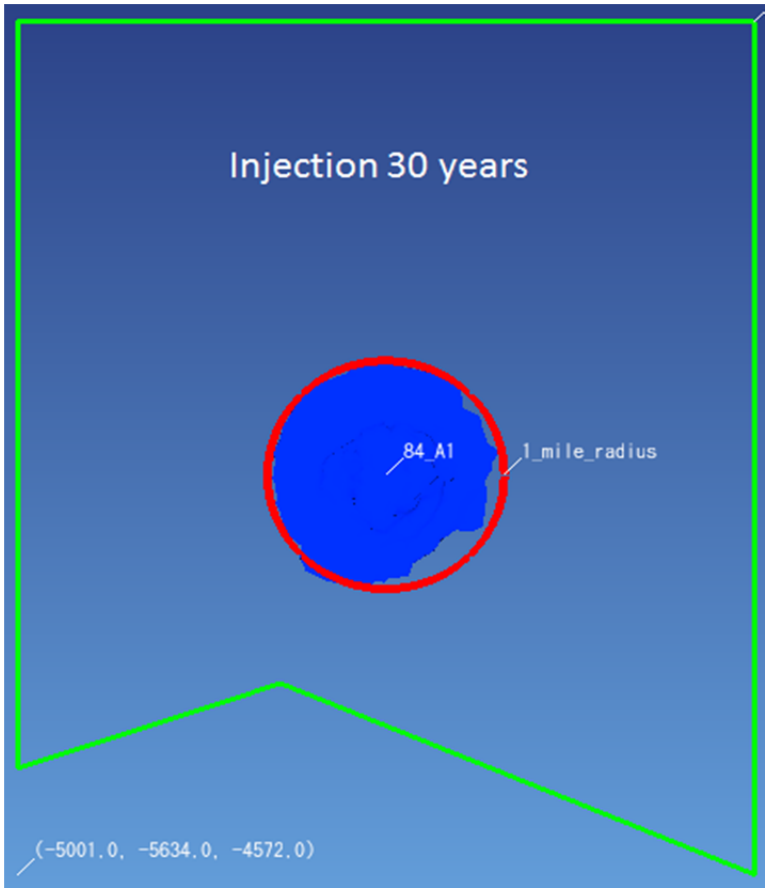

Figure 38 The top view of CO2 Gas plume after 30 years injection, 84_M_sim10 of Miocene-non-isothermal, Ship Shoal Block 84 field

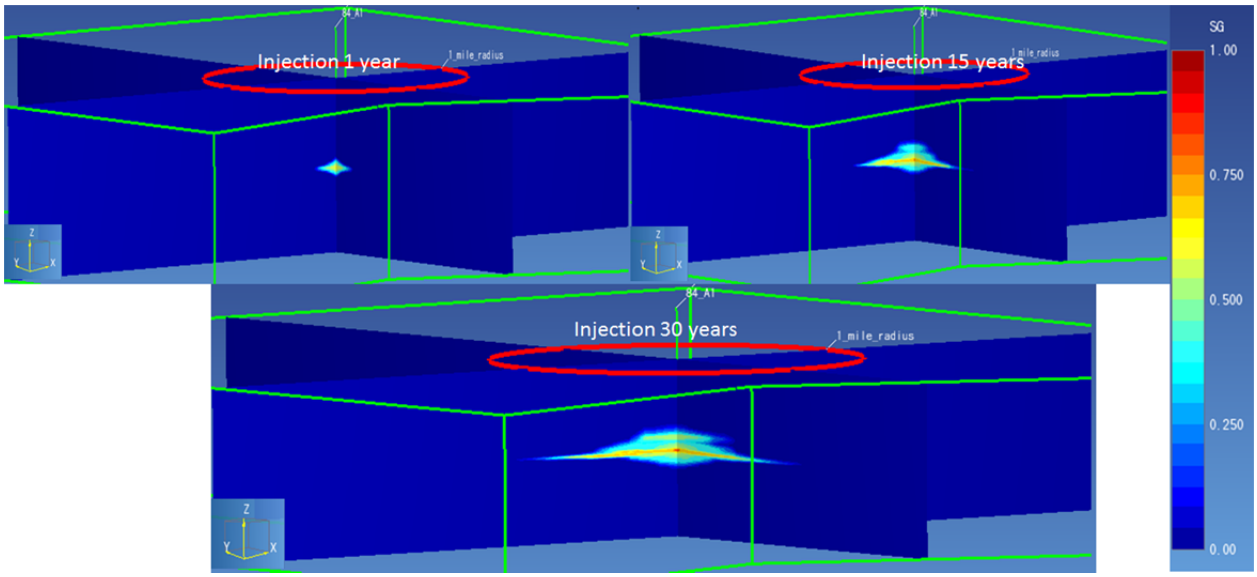

Figure 39 The cross-sections of Gas Saturation after 1, 15, 30 years injection, 84_M_sim11 of Miocene-non-isothermal, Ship Shoal Block 84 field

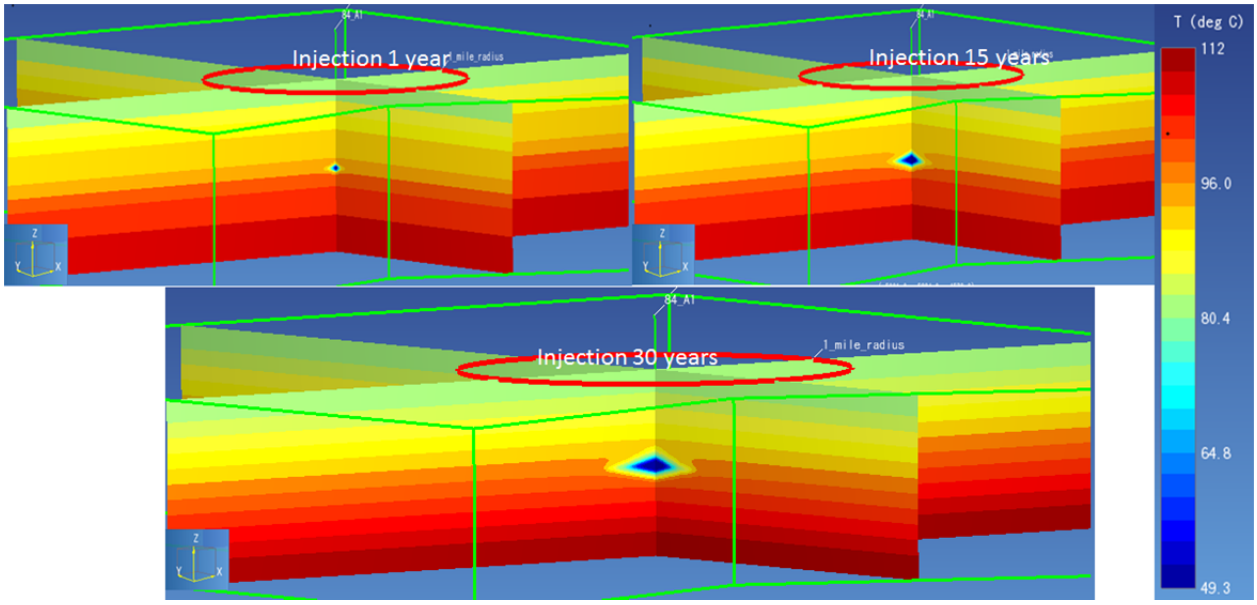

Figure 40 The cross-sections of temperature after 1, 15, 30 years injection, 84_M_sim11 of Miocene-non-isothermal, Ship Shoal Block 84 field

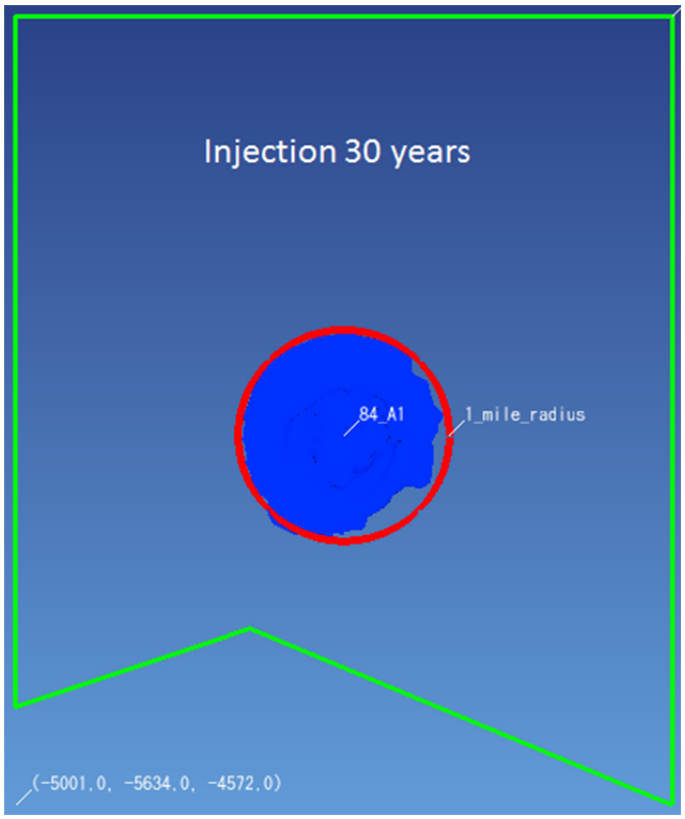

Figure 41 The top view of CO2 Gas plume after 30 years injection, 84_M_sim11 of Miocene-non-isothermal, Ship Shoal Block 84 field

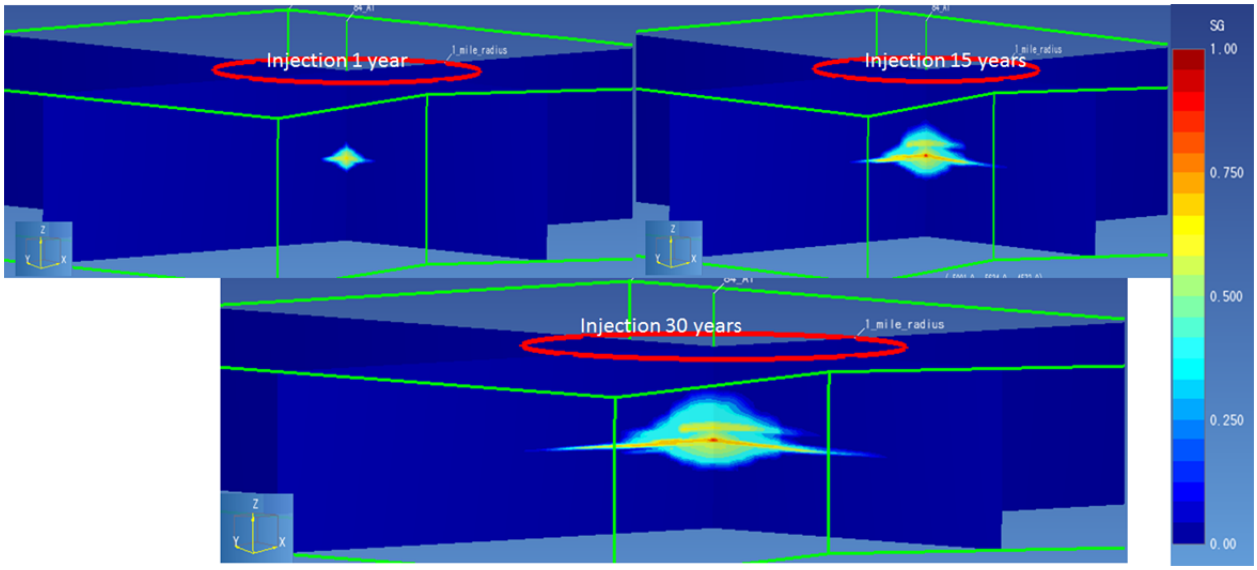

Figure 42 The cross-sections of Gas Saturation after 1, 15, 30 years injection, 84_M_sim12 of Miocene-non-isothermal, Ship Shoal Block 84 field

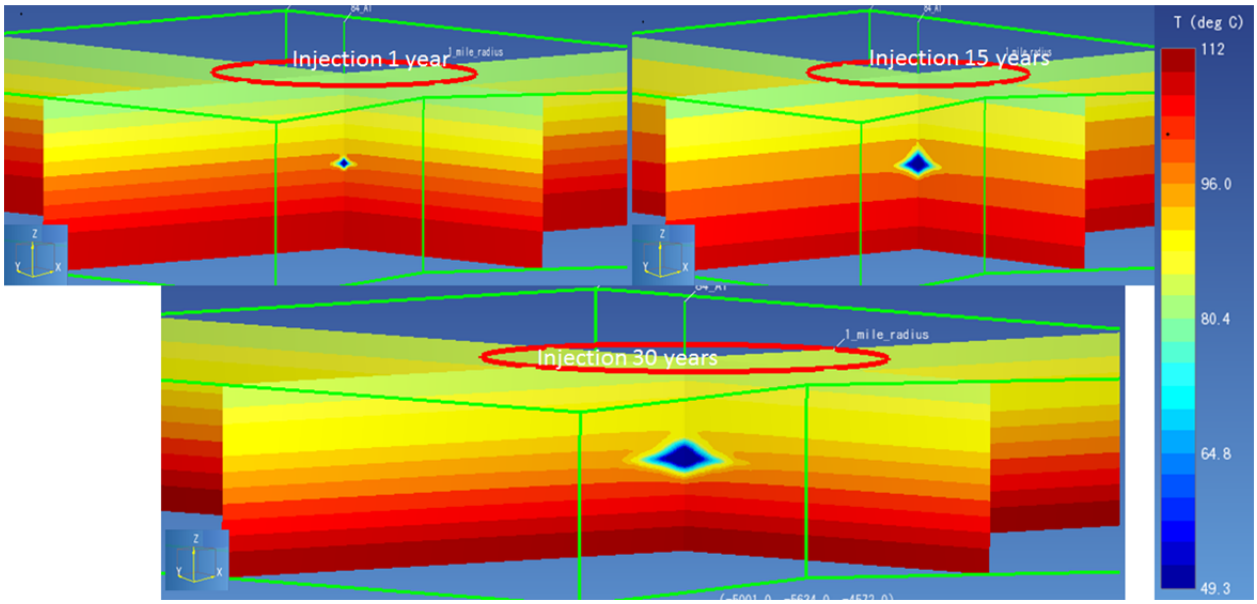

Figure 43 The cross-sections of temperature after 1, 15, 30 years injection, 84_M_sim12 of Miocene-non-isothermal, Ship Shoal Block 84 field

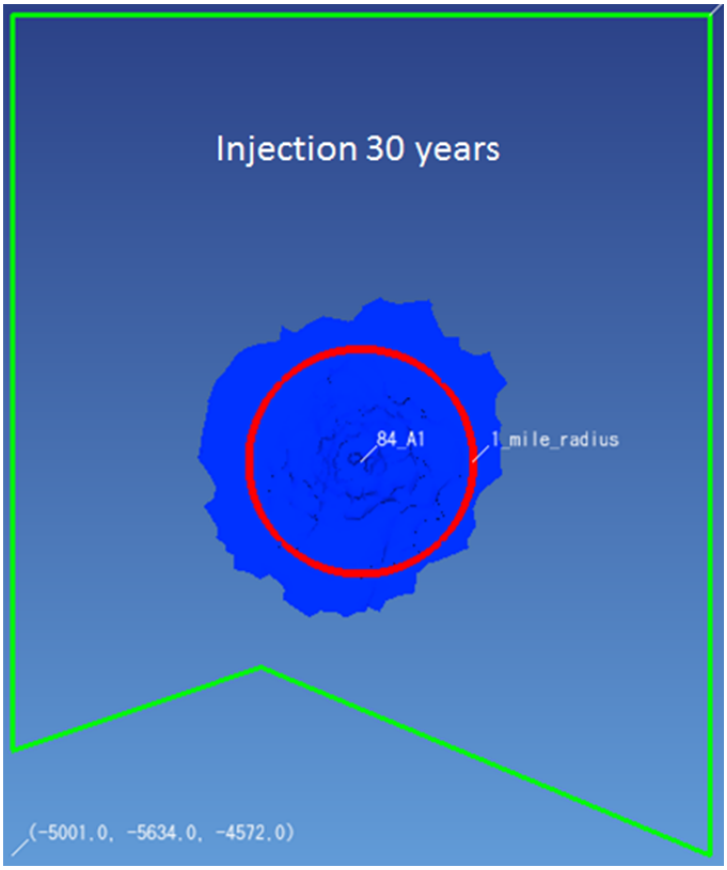

Figure 44 The top view of CO2 Gas plume after 30 years injection, 84_M_sim12 of Miocene-non-isothermal, Ship Shoal Block 84 field

Figure 45 indicates the comparison of pressure profiles across the injection well through the middle of the injection interval (=-3832.4 m), at in-situ conditions and after 30 years of injection. We can see that 84_M_sim12 (double injection rate) reaches higher pressure after 30 years constant rate of CO_2 injection, and 84_M_sim09 (contains no capillary pressure) has the lowest pressure after 30 years of constant CO_2 injection. All other scenarios have close pressure profiles.

Figure 46 plots the comparison of temperature profiles across the injection well through the middle of the injection interval (=-3832.4 m), at in-situ conditions and after 30 years of injection. We can see that the temperature is fixed at 60 ^{0}C at the wellbore for all scenarios during the injection, and 84_M_sim12 (double injection rate) has the lowest temperature profile around the injection well after 30 years of constant CO_2 injection, and all other scenarios have a similar temperature profile around the injection well.

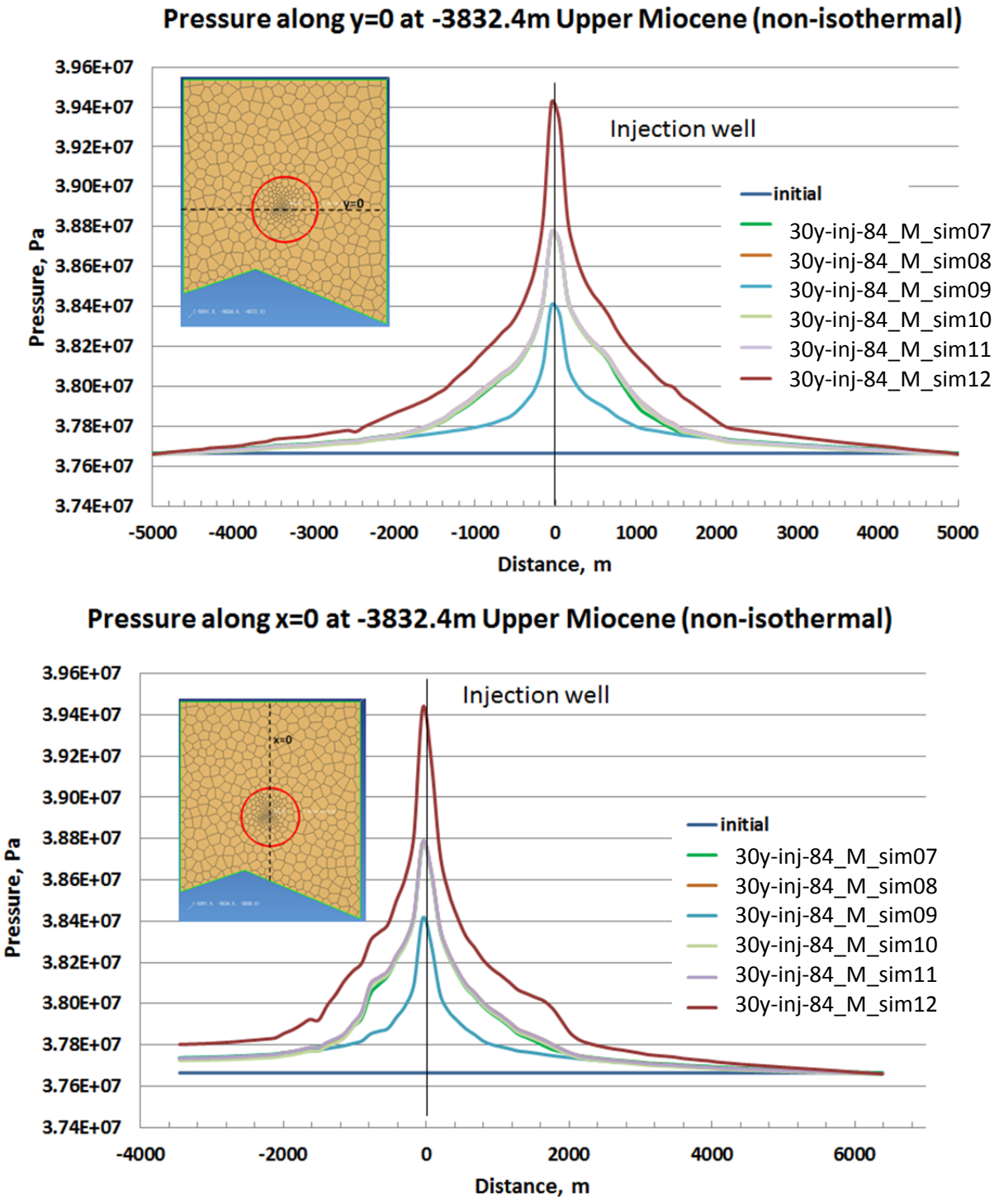

Figure 45 Comprison of pressure profiles across injection well through the middle of injection interval, at initial and after 30 years injection into the Miocene-non-isothermal – Ship Shoal Block 84 field

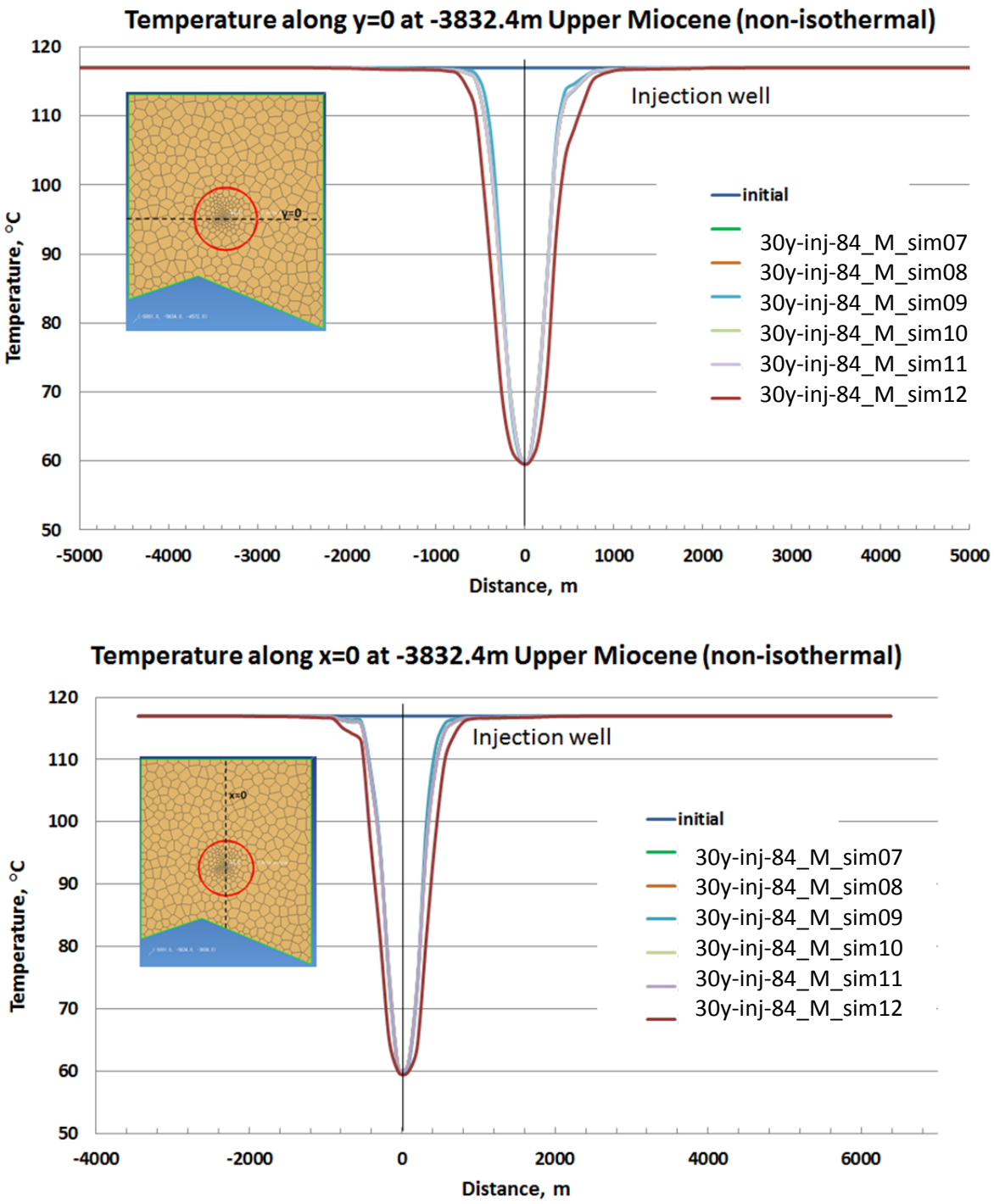

Figure 46 Comprison of temperature profiles across injection well through the middle of injection interval, at initial and after 30 years injection into the Miocene-non-isothermal – Ship Shoal Block 84 field

Figure 21 to Figure 26 compare the pressure profiles across injection well through middle of injection interval (=-3832.4m), after 30 years of injection of each scenario respectively, between the isothermal and non-isothermal effects. We can see that the pressure profiles of simulations run in isothermal mode are slightly higher than the ones of running in non-isothermal mode. Around the injection well in scenarios sim01 and sim06, and the difference is less than 2%; for the other scenarios, pressure profiles with temperature effect are slightly higher than isothermal, and the difference is about 1%.

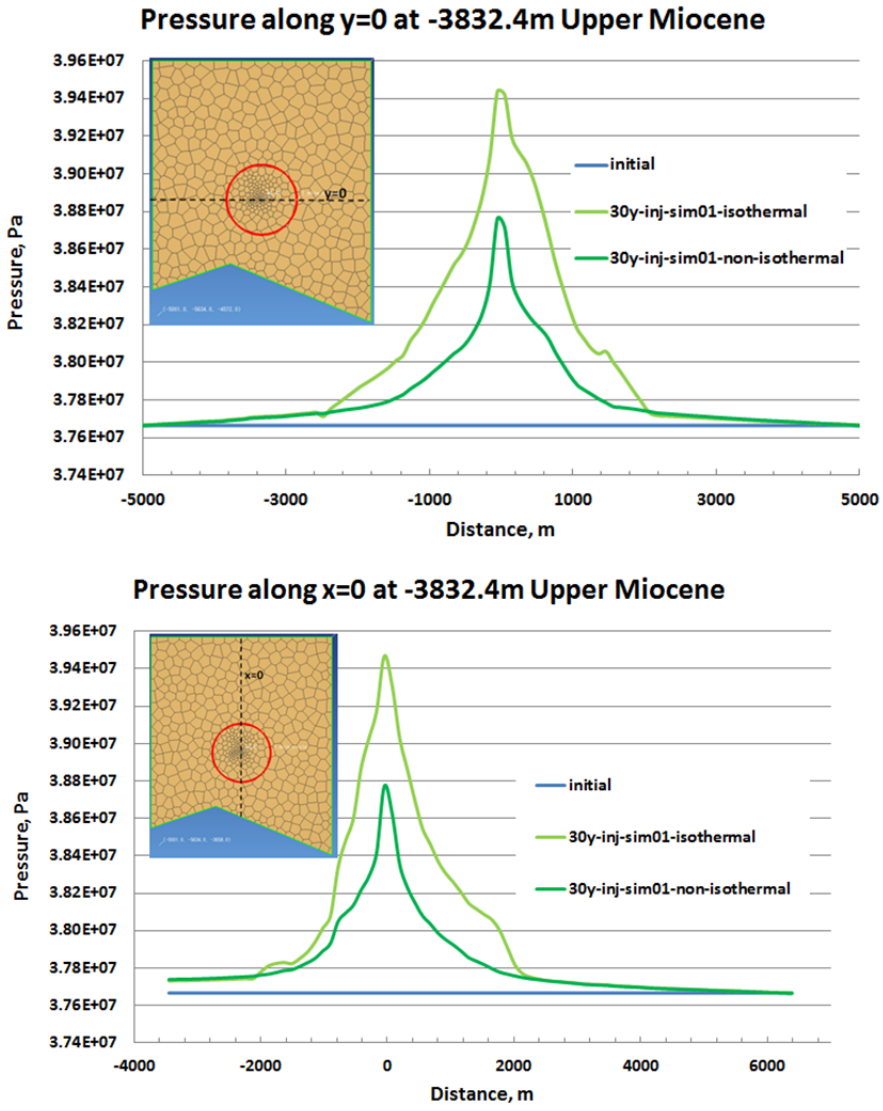

Figure 47 Comprison of pressure profiles across injection well through the middle of injection interval, after 30 years injection into the Upper Miocene, baseline case 84_M_sim01-isothermal and non-isothermal 84_M_sim07 – Ship Shoal Block 84 field

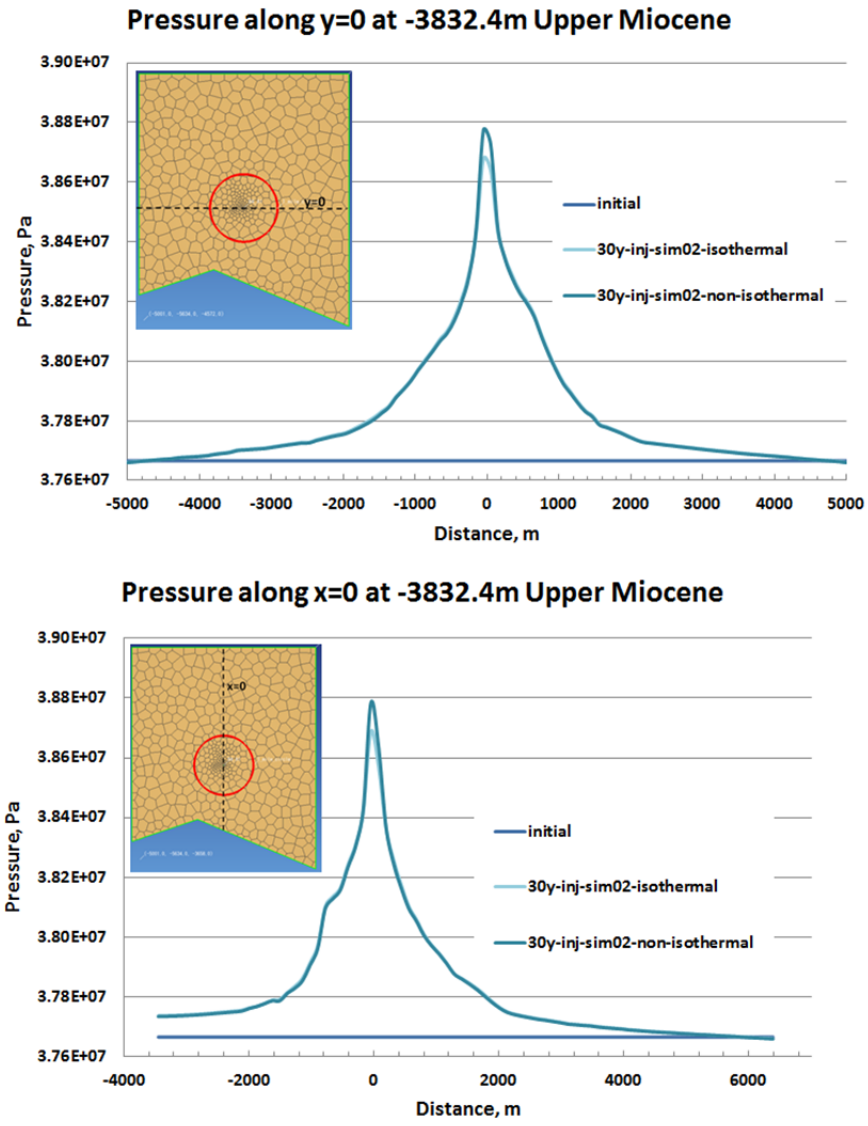

Figure 48 Comprison of pressure profiles across injection well through the middle of injection interval, after 30 years injection into the Upper Miocene, 84_M_sim02 -isothermal and non-isothermal 84_M_sim08 – Ship Shoal Block 84 field

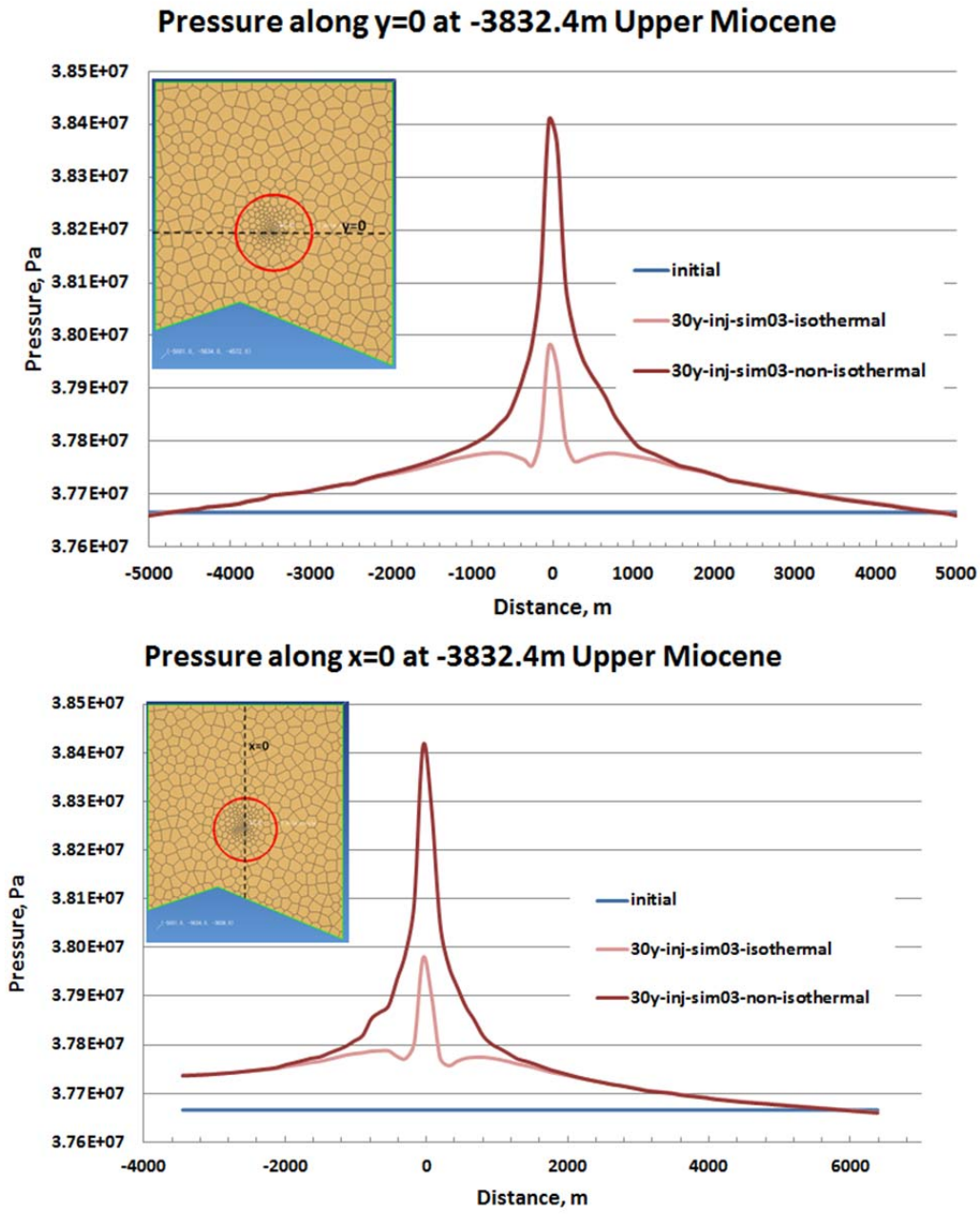

Figure 49 Comprison of pressure profiles across injection well through the middle of injection interval, after 30 years injection into the Upper Miocene, 84_M_sim03 -isothermal and non-isothermal 84_M_sim09 – Ship Shoal Block 84 field

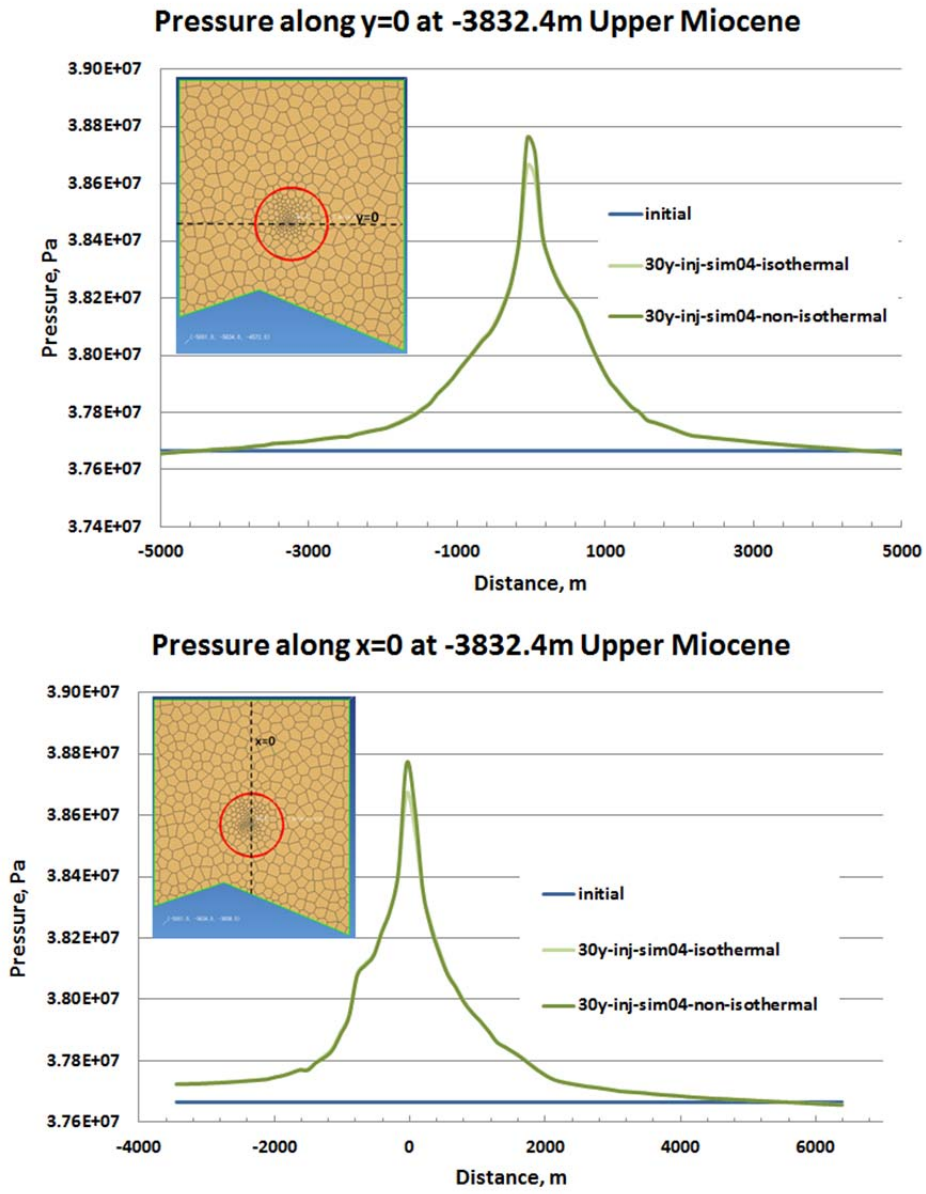

Figure 50 Comprison of pressure profiles across injection well through the middle of injection interval, after 30 years injection into the Upper Miocene, 84_M_sim04 -isothermal and non-isothermal 84_M_sim10 – Ship Shoal Block 84 field

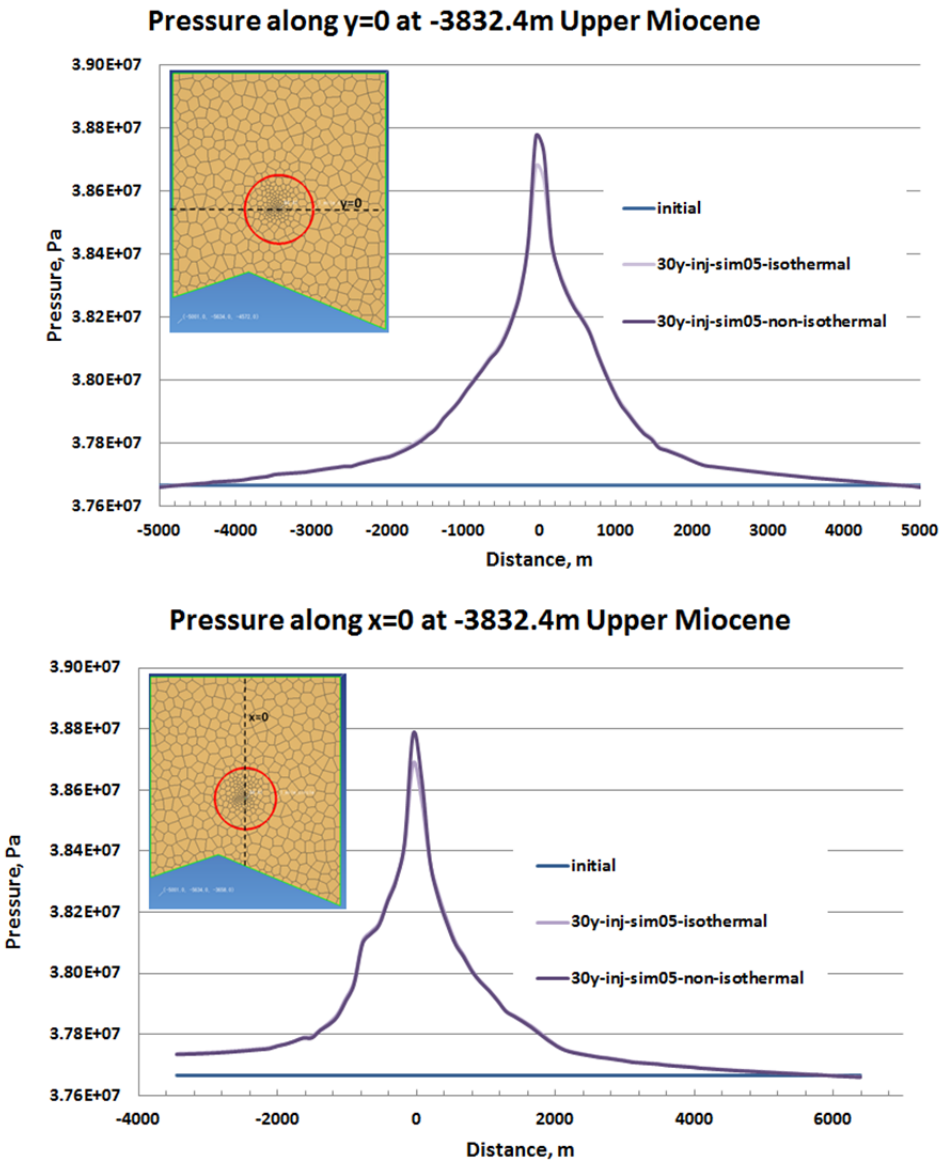

Figure 51 Comprison of pressure profiles across injection well through the middle of injection interval, after 30 years injection into the Upper Miocene, 84_M_sim05 -isothermal and non-isothermal 84_M_sim11 – Ship Shoal Block 84 field

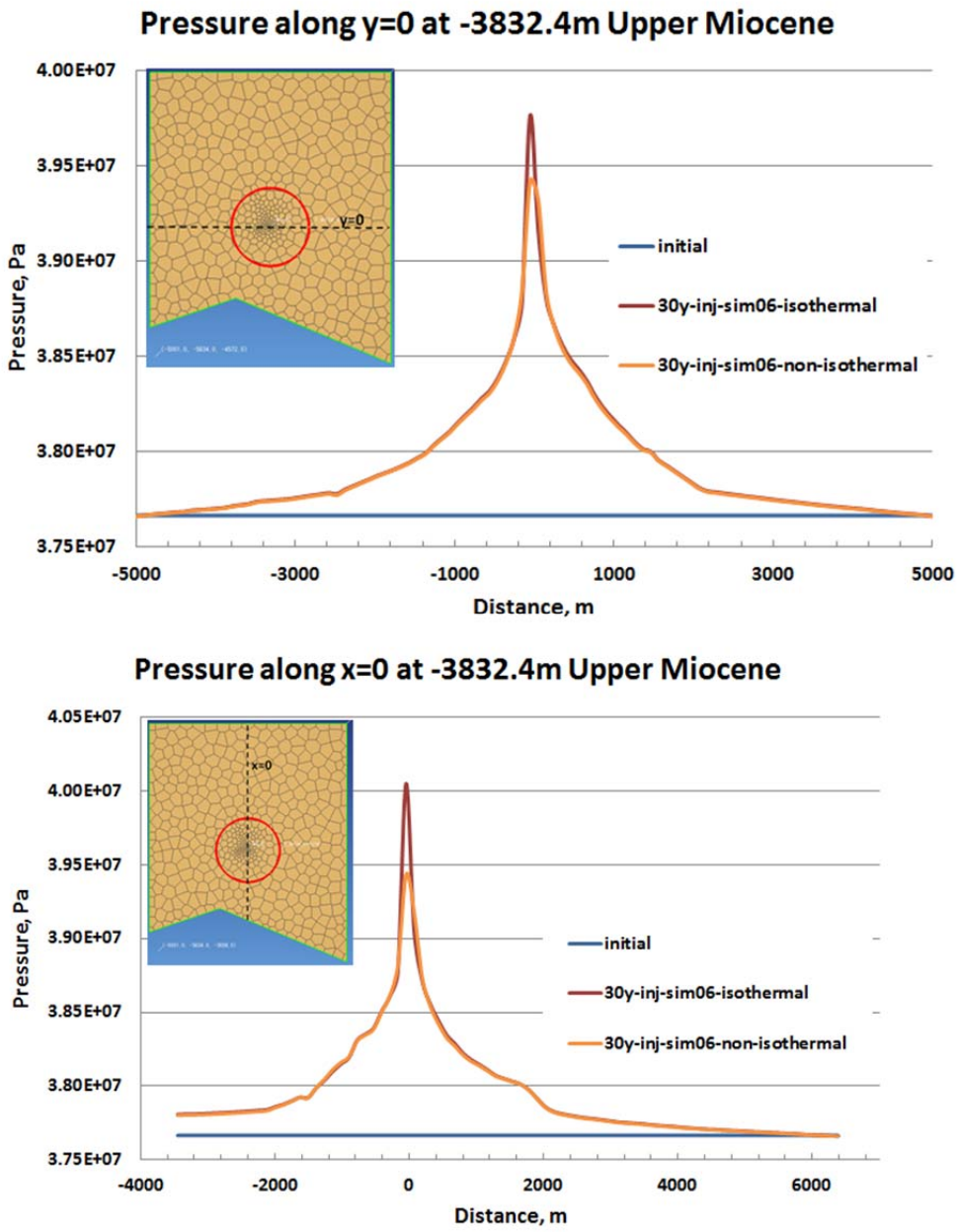

Figure 52 Comprison of pressure profiles across injection well through the middle of injection interval, after 30 years injection into the Upper Miocene, 84_M_sim06 -isothermal and non-isothermal 84_M_sim12 – Ship Shoal Block 84 field